frontiers | Research Topics

Microbiome associated with plant pathogens, pathogenesis, and their applications in developing sustainable agriculture

Edited by
Baoyu Tian, Jian-Wei Guo, Xiao Lin Wang, Dilfuza Egamberdieva and Osama Abdalla Abdelshafy Mohamad

Published in
Frontiers in Microbiology

ISSN 1664-8714
ISBN 978-2-8325-4960-5
DOI 10.3389/978-2-8325-4960-5

About Frontiers

Frontiers is more than just an open access publisher of scholarly articles: it is a pioneering approach to the world of academia, radically improving the way scholarly research is managed. The grand vision of Frontiers is a world where all people have an equal opportunity to seek, share and generate knowledge. Frontiers provides immediate and permanent online open access to all its publications, but this alone is not enough to realize our grand goals.

Frontiers journal series

The Frontiers journal series is a multi-tier and interdisciplinary set of open-access, online journals, promising a paradigm shift from the current review, selection and dissemination processes in academic publishing. All Frontiers journals are driven by researchers for researchers; therefore, they constitute a service to the scholarly community. At the same time, the *Frontiers journal series* operates on a revolutionary invention, the tiered publishing system, initially addressing specific communities of scholars, and gradually climbing up to broader public understanding, thus serving the interests of the lay society, too.

Dedication to quality

Each Frontiers article is a landmark of the highest quality, thanks to genuinely collaborative interactions between authors and review editors, who include some of the world's best academicians. Research must be certified by peers before entering a stream of knowledge that may eventually reach the public - and shape society; therefore, Frontiers only applies the most rigorous and unbiased reviews. Frontiers revolutionizes research publishing by freely delivering the most outstanding research, evaluated with no bias from both the academic and social point of view. By applying the most advanced information technologies, Frontiers is catapulting scholarly publishing into a new generation.

What are Frontiers Research Topics?

Frontiers Research Topics are very popular trademarks of the *Frontiers journals series*: they are collections of at least ten articles, all centered on a particular subject. With their unique mix of varied contributions from Original Research to Review Articles, Frontiers Research Topics unify the most influential researchers, the latest key findings and historical advances in a hot research area.

Find out more on how to host your own Frontiers Research Topic or contribute to one as an author by contacting the Frontiers editorial office: frontiersin.org/about/contact

Microbiome associated with plant pathogens, pathogenesis, and their applications in developing sustainable agriculture

Topic editors

Baoyu Tian – Fujian Normal University, China

Jian-Wei Guo – Kunming University, China

Xiao Lin Wang – Center for Excellence in Molecular Plant Sciences, Chinese Academy of Sciences (CAS), China

Dilfuza Egamberdieva – Leibniz Center for Agricultural Landscape Research (ZALF), Germany

Osama Abdalla Abdelshafy Mohamad – Xinjiang Institute of Ecology and Geography, Chinese Academy of Sciences (CAS), China

Citation

Tian, B., Guo, J.-W., Wang, X. L., Egamberdieva, D., Mohamad, O. A. A., eds. (2024). *Microbiome associated with plant pathogens, pathogenesis, and their applications in developing sustainable agriculture*. Lausanne: Frontiers Media SA. doi: 10.3389/978-2-8325-4960-5

Table of contents

frontiers | Frontiers in Microbiology

TYPE Editorial
PUBLISHED 21 May 2024
DOI 10.3389/fmicb.2024.1423961

OPEN ACCESS

EDITED AND REVIEWED BY
Jesús Navas-Castillo,
CSIC, Spain

*CORRESPONDENCE
Baoyu Tian
✉ tianby@fjnu.edu.cn

RECEIVED 26 April 2024
ACCEPTED 09 May 2024
PUBLISHED 21 May 2024

CITATION
Guo J-W, Mohamad OAA, Wang X, Egamberdieva D and Tian B (2024) Editorial: Microbiome associated with plant pathogens, pathogenesis, and their applications in developing sustainable agriculture.
Front. Microbiol. 15:1423961.
doi: 10.3389/fmicb.2024.1423961

Editorial: Microbiome associated with plant pathogens, pathogenesis, and their applications in developing sustainable agriculture

Jian-Wei Guo[1,2], Osama Abdalla Abdelshafy Mohamad[2,7], Xiaolin Wang[3], Dilfuza Egamberdieva[4,6] and Baoyu Tian[5]*

[1]College of Agronomy and Life Sciences, Yunnan Urban Agricultural Engineering and Technological Research Center, Kunming University, Kunming, China, [2]State Key Laboratory of Desert and Oasis Ecology, Xinjiang Institute of Ecology and Geography, Chinese Academy of Sciences, Urumqi, China, [3]College of Agriculture, South China Agricultural University, Guangzhou, China, [4]Faculty of Biology, National University of Uzbekistan, Tashkent, Uzbekistan, [5]Fujian Key Laboratory of Developmental and Neural Biology, College of Life Sciences, Fujian Normal University, Fuzhou, China, [6]Institute of Fundamental and Applied Research, National Research University TIIAME, Tashkent, Uzbekistan, [7]Department of Environmental Science, Institute of Environmental Studies, Arish University, El-Arish, Egypt

KEYWORDS

plant pathology, plant or pathogen associated microbiome, phytopathogenesis, plant-microbe-pahtogen interaction, sustainable agriculture

Editorial on the Research Topic
Microbiome associated with plant pathogens, pathogenesis, and their applications in developing sustainable agriculture

Plants are susceptible to diverse pathogens and pests, including viral, bacterial, and fungal pathogens, as well as nematodes and other pests. Studies have demonstrated that more than 50,000 parasitic or pathogenic plant diseases are reported worldwide, causing over 40% of total production losses in agriculture in most developing countries (Khaled et al., 2017; Jongman et al., 2020). Phytopathogens and pests pose some of the most devastating threats to productivity and yield, causing destructive plant diseases or damage in both natural and agricultural environments (Egamberdieva et al., 2011; Thynne et al., 2015). Identifying the causal organisms responsible for devastating crop diseases, understanding how they have emerged, and their population epidemiology is of vital importance for enhancing agronomic practice efficiency, ensuring food safety, and developing sustainable agricultural system. Recent advancements in culture-independent techniques, particularly high-throughput sequencing (HTS)-based whole genomic and metagenomic analysis, have provided us with novel insights into the pathogenesis of plant diseases. This shift has moved the focus from individual microbes to a pathobiome paradigm, or systems-based plant pathology (Ray et al., 2020; Mannaa and Seo, 2021). Research focusing on the widely accepted pathogen-disease hypothesis has led to many breakthroughs, such as the identification of multi-origin pathogens of plant known or novel diseases (Ray et al., 2020). Wang X. et al. (2022) and Wang Y. et al. (2022) discovered the soybean stay-green associated virus through the multi-omic integration of bacterial, fungal and viral microbiome data. Furthermore, this disease was associated

with a dramatic increase microbial loads and dysbiosis of the bacterial microbiota in seeds. Furthermore, community analysis has allowed us to observe the pathogen-disease paradigm in detail, considering not only the pathogens capable of growing *in vitro* culture, but also systems-based plant pathology, where communities and their interactions are considered rather than individual organisms (Jongman et al., 2020; Mannaa and Seo, 2021). Phytopathogenesis is not only the outcome of the interactions between pathogens or pests and their host plants and but also the result of interactions with the microbiomes associated with plant hosts and pathogens. Among these, the microbiome associated with the plant host and pathogen plays a central role in regulating plant health and pathogen infection.

The plant microbiome including endophytic, epiphytic, and rhizosphere microbiomes, has shown great potential in agricultural systems for desired agronomic and ecological functions (Carrion et al., 2019; Shen et al., 2024). Plants can recruit specific microbial taxa to adapt to environmental stress. In return, the microbiome can activate genes related to host plants to obtain required nourishment and indirectly improve the fitness of host plants under environmental stress such as nitrogen deficiency and pathogen invasion. For example, the abundance of the genus *Massilia* showed a negative correlation with soil nitrogen content, revealing *Massilia* as a key taxon that drives root microbiota assembly under nitrogen deficiency. Additionally, the inoculation of *Massilia* enhanced both root and shoot growth of *zm00001d048945* mutants under conditions of nitrogen deficiency (He et al., 2024). Microbiome-related genes such as *NRT1.1B* in rice, have been shown to effectively improve the establishment of the rice root microbiome and nitrogen use efficiency (Zhang et al., 2019). Accordingly, the plant-associated microbiome has been regarded as the plant's second genome (Mendes et al., 2011; Berendsen et al., 2012; Wang et al., 2021). The collective genome of the host organism and its symbiotic microbiome is considered as the "hologenome," jointly facilitating the development of new varieties with higher yields and increased pathogen resistance (Li et al., 2024).

However, microbiomes do not always interact with host plants as favorable partners. Growing evidence suggests that disease occurrence in plants is often accompanied by changes in the associated microbiome (Tian et al., 2015; Kwak et al., 2018). Microbiomes may also detrimentally affect plant health or promote parasitism or pathogenicity by establishing symbiotic or mutual relationships with pathogens or pests, thereby facilitating the occurrence of plant diseases (Ray et al., 2020; Mannaa and Seo, 2021). Li et al. (2023) suggested that the community structure and assembly of root endophytic microbiota were significantly affected by root-knot nematodes (RKN) parasitism, revealing an association of nitrogen-fixing bacteria with RKN infection. Liu et al. (2024) identified that non-pathogenic *Pseudomonas syringae* could induce a "cry for help" response from the host plant, leading to the assembly of growth-promoting and disease-suppressing rhizomicrobiomes. Understanding interactions among plants, pathogens and microbiomes will help us develop novel plant disease control strategies (Xun et al., 2022; Zhou et al., 2022; Li et al., 2023).

We organized this topic, "*Microbiome associated with plant pathogens, pathogenesis, and their applications in developing sustainable agriculture*" to consolidate recent findings and perspectives encompassing a broad spectrum of plant pathology, ranging from individual microbes to pathobiomes, or systems-based plant pathology. This includes research on the identification of plant pathogens, pathogenesis, microbiomes associated with plants and pathogens, nematodes or pests, as well as biological control of plant diseases or the enhancement of healthy plant microbiomes to foster sustainable agriculture, among other aspects. We extend our gratitude to all the authors and reviewers for their valuable contributions to this topic, which comprised of two mini-reviews and fourteen original research articles.

Chen et al. conducted a review on the occurrence, corresponding pathogens and geographical distribution of fungal diseases on *Camellia oleifera*. They proposed an integrated approach to control these fungal diseases, which includes establishing monitoring and forecasting systems, breeding disease-resistant varieties, implementing biological control techniques, and employing a rational application of chemical fungicides. Zhou et al. provided a summary detailing the strategies employed by various hemibiotrophic pathogens interacted with host immune receptors to activate plant immunity. They highlighted the significant role of the plasma membrane in plant immune responses, as well as the current obstacles and potential future research directions.

Wang et al. discovered that leaf crinkle of *Lycium barbarum* was caused by a novel cytorhabdovirus named as "goji cytorhabdovirus A (GCVA)" identified using HTS. The virus possesses a linear, negative sense single-stranded RNA genome of 14,812 nucleotides and encodes six open reading frames. Then two phylogenetic analyses of the L protein and N protein demonstrate that GCVA should be classified as a new species in the genus *Cytorhabdovirus*. Additionally, the RT-PCR detection and RT-LAMP assay were effectively developed to detect the new virus. Liu C. et al. reported that *Fusarium oxysporum* was identified by the morphological and molecular characteristics as the causal agent of bulbous rot on *Lilium davidii* var. *willmottiae*. They found that the most suitable temperature for mycelial growth was 28°C, while the optimal relative humidity for spore production was 55%. Additionally, cinnamon essential oil exhibited superior antifungal efficacy against the pathogen.

Guo Z. et al. and Liu F. et al. unveiled pathogenesis and pathogenicity using different pathogen-disease plant models, separately from pathogen and host plant. Guo Z. et al. obtained three mutants (*Cm699*, *Cm854*, and *Cm1078*) of *Colletotrichum magnum*, which caused fruit rot on watermelon. They found that the mutant completely lost pathogenicity, producing significantly fewer or no conidia than the WT strain. Additionally, six potential virulence genes related to pathogenicity and sporulation were identified. In another study, the transcriptome and proteome of the highly resistant cultivar "Renong No. 1" and cultivar "Keitt" in response to *Xanthomonas citri* pv. *mangiferaeindicae* infection at different stages were compared, resulting in 14,397 differentially expressed genes (DEGs) and 3,438 differentially expressed proteins (DEPs). Finally, three hub genes/proteins (SAG113, SRK2A, and ABCB1), which play an important role in plant hormone signal transduction, were identified (Liu F. et al.).

Systems-based plant pathology has demonstrated that pathogenesis and parasitism in plants have significant effects on

the taxonomy, composition, and assembly of pathogen-disease associated microbial communities. Diseased strawberries had a higher microbial diversity than those of healthy ones in both the root surface and root rhizosphere soils. The relative abundances of the genus *Colletotrichum* in diseased roots increased 5–6 times more than those in healthy roots, implicating *Colletotrichum* as the major pathogen in strawberry fields. Additionally, strawberry root rot resulted in the decreased microbial interaction network stability, and more endophytic-plant pathogenic and saprophytic groups (Zhang et al.). Tie et al. revealed that the invasion of *Verticillium dahliae* on tomato plants might specifically recruit beneficial microbiomes, including *Pseudomonas*. Moreover, resistant cultivars had a more complex bacterial community network relationship than susceptible cultivars. Cao et al. found that RKN-infected tobacco exhibited a richer and more diverse rhizosphere soil bacterial community rather than healthy tobacco in most planting areas. Soil pH was the key factor affecting both the microbial composition of tobacco rhizosphere microbiome and the occurrence of RKN disease in the tobacco-growing areas. Zhu et al. showed that the age of the peach trees had a significant impact on the yeast community structure of non-rhizosphere and rhizosphere soils of peach trees. Additionally, soil pH and conductivity were also key factors contributing to changes in soil yeast community structure in the peach orchards.

Application of bio-agents, organic fertilizers and cropping management for developing efficient plant disease control strategies, as well as the improving healthy plant microbiomes, is necessary for achieving sustainable agriculture. Cui et al. isolated antagonistic bacteria from the V-Ti magnetite tailings and elucidated their control effects on *Corynespora cassiicola*, which was the pathogen of kiwifruit brown spot. Among 136 bacterial strains isolated, 18 strains demonstrated inhibitory activity against *C. cassiicola*. Notably, *Bacillus* sp. KT10 exhibited effective control of kiwifruit brown spot in both pot and field experiments. The application of *Bacillus amyloliquefaciens* Ba13 with RNAi modulation enhanced plant growth and host resistance to tomato yellow leaf curl virus (TYLCV) by enhancing RNAi-related gene expression and increasing viral genome methylation levels, suggesting a novel efficient tool and strategy to control viral plant diseases using the RNAi-based antiviral system in the presence of microbial agents. The inoculation of *B. amyloliquefaciens* Ba13 in tomato plants with viral infection promoted a 15.4% increase in plant height, and the relative abundance of the TYLCV gene in tomato leaves decreased by 70.1%, compared with those of non-inoculated controls (Guo Q. et al.). Arbuscular mycorrhizal fungi (AMF) is another promising microbial agent used in agriculture to enhance plant growth and productivity, and control plant diseases. The bioinoculants of AM *Funneliformis mosseae*, *Gigaspora gigantea* and *Acaulospora laevis* led to the increased plant development, yield, quality of beetroot and gene expression analysis (ALDH7B4 and ALDH3I1) (Yadav et al.). Besides microbial agent, biofertilizers and cropping management were also among the most efficient and economical agricultural practices for the establishing a sustainable agriculture system. Oyster shell powder and oyster shell powder with organic microbial fertilizer significantly increased soil total nitrogen (16.2% and 59.9%), soil total carbon (25.8% and 27.7%), pH (56.9% and 55.8%), and electrical conductivity (377.5% and 311.7%), facilitated tomato seed germination, and increased the relative abundance of beneficial bacteria like *Massilia*, *Brevundimonas*, and *Lysobacter*, while decreasing the pathogenic bacteria unidentified_*Burkholderiaceae* (Zheng et al.). Shi et al. investigated the effect of field fertilization treatments on soil microbial communities and plant health at different growth stages of cotton. The results showed that reducing chemical fertilizer combined with the usage of organic fertilizer significantly increased soil available nitrogen and phosphorus, affecting the composition and diversity of bacterial and fungal communities throughout the entire cotton growth period. Evaluating effects of plant cropping systems on soil properties, microbial communities, and crop yield indicated that soybean and maize crop rotation, especially using soybean-maize-maize and maize-soybean-soybean planting systems, could increase soil total organic carbon and nutrients, and promote soybean and maize yield. Moreover, the soybean-maize-maize significantly increased the proportion of some beneficial microorganisms and reduced the soil-borne animal and plant pathogens (Sun et al.).

Author contributions

J-WG: Writing—original draft. OAAM: Writing—review & editing. XW: Writing—review & editing. DE: Writing—review & editing. BT: Writing—review & editing.

Funding

The author(s) declare financial support was received for the research, authorship, and/or publication of this article. This work has been funded by National Natural Science Foundation of China (grant nos. 31860026 and 32100227), Kunming University Talent Program (grant no. XJ20230077), Major Science and Technology Special Plan of Yunnan Province (grant no. 202202AE090035), and Ministry of Science and Technology the People's Republic of China (grant no. 2022xjkk1204).

Acknowledgments

Great thanks to all the contributing authors and reviewers, regardless of whether their submitted manuscripts and advices were accepted for publication and to the Frontiers team for their constant supporting in this Research Topic.

Conflict of interest

The authors declare that the research was conducted in the absence of any commercial or financial relationships that could be construed as a potential conflict of interest.

Publisher's note

the editors and the reviewers. Any product that may be evaluated in this article, or claim that may be made by its manufacturer, is not guaranteed or endorsed by the publisher.

References

Berendsen, R. L., Pieterse, C. M., and Bakker, P. A. (2012). The rhizosphere microbiome and plant health. *Trends Plant Sci.* 17, 478–486. doi: 10.1016/j.tplants.2012.04.001

Carrion, V. J., Perez-Jaramillo, J., Cordovez, V., Tracanna, V., de Hollander, M., Ruiz-Buck, D., et al. (2019). Pathogen-induced activation of disease-suppressive functions in the endophytic root microbiome. *Science* 366, 606–612. doi: 10.1126/science.aaw9285

Egamberdieva, D., Kucharova, Z., Davranov, K., Berg, G., Makarova, N., and Azarova, T. (2011). Bacteria able to control foot and root rot and to promote growth of cucumber in salinated soils. *Biol. Fer. Soils* 47, 197–205. doi: 10.1007/s00374-010-0523-3

He, X., Wang, D., Jiang, Y., Huang, Y., Zhang, S., Shen, L., et al. (2024). Heritable microbiome variation is correlated with source environment in locally adapted maize varieties. *Nat. Plants* 10, 598–617. doi: 10.1038/s41477-024-01654-7

Jongman, M., Carmichael, P. C., and Bill, M. (2020). Technological advances in phytopathogen detection and metagenome profiling techniques. *Curr. Microbiol.* 77, 675–681. doi: 10.1007/s00284-020-01881-z

Khaled, A. Y., Aziz, S. A., Bejo, S. K., Navi, N. M., Seman, I. A., Onwude, D. I., et al. (2017). Early detection of diseases in plant tissue using spectroscopy-applications and limitations. *Appl. Spectr. Rev.* 53, 36–64. doi: 10.1080/05704928.2017.1352510

Kwak, M. J., Kong, H., Choi, K., Kwon, S. K., Song, J. Y., Lee, J., et al. (2018). Rhizosphere microbiome structure alters to enable wilt resistance in tomato. *Nat. Biotechnol.* 36, 1100–1109. doi: 10.1038/nbt.4232

Li, X., Zheng, X., Yadav, N., Saha, S., Salama, E. S., Li, X., et al. (2024). Rational management of the plant microbiome for the second green revolution. *Plant Commun.* 5:100812. doi: 10.1016/j.xplc.2024.100812

Li, Y., Lei, S., Cheng, Z., Jin, L., Zhang, T., Liang, L. M., et al. (2023). Microbiota and functional analyses of nitrogen-fixing bacteria in root-knot nematode parasitism of plants. *Microbiome* 11:48. doi: 10.1186/s40168-023-01484-3

Liu, Y., Zhang, H., Wang, J., Gao, W., Sun, X., Xiong, Q., et al. (2024). Nonpathogenic *Pseudomonas syringae* derivatives and its metabolites trigger the plant "cry for help" response to assemble disease suppressing and growth promoting rhizomicrobiome. *Nat. Commun.* 15:1907. doi: 10.1038/s41467-024-46254-3

Mannaa, M., and Seo, Y. S. (2021). Plants under the attack of allies: moving towards the plant pathobiome paradigm. *Plants* 10:125. doi: 10.3390/plants10010125

Mendes, R., Kruijt, M., de Bruijn, I., Dekkers, E., van der Voort, M., Schneider, J. H. M., et al. (2011). Deciphering the rhizosphere microbiome for disease-suppressive bacteria. *Science* 332, 1097–1100. doi: 10.1126/science.1203980

Ray, P., Lakshmanan, V., Labbé, J. L., and Craven, K. D. (2020). Microbe to microbiome: a paradigm shift in the application of microorganisms for sustainable agriculture. *Front. Microbiol.* 11:622926. doi: 10.3389/fmicb.2020.622926

Shen, J., Wang, M., and Wang, E. (2024). Exploitation of the microbiome for crop breeding. *Nat. Plants* 10, 533–534. doi: 10.1038/s41477-024-01657-4

Thynne, E., McDonald, M. C., and Solomon, P. S. (2015). Phytopathogen emergence in the genomics era. *Trends Plant Sci.* 20, 246–255. doi: 10.1016/j.tplants.2015.01.009

Tian, B., Cao, Y., and Zhang, K. Q. (2015). Metagenomic insights into communities, functions of endophytes, and their associates with infection by root-knot nematode, *Meloidogyne incognita*, in tomato roots. *Sci. Rep.* 5:17087. doi: 10.1038/srep17087

Wang, X., Feng, H., Wang, Y., Wang, M., Xie, X., Chang, H., et al. (2021). Mycorrhizal symbiosis modulates the rhizosphere microbiota to promote rhizobia–legume symbiosis. *Mol. Plant* 14, 503–516. doi: 10.1016/j.molp.2020.12.002

Wang, X., Wang, M., Wang, L., Feng, H., He, X., Chang, S., et al. (2022). Whole-plant microbiome profiling reveals a novel geminivirus associated with soybean stay-green disease. *Plant Biotechnol. J.* 20, 2159–2173. doi: 10.1111/pbi.13896

Wang, Y., Wang, X., Sun, S., Jin, C., Su, J. M., Wei, J., et al. (2022). GWAS, MWAS and mGWAS provide insights into precision agriculture based on genotype-dependent microbial effects in foxtail millet. *Nat. Commun.* 13:5913. doi: 10.1038/s41467-022-33238-4

Xun, W., Ren, Y., Yan, H., Ma, A., Liu, Z., Wang, L., et al. (2022). Sustained inhibition of maize seed-borne *Fusarium* using a *Bacillus*-dominated rhizospheric stable core microbiota with unique cooperative patterns. *Adv. Sci.* 10:2205215. doi: 10.1002/advs.202205215

Zhang, J., Liu, Y. X., Zhang, N., Hu, B., Jin, T., Xu, H., et al. (2019). *NRT1.1B* is associated with root microbiota composition and nitrogen use in field-grown rice. *Nat. Biotechnol.* 37, 676–684. doi: 10.1038/s41587-019-0104-4

Zhou, X., Wang, J., Liu, F., Liang, J., Zhao, P., Tsui, C. K. M., et al. (2022). Cross-kingdom synthetic microbiota supports tomato suppression of *Fusarium wilt* disease. *Nat. Commun.* 13:7890. doi: 10.1038/s41467-022-35452-6

frontiers | Frontiers in Microbiology

TYPE Original Research
PUBLISHED 16 February 2023
DOI 10.3389/fmicb.2023.1095688

OPEN ACCESS

EDITED BY
Jian-Wei Guo,
Kunming Institute of Botany (CAS), China

REVIEWED BY
Zhihui Xu,
Nanjing Agricultural University,
China
Asit Mandal,
Indian Institute of Soil Science (ICAR), India

*CORRESPONDENCE
Xiao-Yang Cui
✉ c_xiaoyang@126.com
Dan Wei
✉ wd2087@163.com

†These authors have contributed equally to this work

SPECIALTY SECTION
This article was submitted to Microbe and Virus Interactions with Plants, a section of the journal Frontiers in Microbiology

RECEIVED 11 November 2022
ACCEPTED 30 January 2023
PUBLISHED 16 February 2023

CITATION
Sun L, Wang S, Narsing Rao MP, Shi Y, Lian Z-H, Jin P-J, Wang W, Li Y-M, Wang K-K, Banerjee A, Cui X-Y and Wei D (2023) The shift of soil microbial community induced by cropping sequence affect soil properties and crop yield. *Front. Microbiol.* 14:1095688. doi: 10.3389/fmicb.2023.1095688

The shift of soil microbial community induced by cropping sequence affect soil properties and crop yield

Lei Sun[1,2†], Shuang Wang[2†], Manik Prabhu Narsing Rao[3], Yu Shi[4], Zheng-Han Lian[5], Pin-Jiao Jin[2], Wei Wang[2], Yu-Mei Li[2], Kang-Kang Wang[2], Aparna Banerjee[6], Xiao-Yang Cui[1*] and Dan Wei[7*]

[1]Key Laboratory of Sustainable Forest Ecosystem Management-Ministry of Education, School of Forestry, Northeast Forestry University, Harbin, China, [2]Heilongjiang Academy of Black Soil Conservation and Utilization, Harbin, China, [3]Programa de Doctorado en Ciencias Aplicadas, Universidad Autónoma de Chile, Talca, Chile, [4]State Key Laboratory of Crop Stress Adaptation and Improvement, School of Life Sciences, Henan University, Kaifeng, China, [5]State Key Laboratory of Biocontrol, Guangdong Provincial Key Laboratory of Plant Resources and Southern Marine Science and Engineering Guangdong Laboratory (Zhuhai), School of Life Sciences, Sun Yat-sen University, Guangzhou, China, [6]Centro de Investigación de Estudios Avanzados del Maule (CIEAM),Vicerrectoría de Investigación y Postgrado, Universidad Católica del Maule, Talca, Chile, [7]Institute of Plant Nutrition and Resources, Beijing Academy of Agriculture and Forestry Sciences, Beijing, China

Rational cropping maintains high soil fertility and a healthy ecosystem. Soil microorganism is the controller of soil fertility. Meanwhile, soil microbial communities also respond to different cropping patterns. The mechanisms by which biotic and abiotic factors were affected by different cropping sequences remain unclear in the major grain-producing regions of northeastern China. To evaluate the effects of different cropping sequences under conventional fertilization practices on soil properties, microbial communities, and crop yield, six types of plant cropping systems were performed, including soybean monoculture, wheat-soybean rotation, wheat-maize-soybean rotation, soybean-maize-maize rotation, maize-soybean-soybean rotation and maize monoculture. Our results showed that compared with the single cropping system, soybean and maize crop rotation in different combinations or sequences can increase soil total organic carbon and nutrients, and promote soybean and maize yield, especially using soybean-maize-maize and maize-soybean-soybean planting system. The 16S rRNA and internal transcribed spacer (ITS) amplicon sequencing showed that different cropping systems had different effects on bacterial and fungal communities. The bacterial and fungal communities of soybean monoculture were less diverse when compared to the other crop rotation planting system. Among the different cropping sequences, the number of observed bacterial species was greater in soybean-maize-maize planting setup and fungal species in maize-soybean-soybean planting setup. Some dominant and functional bacterial and fungal taxa in the rotation soils were observed. Network-based analysis suggests that bacterial phyla *Acidobacteria* and *Actinobacteria* while fungal phylum *Ascomycota* showed a positive correlation with other microbial communities. The phylogenetic investigation of communities by reconstruction of unobserved states (PICRUSt) result showed the presence of various metabolic pathways. Besides, the soybean-maize-maize significantly increased the proportion of some beneficial microorganisms in the soil and reduced the soil-borne animal and plant pathogens. These results warrant further investigation into the mechanisms driving responses of beneficial microbial communities and their capacity on improving soil fertility during legume cropping. The present study extends our understanding of how different crop rotations effect soil parameters, microbial diversity, and metabolic functions, and reveals the importance of crop rotation sequences. These findings could be used

to guide decision-making from the microbial perspective for annual crop planting and soil management approaches.

KEYWORDS

crop rotation, soybean, wheat, maize, microbial community structure

Introduction

China is the world's largest soybean consumer and importer and is regarded as an important food crop, oil crop, and feed source (Yao et al., 2020). To attain overall soybean self-sufficiency in China, the government encourages farmers to cultivate more soybean crops (Tan et al., 2021). Statistical data showed that the world's soybean production increased approximately 13-fold from 1961 to 2017 (Liu S. et al., 2020) Heihe city, in the Northeast of the country, has the largest area under soybean cultivation and the highest total yield in the country, the unique geographical and climatic location, soil composition, water, and air quality are all conducive to the production of green edible soybeans. However, continuous soybean planting caused soil acidification, aggravation of soil-borne diseases, a decrease in soil enzyme activity, and the accumulation of toxins in the soil (Yuan et al., 2021). To overcome this issue many plant cultivation models have been developed and among them crop rotation is one of the essential management approaches used by farmers (Neupane et al., 2021).

Crop rotation is the practice of planting different crops on the same land during successive growth/seeding cycles (Bullock, 1992; Yu et al., 2022). Since ancient times, crop rotation is a common management method used to improve soil nutrient and water availability, reduce weeds and pests, and improve the ecological and economic sustainability of cropping systems (Yang et al., 2021). Diversified crop rotation can even reduce the consequences of increased drought intensity and heatwaves even in drought circumstances (Bowles et al., 2020). Studies have shown that crop rotation enhances soybean yields. Using corn and winter wheat (with or without red clover) plants, Agomoh et al. (2021) investigated the effects of crop rotation on soybean production and discovered that soybeans grown in 3 years of rotations with corn and winter wheat provided the highest yields. Growing soybeans 1 year out of three in three-year cycles, such as corn–soybean–wheat, increased the yield of soybean (Lund et al., 1993). Studies also suggest that the practice of crop rotation helps to control the soybean cyst nematode (Sasser and Uzzell, 1991). In recent years, it has also been found that crop rotation effect subsurface microbial communities (Paungfoo-Lonhienne et al., 2017; Xie et al., 2020; Yu et al., 2021; Wang et al., 2022).

Microorganisms are an integral part of almost all soil, and some agronomic practices, such as fertilization and crop rotation, affect soil microbial communities and functions. Xie et al. (2022) found that the crop rotation stage strongly affected the soil microbial community structure and assembly compared to that of the fertilization regime. The cropping sequences within the rotation can change soil microbial communities and give favorable impacts for increased agronomic performance (Bolaji et al., 2021). Microorganisms have been shown to improve plant development by secreting metabolites, mobilizing nutrients, and alleviating biotic and abiotic stresses (Tahir et al., 2017; Bolaji et al., 2021). Crop rotation sequences appear to have a direct impact on the structure of microbial communities associated with soil and plants (Zhang et al., 2019; Neupane et al., 2021). The most diverse crop rotation showed the most diverse and active soil microbial biota (D'Acunto et al., 2018). Crop rotations can improve disease suppression capacity by influencing soil bacterial composition or increasing the quantity of disease-suppressive microorganisms (Peralta et al., 2018). Previous studies have shown that crop rotation strategies changed microbial communities over time due to cropping sequence practices (Bolaji et al., 2021; Meier et al., 2021). In wheat-soybean rotation, soybean planting increased the relative abundance of *Firmicutes* and *Glomeromycota* (Guo et al., 2020). Although there have been numerous studies on soybean crop rotation management, the effects of crop rotation order on soil microbial communities under conventional fertilization methods for different food crops, including soybean, are not well understood.

The choice of crop planting sequence is often related to the farmer's goal looking to achieve with the rotation, which could be weed management, pest and disease control, increasing available nitrogen in the soil, controlling soil erosion, improving soil structure, and increasing economic benefits (Boincean and Dent, 2019). The local department of agriculture of Heilongjiang has also introduced a pilot scheme for crop rotation and fallow, including the "three-three system" of crop rotation (corn-soybean-wheat, corn-soybean-potato, corn-soybean-grain, etc.), and the "two-two system" of crop rotation (corn-soybean, corn-wheat, corn-potato, and so on) allowed.[1]

In the present study, six planting sequence setups were tested over five years in northeastern China. Planting 1 setup includes only soybean, planting 2 setup includes wheat and soybean, planting 3 set up includes wheat, maize, and soybean, planting 4 setup includes soybean and maize, planting 5 setup includes maize and soybean, and planting 6 setup includes only maize. Marker-based Illumina sequencing and bioinformatics analyses were carried out to understand cropping sequence and its effect on soil properties and crop yields-associated microbial communities. Our objectives were to explore some scientific questions: (i) does the planting sequence effect soil microorganisms? (ii) If so, are there core beneficial microorganisms that could increase crop yields? The answer to these questions can provide recommendations for reasonable crop rotation for local farmers and agricultural managers.

Materials and methods

Experimental setup and fertilization management

In the spring of 2012, the field positioning experiment of the new rotation system, wheat, maize and soybean was established in Sinograin's agriculture demonstration zone (E 49°33′35″, N 125°27′5″, 225 m a.s.l.;

1 https://heilongjiang.dbw.cn/system/2018/03/01/057939012.shtml

soil type: dark brown soil) of Heihe city, China. The site lies within mid temperate semi-humid continental monsoon climate, characterized by low annual average temperature, and a short frost-free period that follows dry, long, and cold winters. In the last four decades, the annual precipitation average was 481 mm, while the mean annual temperature was 0.5°C, with a minimum and maximum monthly average of −29.2°C and 26.6°C, respectively. In this climate, each grain crop can only be planted one season a year.

The long-term field experiment was set up as a strip-plot design. The experiment includes six planting setups. Planting 1 setup includes only soybean (designated as sss), planting 2 setup includes wheat and soybean (designated as wsw), planting 3 setup includes wheat, maize and soybean (designated as wms), planting 4 setup includes soybean and maize (designated as smm), planting 5 setup includes maize and soybean (designated as mss) and planting 6 setup includes only maize (designated as mmm). Each type of cropping consists of three plots, there were 18 plots, each plot area of 87.75 m^2. More details of the crop rotation system are mentioned in Figure 1. The application dosages of chemical fertilizers were set according to the soil testing and fertilizer recommendation and they were applied as base fertilizer when seeds were sown. For maize, soybean, and wheat, N-P_2O_5-K_2O were 135-67.5-45, 50-60-45, and 75-80-45 kg/hm^2, respectively.

Crop harvest, sample collection, and soil properties analysis

After 5 years of crop cultivation, all crops in each plot were harvested and the yields were calculated with dry weight. Soil samples were taken from 0 to 15 cm soil depth in each plot after crop harvesting. Five subsamples were collected randomly from each plot and mixed evenly to form a bulked sample. A total of 18 samples (six treatments with three replicates) were collected and transported to the laboratory in a cooler with ice packs immediately. Each soil sample was passed through a 2-mm sieve, homogenized and plant roots and large rocks were removed. All the samples were divided into two parts: the first was air-dried, ground, and sieved (<0.25 mm) for soil physical and chemical properties analysis, and the second was stored at −70°C until DNA extraction.

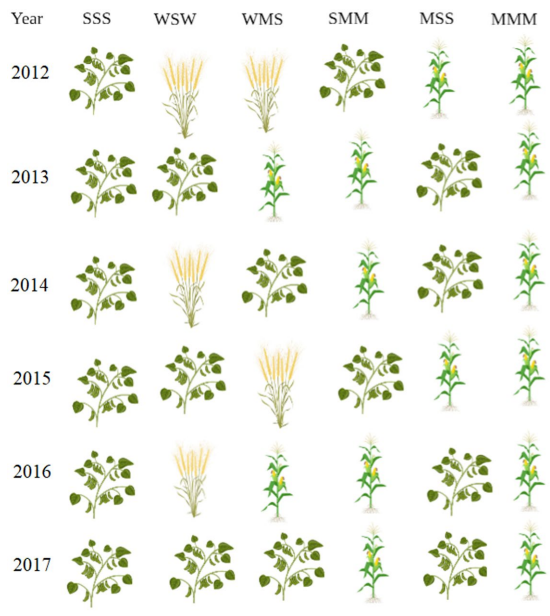

FIGURE 1
Crop rotation planting pattern once a year. Figure is created with BioRender.com.

Soil moisture (MO) was determined by gravimetrical methods. Soil pH was measured using a compound electrode at a 1:2.5 mass/volume soil-water suspension. Soil total organic carbon (TOC), total nitrogen (TN), total phosphorus (TP), total potassium (TK), available nitrogen (AN), available phosphorus (AP) and available potassium (AK) content were measured as described by Lu (2000).

DNA extraction, PCR amplification, and sequencing

Total genomic DNA was extracted from the samples using the PowerSoil DNA isolation kit (MoBio) following the manufacturer's instructions. The final DNA concentration and its purity was evaluated using NanoDrop 2000 UV VIS spectrophotometer (Thermo Scientific, Wilmington, United States). The DNA quality was checked using 1% agarose gel electrophoresis or by separating the DNA macromolecules in a matrix of agarose (Marcos et al., 2016).

The polymerase chain reaction (PCR) was carried out by the Phusion R High-Fidelity PCR Master Mix with GC Buffer (New England Biolabs) using specific primers with a barcode. The bacterial 16S rRNA genes with V3–V4 hypervariable regions were amplified with two primers 341F (5'-CCTAYGGGRBGCASCAG-3') and 806R (5'-GGACTACNNGGGTATCTAAT-3') (Yu et al., 2005). The fungal internal transcribed spacer (ITS) region was amplified using the primer pair ITS1F (5'-CTTGGTCATTTAGAGGAAGTAA-3')/ITS2R (5'-GCTGCGTTCTTCATCGATGC-3') (White et al., 1990). The PCR conditions used for the amplification of the16S rRNA genes and ITS region were as follows: 5 min of denaturation at 95°C, followed by 27 cycles of 30 s at 95°C, 30 s at 55°C for annealing, and 45 s at 72°C for elongation and ending with a final extension at 72°C for 10 min. The reaction mixture consists of 20 µl mixtures, each containing 4 µl of 5 × FastPfu Buffer, 2 µl of 2.5 mM dNTPs, 0.8 µl of each primer (5 µM), 0.4 µl of FastPfu polymerase, and 10 ng of template DNA (Tian et al., 2022). The obtained PCR products were checked on 2% agarose gel and further purified using an AxyPrep DNA Gel Extraction Kit (Axygen Biosciences, United States) and quantified using QuantiFluor™-ST (Promega, United States) according to the manufacturer's instruction. The purified PCR products were pooled in equimolar ratios and paired-end sequenced using the HiSeq 2500 platform (Illumina, United States) at Biozeron Technology Co., Ltd. (Shanghai, China).

Illumina sequence analysis

The raw FASTQ files were demultiplexed and quality-filtered using Trimmomatic (a flexible read trimming tool) (Bolger et al., 2014) and then the sequences data were merged using the FLASH (Fast Length Adjustment of Short reads) tool (Magoč and Salzberg, 2011). Chimeric sequences were identified and removed by applying UCHIME (Edgar et al., 2011). Operational taxonomic units (OTUs) were clustered at a 97% sequence identity cut-off *via* UPARSE (Edgar, 2013). The OTU representative sequences of bacteria and fungi were identified taxonomically using the Ribosomal Database Project (RDP) Classifier

(Wang et al., 2007) and UNITE databases (Nilsson et al., 2018). The detected taxa were averaged across three biological replicates.

The QIIME 2 software was used to calculate the observed species (Bolyen et al., 2019), and the R software (version 2.15.3)[2] was used to draw the species accumulation curve. Bacterial and fungal alpha diversity including richness estimators (Chao and ACE) and diversity indices (Shannon and Simpson) were calculated using Mothur v.1.41.1[3]. The principal coordinate analysis (PCoA) map was drawn by the R software (see footnote 2) using the WGCNA, stats, and ggplot2 software packages (Wickham, 2009). Molecular ecological network analyses were conducted to reveal the variations in the interactions between phylotypes responding to different cropping sequences, according to an online pipeline (Zhou et al., 2010; Xiao et al., 2022). The correlation network was visualized using the R package igraph. FUNGuild was used to predict fungal function based on ITS sequence data (Nguyen et al., 2016). The functional composition prediction was performed using PICRUSt (phylogenetic investigation of communities by reconstruction of unobserved states) (Langille et al., 2013).

The raw sequences for all samples have been deposited in the NCBI Sequence Read Archive (SRA) database with accession numbers PRJNA883616 and PRJNA884493 for bacteria and fungi, respectively.

Statistical analysis

The soil properties (including pH value, moisture, total carbon, total nitrogen, and total phosphorus, total potassium, available nitrogen, available phosphorus and available potassium in soil) were analysed by one-way analysis of variance (ANOVA) in SPSS v22.0. The relationship between the alpha diversity of soil bacteria and fungi and soil properties was examined using corrplot in R software (version 4.1.0). Community composition was visualised using Redundancy analysis (RDA) with soil properties fitted onto the RDA ordination as vectors.

Results and discussion

Crop sequence affected soil physicochemical properties and crop yields

Experiencing the 5 years monoculture and rotation experiment, the soil properties such as pH, water content and total organic carbon, potassium, phosphorus, and nitrogen were significantly changed (Supplementary Table S1). All crop rotations increased soil TOC, TN and AN content. Soil TOC and TN were similar between smm and mss, but AN was higher in mss, AP and AK was higher in smm. In our design of planting patterns, compared with monocultures, soybean and maize increased the yield regardless of crop combinations and rotation sequence. Soybean-maize rotation (mss) increased soybean yield by 11.27% compared with continuous soybean cropping (sss). Compared with continuous cropping (mmm), wms and smm increased maize yield by 1.64 and 23.06%, respectively (Supplementary Table S2), and smm was the most significant. Obvious changes related to soil pH was noticed in wms and wsw planting systems, wms can maintain an almost neutral soil pH, however, wsw made soil pH similar to soybean monoculture (sss).

Earlier studies suggest that continuous single cropping has resulted in the deterioration of soil chemical properties and nutrient imbalance (Liu et al., 2012; Liu Z. et al., 2020) and crop rotation has a significant impact on soil pH (Karlen et al., 2006; Liu Z. et al., 2020). In the present study, soybean and maize rotation in different ways can significantly increase soil pH compared to soybean and wheat rotation. Although we were unable to compare soybean yields under the wheat-soybean rotation (wsw) pattern, however, based on the data from soil nutrients, we predicted that soybean yield may not exceed smm and smm in the next year, moreover wsw rotation made soil pH similar to soybean monoculture (sss), and this type of rotation does not play any role in preventing soil acidification. In a study, Martens (2000) reported that crop rotation significantly increased soil organic carbon content, while it did not happen in monoculture soybeans. Similarly, our findings showed that different crop rotations increased total organic carbon content compared to monocultures (sss and mmm), which decreased total potassium, phosphorus, and nitrogen content (Supplementary Table S1).

Cropping sequences changed the diversity and composition of the soil microbial community

Using the Illumina HiSeq 2500 platform, a total of 799,070 bacterial and 790,459 fungal high-quality clean reads were obtained from the six cropping patterns and grouped into 7,564 OTUs for the bacteria, and 2,895 OTUs for the fungi. The alpha diversity (Supplementary Figures S1A,B) result showed that the rarefaction curves approached a plateau, indicating that the number of OTUs was sufficient to reveal the authentic bacterial and fungal communities within each sample.

Alpha diversity of bacterial and fungal community among all cropping sequences are observed in Supplementary Table S3. The number of observed bacterial species was greater in smm planting setup when compared with the other planting setup, mss planting showed the least number of observed bacterial species (Supplementary Figure S1C). In contrast to the number of observed bacterial species, the number of observed fungal species was greater in mss planting setup (Supplementary Figure S1D). Compared with continuous planting of maize (mmm), planting soybean could significantly increase the soil bacterial richness, which was the highest in smm, but there was no significant difference compared to other soybean cropping sequences. There was a significant difference in Simpson index and Shannon index between mss and wsw, wms, and mmm in bacteria, but no significant difference in Simpson index in fungi, and significant difference in Shannon index between smm and wsw and mmm. According to the findings, different cropping systems had different effects on bacterial and fungal communities, especially between rotation and monoculture.

Some studies have shown that intensive land use can lead to homogenization of soil microbial communities, reduction of taxa and/or dominance of nutrient groups, and decline of overall diversity (Banerjee and van der Heijden, 2023). In this study, there was no significant difference in Chao and ACE among soybean varieties planted in different sequences, including continuous cropping and rotation, which was consistent with findings in previous studies that legume crop rotation had little effect on soil bacterial richness perhaps due to low

2 http://www.r-project.org/

3 http://www.mothur.org/wiki

diversity of the host-specific microbes associated with legumes relative to free-living microorganisms (Venter et al., 2016; Paungfoo-Lonhienne et al., 2017). In two different rotation patterns (smm and mss; designed for soybean and maize) mss significantly increased bacterial diversity while decreased fungal diversity. Similarly, Neupane et al. (2021) evaluated long-term crop rotation effect on subsequent soybean yield, they found significant differences in the alpha diversity for root-associated bacterial and fungal communities among the four treatments (continuous corn, corn/corn/soybean, corn/soybean, and soybean/corn). In addition, some report suggests that alpha diversity of both bacterial and fungal communities was lower in continuous single cropping when compared to different plant crop rotation (Liu Z. et al., 2020). Similar results were obtained in this study, especially the α-diversity of fungi, which was lowest in sss.

The composition of the soil microbial community showed that the top fifteen phyla in all samples were *Proteobacteria*, *Acidobacteria*, *Actinobacteria*, *Chloroflexi*, *Gemmatimonadetes*, *Verrucomicrobia*, *Bacteroidetes*, *Saccharibacteria*, *Firmicutes*, *Planctomycetes*, *Nitrospirae*, *Cyanobacteria*, *Thaumarchaeota*, *Latescibacteria*, and *Armatimonadetes* but their proportion varied (Figure 2A). Researchers found that the phyla *Acidobacteria* and *Proteobacteria* make up the majority of the soil bacterial community in crop rotation systems (Chamberlain et al., 2020). In the present study also a similar microbial abundance was found. Analogously, Bolaji et al. (2021) reported *Actinobacteria*, *Proteobacteria*, and *Acidobacteria* as the dominant taxa in canola, corn, and soybean crop rotation planting systems.

When compared to the other crop rotation systems, the relative abundance of *Proteobacteria* was higher in the maize and soybean (mss and smm) crop rotation systems, *Thaumarchaeota* was noticed in some planting systems (Figure 2A). Recently, the abundance of *Thaumarchaeota* in the plant rhizosphere was detected and suggested their role in nitrogen cycling (Zhang et al., 2020). The sss planting system had a high abundance of *Acidobacteria* while mss planting system had a lower abundance when compared to other planting systems. *Verrucomicrobia* abundance was noticed in wms planting system. A similar study was conducted to evaluate the impact of crop rotation management of soybean-wheat and maize-wheat on microbial diversity. It was noticed that soybean-wheat rotation increased the relative abundances of *Firmicutes* and *Bacteroidetes* and reduced *Actinobacteria*, *Verrucomicrobia*, and *Chloroflexi* compared to maize-wheat rotation (Yu et al., 2021). Strong positive correlations were observed between Proteobacteria and TN, AK; *Actinobacteria* *Verrucomicrobia* and *Chloroflexi* and AP. These taxa play a major role in soil nutrient cycling, to improve nutrient uptake and productivity in crop rotation.

At the genus level, the majority of the OTUs were unclassified, suggesting they might be novel candidates (Figure 2B). The relative abundance of *Acidobacteriaceae* was high in sss planting system, which could due to low soil pH (Supplementary Table S1). The abundance of "*Candidatus* Solibacter" was noticed in all planting systems. A little information was available regarding "*Candidatus* Solibacter" and our future research will focus on its role in soybean crop rotation. Taxa like

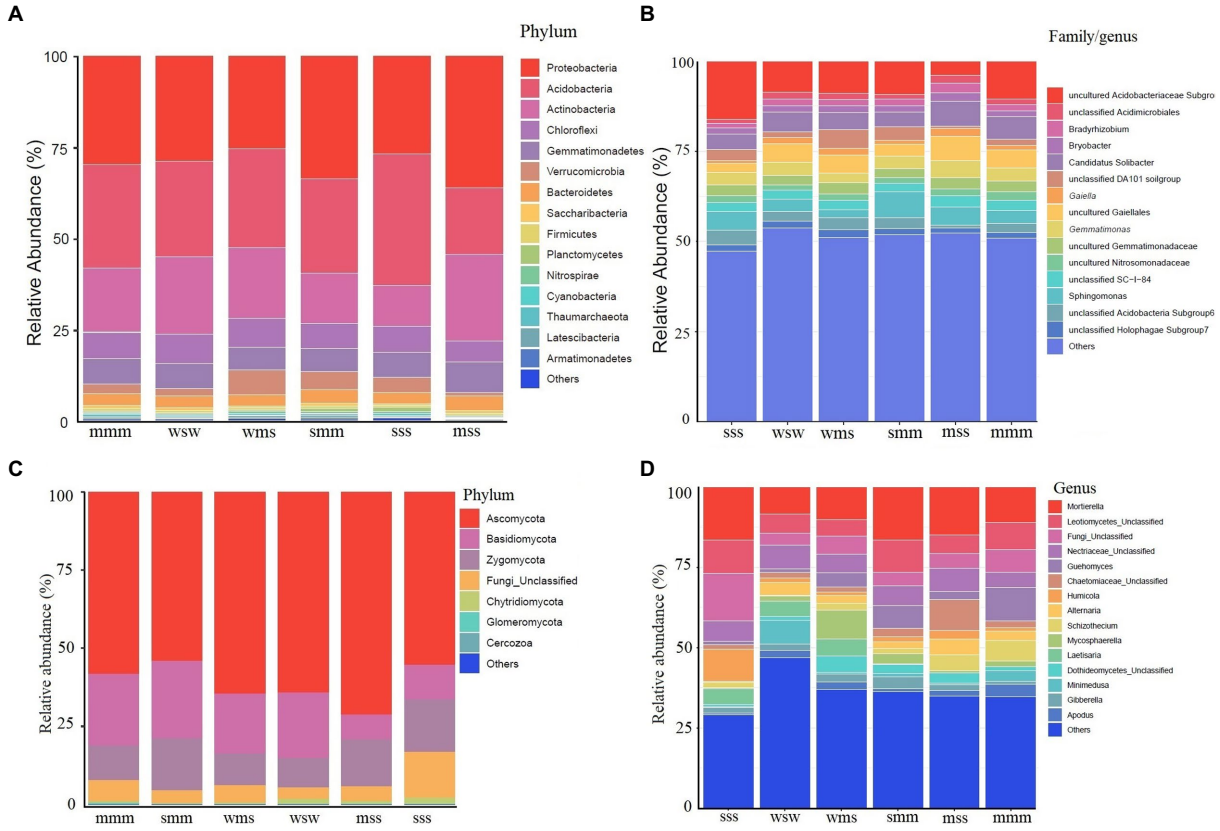

FIGURE 2
Relative abundance of microbial communities in different planting systems: **(A, C)** phylum level, **(B, D)** family/genus level. The x-axis represents samples and the y-axis represents relative abundance presented as a percentage.

Gemmatimonas and *Gaiella* were reported to be abundant under standard nitrogen fertilization (Meier et al., 2021). *Gemmatimonas* and *Gaiella* were also noticed in the present study planting systems (Figure 2B). Such taxa were reported to be key players in nitrification and nitrogen assimilation (Dong et al., 2016; Morrissey et al., 2018).

The abundance of fungi was less when compared with bacteria in all planting systems. The top phyla were *Ascomycota*, *Basidiomycota*, *Zygomycota*, *Chytridiomycota*, *Glomeromycota*, and *Cercozoa* (Figure 2C). Similarly, Narayana et al. (2022) noticed *Ascomycota* and *Basidiomycota* abundance in maize and soybean rotation. *Mortierella* abundance was noticed in almost all planting systems (Figure 2D). Members of the genus *Mortierella* have an impact on the control of plant diseases. It has been demonstrated that some *Mortierella* species were effective at preventing clubroot disease (Narisawa et al., 1998). *Guehomyces* abundance was noticed in maize planting system when compared to other plant crop rotations (Figure 2D) indicating plant-specific abundance. Detailed fungal abundance in different planting systems is depicted in Figure 2.

Soil microbial communities are closely related to soil properties and crop yields

The linear relationships between microbial alpha diversity and soil properties revealed that the bacterial Shannon index was significantly and positively correlated with soil TK content ($p < 0.05$), and Simpson index was significantly and positively correlated with TN ($p < 0.05$) and AP ($p < 0.01$). The Shannon index and Simpson index of fungi were significantly and positively and negatively correlated with AK content (0.05 level), respectively, but had no correlation with other soil properties (Figure 3).

The RDA axis separated the soil bacterial communities of continuous and rotation cropping systems, the results also showed that soil total organic carbon (TOC), total nitrogen (TN) and total phosphorous (TP) had significant effects on soil bacterial community structure of soybean and maize in different cropping sequence (Figure 4A). However, the change of soil pH caused by different types of crops and their different cropping sequences are the main factor affecting the change in fungal community (Figure 4B). This was in agreement with findings by Ai et al. (2018) that bacterial community structure was more sensitive to changes in soil nutrient levels induced by fertilization than fungal community structure.

Microorganisms participate in multiple inter- and intra- kingdom interactions. In particular, network-based techniques have been proven useful in interpreting complex microbial interaction patterns (Matchado et al., 2021). Network-based analysis suggests that phyla *Acidobacteria* and *Actinobacteria* showed a positive correlation with other members (Figure 5A) while *Proteobacteria* in most cases showed a negative correlation with other members. In fungal network analysis, *Ascomycota* showed a positive correlation with other members (Figure 5B). We used PICRUSt to predict the functional composition. The PICRUSt result (Figure 6) showed the presence of various metabolic pathways. The planting setup mss showed the highest pathway abundance while wsw, smm and mmm showed similar pathway abundance (Figure 6).

Moreover, we used FunGuild (spearman correlation coefficient) to perform a functional classification of fungal ITS data, the results of which are shown in Figure 7. Different cropping sequences affected the mean proportion of animal and plant pathogens in soil, it was mss < mmm < smm < wsm < wsw < sss. Some beneficial microorganisms, such as like endophyte, ectomycorrhizal and arbuscular mycorrhizal, were found to have the highest proportion in mss, followed by smm. The wms had the lowest proportion of beneficial microorganisms in all cropping patterns, probably due to the low soil pH in it.

One of the most well-known examples of plant beneficial microorganisms were the mycorrhizal fungi, which form symbiotic associations with nearly 90% of land plants, including many crops (van der Heijden et al., 2015). These fungi help plants obtain water and essential micronutrients and macronutrients from the soil to promote plant growth (Hoeksema et al., 2010). These findings in our study suggest that soybean-maize rotation (mss and smm) can reduce the potential risk of soil-borne animal and plant diseases, increase beneficial functional groups, and maintain a healthy soil ecosystem.

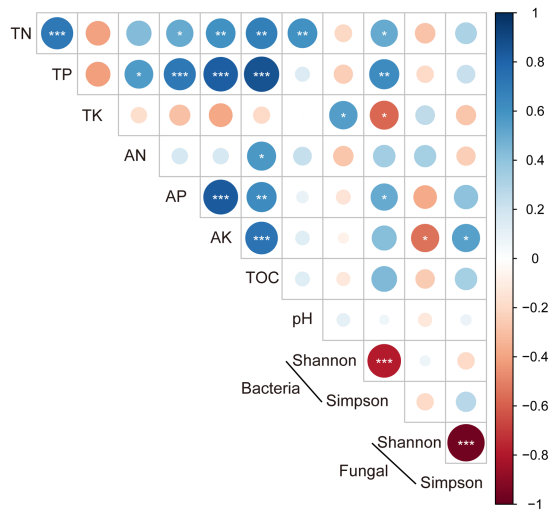

FIGURE 3
The relationship between the alpha diversity and soil properties (*, ≤0.05; **, ≤0.01; ***, ≤0.001).

Conclusion

Crop rotation is one of the effective agricultural management approaches used by farmers to avoid soil degradation and yield decline. The present study evaluated six crop sequences (sss, wsw, wms, smm, mss, and mmm) performed for 5 years. The crop rotation affected the soil physicochemical parameters, which showed soybean and maize rotation (smm and mss) can increase soil organic matter, nitrogen, phosphorus and potassium, which is helpful to increase the yield of soybean and maize. The cropping sequence also changed the diversity and composition of soil microbial community. However, the effects of different cropping sequences on soil bacterial and fungal diversity were not significant. Functional and microbial diversity analysis showed that the present crop rotation planting system showed the presence of nitrogen-fixing bacteria and taxa that inhibit plant pathogens. Interestingly, the highest maize production was noticed in smm planting system, smm can help soil to obtain a lower proportion of pathogens and a higher proportion of beneficial microorganisms. Finally, our findings might be used to guide decision-making for yearly crop and soil management strategies in major grain-producing regions of northeast China.

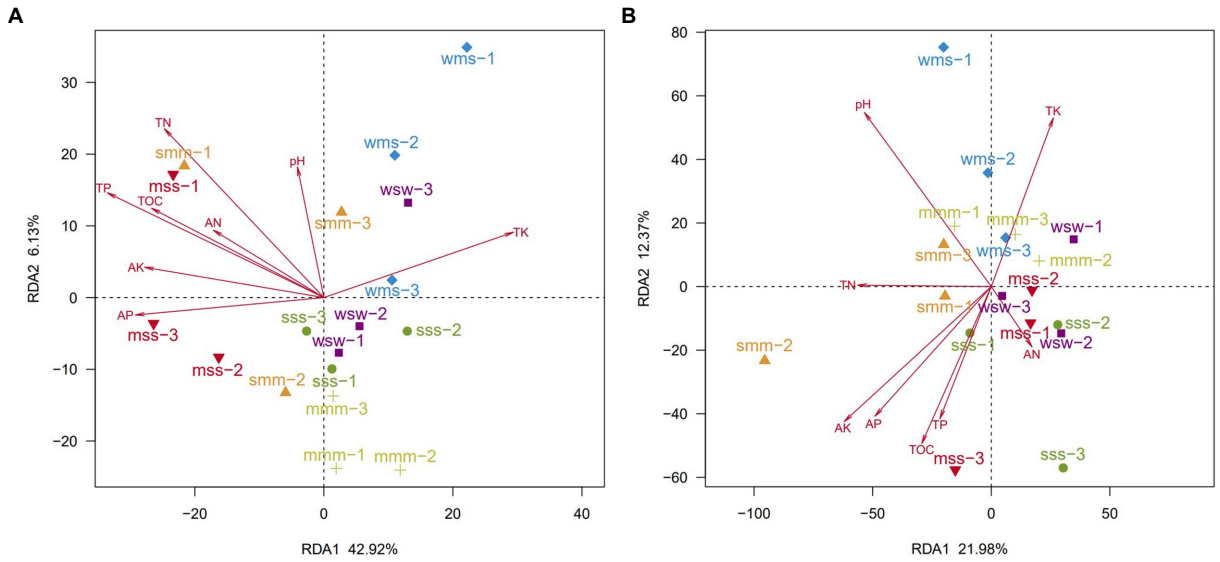

FIGURE 4
Redundancy analysis (RDA) of bacterial **(A)** and fungal **(B)** community compositions and soil chemical properties in all cropping sequences. (OTUs with a relative abundance of more than 0.01%).

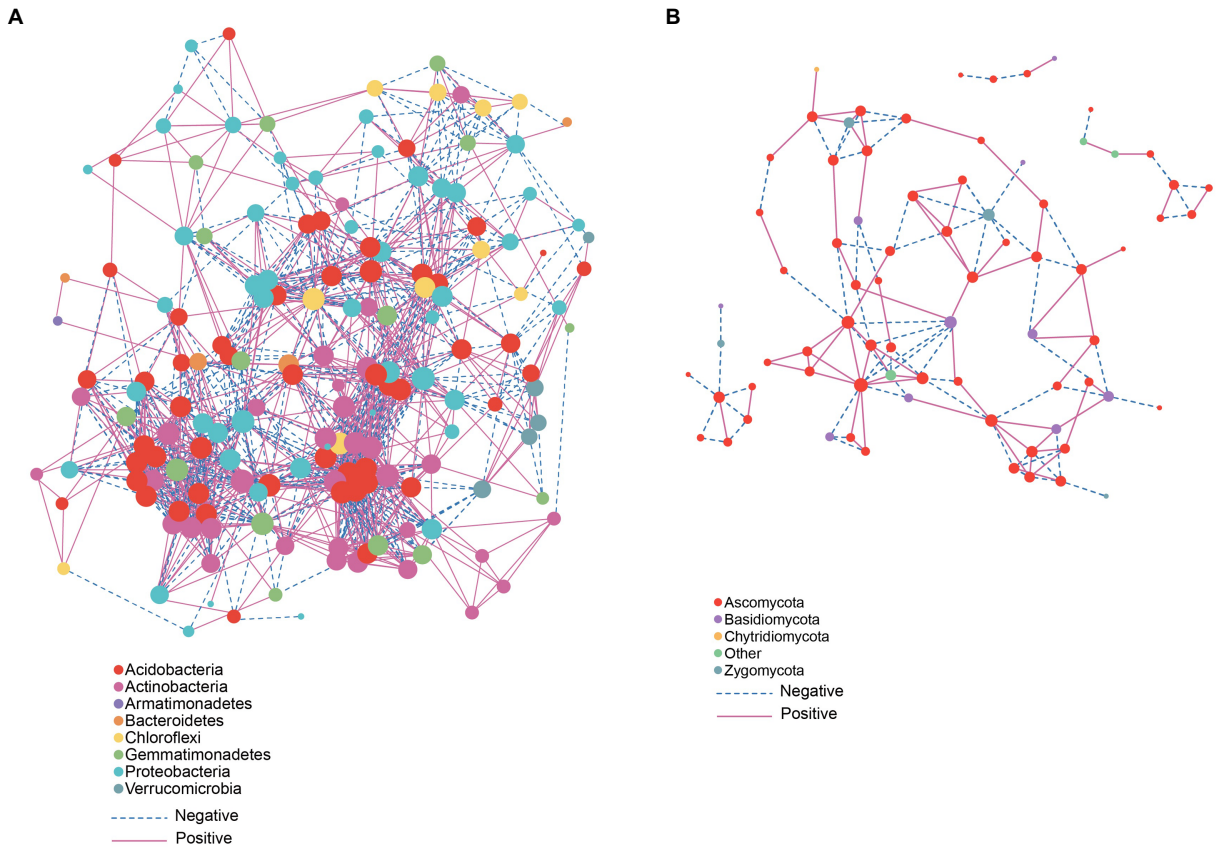

FIGURE 5
Network-based analysis: **(A)** Bacterial communities and **(B)** fungal communities.

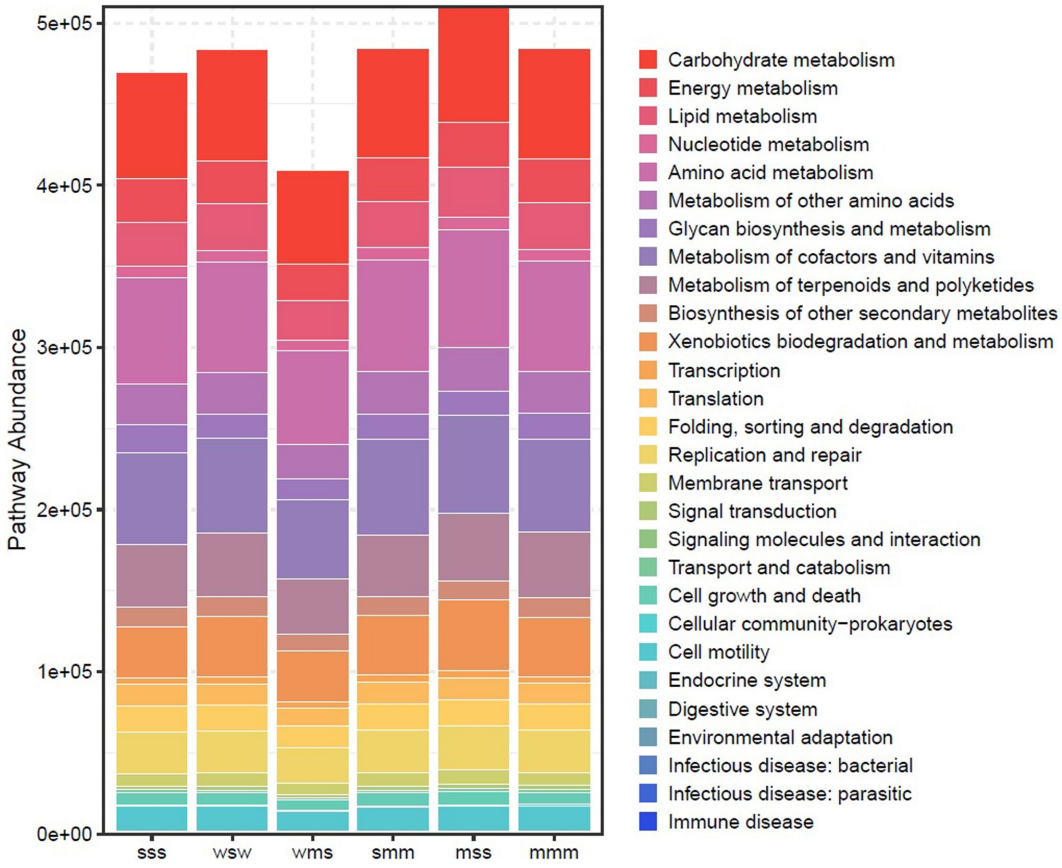

FIGURE 6
PICRUSt based predicted functional composition.

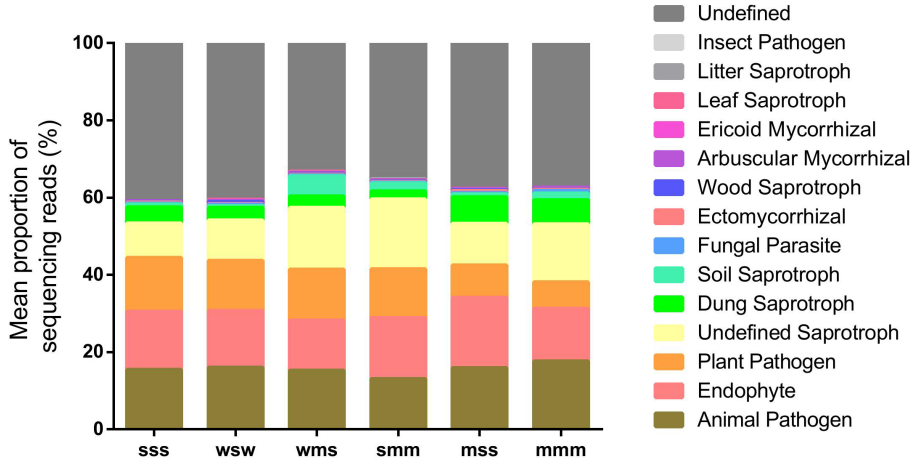

FIGURE 7
Proportion of fungal taxa based on functional annotation by FUNGuild (spearman correlation coefficient).

Data availability statement

The datasets presented in this study can be found in online repositories. The names of the repository/repositories and accession number(s) can be found at: https://www.ncbi.nlm.nih.gov/, PRJNA883616 and https://www.ncbi.nlm.nih.gov/, PRJNA884493.

Author contributions

LS and SW designed the research and project outline. YS, Z-HL, P-JJ, WW, Y-ML, and K-KW performed the DNA extraction and raw data analysis. MN and AB drafted the manuscript. X-YC and DW supervised the study. All authors contributed to the article and approved the submitted version.

Funding

This work was supported by National Key R&D Program of China MOST (no. 2021YFD1500300), China Agriculture Research System of MOF and MARA (CARS-04-PS17), Heilongjiang Science and Technology Project (2021ZXJ05B011), Heilongjiang Academy of Agricultural Sciences Research Project (2020FJZX001 and 2021QKPY008), and UNDP Project (cpr/21/401).

Conflict of interest

The authors declare that the research was conducted in the absence of any commercial or financial relationships that could be construed as a potential conflict of interest.

Publisher's note

Supplementary material

The Supplementary material for this article can be found online at: https://www.frontiersin.org/articles/10.3389/fmicb.2023.1095688/full#supplementary-material

References

Agomoh, I. V., Drury, C. F., Yang, X., Phillips, L. A., and Reynolds, W. D. (2021). Crop rotation enhances soybean yields and soil health indicators. *Soil Sci. Soc. Am. J.* 85, 1185–1195. doi: 10.1002/saj2.20241

Ai, C., Zhang, S., Zhang, X., Guo, D., Zhou, W., and Huang, S. (2018). Distinct responses of soil bacterial and fungal communities to changes in fertilization regime and crop rotation. *Geoderma* 319, 156–166. doi: 10.1016/j.geoderma.2018.01.010

Banerjee, S., and van der Heijden, M. G. A. (2023). Soil microbiomes and one health. *Nat. Rev. Microbiol.* 21, 6–20. doi: 10.1038/s41579-022-00779-w

Boincean, B., and Dent, D. (2019). "Crop rotation" in *Farming the Black Earth* (Cham: Springer)

Bolaji, A. J., Wan, J. C., Manchur, C. L., Lawley, Y., de Kievit, T. R., Fernando, W. G. D., et al. (2021). Microbial community dynamics of soybean (Glycine max) is affected by cropping sequence. *Front. Microbiol.* 12:632280. doi: 10.3389/fmicb.2021.632280

Bolger, A. M., Lohse, M., and Usadel, B. (2014). Trimmomatic: a flexible trimmer for Illumina sequence data. *Bioinformatics* 30, 2114–2120. doi: 10.1093/bioinformatics/btu170

Bolyen, E., Rideout, J. R., Dillon, M. R., Bokulich, N. A., Abnet, C. C., al-Ghalith, G. A., et al. (2019). Reproducible, interactive, scalable and extensible microbiome data science using QIIME 2. *Nat. Biotechnol.* 37, 852–857. doi: 10.1038/s41587-019-0209-9

Bowles, T. M., Mooshammer, M., Socolar, Y., Calderón, F., Cavigelli, M. A., Culman, S. W., et al. (2020). Long-term evidence shows that crop-rotation diversification increases agricultural resilience to adverse growing conditions in North America. *One Earth.* 2, 284–293. doi: 10.1016/j.oneear.2020.02.007

Bullock, D. G. (1992). Crop rotation. Crit rev. *Plant Sci.* 11, 309–326. doi: 10.1080/07352689209382349

Chamberlain, L. A., Bolton, M. L., Cox, M. S., Suen, G., Conley, S. P., and Ane, J. M. (2020). Crop rotation, but not cover crops, influenced soil bacterial community composition in a corn-soybean system in southern Wisconsin. *Appl. Soil Ecol.* 154:103603. doi: 10.1016/j.apsoil.2020.103603

D'acunto, L., Andrade, J. F., Poggio, S. L., and Semmartin, M. (2018). Diversifying crop rotation increased metabolic soil diversity and activity of the microbial community. *Agric. Ecosyst. Environ.* 257, 159–164. doi: 10.1016/j.agee.2018.02.011

Dong, W., Lu, G., Yan, L., Zhang, Z., and Zhang, Y. (2016). Characteristics of pellets with immobilized activated sludge and its performance in increasing nitrification in sequencing batch reactors at low temperatures. *J. Environ. Sci.* 42, 202–209. doi: 10.1016/j.jes.2015.09.002

Edgar, R. C. (2013). UPARSE: highly accurate OTU sequences from microbial amplicon reads. *Nat. Methods* 10, 996–998. doi: 10.1038/nmeth.2604

Edgar, R. C., Haas, B. J., Clemente, J. C., Quince, C., and Knight, R. (2011). UCHIME improves sensitivity and speed of chimera detection. *Bioinformatics* 27, 2194–2200. doi: 10.1093/bioinformatics/btr381

Guo, Z., Wan, S., Hua, K., Yin, Y., Chu, H., Wang, D., et al. (2020). Fertilization regime has a greater effect on soil microbial community structure than crop rotation and growth stage in an agroecosystem. *Appl. Soil Ecol.* 149:103510. doi: 10.1016/j.apsoil.2020.103510

Hoeksema, J. D., Chaudhary, V. B., Gehring, C. A., Johnson, N. C., Karst, J., Koide, R. T., et al. (2010). A meta-analysis of context dependency in plant response to inoculation with mycorrhizal fungi. *Ecol. Lett.* 13, 394–407. doi: 10.1111/j.1461-0248.2009.01430.x

Karlen, D. L., Hurley, E. G., Andrews, S. S., Cambardella, C. A., Meek, D. W., Duffy, M. D., et al. (2006). Crop rotation effects on soil quality at three northern corn/soybean belt locations. *Agron. J.* 98, 484–495. doi: 10.2134/agronj2005.0098

Langille, M. G., Zaneveld, J., Caporaso, J. G., McDonald, D., Knights, D., Reyes, J. A., et al. (2013). Predictive functional profiling of microbial communities using 16S rRNA marker gene sequences. *Nat. Biotechnol.* 31, 814–821. doi: 10.1038/nbt.2676

Liu, X. B., Li, Y. S., Han, B. J., Zhang, Q. Y., Zhou, K. Q., Zhang, X. Y., et al. (2012). Yield response of continuous soybean to one-season crop disturbance in a previous continuous soybean field in Northeast China. *Field Crop Res.* 138, 52–56. doi: 10.1016/j.fcr.2012.09.012

Liu, Z., Liu, J., Yu, Z., Yao, Q., Li, Y., Liang, A., et al. (2020). Long-term continuous cropping of soybean is comparable to crop rotation in mediating microbial abundance, diversity and community composition. *Soil Tillage Res.* 197:104503. doi: 10.1016/j.still.2019.104503

Liu, S., Zhang, M., Feng, F., and Tian, Z. (2020). Toward a "green revolution" for soybean. *Mol. Plant* 13, 688–697. doi: 10.1016/j.molp.2020.03.002

Lu, R. (2000). *Soil and Agricultural Chemistry Analysis*. Beijing: China Agricultural.

Lund, M., Carter, P., and Oplinger, E. (1993). Tillage and crop rotation affect corn, soybean, and winter wheat yields. *J. Prod. Agric.* 6, 207–213. doi: 10.2134/jpa1993.0207

Magoč, T., and Salzberg, S. L. (2011). FLASH: fast length adjustment of short reads to improve genome assemblies. *Bioinformatics* 27, 2957–2963. doi: 10.1093/bioinformatics/btr507

Marcos, P. L., Keith, A. C., and Robert, J. F. (2016). Comparison of two commercial DNA extraction kits for the analysis of nasopharyngeal bacterial communities. *AIMS Microbiol.* 2, 108–119. doi: 10.3934/microbiol.2016.2.108

Martens, D. A. (2000). Plant residue biochemistry regulates soil carbon cycling and carbon sequestration. *Soil Biol. Biochem.* 32, 361–369. doi: 10.1016/S0038-0717(99)00162-5

Matchado, M. S., Lauber, M., Reitmeier, S., Kacprowski, T., Baumbach, J., Haller, D., et al. (2021). Network analysis methods for studying microbial communities: a mini review. *Comput. Struct. Biotechnol. J.* 19, 2687–2698. doi: 10.1016/j.csbj.2021.05.001

Meier, M. A., Lopez-Guerrero, M. G., Guo, M., Schmer, M. R., Herr, J. R., Schnable, J. C., et al. (2021). Rhizosphere microbiomes in a historical maize-soybean rotation system respond to host species and nitrogen fertilization at the genus and subgenus levels. *Appl. Environ. Microbiol.* 87:e0313220. doi: 10.1128/aem.03132-20

Morrissey, E. M., Mau, R. L., Schwartz, E., Koch, B. J., Hayer, M., and Hungate, B. A. (2018). Taxonomic patterns in the nitrogen assimilation of soil prokaryotes: nitrogen assimilation of soil prokaryotes. *Environ. Microbiol.* 20, 1112–1119. doi: 10.1111/1462-2920.14051

Narayana, N. K., Kingery, W. L., Jacobs, A. A., Allison, J. K., and Shanmugam, S. G. (2022). Effects of tillage and winter cover management in a maize soybean rotation on soil bacterial and fungal community composition. *Land.* 11:2259. doi: 10.3390/land11122259

Narisawa, K., Tokumasu, S., and Hashiba, T. (1998). Suppression of clubroot formation in Chinese cabbage by the root endophytic fungus, *Heteroconium chaetospira*. *Plant Pathol.* 47, 206–210. doi: 10.1046/j.1365-3059.1998.00225.x

Neupane, A., Bulbul, I., Wang, Z., Lehman, R. M., Nafziger, E., and Marzano, S. Y. L. (2021). Long term crop rotation effect on subsequent soybean yield explained by soil and root-associated microbiomes and soil health indicators. *Sci. Rep.* 11:9200. doi: 10.1038/s41598-021-88784-6

Nguyen, N. H., Song, Z., Bates, S. T., Branco, S., Tedersoo, L., Menke, J., et al. (2016). FUNGuild: an open annotation tool for parsingfungal community datasets by ecological guild. *Fungal Ecol.* 20, 241–248. doi: 10.1016/j.funeco.2015.06.006

Nilsson, R. H., Larsson, K. H., Taylor, A. F. S., Bengtsson-Palme, J., Jeppesen, T. S., Schigel, D., et al. (2018). The UNITE database for molecular identification of fungi: handling dark taxa and parallel taxonomic classifications. *Nucleic Acids Res.* 47, D259–D264. doi: 10.1093/nar/gky1022

Paungfoo-Lonhienne, C., Wang, W., Yeoh, Y. K., and Halpin, N. (2017). Legume crop rotation suppressed nitrifying microbial community in a sugarcane cropping soil. *Sci. Rep.* 7:16707. doi: 10.1038/s41598-017-17080-z

Peralta, A. L., Sun, Y., Mcdaniel, M. D., and Lennon, J. T. (2018). Crop rotational diversity increases disease suppressive capacity of soil microbiomes. *Ecosphere.* 9:e02235. doi: 10.1002/ecs2.2235

Sasser, J. N., and Uzzell, G. (1991). Control of the soybean cyst nematode by crop rotation in combination with a nematicide. *J. Nematol.* 23, 344–347. PMID: 19283137

Tahir, H. A., Gu, Q., Wu, H., Raza, W., Hanif, A., Wu, L., et al. (2017). Plant growth promotion by volatile organic compounds produced by *Bacillus subtilis* SYST2. *Front. Microbiol.* 8:171. doi: 10.3389/fmicb.2017.00171

Tan, Q., Liu, Y., Dai, L., and Pan, T. (2021). Shortened key growth periods of soybean observed in China under climate change. *Sci. Rep.* 11:8197. doi: 10.1038/s41598-021-87618-9

Tian, B., Zhu, M., Pei, Y., Ran, G., Shi, Y., and Ding, J. (2022). Climate warming alters the soil microbial association network and role of keystone taxa in determining wheat quality in the field. *Agric. Ecosyst. Environ.* 326:107817. doi: 10.1016/j.agee.2021.107817

van der Heijden, M. G. A., Martin, F. M., Selosse, M. A., and Sanders, I. R. (2015). Mycorrhizal ecology and evolution: the past, the present, and the future. *New Phytol.* 205, 1406–1423. doi: 10.1111/nph.13288

Venter, Z. S., Jacobs, K., and Hawkins, H. J. (2016). The impact of crop rotation on soil microbial diversity: a meta-analysis. *Pedobiologia* 59, 215–223. doi: 10.1016/j.pedobi.2016.04.001

Wang, X. Y., Duan, Y., Zhang, J., Ciampitti, I. A., Cui, J. W., Qiu, S. J., et al. (2022). Response of potato yield, soil chemical and microbial properties to different rotation sequences of green manure-potato cropping in North China. *Soil Till Res.* 217:105273. doi: 10.1016/j.still.2021.105273

Wang, Q., Garrity, G. M., Tiedje, J. M., and Cole, J. R. (2007). Naive Bayesian classifier for rapid assignment of rRNA sequences into the new bacterial taxonomy. *Appl. Environ. Microbiol.* 73, 5261–5267. doi: 10.1128/aem.00062-07

White, T. J., Bruns, T., Lee, S., and Taylor, J. (1990). Amplification and direct sequencing of fungal ribosomal RNA genes for phylogenetics. *PCR Protoc. Guide Methods Appl.* 18, 315–322. doi: 10.1016/B978-0-12-372180-8.50042-1

Wickham, H. (2009). *ggplot2: Elegant Graphics for Data Analysis*. Springer-Verlag, New York.

Xiao, N., Zhou, A., Kempher, M. L., Zhou, B. Y., Shi, Z. J., Yuan, M., et al. (2022). Disentangling direct from indirect relationships in association networks. *Proc. Natl. Acad. Sci.* 119:2109995119. doi: 10.1073/pnas.2109995119

Xie, Y. N., Ouyang, Y., Han, S., Se, J., Tang, S., Yang, Y. F., et al. (2022). Crop rotation stage has a greater effect than fertilization on soil microbiome assembly and enzymatic stoichiometry. *Sci. Total Environ.* 815:152956. doi: 10.1016/j.scitotenv.2022.152956

Xie, Y., Wang, F., Wang, K., Yue, H., and Lan, X. (2020). Responses of bacterial phoD gene abundance and diversity to crop rotation and feedbacks to phosphorus uptake in wheat. *Appl. Soil Ecol.* 154:103604. doi: 10.1016/j.apsoil.2020.103604

Yang, T., Evans, B., and Bainard, L. D. (2021). Pulse frequency in crop rotations alters soil microbial community networks and the relative abundance of fungal plant pathogens. *Front. Microbiol.* 12:667394. doi: 10.3389/fmicb.2021.667394

Yao, H., Zuo, X., Zuo, D., Lin, H., Huang, X., and Zang, C. (2020). Study on soybean potential productivity and food security in China under the influence of COVID-19 outbreak. *Geogr Sustain.* 1, 163–171. doi: 10.1016/j.geosus.2020.06.002

Yu, Y., Lee, C., Kim, J., and Hwang, S. (2005). Group-specific primer and probe sets to detect methanogenic communities using quantitative real-time polymerase chain reaction. *Biotechnol. Bioeng.* 89, 670–679. doi: 10.1002/bit.20347

Yu, T., Mahe, L., Li, Y., Wei, X., Deng, X., and Zhang, D. (2022). Benefits of crop rotation on climate resilience and its prospects in China. *Agronomy* 12:436. doi: 10.3390/agronomy12020436

Yu, H., Wang, F., Shao, M., Huang, L., Xie, Y., Xu, Y., et al. (2021). Effects of rotations with legume on soil functional microbial communities involved in phosphorus transformation. *Front. Microbiol.* 12:661100. doi: 10.3389/fmicb.2021.661100

Yuan, M., Yu, T., Shi, Q., Han, D., Yu, K., Wang, L., et al. (2021). Rhizosphere soil bacterial communities of continuous cropping-tolerant and sensitive soybean genotypes respond differently to long-term continuous cropping in mollisols. *Front. Microbiol.* 12:729047. doi: 10.3389/fmicb.2021.729047

Zhang, M., Chai, L., Huang, M., Jia, W., Guo, J., and Huang, Y. (2020). Deciphering the archaeal communities in tree rhizosphere of the Qinghai-Tibetan plateau. *BMC Microbiol.* 20:235. doi: 10.1186/s12866-020-01913-5

Zhang, P., Sun, J., Li, L., Wang, X., Li, X., and Qu, J. (2019). Effect of soybean and maize rotation on soil microbial community structure. *Agronomy* 9:42. doi: 10.3390/agronomy9020042

Zhou, J. Z., Deng, Y., Luo, F., He, Z. L., Tu, Q. C., and Zhi, X. Y. (2010). Functional molecular ecological networks. *mBio* 1:00169-10. doi: 10.1128/mBio.00169-10

frontiers | Frontiers in Microbiology

TYPE Original Research
PUBLISHED 03 July 2023
DOI 10.3389/fmicb.2023.1196101

OPEN ACCESS

EDITED BY
Jian-Wei Guo,
Chinese Academy of Sciences (CAS), China

REVIEWED BY
Dilfuza Jabborova,
Academy of Sciences Republic of Uzbekistan (UzAS), Uzbekistan
Rahul Kumar Tiwari,
Central Potato Research Institute (ICAR), India

*CORRESPONDENCE
Deepanshu Jayaswal
✉ jayaswaldeepanshu@gmail.com
Radha Krishna Jha
✉ radhakrishnajha1959@gmail.com

RECEIVED 29 March 2023
ACCEPTED 30 May 2023
PUBLISHED 03 July 2023

CITATION
Yadav VK, Kumar D, Jha RK, Bairwa RK, Singh R, Mishra G, Singh JP, Kumar A, Vinesh B, Jayaswall K, Rai AK, Singh AN, Kumar S, Rajavat MVS and Jayaswal D (2023) Mycorrhizae set the stage for plants to produce a higher production of biomolecules and stress-related metabolites: a sustainable alternative of agrochemicals to enhance the quality and yield of beetroot (*Beta vulgaris L.*). *Front. Microbiol.* 14:1196101. doi: 10.3389/fmicb.2023.1196101

Mycorrhizae set the stage for plants to produce a higher production of biomolecules and stress-related metabolites: a sustainable alternative of agrochemicals to enhance the quality and yield of beetroot (*Beta vulgaris L.*)

Vinod Kumar Yadav[1], Deepesh Kumar[2], Radha Krishna Jha[1]*, Rakesh Kumar Bairwa[3], Rajan Singh[4], Gaurav Mishra[5], Jyoti Prakash Singh[6], Adarsh Kumar[6], Banoth Vinesh[7], Kuldip Jayaswall[7], Abhishek Kumar Rai[7], Arvind Nath Singh[7], Sanjay Kumar[7], Mahendra Vikram Singh Rajavat[6] and Deepanshu Jayaswal[7]*

[1]University Department of Botany, Ranchi University, Ranchi, Jharkhand, India, [2]ICAR-National Institute for Plant Biotechnology, New Delhi, India, [3]ICAR-Indian Institute of Wheat and Barley Research, Karnal, India, [4]ICAR-Indian Institute of Vegetable Research, Varanasi, India, [5]Chandra Shekhar Azad University of Agriculture and Technology, Kanpur, India, [6]ICAR-National Bureau of Agriculturally Important Microorganism, Mau, Uttar Pradesh, India, [7]ICAR-Indian Institute of Seed Science, Mau, Uttar Pradesh, India

Population explosions, environmental deprivation, and industrial expansion led to an imbalanced agricultural system. Non-judicial uses of agrochemicals have decreased agrodiversity, degraded agroecosystems, and increased the cost of farming. In this scenario, a sustainable agriculture system could play a crucial role; however, it needs rigorous study to understand the biological interfaces within agroecosystems. Among the various biological components with respect to agriculture, mycorrhizae could be a potential candidate. Most agricultural crops are symbiotic with arbuscular mycorrhizal fungi (AMF). In this study, beetroot has been chose to study the effect of different AMFs on various parameters such as morphological traits, biochemical attributes, and gene expression analysis (ALDH7B4 and ALDH3I1). The AMF Gm-*Funneliformis mosseae* (*Glomus mosseae*), *Acaulospora laevis,* and GG-*Gigaspora gigantean* were taken as treatments to study the effect on the above-mentioned parameters in beetroot. We observed that among all the possible combinations of mycorrhizae, Gm+Al+GG performed best, and the Al-alone treatment was found to be a poor performer with respect to all the studied parameters. This study concluded that the more the combinations of mycorrhizae, the better the results will be. However, the phenomenon depends on the receptivity, infectivity, and past nutrient profile of the soil.

KEYWORDS

ALDH7B4, ALDH3I1, beetroot, *Glomus mosseae*, *Gigaspora gigantea*, mycorrhizal inoculation, *Acaulospora laevis*, soil

Introduction

The increasing population worldwide has created huge pressure on the agriculture system due to the high demand for grain for pulses, vegetables, and fruits. During the green revolution in the 1960s, several chemical fertilizers, pesticides, and herbicides were used to meet the high demand for food (Singh, 2000). The ultimate result was increased agricultural production with the uncontrolled use of agrochemicals led to the imbalanced bio-physiochemical properties of the soil. In the current scenario, when climate change is the major cause of several biotic and abiotic stresses, a second green revolution in a sustainable way is the need of the hour (Bhatt et al., 2016). The application of biofertilizer instead of chemical fertilizer could be the major contributor to attaining the second green revolution.

Vegetables, particularly beetroot (*Beta vulgaris* L.), are being used in the food, pharmaceutical, and sugar industries (El-Beltagi et al., 2022). Considering the yield and quality parameters, it is clearly evident that beetroot produced without agrochemicals is highly desirable for human consumption, which could be achieved using biological organisms, such as mycorrhizae and other soil bacteria, without compromising the yield and quality of the beetroot. Beetroot is a biennial flowering plant that belongs to the Amaranthaceae family and originated in Asia and Europe (Avetisyan et al., 2022; Thakur and Singh, 2022). Approximately 1,400 species in 105 genera of beetroot have been reported worldwide to date (Lazăr et al., 2021). Looking at the nutrient profile of the beetroot, it contains a variety of biomolecules and active ingredients such as highly active pigments, dietary fibers, vitamins, and secondary metabolites including carotenoids, polyphenols, flavonoids, and saponins (Chhikara et al., 2019). The multiple biomolecules and secondary metabolites of the beetroot play a significant role as antioxidants, anti-inflammatory agents, anti-cancer agents, and anti-diabetic agents. It is reported that these active ingredients can help reduce cardiovascular disease, promote wound healing, and provide several other health benefits (Sun and Lu, 2019).

While going through the health benefits of beetroot, several studies were carried out focusing on its growth and development, crop improvement through conventional and molecular breeding, nutrient profiling, cell suspension culture, and metabolic profiling, along with its regulation (Abu-Ellail et al., 2021; Carrera et al., 2021; Wikandari et al., 2021; Wang et al., 2022). The underutilized part of getting the maximum yield in a sustainable way is the application of bioprospecting. Therefore, the study of novel mycorrhizae to observe their effect on the physiological and biochemical aspects of beetroot is crucial. In some studies, it is reported that mycorrhizae, particularly arbuscular mycorrhizal fungi (AMF), could be used to enhance plant growth, biotic and abiotic stress tolerance, and ultimately productivity (Khaliq et al., 2022). The AMF is among the best examples of obligate symbionts, where the fungal partner provides water to the plant and absorbs nutrients from the soil for the host (Manga et al., 2022). In an agricultural context, AMF alters the soil structure by crosslinking highly dense mycelium with soil particles, which reduces soil erosion, and enhances soil water retention capacity (Leifheit et al., 2014). According to Van Der Heijden et al. (2006), AMF do not directly increase plant productivity; rather, they significantly help in phosphorus and nitrogen acquisition and the survival of different plant species. The environmental conditions and availability of phosphorus and nitrogen in soil affect the successful colonization of AMF and symbiosis (Baar, 2008).

The AMF are of key importance for the plant's physiology, *viz*., the biomass of the root, osmotic balance, mineral contents, chlorophyll content, stomatal conductance, photosynthetic, and respiration rates, as well as antioxidant activities (Liu et al., 2014; Pedranzani et al., 2016). The resulting effects of these AMF on plants are increased nutritional content and rapid plant growth (Jabborova et al., 2021a,b). In this line, several researchers have concluded that mycorrhizae alone and in combination with other microorganisms could be used in the agriculture sector to enhance crop yield by modifying plant physiology, including height, leaf, and root parameters (Mathur and Sharma, 2018). Recent studies on the effect of AMF on the physiology of several crops have proven that AMF plays a significant role in increasing the total chlorophyll, carotenoid, nutrient, phytohormones, antioxidants, SODs, and peroxidases, ultimately affecting the overall metabolism of the plants, and resulting in high yields from the concerned crops (Basu et al., 2021; Jabborova et al., 2021c, 2022; Jabborova, 2022).

Therefore, in this study, we proposed the hypothesis that bioinoculants (Gm-*Funneliformis mosseae*, Al-*Acaulospora laevis,* and G_G-*Gigaspora gigantean)* act on (i) morphological and food storage parameters of *Beta vulgaris;* (ii) biochemical and physiological attributes of *Beta vulgaris;* (iii) stress physiological attributes of *Beta vulgaris;* (iv) mineral content of *Beta vulgaris;* and (v) aldehyde dehydrogenase gene expression.

Materials and methods

Field preparation and selection of beetroot cultivar

Before initiating the seed sowing and microbial treatment, the net house conditions were optimized. The desired conditions of 24°C and 49–66% relative humidity were established in the greenhouse. The soil was prepared by making a mixture of alluvial soil and sand in a ratio of 3:1 with 70.8% sand, 24.5% silt, and 4.0% clay. The chemical composition of the soil was analyzed (0.042% N, 0.017% P, 0.06% organic carbon, and a pH of 7.4) and found to be suitable for the cultivation of beetroot. Furthermore, the soil was autoclaved at 121°C to eliminate the seeds of weeds and microbial inoculums. The beetroot cultivar Crimson Globe was taken for sowing in pots during the month of October 2020. Furthermore, a randomized complete block design was chosen to give the desired treatments in triplicate, with 15 plants in each replication. The agronomical practices were followed by Yadav et al. (2021).

Microbial inoculums preparation and treatments on beetroot

In this study, three microbial inoculums were taken for the treatment of beetroot in different combinations. The inoculum of *Funneliformis mosseae* (Gm) with 80–86% colonization (root

pieces) and 780–800 AM spores (w/w) was procured from the Department of Botany, Kurukshetra University, Kurukshetra. The inoculum of *Gigaspora gigantea* (Gg) with 75–79% colonization (root pieces) and 870–890 AM spores (w/w) and *Acaulospora laevis* was procured from the Forest Pathology Discipline, Forest Protection Division, FRI, Dehradun, India. To get the starter inoculum for the experiment, both inoculums (*Funneliformis mosseae* and *Gigaspora gigantea*) were then mass multiplied using maize as a host for 3 months. After mass production, the inoculum containing 77–82% colonization/infection (maize root pieces) and 820–860 *Funneliformis mosseae* spores (w/w), and 74–78% colonization/infection (maize root pieces) and 840–880 *Gigaspora gigantea* spores (w/w) were taken. *Acaulospora laevis* was multiplied in a nutrient broth medium containing beef extract, peptone, and NaCl at 3 g/L, 5 g/L, and 5 g/L, respectively, and incubated at 32°C for 48 h for proper growth of AMF.

TABLE 1 Treatments with single and different microbial combinations given to beetroot along with control.

Treatment	Microbial inoculation
C	Control
T1	Funneliformis mosseae (Gm)
T2	Acaulospora laevis (Al)
T3	Gigaspora gigantea (GG)
T4	Gm + Al
T5	Gm + GG
T6	Al + GG
T7	Gm + Al + GG (consortium)

In total, 10 g of each inoculum was added per pot for a single treatment, and 5 + 5 g (*Funneliformis mosseae* + *Gigaspora gigantea*) was added for dual and consortium treatments. For the *Acaulospora laevis* treatment, all the seeds of beetroot except the control were dipped in the nutrient broth medium for 10 min (Saini et al., 2019). Microbial inoculums used in this study are shown in Table 1. The following seven treatments (Tt) were investigated to inoculate beetroot alongside the control.

Morphological and food storage parameters of beetroot

With all the treatments alone and in combinations, morphological and food storage parameter data, such as shoot length (cm), root weight (g), shelf life (days), root circumference (cm), protein (mg/100 mg FW), and carbohydrate (mg/100 mg FW), were recorded and statistically analyzed (Figure 1, Supplementary Table 1). To analyze the AMF colonization, beetroot roots were washed with water and chopped into small pieces. The digestion and clearance were carried out in KOH and stained with trypan blue (0.05%). Thereafter, AMF colonization was measured with a microscope. Based on the fungal hyphal infection, the frequency distribution method was followed to study the colonization (number of arbuscules) in the beetroot segments (Phillips, 1970; Giovannetti, 1980; Biermann, 1981; Koske, 1989).

Biochemical and physiological attributes of beetroot

Several biochemical tests were performed (50 days after sowing) to measure total chlorophyll (mgFW-g), total anthocyanin

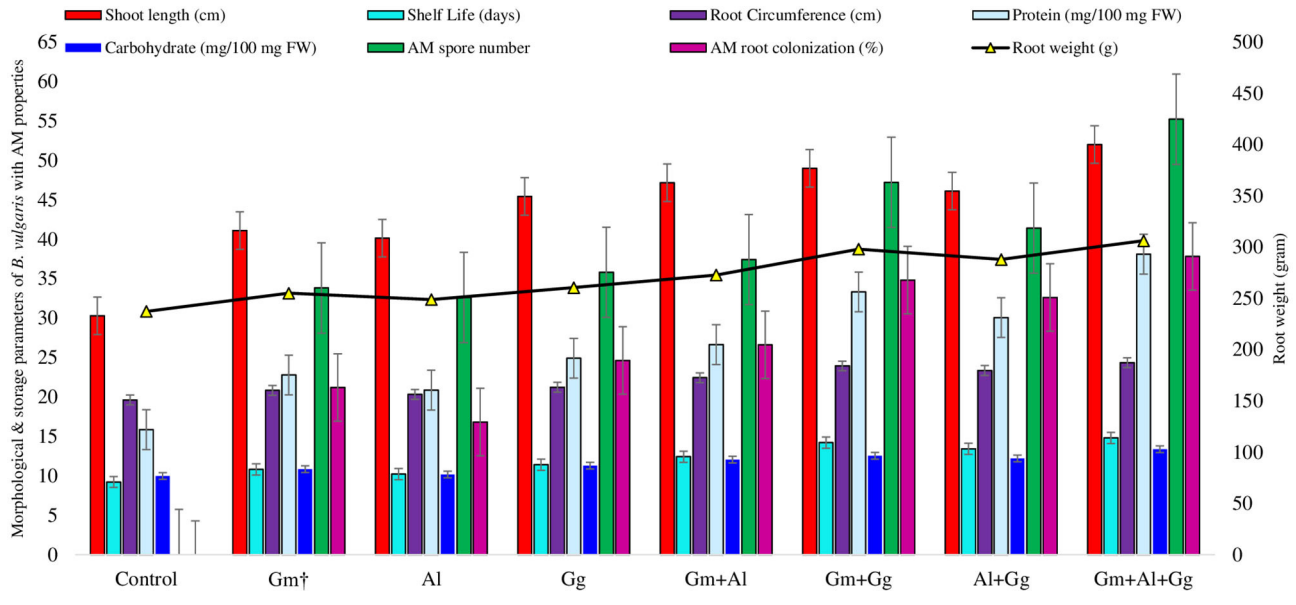

FIGURE 1
Morphological and food storage parameters of beetroot with AMF properties.

(mgFW-g), phosphorus content (%) in root and shoot, and phosphatase (IU/g FW) from beetroot samples in triplicates (Supplementary Table 2). The absorbance of the supernatant was recorded at 645 nm and 663 nm for chlorophyll a and b, respectively, using a UV–vis spectrophotometer (Specord 205 Analytik Jena AG, Jena, Germany). Anthocyanin was measured at 520 nm using acetone (80%) as a blank (McGonigle et al., 1990). The recorded data were analyzed statistically using SPSS (version 11.5), and inferences were made.

Measurement of stress-related attributes and mineral contents of beetroot

The peroxide content, electrolyte leakage, proline, catalase, ascorbate peroxidase, and superoxide dismutase (SOD) were measured following the protocol (Plenchette et al., 2005). The recorded data were statistically analyzed (Supplementary Table 3). In the control plants, individual inoculum-treated plants, consortium-treated plants, mineral levels, such as potassium (K), calcium (Ca), magnesium (Mg), iron (Fe), and manganese (Mn), were measured (Mitchell and Bingham, 1974; Kurt and Kizildag, 2018; Saini et al., 2020).

RNA isolation and cDNA synthesis

The fresh leaf samples from all the treatments and control plants were procured in liquid nitrogen. The leaf samples were collected after 3 days of treatment. Total RNA was isolated from all the collected leaf samples using the Trizol method. The DNase (RNase-free) treatment was given to the isolated total RNA. The quantification of isolated RNA was performed by Nanodrop (Thermo Scientific Nanodrop 2000) along with a quality check by 1.2% denaturing agarose gel electrophoresis. For cDNA synthesis, the Thermo Scientific cDNA synthesis kit was used as per the protocol given by the manufacturers. All the samples were collected in triplicate.

Gene expression analysis using *Arabidopsis thaliana* aldehyde dehydrogenase 7B4 and *Arabidopsis thaliana* aldehyde dehydrogenase 3I1

The primers for both the genes ALDH7B4 and ALDH3I1 (Table 2) were designed from *Arabidopsis thaliana* transcripts NM¬_179476.3:121-1647 and NM¬_001342263.1:749-1975, respectively, using IDT software.

The PCR reaction was set up in a 96-well PCR plate containing 2 μl of template, 0.5 μl primers, 10 μl SYBR green, and DEPC water. The qRTPCR reaction condition was denaturation at 94 °C for 3 min, 35 cycles of 94 °C for 30 s, 60 °C for 20 s, and 72 °C for 30 s. Actin was used as an internal control. Three technical replicates were taken for each sample, and "the comparative Ct method" was used to calculate the relative expression of each sample.

TABLE 2 Primer sequences of ALDH7B4, ALDH3I1 used for gene expression analysis.

S.N.	Genes	Primer sequence
1	*ALDH7B4*	Forward: AAGCAGTCGAAGGTGAAGGA
		Reverse: GTTTTCAGGGTTCCGAGTGA
2	*ALDH3I1*	Forward: GAGGGAGGAGTCCCTGAAAC
		Reverse: TCCTCCTAGCAGCCACTTGT
3	*Actin*	Forward: TGTGCCAATCTACGAGGGTT
		Reverse: ACAACGGCACTACTGGATCA

Result and discussion

Environmental degradation, population explosion, and industrial globalization have created a situation in which we have to reconsider the agricultural system *via* restoration and reclamation of soil microbiota, bio-prospecting, and cutting-edge technology (Ortas, 2012). The unjudicial use of chemical fertilizers and pesticides led to an environmental loss, an unbalanced agroecosystem, and non-profitable crop cultivation. Before replacing the current system of agriculture with a sustainable agriculture system, we have to understand the deep biological interactions among plant and soil microbiota (Chun et al., 2018). With the conclusion of previous studies, it is now well known that mycorrhizae, which are symbiotic associations between fungi and plant roots, are very helpful in biotic and abiotic stress tolerance and mineral absorption, ultimately assisting in the enhanced productivity of various crops (Amirnia et al., 2019; Adeyemi et al., 2020; Wang et al., 2020). The AMF positively affects plant growth by balancing ROS levels in the cells, improving nutrient uptake by altering the root architecture, and increasing antioxidant levels (Augé, 2001; He et al., 2020). The AMF symbiosis also regulates the homeostasis of hormones in the plants that are responsible for changes in their physiology (Pozo et al., 2015). Due to AMF, the increasing amount of minerals, such as P, regulates gas exchange, transpiration, and drought stress (Pozo et al., 2015). Even though the importance of mycorrhizae in agricultural systems is well established, their implementation is very rare. Therefore, it is the need of the hour to do rigorous research on interactions between mycorrhizae and different crop roots, infectivity, and receptivity of mycorrhizae to the soil. With this background, we have tried to analyze our hypothesis on beetroot.

Effect of bioinoculants on morphological and food storage parameters of beetroot

The morphological, biochemical, shelf life (days), and AMF root colonization (%) data in control and treated beetroot were recorded and analyzed (Figure 1, Supplementary Table 1). The shoot length of the beetroot was the highest, i.e., 51.974 cm, in the combination of treatments having G_m- *Funneliformis mosseae*, Al-*Acaulo sporalaevis,* and G_G-*Gigaspora gigantean,* followed by 48.974 cm in the treatment having G_m+G_G, 47.148 cm in G_m+A_l, 45.426 cm in G_G, 40.118 cm in A_l, 41.088 cm in Gm, and 30.280 cm in the control (Supplementary Table 1). The highest root weight

was recorded in the treatment having Gm+Al+GG, i.e., 306.102 grams, and the least in Al, i.e., 248.716 grams (Figure 1). The highest root circumference was observed in the $G_m+A_l+G_G$ treatment, i.e., 24.320 cm, and the least was in the A_l treatment at 20.310 cm (Supplementary Table 1). The shelf life of the beetroot was found to be the highest in the $G_m+A_l+G_G$ treatment and the lowest in the A_l treatment. Looking into the nutrient profiling, i.e., protein and carbohydrate (mg/100 mg fresh weight), the highest protein and carbohydrate were observed in the $G_m+A_l+G_G$ treatment, i.e., 38.092 and 13.352, respectively, and the least was in Al, i.e., 20.841 and 10.142, respectively (Supplementary Table 1). In this sequence, following the same pattern, AM spore number and AM root colonization (%) were the highest in the $G_m+A_l+G_G$ treatment, i.e., 55.200 and 37.800, respectively, and the lowest in the Al treatment, i.e., 32.600 and 16.800, respectively. The values recorded for all the parameters were found to be the lowest in the control plants (Figure 1). The mentioned values related to all the parameters are given in Supplementary Table 1.

Our findings suggested that among the single and combinations of mycorrhizal treatments, the $G_m+A_l+G_G$ treatment showed significant results for all the parameters. The most probable reason would be the synergistic effect of the mycorrhizae on beetroot. In most of the parameters, the performance of the A_l treatment was the lowest among all the treatments. This would be because the soil has less mycorrhizal infectivity and/or receptivity. As the control plants showed the least value for all the parameters, it could be because of the low or unbalanced nutrient profile of the soil. With this observation, it may be concluded that a more compatible combination of mycorrhizae could lead to an increased value of the studied parameters. This could not be the case when the soil is already rich in nutrients or has a past record of cropping patterns that lead to soil enrichment up to a threshold, such as azotrophs and/or mycorrhizal associations (Saboor et al., 2021).

Effect of bioinoculants on biochemical and physiological attributes of beetroot

For many years, research on the effect of mycorrhizae on chlorophyll and anthocyanin contents in various crops has been conducted. The research findings indicate that these biofertilizers enhance the different plant pigments to enhance immunity against different stresses and chlorophyll content to increase the number of photosynthates along with phosphorus and phosphatase contents (Lingua et al., 2013; Zare-Maivan et al., 2017; Begum et al., 2019a; Mahmud et al., 2021). Compared with the control plants, AMF-treated plants contain more chlorophyll because of antioxidants and supporting minerals, viz., N and Mg (to help in the biosynthesis and stabilization of necessary pigments). Due to this, more photosynthates (carbohydrates) as a carbon sink could enhance the photosynthesis rate. This is the first report on the effect of selected mycorrhizae on chlorophyll, anthocyanin, phosphate (in both shoot and root), and phosphatase content in beetroot. In this sequence, looking at the research findings, the total chlorophyll and anthocyanin contents were the highest, i.e., 25.346 and 27.912 mg FW^{-g} in the $G_m+A_l+G_G$ treatment on beetroot, respectively, and the lowest in the A_l treatment, i.e., 21.452 and 24.028 mg FW^{-g}, respectively (Supplementary Table 2). After looking into the phosphorus content in the shoot and root of the beetroot, the phosphorus content in the shoot and root was recorded as the highest in the Gm+Al+GG treatment, i.e., 1.007 and 2.849 (%), respectively. Following the same pattern, phosphorus content was the lowest, i.e., 0.737 and 1.134%, in the shoot and root of the beetroot, respectively. The phosphatase content (IU g-1 FW) in both acidic and alkaline forms was observed in all the treatments, and it was found that the Gm+Al+GG treatment had the highest phosphatase content in acidic and alkaline forms, i.e., 20.153 and 25.239, respectively. Again, the A_l treatment showed poor phosphatase content (acidic and alkaline forms), i.e., 17.221 and 21.743, respectively (Supplementary Table 2).

The analysis of the observed parameters indicates that among all the single and combined mycorrhizal treatments, the $G_m+A_l+G_G$ treatment performed very well, and the A_l treatment performed poorly. Although, the findings suggest some good and poor performers of mycorrhizal treatment, the results may vary depending on soil health and crop-to-crop interaction (Pal and Pandey, 2015; Tsoata et al., 2015; Zhao et al., 2015). The enzyme phosphatase acts on the insoluble phosphate present in the soil and makes it available for plants. In this study, the Gm+Al+GG treatment showed the highest phosphorus and phosphatase contents, which may be because of the synergistic effect of all the AMF. All the treatments had higher values for all the observed parameters in comparison to the control (Supplementary Table 2).

Effect of bioinoculants on stress physiological attributes of beetroot

Under different biotic and abiotic stresses, peroxidation and electrolyte leakage are the major contributors to creating imbalances in the plant defense system (Talaat and Shawky, 2014; EshaghiGorgi et al., 2022; Haghighi and Saharkhiz, 2022). The application of mycorrhizae to study the level of peroxide content ($\mu mol\ g^{-1}$ FW) and electrolyte leakage (%) on beetroot was recorded (Supplementary Table 3). In the experiment, we observed that the lowest peroxide and electrolyte leakage were found in the $G_m+A_l+G_G$ treatment, i.e., 11.173 and 31.913, respectively, while the highest peroxide and electrolyte leakage were observed in the A_l treatment, i.e., 16.287 and 36.257, respectively (Figure 2). Along with this, we have also recorded the proline content (μmol g-1 FW) of the beetroot. It was observed that the highest level of proline was found in the $G_m+A_l+G_G$ treatment, i.e., 134.788, and the lowest in the A_l treatment, i.e., 130.114 μmol g-1 FW (Figure 2). Furthermore, in this study, enzymatic activity was measured in beetroot, such as catalase (U mg-1 protein), ascorbate peroxidase (mg protein min-10), and superoxide dismutase (U mg-1 protein) (Supplementary Table 3). All three enzyme levels were the highest in the $G_m+A_l+G_G$ treatment, i.e., 181.876, 0.809, and 140.333, respectively (Figure 3). Peroxidation and electrolyte leakage must be low to avoid any metabolic imbalance in the plant system (Chun et al., 2018). Therefore, we have given different treatments to record the levels of peroxidase and electrolyte leakage in control and treated beetroot. Our finding suggests that the use

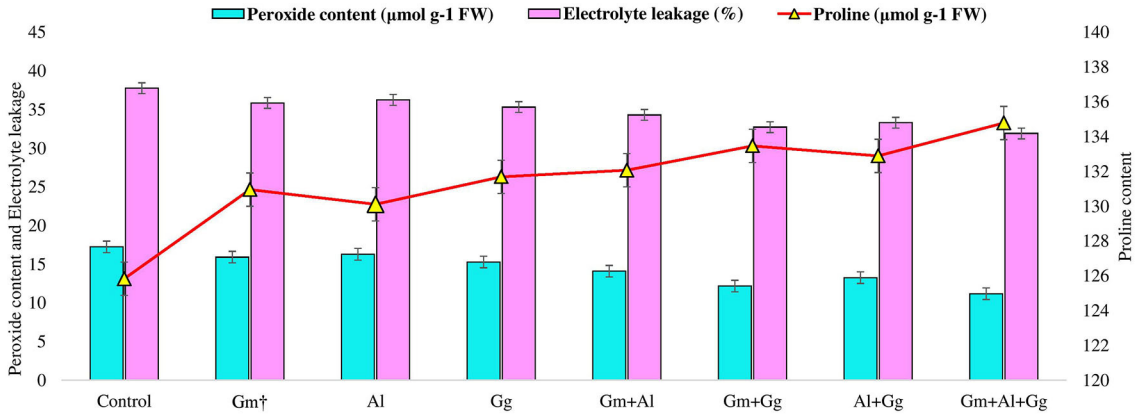

FIGURE 2
Peroxide content, electrolyte leakage, and proline content in control and treatment beetroot plant.

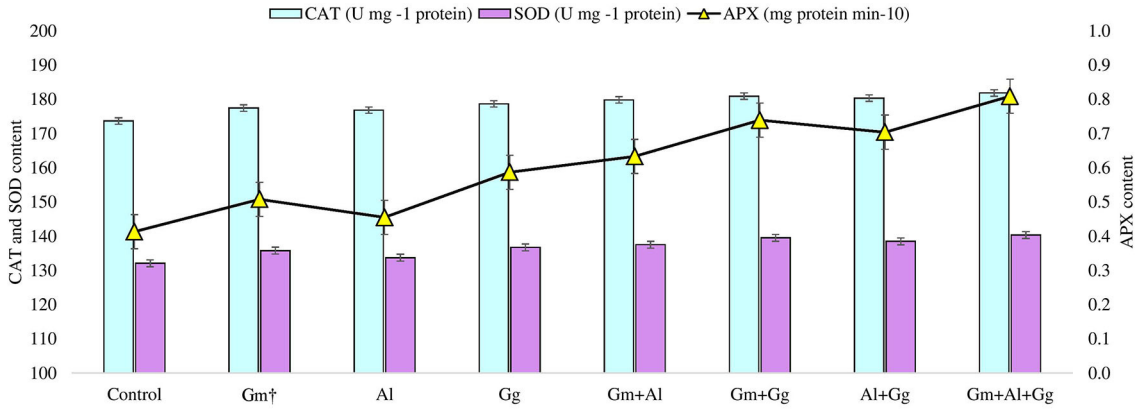

FIGURE 3
Catalase, superoxide dismutase, and ascorbate peroxidase content in control and treatment beetroot plant.

of biofertilizer and mycorrhizae in different combinations gives the best outputs, i.e., less peroxidase will be produced, leading to minimal lipid peroxidation and less electrolyte leakage. In the same way, proline content was measured. It is well known that proline is the major osmolyte, which plays an important role in maintaining the osmotic balance of the cell during various stresses, and different mycorrhizae boost the immune system of the plants by enhancing the level of proline in both unstressed and stressed conditions (Ortiz et al., 2015; Kulczyk-Skrzeszewska and Kieliszewska-Rokicka, 2022; Zahedi et al., 2022). Here, after treatment with mycorrhizae, it was found that proline concentration was increasing with the increasing mycorrhizal combination. The probable explanation for this could be that the single selected mycorrhiza could induce the production of proline minimally due to several reasons (Jeevan Kumar et al., 2015). However, when the mycorrhizal combination meets together, they might be associating symbiotically with plant roots, leading to the induction of genes to produce more proline in plants. There are various metabolic processes, such as photosynthesis and respiration, in the plant system during which different reactive oxygen species are produced. Reactive oxygen species (ROS) are not always harmful. Their balanced amount of ROS in the plant system is essential for successful metabolic activity inside various tissues (Haghighi et al., 2022). Even in open environments, stresses are always there for plants; hence, ROS levels are high all the time and increase exponentially, which damages biomolecules. In our findings, we have measured the levels of catalase, ascorbate peroxidase, and superoxide dismutase in beetroot plants in control (no treatment) and treatment conditions. We found that the levels of all three enzymes were the highest in the $G_m+A_l+G_G$ treatment and the lowest in the A_l treatment (Figure 3). Previous studies also support our finding that mycorrhizal treatment enhances the level of these enzymes in different conditions to tackle the adverse effect of ROS (Jeevan Kumar et al., 2015; Ait-El-Mokhtar et al., 2022; Li et al., 2022; Naseri Rad and Naseri, 2022; Razvi et al., 2022). All the treatments showed more value than the control, indicating that no selected mycorrhiza is implicated in negative impacts on the beetroot.

TABLE 3 Effect of bioinoculants on mineral contents of *Beta vulgaris*.

Parameters → Treatments ↓	K (mg/100 g FW)	Ca (mg/100 g FW)	Mg (mg/100 g FW)	Fe (mg/100 g FW)	Mn (mg/100 g FW)
Control	231.677 ± 1.182^{f}	20.742 ± 1.27^{e}	29.624 ± 0.661^{e}	0.959 ± 0.118^{e}	0.425 ± 0.844^{d}
G_m†	234.546 ± 0.967^{d}	23.424 ± 1.02^{c}	33.246 ± 1.018^{cd}	1.293 ± 0.114^{c}	0.484 ± 0.077^{bcd}
A_l	233.971 ± 0.785^{e}	22.462 ± 1.57^{d}	32.524 ± 1.068^{d}	1.104 ± 0.172^{d}	0.456 ± 0.052^{cd}
G_G	235.592 ± 2.215^{cd}	24.018 ± 1.46^{bc}	33.722 ± 1.153^{bcd}	1.381 ± 0.125^{c}	0.587 ± 0.044^{ab}
G_m+A_l	235.501 ± 1.165^{bc}	24.242 ± 1.18^{b}	34.322 ± 0.924^{ab}	1.564 ± 0.073^{b}	0.508 ± 0.064^{bcd}
G_m+G_G	237.561 ± 2.602^{b}	25.194 ± 2.55^{b}	34.992 ± 0.828^{ab}	1.689 ± 0.135^{ab}	0.572 ± 0.114^{ab}
A_l+G_G	236.549 ± 1.683^{bc}	24.876 ± 1.88^{b}	34.878 ± 1.351^{ab}	1.635 ± 0.101^{ab}	0.521 ± 0.113^{bcd}
$G_m+A_l+G_G$	240.335 ± 1.257^{a}	25.492 ± 1.05^{a}	35.506 ± 1.128^{a}	1.761 ± 0.075^{a}	0.662 ± 0.093^{a}
LSD ($P \leq 0.05$)	2.057	1.441	1.334	0.152	0.108
ANOVA (Biermann, 1981; Lazăr et al., 2021)	13.051	9.991	16.520	29.782	4.168

†G_m, *Glomus mosseae*; A_l, *Acaulospora laevis*; G_G, *Gigaspora gigantean*. ±, Standard deviation; LSD, least significant difference test; FW, Fresh Weight.

Effect of bioinoculants on the mineral content of beetroot

The treatments of various mycorrhizae have been given to study the effect of mycorrhizae on mineral uptake in plants that affects plant growth and development is well-known for many years. However, their implementations in agroecosystems have not been much explored. This study has shown the effect of mycorrhizal treatment in single and combination on the beetroot nutrient profile (Table 3). We analyzed the calcium, magnesium, potassium, iron, and manganese content (mg/100 g FW) in beetroot under control and treatment with different combinations of mycorrhizae. The best result was found in the $G_m+A_l+G_G$ treatment in terms of nutrient uptake, such as potassium, calcium, magnesium, iron, and manganese in beetroot, while the least was observed in the Al treatment (Table 3). Our finding suggests that AMFs are very helpful in nutrient uptake from the soil, which will be available for plants. These minerals lead to biomass enhancement during the developmental process of the plants. In previous studies, single and combinatorial effects of mycorrhizae have been explored that strongly suggests that these mycorrhizae could be used as a biofertilizer (Liu et al., 2021; Rodrigues et al., 2021; Zhao et al., 2021; Ortas and Bilgili, 2022; Paredes-Jácome et al., 2022; Tereucán et al., 2022).

Gene expression analysis

Gene expression analysis was performed using ALDH7B4 and ALDH3I1 primers. With the findings of biochemical analysis, it was evident that different treatments had variable responses on peroxide content, proline, catalase, ascorbate peroxidase, and superoxide dismutase levels. Furthermore, to validate the findings, we have performed aldehyde dehydrogenase gene expression that could lead to the lowering of peroxide content. In control beetroot plants, the ALDH7B4 gene was minimally expressed, while in all treatments, a different fold change in gene expression was observed (Figure 4). Among all treatments, the least gene expression was found in T2 (4.3 X) and the highest in T7 (7.2 X). The relative fold change of gene expression in T1 was 5.1X, T2 was 4.3X, T3 was 5.3X, T4 was 5.6X, T5 was 6.5X, T6 was 6.07X, and in T7, it was 7.2X. The chronology of treatment effects on *ALDH7B4* gene expression was C<T2<T1<T3<T4<T6<T5<T7. The second gene, ALDH3I1, was analyzed for gene expression. The least expression was observed in control plants (1X), followed by T2 (3.7X), while the highest gene expression was observed in T7 (5.6X). The relative fold change of gene expression in T1 was 3.7 X, T3 was 4.5 X, T4 was 4.7 X, T5 was 4.9 X, and in T6, it was 4.4 X. The fold change in T6 and T3 was almost equal (4.4 and 4.5, respectively). The chronology of treatment effects on ALDH3I1 gene expression was C<T2<T1<T6<T3<T4<T5<T7 (Figure 4). Aldehyde dehydrogenases are well known for their crucial role in aldehyde detoxification and scavenging ROS in plants (Kotchoni et al., 2006; Bhantana et al., 2021). In this study, upon various combinations of mycorrhizae treatment on beetroot plants, we observed different parameters such as peroxide content, proline, catalase, ascorbate peroxidase, and superoxide dismutase concentration (Supplementary Table 3). Begum et al. (2019b) studied the effect of AMF inoculation on catalase, peroxidase, and SOD synthesis against drought tolerance in maize. Similarly, the effect of AMF on antioxidants and their ROS scavenging capacity has been reported in the literature (Evelin et al., 2019). In our study, after mycorrhizal treatment, the peroxide level was observed to be higher in the control plants than in all the treated plants. The levels of proline, catalase, ascorbate peroxidase, and SOD were lowest in control plants, whereas in treated plants, the levels were significantly different and higher than in controls (Supplementary Table 3). Aldehyde dehydrogenases regulate the ROS level in organisms. Therefore, to know the probable reason for high levels of ROS in control and less ROS in treatments, we have analyzed the *ALDH7B4* and *ALDH3I1* gene expression. With the qRTPCR results, it is evident that different

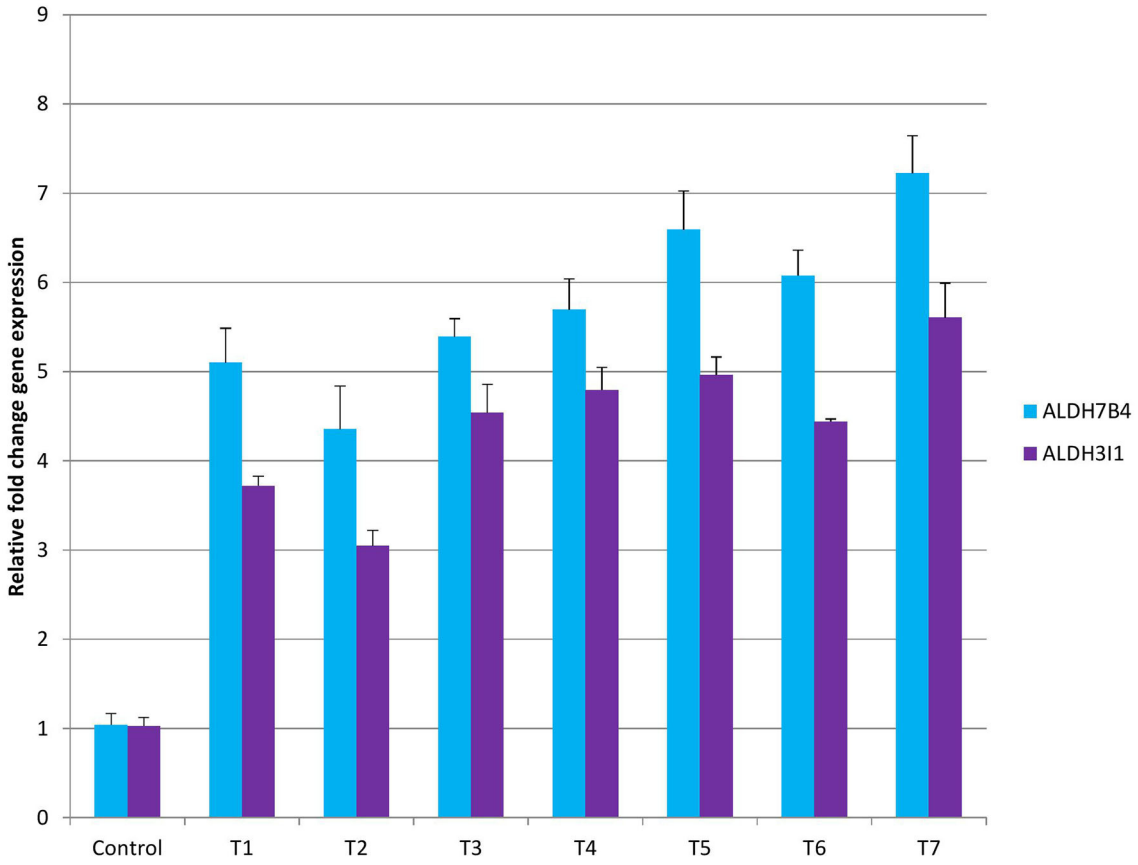

FIGURE 4
Gene expression analysis with ALDH7B4 and ALDH3I1 primers in control and treatment beetroot plant.

AMF treatments had different levels of effects on gene expression. The best-performing AMF combination was T7, which resulted in the highest *ALDH7B4* and *ALDH3I1* gene expression. This analysis supports our biochemical findings, where coherent results were obtained.

With the morphological, biochemical, and molecular analyses of the effect of different AMFs alone and in combinations on beetroot crops, the present study showed that AMFs are very effective for higher shelf life, higher production, and better resistance capacity. Therefore, with the current scenario of an increasing global population, high demand for foods, decreasing agricultural land area, high demand for organic foods, and environmental protection, the application of mycorrhizae for agricultural production is the best alternative to agrochemicals.

Conclusion

The AMF treatment appears to be promising for beetroot production. In this direction, the AMF seems to be in a position to increase plant development, yield, and quality of beetroot. The optimum values for the biochemical and morphological traits have been based on the treatment with *G. mosseae*, *G. gigantean,* and *A. laevis*. The gene expression analysis validated the conclusions drawn based on morphological and biochemical data that the Gm+Al+GG consortium was the best among all combinations. Overall, our study could be a guide to exploring more microbes and mycorrhizal fungi for profitable beetroot production.

Data availability statement

The original contributions presented in the study are included in the article/Supplementary material, further inquiries can be directed to the corresponding author.

Author contributions

VY, DK, RJ, JS, AK, and AR have performed morphological, biochemical, and molecular work. RB, JS, GM, BV, and KJ have analyzed the data and performed the statistical analysis. AS and SK assisted in the proofreading of the MS. VY, DJ, and MR have written the MS and finalized it. All authors contributed to the article and approved the submitted version.

Acknowledgments

RJ and DJ extend their appreciation to the Head of the University Department of Botany, Ranchi University, Ranchi, Jharkhand, India.

Conflict of interest

The authors declare that the research was conducted in the absence of any commercial or financial relationships that could be construed as a potential conflict of interest.

Publisher's note

All claims expressed in this article are solely those of the authors and do not necessarily represent those of their affiliated organizations, or those of the publisher, the editors and the reviewers. Any product that may be evaluated in this article, or claim that may be made by its manufacturer, is not guaranteed or endorsed by the publisher.

Supplementary material

The Supplementary Material for this article can be found online at: https://www.frontiersin.org/articles/10.3389/fmicb.2023.1196101/full#supplementary-material

References

Abu-Ellail, F. F., Salem, K. F., Saleh, M. M., Alnaddaf, L. M., and Al-Khayri, J. M. (2021). "Molecular breeding strategies of *Beeta vulgaris* (*Beta vulgaris ssp*. vulgaris var. conditivaAlefeld)," in *Advances in Plant Breeding Strategies: Vegetable Crops* (Cham: Springer) 157–212. doi: 10.1007/978-3-030-66965-2_4

Adeyemi, N. O., Atayese, M. O., Olubode, A. A., and Akan, M. E. (2020). Effect of commercial arbuscularmycorrhizal fungi inoculant on growth and yield of soybean under controlled and natural field conditions. *J. Plant Nutr.* 43, 487–499. doi: 10.1080/01904167.2019.1685101

Ait-El-Mokhtar, M., Ben-Laouane, R., Boutasknit, A., Anli, M., El-Amerany, F., Toubali, S., et al. (2022). "The Beneficial Effects of Arbuscular Mycorrhizal Fungi and Compost on Plant Tolerance to Drought and Salinity Stresses: A Study on Date Palm and Alfalfa," in *Microbial BioTechnology for Sustainable Agriculture* (Singapore: Springer) 369–406. doi: 10.1007/978-981-16-4843-4_12

Amirnia, R., Ghiyasi, M., SiavashMoghaddam, S., Rahimi, A., Damalas, C. A., and Heydarzadeh, S. (2019). Nitrogen-fixing soil bacteria plus mycorrhizal fungi improve seed yield and quality traits of lentil (Lens culinarisMedik). *J. Soil Sci. Plant Nutr.* 19, 592–602. doi: 10.1007/s42729-019-00058-3

Augé, R. M. (2001). Water relations, drought and vesicular-arbuscular mycorrhizal symbiosis. *Mycorrhiza* 11, 3–42. doi: 10.1007/s005720100097

Avetisyan, A., Aloyan, T., Iskandaryan, A., Harutyunyan, M., Jaakola, L., and Melikyan, A. (2022). Distribution of biodiversity of wild beet species (*Genus Beta L.*) in Armenia under ongoing climate change conditions. *Plants* 11, 2502. doi: 10.3390/plants11192502

Baar, J. (2008). "From production to application of arbuscular mycorrhizal fungi in agricultural systems: requirements and needs," in *Mycorrhiza* (Berlin, Heidelberg: Springer) 361–373. doi: 10.1007/978-3-540-78826-3_18

Basu, A., Prasad, P., Das, S. N., Kalam, S., Sayyed, R. Z., Reddy, M. S., et al. (2021). Plant growth promoting rhizobacteria (PGPR) as green bioinoculants: recent developments, constraints, and prospects. *Sustainability* 2213, 1140. doi: 10.3390/su13031140

Begum, N., Ahanger, M. A., Su, Y., Lei, Y., Mustafa, N. S. A., Ahmad, P., et al. (2019b). Improved drought tolerance by AMF inoculation in maize (*Zea mays*) involves physiological and biochemical implications. *Plants* 8, 579. doi: 10.3390/plants8120579

Begum, N., Qin, C., Ahanger, M. A., Raza, S., Khan, M. I., Ashraf, M., et al. (2019a). Role of arbuscular mycorrhizal fungi in plant growth regulation: implications in abiotic stress tolerance. *Front. Plant Sci.* 10, 1068. doi: 10.3389/fpls.2019.01068

Bhantana, P., Rana, M. S., Sun, X. C., Moussa, M. G., Saleem, M. H., Syaifudin, M., et al. (2021). Arbuscular mycorrhizal fungi and its major role in plant growth, zinc nutrition, phosphorous regulation and phytoremediation. *Symbiosis* 84, 19–37. doi: 10.1007/s13199-021-00756-6

Bhatt, B. P., Mishra, J. S., Dey, A., Singh, A. K., and Kumar, S. (2016). *Second Green Revolution in Eastern India: Issues and Initiatives*. Patna, India: Policy Document Indian Council of Agricultural Research, Research Complex for Eastern Region.

Biermann, B. (1981). Quantifying vesicular-arbuscular mycorrhizae: a proposed method towards standardization. *New Phytol.* 87, 63–67. doi: 10.1111/j.1469-8137.1981.tb01690.x

Carrera, F. P., Noceda, C., Maridueña-Zavala, M. G., and Cevallos-Cevallos, J. M. (2021). Metabolomics, a powerful tool for understanding plant abiotic stress. *Agronomy* 11, 824. doi: 10.3390/agronomy11050824

Chhikara, N., Kushwaha, K., Sharma, P., Gat, Y., and Panghal, A. (2019). Bioactive compounds of beeta vulgaris and utilization in food processing industry: A critical review. *Food Chem.* 272, 192–200. doi: 10.1016/j.foodchem.2018.08.022

Chun, S. C., Paramasivan, M., and Chandrasekaran, M. (2018). Proline accumulation influenced by osmotic stress in Arbuscular mycorrhizal symbiotic plants. *Front. Microbiol.* 9, 2525. doi: 10.3389/fmicb.2018.02525

El-Beltagi, H. S., El-Mogy, M. M., Parmar, A., Mansour, A. T., Shalaby, T. A., Ali, M. R., et al. (2022). Phytochemical characterization and utilization of dried red beeta vulgaris (*Beta vulgaris*) peel extract in maintaining the quality of Nile Tilapia fish fillet. *Antioxidants* 11, 906. doi: 10.3390/antiox11050906

EshaghiGorgi, O., Fallah, H., Niknejad, Y., and BarariTari, D. (2022). Effect of Plant growth promoting rhizobacteria (PGPR) and mycorrhizal fungi inoculations on essential oil in Melissa officinalis L. under drought stress. *Biologia* 77, 11–20. doi: 10.1007/s11756-021-00919-2

Evelin, H., Devi, T. S., and Gupta, S. (2019). Mitigation of salinity stress in plants by arbuscular mycorrhizal symbiosis: current understanding and new challenges. *Front. Plant Sci.* 10, 470. doi: 10.3389/fpls.2019.00470

Giovannetti, M. (1980). An evaluation of techniques for measuring vesicular arbuscular mycorrhizal infection in roots. *New Phytol.* 489–500. doi: 10.1111/j.1469-8137.1980.tb04556.x

Haghighi, T. M., and Saharkhiz, M. J. (2022). Mycorrhizal colonization and silicon nutrition mitigates drought stress in Licorice (Glycyrrhizaglabra L.) with morphophysiological and biochemical perspectives. *Ind. Crops Products* 178, 114650. doi: 10.1016/j.indcrop.2022.114650

Haghighi, T. M., Saharkhiz, M. J., and Kavoosi, G. (2022). Monitoring amino acid profile and protein quality of Licorice (*Glycyrrhiza glabra L.*) under drought stress, silicon nutrition and mycorrhiza inoculation. *Sci. Hortic.* 295, 110808. doi: 10.1016/j.scienta.2021.110808

He, J. D., Zou, Y. N., and Wu, Q. S. (2020). Mycorrhizas enhance drought tolerance of trifoliate orange by enhancing activities and gene expression of antioxidant enzymes. *Sci. Hortic.* 262, 108745. doi: 10.1016/j.scienta.2019.108745

Jabborova, D. (2022). The effects of Pseudomonas koreensis IGPEB 17 and arbuscular mycorrhizal fungi on growth and physiological properties of ginger. *Turkish J. Agric. Forestry* 46, 488–495. doi: 10.55730/1300-011X.3020

Jabborova, D., Annapurna, K., Al-Sadi, A. M., Alharbi, S. A., and Datta, R. (2021b). Biochar and Arbuscular mycorrhizal fungi mediated enhanced drought tolerance in Okra (Abelmoschus esculentus) plant growth, root morphological traits and physiological properties. *Saudi J. Biol. Sci.* 28, 5490–5499. doi: 10.1016/j.sjbs.2021.08.016

Jabborova, D., Annapurna, K., Choudhary, R., Bhowmik, S. N., Desouky, S. E., Selim, S., et al. (2021c). Interactive impact of biochar and arbuscular mycorrhizal on root morphology, physiological properties of fenugreek (Trigonella foenum-graecum L.) and soil enzymatic activities. *Agronomy* 11, 2341. doi: 10.3390/agronomy11112341

Jabborova, D., Annapurna, K., Paul, S., Kumar, S., Saad, H. A., Desouky, S., et al. (2021a). Beneficial features of biochar and arbuscular mycorrhiza for improving

spinach plant growth, root morphological traits, physiological properties, and soil enzymatic activities. *J. Fungi* 7, 571. doi: 10.3390/jof7070571

Jabborova, D., Davranov, K., Jabbarov, Z., Bhowmik, S. N., Ercisli, S., Danish, S., et al. (2022). Dual Inoculation of Plant Growth-Promoting Bacillus endophyticus and Funneliformis mosseae Improves Plant Growth and Soil Properties in Ginger. *ACS omega* 7, 34779–34788. doi: 10.1021/acsomega.2c02353

Jeevan Kumar, S. P., Rajendra Prasad, S., Banerjee, R., and Thammineni, C. (2015). Seed birth to death: dual functions of reactive oxygen species in seed physiology. *Ann. Botany* 116, 663–668. doi: 10.1093/aob/mcv098

Khaliq, A., Perveen, S., Alamer, K. H., Zia Ul Haq, M., Rafique, Z., Alsudays, I. M., et al. (2022). Arbuscular mycorrhizal fungi symbiosis to enhance plant–soil interaction. *Sustainability* 14, 7840. doi: 10.3390/su14137840

Koske, R. E. (1989). A modified procedure for staining roots to detect VA mycorrhizas. *Mycol. Res.* 92, 486. doi: 10.1016/S0953-7562(89)80195-9

Kotchoni, S. O., Kuhns, C., and Ditzer, A., Kirch, H. H., Bartels, D. (2006). Over-expression of different aldehyde dehydrogenase genes in Arabidopsis thaliana confers tolerance to abiotic stress and protects plants against lipid peroxidation and oxidative stress. *Plant, Cell Environ.* 29, 1033–1048. doi: 10.1111/j.1365-3040.2005.01458.x

Kulczyk-Skrzeszewska, M., and Kieliszewska-Rokicka, B. (2022). Influence of drought and salt stress on the growth of young Populusnigra 'Italica' plants and associated mycorrhizal fungi and non-mycorrhizal fungal endophytes. *New Forests* 53, 679–694. doi: 10.1007/s11056-021-09879-6

Kurt, C., and Kizildag, N. (2018). Determination of content of micronutrients in some sesame (Sesamum indicum L.) accession. *Fresenius Environ. Bull.* 27, 8456–8462.

Lazăr, S., Constantin, O. E., Stănciuc, N., Aprodu, I., Croitoru, C., Râpeanu, G., et al. (2021). Optimization of betalain pigments extraction using beeta vulgaris by-products as a valuable source. *Inventions* 6, 50. doi: 10.3390/inventions6030050

Leifheit, E. F., Veresoglou, S. D., Lehmann, A., Morris, E. K., and Rillig, M. C. (2014). Multiple factors influence the role of arbuscular mycorrhizal fungi in soil aggregation—a meta-analysis. *Plant Soil* 374, 523–537. doi: 10.1007/s11104-013-1899-2

Li, Q. S., Xie, Y. C., Rahman, M. M., Hashem, A., AbdAllah, E. F., and Wu, Q. S. (2022). Arbuscular mycorrhizal fungi and endophytic fungi activate leaf antioxidant defence system of lane late navel orange. *J. Fungi* 8, 282. doi: 10.3390/jof8030282

Lingua, G., Bona, E., Manassero, P., Marsano, F., Todeschini, V., Cantamessa, S., et al. (2013). Arbuscular mycorrhizal fungi and plant growth-promoting pseudomonads increases anthocyanin concentration in strawberry fruits (Fragaria x ananassa var. Selva) in conditions of reduced fertilization. *Int. J. Molec. Sci.* 14, 16207–16225. doi: 10.3390/ijms140816207

Liu, L., Gong, Z., and Zhang, Y. (2014). Growth, cadmium uptake and accumulation of maize (*Zea mays L.*) under the effects of arbuscular mycorrhizal fungi. *Ecotoxicology* 23, 1979–1986. doi: 10.1007/s10646-014-1331-6

Liu, S., Liu, M., Liao, Q. G., Lü, F. B., and Zhao, X. L. (2021). Effects of inoculated mycorrhizal fungi and non-mycorrhizal beneficial micro-organisms on plant traits, nutrient uptake and root-associated fungal community composition of the Cymbidium hybridum in greenhouse. *J. Appl. Microbiol.* 131, 413–424. doi: 10.1111/jam.14967

Mahmud, K., Missaoui, A., Lee, K., Ghimire, B., and Presley, H. W. (2021). Rhizosphere microbiome manipulation for sustainable crop production. *Curr. Plant Biol.* 27, 100210. doi: 10.1016/j.cpb.2021.100210

Manga, A. G., Ndiaye, M., Ndiaye, M. A., Sané, S., Diop, T. A., Diatta, A. A., et al. (2022). Arbuscular mycorrhizal fungi improve growth and phosphate nutrition of acacia seyal (delile) under saline conditions. *Soil Syst.* 6, 79. doi: 10.3390/soilsystems6040079

Mathur, S., and Sharma, M. P. (2018). Improved photosynthetic efficacy of maize (Zea mays) plants with arbuscular mycorrhizal fungi (AMF) under high temperature stress. *J. Photochem. Photobiol.* 180, 149–154. doi: 10.1016/j.jphotobiol.2018.02.002

McGonigle, T. P., Miller, M. H., Evans, D. G., Fairchild, G. L., and Swan, J. A. (1990). A new method which gives an objective measure of colonization of roots by vesicular—arbuscular mycorrhizal fungi. *New Phytol.* 115, 495–501. doi: 10.1111/j.1469-8137.1990.tb00476.x

Mitchell, G. A., and Bingham, F. T. (1974). Growth, mineral composition and seed characteristics of sesame as affected by nitrogen, phosphorus, and potassium nutrition. *Soil Sci. Soc. Am. J.* 38, 925–931. doi: 10.2136/sssaj1974.03615995003800060026x

Naseri Rad, H., and Naseri, R. (2022). Evaluation of some root growth traits and activity of enzyme and non-enzyme antioxidants of different cultivars of durum wheat (Triticumturgidum var. durum) effected by phosphorous fertilizer and mycorrhizal fungi in rainfed condition. *J. Iranian Plant Ecophysiol. Res.* 17, 1–23.

Ortas, I. (2012). The effect of mycorrhizal fungal inoculation on plant yield, nutrient uptake and inoculation effectiveness under long-term field conditions. *Field Crops Res.* 125, 35–48. doi: 10.1016/j.fcr.2011.08.005

Ortas, I., and Bilgili, G. (2022). Mycorrhizal species selectivity of sweet sorghum genotypes and their effect on nutrients uptake. *Acta Agric. Scandin. Section B—Soil Plant Sci.* 72, 733–743. doi: 10.1080/09064710.2022.2063167

Ortiz, N., Armada, E., Duque, E., and Roldán, A. (2015). Contribution of arbuscular mycorrhizal fungi and/or bacteria to enhancing plant drought tolerance under natural soil conditions: effectiveness of autochthonous or allochthonous strains. *J. Plant Physiol.* 174, 87–96. doi: 10.1016/j.jplph.2014.08.019

Pal, A., and Pandey, S. (2015). Role of arbuscularmycorrhizal fungi on plant growth and reclamation of barren soil with wheat (*Triticumaestivum* L.) crop. *Int. J. Soil Sci.* 12, 25–31. doi: 10.3923/ijss.2017.25.31

Paredes-Jácome, J. R., Hernández-Montiel, L. G., Robledo-Torres, V., González-Fuentes, J. A., Chiquito-Contreras, R. G., Mendoza-Villarreal, R., et al. (2022). Arbuscularmycorrhizal fungus and organics substrates effect on bean plant morphology and minerals. *Rev. Terra Latinoamericana* 40, 1012. doi: 10.28940/terra.v40i0.1012

Pedranzani, H., Rodríguez-Rivera, M., Gutiérrez, M., Porcel, R., and Hause, B. (2016). Arbuscular mycorrhizal symbiosis regulates physiology and performance of Digitaria eriantha plants subjected to abiotic stresses by modulating antioxidant and jasmonate levels. *Mycorrhiza* 26, 141–152. doi: 10.1007/s00572-015-0653-4

Phillips, J. M. (1970). Improved procedures for clearing roots and staining parasitic and vesicular-arbuscular mycorrhizal fungi for rapid assessment of infection. *Trans. Br. Mycol. Soc.* 55, 158–161. doi: 10.1016/S0007-1536(70)80110-3

Plenchette, C., Clermont-Dauphin, C., Meynard, J. M., and Fortin, J. A. (2005). Managing arbuscular mycorrhizal fungi in cropping systems. *Canadian J. Plant Sci.* 85, 31–40. doi: 10.4141/P03-159

Pozo, M. J., López-Ráez, J. A., Azcón-Aguilar, C., and García-Garrido, J. M. (2015). Phytohormones as integrators of environmental signals in the regulation of mycorrhizal symbioses. *New Phytol.* 205, 1431–1436. doi: 10.1111/nph.13252

Razvi, S. M., Singh, N., Mushtaq, A., and Shahnawaz, D. A. R. (2022). Arbuscular Mycorrhizal Fungi—alleviator for salinity stress: A review. *Pedosphere* 104, 1263–1280.

Rodrigues, M. Â., Piroli, L. B., Forcelini, D., Raimundo, S., da Silva, D., Cassol, L., et al. (2021). Use of commercial mycorrhizal fungi in stress-free growing conditions of potted olive cuttings. *Sci. Hortic.* 275, 109712. doi: 10.1016/j.scienta.2020.109712

Saboor, A., Ali, M. A., Danish, S., Ahmed, N., Fahad, S., Datta, R., et al. (2021). Effect of Arbuscular mycorrhizal fungi on the physiological functioning of maize under zinc-deficient soils. *Sci. Rep.* 11, 1–11. doi: 10.1038/s41598-021-97742-1

Saini, I., Aggarwal, A., and Kaushik, P. (2019). Inoculation with mycorrhizal fungi and other microbes to improve the morpho-physiological and floral traits of Gazania rigens (L.) Gaertn. *Agriculture* 9, 51. doi: 10.3390/agriculture9030051

Saini, I., Yadav, V. K., Aggarwal, A., and Kaushik, P. (2020). Effect of superphosphate, urea and bioinoculants on Zinnia elegans Jacq. *Indian J. Exper. Biol.* 58, 730–737.

Singh, R. B. (2000). Environmental consequences of agricultural development: a case study from the Green Revolution state of Haryana, India. *Agric. Ecosyst. Environ.* 82, 97–103. doi: 10.1016/S0167-8809(00)00219-X

Sun, Q., and Lu, P. (2019). Bioactive compounds in beeta vulgaris and their utilization in food processing industry. *China Condiment* 44, 164–167.

Talaat, N. B., and Shawky, B. T. (2014). Protective effects of arbuscularmycorrhizal fungi on wheat (Triticumaestivum L.) plants exposed to salinity. *Environ. Exper. Botany* 98, 20–31. doi: 10.1016/j.envexpbot.2013.10.005

Tereucán, G., Ruiz, A., Nahuelcura, J., Oyarzún, P., Santander, C., Winterhalter, P., et al. (2022). Shifts in biochemical and physiological responses by the inoculation of arbuscular mycorrhizal fungi in Triticum aestivum growing under drought conditions. *J. Sci. Food Agric.* 102, 1927–1938. doi: 10.1002/jsfa.11530

Thakur, N. S., and Singh, S. P. (2022). Nutritional quality of beeta vulgaris and multi seeds for chips. *Magnesium (mg)* 23, 2.

Tsoata, E., Njock, S. R., Youmbi, E., and Nwaga, D. (2015). Early effects of water stress on some biochemical and mineral parameters of mycorrhizal *Vignasubterranea* (L.) Verdc. (Fabaceae) cultivated in Cameroon. *Int. J. Agron. Agric. Res.* 7, 21–35.

Van Der Heijden, M. G., Streitwolf-Engel, R., Riedl, R., Siegrist, S., Neudecker, A., Ineichen, K., et al. (2006). The mycorrhizal contribution to plant productivity, plant nutrition and soil structure in experimental grassland. *New Phytol.* 172, 739–752. doi: 10.1111/j.1469-8137.2006.01862.x

Wang, L., Huang, X., Li, J., Huang, J., Bao, S., He, C., et al. (2022). Metabolites of zearalenone and phytohormones secreted by endophytic fungus strain TH15 regulating the root development in *Tetrastigma hemsleyanum*. *Plant Cell, Tissue Organ Cult.* 25, 1–2. doi: 10.1007/s11240-022-02321-5

Wang, X. X., Hoffland, E., Feng, G., and Kuyper, T. W. (2020). Arbuscularmycorrhizal symbiosis increases phosphorus uptake and productivity of mixtures of maize varieties compared to monocultures. *J. Appl. Ecol.* 57, 2203–2211. doi: 10.1111/1365-2664.13739

Wikandari, R., Manikharda, B. S., Ningrum, A., and Taherzadeh, M. J. (2021). Application of cell culture technology and genetic engineering for production of future foods and crop improvement to strengthen food security. *Bioengineered* 12, 11305–11330. doi: 10.1080/21655979.2021.2003665

Yadav, V. K., Jha, R. K., Kaushik, P., Altalayan, F. H., Al Balawi, T., Alam, P., et al. (2021). Traversing arbuscular mycorrhizal fungi and *Pseudomonas fluorescens* for carrot production under salinity. *Saudi J. Biol. Sci.* 28, 4217–4223. doi: 10.1016/j.sjbs.2021.06.025

Zahedi, M., Sarcheshmehpour, M., and Farahmand, H. (2022). Effect of native mycorrhizal fungi on morphological and physiological traits of judas tree (CercisSiliquastrum) and Mesquite (Prosopis Cineraria) seedlings under drought stress conditions. *Int. J. Hortic. Sci. Technol.* 9, 429–444.

Zare-Maivan, H., Khanpour-Ardestani, N., and Ghanati, F. (2017). Influence of mycorrhizal fungi on growth, chlorophyll content, and potassium and magnesium uptake in maize. *J. Plant Nutr.* 40, 2026–2032. doi: 10.1080/01904167.2017.1346119

Zhao, R., Guo, W., Bi, N., Guo, J., Wang, L., Zhao, J., et al. (2015). Zhang, J.Arbuscularmycorrhizal fungi affect the growth, nutrient uptake and water status of maize (*Zea mays*, L.) grown in two types of coal mine spoils under drought stress. *Appl. Soil Ecol.* 88, 41–49. doi: 10.1016/j.apsoil.2014.11.016

Zhao, Z., Chen, L., and Xiao, Y. (2021). The combined use of arbuscularmycorrhizal fungi, biochar and nitrogen fertilizer is most beneficial to cultivate *Cichoriumintybus L.* in Cd-contaminated soil. *Ecotoxicol. Environ. Safety* 217, 112154. doi: 10.1016/j.ecoenv.2021.112154

frontiers | Frontiers in Microbiology

TYPE Methods
PUBLISHED 04 July 2023
DOI 10.3389/fmicb.2023.1220101

OPEN ACCESS

EDITED BY
Jian-Wei Guo,
Chinese Academy of Sciences (CAS), China

REVIEWED BY
Yanguo Ke,
Kunming University, China
Jiejun Peng,
Ningbo University, China

*CORRESPONDENCE
Quansheng Yao
✉ yqsh1028@163.com
Ru-lin Zhan
✉ zhanrulin555@163.com

†These authors have contributed equally to this work

RECEIVED 10 May 2023
ACCEPTED 21 June 2023
PUBLISHED 04 July 2023

CITATION
Liu F, Sun X, Wang L, Zhou K, Yao Q and Zhan R-l (2023) Transcriptomic and proteomic analyses of *Mangifera indica* in response to *Xanthomonas critis* pv. *mangiferaeindicae*. *Front. Microbiol.* 14:1220101. doi: 10.3389/fmicb.2023.1220101

Transcriptomic and proteomic analyses of *Mangifera indica* in response to *Xanthomonas critis* pv. *mangiferaeindicae*

Feng Liu[1†], Xin Sun[1†], Lulu Wang[1], Kaibing Zhou[2], Quansheng Yao[1*] and Ru-lin Zhan[1*]

[1]Key Laboratory of Hainan Province for Postharvest Physiology and Technology of Tropical Horticultural Products, Key Laboratory of Tropical Fruit Biology, Ministry of Agriculture, South Subtropical Crops Research Institute, Chinese Academy of Tropical Agricultural Sciences, Zhanjiang, Guangdong, China, [2]College of Horticulture, Hainan University, Haikou, China

Mango is an important tropical fruit with the reputation of "Tropical Fruit King." It is widely cultivated in tropical and subtropical regions. Mango bacterial leaf spot, which is caused by *Xanthomonas critis* pv. *mangiferaeindicae* (*Xcm*), poses a great threat to the development of mango planting industry. In this study, we used RNA sequencing and data-independent acquisition techniques to compare the transcriptome and proteome of the highly resistant cultivar "Renong No.1" (RN) and the highly susceptible cultivar "Keitt" (KT) in response to *Xcm* infection at different stages (0, 2, and 6 days). A total of 14,397 differentially expressed genes (DEGs) were identified in the transcriptome of the two varieties, and 4,400 and 8,926 genes were differentially expressed in RN and KT, respectively. Among them, 217 DEGs were related to plant hormone signaling pathway, and 202 were involved in the maintenance of cellular redox homeostasis. A total of 3,438 differentially expressed proteins (DEPs) were identified in the proteome of the two varieties. Exactly 1,542 and 1,700 DEPs were detected in RN and KT, respectively. In addition, 39 DEPs were related to plant hormone signaling pathway, whereas 68 were involved in the maintenance of cellular redox homeostasis. Through cross-validation of the two omics, 1,470 genes were found to be expressed in both groups, and a large number of glutathione metabolism-related genes, such as *HSP26-A*, *G6PD4*, and *GPX2*, were up-regulated in both omics. Peroxisome-related genes, such as *LACS6*, *LACS9*, *PED1*, *GLO4*, and *HACL*, were up-regulated or down-regulated in both omics. *ABCB11*, *SAPK2*, *MYC2*, *TAG7*, *PYL1*, and other genes related to indole-3-acetic acid and abscisic acid signal transduction and plant-pathogen interaction were up-regulated or down-regulated in both omics. We also used weighted gene co-expression network analysis to combine physiological and biochemical data (superoxide dismutase and catalase activity changes) with transcriptome and proteome data and finally identified three hub

genes/proteins (*SAG113*, *SRK2A*, and *ABCB1*) that play an important role in plant hormone signal transduction. This work was the first study of gene/protein changes in resistant and susceptible mango varieties, and its results improved our understanding of the molecular mechanism of mango resistance to *Xcm*.

KEYWORDS

mango bacterial leaf spot, proteomics, transcriptomics, plant hormone signaling, cellular redox homeostasis

Introduction

Mango (*Mangifera indica* L.) is a kind of evergreen tree, originated in Malaysia, India. It has a long history of planting in China and is an important agricultural industry in tropical regions. Its fruit is not only rich in nutrients such as vitamin A, vitamin C and amino acids, but also its branches, leaves and peels contain a large number of bioactive substances, such as polyphenols, terpenes, carotene and phytosterols, which have certain edible value and medical value (Lebaka et al., 2021). Studies have shown that these active substances in mango have anti-inflammatory, immunomodulatory, antibacterial, anti-diabetic, anti-obesity and anti-cancer effects in medicine (Mirza et al., 2021).

Mango bacterial leaf spot (MBLS), which is caused by *Xanthomonas critis* pv. *mangiferaeindicae* (*Xcm*), can cause serious damage to fruit health, which results in reduced or zero mango yield. At present, disease-resistance breeding is the most economical and effective control method for disease resistance (Zandalinas et al., 2021). Therefore, studying the changes in gene and protein expression in mango during *Xcm* infection can not only lead to complete understanding of the molecular mechanism of mango resistance to MBLS but also provide valuable genetic resources for the breeding of disease-resistant mango varieties.

Plant hormones, such as ethylene (ETH), jasmonic acid (JA), salicylic acid, auxin, indole-3-acetic acid (IAA), abscisic acid (ABA), and gibberellin (GA), are key regulators of plant immunity (Li et al., 2019). They interact in complex networks to respond to pathogen invasion and thus exhibit resistance to pathogens (Denancé et al., 2013). Anderson et al. (2004) observed that the transcription level of *AtMYC2*, a positive regulator of ABA signal transduction in *Arabidopsis thaliana*, was induced in the early stage of soil-borne pathogenic fungus *Fusarium oxysporum* infection by reverse transcription-quantitative polymerase chain reaction (PCR). Further overexpression of *AtMYC2* showed that the levels of ETH and JA were significantly lower than those in the control group, which indicates the antagonistic effect of ABA on JA and ETH. Their interaction regulated the expression of *Arabidopsis* defense and stress genes in response to biological stress. Li et al. (2013) used Illumina technology to analyze the transcriptome changes of roots of Cavendish banana varieties infected with *Fusarium oxysporum* f. sp. *Cubense* (*Foc*). The two genes encoding ETH biosynthesis enzyme aminocyclopropanecarboxylate oxidase and several ETH-responsive transcription factors were one of the strongly induced genes of *Foc*, which indicates that ETH synthesis and signaling pathways were activated in response to Foc infection. Djami-Tchatchou et al. (2022) conducted a global transcriptomic analysis of tomato strain DC3000 (*Pto*DC3000) and observed that IAA inhibited the expression of genes involved in the type III secretion system and exercise; thus, IAA is a signal molecule for gene expression in *Pto*DC3000.

Under pathogen attack, reactive oxygen species (ROS) will accumulate in plants, and excessive accumulation will cause serious damage to plant proteins, DNA, and other cellular components, thus promoting the invasion of pathogens (Sies, 2018). At this point, the enzymatic systems, including catalase (*CAT*), superoxide dismutase (*SOD*), glutathione peroxidase (*GPX*), and glutathione S-transferase (*GST*), and non-enzymatic system, such as ascorbic acid, glutathione (GSH), mannitol, and flavonoids, play important roles in plants (Bela et al., 2015; Meitha et al., 2020). Xue et al. (2020) discovered that after phytoplasma caused red date witch broom disease, the genes involved in GSH cycle and thioredoxin synthesis in jujube leaves were up-regulated at the transcriptional and metabolic levels. The activities of *GST* and *GPX* in disease-resistant varieties were higher than those in susceptible varieties, which indicates that the antioxidant defense system plays an important role in plant pathogen invasion. Akbar et al. (2020) reported differences in the transcription levels of ROS-related genes between the disease-resistant sugarcane variety (B-48) infected with *Sugarcane mosaic virus* and the susceptible sugarcane variety (Badila). Compared with Badila, the expression of *GST* was significantly reduced, whereas those of transcription factors, such as *WRKY*, *AP2*, and *bHLH*, were significantly increased in B-48. Therefore, the genes involved in the ROS detoxification pathway can be used as key indicators for pathogen attack in plants.

Next-generation RNA sequencing (RNA-Seq) and data-independent acquisition (DIA) are currently the most advanced high-throughput technologies, and they can perform global analysis of gene and protein expressions in a large number of biological samples. Joint analysis of transcriptome and proteome is widely used to address plant responses to various biotic stresses. Cucumber fusarium wilt caused by *Fusarium oxysporum f.* sp. *cucumerinum* (*FOC*) is one of the most important

Abbreviations: ABA, abscisic acid; CAT, catalase; DDA, data dependent acquisition; DEGs, differentially expressed genes; DEPs, differentially expressed proteins; DIA, data independent acquisition; ETH, ethylene; *Foc*, *Fusarium oxysporum* f. sp. *Cubense*; GA, gibberellin; GPX, glutathione peroxidase; GSH, glutathione; GST, glutathione S-transferase; IAA, indoleacetic acid; JA, jasmonic acid; KT, mango varieties of "Keitt"; LB, lysogeny broth; PCD, programmed cell death; ROS, reactive oxygen species; RN, mango varieties of "Renong No.1"; SOD, superoxide dismutase; Trx, thioredoxin; WGCNA, weighted gene co-expression network analysis; *Xcm*, *Xanthomonas critis* pv. *Mangiferaeindicae*.

diseases in cucumber cultivation. In the exploration of the molecular mechanism of cucumber response to *FOC* infection, combined transcriptome and proteome analyses of cucumber leaves inoculated with *FOC* at 2 and 4 days showed that *FOC* infection activated plant hormone signals and transcription factors and inhibited wax biosynthesis and photosynthesis. The accumulation of redox proteins also plays a key role in cucumber resistance to *FOC* (Xie et al., 2022). Kiwifruit is an important tropical fruit in China. Kiwifruit bacterial canker caused by *Pseudomonas syringae* pv. *Actinidiae* (*Psa*) is an important disease in the kiwifruit seed industry. The transcriptome and proteome analyses of the resistant variety "Jinkui" and the susceptible variety "Hongtao" showed that the pathways of "phytohormone signal transduction" and "phenylpropanol biosynthesis" were activated at the protein and transcriptional levels after *Psa* infection. The transient expression of *AcMYB16* gene in "Jinkui" induced *Psa* infection (Wang et al., 2021). However, reports on the response of mango to *Xcm* are limited.

At present, the research on MBLS mainly focuses on the comprehensive treatment of MBLS and the isolation and identification of MBLS pathogens (Gagnevin and Pruvost, 2001; Sanahuja et al., 2016). The research on the molecular mechanism of mango resistance to MBLS is still in its infancy. This work is the first to study the changes in gene and protein expressions in mango during *Xcm* infection. Our findings will provide new ideas for MBLS resistance and valuable genetic resources for the breeding of MBLS-resistant mango.

Methods

Preparation of bacterial solution

Single colonies of activated *Xcm* cultured for 48 h were picked into LB and incubated at 200 rmp at 28°C for 2 days before inoculation. The concentration of pathogen was about 1×10^9 CFU/mL determined by plate colony counting method.

Treatment of plant material

The resistant and susceptible mango varieties "Renong No.1" (RN) and "Keitt" (KT) were used as plant materials. *Xcm* was identified by pathogenicity determination, morphology, and 16S ribosomal RNA (16S) from the susceptible leaves of KT mango in the mango germplasm resource nursery of the South Subtropical Crops Institute of the Chinese Academy of Tropical Agricultural Sciences. We selected healthy fruits with the same size and maturity, soaked them in 1% sodium hypochlorite for 2 min for disinfection, washed them thrice with sterile water, and then placed them in an alcohol-disinfected plastic box to dry naturally. Plum blossom needles were used for acupuncture inoculation, and 60 μL mixed bacterial solution was added at each inoculation point. The inoculated fruits were placed in a fresh keeping box at 28°C and 100% humidity to be sampled, and the same treatment with LB liquid medium was used for the control. Each fruit was inoculated in three places, seven points were inoculated in each place, and three fruits were inoculated as triplicate. On days 0, 2, and 6 of inoculation with *Xcm*, the mango epidermis with a thickness of 1–2 mm on the surface of the inoculation point was used as the experimental sample and stored at −80°C for use.

SOD and CAT analyses

For the determination of superoxide dismutase (SOD) and catalase (CAT) activities, based on the ratio of experimental sample weight (g):volume (mL) = 1:9, phosphate buffer solution 9 times the volume of the sample was added (0.1 mol/L, pH 7.0–7.4). Then, the sample was homogenized in an ice water bath and centrifuged at 12,000 rpm for 15 min at 4°C, and the supernatant was collected for measurement. An ultraviolet spectrophotometer or a Tecan Spark microplate reader was used to measure the absorbance value of the reaction solution, and the result was inputted into the formula to calculate the SOD and CAT activities. The analyses at each time point were repeated thrice.

RNA extraction, library construction, and sequencing

Total RNA was extracted using Trizol reagent kit (Invitrogen, Carlsbad, CA, USA), in accordance with the manufacturer's protocol (Poyraz et al., 2010). RNA quality was assessed on an Agilent 2100 Bioanalyzer (Agilent Technologies, Palo Alto, CA, USA) and checked using RNase-free agarose gel electrophoresis. After the total RNA was extracted, eukaryotic mRNA was enriched by Oligo(dT) beads. Then, the enriched mRNA was broken into short fragments using fragmentation buffer and reverse transcribed into cDNA using NEBNext Ultra RNA Library Prep Kit for Illumina sequencing (NEB #7530, New England Biolabs, Ipswich, MA, USA) (Salmela and Rivals, 2014). The purified double-stranded cDNA fragments were end repaired, added with A base, and ligated to Illumina sequencing adapters. The ligation reaction was purified with AMPure XP Beads (1.0X). The ligated fragments were subjected to size selection by agarose gel electrophoresis and PCR amplification. The resulting cDNA library was sequenced using Illumina Novaseq6000 by Gene *Denovo* Biotechnology Co. (Guangzhou, China).

Transcriptome data analysis

The raw readings produced by transcriptome sequencing were quality controlled by fastp (version 0.18.0) (Chen et al., 2018), and the comparison tool Bowtie (version 2.2.8) (Langmead and Salzberg, 2012) was used to remove low-quality reads. Then, the clean reads were compared with the mango genome of each sample by HISAT (version 2.2.4) (Kim et al., 2015). No more than three base mismatches were observed. To analyze the gene expression in mango, mango variety "Hong Xiang Ya" was used as the reference genome,[1] the total number of valid reads obtained from all samples was 1,456,435,960, and the number of reads that

1 https://ngdc.cncb.ac.cn/search/?dbId=gwh&q=PRJCA002248

could be mapped to the mango genome was 1,325,116,148. After counting the reads for each gene, the set of genes expressed in each time period was counted for each cultivar, and differences between cultivars were analyzed by Venn diagram. At the same time, the sample cluster diagram was used to cluster the samples in different time periods to ensure the reliability of the subsequent analysis results. Finally we used the fragments per kilobase of transcript per million mapped reads (FPKM) method for normalization (Li and Dewey, 2011). Low-expression genes were filtered (<5 FPKM), and RNA differential expression analysis was performed between two different groups by DESeq2 (Love et al., 2014) (and by edgR between two samples) (Ashburner et al., 2000; Robinson et al., 2010). The genes with false discovery rate (FDR) below 0.05 and absolute fold change (FC) $\geq$ 2 were considered differentially expressed genes (DEGs).

Protein sample preparation

Sample preparation involved protein denaturation, reduction, alkylation, tryptic digestion, and peptide cleanup. Commercially available iST Sample Preparation kit (PreOmics GmbH, Planegg, Germany) was used following the protocols provided. Briefly, after the samples were ground with liquid nitrogen, 50 μL lysis buffer was added and heated at 95°C for 10 min at 1,000 rpm with agitation. After cooling the sample to room temperature, trypsin digestion buffer was added, and the sample was incubated at 37°C for 2 h at 500 rpm with shaking. The digestion process was stopped with a stop buffer. Sample clean-up and desalting were carried out in the iST cartridge using the recommended wash buffers. Peptides were eluted with elution buffer (2 × 100 μl) and then lyophilized by SpeedVac.

DIA protein detection

Before mass spectrometry detection, Biognosys quality control reagent from the iRT Kit was added to each sample, and calibration was performed based on the retention time of the polypeptide in chromatography. QuiC (Biognosys) software was used to control the original mass spectrometry data to investigate the similarity in the quality control indicators between each sample. If the index results were similar, the detection repeatability was good. Then, Pulsar software was used to build a database of the data obtained from the date-dependent acquisition (DDA) mode, and the date-independent acquisition (DIA) data were analyzed based on the DDA reference database to identify proteins. When at least one sample detected a protein, the qualitative results of the protein and quantitative results in all samples were outputted.

Qualitative analysis of proteins was conducted to detect proteins in the sample and identify their types. To ensure the reliability of results, we checked whether protein qualitative analysis results meet the following identification criteria: precursor threshold of 1.0% FDR and protein threshold of 1.0% FDR at the peptide and protein levels, respectively. The average peak area of the first three MS1 peptides with the FDR of less than 1.0% was screened for protein quantification.

After counting the reads for each protein, the set of genes expressed in each time period was counted for each cultivar, and differences between cultivars were analyzed by Venn diagram. Finally, according to the results of protein quantification, the proteins with significant changes in abundance between the comparison groups were screened. Statistical test FDR value and fold change log2FC were used to screen proteins with significant differences. The default threshold was FDR $<$ 0.05, $|\log2(fc)| > 0.58$. This part can visualize the results of difference analysis in the form of chart interaction.

Functional analysis

Gene Ontology (GO) enrichment analysis provided all GO terms that were significantly enriched in DEGs/differentially expressed proteins (DEPs) compared with the genome background, whereas the DEGs/DEPs that corresponded to biological functions were filtered (Young et al., 2010). First, all DEGs/DEPs were mapped to the GO terms in the GO database,[2] and gene and protein numbers were calculated for every term (Chen et al., 2017). Significantly enriched GO terms in DEGs/DEPs compared with the genome background were defined by hypergeometric test. Kyoto Encyclopedia of Genes and Genomes (KEGG)[3] is a major public pathway-related database (Kanehisa and Goto, 1999; Fang et al., 2021). Pathway enrichment analysis identified significantly enriched metabolic pathways or signal transduction pathways in DEGs/DEPs compared with the whole genome or proteome background. The formula was the same as that in GO analysis (Kanehisa and Goto, 1999). The calculated *p*-value was subjected to FDR correction, with FDR $\leq$ 0.05 as a threshold (Anders and Huber, 2010).

Network construction

To identify genes or proteins related to CAT, and SOD changes, we performed a weighted gene co-expression network analysis (WGCNA) on the genes and proteins. Co-expression networks were constructed using WGCNA (v1.47) package in R (Langfelder and Horvath, 2008). After filtering genes and proteins (<1 reads per kilobase per million mapped reads), gene/protein expression values were imported into WGCNA to construct co-expression modules using the automatic network construction function BlockwiseModules with default settings, except that the power was 13, and minimum module size was 50. Genes/proteins were clustered into 20 correlated modules (Botía et al., 2017).

Module and gene selection

To detect biologically significant modules, we used module eigengenes to calculate the correlation coefficient with samples or sample traits. Correlation analysis was performed using a module eigengene with data for specific traits or phenotypes (Niemira et al., 2019). Pearson correlation between each gene and trait

2 http://www.geneontology.org/
3 https://www.kegg.jp

data under the module were also calculated for the most relevant module (positive and negative correlations) corresponding to each phenotype data.

Quantitative RT-PCR analysis

Premier 6 was used to design gene qRT-PCR primers based on the CDS sequence of the differential genes (**Supplementary Table 1**). The reverse transcribed C-DNA of total RNA (the same sample as transcriptome sequencing) of mango fruit inoculated with the pathogen of mango bacterial keratitis at 0, 2, and 6 days was used as the template. The mango actin gene was used as the reference gene, and the dye kit method was used to verify the results. The entire RNA reverse transcription step was performed according to the reverse transcription kit instructions (Taylor et al., 2019). Expression was calculated using the $2^{-\Delta\Delta Ct}$ method (Livak and Schmittgen, 2001).

Results

Symptoms after LB and *Xcm* treatments

After inoculation with *Xcm* and LB liquid medium by needling method, the phenotypic changes of the two varieties were observed at 0, 2 and 6 days (**Figure 1**). It was found that after inoculation with LB liquid medium, the color of the inoculation point of "Keitt" and "Renong No.1" gradually turned brown over time, but the changes at the inoculation point of the two varieties were not obvious. During the whole experimental period of *Xcm* inoculation, the changes of symptoms of the two varieties were consistent with their disease resistance. The specific manifestations were as follows: on day 2 after inoculation, black spots began to appear at the inoculation sites of the two varieties, and the symptoms were similar at this time. On the sixth day after inoculation, the symptoms of the two varieties at the indirect seeding sites were obviously different. The black spots of "Renong 1" were deepened and slightly spread. "Kate" was more widespread, showing the typical 'crisscross volcanic' pattern of bacterial corner spot in mango orchards. The results suggest that 0, 2, and 6 days after *Xcm* inoculation may be key sampling time points to explore the mechanisms of resistance to bacterial keratosis in mangoes with different resistance.

Overview of mango fruit transcriptome

To study the changes in gene expressions in fruits of KT and RN after inoculation with *Xcm*, we obtained the pericarp tissues of two resistant and susceptible germplasms at 0, 2, and 6 days after inoculation with pathogens. Then, we used TRIzol reagent to extract the total RNA of each sample and sequenced them by Illumina HiSeq 2000 platform. Initially, transcriptome sequencing generated about 59,160,000 original reads and about 59,040,000 clean reads for all samples. Then, the clean reads were aligned with the mango genome sequence, which resulted in 90.15–92.13% clean reads with no more than three base mismatches. To analyze mango gene expressions, we calculated the number of clean reads aligned with mango gene sequences (36,065 sequences) and normalized them using the FPKM method. After filtering the low-expression genes (<5 FPKM), we identified 28,704 genes (about 79.59% of all mango genes) in all samples.

After counting the readings, to exclude the influence of genetic background differences between KT and RN on subsequent analyses, we analyzed the expression of KT and RN overall genes under LB treatment. A Venn diagram (**Supplementary Figure 1**) showed that 7,057 genes were expressed, and no genes were detected that were expressed specifically at a single time point. This ruled out the possibility of misinterpretation of gene expression data generated during the natural growth of mango.

DEGs in resistant and susceptible mango fruits

To analyze mango fruit gene expression, we used Deseq2 software to calculate *P*- and FDR values and the default FDR < 0.05; $|\log2FC| > 1$ indicated differential genes. We identified 14,397 DEGs in the KT and RN. A total of 8,926 DEGs were identified in KT. Compared with KT0d, 5,276 (3,623 up-regulated and 1,653 down-regulated) and 6,809 DEGs (3,583 up-regulated and 3,226 down-regulated) were identified in KT2d and KT6d, respectively. Compared with KT2d, we identified 2,977 DEGs in KT6d (595 up-regulated and 2,382 down-regulated). We identified 4,400 DEGs in RN. Compared with RN0d, we identified 2,045 (1,118 up-regulated and 927 down-regulated) and 3,043 DEGs (1,019 up-regulated and 2,044 down-regulated) in RN2d and RN6d, respectively. Compared with RN2d, we identified 1,996 DEGs (386 up-regulated and 1,610 down-regulated) in RN6d. In the further comparison of RN2d with KT2d and RN6d with KT6d, we identified 7,523 (2,228 up-regulated and 5,295 down-regulated) and 9,380 DEGs (3,120 up-regulated and 6,260 down-regulated) in the RNs, respectively (**Figure 2A**). Venn diagram (**Figure 2B**) showed that 626 DEGs were continuously differentially expressed during the whole infection period of KTs, and 242 DEGs were continuously differentially expressed during the whole experimental period of RNs. Furthermore, 5,975 DEGs were shared between KTs and RNs. A total of 3,650 out of 8,926 DEGs identified in KTs (40.89%) and 2,355 out of 4,400 DEGs identified in RNs (53.52%) were specifically expressed on day 6, which indicated that the transcriptome of mango changed significantly on day 6 after *Xcm* infection.

To understand the possible pathways and functions of these DEGs in mango response to *Xcm*, we performed GO and KEGG enrichment analyses on the DEGs (**Figure 3**; **Supplementary Tables 2**, **3**). GO enrichment analysis showed that a large number of DEGs in KTs and RNs were annotated to metabolic process (GO: 0008152), cellular process (GO: 0009987), catalytic activity (GO: 0003824), biological regulation (GO: 0065007), response to stimulus (GO: 0050896), membrane (GO: 0016020), and cell part (GO: 0044464). These significantly enriched GO terms were associated with the symptoms of MBLS, including "cross-shaped volcanic lesions" and black spots. KEGG enrichment analysis revealed that a large number of DEGs of RNs and KTs are involved in GSH metabolism, phenylalanine metabolism, peroxisome, and other important pathways. However, several differences were observed in the pathways involved in certain DEGs enriched by

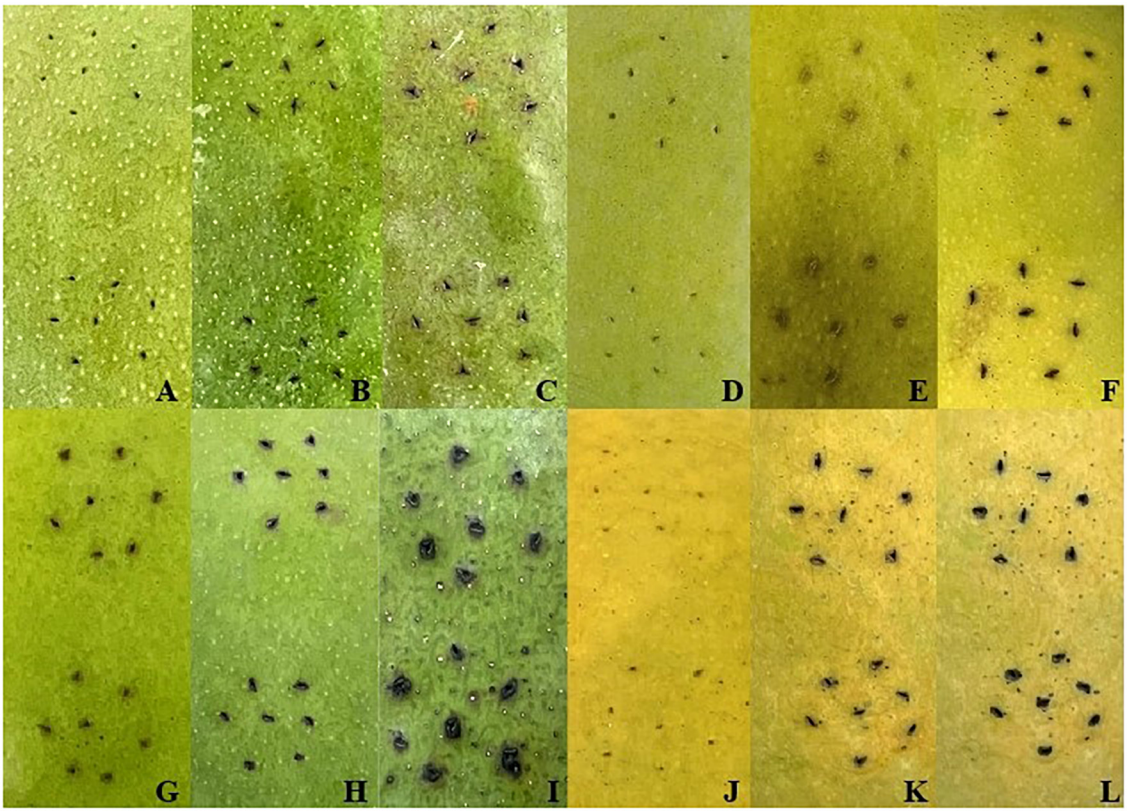

FIGURE 1
Symptoms after LB and *Xcm* treatments. Panels **(A–C)** and **(D–F)** were the symptoms of "Keitt" and "Renong No.1" after 0 days, 2 days, and 6 days of LB liquid medium treatment, respectively. Panels **(G–I)** and **(J–L)** were the symptoms of "Keitt" and "Renong No.1" after 0 days, 2 days, and 6 days of treatment with bacterial solution containing *Xcm*, respectively.

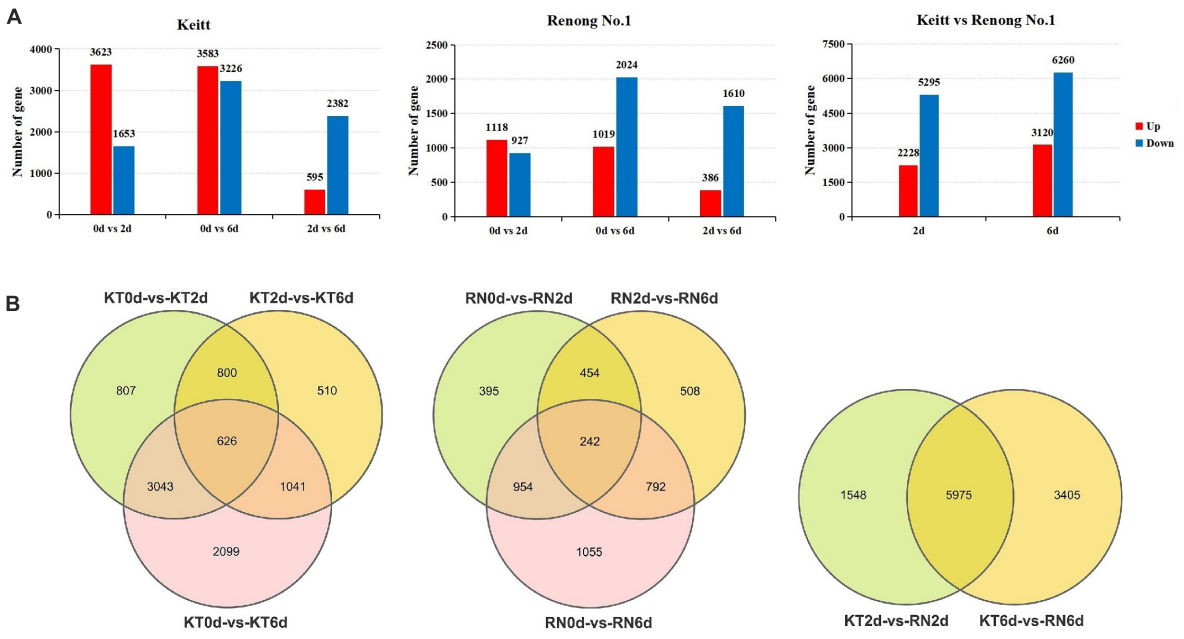

FIGURE 2
DEGs of RN and KT. Panel **(A)** is the expression summary of DEGs in RN and KT, red represents upregulation and blue represents downregulation; Panel **(B)** is the distribution of DEGs in KT and RN, the left is DEGs in KT, the middle is the DEGs in RN, and the right is DEGs in RN at different stages after inoculation (relative to KT).

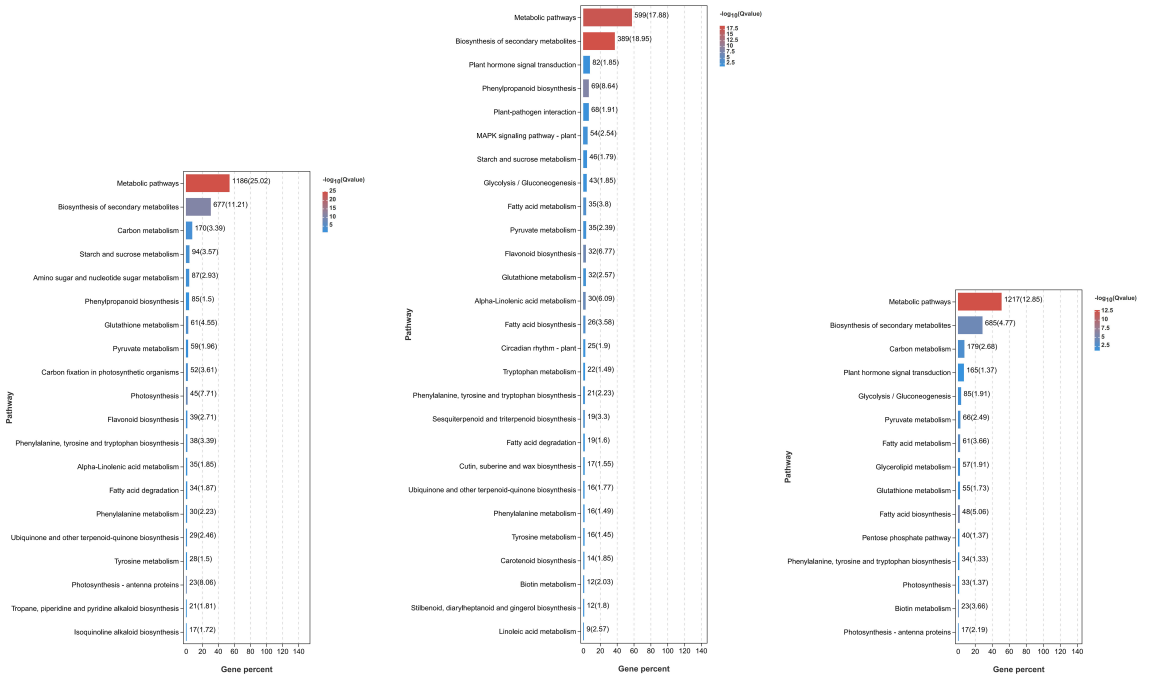

FIGURE 3
Significant KEGG pathways of DEGs identified in RN and KT. Different pathways and their *p*-values of the number of genes contained and the degree of enrichment significance were plotted, and only the pathway that met the threshold was selected for plotting. Each column represents a pathway, and the color of the column represents the enrichment significance of that Pathway. The numbers outside the brackets next to the columns represent the number of genes belonging to the pathway in the module. The values in parentheses next to the columns represent the degree of enrichment and are −log10(*p*-value) and correspond to the color of the columns. In the significance bars, the order "from large to small" was selected according to the number of genes enriched in the pathway.

KTs and RNs. Specific pathways were only found in RN enrichment results, and these pathways included plant mitogen-activated protein kinase signaling pathway, plant-pathogen interaction, plant hormone signal transduction, and cutin, suberin, and wax biosynthesis. Thus, the DEGs of RNs and KTs are involved in different pathways in response to *Xcm* infection.

Genes in the plant hormone signaling pathway

A total of 217 DEGs were found to be related to plant hormone signal transduction pathway (**Supplementary Table 4**). These DEGs included 63 IAA-related genes, such as auxin-responsive protein (*IAA26*, *LAX2*, *ARF9*, and *AUX22D*) and IAA amido synthetase (*GH3.1*, *GH3.6*, and *GH3.10*), of which 22 were down-regulated in RN and KT. Twelve genes were associated with ABA; two of them (*ABF2* and *PYL8*) decreased, and three (*DPBF2*, *PYL1*, and *PYL3*) increased in RN and KT. A total of 6 and 14 ETH-related genes (*EIL3*, *EIL1*, *EIN3*, and *ETR1*) decreased in KT and RN, respectively, and the remaining 8 genes showed different expression trends in various mango varieties. A total of 12 genes were related to GA, 4 (*GAIPB*, *GID1B*, *GID2*, and *GAI*) were down-regulated in RN and KT, and the remaining 7 genes showed different expression patterns in various mango species. In addition, 10 and 17 TF genes (1 *TGA*, 2 *PIF*, 5 *MYC*, and 1 *HBP-1b*) were down-regulated in RN and KT, respectively. A total of 7 were down-regulated (4 serine/threonine-protein kinase, 1 *MKK*, and 2 *BAK*), and 3 kinases (*MKK*, serine/threonine-protein kinase, and *AHK*) were up-regulated. The up-regulation and down-regulation of these genes indicated that hormone signaling was induced by *Xcm* infection in mango tissues, and the levels of plant hormones may play an important role in this process.

Genes involved in the maintenance of cellular redox homeostasis

Among the 14,397 DEGs, 202 were found to be involved in the redox process or play a regulatory role in cellular redox homeostasis (**Supplementary Table 5**). A total of 74 genes were annotated to peroxisomes, and 32 genes were up-regulated in RN but down-regulated in KT. CAT isozyme (*CAT1*), Nudix hydrolase family (*NUDT15*, *NUDT19*), and other enzymes were annotated as fatty acyl-CoA reductase, phytanoyl-CoA dioxygenase, and long chain acyl-CoA synthetase. A total of 81 DEGs were involved in GSH metabolism, including those of L-ascorbate peroxidase (*APX3*, *APXS* and *APXT*), glucose-6-phosphate 1-dehydrogenase (*G6PD2*, *G6PD4*, and *G6PDH*), and 20 of them were continuously up-regulated in RN; their expression levels were significantly higher than those in KT. After *Xcm* infection, 18 redox proteins (3 CAT isozymes, 10 ferredoxin (Fd), and 5 SOD) were induced, among which *CAT1*, *FD3*, and *Os07g0147900* were up-regulated in RN and down-regulated in KT. The expression levels of 11 photosystem I (PSI) reaction center subunits and 8 PSII proteins generally

increased in resistant and susceptible varieties, but the changes in KT were more significant.

Overview of mango fruit proteome

Proteomics technology is widely used in the study of protein differential expression and various post-translational modifications (Haverland et al., 2014; Sidoli et al., 2015). In this study, we used DIA (a new holographic quantitative technique based on electrostatic field orbitrap) to investigate the protein expression changes in KT and RN mango during *Xcm* infection (0, 2, and 6 days). To ensure the reliability of the results, we checked whether the protein qualitative analysis findings met the identification criteria, namely, precursor threshold of 1.0% FDR and protein threshold of 1.0% FDR, at the peptide and protein levels, respectively. Finally, 12,260 peptides and 12,877 proteins were identified from the two mango varieties.

As with the transcriptome analysis, after counting, we analyzed KT and RN total protein expression under LB treatment. The Venn diagram (**Supplementary Figure 2**) shows that 11,329 proteins were co-expressed across all tested time points, and no more than 35 proteins were specifically expressed at each tested time point. For reliability of subsequent analysis, 11,329 co-expressed proteins were selected for subsequent analysis.

DEPs in resistant and susceptible mango fruits

We aimed to understand the differences in protein expression levels in response to *Xcm* in different mango varieties. According to the screening threshold of DEPs, the absolute value of the FC was greater than 1.5 times ($|\log2(1.5)| \approx 0.58$ corrected *P*-value (Q value) < 0.05). The proteins with significant differences between groups (KT0d vs. KT2d, KT0d vs. KT6d, KT2d vs. KT6d, RN0d vs. RN2d, RN0d vs. RN6d, RN2d vs. RN6d, KT2d vs. RN2d, and KT6d vs. RN6d) were screened. A total of 1,700 DEPs were identified in KT. Compared with KT0d, 1,101 (578 up-regulated and 523 down-regulated) and 1,044 (509 up-regulated and 535 down-regulated) DEPs were identified in KT2d and KT6d, respectively. Compared with KT2d, 296 DEPs were identified in KT6d (102 up-regulated and 194 down-regulated). A total of 1,542 DEPs were identified in RNs. Compared with RN0d, 650 (391 up-regulated and 259 down-regulated) and 337 DEPs (206 up-regulated and 131 down-regulated) were identified in RN2d and RN6d, respectively. Compared with RN2d, 1,221 DEPs (635 up-regulated and 586 down-regulated) were identified in RN6d (**Figure 4A**). The Venn diagram (**Figure 4B**) showed that 65 and 94 DEPs were significantly differentially expressed after KTs and RNs were infected with *Xcm*, respectively. A total of 1,800 DEPs were detected between KTs and RNs. Similar to the transcriptome results, the expression of DEPs induced on the 6th day of *Xcm* infection was higher than that of all DEPs. A total of 1,243 DEPs (50.92%) were observed in KT6d and 1,340 (60.69%) in RN6d. Thus, the 6th day of *Xcm* infection not only caused great changes in the transcriptome of mango but also the expression of its proteins.

To understand the function of DEPs in RNs and KTs and the pathways involved in regulation, we also conducted GO and KEGG enrichment analyses on DEPs (**Figure 5**; **Supplementary Tables 6**, **7**). GO enrichment results showed a large number of organism metabolic process proteins in both cultivars (GO: 0044710), including oxoacid metabolic process (GO: 0043436), cellular homeostasis (GO: 0019725), regulation of hormone levels (GO: 0010817), and other biological processes, such as oxidoreductase activity (GO: 0016491), catalytic activity (GO: 0003824), antioxidant activity (GO: 0016209), and other molecular functions that neutralize cell-cell junction (GO: 0005911); cell periphery (GO: 0071944), cytoplasmic part (GO: 0044444), and other cellular components. We speculate that *Xcm* may act mainly on the membrane of mango cells or accelerate the process of infection by secreting special substances or degrading normal mango cell structures to bind them to cells. KEGG enrichment analysis showed that a large number of proteins are involved in metabolic pathways, biotin metabolism, carbon metabolism, and other pathways. DEPs in RNs were also significantly enriched in important pathways, such as peroxisome and GSH metabolism. We suggest that mango infection may trigger a series of physiological and chemical reactions, such as the synthesis of plant hormones and lignin, antioxidant production, and changes in ROS.

Proteins in the plant hormone signaling pathway

Similar to the transcriptome analysis, we identified 39 DEPs associated with plant hormone signaling pathway (**Supplementary Table 8**). Among these DEPs, several were identified together with their transcriptomes, two were associated with IAA (*IAA26* and *LAX2* were up-regulated in RN and down-regulated in KT), seven were associated with ABA, and six (*PYL1*, *PYL2*, 2 *PYL9*, and 2 *ABF2*) were generally down-regulated in KT and RN. One DEP (*PYL8*) was up-regulated in RN but down-regulated in KT. Several transcription factors (*TGA7*, *TGA21*, and *MYC2*) were down-regulated in RN and KT, and the proteome-specific protein *TGAL1* was identified (down-regulated in RN and up-regulated in KT). In addition, we observed that eight classes of kinases (*BSK7*, *SAPK3*, *SRK2A*, *SRK2E*, *BSK2*, *SAPK2*, *ASK7*, and *BSK1*) (*BSK1* and *ASK7* were up-regulated in RN and down-regulated in KT, and the others were down-regulated in KT and RN). The pathogenesis-related protein *PRB1* was up-regulated in KT and RN but was more evident in RN. The findings indicate that the regulatory pathways involving several transcription factors and kinases and IAA and ABA signaling pathways are the keys to mango response to *Xcm*.

Proteins involved in the maintenance of cellular redox homeostasis

A total of 68 DEPs were identified to be related to the maintenance of cellular redox homeostasis (**Supplementary Table 9**). These DEPs included 5 redox proteins (3 *FD3* and 2 *CAT1* were up-regulated in RN but down-regulated in KT; *FSD2* was down-regulated in KT and RN), of which 38 are involved in the production of peroxisomes, including *PED1*, *PMP22*, *ACX3*, *ACX4*, and *ACX2*, and were up-regulated in KT and RN, with a stronger response observed in RN. A total of 49 genes are

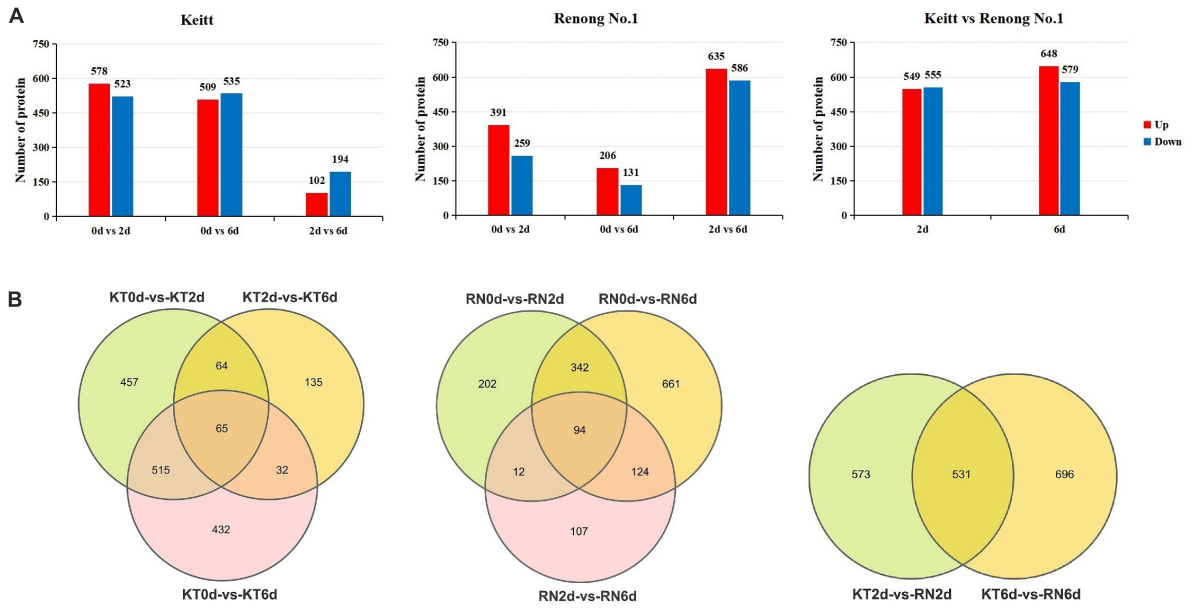

FIGURE 4
DEPs of RN and KT. Panel **(A)** is the expression summary of DEPs in RN and KT, red represents upregulation and blue represents downregulation; Panel **(B)** is the distribution of DEPs in KT and RN, the left is DEPs in KT, the middle is the DEPs in RN, and the right is DEPs in RN at different stages after inoculation (relative to KT).

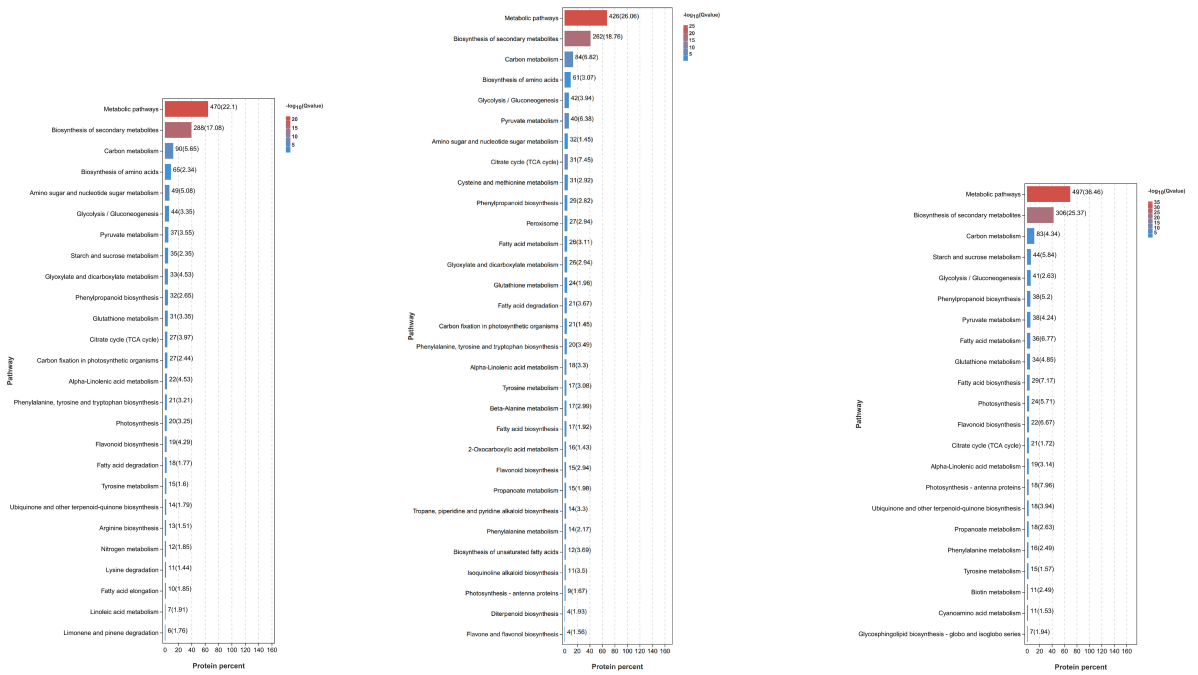

FIGURE 5
Significant KEGG pathways of DEPs identified in RN and KT. Different pathways and their *p*-values of the number of proteins contained and the degree of enrichment significance were plotted, and only the pathway that met the threshold was selected for plotting. Each column represents a pathway, and the color of the column represents the enrichment significance of that pathway. The numbers outside the brackets next to the columns represent the number of proteins belonging to the pathway in the module. The values in parentheses next to the columns represent the degree of enrichment and are −log10(*p*-value) and correspond to the color of the columns. In the significance bar, the order "from large to small" was selected according to the number of enriched proteins in the pathway.

10.3389/fmicb.2023.1220101

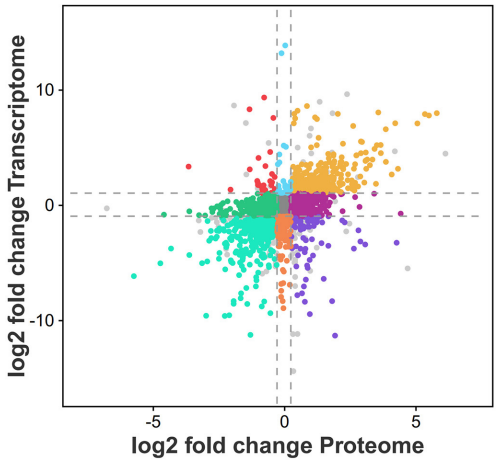

FIGURE 6
Nine quadrant map of common differential genes between transcriptome and proteome. The abscission is the log2 value of protein fold change, and the ordinate is the log2 value of transcriptome fold change. The dashed line represents the log2 value of the difference multiple specified in the difference analysis. In the figure, each colored point represents the collection of a class of genes, in which the colored points represent genes that meet the differential analysis threshold range (that is, meet the screening conditions for differential mRNA and differential protein), and the gray points represent genes that do not meet the analysis threshold.

related to GSH metabolism, and 29 genes, such as GST (*HSP26-A*, *GSTU7* and *PARC*), 6-phosphogluconate dehydrogenase (*PGD3*), and phospholipid hydroperoxide GSH (*GPX1* and *GPX2*), were up-regulated in RN and KT. Nine PSI- and three PSII-related proteins, such as *PSAA*, *PSAH2*, and *PSB27-1*, were continuously down-regulated in RN but were significantly increased in KT on day 6 after *Xcm* stress. Proteins involved in the regulation of antioxidant enzymes and peroxisome biosynthesis were also identified in the transcriptome, and the expression patterns of PS-related proteins differed between KT and RN. These results indicate that proteins from these three pathways may play important roles in the resistance of mango to *Xcm* invasion.

Cross-validation of transcriptomics and proteomics

To screen the gene set with the same or opposite expression trend in the two groups, based on the results of transcriptome and proteome difference analyses, we selected the common genes in the two omics for nine-quadrant analysis (Figure 6). The results showed that 1,470 genes were detected in the differential analysis of the two omics (Supplementary Table 10), and the expression patterns of 663 DEGs and DEPs were consistent (306 up-regulated and 357 down-regulated). The expression patterns of 95 DEGs were opposite those of DEPs (24 were up-regulated at the transcriptional level and down-regulated at the protein level; 71 were up-regulated at the protein level and down-regulated at the transcriptional level). A total of 580 genes were differentially expressed only at the protein level (271 up-regulated and 309 down-regulated). In addition, 132 genes were only differentially expressed at the transcriptional level

TABLE 1 Data statistics for CAT and SOD.

Name of sample	Activity of SOD (U/g FW)	Activity of CAT (U/g FW)
KT0-CK-1	116.7192	146.1181
KT0-CK-2	101.1579	147.3061
KT0-CK-3	108.9385	146.7121
RN0-CK-1	68.7029	101.7278
RN0-CK-2	61.1496	116.3664
RN0-CK-3	75.1006	109.0471
KT2-CK-1	51.3421	146.4533
KT2-CK-2	43.0272	150.7463
KT2-CK-3	47.1847	148.5999
RN2-CK-1	64.8143	103.0125
RN2-CK-2	69.9055	106.6258
RN2-CK-3	73.3733	104.8196
KT6-CK-1	127.6464	137.9829
KT6-CK-2	95.9465	122.1177
KT6-CK-3	111.7965	130.0503
RN6-CK-1	123.1138	126.6759
RN6-CK-2	92.8053	121.7515
RN6-CK-3	107.9596	116.8271
KT2-1	60.9331	221.6349
KT2-2	77.7148	220.1284
KT2-3	56.0119	229.9195
RN2-1	96.6945	151.8826
RN2-2	83.0136	153.2427
RN2-3	89.8540	152.5627
KT6-1	318.2606	207.4966
KT6-2	407.8865	209.8200
KT6-3	363.0736	208.6583
RN6-1	591.5970	314.2697
RN6-2	467.4140	307.9936
RN6-3	529.5055	311.1317

(34 up-regulated and 98 down-regulated). Notably, a large number of DEGs/DEPs, including GST (*HSP26-A* and *PARC*), glucose-6-phosphate 1-dehydrogenase (*G6PD2* and *G6PD4*) and GPX (*GPX2*), were found to be associated with GSH metabolism. Some DEGs/DEPs were also found to be associated with peroxisomes, including co-upregulated (*LACS6*, *LACS9*, and *PED1*) and co-downregulated (*GLO4* and *HACL*) genes, which are involved in the regulation of cellular redox homeostasis and protect cells from stress-induced oxidative damage. Four ABC transporter families, including *ABCB11*, *ABCB26*, and *ABCB28*, were up-regulated in both omics. *MYC2* and *TGA7* transcription factors related to plant IAA and ABA signal transduction were down-regulated in both omics. *PYL1* and *PYL9* were down-regulated, and *SAPK2* was up-regulated in both omics; these genes are related to plant ABA signaling and plant-pathogen interaction.

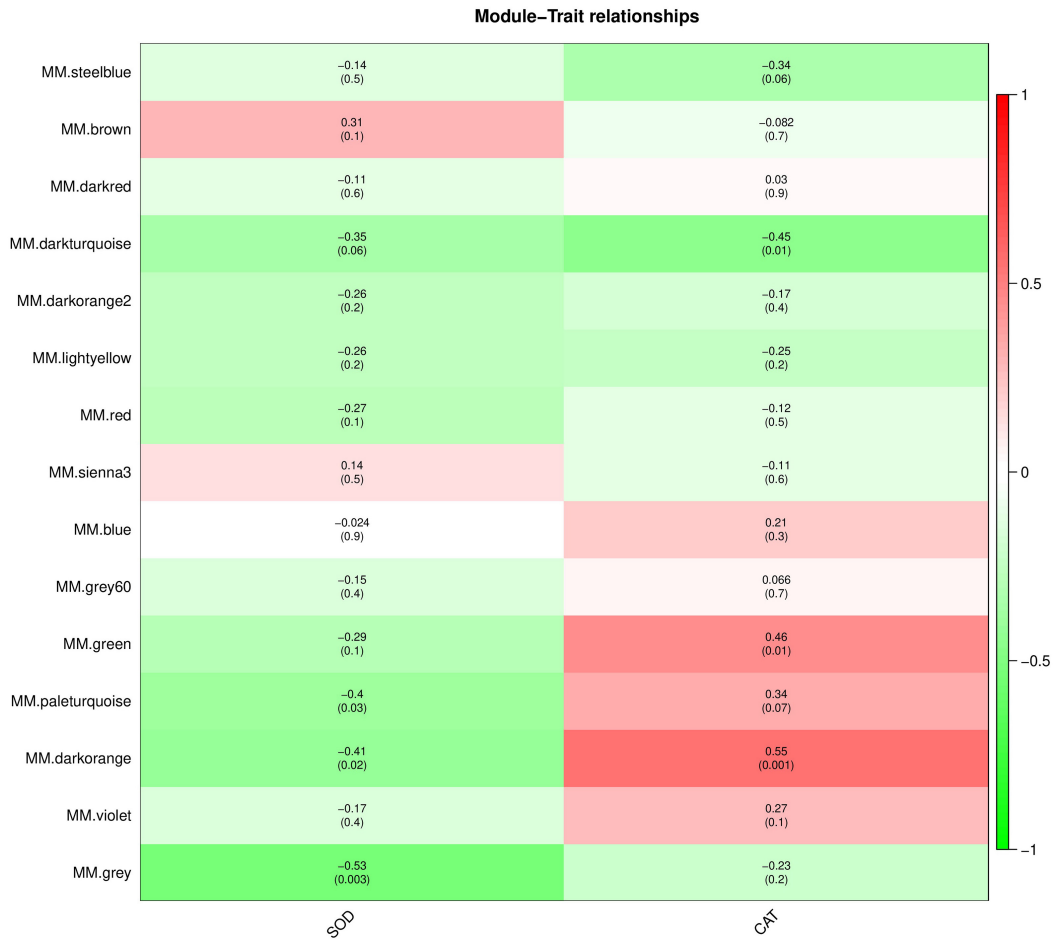

FIGURE 7
Module-trait relationships of co-expressed genes. The abscissa is the trait, the ordinate is the module, and the module eigenvalues and trait data are plotted using Pearson correlation coefficients. In the figure, red represents positive correlation, green represents negative correlation, and darker colors indicate stronger correlation.

Differential accumulation of SOD and CAT in two mango cultivars after *Xcm* inoculation

Transcriptome and proteome analyses showed that SOD and CAT constantly run through them. Thus, these antioxidant enzymes are significant for mango response to *Xcm*. Therefore, the activities of SOD and CAT in diseased mango fruits were determined at different time points (0, 2, and 6 days) (**Table 1**).

The results showed that SOD and CAT activities increased in both cultivars after *Xcm* inoculation at different times. In addition, significant differences (P-value < 0.0001) were observed in the changes of the same index among different varieties (**Supplementary Figure 3**). The results indicated that the two varieties may have different response mechanisms to *Xcm* stress.

Co-expressed genes/proteins by WGCNA

The interaction between plants and pathogens usually leads to the rapid accumulation of ROS in plants (Fichman and Mittler, 2021; Mittler et al., 2022). Several antioxidant enzymes play a key role in detoxification of ROS produced by plant stress response (Czarnocka and Karpiński, 2018). Therefore, we used WGCNA to screen the genes and proteins with the strongest correlation with SOD and CAT activity changes to further understand the co-expression relationship between KT and RN genes/proteins related to antioxidant enzymes. We selected the module with the highest Pearson r between the module and physiological and biochemical data as the key module. Removing the outlier grey module, in the gene co-expression network analysis, we observed that the brown and dark orange gene modules were most positively/negatively correlated with the SOD activity change pattern (brown: cor = 0.31, P-value = 0.1; dark orange: cor = −0.41; P-value = 0.02), containing 2,062 and 259 genes, respectively. The dark-orange and dark-turquoise gene modules were most positively/negatively correlated with CAT activity change patterns (dark orange: cor = 0.55, P-value = 0.001; dark-turquoise: cor = −0.45, P-value = 0.01). The dark-turquoise gene module contained 176 genes (**Figure 7**). In the protein co-expression network analysis, the dark-orange and grey60 modules exhibited the most positive/negative correlation with the change pattern of

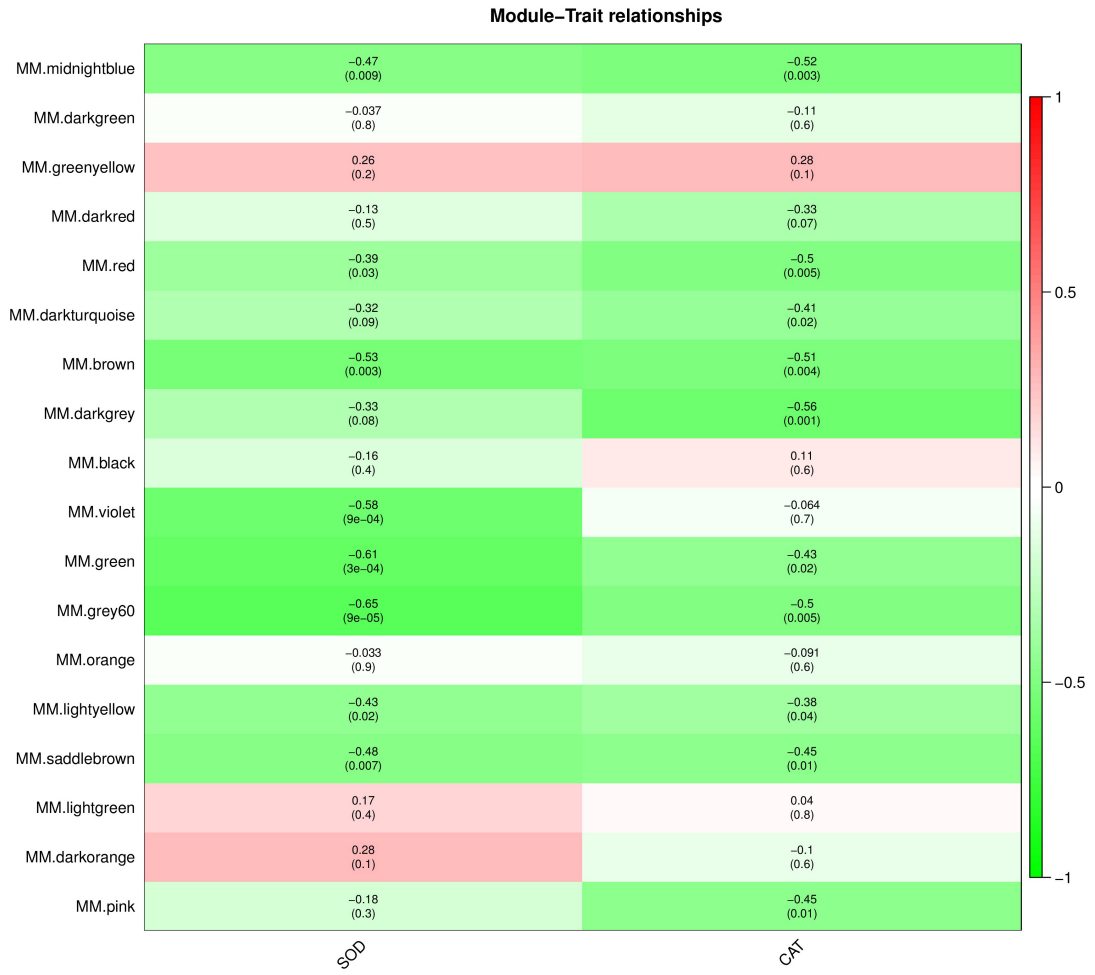

FIGURE 8
Module-trait relationships of co-expressed proteins. The abscissa is the trait, the ordinate is the module, and the module eigenvalues and trait data are plotted using Pearson correlation coefficients. In the figure, red represents positive correlation, green represents negative correlation, and darker colors indicate stronger correlation.

SOD activity (dark orange: cor = 0.28, *P*-value = 0.1; grey60 module: cor = −0.65, *P*-value = 9e-05), containing 217 and 180 proteins, respectively. The green-yellow and dark-gray modules had the most positive/negative correlation with CAT activity change pattern (green-yellow: cor = 0.28, *P*-value = 0.1; darkgray: cor = −0.56, *P*-value = 0.001), containing 261 and 131 proteins, respectively (**Figure 8**). KEGG pathway analysis showed that all three co-expressed gene modules were involved in "Glutathione metabolism," which plays an important role in plant antioxidant and integrated detoxification functions (Bela et al., 2015). We also found 17 genes involved in "Peroxisome," which is an important component of the plant antioxidant system, in the brown module (Yun and Kim, 2018). Next, we analyzed the co-expressed protein modules. The dark-orange module was annotated to "Metabolic pathways" and "Carbon metabolism," grey60 to "Spliceosome" and "RNA degradation," and green-yellow to "Flavonoid biosynthesis." The dark-gray module was annotated to "Phenylpropanoid biosynthesis," "Biotin metabolism," and "Diterpenoid biosynthesis." These findings indicate that the gene/protein modules are involved in different pathways to respond to *Xcm* invasion and may play an important role in maintaining cellular oxidative balance and biological regulation through these pathways.

Comparison of WGCNA results identified 58 co-expressed genes/proteins at the mRNA and protein levels. A total of 58 genes were compared with the DEGs identified in this study (**Table 2**). Exactly 20 and 19 DEGs were detected in KT and RN, respectively, of which 8 were dysregulated in RN (**Table 3**). Compared with DEPs, 31 proteins were differentially expressed in two mango cultivars; 13 and 11 of these proteins were differentially expressed in KT and RN, respectively, and 5 were dysregulated in RN (**Table 4**). These results indicate that differential genes/proteins may interact with non-differential ones. These proteins are not only related to mango antioxidant and certain biosynthesis but also may be related to mango disease resistance.

Among the DEGs obtained in WGCNA, three are related to plant hormone signal transduction (*SAG113*, *SRK2A*, and *ABCB1*). One gene, which was annotated as GSH dehydrogenase (*At5g42250*), is related to the regulation of redox homeostasis in plant cells and involved in GSH metabolism. One protein (*SAG113*) related to plant hormone signal transduction and one (*At5g42250*) regulating cell redox homeostasis were also found in the 31 DEPs

TABLE 2 A total of 58 co-expressed genes and proteins were identified by WGCNA results.

	Gene expression level							Protein expression level					
Id	Symbol	RN0d	RN2d	RN6d	KT0d	KT2d	KT6d	RN0d	RN2d	RN6d	KT0d	KT2d	KT6d
mango000296	CYP98A2	9.077	45.163	7.223	28.54	135.043	29.203	120449.669	336072.583	400800.042	254158.284	1019853.219	1696598.542
mango000839	SAG113	932.533	670.88	624.033	254.743	335.347	309.333	631877.458	455194.052	434339.406	683416	167780.609	124673.814
mango003892	CYP75A1	3.343	75.497	13.91	35.847	129.567	34.317	236681.745	1493866.958	2342342.417	339446.219	5058423.667	4947420.667
mango004150	THFS	49.22	60	38.217	32.26	67.733	37.697	11576418.67	9818077.333	11823384	9814331.667	8291622	9367840
mango005596	CYP86A22	46.457	53.637	64.88	2.973	9.297	16.103	1515010.354	816778.292	253823.823	850163.25	169501.807	259646.812
mango005775	ELF5	29.387	26.813	26.037	0.1	0.257	0.077	608604.5	437408.49	448061.917	652486.052	603007.802	461195.115
mango006296	4CL2	15.937	81.573	25.067	39.437	185.467	45.13	267768.224	1657512.75	2795836.583	225517.089	6310093.667	7322742.833
mango006430	GC5	28.737	35.537	45.947	16.92	19.077	14.26	551177.49	346006.497	168726.192	210471.427	239766.174	272378.44
mango006938	At3g47520	102.743	106.617	161.383	51.213	36.82	49.63	11182567.33	11850842	13976115.67	8119996.667	6680809.833	7291565.667
mango007487	UAH	9.41	12.19	7.76	5.117	10.513	5.913	3059991.667	2540401.833	2867465.25	2088687.208	1974811.583	2077584.917
mango008372	GLIP5	39.963	49.117	35.507	20.78	20.93	17.393	639855.354	623948.417	819532.771	334714.906	301998.797	376429.344
mango008492	CKL1	25.397	26.27	31.577	0.073	0.247	0.033	425939.167	230623.167	228819.406	379393.182	145321.557	149100.297
mango008818	BRIZ1	0.763	0.573	0.557	29.807	22.913	18.11	240898.339	298488.969	178607.548	225951.594	329491.573	254470.734
mango009044	–	68.547	109.253	32.673	43.683	132.607	40.69	2286412.917	2726363.583	2348346.917	1447527.583	3331601.917	4125099.167
mango011025	MC410	29.327	16.913	17.647	0.047	0.09	0	130390.026	88184.142	66171.405	99272.096	60717.603	54723.872
mango012295	RCOM_1506700	10.373	14.467	21.237	4.343	7.463	8.597	802806.979	708689.208	841368.208	675084.917	411557.135	555602.979
mango012298	MVD2	60.73	79.223	100.39	30.483	30.51	27.407	4598980.5	4295668.75	5038793	3759557.167	3429621.583	3287508.333
mango012341	SPBC776.07	4.817	5.737	3.673	9.85	9.967	9.53	1180885.667	976157.25	1187463.333	892162.625	776807.417	950840.375
mango012352	RTM2	0.507	0.387	3.96	0.253	0.073	0	435499.844	464847.885	331642.167	416058.344	276312.526	242228.646
mango012477	tal	393.79	559.74	637.897	233.253	289.607	195.803	11053258	10469292	13088137	8039736	7254753.667	7475896.5
mango013678	KAS1	52.033	76.32	97.343	39.407	26.873	28.02	4089943.333	2669365.333	3076852	3255481.833	2750220.333	3036436.417
mango013911	–	99.383	116.91	143.463	41.58	56.157	66.46	3339037.083	3102724	2848404.833	3595689.167	1778566.875	2227503.875
mango015130	SRK2A	13.223	8.907	10.103	39.007	35.01	35.897	364706.802	245055.76	173405.807	365675.781	201554.737	184828.219
mango017964	RTNLB8	17.583	23.377	14.03	9.523	25.83	13.333	892079.771	1053576.51	265746.654	1506117.625	1298243.458	600708.497
mango018070	SUMO2	3.64	4.283	3.76	1.68	0.97	2.07	605803.062	425804.167	416404.781	501482.458	307870.026	337847.292
mango018604	GF14D	164.24	222.787	174.74	125.323	252.17	166.763	32110846	26634130.67	29684760.67	23849617.33	23407323.33	29048290
mango018984	PAE8	20.477	114.597	16.65	6.75	90.6	9.203	14259275.67	9416066	9666316.333	9980805	10416728	8661339.167
mango020228	AFB2	58.567	62.18	89.82	37.887	38.09	32.177	544816.146	423586.354	326912.156	523882.51	422021.208	267861.823

(Continued)

10.3389/fmicb.2023.1220101

TABLE 2 (Continued)

	Gene expression level							Protein expression level					
Id	Symbol	RN0d	RN2d	RN6d	KT0d	KT2d	KT6d	RN0d	RN2d	RN6d	KT0d	KT2d	KT6d
mango020536	DBR	14.047	3.567	1.4	2.497	4.22	5.127	1327042.792	963911.958	489440.458	1111487.875	531932.365	427321.708
mango021031	HEXO2	15.157	32.947	11.707	26.427	34.927	16.99	151324.245	439039.583	416883.708	372989.229	879524.708	819515.25
mango021699	PLT5	19.467	54.62	37.61	30.247	99.233	26.93	667121.625	738229.729	662353.208	269335.333	1002994.146	1141336.271
mango022055	ABCB20	22.193	17.357	14.127	31.92	29.63	28.647	352198.042	398142	246857.323	426489.229	410300.302	325395.583
mango022508	ADCK1	48.847	15.487	10.243	36.453	24.97	23.143	147165.857	192104.661	181896.562	156913.062	298447.896	278558.891
mango023351	HCS1	45.403	41.58	51.943	22.843	21.87	23.69	520459.594	426767.615	297574.5	490239.083	337919.406	299679.25
mango023529	XK2	11.023	14.383	24.583	8.207	15.717	13.29	4484826.25	3297040.083	5104332.333	3658099.167	3117518.25	3054485.167
mango023835	SCP2	65.787	92.243	79.777	19.347	51.837	41.58	1972901.833	1787336.958	1749565.875	2421409.417	1098470.312	1508311.292
mango024212	At5g42250	1.323	4.267	3.45	2.543	5.167	3.46	160343.128	154011.594	295552.198	197642.305	342618.052	528385.219
mango024861	TFT7	63.79	67.6	75.36	10.187	27.02	29.803	730657.021	629114.354	746246.938	404433.219	380753.344	407370.042
mango026117	PGL3	10.34	8.013	13.213	4.267	5.69	4.417	547663.844	484599.74	445614.302	547793.781	242155.807	113928.124
mango026233	POR1	171.973	175.867	175.513	71.66	87.68	90.32	5275425.5	5293905.667	6443040.667	3263134.917	3106708.333	3300088.25
mango027123	At2g47970	78.183	63.787	38.19	89.54	96.82	83.147	984970.667	688723.688	593986.25	568024.156	611011.042	705327.167
mango027688	EO	804.393	1005.29	2212.13	40.2	192.4	1099.877	59746497.33	42094121.33	85985816	25247409.67	12017303.33	29097208.67
mango028314	MRF3	40.197	41.257	25.363	69.23	67.037	56.547	1408370.708	1592967.75	1269272.167	1986596.375	1940101.417	1813735.958
mango028849	Os02g0773300	13.667	18.103	22.68	7.217	9.337	7.893	1080241.396	933833.125	1019609.667	934037.188	718257.438	738553.396
mango029750	accB	27.31	38.997	52.19	19.623	19.493	22.76	1206027.833	1020100.625	1381977.667	771260.729	650144.271	757788.625
mango030037	ABCC8	18.903	2.487	0.28	1.193	4.807	4.217	363506.167	224265.036	86538.34	224485.807	159032.712	46309.887
mango031069	At1g06840	130.743	55.35	67.847	39.507	32.333	52.103	551076.917	466507.385	422713.052	458934.552	123791.948	245752.318
mango031169	RE	41.077	38.94	45.277	99.343	104.49	106.757	354674.052	398554.365	435910.01	418370.448	549467.938	559465.01
mango031532	ENO2	525.77	631.473	660.98	363.07	519.947	310.293	47112662.67	39513638.67	56960532	32152804.67	40807095.33	34221342
mango031829	VPS39	17.85	18.27	30.207	5.713	7.343	6.987	327551.771	415177.927	284328.375	407020.979	499444.552	324789.109
mango032009	SAC6	0.32	0.07	0.13	0.207	0.413	0.087	8726167.333	3168066.917	13242061	7535093	3510093.583	5190783
mango032095	exgA	2.463	2.453	12.647	1.543	5.523	4.377	726082.302	417935.958	605397.417	340726.146	316432.448	420246.802
mango032622	SPP2	106.24	100.547	169.077	28	61.943	60.087	3824173.833	3728226.667	4532774.75	2030338.542	1666033.333	1999753.458
mango033221	–	29.137	67.26	86.993	13.183	26.657	41.75	407787.885	164688.378	230557.328	216012.471	156628.076	102896.935
mango033409	FTSZ1	23.363	25.213	42.57	8.72	10.48	13.19	834630.917	637751.073	1093706.229	249376.729	228567.771	299652.328
mango034889	MTB	3.987	4.823	2.947	9.093	10.003	8.687	140038.404	125819.164	80701.871	142846.672	145785.974	115555.281
mango035105	SKP20	7.073	12.49	11.507	4.683	4.047	2.957	2534340.083	2353001.625	2375078.5	2237931.625	1963994.292	1739793.25
mango035149	At1g79260	14.97	26.47	26.68	4.42	10.743	11.28	2437932.083	2600219.792	1519332.604	2652060.667	1895509.958	2298095.917

10.3389/fmicb.2023.1220101

10.3389/fmicb.2023.1220101

TABLE 3 A total of 58 DEGs screened by WGCNA.

Id	Symbol	DEGs express level					
		RN0d	RN2d	RN6d	KT0d	KT2d	KT6d
mango000296	CYP98A2	9.077	45.163	7.223	28.54	135.043	29.203
mango000839	SAG113	932.533	670.88	624.033	254.743	335.347	309.333
mango003892	CYP75A1	3.343	75.497	13.91	35.847	129.567	34.317
mango004150	THFS	49.22	60	38.217	32.26	67.733	37.697
mango005596	CYP86A22	46.457	53.637	64.88	2.973	9.297	16.103
mango005775	ELF5	29.387	26.813	26.037	0.1	0.257	0.077
mango006296	4CL2	15.937	81.573	25.067	39.437	185.467	45.13
mango006430	GC5	28.737	35.537	45.947	16.92	19.077	14.26
mango006938	At3g47520	102.743	106.617	161.383	51.213	36.82	49.63
mango007487	UAH	9.41	12.19	7.76	5.117	10.513	5.913
mango008372	GLIP5	39.963	49.117	35.507	20.78	20.93	17.393
mango008492	CKL1	25.397	26.27	31.577	0.073	0.247	0.033
mango008818	BRIZ1	0.763	0.573	0.557	29.807	22.913	18.11
mango009044	–	68.547	109.253	32.673	43.683	132.607	40.69
mango011025	MC410	29.327	16.913	17.647	0.047	0.09	0
mango012295	RCOM_1506700	10.373	14.467	21.237	4.343	7.463	8.597
mango012298	MVD2	60.73	79.223	100.39	30.483	30.51	27.407
mango012341	SPBC776.07	4.817	5.737	3.673	9.85	9.967	9.53
mango012352	RTM2	0.507	0.387	3.96	0.253	0.073	0
mango012477	tal	393.79	559.74	637.897	233.253	289.607	195.803
mango013678	KAS1	52.033	76.32	97.343	39.407	26.873	28.02
mango013911	–	99.383	116.91	143.463	41.58	56.157	66.46
mango015130	SRK2A	13.223	8.907	10.103	39.007	35.01	35.897
mango017964	RTNLB8	17.583	23.377	14.03	9.523	25.83	13.333
mango018070	SUMO2	3.64	4.283	3.76	1.68	0.97	2.07
mango018604	GF14D	164.24	222.787	174.74	125.323	252.17	166.763
mango018984	PAE8	20.477	114.597	16.65	6.75	90.6	9.203
mango020228	AFB2	58.567	62.18	89.82	37.887	38.09	32.177
mango020536	DBR	14.047	3.567	1.4	2.497	4.22	5.127
mango021031	HEXO2	15.157	32.947	11.707	26.427	34.927	16.99
mango021699	PLT5	19.467	54.62	37.61	30.247	99.233	26.93
mango022055	ABCB1	22.193	17.357	14.127	31.92	29.63	28.647
mango022508	ADCK1	48.847	15.487	10.243	36.453	24.97	23.143
mango023351	HCS1	45.403	41.58	51.943	22.843	21.87	23.69
mango023529	XK2	11.023	14.383	24.583	8.207	15.717	13.29
mango023835	SCP2	65.787	92.243	79.777	19.347	51.837	41.58
mango024212	At5g42250	1.323	4.267	3.45	2.543	5.167	3.46
mango024861	TFT7	63.79	67.6	75.36	10.187	27.02	29.803
mango026117	PGL3	10.34	8.013	13.213	4.267	5.69	4.417
mango026233	POR1	171.973	175.867	175.513	71.66	87.68	90.32
mango027123	At2g47970	78.183	63.787	38.19	89.54	96.82	83.147
mango027688	EO	804.393	1005.29	2212.13	40.2	192.4	1099.877
mango028314	MRF3	40.197	41.257	25.363	69.23	67.037	56.547

(Continued)

TABLE 3 (Continued)

Id	Symbol	DEGs express level					
		RN0d	RN2d	RN6d	KT0d	KT2d	KT6d
mango028849	Os02g0773300	13.667	18.103	22.68	7.217	9.337	7.893
mango029750	accB	27.31	38.997	52.19	19.623	19.493	22.76
mango030037	ABCC8	18.903	2.487	0.28	1.193	4.807	4.217
mango031069	At1g06840	130.743	55.35	67.847	39.507	32.333	52.103
mango031169	RE	41.077	38.94	45.277	99.343	104.49	106.757
mango031532	ENO2	525.77	631.473	660.98	363.07	519.947	310.293
mango031829	VPS39	17.85	18.27	30.207	5.713	7.343	6.987
mango032009	SAC6	0.32	0.07	0.13	0.207	0.413	0.087
mango032095	exgA	2.463	2.453	12.647	1.543	5.523	4.377
mango032622	SPP2	106.24	100.547	169.077	28	61.943	60.087
mango033221	–	29.137	67.26	86.993	13.183	26.657	41.75
mango033409	FTSZ1	23.363	25.213	42.57	8.72	10.48	13.19
mango034889	MTB	3.987	4.823	2.947	9.093	10.003	8.687
mango035105	SKP20	7.073	12.49	11.507	4.683	4.047	2.957
mango035149	At1g79260	14.97	26.47	26.68	4.42	10.743	11.28

obtained in WGCNA. Notably, two DEPs, namely, *SAG113* and *At5g42250*, ran through the transcriptome and proteome of the study and were annotated to GSH metabolism and plant hormone signal transduction. Thus, these pathways may be important means for mango resistance to *Xcm*.

Real-time polymerase chain reaction validation

We performed real-time polymerase chain reaction analysis of three plant hormone-related DEGs/DEPs obtained by WGCNA to validate the RNA-seq results, and these genes showed different expression patterns at 0, 2, and 6d. The expression patterns of these genes obtained by qRT-PCR largely confirmed the transcriptome data (**Supplementary Figure 4**).

Discussion

In our study, RNA-seq and DIA techniques were used to holographically identify the changes in mRNA and protein levels in mango at different stages of *Xcm* infection. A total of 28,704 RNA data and 12,877 protein information were obtained. After differential analysis, 14,397 DEGs and 3,438 DEPs were obtained, and a large number of differential genes were shared between the two varieties of mango. This paper focused on DEGs/DEPs involved in redox homeostasis regulation and plant hormone signal transduction in mango cells. Given the great contribution of SOD and CAT in plant oxidative stress, we analyzed the correlation between the changes in SOD and CAT levels and changes in transcriptome and proteome in mango to explore the important genes related to trait indicators.

Photosynthesis, GSH metabolism, and peroxisomes play important regulatory roles in plant cell redox homeostasis during plant resistance to pathogens. Photosynthesis is an important source of ATP and carbohydrates in plants. A series of genes involved in photosynthesis can participate in the production and signal transduction of plant hormone signaling molecules, such as ABA, ETH, IAA, GA, etc., and the production and signal transduction of non-hormone signaling molecules. PSI and PSII are the main sources of ROS production and play a crucial role in the balanced synthesis of ROS and NO (Apel and Hirt, 2004; Asada, 2006; Del Río, 2015; Lu and Yao, 2018). In mango, more than 80% of DEGs and DEPs involved in PSI and PSII were generally up-regulated in KT and RN. However, the change in RN was always negligible, and that of related genes in KT continuously increased (**Table 5**). The general imbalance of photosynthetic genes may hinder the stability of photosynthesis in susceptible plants; it was also encountered in chickpeas infected with *F. oxysporum f.* sp. *ciceri* race 1 (Bhar et al., 2017) and *Cucurbita ficifolia* Bouché infected with *Fusarium oxysporum f.* sp. *cucumerinum*. In addition, DEGs *FD3* and *Os07g0147900*, which were annotated as Fd, were up-regulated in RN and down-regulated in KT, and DEPs, including *FD3*, *SIR1*, and *FTRC*, were annotated as Fd and up-regulated in RN and KT. However, the change in RN was more significant.

The plant-type redox system composed of Fd-NADP (+) reductase and its redox partner Fd can play an important role in plant-pathogen interaction (Iyanagi, 2022). Fd can interact with the HC-Pro protein of *sugar cane mosaic virus* (*SCMV*) in maize infected with *SCMV* and may interfere with the post-translational modification of Fd in the chloroplast of maize sheath cells, which will disturb chloroplast structure and function (Cheng et al., 2008). Fd may activate hypersensitivity related events, such as H_2O_2 accumulation, through the recognition of interacting proteins in mango to enhance the plant's resistance. Overexpression of Fd also

10.3389/fmicb.2023.1220101

TABLE 4 A total of 31 DEPs screened by WGCNA.

Protein_id	Symbol	RN0d	RN2d	RN6d	KT0d	KT2d	KT6d
mango000296	CYP98A2	120449.669	336072.583	400800.042	254158.284	1019853.219	1696598.542
mango000839	SAG113	683416	124673.814	167780.609	434339.406	631877.458	455194.052
mango003892	CYP75A1	236681.745	1493866.958	2342342.417	339446.219	5058423.667	4947420.667
mango005596	CYP86A22	1515010.354	816778.292	253823.823	850163.25	169501.807	259646.812
mango006296	4CL2	267768.224	1657512.75	2795836.583	225517.089	6310093.667	7322742.833
mango006938	At3g47520	11182567.33	11850842	13976115.67	8119996.667	6680809.833	7291565.667
mango008372	GLIP5	639855.354	623948.417	819532.771	334714.906	301998.797	376429.344
mango008492	CKL1	425939.167	230623.167	228819.406	379393.182	145321.557	149100.297
mango009044	–	2286412.917	2726363.583	2348346.917	1447527.583	3331601.917	4125099.167
mango012295	RCOM_1506700	802806.979	708689.208	841368.208	675084.917	411557.135	555602.979
mango012298	MVD2	4598980.5	4295668.75	5038793	3759557.167	3429621.583	3287508.333
mango012477	tal	11053258	10469292	13088137	8039736	7254753.667	7475896.5
mango013678	KAS1	4089943.333	2669365.333	3076852	3255481.833	2750220.333	3036436.417
mango013911	–	3339037.083	3102724	2848404.833	3595689.167	1778566.875	2227503.875
mango020536	DBR	1327042.792	963911.958	489440.458	1111487.875	531932.365	427321.708
mango021031	HEXO2	151324.245	439039.583	416883.708	372989.229	879524.708	819515.25
mango021699	PLT5	667121.625	738229.729	662353.208	269335.333	1002994.146	1141336.271
mango022508	ADCK1	147165.857	192104.661	181896.562	156913.062	298447.896	278558.891
mango023351	HCS1	520459.594	426767.615	297574.5	490239.083	337919.406	299679.25
mango023529	XK2	4484826.25	3297040.083	5104332.333	3658099.167	3117518.25	3054485.167
mango023835	SCP2	1972901.833	1787336.958	1749565.875	2421409.417	1098470.312	1508311.292
mango024212	At5g42250	197642.305	342618.052	528385.219	160343.128	154011.594	295552.198
mango024861	TFT7	730657.021	629114.354	746246.938	404433.219	380753.344	407370.042
mango026233	POR1	5275425.5	5293905.667	6443040.667	3263134.917	3106708.333	3300088.25
mango027123	At2g47970	984970.667	688723.688	593986.25	568024.156	611011.042	705327.167
mango027688	EO	59746497.33	42094121.33	85985816	25247409.67	12017303.33	29097208.67
mango029750	accB	1206027.833	1020100.625	1381977.667	771260.729	650144.271	757788.625
mango030037	ABCC8	363506.167	224265.036	86538.34	224485.807	159032.712	46309.887
mango031069	At1g06840	551076.917	466507.385	422713.052	458934.552	123791.948	245752.318
mango032622	SPP2	3824173.833	3728226.667	4532774.75	2030338.542	1666033.333	1999753.458
mango033409	FTSZ1	834630.917	637751.073	1093706.229	249376.729	228567.771	299652.328

enhances the resistance of *Arabidopsis* (Ger et al., 2014), sweet pepper (Dayakar et al., 2003), and tobacco (Huang et al., 2007).

Glutathione metabolism is the metabolic process of gamma-glutamyl-cysteinyl-glycine (GSH) in plants. GSH is an antioxidant that can resist free radical damage, support the dynamic relationship with ROS, redox regulation, and signal transduction, and protect cells from external factors (Diaz-Vivancos et al., 2015; Noctor et al., 2023). GSH activates the potato defense system by reducing potential damage to host cells in *Potato virus* Y NTN medical record system, which results in reduced virus concentration and limits systemic infection of potatoes caused by oxidative stress (Otulak-Kozieł et al., 2022). In our study, 81 genes were involved in GSH metabolism, of which 20 genes, such as L-ascorbate peroxidase (*APX1*), were consistently expressed at mRNA and protein levels. GST (*HSP26-A*, *PARC*, *GSTU8*, and *GSTL3*) and GSH dehydrogenase/transferase (*DHAR2*) were down-regulated in resistant and susceptible mango cultivars. Glucose-6-phosphate 1-dehydrogenase (*G6PD2* and *G6PD4*) and GPX (*GPX2*) were up-regulated, and the expression trends of the three genes in the two omics were opposite. Gamma-glutamyltranspeptidase (*GGT2*) was down-regulated in the transcriptome and up-regulated at the protein level. Two GSTs (*GSTF11* and *GSTU17*) showed the opposite result, and one GSH dehydrogenase (*At5g42250*) was found in WGCNA and differentially expressed in the two omics. Thus, the metabolic process of GSH is very important for mango to resist *Xcm* invasion, and its related genes regulate its metabolic process at different levels, thus protecting mango cells from the oxidative stress caused by *Xcm* infection.

Peroxisome is an important organelle in ROS metabolism, mainly producing superoxide anion (O_2^-) and hydrogen peroxide

10.3389/fmicb.2023.1220101

TABLE 5 DEGs and DEPs in photosystem 1 and photosystem 2.

Id	Symbol	DEGs express level					
		RN0d	RN2d	RN6d	KT0d	KT2d	KT6d
mango000380	PSAO	28.067	46.73	42.25	5.197	100.017	121.05
mango003053	psaD	0.063	0.04	0.103	0.093	2.73	2.85
mango006427	PSAH2	3.143	4.42	1.913	6.647	35.077	30.883
mango007574	psaD	84.55	102.213	125.847	32.657	96.63	155.057
mango010109	PSAN	4.937	15.983	7.387	2.78	44.307	73.97
mango015793	PSBY	0.793	1.65	0.93	0.66	18.933	39.063
mango018113	PSAE	20.483	19.163	14.077	12.933	35.727	52.393
mango018135	PSB28	15.29	31.427	34.053	2.483	12.833	10.91
mango019341	PSBW	11.713	17.093	14.37	0.83	16.127	18.343
mango019347	PSBW	0	0	0.203	0.97	23.453	39.36
mango020695	PSBW	133.573	198.41	336.833	61.183	226.493	252.927
mango020754	PSAL	43.027	55.49	36.457	17.483	149.747	210.073
mango025005	PSBS	50.043	72.147	99.383	18.66	75.52	61.463
mango026466	PSBY	32.703	50.273	48.007	10.027	58.307	78.193
mango026761	PSB28	1.143	3.85	2.467	0.677	5.683	2.937
mango026786	PSAEA	66.377	78.883	71.193	23.287	79.123	117.487
mango029879	PSAH2	12.33	26.457	20.117	5.76	58.56	66.347
mango030680	PSAF	95.027	140.253	162.19	42.743	134.8	146.973
mango032227	PSAN	0	0.053	0	0	0.2	0.877
Protein_id	Symbol	DEPs express level					
		RN0d	RN2d	RN6d	KT0d	KT2d	KT6d
mango006427	PSAH2	2701098.292	712847.542	1326046.208	13895611.17	4650683.375	10251425.67
mango029879	PSAH2	2701098.292	712847.542	1326046.208	13895611.17	4650683.375	10251425.67
mango007574	psaD	6829527.667	3117529.667	3623329.292	31275804.67	14579772.67	21904209.33
mango010025	psaA	11205578.5	3604213.917	3367035.833	44034390.67	20162870	35687958.67
mango015142	LHCA3	2531327.75	668129.188	918001.333	13884698.33	5543263.167	8379549.833
mango015191	LHCA3	2531327.75	668129.188	918001.333	13884698.33	5543263.167	8379549.833
mango016666	psbB	7404652.833	4324037.917	4967177.083	15096296	10150018.17	15987511.67
mango018113	PSAE	266476.005	205574.255	56204.501	2521959.5	793993.719	1646594.167
mango020436	PSB27-1	2957401.5	1727613.333	1635928.833	3728865.583	2361803.708	2865011.208
mango020754	PSAL	219881.568	82765.891	108931.694	765285.792	424844.661	754995.906
mango022823	psbB	3362773.917	1869271.75	1268698.5	6328656.917	3476546.333	5686411.5
mango023837	LHCA5	35759.461	NA	1.032	190346.31	621114.688	262428.484
mango026786	PSAEA	1427598.792	788556.125	475287.797	6385375.833	2773814.167	5008947.25
mango030680	PSAF	13723842.33	4954353.583	6383658.583	50647948	21665666	38667322.67
mango032227	PSAN	6035151.833	1928648.958	2417696.083	25466472	8873263.667	12152935.67

(H_2O_2) (Corpas et al., 2020). Peroxisome is involved in a series of ROS generation and scavenging mechanisms, and participates in programmed cell death of plant cells to resist environmental stresses (Huang et al., 2022). In our study, at the transcriptome level, nearly half of the peroxisome-related DEGs changed more significantly in RN, whereas at the proteome level, 30 out of 38 DEPs, including POD (*CAT1*) and SOD (*FSD2*), were up-regulated in RN, and the change range was more than that observed KT. Thus, several multifunctional genes can regulate the balance of ROS in mango by positively regulating the biosynthesis of peroxisomes.

Hormones play a vital role in plant disease resistance. The signaling pathways of multiple hormones are not independent of each other in the disease resistance response; however, the interaction between hormones forms a complex regulatory network that enables plants to efficiently coordinate different hormones in the body to improve plant resistance, which is an effective

method to resist pathogen invasion (Verma et al., 2016). In this study, a large number of genes were found to be involved in the signal transduction of plant hormones, such as IAA, ABA, GA, ETH, and so on, at the transcriptional and protein levels. The expression levels of these plant hormone-related DEGs in RN were relatively low and generally down-regulated. The related proteins with large differences in expression in the proteome were similar to the transcriptome, mainly that of KT. Through cross-validation of transcriptome and proteomics and WGCNA, three key genes (*SAG113*, *SRK2A*, and *ABCB1*) that were co-expressed in two groups were finally screened out, and they were related to the changes in SOD and CAT activities. *SAG113* was also identified in WGCNA of the proteome. Thus, these three genes are not only involved in the signal transduction of plant hormones but may also regulate the redox homeostasis of mango cells during stress response through signal transduction.

Conclusion

The response of mango fruit to Xcm is a complex process, and our understanding of MBLS pathology is limited. The symptoms of disease-resistant varieties and susceptible varieties appeared on the 2nd day and differentiated on the 6th day of the experiment. To determine the positively or negatively affected genes, we mainly analyzed the significantly DEGs that maintained a consistent trend from day 0 to day 6. The genes and proteins identified in this study provide valuable resources for mango resistance to MBLS breeding and can benefit researchers in this field.

Data availability statement

The authors acknowledge that the data presented in this study must be deposited and made publicly available in an acceptable repository, prior to publication. Frontiers cannot accept a manuscript that does not adhere to our open data policies.

Author contributions

FL and R-LZ contributed to the conception and design of the study. XS wrote the first draft of the manuscript. QY and KZ provided scientific advice. LW performed the statistical analysis. All authors contributed to the manuscript revision and read and approved the submitted version.

Funding

This research was supported by the Key-Area Research and Development Program of Guangdong Province (2022B0202070002), the Yunnan Innovation Guidance and Technological Enterprise Cultivation Plan Project (202104BI090012), and the Chinese Special Fund of Basic Scientific Research Projects for State Level and Public Welfare-Scientific Research Institutes (1630062021014).

Acknowledgments

We thank Gene Denovo at Guangzhou for its assistance in original data processing and related bioinformatics analysis.

Conflict of interest

The authors declare that the research was conducted in the absence of any commercial or financial relationships that could be construed as a potential conflict of interest.

Publisher's note

Supplementary material

The Supplementary Material for this article can be found online at: https://www.frontiersin.org/articles/10.3389/fmicb.2023.1220101/full#supplementary-material

SUPPLEMENTARY FIGURE 1
Venn diagram of transcriptome sample abundance. Each set in the figure is filled with different colors and labeled with the number of genes contained in each set. The overlapping parts of the set represent the number of genes shared between groups, while the non-overlapping parts represent the unique genes of each group.

SUPPLEMENTARY FIGURE 2
Venn diagram of proteome sample abundance. Each group in the figure is filled with a different color and marked with the number of proteins each group contains. The overlapping part of the set represents the number of proteins shared between groups, and the non-overlapping part represents the genes unique to each group.

SUPPLEMENTARY FIGURE 3
Changes of SOD and CAT activity in fruits of different mango varieties under Xcm stress. The mark above the error line is the difference analysis result between the treatment group and the control group.

SUPPLEMENTARY FIGURE 4
Validation of the transcriptome data. The ordinate in the figure represents the relative expression of differentially expressed genes in qRT-PCR. The abscissa represents the different treatment groups; Error bars are standard deviations.

SUPPLEMENTARY TABLE 1
Primer sequences used for qRT-PCR.

SUPPLEMENTARY TABLE 2
GO annotation results of DEGs.

SUPPLEMENTARY TABLE 3
Results of KEGG enrichment analysis of DEGs.

SUPPLEMENTARY TABLE 4
Genes involved in plant hormone signaling.

SUPPLEMENTARY TABLE 5
Redox-related genes.

SUPPLEMENTARY TABLE 6
GO annotation results of DEPs.

SUPPLEMENTARY TABLE 7
Results of KEGG enrichment analysis of DEPs.

SUPPLEMENTARY TABLE 8
Proteins involved in plant hormone signaling.

SUPPLEMENTARY TABLE 9
Redox-related proteins.

SUPPLEMENTARY TABLE 10
Cross-validation of transcriptomics and proteomics.

References

Akbar, S., Wei, Y., Yuan, Y., Khan, M. T., Qin, L., Powell, C. A., et al. (2020). Gene expression profiling of reactive oxygen species (ROS) and antioxidant defense system following *Sugarcane mosaic virus* (*SCMV*) infection. *BMC Plant Biol.* 20:532. doi: 10.1186/s12870-020-02737-1

Anders, S., and Huber, W. (2010). Differential expression analysis for sequence count data. *Genome Biol.* 11:R106.

Anderson, J. P., Badruzsaufari, E., Schenk, P. M., Manners, J. M., Desmond, O. J., Ehlert, C., et al. (2004). Antagonistic interaction between abscisic acid and jasmonate-ethylene signaling pathways modulates defense gene expression and disease resistance in *Arabidopsis*. *Plant Cell* 16, 3460–3479. doi: 10.1105/tpc.104.025833

Apel, K., and Hirt, H. (2004). Reactive oxygen species: Metabolism, oxidative stress, and signal transduction. *Annu. Rev. Plant Biol.* 55, 373–399. doi: 10.1146/annurev.arplant.55.031903.141701

Asada, K. (2006). Production and scavenging of reactive oxygen species in chloroplasts and their functions. *Plant Physiol.* 141, 391–396. doi: 10.1104/pp.106.082040

Ashburner, M., Ball, C. A., Blake, J. A., Botstein, D., Butler, H., Cherry, J. M., et al. (2000). Gene ontology: Tool for the unification of biology. The gene ontology consortium. *Nat. Genet.* 25, 25–29. doi: 10.1038/75556

Bela, K., Horváth, E., Gallé, Á, Szabados, L., Tari, I., and Csiszár, J. (2015). Plant glutathione peroxidases: Emerging role of the antioxidant enzymes in plant development and stress responses. *J. Plant Physiol.* 176, 192–201. doi: 10.1016/j.jplph.2014.12.014

Bhar, A., Gupta, S., Chatterjee, M., Sen, S., and Das, S. (2017). Differential expressions of photosynthetic genes provide clues to the resistance mechanism during *Fusarium oxysporum*, fsp *ciceri*, race 1 (*Foc*1) infection in chickpea (*Cicer arietinum L*). *Eur. J. Plant Pathol.* 148, 533–549. doi: 10.1007/s10658-016-1109-1

Botía, J. A., Vandrovcova, J., Forabosco, P., Guelfi, S., D'Sa, K., United Kingdom Brain Expression Consortium, et al. (2017). An additional k-means clustering step improves the biological features of WGCNA gene co-expression networks. *BMC Syst. Biol.* 11:47. doi: 10.1186/s12918-017-0420-6

Chen, L., Zhang, Y. H., Wang, S., Zhang, Y., Huang, T., and Cai, Y. D. (2017). Prediction and analysis of essential genes using the enrichments of gene ontology and KEGG pathways. *PLoS One* 12:e0184129. doi: 10.1371/journal.pone.0184129

Chen, S., Zhou, Y., Chen, Y., and Gu, J. (2018). fastp:an ultra-fast all-in-one FASTQ preprocessor. *Bioinformatics* 34, i884–i890. doi: 10.1093/bioinformatics/bty560

Cheng, Y. Q., Liu, Z. M., Xu, J., Zhou, T., Wang, M., Chen, Y. T., et al. (2008). HC-Pro protein of sugar cane mosaic virus interacts specifically with maize ferredoxin-5 in vitro and in planta. *J. Gen. Virol.* 89, 2046–2054. doi: 10.1099/vir.0.2008/001271-0

Corpas, F. J., González-Gordo, S., and Palma, J. M. (2020). Plant peroxisomes: Afactory of reactive species. *Front. Plant Sci.* 11:853. doi: 10.3389/fpls.2020.00853

Czarnocka, W., and Karpiński, S. (2018). Friend or foe? Reactive oxygen species production, scavenging and signaling in plant response to environmental stresses. *Free Radic. Biol. Med.* 122, 4–20. doi: 10.1016/j.freeradbiomed.2018.01.011

Dayakar, B. V., Lin, H. J., Chen, C. H., Ger, M. J., Lee, B. H., Pai, C. H., et al. (2003). Ferredoxin from sweet pepper (*Capsicum annuum* L.) intensifying harpin(pss)-mediated hypersensitive response shows an enhanced production of active oxygen species (AOS). *Plant Mol. Biol.* 51, 913–924. doi: 10.1023/a:1023061303755

Del Río, L. A. (2015). ROS and RNS in plant physiology: An overview. *J. Exp. Bot.* 66, 2827–2837. doi: 10.1093/jxb/erv099

Denancé, N., Sánchez-Vallet, A., Goffner, D., and Molina, A. (2013). Disease resistance or growth: The role of plant hormones in balancing immune responses and fitness costs. *Front. Plant Sci.* 4:155. doi: 10.3389/fpls.2013.00155

Diaz-Vivancos, P., de Simone, A., Kiddle, G., and Foyer, C. H. (2015). Glutathione-linking cell proliferation to oxidative stress. *Free Radic. Biol. Med.* 89, 1154–1164. doi: 10.1016/j.freeradbiomed.2015.09.023

Djami-Tchatchou, A. T., Li, Z. A., Stodghill, P., Filiatrault, M. J., and Kunkel, B. N. (2022). Identification of Indole-3-Acetic Acid-Regulated Genes in *Pseudomonas syringae* pv. tomato strain DC3000. *J. Bacteriol.* 204:e0038021. doi: 10.1128/JB.00380-21

Fang, X., Zeng, X., Wang, M., Qin, L., Tan, C., and Wu, J. (2021). Enrichment analysis of differentially expressed genes in chronic heart failure. *Ann. Palliat. Med.* 10, 9049–9056. doi: 10.21037/apm-21-1854

Fichman, Y., and Mittler, R. (2021). A systemic whole-plant change in redox levels accompanies the rapid systemic response to wounding. *J. Plant Physiol.* 186, 4–8. doi: 10.1093/plphys/kiab022

Gagnevin, L., and Pruvost, O. (2001). Epidemiology and control of mango bacterial black spot. *Plant Dis.* 85, 928–935. doi: 10.1094/PDIS.2001.85.9.928

Ger, M. J., Louh, G. Y., Lin, Y. H., Feng, T. Y., and Huang, H. E. (2014). Ectopically expressed sweet pepper ferredoxin PFLP enhances disease resistance to *Pectobacterium carotovorum* subsp. *carotovorum* affected by harpin and protease-mediated hypersensitive response in *Arabidopsis*. *Mol. Plant Pathol.* 15, 892–906. doi: 10.1111/mpp.12150

Haverland, N. A., Fox, H. S., and Ciborowski, P. (2014). Quantitative proteomics by SWATH-MS reveals altered expression of nucleic acid binding and regulatory proteins in HIV-1-infected macrophages. *J. Proteome Res.* 13, 2109–2119. doi: 10.1021/pr4012602

Huang, H. E., Ger, M. J., Chen, C. Y., Pandey, A. K., Yip, M. K., Chou, H. W., et al. (2007). Disease resistance to bacterial pathogens affected by the amount of ferredoxin-I protein in plants. *Mol. Plant Pathol.* 8, 129–137. doi: 10.1111/j.1364-3703.2006.00378.x

Huang, L., Liu, Y., Wang, X., Jiang, C., Zhao, Y., Lu, M., et al. (2022). Peroxisome-mediated reactive oxygen species signals modulate programmed cell death in plants. *Int. J. Mol. Sci.* 23:10087. doi: 10.3390/ijms231710087

Iyanagi, T. (2022). Roles of ferredoxin-NADP+ oxidoreductase and flavodoxin in NAD(P)H-dependent electron transfer systems. *Antioxidants (Basel)* 11:2143. doi: 10.3390/antiox11112143

Kanehisa, M., and Goto, S. (1999). KEGG: Kyoto encyclopedia of genes and genomes. *Nucleic Acids Res.* 27, 29–34. doi: 10.1093/nar/27.1.29

Kim, D., Langmead, B., and Salzberg, S. L. (2015). HISAT: A fast spliced aligner with low memory requirements. *Nat. Methods* 12:357. doi: 10.1038/nmeth.3317

Langfelder, P., and Horvath, S. (2008). WGCNA: An R package for weighted correlation network analysis. *BMC Bioinformatics* 9:559. doi: 10.1186/1471-2105-9-559

Langmead, B., and Salzberg, S. L. (2012). Fast gapped-read alignment with Bowtie 2. *Nat. Methods* 9, 357–359. doi: 10.1038/nmeth.1923

Lebaka, V. R., Wee, Y.-J., Ye, W., and Korivi, M. (2021). Nutritional composition and bioactive compounds in three different parts of mango fruit. *Int. J. Environ. Res. Public Health* 18:741. doi: 10.3390/ijerph18020741

Li, B., and Dewey, C. N. (2011). RSEM: Accurate transcript quantification from RNA-Seq data with or without a reference genome. *BMC Bioinformatics* 12:323. doi: 10.1186/1471-2105-12-323

Li, C., Shao, J., Wang, Y., Li, W., Guo, D., Yan, B., et al. (2013). Analysis of banana transcriptome and global gene expression profiles in banana roots in response to infection by race 1 and tropical race 4 of *Fusarium oxysporum* f. sp. *cubense*. *BMC Genomics* 14:851. doi: 10.1186/1471-2164-14-851

Li, N., Han, X., Feng, D., Yuan, D., and Huang, L. J. (2019). Signaling crosstalk between salicylic acid and ethylene/jasmonate in plant defense: Do we understand what they are whispering? *Int. J. Mol. Sci.* 20:671. doi: 10.3390/ijms20030671

Livak, K. J., and Schmittgen, T. D. (2001). Analysis of relative gene expression data using real-time quantitative PCR and the 2(-Delta Delta C(T)) Method. *Methods* 25, 402–408. doi: 10.1006/meth.2001.1262

Love, M. I., Huber, W., and Anders, S. (2014). Moderated estimation of fold change and dispersion for RNA-seq data with DESeq2. *Genome Biol.* 15:550. doi: 10.1186/s13059-014-0550-8

Lu, Y., and Yao, J. (2018). Chloroplasts at the crossroad of photosynthesis, pathogen infection and plant defense. *Int. J. Mol. Sci.* 19:3900. doi: 10.3390/ijms19123900

Meitha, K., Pramesti, Y., and Suhandono, S. (2020). Reactive oxygen species and antioxidants in postharvest vegetables and fruits. *Int. J. Food Sci.* 2020:8817778. doi: 10.1155/2020/8817778

Mirza, B., Croley, C. R., Ahmad, M., Pumarol, J., Das, N., Sethi, G., et al. (2021). Mango (*Mangifera indica* L.): A magnificent plant with cancer preventive and anticancer therapeutic potential. *Crit. Rev. Food Sci. Nutr.* 61, 2125–2151. doi: 10.1080/10408398.2020.1771678

Mittler, R., Zandalinas, S. I., Fichman, Y., and Van Breusegem, F. (2022). Reactive oxygen species signalling in plant stress responses. *Nat. Rev. Mol. Cell Biol.* 23, 663–679. doi: 10.1038/s41580-022-00499-2

Niemira, M., Collin, F., Szalkowska, A., Bielska, A., Chwialkowska, K., Reszec, J., et al. (2019). Molecular signature of subtypes of non-small-cell lung cancer by large-scale transcriptional profiling: Identification of key modules and genes by weighted gene co-expression network analysis (WGCNA). *Cancers (Basel)* 12:37. doi: 10.3390/cancers12010037

Noctor, G., Cohen, M., Trémulot, L., Van Breusegem, F., and Mhamdi, A. (2023). Quantitative measurements of biochemical and molecular markers of oxidative stress signaling and responses. *Methods Mol. Biol.* 2642, 197–214. doi: 10.1007/978-1-0716-3044-0_11

Otulak-Kozieł, K., Kozieł, E., Przewodowski, W., Ciacka, K., and Przewodowska, A. (2022). Glutathione modulation in PVYNTN susceptible and resistant potato plant interactions. *Int. J. Mol. Sci.* 23:3797. doi: 10.3390/ijms23073797

Poyraz, I., Sözen, E., and Arslanyolub, M. (2010). Isolation of quality total RNA from the aromatic plant *Origanum onites*. *Z. Naturforsch. C J. Biosci.* 65, 266–270. doi: 10.1515/znc-2010-3-415

Robinson, M. D., McCarthy, D. J., and Smyth, G. K. (2010). edgeR: A bioconductor package for differential expression analysis of digital gene expression data. *Bioinformatics* 26, 139–140. doi: 10.1093/bioinformatics/btp616

Salmela, L., and Rivals, E. (2014). LoRDEC:accurate and efficient long read error correction. *Bioinformatics* 30, 3506–3514. doi: 10.1093/bioinformatics/btu538

Sanahuja, G., Ploetz, R. C., Lopez, P., Konkol, J. L., Palmateer, A. J., and Pruvost, O. (2016). *Mangifera indica*, caused by *Xanthomonas citri* pv. *mangiferaeindicae*, confirmed for the first time in the Americas. *Plant Dis.* 100:2520. doi: 10.1094/PDIS-03-16-0412-PDN

Sidoli, S., Lin, S., Xiong, L., Bhanu, N., Karch, K., Johansen, E., et al. (2015). Sequential window acquisition of all theoretical mass spectra (swath) analysis for characterization and quantification of histone post-translational modifications. *Mol. Cell. Proteomics* 14, 2420–2428. doi: 10.1074/mcp.O114.046102

Sies, H. (2018). On the history of oxidative stress: Concept and some aspects of current development. *Curr. Opin. Toxicol.* 7, 122–126. doi: 10.1016/j.cotox.2018.01.002

Taylor, S. C., Nadeau, K., Abbasi, M., Lachance, C., Nguyen, M., and Fenrich, J. (2019). The Ultimate qPCR experiment: Producing publication quality, reproducible data the first time. *Trends Biotechnol.* 37, 761–774. doi: 10.1016/j.tibtech.2018.12.002

Verma, V., Ravindran, P., and Kumar, P. P. (2016). Plant hormone-mediated regulation of stress responses. *BMC Plant Biol.* 16:86. doi: 10.1186/s12870-016-0771-y

Wang, X., Li, Y., Liu, Y., Zhang, D., Ni, M., Jia, B., et al. (2021). Transcriptomic and proteomic profiling reveal the key role of AcMYB16 in the response of *Pseudomonas syringae* pv. *actinidiae* in Kiwifruit. *Front. Plant Sci.* 10:756330. doi: 10.3389/fpls.2021.756330

Xie, J., Ding, Y., Gao, T., He, S., Zhao, K., Yang, X., et al. (2022). Transcriptomic and proteomic analyses of *Cucurbita ficifolia* Bouché (Cucurbitaceae) response to *Fusarium oxysporum* f.sp. *cucumerium*. *BMC Genomics* 23:436. doi: 10.1186/s12864-022-08674-7

Xue, C., Liu, Z., Wang, L., Li, H., Gao, W., Liu, M., et al. (2020). The antioxidant defense system in Chinese jujube is triggered to cope with phytoplasma invasion. *Tree Physiol.* 40, 1437–1449. doi: 10.1093/treephys/tpaa067

Young, M. D., Wakefield, M. J., Smyth, G. K., and Oshlack, A. (2010). Gene ontology analysis for RNA-seq: Accounting for selection bias. *Genome Biol.* 11:R14. doi: 10.1186/gb-2010-11-2-r14

Yun, T. K., and Kim, L. (2018). Gonzalez, Bonnie bartel, peroxisome function, biogenesisand dynamics in plants. *J. Plant Physiol.* 176, 162–177. doi: 10.1104/pp.17.01050

Zandalinas, S. I., Fritschi, F. B., and Mittler, R. (2021). Global warming, climate change, and environmental pollution: Recipe for a multifactorial stress combination disaster. *Trends Plant Sci.* 26, 588–599. doi: 10.1016/j.tplants.2021.02.011

frontiers | Frontiers in Microbiology

TYPE Original Research
PUBLISHED 20 July 2023
DOI 10.3389/fmicb.2023.1220116

OPEN ACCESS

EDITED BY
Jian-Wei Guo,
Chinese Academy of Sciences (CAS), China

REVIEWED BY
Lian-Ming Liang,
Yunnan University, China
Rasappa Viswanathan,
Indian Council of Agricultural Research (ICAR), India

*CORRESPONDENCE
Chaoxi Luo
✉ cxluo@mail.hzau.edu.cn
Qinsheng Gu
✉ guqinsheng@caas.cn

RECEIVED 10 May 2023
ACCEPTED 04 July 2023
PUBLISHED 20 July 2023

CITATION
Guo Z, Wu H, Peng B, Kang B, Liu L, Luo C and Gu Q (2023) Identifying pathogenicity-related genes in the pathogen *Colletotrichum magnum* causing watermelon anthracnose disease *via* T-DNA insertion mutagenesis. *Front. Microbiol.* 14:1220116. doi: 10.3389/fmicb.2023.1220116

Identifying pathogenicity-related genes in the pathogen *Colletotrichum magnum* causing watermelon anthracnose disease *via* T-DNA insertion mutagenesis

Zhen Guo[1,2], Huijie Wu[1], Bin Peng[1], Baoshan Kang[1], Liming Liu[1], Chaoxi Luo[2]*and Qinsheng Gu[1]*

[1]National Key Laboratory for Germplasm Innovation and Utilization of Horticultural Crops, Zhengzhou Fruit Research Institute, Chinese Academy of Agricultural Sciences, Zhengzhou, China, [2]National Key Laboratory for Germplasm Innovation and Utilization for Fruit and Vegetable Horticultural Crops, College of Plant Science and Technology, Huazhong Agricultural University, Wuhan, China

Fruit rot caused by *Colletotrichum magnum* is a crucial watermelon disease threatening the production and quality. To understand the pathogenic mechanism of *C. magnum*, we optimized the *Agrobacterium tumefaciens*-mediated transformation system (ATMT) for genetic transformation of *C. magnum*. The transformation efficiency of ATMT was an average of around 245 transformants per 100 million conidia. Southern blot analysis indicated that approximately 75% of the mutants contained a single copy of T-DNA. Pathogenicity test revealed that three mutants completely lost pathogenicity. The T-DNA integration sites (TISs) of three mutants were Identified. In mutant Cm699, the TISs were found in the intron region of the gene, which encoded a protein containing AP-2 complex subunit σ, and simultaneous gene deletions were observed. Two deleted genes encoded the transcription initiation protein SPT3 and a hypothetical protein, respectively. In mutant Cm854, the TISs were found in the 5′-flanking regions of a gene that was similar to the *MYO5* encoding Myosin I of *Pyricularia oryzae* (78%). In mutant Cm1078, the T-DNA was integrated into the exon regions of two adjacent genes. One was 5′-3′ exoribonuclease 1 encoding gene while the other encoded a WD-repeat protein retinoblastoma binding protein 4, the homolog of the MSl1 of *Saccharomyces cerevisiae*.

KEYWORDS

fungal transformation, ATMT, T-DNA integration, virulence gene, *Colletotrichum magnum*

Introduction

Colletotrichum magnum, is one of the major pathogens causing watermelon anthracnose (Rossman et al., 2016; Damm et al., 2019; Guo et al., 2022). Recently, it was reported on *Cucumis sativus*, *Capsicum* spp., *Lagenaria siceraria*, *Lobelia chinensis*, and *Luffa cylindrica* in China (Tsay et al., 2010; Li et al., 2013; Liu F. et al., 2022). *C. magum*, whoes conidia were larger than those of other *Colletotrichum* species, belongs to *C. magum* species complex (Damm et al., 2019). When *Colletotrichum* species infect the host, they establish biotrophic and necrotrophic lifestyles (Munch et al., 2008). To colonize host tissues, pathogens of *Colletotrichum* species generally

form appressoria which penetrate the epidermis of the host using penetration pegs. The formation of appressoria usually begins with the germination of conidia (Tucker and Talbot, 2001). In the biotrophic phase of the pathogen, the primary hyphae infect the epidermal and mesophyll cells and do not cause macroscopically visible damage to the host (De Silva et al., 2017). Subsequently, when differentiation of the primary hyphae produces secondary hyphae that spread throughout host tissue, the necrotrophic infection phase occurs (Wharton et al., 2001; Moraes et al., 2015).

The taxonomy, population structure, and disease epidemiology of *C. magnum* have been extensively studied (Damm et al., 2019). However, little is known about the pathogenicity of *C. magnum*. *Agrobacterium tumefaciens*-mediated transformation (ATMT) allows the study of numerous fungi to discover candidate pathogenic genes (Tsuji et al., 2003; Lawrence et al., 2010; Zhang et al., 2013; Martinez-Cruz et al., 2017; Li et al., 2019; Binh et al., 2021; Chauhan et al., 2021). Compared to conventional transformation methods, this approach provides a high percentage of T-DNA single-copy integration (De Groot et al., 1998; Münch et al., 2011) and is suitable for random insertional mutagenesis. The T-DNA integration sites (TISs) of transformants labeled with T-DNA can be easily identified (Liu et al., 1995; Sun et al., 2019).

The molecular determinants of fungal pathogenicity remain to be clarified and require more attention. Depending on the method of plant infection and the genome size of the fungus, fungi presumably containing 60–360 virulence genes (Idnurm and Howlett, 2001). Some genes that play important roles in signal cascades, cell wall degradation, the formation of infection structures, respond to the host environment, participat in the synthesis of toxins, and avoid and overcom plant defenses, have been identified as virulence or pathogenicity genes (Idnurm and Howlett, 2001; Werner et al., 2007; Gong et al., 2022; Jiao et al., 2022). To form an infection structure, fungi secrete effector molecules, such as the mutant of *C. higginsianum* is deficient in dihydroxynaphthalene melanin metabolism and is unable to form mature and infectious appressoria, thereby exhibiting reduced pathogenicity (Liu et al., 2013). In *C. gloeosporioides* and *Magnaporthe grisea*, the protein encoded by the protein kinase A is necessary for the mature appressorium to mediated plant infection (Gilbert et al., 2006; Cai et al., 2013). In *C. lindemuthianum*, the transcriptional activator gene (*CLTA1*) is disrupted, and mutant H433 cannot form necrotrophic secondary hyphae (Dufresne et al., 2000). Furthermore, allantoicase genes may participate in appressorium formation in *C. graminicola* (Münch et al., 2011).

In the present study, we established a stable ATMT protocol for *C. magnum* and generated a library of hygromycin B transformants. In the virulence assays on leaves, three mutants with defective pathogenicity were generated. The TISs of the three mutants were identified. Six putative pathogenic genes were identified.

Materials and methods

Fungus and plasmid preparation

The *C. magnum* wild-type (WT) strain CAASZK4 was isolated from watermelons in Kaifeng City, Henan Province, China (Guo et al., 2022). The strain AGL-1 of *A tumefaciens*, containing plasmid pATMT1 which carries a hygromycin B resistance cassette, was used as a T-DNA donor for fungal transformation (Zheng et al., 2011; Li et al., 2019).

ATMT of *Colletotrichum magnum*

The WT strain (CAASZK4) were grown on potato dextrose agar (PDA) medium complemented with a range of hygromycin B concentrations (0, 20, 40, 60, 80, 100, 150, 200, and 250 mg/L) and were incubated at 27°C in darkness for 7 d.

ATMT-based transformation of *C. magnum* was performed according to the protocol described by Cai et al. with slight modifications (Cai et al., 2013). The AGL-1 strain grew at 28°C in 5 mL of Luria–Bertani (LB) medium supplemented 25 mg/L rifampicin and 50 mg/L kanamycin. Cultures were centrifuged again. Finally, the cells were resuspended in induction medium (IM, Bundock et al., 1995) supplemented with acetosyringone (AS, 200 μM), and incubated for 6 h to achieve OD600 nm values (0.6–0.8).

C. magnum grew on synthetic nutrient-poor agar medium (SNA, Nirenberg, 1976) for 25 d at 27°C in the dark. Subsequently, the conidia of *C. magnum* were cleaned thrice sterile water and diluted in IM to achieve different concentrations (1×10^6–1×10^8 spores/ml). Aliquots of 100 μL of bacterial culture and 100 μL of conidial suspension were plated onto the 0.45 μm pore nitrocellulose filter of the co-cultivation medium (CM) containing 200 μM AS. After cocultivation for 84 h at 23°C in the dark, the membranes were transferred to PDA containing 200 mg/L cefotaxime, 100 mg/L timentin, and 80 mg/L hygromycin B, and cultured for 18 d at 27°C in the dark. Mycelial plugs from the edges where fresh mycelia were cultured on PDA containing 80 mg/L hygromycin B were used to confirm resistance. To determine the mitotic stability of the transformants, 40 randomly selected transformants were cultured on PDA without hygromycin B for four generations and then transferred back to PDA with hygromycin B.

DNA extraction and sequence analysis

The transformants and the WT strains of *C. magnum* were transferred to 100 mL fresh liquid PDA and cultured for 20 d at 27°C in the dark. Genomic DNA of 40 transformants and the WT strains of *C. magnum* were extracted by CTAB (Sangon Biotech, China).

To analyze genome integration of the transferred genes, the *hph* gene was amplified using the primer pair hph-F + hph-R (Table 1) and sequenced. PCR was were performed according to the protocol described by Guo et al. with slight modifications (Guo et al., 2022). The annealing temperature of *hph* was 60°C. PCR amplicons were purified and sequenced by Sangon Biotech Company (Shanghai, China).

The digestion of genomic DNA from 40 transformants or WT strains with *Eco*RI and *Hind*III (NEB, Ipswich, United States), electrophoresised on 0.75% agarose, were depurated, and transferred to nylon membranes (Hybond-N+; General Electric Company, Boston, United States). In the hybridization experiments, the digoxigenin (DIG) labeled probe corresponded to 1,380 bp *hph* of T-DNA from plasmid pATMT1 (Figure 1), and the *hph* gene was amplified using the primers hph-F and hph-R. Hybridization and chemiluminescence detection of the hybridized Dig-labeled probes were performed using the DIG High Prime DNA Labeling and Detection Starter Kit (Roche, Germany).

Pathogenicity assay and morphological characterization of transformants

Mycelial plugs (5 mm) from 1,460 transformants and WT strains of *C. magnum* were cultured in PDA at 27°C in the dark for 5–15 d. The pathogenicity of these transformants and WT strain was evaluated on healthy detached watermelon leaves (*Citrullus lanatus* cv. Hongheping, 5–6 true leaves), which were previously washed with tap water, surface-sterilized with 75% ethanol for 30 s, and rinsed thrice with sterile water. Mycelial discs (5 mm in diameter) were individually placed on the right half of the leaves. PDA blocks (5 mm in diameter) were placed on the left half of the same leaves as controls. All leaves were incubated in sealed sterile plastic plates at 27°C in the dark. Leaf symptoms were assessed at 4 d post-inoculation. All transformants and WT strains were tested in triplicates.

TABLE 1 Primer list used in TAIL-PCR.

Name	Sequence (5′ → 3′)	Reference
hph-F	ATTGAAGGAGCATTTTTTGGGC	This study
hph-R	CTATTCCTTTGCCCTCGGAC	This study
L1	GGGTTCCTATAGGGTTTCGCTCATG	Mullins et al. (2001)
L2	CATGTGTTGAGCATATAAGAAACCCT	Mullins et al. (2001)
L3	GAATTAATTCGGCGTTAATTCAGT	Mullins et al. (2001)
R1	GGCACTGGCCGTCGTTTTACAAC	Mullins et al. (2001)
R2	AACGTCGTGACTGGGAAAACCCT	Mullins et al. (2001)
R3	CCCTTCCCAACAGTTGCGCA	Mullins et al. (2001)
AD1[a]	NGTCGASWGANAWGAA	Liu et al. (1995)
AD2	NTCGASTWTSGWGTT	Liu et al. (1995)
AD3	TGWGNAGSANCASAGA	Sessions et al. (2002)

Mycelial plugs (5 mm) from transformants and WT strains were transferred on 60 mm Petri dishes containing SNA medium, and incubated in the dark at 27°C for 25 d. The mycelia, conidia, and appressoria were observed under a light microscopy (Olympus BX51, Japan). The conidia formed in 60-mm Petri dishes were cleaned thrice with sterile water and resuspended in 1 mL sterile water. The number of conidia was calculated using a hemocytometer. To induce the formation of appressoria, the conidia were suspended in 1% glucose and incubated at 27°C in the dark. After 48 h, the germination rate of the conidia was measured. All transformants and WT strains were tested in triplicates.

Cloning and sequencing of flanking T-DNA sequences

The T-DNA flanking sequences inserted into the genome were cloned using thermal asymmetric interlaced PCR (TAIL-PCR) protocol with minor modification (Liu et al., 1995; Mullins et al., 2001). Right border primers (R1, R2, and R3) and left border primers (L1, L2, and L3) and arbitrary degenerate primers (AD1, AD2, and AD-3) were utilized for TAIL-PCR (Table 1). PCR conditions were set as described by Mullins and Sessions (Mullins et al., 2001; Sessions et al., 2002), with minor modifications (Supplementary Table S1). The third TAIL-PCR products of all transformants displaying the highest brightness were purified using the FastPure Gel DNA Extraction Mini Kit (Vazyme, China). This fragment was ligated to the vector pTOPO-Blunt, which was transferred into *Escherichia coli* strain Top10 using a CV16-Zero Background pTOPO-Blunt Cloning Kit (Aidlab, China). *E. coli* harboring the pTOPO-Blunt vector was sequenced by Sangon Biotech Company (Shanghai, China). To isolate the tagged genes, the sequences flanking the T-DNA of each transformant were used

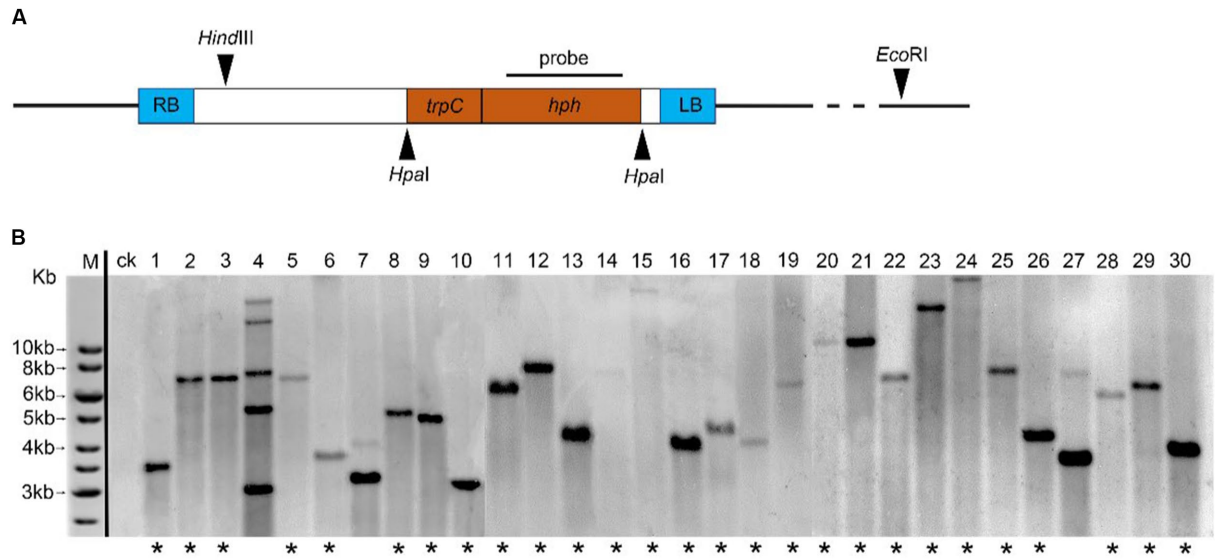

FIGURE 1
Analysis of T-DNA copy number in *C. magnum* transformants generated by *Agrobacterium tumefaciens*-mediated transformation (ATMT). **(A)** Probe used for hybridization, *Hind*III and *Eco*RI restriction sites are indicated; **(B)** Genomic Southern blot analysis of 30 transformants of *C. magnum* (1–30) generated by ATMT. Genomic DNA was restricted with *Hind*III and *Eco*RI. One band (lanes marked with an asterisk) represents a single T-DNA integration event 20, 22, and 28 represent genomic Southern blot analysis of Cm699, Cm854, and Cm1078, respectively.

to search the local genome database of WT *C. magnum* by BLAST+.[1] Gene structure was predicted using the *C. fioriniae*, *C. gloeosporioides*, *C. graminicola*, *C. higginsianum*, *C. orbiculare*, and *C. sublineola* by the FGENESH program.[2]

Whole-genome resequencing and analyses

Four micrograms of high-quality genomic DNA from three transformants (Cm699, Cm854, and Cm1078) were extracted from fresh mycelia using CTAB (Sangon Biotech, China) and used to construct a sequencing library, following the manufacturer's instructions (Illumina Inc.). Paired-end sequencing libraries with an insert size of approximately 200 or 400 bp were sequenced using an Illumina HiSeq 2,500, NovaSeq 6,000, or MiSeq sequencer, with a reading length of 150 bp. In total, more than 6 GB of sequence data were generated for each transformant. The upstream and downstream genome sequences (500 bp) of the TISs were obtained using a comprehensive approach called TDNAscan[3] searches against the genome database of WT *C. magnum* CAASZK4 (Sun et al., 2019). Using the GFF3 file of WT *C. magnum* as a reference genome organism, TDNAscan annotated all identified T-DNA insertions. Sequence homology searches were performed using NCBI protein database.[4]

Primers were designed to validate the TISs, T-DNA integration patterns, and deleted genes of Cm699, (Supplementary Table S2).

Results

Establishing a transformant library of *Colletotrichum magnum* using ATMT

To determine the hygromycin B sensitivity of *C. magnum*, the CAASZK4 strain was incubated on PDA supplemented with various concentrations of hygromycin B. These results indicate that the growth of *C. magnum* was inhibited by 60 mg/L hygromycin (Supplementary Figure S1). To exclude the possibility of false-positive transformants, 70 mg/L was chosen for the subsequent selection of resistant transformants.

Using the modified ATMT protocol, we obtained a library containing 1,460 transformants of the watermelon pathogen *C. magnum*. On an average, 245 transformants were generated from 10^8 conidia. Analysis of 40 randomly selected transformants harboring hygromycin B resistance revealed that all 40 transformants showed mitotically stable integrated T-DNA. These transformants, which were successively cultured for four generations on PDA medium without the selection marker hygromycin B, did not result in the loss of integrated T-DNA, as shown by the ability of all 40 transformants to grow on the screening medium containing hygromycin B and *hph* gene amplification analysis (Supplementary Figures S2, S3).

T-DNA copy number variation of transformants

To effectively identify the T-DNA integration events in the mutant library, 40 randomly selected transformants and WT strains were subjected to genomic Southern blot hybridization. Genomic DNA digested using *Eco*RI and *Hind*III was detected with the digoxigenin (Dig)-labeled probe harboring 1,380 bp *hph* gene (Figure 1A). Of the tested transformants, 30 displayed single-site TISs, nine harbored two TISs, and one harbored more than two TISs. Representative selections of 30 transformants are shown in Figure 1B.

Identification of transformants with reduced pathogenicity

In total 1,460 transformants were analyzed for pathogenicity on detached leaves. Fourteen transformants were screened out for their strongly reduced virulence and further identified and analyzed on watermelon leaves. The three transformants of the 14 strains exhibited strongly reduced virulence in leaves assays. Interestingly, the three transformants (Cm699, Cm854, and Cm1078) caused no visible disease symptoms in watermelon leaves (Figure 2).

Morphological and growth characterization of transformants with reduced pathogenicity

Three transformants (Cm699, Cm854, and Cm1078) exhibited significant morphology alterations compared to the WT strain (Figure 2). Of the three transformants, the hyphae of Cm699 showned severe deformity and pigment deposition compared to those of the WT strain (Figure 2); Cm699 and Cm1078 did not produce conidia, whereas Cm854 produced significantly fewer conidia than the WT strain (Figure 3A). In addition, the conidia germination rates of Cm854 were significantly lower than those of the WT strain (Figure 3B).

The growth rates of Cm699 (2.5) and Cm854 (10.8) were significantly lower than those of the WT strain (11.9), and there was no significant difference between the Cm1078 (11.6) and WT strains (Figure 4).

Identification of T-DNA insertion sites

According to genomic Southern blot experiments, three transformants (Cm699, Cm854, and Cm1078) harbored single T-DNA integrations (Figure 1B). To identify the genomic loci of the transformants where T-DNA was inserted, TAIL-PCR was performed on three pathogenic transformants. PCR fragments displayed more specific and higher intensity bands in the third round than those in the first and second of TAIL-PCRs (Supplementary Figure S5). Thus, PCR amplicons resulting from the third round of TAIL-PCR were cloned and sequenced. Three genomic DNA sequences flanking the left and right border of the T-DNA ranging from 0.7 to 3.0 kb were obtained, respectively. In two transformants (Cm699 and Cm1078),

1 https://blast.ncbi.nlm.nih.gov/Blast.cgi
2 http://linux1.softberry.com/berry.phtml
3 https://github.com/BCH-RC/TDNAscan
4 http://www.ncbi.nlm.nih.gov

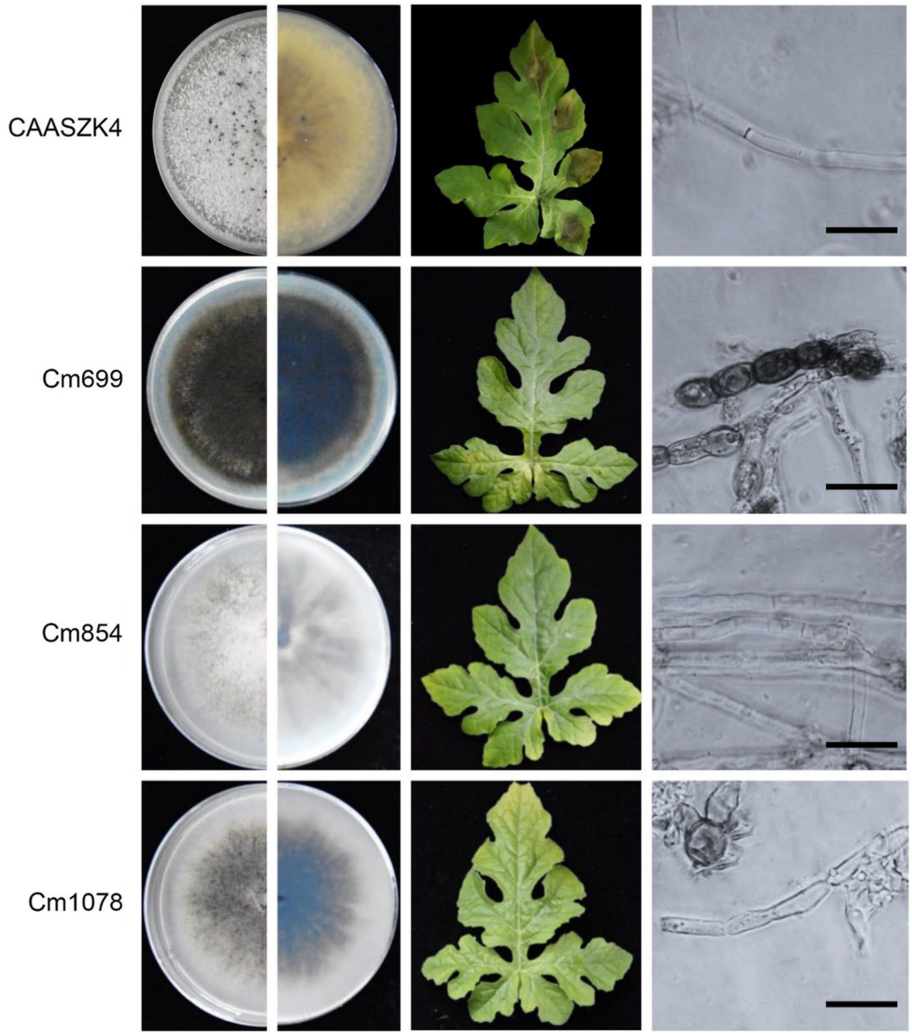

FIGURE 2
Phenotype and pathogenic development of *C. magnum* transformants produced by *Agrobacterium tumefaciens*-mediated transformation (ATMT). The phenotype during axenic growth on PDA is shown in the left panel. Pathogenicity assays on detached watermelon leaves (4 days post-inoculation (dpi)). Structure of *C. magnum* transformants mycelia. Bars represent 50 μm.

comparison of the sequences flanking the left and right border of the T-DNA with the genome sequence of WT *C. magnum* revealed significant similarities (Table 2). However, the sequence flanking the T-DNA of Cm854 showed no significant similarity with the genomic sequence of WT *C. magnum*. A analysis of T-DNA insertions demonstrated that two transformants (Cm699 and Cm1078) had interrupted protein-coding genes (Table 3).

To further localize and characterize the TISs, whole-genome resequencing data from three transformants (Cm699, Cm854, and Cm1078) were utilized. Six T-DNA insertions in the three transformants were identified using TDNAscan (Table 4). However, all T-DNA insertions in the two transformants (Cm854 and Cm1078) were truncated (Table 5; Supplementary Figure S5). Furthermore, two T-DNA integration patterns, single-copy T-DNA with complete LB and RB and truncated tandem T-DNA repeats of LB or RB, were found in *C. magnum* (Figure 5). Using the local genome database of WT *C. magnum* as a reference genome, we found that T-DNA integration of transformant Cm699 occurred in the intron region starting 1,336-bp downstream of the start codon of the AP-2 complex subunit σ gene, and two genes were deleted, in the integration process. (Figure 5A). Based on whole-genome resequencing data, the two deleted genes were predicted to be the transcription initiation protein gene and hypothetical gene, respectively (Table 5). Furthermore, integration occurred within the promoter region 217-bp upstream of the start codon of the Myosin I gene in the transformant Cm854 (Figure 5B). In the Cm1078 transformant, the integration had in the exon region of two adjacent genes, one exon region starting 893-bp downstream of the start codon of WD-repeat protein retinoblastoma binding protein 4 gene (*RBBP4*), while the other exon region starting 4,812-bp upstream of the termination codon of 5′-3′exoribonuclease 1 gene (*XRN1*) (Figure 5C).

Discussion

C. magnum is a crcucial fungus that induces watermelon anthracnose (Damm et al., 2019). Understanding the mechanisms

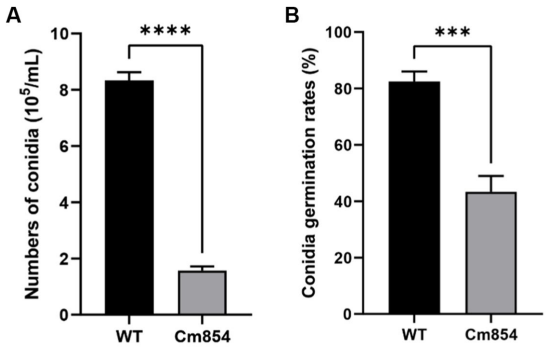

FIGURE 3
Numbers of conidia and the conidia germination rates of the wild-type (WT) strain CAASZK4 and of mutant Cm854. **(A)** Numbers of conidia of the wild-type (WT) strain and of mutant Cm854; **(B)** Conidia germination rates of the wild-type (WT) strain CAASZK4 and of mutant Cm854. Data were analysed with GraphPad Prism 9.0 (https://www.graphpad.com/). Asterisks over the error bars indicate the significant difference at the $p = 0.05$ level.

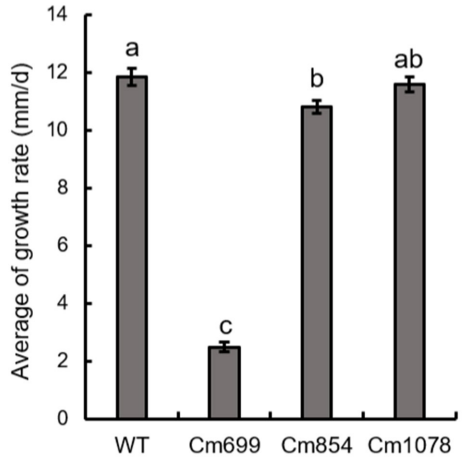

FIGURE 4
The growth rate of the three pathogenicity mutants and WT strains obtained in this study. Data were analysed with SPSS Statistics 19.0 (WinWrap Basic; http://www.winwrap.com) by one-way analysis of variance, and means were compared using Duncan's test at a significance level of $p = 0.05$. Letters over the error bars indicate the significant difference at the $p = 0.05$ level.

of its pathogenesis will facilitate disease management. ATMT is an effective method for exploring pathogenicity associated genes in pathogenic fungi (Fitzgerald et al., 2003; Leclerque et al., 2004; White and Chen, 2006; Zhang et al., 2013; Li et al., 2019; Villena et al., 2020; Binh et al., 2021; Casado-Del Castillo et al., 2021; Chauhan et al., 2021; Liu et al., 2021). Howerever, this method has not been applied to *C. magnum*. In this study, we optimized the ATMT protocol for the stable transformation of *C. magnum*, yielding130–360 (average = 245) transformants per 10^8 spores.

The mode and frequency of T-DNA insertions into the pathogenic genome are vital for the identification of disrupted genes. In *Magnaporthe oryzae*, not only single-copy T-DNA integration into genome, but multi-copy integration of the entire Ti-plasmid was found (Li et al., 2007). In this study, 75% of the transfromants had a single copy of T-DNA randomly located in the genome, whereas only approximately 2% multi-copy integration was found, which was consistent with previous reports (Münch et al., 2011). The transformants generated using the ATMT protocol, in combination with the identification of TISs, were used to determine the virulence factors of *C. magnum*, which can be applied in forward genetics.

Pathogenically defective transformants were predicted through the pathogenicity assay of the transformants, which were obtained using ATMT protocol for *C. magnum*. The penetration barriers (cuticle and epidermis) of the host are the main structures that defend against pathogenic infections. If both penetration barriers are destroyed and the quiescent infection is dispruted, the transformants are capable of colonizing the host tissues (Takano et al., 2000; Tsuji et al., 2003). Beacuse the defense reaction of young leaves is incomplete compared to that of old leaves when the host is infected by fungi, young leaves are more suitable for screening and assessing the pathogenicity of transformants (Cai et al., 2013). In this study, pathogenicity assay for all transformants was conducted on healthy and wounded watermelon leaves (5–6 true leaves), and the mycelium of the pathogen was used to inoculate watermelon leaves. Of these, compared with the WT strain, three transformants revealed no pathogenicity and 11 transformants showed impaired pathogenicity on healthy detached watermelon leaves (Figure 2; Supplementary Figure S6). It may be that potential pathogenic genes of three transformants affected the ability of the mycelium to infect the host.

As the integration of T-DNA into the genome of the pathogen affected the expression of pathogenic genes of pathogen, defective transformants were obtained. Hence, the TISs analysis was necessary. To identify the location and mode of the T-DNA insertions into the fungal genome, flanking sequence analysis was performed *via* TAIL-PCR (Huser et al., 2009; Liu et al., 2013). However, the application of TAIL-PCR for the identification of TISs was limited because the left and/or right ends of T-DNA can be truncated before insertion into the genome (Schouten et al., 2017). In this study, no LB-or RB-flanking sequences were cloned from the Cm854 transformants. For the Cm1078 transformants, LB flanking sequences were not cloned. This result may be explained by the truncation of LB, similar to observations in other fungi (Maruthachalam et al., 2008; Cai et al., 2013). Next-generation sequencing technologies have complemented the deficiency of TAIL-PCR for T-DNA site identification. The TISs of three transformants (Cm699, Cm854, and Cm1078) were successfully identified using whole-genome resequencing data (Table 5). Moreover, the sequences of 500 bp flanking TISs and the position of TISs in the genome of *C. magnum* were obtained using TDNAscan. Notably, the TISs of Cm699 and Cm1078 examined using TDNAscan were consistent with those obtained using TAIL-PCR (Tables 3, 5).

Some genes regulate infection-related morphogenesis during pathogenesis (Idnurm and Howlett, 2001). In the present study, six potentially pathogenic genes were identified. One potential pathogenicity gene encoded a protein containing the AP-2 complex subunit σ. AP-2 complexes were composed of four subunits: two large subunits (β2 and α), a medium subunit μ, and

a small subunit σ (Liu C. et al., 2022). In *S. cerevisiae*, AP2 has been shown to facilitate the formation of the major class of endocytic vesicles (Myers and Payne, 2013; Lu et al., 2016). Moreover, we found that two genes were deleted in the transformant Cm699 (Figure 5A), which was probably a result of T-DNA integration employing double-strand break repair (Kleinboelting et al., 2015). These two genes may also be potential pathogenic genes that are not similar to known genes in fungi, and may be novel fungal pathogenic factors. T-DNA insertion into the promoter region of the potential pathogenicity gene was probably the main element responsible for the observed pathogenic defect in the transformant (Lee et al., 1990). In the transformant Cm854, the observed pathogenicity defect was presumably the reason for the disruption of the promoter region of a gene encoding Myosin I, which shares sequence homology with *MYO5* of *Pyricularia oryzae* (78%) by T-DNA integration. In *S. cerevisiae*, although the

TABLE 2 The sequences flanking left border and the right border of the T-DNA were aligned to the genome sequence of WT *C. magnum* by BLAST+.

Sequence	Chromosome	Position	Alignment length	Identify (%)	*e*-value
The left border of Cm699	Contig00001	4,448,487–4,450,001(−)	1,517	99.67	0
The right border of Cm699	Contig00001	4,438,996–4,439,880(−)	893	99.78	0
The right border of Cm1078	Contig00001	2,064,712–2,065,424(−)	715	99.02	0

TABLE 3 Summary of *C. magnum* genes identified from T-DNA flanking sequences.

Mutant	Open reading frame (ORF) predicted		Best BLAST match with functional annotation		
	T-DNA insertion[c]	Score	Putative function (NCBI accession no.)	Organism	*e*-value
Cm699-L[a]	1,583 bp upstream	35.71	Pro-apoptotic serine protease (XP_045270804.1)	*Colletotrichum gloeosporioides*	0
Cm699-R[b]	In ORF	53.30	AP-2 complex subunit σ(XP_045270800.1)	*Colletotrichum gloeosporioides*	7.00E-118
Cm1078-R	In ORF	32.45	histone-binding protein RBBP4 (XP_038750499.1)	*Colletotrichum karsti*	3.00E-108

[a]Genomic DNA sequences flanking the left border of the T-DNA.
[b]Genomic DNA sequences flanking the right border of the T-DNA.
[c]Putative position relative to open reading frame (ORF). Distance upstream of predicted start codon of predicted stop codon.

TABLE 4 T-DNA insertions identified by TDNAscan.

Mutant	Chromosome	Position	Informative reads	T-DNA truncation	Strand	Freq	Annotation
Cm699	Contig00001	4,439,884	CLR:8, DIR:0	tdna_st:-, tdna_end:282	–	1	intron
	Contig00001	4,448,487	CLR:18, DIR:3	tdna_st:6579, tdna_end:-	–	1	–
Cm854	Contig00005	7,323,116	CLR:55, DIR:0	tdna_st:-, tdna_end:282	–	1	–
	Contig00005	7,323,128	CLR:43, DIR:1	tdna_st:-, tdna_end:281	+	1	–
Cm1078	Contig00001	2,065,426	CLR:58, DIR:0	tdna_st:-, tdna_end:276	–	1	exon
	Contig00001	2,066,904	CLR:43, DIR:0	tdna_st:-, tdna_end:283	+	1	exon

TABLE 5 Summary of *C. magnum* genes identified from whole genome re-sequencing.

Mutant	Chromosome	Position	Annotation	Putative function
Cm699	Contig00001	4,438,548–4,440,264(−)	EVM0011112	AP-2 complex subunit σ
	Contig00001	4,441,377–4,445,085(−)	EVM0004795	Transcription initiation protein SPT3
	Contig00001	4,446,661–4,447,361(−)	EVM0008660	Hypothetical protein
	Contig00001	4,449,487–4,453,700(+)	EVM0012133	Pro-apoptotic serine protease
Cm854	Contig00005	7,319,862–7,322,530(+)	EVM0006621	Hypothetical protein
	Contig00005	7,323,345–7,327,847(+)	EVM0013725	Myosin I
Cm1078	Contig00001	2,064,140–2,066,069(−)	EVM0005516	Histone-binding protein RBBP4
	Contig00001	2,066,586–2,071,716(+)	EVM0003471	5′-3′ exoribonuclease 1

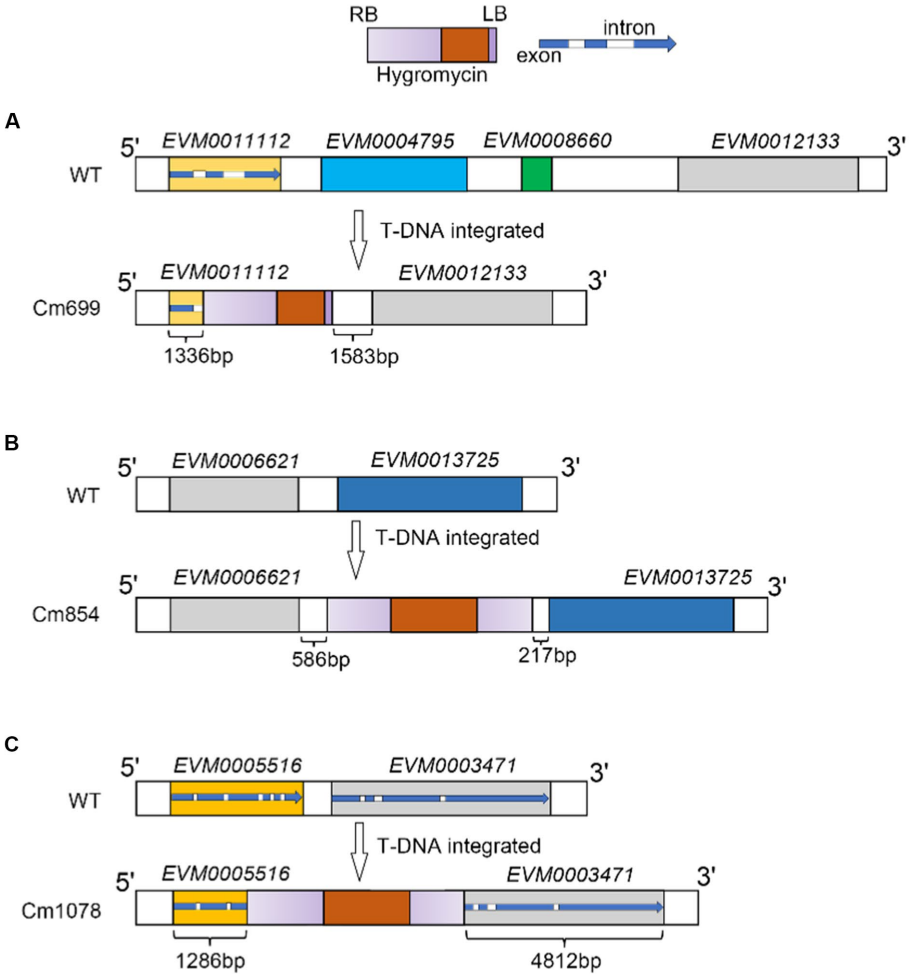

FIGURE 5
T-DNA integration sites patterns of T-DNA integration and in transformants Cm699, Cm854, and Cm1078. **(A)**, **(B)**, **(C)** Illustration of T-DNA integration into Cm699, Cm854, and Cm1078, respectively. The rectangle in gradient purple represents the ideal T-DNA between LB and RB. The rectangle in orange represents the T-DNA fragment coding the hygromycin resistance gene. In the blue arrow, the blue represents the exon as well as the white represents the intron. The integration sites were identified by whole genome re-sequencing in the text.

phenotype of *MYO5* deletion mutants did not change, growth and actin cytoskeletal organization were affected (Goodson et al., 1996). The observed pathogenicity defect in the transformant Cm1078 was possibly a result of a T-DNA insertion into the region of between two adjacent genes, which were simultaneously disrupted. One gene encoded a WD-repeat protein RBBP4, which also known as chromatin-remodeling factor RBAP48, shares sequence homology with MSl1 of *S. cerevisiae* (Ruggieri et al., 1989; Qian et al., 1993; Miao et al., 2020). Furthermore, the *MSl1* gene could suppress the defects in *S. cerevisiae* sporulation (Ruggieri et al., 1989). The other gene encoded a protein, which exhibited homology with the *XRN1* of *S. cerevisiae*, was not only involved in the termination of DNA transcription, but also in RNA degradation (Hsu and Stevens, 1993; Kim et al., 2004; Sharma et al., 2022).

In summary, the modified ATMT protocol is suitable for identifying novel genes required for the pathogenicity of the watermelon pathogen *C. magnum*. Six potential virulence genes were identified in *C. magnum*. These findings provide foundation for the pathogenic mechanism of *C. magnum*.

Data availability statement

The datasets presented in this study can be found in online repositories. The names of the repository/repositories and accession number(s) can be found in the article/Supplementary material.

Author contributions

QG and ZG conceptualized the study and designed the experiments. ZG performed the experiments, acquired and analyzed the data, and drafted the original manuscript. HW, CL, and QG reviewed and edited the manuscript. BP, BK, LL, HW, and QG supervised the work. All authors contributed to the article and approved the submitted version.

Funding

This work was financially supported by Agricultural Science and Technology Innovation Program (CAAS-ASTIP-2022-ZFRI-09).

Conflict of interest

The authors declare that the research was conducted in the absence of any commercial or financial relationships that could be construed as a potential conflict of interest.

Publisher's note

All claims expressed in this article are solely those of the authors and do not necessarily represent those of their affiliated organizations, or those of the publisher, the editors and the reviewers. Any product that may be evaluated in this article, or claim that may be made by its manufacturer, is not guaranteed or endorsed by the publisher.

Supplementary material

The Supplementary material for this article can be found online at: https://www.frontiersin.org/articles/10.3389/fmicb.2023.1220116/full#supplementary-material

References

Binh, C. T., Thai, H. D., Ha, B. T. V., and Tran, V. T. (2021). Establishment of a new and efficient agrobacterium-mediated transformation system in the nematicidal fungus Purpureocillium lilacinum. *Microbiol. Res.* 249:126773. doi: 10.1016/j.micres.2021.126773

Bundock, P., Den Dulk-Ras, A., Beijersbergen, A., and Hooykaas, P. J. (1995). Trans-kingdom T-DNA transfer from *Agrobacterium tumefaciens* to *Saccharomyces cerevisiae*. *EMBO J.* 14, 3206–3214. doi: 10.1002/j.1460-2075.1995.tb07323.x

Cai, Z., Li, G., Lin, C., Shi, T., Zhai, L., Chen, Y., et al. (2013). Identifying pathogenicity genes in the rubber tree anthracnose fungus Colletotrichum gloeosporioides through random insertional mutagenesis. *Microbiol. Res.* 168, 340–350. doi: 10.1016/j.micres.2013.01.005

Casado-Del Castillo, V., Maccabe, A. P., and Orejas, M. (2021). *Agrobacterium tumefaciens*-mediated transformation of NHEJ mutant aspergillus nidulans conidia: an efficient tool for targeted gene recombination using selectable nutritional markers. *J. Fungi* 7:961. doi: 10.3390/jof7110961

Chauhan, A., Modgil, M., and Rajam, M. V. (2021). Establishment of *Agrobacterium tumefaciens* - mediated genetic transformation of apple pathogen Marssonina coronaria using marker genes under the control of CaMV 35S promoter. *Microbiol. Res.* 253:126878. doi: 10.1016/j.micres.2021.126878

Damm, U., Sato, T., Alizadeh, A., Groenewald, J. Z., and Crous, P. W. (2019). The Colletotrichum dracaenophilum, C. magnum and *C. orchidearum* species complexes. *Stud. Mycol.* 92, 1–46. doi: 10.1016/j.simyco.2018.04.001

De Groot, M. J. A., Bundock, P., Hooykaas, P. J. J., and Beijersbergen, A. G. M. (1998). *Agrobacterium tumefaciens*-mediated transformation of filamentous fungi. *Nat. Biotechnol.* 16, 839–842. doi: 10.1038/nbt0998-839

De Silva, D. D., Crous, P. W., Ades, P. K., Hyde, K. D., and Taylor, P. W. J. (2017). Life styles of Colletotrichum species and implications for plant biosecurity. *Fungal Biol. Rev.* 31, 155–168. doi: 10.1016/j.fbr.2017.05.001

Dufresne, M., Perfect, S., Pellier, A. L., Bailey, J. A., and Langin, T. (2000). A GAL4-like protein is involved in the switch between biotrophic and necrotrophic phases of the infection process of Colletotrichum lindemuthianum on common bean. *Plant Cell* 12, 1579–1589. doi: 10.1105/tpc.12.9.1579

Fitzgerald, A. M., Mudge, A. M., Gleave, A. P., and Plummer, K. M. (2003). Agrobacterium and PEG-mediated transformation of the phytopathogen Venturia inaequalis. *Mycol. Res.* 107, 803–810. doi: 10.1017/s0953756203008086

Gilbert, M. J., Thornton, C. R., Wakley, G. E., and Talbot, N. J. (2006). A P-type ATPase required for rice blast disease and induction of host resistance. *Nature* 440, 535–539. doi: 10.1038/nature04567

Gong, Z., Ning, N., Li, Z., Xie, X., Wilson, R. A., and Liu, W. (2022). Two Magnaporthe appressoria-specific (MAS) proteins, MoMas3 and MoMas5, are required for suppressing host innate immunity and promoting biotrophic growth in rice cells. *Mol. Plant Pathol.* 23, 1290–1302. doi: 10.1111/mpp.13226

Goodson, H. V., Anderson, B. L., Warrick, H. M., Pon, L. A., and Spudich, J. A. (1996). Synthetic lethality screen identifies a novel yeast myosin I gene (MYO5): myosin I proteins are required for polarization of the actin cytoskeleton. *J. Cell Biol.* 133, 1277–1291. doi: 10.1083/jcb.133.6.1277

Guo, Z., Luo, C. X., Wu, H. J., Peng, B., Kang, B. S., Liu, L. M., et al. (2022). Colletotrichum species associated with anthracnose disease of watermelon (*Citrullus lanatus*) in China. *J. Fungi* 8:790. doi: 10.3390/jof8080790

Hsu, C. L., and Stevens, A. (1993). Yeast cells lacking 5′-->3′ exoribonuclease 1 contain mRNA species that are poly (a) deficient and partially lack the 5′ cap structure. *Mol. Cell. Biol.* 13, 4826–4835. doi: 10.1128/mcb.13.8.4826-4835.1993

Huser, A., Takahara, H., Schmalenbach, W., and O'connell, R. (2009). Discovery of pathogenicity genes in the crucifer anthracnose fungus Colletotrichum higginsianum, using random insertional mutagenesis. *Mol. Plant-Microbe Interact.* 22, 143–156. doi: 10.1094/mpmi-22-2-0143

Idnurm, A., and Howlett, B. J. (2001). Pathogenicity genes of phytopathogenic fungi. *Mol. Plant Pathol.* 2, 241–255. doi: 10.1046/j.1464-6722.2001.00070.x

Jiao, W., Yu, H., Cong, J., Xiao, K., Zhang, X., Liu, J., et al. (2022). Transcription factor SsFoxE3 activating SsAtg8 is critical for sclerotia, compound appressoria formation, and pathogenicity in Sclerotinia sclerotiorum. *Mol. Plant Pathol.* 23, 204–217. doi: 10.1111/mpp.13154

Kim, M., Krogan, N. J., Vasiljeva, L., Rando, O. J., Nedea, E., Greenblatt, J. F., et al. (2004). The yeast Rat1 exonuclease promotes transcription termination by RNA polymerase II. *Nature* 432, 517–522. doi: 10.1038/nature03041

Kleinboelting, N., Huep, G., Appelhagen, I., Viehoever, P., Li, Y., and Weisshaar, B. (2015). The structural features of thousands of T-DNA insertion sites are consistent with a double-strand break repair-based insertion mechanism. *Mol. Plant* 8, 1651–1664. doi: 10.1016/j.molp.2015.08.011

Lawrence, G. J., Dodds, P. N., and Ellis, J. G. (2010). Transformation of the flax rust fungus, Melampsora lini: selection via silencing of an avirulence gene. *Plant J.* 61, 364–369. doi: 10.1111/j.1365-313X.2009.04052.x

Leclerque, A., Wan, H., Abschutz, A., Chen, S., Mitina, G. V., Zimmermann, G., et al. (2004). Agrobacterium-mediated insertional mutagenesis (AIM) of the entomopathogenic fungus Beauveria bassiana. *Curr. Genet.* 45, 111–119. doi: 10.1007/s00294-003-0468-2

Lee, H., Fu, Y. H., and Marzluf, G. A. (1990). Nucleotide sequence and DNA recognition elements of alc, the structural gene which encodes allantoicase, a purine catabolic enzyme of Neurospora crassa. *Biochemistry* 29, 8779–8787. doi: 10.1021/bi00489a039

Li, J. X., Hong, N., Peng, B., Wu, H. J., and Gu, Q. S. (2019). Transformation of Corynespora cassiicola by *Agrobacterium tumefaciens*. *Fungal Biol.* 123, 669–675. doi: 10.1016/j.funbio.2019.05.011

Li, Q. L., Mo, J. Y., Huang, S. P., Guo, T. X., and Hsiang, T. (2013). First report of leaf spot disease caused by Glomerella magna on *Lobelia chinensis* in China. *Plant Dis.* 97:1383. dio. doi: 10.1094/PDIS-03-13-0346-PDN

Li, G., Zhou, Z., Liu, G., Zheng, F., and He, C. (2007). Characterization of T-DNA insertion patterns in the genome of rice blast fungus Magnaporthe oryzae. *Curr. Genet.* 51, 233–243. doi: 10.1007/s00294-007-0122-5

Liu, R., Kim, W., Paguirigan, J. A., Jeong, M. H., and Hur, J. S. (2021). Establishment of *Agrobacterium tumefaciens*-mediated transformation of *Cladonia macilenta*, a odmel lichen-ofrming ufngus. *J. Fungi* 7:252. doi: 10.3390/jof7040252

Liu, C., Li, Z., Tian, D., Xu, M., Pan, J., Wu, H., et al. (2022). AP1/2beta-mediated exocytosis of tapetum-specific transporters is required for pollen development in *Arabidopsis thaliana*. *Plant Cell* 34, 3961–3982. doi: 10.1093/plcell/koac192

Liu, F., Ma, Z. Y., Hou, L. W., Diao, Y. Z., Wu, W. P., Damm, U., et al. (2022). Updating species diversity of Colletotrichum, with a phylogenomic overview. *Stud. Mycol.* 101, 1–56. doi: 10.3114/sim.2022.101.01

Liu, Y.-G., Mitsukawa, N., Oosumi, T., and Whittier, R. F. (1995). Efficient isolation and mapping of *Arabidopsis thaliana* T-DNA insert junctions by thermal asymmetric interlaced PCR. *Plant J.* 8, 457–463. doi: 10.1046/j.1365-313X.1995.08030457.x

Liu, L., Zhao, D., Zheng, L., Hsiang, T., Wei, Y., Fu, Y., et al. (2013). Identification of virulence genes in the crucifer anthracnose fungus Colletotrichum higginsianum by insertional mutagenesis. *Microb. Pathog.* 64, 6–17. doi: 10.1016/j.micpath.2013.06.001

Lu, R., Drubin, D. G., and Sun, Y. (2016). Clathrin-mediated endocytosis in budding yeast at a glance. *J. Cell Sci.* 129, 1531–1536. doi: 10.1242/jcs.182303

Martinez-Cruz, J., Romero, D., De Vicente, A., and Perez-Garcia, A. (2017). Transformation of the cucurbit powdery mildew pathogen Podosphaera xanthii by *Agrobacterium tumefaciens*. *New Phytol.* 213, 1961–1973. doi: 10.1111/nph.14297

Maruthachalam, K., Nair, V., Rho, H. S., Choi, J., Kim, S., and Lee, Y. H. (2008). *Agrobacterium tumefaciens*-mediated transformation in Colletotrichum falcatum and *C. acutatum*. *J. Microbiol. Biotechnol.*. 18: 234–241. dio:

Miao, X., Sun, T., Barletta, H., Mager, J., and Cui, W. (2020). Loss of RBBP4 results in defective inner cell mass, severe apoptosis, hyperacetylated histones and

preimplantation lethality in micedagger. *Biol. Reprod.* 103, 13–23. doi: 10.1093/biolre/ioaa046

Moraes, S. R. G., Escanferla, M. E., and Massola, N. S. Jr. (2015). Prepenetration and penetration of Colletotrichum gloeosporioides into guava fruit (*Psidium guajava* L.): effects of temperature, wetness period and fruit age. *J. Phytopathol.* 163, 149–159. doi: 10.1111/jph.12294

Mullins, E., Chen, X., Romaine, P., Raina, R., Geiser, D., and Kang, S. (2001). Agrobacterium-mediated transformation ofFusarium oxysporum: an efficient tool for insertional mutagenesis and gene transfer. *Phytopathology* 91, 173–180. doi: 10.1094/PHYTO.2001.91.2.173

Munch, S., Lingner, U., Floss, D. S., Ludwig, N., Sauer, N., and Deising, H. B. (2008). The hemibiotrophic lifestyle of Colletotrichum species. *J. Plant Physiol.* 165, 41–51. doi: 10.1016/j.jplph.2007.06.008

Münch, S., Ludwig, N., Floss, D. S., Sugui, J. A., Koszucka, A. M., Voll, L. M., et al. (2011). Identification of virulence genes in the corn pathogen Colletotrichum graminicola by *Agrobacterium tumefaciens*-mediated transformation. *Mol. Plant Pathol.* 12, 43–55. doi: 10.1111/j.1364-3703.2010.00651.x

Myers, M. D., and Payne, G. S. (2013). Clathrin, adaptors and disease: insights from the yeast *Saccharomyces cerevisiae*. *Front. Biosci.* 18, 862–891. doi: 10.2741/4149

Nirenberg, H. (1976). Untersuchungen über die morphologische und biologische differenzierung in der Fusarium-Sektion Liseola. *Mitt. Biol. Bundesanst. für Land-und Forstwirtsch Berlin-Dahlem.* 169, 1–117.

Qian, Y. W., Wang, Y. C., Hollingsworth, R. E. Jr., Jones, D., Ling, N., and Lee, E. Y. (1993). A retinoblastoma-binding protein related to a negative regulator of Ras in yeast. *Nature* 364, 648–652. doi: 10.1038/364648a0

Rossman, A. Y., Allen, W. C., and Castlebury, L. A. (2016). New combinations of plant-associated fungi resulting from the change to one name for fungi. *IMA Fungus* 7, 1–7. doi: 10.5598/imafungus.2016.07.01.01

Ruggieri, R., Tanaka, K., Nakafuku, M., Kaziro, Y., Toh-e, A., and Matsumoto, K. (1989). MSI1, a negative regulator of the RAS-cAMP pathway in *Saccharomyces cerevisiae*. *Proc. Natl. Acad. Sci. U. S. A.* 86, 8778–8782. doi: 10.1073/pnas.86.22.8778

Schouten, H. J., Vande Geest, H., Papadimitriou, S., Bemer, M., Schaart, J. G., Smulders, M. J., et al. (2017). Re-sequencing transgenic plants revealed rearrangements at T-DNA inserts, and integration of a short T-DNA fragment, but no increase of small mutations elsewhere. *Plant Cell Rep.* 36, 493–504. doi: 10.1007/s00299-017-2098-z

Sessions, A., Burke, E., Presting, G., Aux, G., Mcelver, J., Patton, D., et al. (2002). A high-throughput Arabidopsis reverse genetics system. *Plant Cell* 14, 2985–2994. doi: 10.1105/tpc.004630

Sharma, S., Yang, J., Grudzien-Nogalska, E., Shivas, J., Kwan, K. Y., and Kiledjian, M. (2022). Xrn1 is a deNADding enzyme modulating mitochondrial NAD-capped RNA. *Nat. Commun.* 13:889. doi: 10.1038/s41467-022-28555-7

Sun, L., Ge, Y., Sparks, J. A., Robinson, Z. T., Cheng, X., Wen, J., et al. (2019). TDNAscan: a software to identify complete and truncated T-DNA insertions. *Front. Genet.* 10:685. doi: 10.3389/fgene.2019.00685

Takano, Y., Kikuchi, T., Kubo, Y., Hamer, J. E., Mise, K., and Furusawa, I. (2000). The Colletotrichum lagenarium MAP kinase gene CMK1 regulates diverse aspects of fungal pathogenesis. *Mol. Plant-Microbe Interact.* 13, 374–383. doi: 10.1094/MPMI.2000.13.4.374

Tsay, J. G., Chen, R. S., Wang, W. L., and Weng, B. C. (2010). First report of anthracnose on cucurbitaceous crops caused by Glomerella magna in Taiwan. *Plant Dis.* 94:787. doi: 10.1094/PDIS-94-6-0787A

Tsuji, G., Fujii, S., Fujihara, N., Hirose, C., Tsuge, S., Shiraishi, T., et al. (2003). *Agrobacterium tumefaciens*-mediated transformation for random insertional mutagenesis in Colletotrichum lagenarium. *J. Gen. Plant Pathol.* 69, 230–239. doi: 10.1007/s10327-003-0040-4

Tucker, S. L., and Talbot, N. J. (2001). Surface attachment and pre-penetration stage development by plant pathogenic fungi. *Annu. Rev. Phytopathol.* 39, 385–417. doi: 10.1146/annurev.phyto.39.1.385

Villena, C. I. F., Gomes, R. R., Fernandes, L., Florencio, C. S., Bombassaro, A., Grisolia, M. E., et al. (2020). *Agrobacterium tumefaciens*-mediated transformation of Fonsecaea monophora and Fonsecaea erecta for host-environment interaction studies. *J. Fungi* 6:325. doi: 10.3390/jof6040325

Werner, S., Sugui, J. A., Steinberg, G., and Deising, H. B. (2007). A chitin synthase with a myosin-like motor domain is essential for hyphal growth, appressorium differentiation, and pathogenicity of the maize anthracnose fungus Colletotrichum graminicola. *Mol. Plant-Microbe Interact.* 20, 1555–1567. doi: 10.1094/MPMI-20-12-1555

Wharton, P. S., Julian, A. M., and O'connell, R. J. (2001). Ultrastructure of the infection of *sorghum bicolor* by Colletotrichum sublineolum. *Phytopathology* 91, 149–158. doi: 10.1094/PHYTO.2001.91.2.149

White, D., and Chen, W. (2006). Genetic transformation of Ascochyta rabiei using agrobacterium-mediated transformation. *Curr. Genet.* 49, 272–280. doi: 10.1007/s00294-005-0048-8

Zhang, T., Qi, Z., Wang, Y., Zhang, F., Li, R., Yu, Q., et al. (2013). *Agrobacterium tumefaciens*-mediated transformation of Penicillium expansum PE-12 and its application in molecular breeding. *Microbiol. Res.* 168, 130–137. doi: 10.1016/j.micres.2012.11.001

Zheng, Z., Huang, C., Cao, L., Xie, C., and Han, R. (2011). *Agrobacterium tumefaciens*-mediated transformation as a tool for insertional mutagenesis in medicinal fungus Cordyceps militaris. *Fungal Biol.* 115, 265–274. doi: 10.1016/j.funbio.2010.12.011

frontiers | Frontiers in Microbiology

TYPE Original Research
PUBLISHED 11 August 2023
DOI 10.3389/fmicb.2023.1229454

OPEN ACCESS

EDITED BY
Osama Abdalla Abdelshafy Mohamad,
Chinese Academy of Sciences (CAS), China

REVIEWED BY
Yong-Hong Liu,
Chinese Academy of Sciences (CAS), China
Bao-zhu Fang,
Chinese Academy of Sciences (CAS), China

*CORRESPONDENCE
XueKun Zhang
✉ Zhangxk2459@163.com
Hui Xi
✉ xihui101101@126.com

†These authors have contributed equally to this work and share first authorship

RECEIVED 26 May 2023
ACCEPTED 31 July 2023
PUBLISHED 11 August 2023

CITATION
Tie Z, Wang P, Chen W, Tang B, Yu Y, Liu Z, Zhao S, Khan FH, Zhang X and Xi H (2023) Different responses of the rhizosphere microbiome to *Verticillium dahliae* infection in two cotton cultivars.
Front. Microbiol. 14:1229454.
doi: 10.3389/fmicb.2023.1229454

Different responses of the rhizosphere microbiome to *Verticillium dahliae* infection in two cotton cultivars

Zhanjiang Tie[1†], Peng Wang[2†], Weijian Chen[1], Binghui Tang[3], Yu Yu[2], Zheng Liu[1], Sifeng Zhao[1], Faisal Hayat Khan[1], XueKun Zhang[1*] and Hui Xi[1*]

[1]College of Agriculture, Shihezi University, Shihezi, Xinjiang, China, [2]Xinjiang Academy of Agricultural Reclamation Sciences, Shihezi, Xinjiang, China, [3]Cotton Research Institute, Shihezi Academy of Agricultural Sciences, Shihezi, Xinjiang, China

Verticillium wilt is a disastrous disease caused by *Verticillium dahliae* that severely damages the production of cotton in China. Even under homogeneous conditions, the same cotton cultivar facing *V. dahliae* tends to either stay healthy or become seriously ill and die. This binary outcome may be related to the interactions between microbiome assembly and plant health. Understanding how the rhizosphere microbiome responds to *V. dahliae* infection is vital to controlling Verticillium wilt through the manipulation of the microbiome. In this study, we evaluated the healthy and diseased rhizosphere microbiome of two upland cotton cultivars that are resistant to *V. dahliae*, Zhong 2 (resistant) and Xin 36 (susceptible), using 16S rRNA and ITS high-throughput sequencing. The results showed that the healthy rhizosphere of both resistant cultivar and susceptible cultivar had more unique bacterial ASVs than the diseased rhizosphere, whereas fewer unique fungal ASVs were found in the healthy rhizosphere of resistant cultivar. There were no significant differences in alpha diversity and beta diversity between the resistant cultivar and susceptible cultivar. In both resistant cultivar and susceptible cultivar, bacterial genera such as *Pseudomonas* and *Acidobacteria bacterium LP6*, and fungal genera such as *Cephalotrichum* and *Mortierella* were both highly enriched in the diseased rhizosphere, and *Pseudomonas* abundance in diseased rhizospheres was significantly higher than that in the healthy rhizosphere regardless of the cultivar type. However, cultivar and *V. dahliae* infection can cause composition changes in the rhizosphere bacterial and fungal communities, especially in the relative abundances of core microbiome members, which varied significantly, with different responses in the two cotton cultivars. Analysis of co-occurrence networks showed that resistant cultivar has a more complex network relationship than susceptible cultivar in the bacterial communities, and *V. dahliae* has a significant impact on the bacterial community structure. These findings will further broaden the understanding of plant-rhizosphere microbiome interactions and provide an integrative perspective on the cotton rhizosphere microbiome, which is beneficial to cotton health and production.

KEYWORDS

cotton, *Verticillium dahliae*, rhizosphere microbiome, 16S rRNA, ITS

Introduction

Under heterogeneity of local conditions, such as the genetic background and abundance of pathogens (Campbell, 1985; Genin and Denny, 2012), host genotypes (Kwak et al., 2018), soil or plant-related microbiome, and soil physicochemical properties (Wei et al., 2019), plants facing many pathogens either stay healthy or become seriously ill and die. However, even under homogeneous conditions, plants facing soil-borne pathogens often exhibit binary outcomes. This binary outcome may be the result of early differentiation of the rhizosphere microbiome, which may further lead to different disease inhibition abilities (Gu et al., 2022).

The rhizosphere is a hotspot where plants exchange substances and energy with their surrounding environment, which serves as the first line of defense against various biotic and abiotic stresses (Li et al., 2020, 2022). Therefore, the rhizosphere microbiome is critical to plant growth and health and is considered the second genome of plants (Mendes et al., 2011). The structure of the rhizosphere microbial community is the result of a series of complex interactions between the plant and soil microbiome (Zhalnina et al., 2018), and its composition and function change during plant development. In addition, the composition of the rhizosphere microbial community is influenced by host genotypes, plant growth stages, climate, microbial species pool, soil types, and agricultural management strategies (Berendsen et al., 2012; Gao et al., 2021). In natural ecosystems where roots and rhizosphere microbiomes coevolve over a long period of time, host genotypes have a great effect on microbial communities (Philippot et al., 2013). Disease-resistant cultivars of bean can resist the invasion of pathogens by enriching specific groups of bacteria in the rhizosphere (Mendes et al., 2017). *Flavobacterium* is significantly enriched in the rhizosphere of resistant tomato cultivars, which could change the rhizosphere microbial community to improve resistance to *Pseudomonas solanacearum* (Kwak et al., 2018). Apart from these factors, pathogen invasion has a great influence on species composition and community diversity (Carrion et al., 2019; Gao et al., 2021) and often occurs in conjunction with changes in diversity and function in the rhizosphere microbiome (Wei et al., 2018; Yuan et al., 2018; Shi et al., 2019), as the function and assembly of the rhizosphere microbiome are tightly coupled (Xun et al., 2019; Luan et al., 2020).

China is the world's largest cotton producer, accounting for more than 23% of the world's total output (Meyer and Dew, 2023). However, Verticillium wilt is a kind of plant pathogen with important economic significance that can severely restrict the yield and quality of cotton in China, which can occur during the growing season of cotton, and severe outbreaks can result in yield losses of more than 50% (Ranga et al., 2020; Zhu et al., 2023). Gaining insight into the rhizosphere microbiome's response to *V. dahliae* may contribute to developing environmentally friendly *V. dahliae* control strategies. In this study, the rhizosphere microbiome of two cotton cultivars with different levels of resistance to *V. dahliae* was investigated using 16S rRNA and ITS high-throughput sequencing. We aimed to (i) assess the effects of *V. dahliae* on the bacterial and fungal rhizosphere microbiome of two cotton cultivars and (ii) determine the differences between healthy and diseased cotton rhizosphere microbiomes.

Materials and methods

Experimental design and sample preparation

In this study, two cultivars of upland cotton with different levels of resistance were selected: Zhongzhimian 2 (Zhong 2, resistant to *V. dahliae*) and Xinluzao 36 (Xin 36, highly susceptible to *V. dahliae*). Two cultivars were cultivated in a random arrangement in the Verticillium wilt disease nursery at the Shihezi Academy of Agricultural Sciences, Xinjiang. The field has a continuous cotton growing history of more than 20 years, with a serious and uniform incidence of Verticillium wilt. In April 2021, the seeds of two cultivars were sown in the field, and 18 plants (9 healthy +9 diseased plants for each cultivar) were randomly uprooted with shovels when plants infected with *V. dahliae* showed obvious disease symptoms in August 2021 (Supplementary Figure 1). The disease index (DI) was used to evaluate the severity of cotton Verticillium wilt (Zhang et al., 2012) using the following formula: $DI = [\Sigma$ (disease grades × number of infected plants)/(total checked plants×4)] × 100 (Zhang et al., 2017).

To collect the rhizosphere soil (1–2 mm–thick soil layer surrounding the root after shaking vigorously), the roots were transferred into a 50 mL centrifuge tube containing 15 mL of 1× phosphate buffer solution (PBS), rotated for 5 min and then removed. Next, the tubes were centrifuged at 4000 × *g* and 4°C for 10 min, and the supernatant was discarded. Then, the samples were centrifuged at 8000 × *g* for 5 min, the supernatant was discarded again, and the remaining part was regarded as the rhizosphere soil (Edwards et al., 2018).

Microbiome sample collection, PCR amplification and sequencing

Total DNA of soil was extracted from 36 rhizosphere soil samples according to the instructions using the DNeasy PowerSoil Kit (QIAGEN, Germany). The full-length bacterial 16S rRNA gene and fungal ITS were amplified by PCR using the bacteria-specific primer pair 27F (5′-AGAGTTTGATCMTGGCTCAG-3′)/1492R (5′-ACCTTGTTACGACTT-3′) (Thies, 2007) and the fungi-specific primer pair ITS1F (5′-CTTGGTCATTTAGAGGAAGTAA-3′)/LR3 (5′-CCGTGTTTCAAGACGGG-3′) (Kurtzman and Robnett, 1998), respectively. PCR procedure: 95°C for 2 min; 30 cycles of 95°C for 30 s, 55°C for 30 s, 72°C for 30 s with a final extension of 72°C for 5 min. PCR products were purified by Gel Extraction Kit (OMEGA, USA). Then, the entire 16S rRNA gene and ITS lengths of the community were determined using the PacBio Sequel platform at Personalbio, Inc. (Shanghai, China).

Statistical methods

The sequence data were verified using Quantitative Insights Into Microbial Ecology 2 (QIIME2) and the R software package (version 3.2.0). The QIIME package[1] was used to extract the high-quality

1 http://qiime.org/scripts/pick_oyus.html

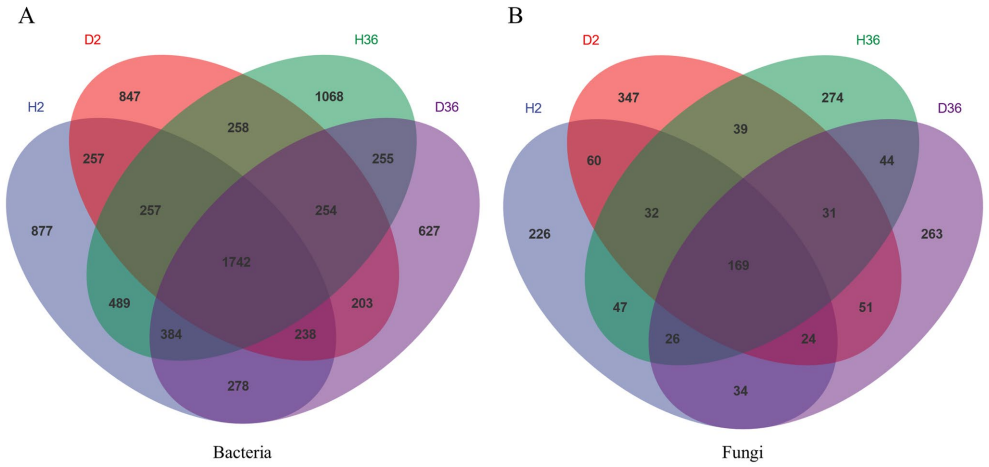

FIGURE 1
Unique and shared ASVs in healthy and diseased rhizosphere microbiomes of two cotton cultivars.

sequences, which were then clustered into amplicon sequence variants (ASVs). Taxonomic assignment of 16S rRNA gene and ITS fragment representative sequences was performed based on the Greengenes database (McDonald et al., 2012) and the UNITE database (Abarenkov et al., 2010). Alpha-diversity analyses included Shannon, Chao1, Simpson, Pielou_e and Observed_species. Beta diversity was calculated by the weighted UniFrac distance and then analyzed by principal coordinate analyses (PCoA) (Lozupone and Knight, 2005). The Kruskal–Wallis test and permutational multivariate analysis of variance (PERMANOVA) with 999 random permutations were used to analyze significant differences in alpha diversity and beta diversity (Anderson, 2001). Venn diagrams were implemented online to show unique and shared ASVs.[2] The abundances of healthy and diseased rhizospheres in two cotton cultivars were statistically compared at different taxonomic levels and visualized by histogram and heatmap. Two-sided analysis of variance with a *t* test was used for two-group comparison analyses using STAMP (v.2.0.0) (Parks et al., 2014). Co-occurrence network analysis was conducted at the genus level based on Spearman correlation with a threshold of $|r| > 0.6$ ($p < 0.05$).

Results

Diversity and structure of the rhizosphere microbiome in response to *Verticillium dahliae* infection in two cotton cultivars

A total of 433,283 high-quality bacterial 16S rRNA reads and 461,403 fungal internal transcribed spacer [ITS] reads were obtained via the PacBio Sequel platform from 18 healthy and 18 diseased samples, respectively. These reads were aggregated into 8,034 bacterial ASVs and 1,667 ITS fungal ASVs.

Venn diagrams show the unique and shared ASVs in the different samples in Figure 1. A total of 1742 bacterial ASVs and 169 fungal ASVs were common to all groups (Figures 1A,B). The healthy rhizosphere of Xin 36 had more unique bacterial (H36, 2072; D36, 1346) and fungal ASVs (H36, 392; D36, 372) than the diseased rhizosphere; the healthy rhizosphere of Zhong 2 had more unique bacterial ASVs than the diseased rhizosphere (H2, 2028; D2, 1562) but fewer unique fungal ASVs than the diseased rhizosphere (H2, 333; D2, 468).

Notably, there was no significant difference in alpha diversity between healthy and diseased rhizospheres of both bacteria and fungi in the two cotton cultivars (Supplementary Figure 3). Principal coordinate analysis (PCoA) was performed based on Bray–Curtis dissimilarity and revealed that bacterial and fungal communities showed no significant difference between healthy and diseased rhizospheres, especially for Xin 36 (Figure 2).

Comparison of rhizosphere community composition between two cotton cultivars

A total of 28 phyla, 72 classes, 133 orders, 266 families, and 505 genera were identified in the bacterial community. In Zhong 2 and Xin 36, the dominant bacterial phyla were *Pseudomonadota* (42.91%), *Acidobacteriota* (15.78%), *Bacteroidota* (6.34%) and *Planctomycetota* (6.18%) (relative abundance ≥5%), accounting for 71.22% (Figure 3A). At the genus level, most of the bacterial ASVs in Zhong 2 were assigned to *Vicinamibacter* (5.51%), *Bacterium* (4.69%), *Pseudomonas* (3.54%), *Lysobacter* (3.39%) and *Novosphingobium* (3.50%), whereas bacterial ASVs in Xin 36 were mainly classified into *Pseudomonas* (6.84%), *Vicinamibacter* (5.69%), *Bacterium* (4.48%), Bacillus (3.40%) and *Lysobacter* (3.24%) (Figure 3C).

A total of 19 phyla, 52 classes, 94 orders, 160 families, and 219 genera were identified in the fungal community. In Zhong 2 and Xin 36, the dominant fungal phyla were *Ascomycota* (23.67%), *Basidiomycota* (14.28%), *Mortierellomycota* (9.69%), and *Rozellomycota* (6.04%), accounting for 53.68% (Figure 3B). At the

2 http://bioinformatics.psb.ugent.be/webtools/Venn/

10.3389/fmicb.2023.1229454

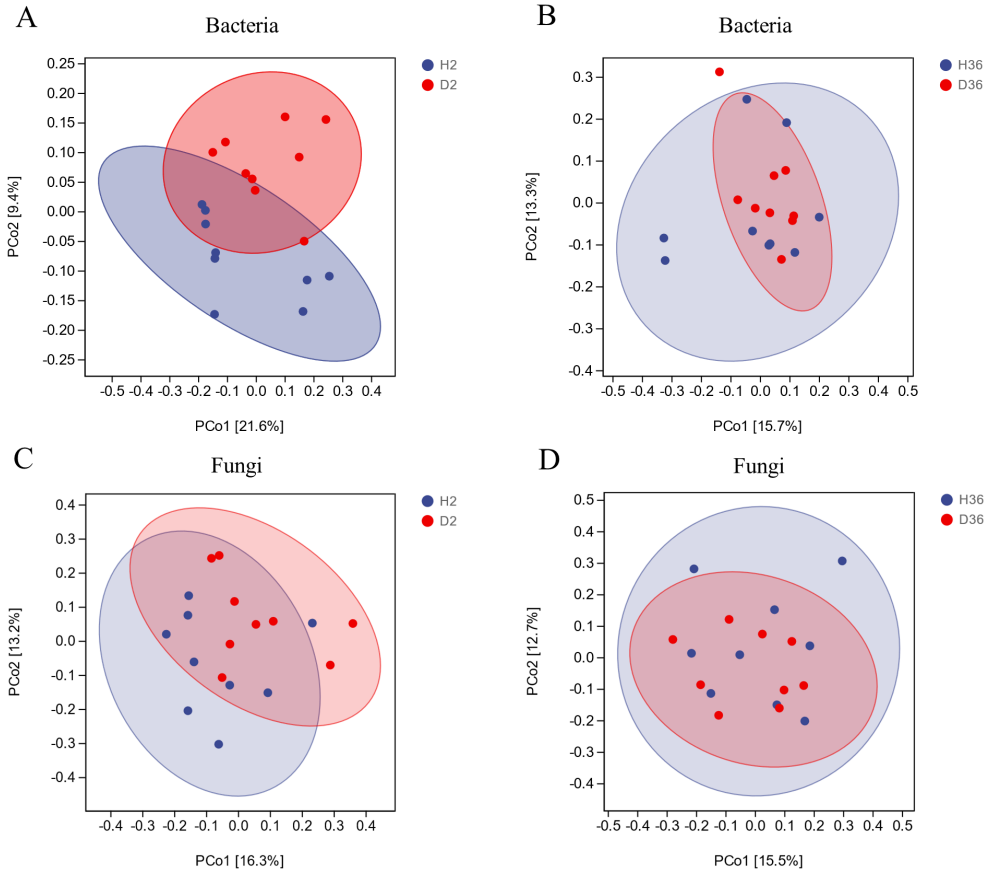

FIGURE 2
PCoA based on Bray–Curtis distance between healthy and diseased rhizosphere microbiomes of two cotton cultivars (n = 36).

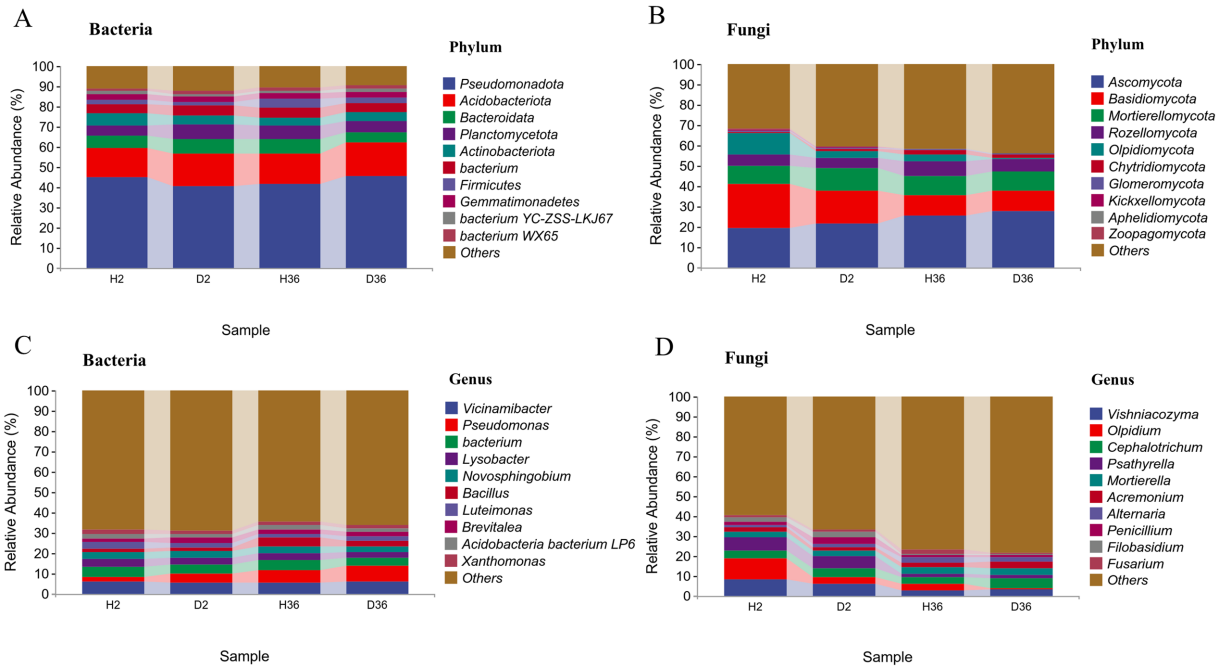

FIGURE 3
Comparison of the compositions between healthy and diseased rhizosphere microbiomes of two cotton cultivars at the phylum and genus levels.

genus level, most of the fungal Zhong 2 ASVs were assigned to *Vishniacozyma* (7.10%), *Olpidium* (6.90%), *Psathyrella* (6.38%) and *Cephalotrichum* (4.19%), whereas fungal ASVs in Xin 36 were mainly classified into *Vishniacozyma* (3.06%), *Cephalotrichum* (4.27%), and *Mortierella* (3.42%) (Figure 3D).

Based on the heatmaps of the top 40 genera, the differences between the healthy and diseased rhizosphere microbiomes of the two cotton cultivars were compared (Figures 4A,B). According to the relative abundances of these genera, D2 and H36 were clustered together in the bacterial community, followed by D36 and H2, whereas H2 and D2, and H36 and D36 were clustered together in the fungal community.

Effects of *Verticillium dahliae* on the composition of rhizosphere microbiomes in two cotton cultivars

We further identified the changes between two cultivars in the taxonomic composition of the rhizosphere microbiomes of the two cultivars. Specifically, the relative abundance of 31 and 18 bacterial orders differed significantly in Zhong 2 (Figure 5A) and Xin 36 (Figure 5B) between healthy and diseased rhizospheres, respectively. In Zhong 2, the relative abundances of bacterium WX65 and Fimbriimonadales significantly increased in D2, while the relative abundances of Caulobacterales, Myxococcales and Nevskiales were significantly reduced. Only Chitinophagales decreased significantly in D36. Furthermore, the relative abundance of Entomophthorales in the fungal order differed significantly in Xin 36 between the healthy and diseased rhizospheres (Figure 5C), and there was no significant change in Zhong 2.

The relative abundance of 40 and 32 bacterial families differed significantly in Zhong 2 (Figure 6A) and Xin 36 (Figure 6B) between healthy and diseased rhizospheres, respectively. In Zhong 2, the relative abundance of bacterium WX65 significantly increased in D2, whereas the relative abundances of Caulobacteraceae, Hyphomicrobiaceae and Steroidobacteraceae were significantly decreased. Only Chitinophagaceae decreased significantly in D36. Furthermore, the relative abundance of Ancylistaceae in the fungal family differed significantly in Xin 36 between the healthy and diseased rhizospheres (Figure 6C), and there was no significant change in Zhong 2. These results indicated that *V. dahliae* infection influenced the distribution and composition of the rhizosphere bacterial and fungal communities of the two cotton cultivars.

Different responses of two cotton cultivars to *Verticillium dahliae* infection

The relative abundance of *Verticillium* was significantly different between healthy and diseased rhizospheres of the two cotton cultivars ($p < 0.05$), with high enrichment in diseased rhizospheres compared with healthy rhizospheres. Notably, in both healthy and diseased rhizospheres, the relative abundance of *Verticillium* was higher in Xin 36 than in Zhong 2 (Supplementary Figure 2A). *Verticillium dahliae* and *Verticillium albo-atrum* are potential pathogens causing cotton Verticillium wilt according to previous studies (Qin et al., 2006, 2008). In the genus *Verticillium*, only *Verticillium dahliae* was identified, and the relative abundance was D36 (0.86%) > H36 (0.14%) > D2 (0.03%) > H2 (0%). This was consistent with the phenotypic results of the field Verticillium wilt investigation (Supplementary Figure 2B).

To determine the effects of *V. dahliae* on rhizosphere microbial co-occurrence patterns between healthy and diseased samples in two cotton cultivars, the genera with the top 20 relative abundances were screened to construct the networks based on correlation relationships (Figure 7). For bacterial communities, the microbial networks in

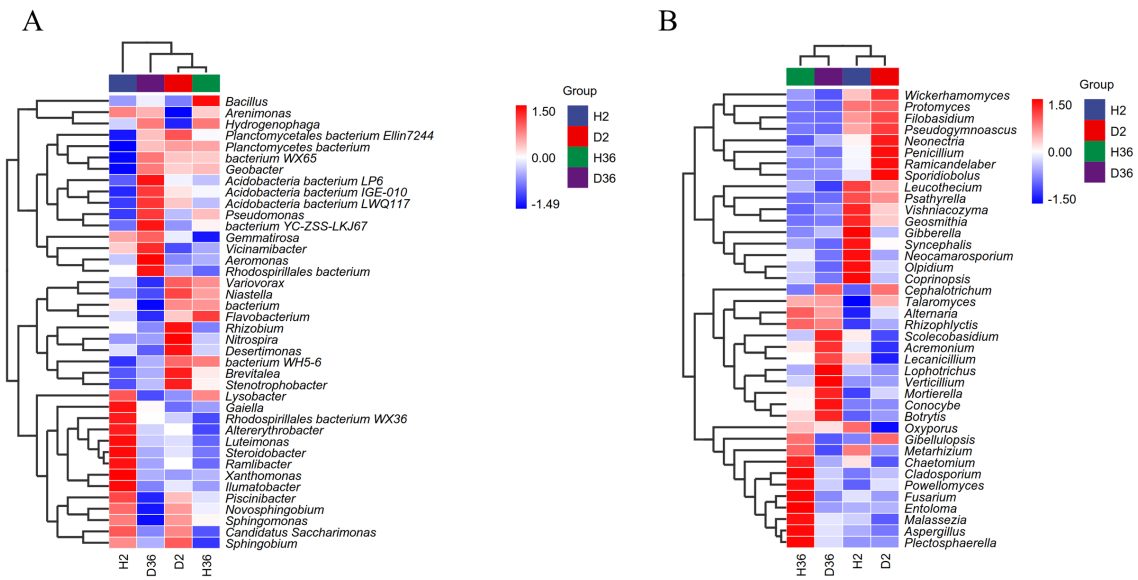

FIGURE 4
Heatmap analysis of rhizosphere bacterial **(A)** and fungal **(B)** communities at the genus level. The average relative abundance of the genus in the top 40 and $p < 0.05$ were used as the screening criteria, $n = 36$.

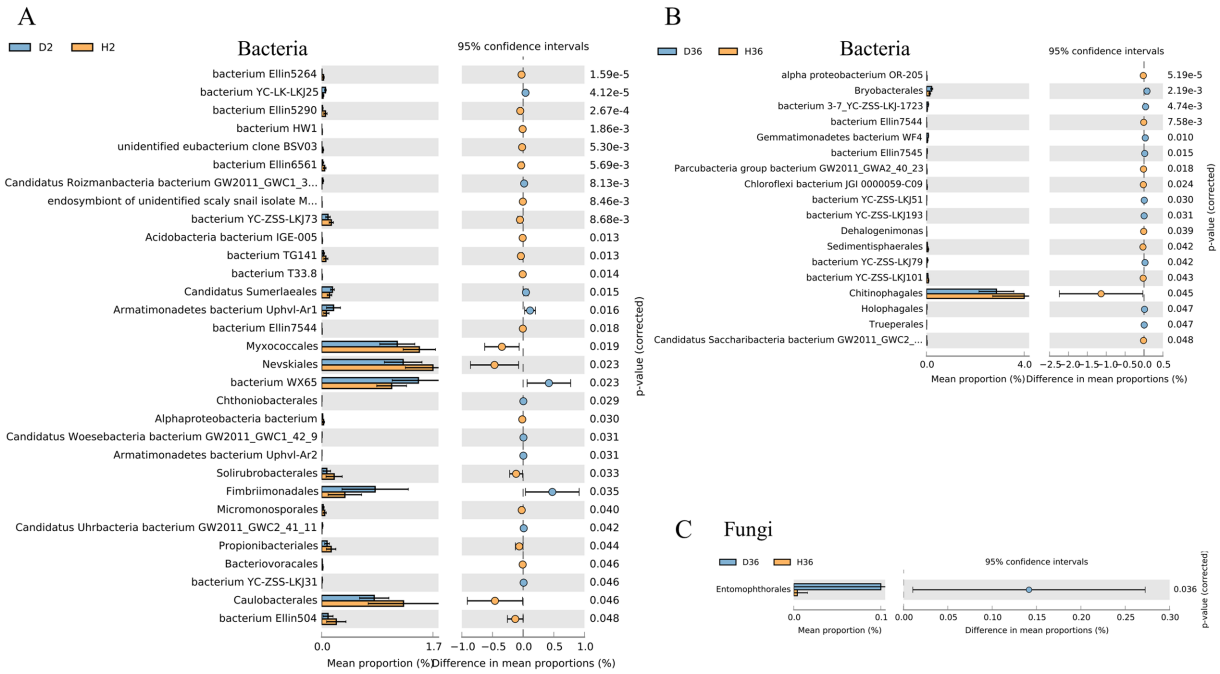

FIGURE 5
Quantification of the abundance of differential bacterial orders between healthy and diseased rhizospheres of two cotton cultivars using a two-sided *t* test. The corrected *p* values are shown.

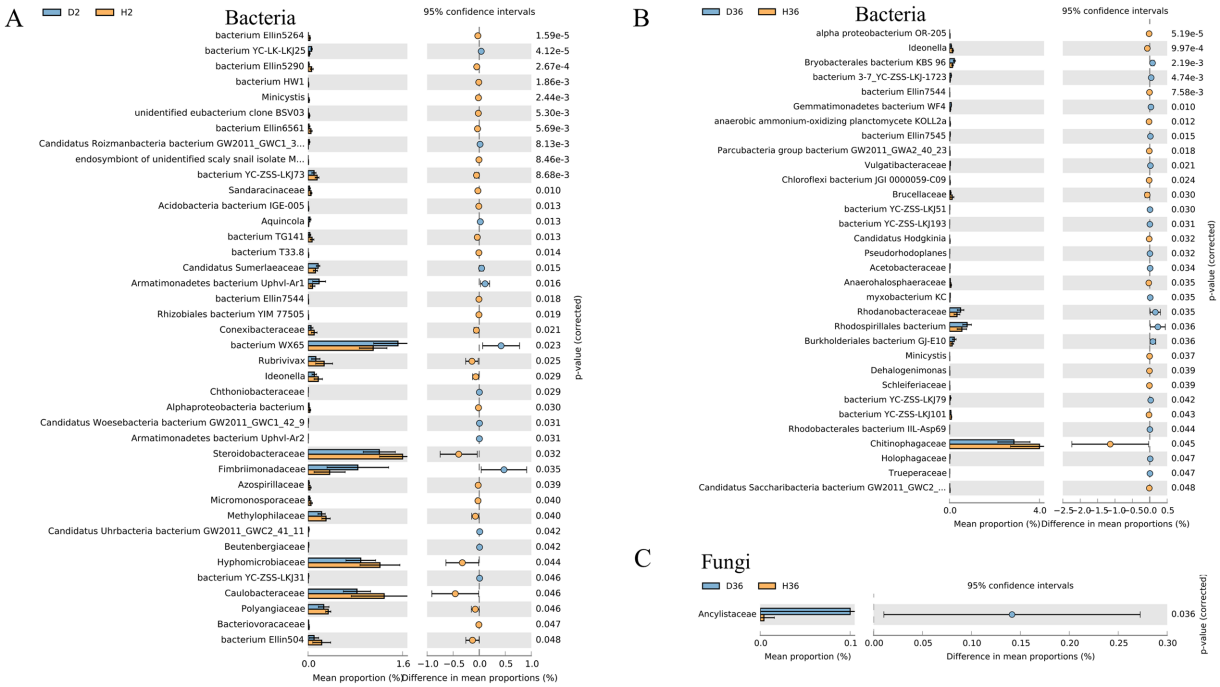

FIGURE 6
Quantification of the abundance of differential bacterial families between healthy and diseased rhizospheres of two cotton cultivars using a two-sided *t* test. The corrected *p* values are shown.

Zhong 2, neither healthy nor diseased rhizospheres, were denser and had a more complex network than those of Xin 36. In contrast, Xin 36 had a more complex network than Zhong 2 in the fungal communities. The results clearly show that the resistance of cotton cultivars has an effect on the complexity of the rhizosphere microbiome. In addition, the influence of *V. dahliae* infection on the

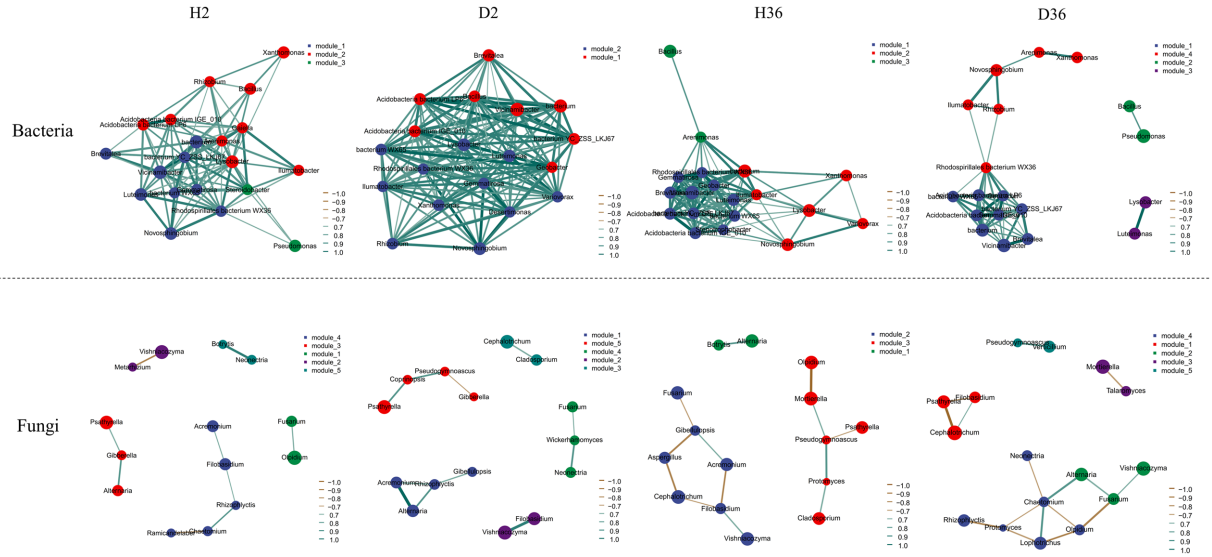

FIGURE 7
Co-occurrence network analysis of rhizosphere bacterial and fungal communities between healthy and diseased samples in two cotton cultivars. $p < 0.05$, $|r| > 0.6$.

complexity of rhizosphere bacterial communities was greater than that of fungal communities.

Discussion

Rhizosphere microorganisms play an important role in the growth and development of plants, and much research on the plant–microbe and microbe–microbe interactions has been reported in the plant rhizosphere (Lu et al., 2018; Ge et al., 2023). The rhizosphere microbiome is considered to be the first line of defense against soil-borne pathogen infection and abiotic stress, which is vital to the health of plants (Mendes et al., 2013; Ahmed et al., 2022). The balance in the rhizosphere during normal plant growth is disturbed under stress conditions, leading to changes in the composition of the rhizosphere community (Qian et al., 2018). However, there are few studies on how rhizosphere microorganisms of different resistant cultivars of cotton respond to *V. dahliae* infection in the natural field. In this study, we analyzed the different responses of rhizosphere microbial communities in two upland cottons with opposite resistance to Verticillium wilt. The results indicated that *V. dahliae* infection and cultivar alter the composition of the rhizosphere communities, with different responses in two cotton cultivars.

Verticillium dahliae infection influences the structure of the rhizosphere microbial community

After *V. dahliae* infection, the unique bacterial and fungal ASVs in the healthy rhizosphere of Xin 36 were higher than those in the diseased rhizosphere, whereas the healthy rhizosphere of Zhong 2 had more unique bacterial ASVs and fewer unique fungal ASVs than the diseased rhizosphere. The results suggested that *V. dahliae* infection may alter the structure of the rhizosphere microbiome, which is consistent with the result that pathogen infection disrupts host control over the rhizosphere microbiome (Wei et al., 2018; Wen et al., 2020).

The occurrence of diseases is usually accompanied by diversity changes in the rhizosphere microbiome (Wei et al., 2018; Yuan et al., 2018; Shi et al., 2019). However, the analysis results of the alpha and beta diversity showed that there were no significant differences between the resistant cultivar and susceptible cultivar, consistent with a previous study (Fernández-González et al., 2020). Such results may be due to differences in plant host, pathogen, soil, agricultural practices, or environmental conditions (Kwak et al., 2018; Gu et al., 2020; Jiang et al., 2021).

Verticillium dahliae infection shifts the composition of rhizosphere microbial communities

This study demonstrated that the relative abundance of many rhizosphere microorganisms in the healthy rhizosphere differed from that in the diseased rhizosphere of each cultivar. The taxonomic composition of the rhizosphere bacterial communities showed that *Pseudomonadota*, *Acidobacteriota*, *Bacteroidota* and *Planctomycetota* were dominant in two cotton cultivars, with *Pseudomonadota* members accounting for 42.91% of the community composition (Trivedi et al., 2020). Zhong 2 was characterized by a higher relative abundance of *Actinomycetota* than Xin 36, which is known as a biocontrol microorganism (Lee et al., 2021). In addition, the rhizosphere fungal community is mainly composed of *Ascomycota* and *Basidiomycota*, which are the most abundant phyla observed in previous studies (Bálint et al., 2015; Coleman-Derr et al., 2016).

Compared with the rhizosphere microbial communities in the healthy rhizosphere of Zhong 2 and Xin 36, *Pseudomonas* and *Acidobacteria bacterium LP6* in the bacterial communities and

Cephalotrichum and *Mortierella* in the fungal communities were both highly enriched in the diseased rhizosphere. *Pseudomonas* abundance in diseased rhizospheres was significantly higher than that in the healthy rhizosphere regardless of the cultivar type. Consistently, a previous study found that *Rhizoctonia solani* invasion alters the rhizosphere microbial community and specifically accumulates beneficial *Pseudomonas* (Yin et al., 2021). Therefore, it is reasonable to speculate that the increase in *Pseudomonas* in diseased rhizospheres may contribute to the potential resistance of their host plants to Verticillium wilt. These results suggest that plants may increase the enrichment of specific microbiomes in response to pathogen infection (Busby et al., 2016), which can be used as antagonistic candidates for Verticillium wilt and need to be confirmed by further culture-based experiments.

Effects of cultivar resistance on the microbial community structure in the cotton rhizosphere

Different microorganisms are recruited by plants to shape their rhizosphere microbiome, and the rhizosphere microflora community structure of the same species changes due to genotype differences (Bressan et al., 2009; Zhang et al., 2021; Yue et al., 2023). The growth and development of different blueberry cultivars were enhanced by recruiting specific rhizosphere microflora based on genotype (Jacoby et al., 2017). Our results showed that the different genotypes of cotton recruited specific rhizosphere microbiomes, suggesting that the rhizosphere microbial community was regulated by host genotypes, consistent with the results in soybean, rice, and barley (Bulgarelli et al., 2015; Singh et al., 2022; Qu et al., 2023). In addition, resistant cultivars may resist pathogen invasion by enriching specific bacterial or fungal groups in the rhizosphere (Mendes et al., 2017; Kwak et al., 2018). The analysis of co-occurrence networks also showed that the resistant cultivar Zhong 2 has a more complex network than the susceptible cultivar Xin 36 in the bacterial communities, and *V. dahliae* has a significant impact on the bacterial community structure compared with fungal communities.

Conclusion

Analyzing the rhizosphere microbial communities of different resistant cotton is conducive to elucidating the interaction mechanism between cotton and *V. dahliae*, which plays an important role in the green and durable control of cotton Verticillium wilt. In the present study, the healthy and diseased rhizosphere microbiome communities were compared between Zhong 2 and Xin 36, which have significant differences in resistance to *V. dahliae*. The results showed that no significant differences were found in alpha diversity and beta diversity between healthy and diseased rhizospheres in the two cotton cultivars. *V. dahliae* infection and cultivar alter the composition of the rhizosphere communities, with different responses in two cotton cultivars. *V. dahliae* invasion may specifically accumulates beneficial microbiomes, such as *Pseudomonas*, which can be used as antagonistic candidates for Verticillium wilt. Additionally, cultivar and Resistant cultivar has a more complex network relationship than susceptible cultivar in the bacterial communities, and *V. dahliae* has a significant impact on the bacterial community structure. This study analyzed the resistance mechanism of cotton from the perspective of microbiology, and the research results will provide a theoretical basis for the green control strategy of cotton Verticillium wilt.

Data availability statement

The datasets presented in this study can be found in online repositories. The names of the repository/repositories and accession number(s) can be found below: NCBI database, under accessions PRJNA980128 and PRJNA980194.

Author contributions

HX and XZ planned and designed the research and experiments. ZT, PW, WC, BT, HX, and XZ performed the experiments. HX analyzed the data. ZT, HX, and XZ wrote the manuscript. HX, ZL, YY, and SZ acquired the funds for the study. All authors have read and approved the final manuscript.

Funding

This work was supported by the Shihezi University high-level talents research project (project number RCZK202016), National key research and development plan project (project number 2022YFD1400305-02), Basic research project of the Corps (project number 2023CB007-08), and Major science and technology special projects of Autonomous region (project number 2022294083).

Conflict of interest

The authors declare that the research was conducted in the absence of any commercial or financial relationships that could be construed as a potential conflict of interest.

Publisher's note

Supplementary material

The Supplementary material for this article can be found online at: https://www.frontiersin.org/articles/10.3389/fmicb.2023.1229454/full#supplementary-material

References

Abarenkov, K., Henrik Nilsson, R., Larsson, K. H., Alexander, I. J., Eberhardt, U., Erland, S., et al. (2010). The UNITE database for molecular identification of fungi – recent updates and future perspectives. *New Phytol.* 186, 281–285. doi: 10.1111/j.1469-8137.2009.03160.x

Ahmed, W., Dai, Z., Liu, Q., Munir, S., Yang, J., Karunarathna, S. C., et al. (2022). Microbial cross-talk: dissecting the core microbiota associated with flue-cured tobacco (*Nicotiana tabacum*) plants under healthy and diseased state. *Front. Microbiol.* 13:845310. doi: 10.3389/fmicb.2022.845310

Anderson, M. J. (2001). A new method for non-parametric multivariate analysis of variance. *Austral Ecol.* 26, 32–46. doi: 10.1046/j.1442-9993.2001.01070.x

Bálint, M., Bartha, L., O'Hara, R. B., Olson, M. S., Otte, J., Pfenninger, M., et al. (2015). Relocation, high-latitude warming and host genetic identity shape the foliar fungal microbiome of poplars. *Mol. Ecol.* 24, 235–248. doi: 10.1111/mec.13018

Berendsen, R. L., Pieterse, C. M. J., and Bakker, P. A. H. M. (2012). The rhizosphere microbiome and plant health. *Trends Plant Sci.* 17, 478–486. doi: 10.1016/j.tplants.2012.04.001

Bressan, M., Roncato, M. A., Bellvert, F., Comte, G., Haichar, F. Z., Achouak, W., et al. (2009). Exogenous glucosinolate produced by *Arabidopsis thaliana* has an impact on microbes in the rhizosphere and plant roots. *ISME J.* 3, 1243–1257. doi: 10.1038/ismej.2009.68

Bulgarelli, D., Garrido-Oter, R., Münch, P. C., Weiman, A., Dröge, J., Pan, Y., et al. (2015). Structure and function of the bacterial root microbiota in wild and domesticated barley. *Cell Host Microbe* 17, 392–403. doi: 10.1016/j.chom.2015.01.011

Busby, P. E., Peay, K. G., and Newcombe, G. (2016). Common foliar fungi of *Populus trichocarpa* modify Melampsora rust disease severity. *New Phytol.* 209, 1681–1692. doi: 10.1111/nph.13742

Campbell, C. (1985). The spatial analysis of soilborne pathogens and root diseases. *Annu. Rev. Phytopathol.* 23, 129–148. doi: 10.1146/annurev.py.23.090185.001021

Carrion, V. J., Perez-Jaramillo, J., Cordovez, V., Tracanna, V., de Hollander, M., Ruiz-Buck, D., et al. (2019). Pathogen-induced activation of disease-suppressive functions in the endophytic root microbiome. *Science* 366, 606–612. doi: 10.1126/science.aaw9285

Coleman-Derr, D., Desgarennes, D., Fonseca-Garcia, C., Gross, S., Clingenpeel, S., Woyke, T., et al. (2016). Plant compartment and biogeography affect microbiome composition in cultivated and native Agave species. *New Phytol.* 209, 798–811. doi: 10.1111/nph.13697

Edwards, J., Santos-Medellín, C., and Sundaresan, V. (2018). Extraction and 16S rRNA sequence analysis of microbiomes associated with rice roots. *Bio Protoc* 8:e2884. doi: 10.21769/BioProtoc.2884

Fernández-González, A. J., Cardoni, M., Cabanás, C. G.-L., Valverde-Corredor, A., and Mercado-Blanco, J. (2020). Linking belowground microbial network changes to different tolerance level towards Verticillium wilt of olive. *Microbiome* 8:11. doi: 10.1186/s40168-020-0787-2

Gao, M., Xiong, C., Gao, C., Tsui, C. K. M., Wang, M. M., Zhou, X., et al. (2021). Disease-induced changes in plant microbiome assembly and functional adaptation. *Microbiome* 9:187. doi: 10.1186/s40168-021-01138-2

Ge, J., Li, D., Ding, J., Xiao, X., and Liang, Y. (2023). Microbial coexistence in the rhizosphere and the promotion of plant stress resistance: a review. *Environ. Res.* 222:115298. doi: 10.1016/j.envres.2023.115298

Genin, S., and Denny, T. P. (2012). Pathogenomics of the *Ralstonia solanacearum* species complex. *Annu. Rev. Phytopathol.* 50, 67–89. doi: 10.1146/annurev-phyto-081211-173000

Gu, Y., Banerjee, S., Dini-Andreote, F., Xu, Y., Shen, Q., Jousset, A., et al. (2022). Small changes in rhizosphere microbiome composition predict disease outcomes earlier than pathogen density variations. *ISME J.* 16, 2448–2456. doi: 10.1038/s41396-022-01290-z

Gu, Y., Dong, K., Geisen, S., Yang, W., Yan, Y., Gu, D., et al. (2020). The effect of microbial inoculant origin on the rhizosphere bacterial community composition and plant growth promotion. *Plant Soil* 452, 105–117. doi: 10.1007/s11104-020-04545-w

Jacoby, R., Peukert, M., Succurro, A., Koprivova, A., and Kopriva, S. (2017). The role of soil microorganisms in plant mineral nutrition-current knowledge and future directions. *Front. Plant Sci.* 8:1617. doi: 10.3389/fpls.2017.01617

Jiang, G., Wang, N., Zhang, Y., Wang, Z., Zhang, Y., Yu, J., et al. (2021). The relative importance of soil moisture in predicting bacterial wilt disease occurrence. *Soil Ecol. Lett.* 3, 356–366. doi: 10.1007/s42832-021-0086-2

Kurtzman, C. P., and Robnett, C. J. (1998). Identification and phylogeny of ascomycetous yeasts from analysis of nuclear large subunit (26S) ribosomal DNA partial sequences. *Antonie Van Leeuwenhoek* 73, 331–371. doi: 10.1023/A:1001761008817

Kwak, M. J., Kong, H. G., Choi, K., Kwon, S. K., Song, J. Y., Lee, J., et al. (2018). Rhizosphere microbiome structure alters to enable wilt resistance in tomato. *Nat. Biotechnol.* 36, 1100–1109. doi: 10.1038/nbt.4232

Lee, S. M., Kong, H. G., Song, G. C., and Ryu, C. M. (2021). Disruption of Firmicutes and Actinobacteria abundance in tomato rhizosphere causes the incidence of bacterial wilt disease. *ISME J.* 15, 330–347. doi: 10.1038/s41396-020-00785-x

Li, P., Liu, J., Saleem, M., Li, G., Luan, L., Wu, M., et al. (2022). Reduced chemodiversity suppresses rhizosphere microbiome functioning in the mono-cropped agroecosystems. *Microbiome* 10:108. doi: 10.1186/s40168-022-01287-y

Li, X., Yao, S., Bian, Y., Jiang, X., and Song, Y. (2020). The combination of biochar and plant roots improves soil bacterial adaptation to PAH stress: insights from soil enzymes, microbiome, and metabolome. *J. Hazard. Mater.* 400:123227. doi: 10.1016/j.jhazmat.2020.123227

Lozupone, C., and Knight, R. (2005). UniFrac: a new phylogenetic method for comparing microbial communities. *Appl. Environ. Microb.* 71, 8228–8235. doi: 10.1128/AEM.71.12.8228-8235.2005

Luan, L., Liang, C., Chen, L., Wang, H., Xu, Q., Jiang, Y., et al. (2020). Coupling bacterial community assembly to microbial metabolism across soil profiles. *mSystems* 5:e00298-20. doi: 10.1128/mSystems.00298-20

Lu, T., Ke, M., Lavoie, M., Jin, Y., Fan, X., Zhang, Z., et al. (2018). Rhizosphere microorganisms can influence the timing of plant flowering. *Microbiome* 6:231. doi: 10.1186/s40168-018-0615-0

McDonald, D., Price, M. N., Goodrich, J., Nawrocki, E. P., DeSantis, T. Z., Probst, A., et al. (2012). An improved Greengenes taxonomy with explicit ranks for ecological and evolutionary analyses of bacteria and archaea. *ISME J.* 6, 610–618. doi: 10.1038/ismej.2011.139

Mendes, L. W., Raaijmakers, J. M., Hollander, M. D., Mendes, R., and Tsai, S. M. (2017). Influence of resistance breeding in common bean on rhizosphere microbiome composition and function. *ISME J.* 12, 1–13. doi: 10.1038/ismej.2017.158

Mendes, R., Garbeva, P., and Raaijmakers, J. M. (2013). The rhizosphere microbiome: significance of plant beneficial, plant pathogenic, and human pathogenic microorganisms. *FEMS Microbiol. Rev.* 37, 634–663. doi: 10.1111/1574-6976.12028

Mendes, R., Kruijt, M., Bruijn, I. D., Dekkers, E., van der Voort, M., Schneider, J. H. M., et al. (2011). Deciphering the rhizosphere microbiome for disease-suppressive bacteria. *Science* 332, 1097–1100. doi: 10.1126/science.1203980

Meyer, L., and Dew, T. (2023). Cotton and wool outlook tables. Available at: https://www.ers.usda.gov/publications/pub-details/?pubid=105597.

Parks, D. H., Tyson, G. W., Hugenholtz, P., and Beiko, R. G. (2014). STAMP: statistical analysis of taxonomic and functional profiles. *Bioinformatics* 30, 3123–3124. doi: 10.1093/bioinformatics/btu494

Philippot, L., Raaijmakers, J. M., Lemanceau, P., and van der Putten, W. H. (2013). Going back to the roots: the microbial ecology of the rhizosphere. *Nat. Rev. Microbiol.* 11, 789–799. doi: 10.1038/nrmicro3109

Qian, H., Zhu, Y., Chen, S., Jin, Y., Lavoie, M., Ke, M., et al. (2018). Interacting effect of diclofop-methyl on the rice rhizosphere microbiome and denitrification. *Pestic. Biochem. Physiol.* 146, 90–96. doi: 10.1016/j.pestbp.2018.03.002

Qin, Q. M., Vallad, G. E., Wu, B. M., and Subbarao, K. V. (2006). Phylogenetic analyses of phytopathogenic isolates of Verticillium spp. *Phytopathology* 96, 582–592. doi: 10.1094/PHYTO-96-0582

Qin, Q. M., Valled, G. E., and Subbarao, K. V. (2008). Characterization of *Verticillium dahliae* and V. tricorpus isolates from lettuce and artichoke. *Plant Dis.* 92, 69–77. doi: 10.1094/PDIS-92-1-0069

Qu, Z., Li, Y. H., Xu, W. H., Chen, W. J., Hu, Y. L., and Wang, Z. G. (2023). Different genotypes regulate the microbial community structure in the soybean rhizosphere. *J. Integr. Agric.* 22, 585–597. doi: 10.1016/j.jia.2022.08.010

Ranga, A., Kak, V., and Darvhankar, M. (2020). Genetic and molecular research of resistance to wilt in cotton: a concise review. *Int. J. Curr. Microbiol. Appl. Sci.* 9, 2410–2422. doi: 10.20546/ijcmas.2020.906.296

Shi, W. C., Li, M. C., Wei, G. S., Tian, R. M., Li, C. P., Wang, B., et al. (2019). The occurrence of potato common scab correlates with the community composition and function of the geocaulosphere soil microbiome. *Microbiome* 7:14. doi: 10.1186/s40168-019-0629-2

Singh, A., Kumar, M., Chakdar, H., Pandiyan, K., Kumar, S. C., Zeyad, M. T., et al. (2022). Influence of host genotype in establishing root associated microbiome of indica rice cultivars for plant growth promotion. *Front. Microbiol.* 13:1033158. doi: 10.3389/fmicb.2022.1033158

Thies, J. E. (2007). Soil microbial community analysis using terminal restriction fragment length polymorphisms. *Soil Sci. Soc. Am. J.* 71, 579–591. doi: 10.2136/sssaj2006.0318

Trivedi, P., Leach, J. E., Tringe, S. G., Sa, T., and Singh, B. K. (2020). Plant-microbiome interactions: from community assembly to plant health. *Nat. Rev. Microbiol.* 18, 607–621. doi: 10.1038/s41579-020-0412-1

Wei, Z., Gu, Y., Friman, V. P., Kowalchuk, G. A., Xu, Y., Shen, Q., et al. (2019). Initial soil microbiome composition and functioning predetermine future plant health. *Sci. Adv.* 5:eaaw0759. doi: 10.1126/sciadv.aaw0759

Wei, Z., Hu, J., Gu, Y. A., Yin, S., Xu, Y., Jousset, A., et al. (2018). *Ralstonia Solanacearum* pathogen disrupts bacterial rhizosphere microbiome during an invasion. *Soil Biol. Biochem.* 118, 8–17. doi: 10.1016/j.soilbio.2017.11.012

Wen, T., Zhao, M., Liu, T., Huang, Q., Yuan, J., and Shen, Q. (2020). High abundance of *Ralstonia solanacearum* changed tomato rhizosphere microbiome and metabolome. *BMC Plant Biol.* 20:166. doi: 10.1186/s12870-020-02365-9

Xun, W., Li, W., Xiong, W., Ren, Y., Liu, Y., Miao, Y., et al. (2019). Diversity-triggered deterministic bacterial assembly constrains community functions. *Nat. Commun.* 10, 3833–3843. doi: 10.1038/s41467-019-11787-5

Yin, C., Casa Vargas, J. M., Schlatter, D. C., Hagerty, C. H., Hulbert, S. H., and Paulitz, T. C. (2021). Rhizosphere community selection reveals bacteria associated with reduced root disease. *Microbiome* 9:86. doi: 10.1186/s40168-020-00997-5

Yuan, J., Zhao, J., Wen, T., Zhao, M. L., Li, R., Goossens, P., et al. (2018). Root exudates drive the soil-borne legacy of aboveground pathogen infection. *Microbiome* 6:156. doi: 10.1186/s40168-018-0537-x

Yue, H., Yue, W. J., Jiao, S., Kim, H., Lee, Y. H., Wei, G. H., et al. (2023). Plant domestication shapes rhizosphere microbiome assembly and metabolic functions. *Microbiome.* 11:70. doi: 10.1186/s40168-023-01513-1

Zhalnina, K., Louie, K. B., Hao, Z., Mansoori, N., Rocha, U. N. D., Shi, S., et al. (2018). Dynamic root exudate chemistry and microbial substrate preferences drive patterns in rhizosphere microbial community assembly. *Nat. Microbiol.* 3, 470–480. doi: 10.1038/s41564-018-0129-3

Zhang, W. W., Jiang, T. F., Cui, X., Qi, F. J., and Jian, G. L. (2012). Colonization in cotton plants by a green fluorescent protein labelled strain of *Verticillium dahliae*. *Eur. J. Plant Pathol.* 135, 867–876. doi: 10.1007/s10658-012-0131-1

Zhang, W., Zhang, H., Liu, K., Jian, G., Qi, F., and Si, N. (2017). Large-scale identification of *Gossypium hirsutum* genes associated with *Verticillium dahliae* by comparative transcriptomic and reverse genetics analysis. *PLoS One* 12:e0181609. doi: 10.1371/journal.pone.0181609

Zhang, Y., Wang, W., Shen, Z., Wang, J., Chen, Y., Wang, D., et al. (2021). Comparison and interpretation of characteristics of rhizosphere microbiomes of three blueberry varieties. *BMC Microbiol.* 21:30. doi: 10.1186/s12866-021-02092-7

Zhu, Y., Zhao, M., Li, T., Wang, L., Liao, C., Liu, D., et al. (2023). Interactions between *Verticillium dahliae* and cotton: pathogenic mechanism and cotton resistance mechanism to Verticillium wilt. *Front. Plant Sci.* 14:1174281. doi: 10.3389/fpls.2023.1174281

frontiers | Frontiers in Microbiology

TYPE Original Research
PUBLISHED 19 September 2023
DOI 10.3389/fmicb.2023.1226142

OPEN ACCESS

EDITED BY
Dilfuza Egamberdieva,
Leibniz Center for Agricultural Landscape Research (ZALF), Germany

REVIEWED BY
Mahendra Vikram Singh Rajawat,
Prabhat Fertilizers and Chemical Works, India
Agnieszka Kuźniar,
The John Paul II Catholic University of Lublin, Poland

*CORRESPONDENCE
YongHui Lei
497976@qq.com
YanFei Sun
81711308@qq.com

†These authors have contributed equally to this work

RECEIVED 20 May 2023
ACCEPTED 31 August 2023
PUBLISHED 19 September 2023

CITATION
Zhu S, Cai Y, Li Y, Xiong J, Lei Y and Sun Y (2023) Effects of temporal and spatial scales on soil yeast communities in the peach orchard. *Front. Microbiol.* 14:1226142. doi: 10.3389/fmicb.2023.1226142

Effects of temporal and spatial scales on soil yeast communities in the peach orchard

ShanShan Zhu[1†], YanLi Cai[2†], Yang Li[2], Jie Xiong[2], YongHui Lei[1*] and YanFei Sun[2*]

[1]Department of Plant Protection, College of Agriculture, Shihezi University, Shihezi, Xinjiang, China, [2]College of Life Sciences, Shihezi University, Shihezi, Xinjiang, China

Shihezi Reclamation Area is located at the southern edge of the Junggar Basin, with natural, soil, and climatic conditions unique to the production of peaches. In turn, peach orchards have accumulated rich microbial resources. As an important taxon of soil fungi, the diversity and community structure changes of yeast in the soil of peach orchards on spatial and temporal scales are still unknown. Here, we aimed to investigate the changes in yeast diversity and community structure in non-rhizosphere and rhizosphere soils of peach trees of different ages in the peach orchard and the factors affecting them, as well as the changes in the yeast co-occurrence network in the peach orchard at spatial and temporal scales. High-through put sequencing results showed that a total of 114 yeast genera were detected in all soil samples, belonging to Ascomycota (60 genera) and Basidiomycota (54 genera). The most dominant genus, *Cryptococcus*, was present in greater than 10% abundance in each sample. Overall, the differences in yeast diversity between non-rhizosphere and rhizosphere soil of peach trees at 3, 8 and 15 years were not significant. Principal coordinate analysis (PCoA) showed that differences in yeast community structure were more pronounced at the temporal scale compared to the spatial scale. The results of soil physical and chemical analysis showed that the 15-year-old peach rhizosphere soil had the lowest pH, while the OM, TN, and TP contents increased significantly. Redundancy analysis showed that soil pH and CO were key factors contributing to changes in soil yeast community structure in the peach orchard at both spatial and temporal scales. The results of co-occurrence network analysis showed that the peach orchard soil yeast network showed synergistic effects as a whole, and the degree of interactions and connection tightness of the 15-year-old peach orchard soil yeast network were significantly higher than the 3- and 8-year-old ones on the time scale. The results reveal the distribution pattern and mechanism of action of yeast communities in peach orchard soils, which can help to develop effective soil management strategies and improve the stability of soil microecology, thus promoting crop growth.

KEYWORDS

yeast community, spatio-temporal scales, high-throughput sequencing, co-occurrence network, orchard soil

1. Introduction

Yeast is known as the first "domesticated microorganism" in human history and is widely used in food fermentation, industry and agriculture, and pharmaceutical production because of its short growth cycle, high metabolic efficiency, and production of beneficial metabolites (Zhao et al., 2004). In recent years, yeasts have been shown to play a key role also in the biosorption of heavy

metal ions in the environment, in building the balance of ecosystems, and in the prevention and control of polluted environments (He et al., 2022; Igwegbe et al., 2022). Yeast has an extremely wide distribution habitat, and since it prefers acidic and sugar-rich habitats, it is usually found in orchards, mainly from different organs of fruit trees such as leaves, flowers and fruits, as well as from orchard soil (Yang and Wang, 2009). Not only can novel yeast species be found in the orchard soil (Chen et al., 2010, 2012), but also many yeasts with excellent performance can be screened to add unique flavor to the fruit wine (Chen et al., 2018; Wang et al., 2022). There are also some orchard soil yeasts that can be used to control fruit tree diseases or to alleviate post-harvest diseases of fruits to extend the shelf life of fruit (Wang et al., 2016; Ferraz et al., 2019). In addition, some soil yeasts can indirectly promote plant root growth and development by enhancing colonization of arbuscular mycorrhizal (AM) fungal in host plants (Boby et al., 2008; Mirabal Alonso et al., 2008), and there are also yeasts that possess the ability to solubilize rock phosphate or produce plant growth regulators to improve plant growth directly (Nassar et al., 2005; El-Tarabily and Sivasithamparam, 2006; Kumla et al., 2020). Because of this, soil conditioners containing yeast have been developed to improve crop productivity (Ito and Ito, 2001). Research is also ongoing on the potential of soil yeast as a biofertilizer, which can also reduce the damage to the soil caused by conventional chemical fertilizers to some extent and rebuild the maintenance capacity of agroecosystems (Hernández-Fernández et al., 2021; Marques et al., 2021). Therefore, the study of yeast diversity in orchard soils is still of great importance and can provide rich strain resources for social production. In fact, in addition to exploring the function of soil yeasts in orchards, the search for relevant factors affecting the diversity and composition of yeast communities has also never stopped.

Soil yeast diversity and community structure are generally influenced by factors such as soil type, type of vegetation covered, climatic conditions, and geographic location (Vadkertiová et al., 2017). For instance, in vineyards, different grape types' cultivated soils varied in their diversity of yeast composition and abundance of the same yeast species, and there was a significant relationship between some yeast species and particular grape varieties (Zhang et al., 2017). Moreover, distinct yeast strains obtained from various vineyard soils resulted in noticeably diverse fermentation flavors, providing directions for future screening of edible grape yeasts and genetic improvement of edible grapes (Wang et al., 2022). Yeast populations living in soil under various fruit tree species varied in species richness and evenness, with the highest species richness in soil next to apricot trees, according to a previous study of yeasts in 200 soil samples from five fruit tree species (apple, pear, plum, peach, and apricot) in two regions of Slovakia (Vadkertiová et al., 2019). Numerous earlier studies have demonstrated that the number of yeast cells tends to decrease as soil depth increases. This is because deeper soil contains less efficient nutrients and soil organic matter, which is unfavorable for the survival of yeast (Starmer and Lachance, 2011; Yurkov, 2018). As well, rhizosphere soil yeasts are more numerous than bulk soil due to their ease of uptake of simple organic carbon compounds secreted by plant roots and their ability to feed on spoilage fruits deposited in the soil (Cloete et al., 2009; Botha, 2011). Understanding the survival mechanism of yeast in orchard soil ecosystem is crucial for the growth and application of yeast resources.

Peach is rich in many essential substances for human body, including protein, crude fiber, various amino acids, carotenoids and minerals such as iron and phosphorus (Yin et al., 2017), and is known as the "first fruit of the world" (Zhou and Zhang, 2009). Shihezi, Xinjiang, is located in the middle of the northern foot of Tianshan Mountains and the southern edge of Junggar Basin (Fan et al., 2006). It has a dry climate, abundant light, heat and water sources, a wide day-night temperature range, long daylight hours, drought, and little rain during the fruiting season of fruit trees, all of which are very conducive to the accumulation of sugar and dry matter in fruits as well as the accumulation of rich yeast resources (Xu et al., 2015). Previous studies on microorganisms in peach orchards have focused either on the biological control of postharvest peach fruit diseases, on the structural analysis of peach leaf-attached yeast communities in peach orchards by a culture-independent method, or on the culturable yeast diversity of soil in peach orchards by a culture-dependent method (Yin et al., 2017; Liu et al., 2019; Wang et al., 2019). However, the yeast diversity and community composition in non-rhizosphere and rhizosphere soils of perennial peach trees containing both culturable and nonculturable yeasts, and whether they are influenced by annual (yearly) variation and soil factors, are not yet known, which will be a bottleneck for studying yeast adaptation mechanisms in peach orchards and their further development and utilization.

As a natural breeding ground for microorganisms, each gram of soil may contain millions of microbial species (Bunge et al., 2006), and most (>99%) are non-culturable microorganisms. Illumina MiSeq high-throughput sequencing technology allows for more comprehensive and accurate detection of species composition compared to traditional culture-dependent methods (Zebin et al., 2016). Here, we studied the diversity and composition of yeast communities associated with the non-rhizosphere and rhizosphere soil of peach trees of different ages based on Illumina MiSeq high-throughput sequencing technology in peach orchard of Shihezi, Xinjiang. The aim was to explore the differences in soil yeast diversity and community structure in the peach orchard at temporal and spatial scales, the correlation between soil factors and yeast communities, the variation of the soil yeast co-occurrence network in the peach orchard at spatial and temporal scales, and the mechanism of yeast action in the network. Our study provides supplemental information for a comprehensive understanding of peach orchard yeast resources, factors affecting soil yeast composition in perennial peach trees, and the mechanisms of action among yeasts in peach orchard soils, as well as some ideas for achieving sustainable agricultural development in the peach orchard.

2. Materials and methods

2.1. Study site and sample collection

Our soil samples were collected from a peach orchard in Shihezi 143rd Regiment (N44°28′, E85°82′, Altitude 450 m), Xinjiang. The soil type is gray desert soil with a medium loamy texture, cultivated at a depth of 80–100 cm with good permeability, and the peach trees are

Abbreviations: OTU, Operational taxonomic units; CO, Conductivity; SWC, Soil water content; OM, Organic matter; TN, Total nitrogen; TP, Total phosphorus; TK, Total potassium; PRECTP, Average annual precipitation; TEMP, Average annual temperature; LST, Average annual land surface temperature; RH, Average annual relative humidity; EVLAND, Average annual evaporation land; PCoA, Principal coordinates analysis; RDA, Redundancy analysis.

TABLE 1 Meteorological data of Shihezi region in the past 10 years.

Year	PRECTP (mm)	TEMP (°C)	LTS (°C)	RH (%)	EVLAND (mm)
2013	18.15 ± 3.743	8.00 ± 2.993	7.08 ± 3.448	48.14 ± 1.463	24.95 ± 4.948
2014	16.19 ± 2.993	6.65 ± 3.320	5.85 ± 3.706	46.33 ± 2.519	22.99 ± 4.833
2015	21.86 ± 3.808	7.81 ± 3.071	6.96 ± 3.546	49.15 ± 2.225	26.20 ± 5.266
2016	22.94 ± 4.876	7.81 ± 3.149	7.00 ± 3.600	52.67 ± 1.970	30.89 ± 6.938
2017	16.83 ± 3.469	7.56 ± 3.152	6.81 ± 3.548	49.31 ± 2.436	24.87 ± 5.440
2018	17.85 ± 3.003	6.29 ± 3.499	5.25 ± 4.025	50.57 ± 2.506	23.02 ± 4.079
2019	17.62 ± 4.083	7.28 ± 3.245	6.28 ± 3.714	50.32 ± 2.436	23.54 ± 4.746
2020	16.45 ± 3.415	7.09 ± 3.143	6.16 ± 3.628	48.30 ± 2.116	24.01 ± 4.651
2021	15.97 ± 2.746	7.54 ± 3.136	6.53 ± 3.611	46.47 ± 2.082	22.56 ± 4.193
2022	13.50 ± 2.042	8.02 ± 3.375	7.26 ± 3.870	44.46 ± 2.731	16.43 ± 3.027

Sample abbreviations are as in Figure 1. Climate factors: Average annual precipitation (PRECTP), Average annual temperature (TEMP), Average annual land surface temperature (LST), Average annual relative humidity (RH), The annual average evaporation land (EVLAND). The values of mean ± SE (standard error) of meteorological data of Shihezi region in the past 10 years are shown in the table.

planted with a spacing of 5.0 m between plants and 6.0 m between rows, with a density of 330 plants per hectare (ha). The site is planted on 500 hectares and has year-round good irrigation conditions. All peach trees of the peach orchard are *Amygdalus persica* L. "Compressa." The climate of the Shihezi region is typical of a temperate continental climate, with long and severe winters and short and hot summers (Han et al., 2008). The climate information of the sampling sites is shown in Table 1. The data of precipitation (PRECTP) and temperature (TEMP) from NOAA—Climate Prediction Center,[1] land surface temperature (LST) and relative humidity (RH) from NASA GES DISC MERRA2—inst1_2d_asm_Nx,[2] evaporation land (EVLAND) from NASA GES DISC MERRA2—tavg1_2d_lnd_Nx (see footnote 2).

Non-rhizosphere and rhizosphere soils were collected from peach trees of 3, 8 and 15 years of age, respectively. Non-rhizosphere soil samples, i.e., bulk soil samples (S3B, S8B, S15B) were collected at a distance of 1 m from the main trunk and at a depth of 30 cm, while rhizosphere soil samples (S3R, S8R, S15R) were collected at a distance of 30 cm from the main trunk and at a depth of 30 cm. Samples were collected using a five-point sampling method. Specifically, five peach trees each of three, eight, and fifteen years of age were randomly selected, and non-rhizosphere and rhizosphere soils were collected from each tree separately according to the previously described requirements, and plant residues and stones were removed with a shovel and sieve. Each of the five soil samples of non-rhizosphere and rhizosphere soils from the same tree age was then homogeneously mixed and divided into three equal parts, respectively. Both non-rhizosphere and rhizosphere soil samples have three replicates for each tree age, for a total of 18 samples. Samples were collected at the fruiting stage. Each sample was stored individually in sterile self-sealing bags and transported to the laboratory immediately, then filtered with a 2 mm sieve. They were divided into two parts: one part stored at room temperature for soil physicochemical analysis; the other part was stored in a −20°C refrigerator for subsequent DNA extraction.

2.2. DNA extraction and PCR amplification

PowerSoil® DNA Isolation Kit (MoBio Laboratories) was used to extract total DNA in triplicate from soil samples (0.25 g) by using manufacturer's protocol. The DNA extractions from the same soil sample were combined, then quantified using a NanoDrop 2000 UV–Vis spectrophotometer (Thermo Scientific, United States). The integrity of the DNA was detected using 0.8% agarose gel electrophoresis. The purity and amount of DNA is shown in Supplementary Table S1. The region D1 of the LSU rRNA gene was amplified with a pair of specific primers with barcode NL1F (5′-GCATATCAATAAGCGGAGGAAAAG-3′) and NL2R (5′-CTTGTTCGCTATCGGTCTC-3′; Liu et al., 2018). The PCR reaction system were performed in 20 μL volume containing 5× Fast*Pfu* Buffer (4 μL), 5 μM forward primer and reverse primer (0.8 μL each), 2.5 mM dNTPs (2 μL), 0.4 μL Fast*Pfu* Polymerase, 0.2 μL BSA, and 10 ng of the template DNA. An equal amount of sterile water instead of template DNA was used as a negative control. Amplification was initiated with 5 min at 98°C, followed by 30 cycles of denaturation at 98°C for 30 s, primer annealing at 52°C for 30 s, extension at 72°C for 45 min, and final extension for 5 min at 72°C. Reactions, performed in triplicate, were combined. The PCR products were purified by using 2% agarose gel electrophoresis followed by the AxyPrep DNA Gel Extraction Kit (Axygen Biosciences, United States) and quantified using QuantiFluor™-ST (Promega, United States; Zhang et al., 2018). High-throughput sequencing with the Illumina MiSeq PE300 platform (Illumina, United States) was performed by using paired-end sequencing, which follows the instructions by Personal Biotechnology Co., Ltd. (Shanghai, China).

2.3. Sequence processing

The raw Illumina sequences were assigned to individual samples based on their unique barcodes. Raw sequence files were then demultiplexed, quality filtered and analyzed by merging Paired-end reads with FLASH and the Quantitative Insight Into Microbial Ecology (QIIME) software package, respectively (Caporaso et al., 2010; Magoč and Salzberg, 2011). Operational taxonomic unit (OTU) were clustered using UPARSE (version 7.1; http://drive5.

1 https://www.cpc.ncep.noaa.gov/

2 https://disc.gsfc.nasa.gov/

com/uparse/) with a threshold of 97% pairwise identity (Edgar, 2013). UCHIME software was used to identify and remove the chimeric sequences. OTUs were classified taxonomically using the Ribosomal Database Project (RDP) classifier (version 2.2; http://sourceforge.net/pro-jects/rdp-classifier/; Wang et al., 2007) against the database of National Centre for Biotechnology Information (NCBI; National Centre for Biotechnology Information, https://www.ncbi.nlm.nih.gov/public/). Any OTUs representing non-yeast sequences were removed before down-stream analysis (Bokulich et al., 2013).

2.4. Determination of soil physical and chemical properties

The soil water suspension was shaken for 30 min and then measured by a glass electrode meter for pH value. Conductivity (CO) was measured by electrode method after mixing a naturally dried soil sample with water at a ratio of 1:5 (M/V). Soil water content (SWC) was measured by the drying method, where a moist soil sample of known weight is dried in an oven and then weighed, and the moisture lost by heating represents the soil moisture in the moist sample. Organic matter (OM) was measured by titration with ferrous sulfate, using o-phenanthroline as the indicator. The total nitrogen (TN) was determined by the Kjeldahl method. Total phosphorus (TP) and total potassium (TK) were measured by acid solubilization (Bao, 2007).

2.5. Data analysis

The observed richness (Sobs), ACE index, Chao1 estimator, Shannon diversity index and Simpson diversity index of the samples were calculated using QIIME (Caporaso et al., 2010). And the rarefaction curve was plotted based on the diversity index using the "vegan" and "ggplot2" packages in R (v4.3.0). Alpha diversity and soil physical and chemical properties were compared between samples by SPSS Statistics v25.0 software (IBM, United States) based on Kruskal-Wallis test. All values are presented as mean ± standard error (mean ± SE). Differences were taken statistically significant at $p < 0.05$. The Venn diagram was drawn using the "VennDiagram" package and the community bar graph was plotted using "ggplot2" and "ggalluvial" packages in R (v4.2.1). Heatmap were created based on the "vegan" and "pheatmap" packages in R (v4.3.0) to analyze the differences in dominant genera across samples. Principal co-ordinate analysis (PCoA) was done based on Bray-Curtis at OTU level to analyze similarities or differences in the community composition of samples using "vegan" and "ape" packages in R (v4.3.0). Tests for differences between groups in PCoA were analyzed using ANOSIM (analysis of similarities) by vegan package in R. Redundancy analysis (RDA) was used to evaluate the relationships between soil factors and yeast communities, and the plot was drawn by the "vegan" and "ggplot2" packages in R (v4.3.0). Construct a co-occurrence network for each sample group based on the absolute abundance of OTUs. Network topological properties were calculated using the "igraph" package in R (v4.3.0). To reduce network complexity and ensure network reliability, the co-occurrence networks at the genus level were constructed by retaining OTUs with relative abundance ≥ 0.01% and Spearman's correlation coefficient $|r| \geq 0.6$, with significance $p < 0.01$. The co-occurrence network was visualized using Gephi (v.0.10.0; Barberán et al., 2012; Meng et al., 2022). The node data and edge data files for each sample used to generate the co-occurrence network graphs are shown in Supplementary Tables S2–S13.

3. Results

3.1. Alpha diversity of yeast

According to the age of the peach trees and the sampling locations, we divided the 18 soil samples into 6 groups, named S3B (3-year-old non-rhizosphere), S3R (3-year-old rhizosphere), S8B (8-year-old non-rhizosphere), S8R (8-year-old rhizosphere), S15B (15-year-old non-rhizosphere), and S15R (15-year-old rhizosphere). Based on high-throughput sequencing of the D1 domain of the large subunit (LSU) rRNA gene, we obtained a total of 968,960 sequences from 18 soil samples after removing chimeras and sequences with low-quality reads, and 48,114 yeast sequence reads after excluding non-yeast sequence reads. All yeast sequence reads were clustered into 3,103 operational taxonomic units (OTUs) based on 97% similarity. The yeast rarefaction curves of all samples tended to be flat, indicating that the sequencing depth of the samples was sufficient and the sampling was reasonable (Figure 1).

The results of alpha diversity analysis showed that there were no significant differences in the observed species richness (Sobs), species richness (Chao1 and ACE indices) and species diversity (Shannon and Simpson indices; $p > 0.05$; Table 2). The OTUs of S3 (3-year rhizosphere and non-rhizosphere), S8 (8-year rhizosphere and non-rhizosphere) and S15 (15-year rhizosphere and non-rhizosphere) were 1,542, 1,568, and 1,581, respectively. We found that 454 OTUs shared between S3, S8 and S15; 700 OTUs are shared between S3 and S8, 755 OTUs between S3 and S15 and 587 OTUs between S8 and S15. The OTUs of non-rhizosphere (S3B, S8B and S15B) and rhizosphere (S3R, S8R, and S15R) were 2,095 and 2,115, respectively. Among them, the OTUs of S3B, S8B, and S15B were 1,037, 1,027, and 985, respectively; 261 OTUs shared between S3B, S8B, and S15B; 426 OTUs are shared between S3B and S8B, 442 OTUs between S3B and S15B and 347 OTUs between S8B and S15B. The OTUs of S3R, S8R, and S15R were 973, 970, and 1,037, respectively; 222 OTUs shared between S3R, S8R, and S15R; 359 OTUs are shared between S3R and S8R, 425 OTUs between S3R and S15R and 303 OTUs between S8R and S15R (Figure 2).

3.2. Yeast community structure in the soil

Next, 3,103 OTUs were identified as two phyla (Ascomycota and Basidiomycota) and 114 genera. Ascomycota contained 60 genera accounting for 44.78% of all yeast sequences, and Basidiomycota had 54 genera accounting for 55.22% (Tables 3, 4). These include 19 dominant genera that accounted for greater than 1% were *Cryptococcus* (21.40%), *Pichia* (9.615%), *Clavispora* (9.249%), *Tausonia* (5.491%), *Zygosaccharomyces* (4.849%), *Solicoccozyma* (4.527%), *Udeniomyces* (3.912%), *Candida* (3.294%), *Filobasidium* (3.284%), *Trigonopsis* (3.124%), *Aureobasidium* (3.024%), *Papiliotrema* (2.822%), *Saturnispora* (2.752%), *Rhodotorula* (2.060%), *Saitozyma* (2.058%),

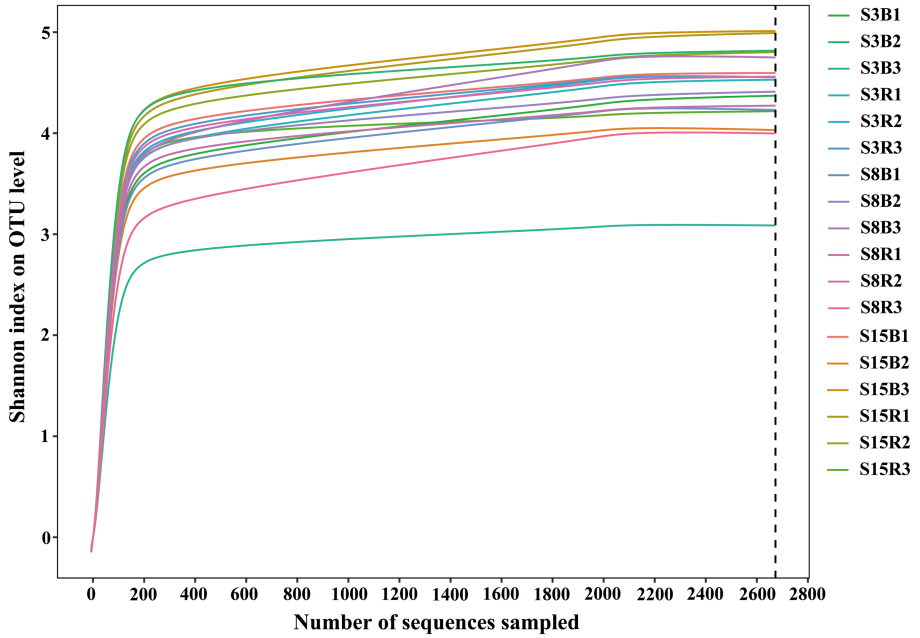

FIGURE 1
Rarefaction curves of all soil samples. Rarefaction curves of OTUs were clustered for a dissimilarity threshold of 3%. S3B, S3R, S8B, S8R, S15B, and S15R represent non-rhizosphere and rhizosphere soil samples from 3-year-old, 8-year-old, and 15-year-old peach trees, respectively. Each sample had three replicates.

TABLE 2 Alpha diversity indices of soil samples in peach orchard.

Sample name	Sobs	Chao1	ACE	Shannon	Simpson
S3B	473.0 ± 60.58a	853.5 ± 66.31a	959.1 ± 99.11a	5.903 ± 0.748a	0.884 ± 0.068a
S3R	470.7 ± 10.68a	843.5 ± 59.85a	938.5 ± 89.50a	6.558 ± 0.012a	0.962 ± 0.005a
S8B	486.0 ± 26.98a	806.0 ± 44.66a	899.5 ± 39.75a	6.440 ± 0.220a	0.953 ± 0.008a
S8R	460.3 ± 26.98a	973.9 ± 67.71a	1054.1 ± 55.16a	6.170 ± 0.234a	0.935 ± 0.012a
S15B	463.0 ± 54.15a	701.5 ± 135.85a	756.3 ± 154.26a	6.559 ± 0.410a	0.949 ± 0.021a
S15R	483.3 ± 36.17a	852.9 ± 81.02a	891.4 ± 84.55a	6.738 ± 0.336a	0.963 ± 0.011a

Samples abbreviations are as in Figure 1. Each sample had three replicates. Sobs index was the observed species richness, Chao1 and ACE indices were used to evaluate species richness, Shannon and Simpson indices were used to evaluate species diversity. The values of mean ± SE (standard error) of three samples are shown in the table. Different lowercase letters indicate a significant difference between groups, while the same lowercase letter indicates no significant difference between groups (Kruskal-Wallis test, $p < 0.05$).

Cyniclomyces (1.567%), *Goffeauzyma* (1.814%), *Naganishia* (1.594%), and *Cyberlindnera* (1.122%). The 19 dominant genera accounted for 87.558% of all yeast sequences. In addition, a total of 15 rare yeast genera (genus with less than 10% frequency of occurrence) were included in all soil samples, accounting for approximately 13.16% of all yeast genera. 33 yeast genera were shared by 18 soil samples, and 24 yeast genera were significantly different among S3B, S3R, S8B, S8R, S15B, and S15R groups ($p < 0.05$; Tables 3, 4).

After that, we show the proportions of 19 dominant genera in each group of soil samples to reveal the differences in yeast community composition between non-rhizosphere and rhizosphere soils of peach trees at different ages (Figure 3). The results showed that the top three dominant genera in S3 were *Cryptococcus* (21.77%), *Clavispora* (15.47%) and *Pichia* (13.27%) in that order; *Cryptococcus* (27.90%), *Zygosaccharomyces* (12.98%) and *Pichia* (9.696%) in S8; and *Cryptococcus* (14.53%), *Tausonia* (7.052%), and *Clavispora* (6.996%) in S15 (Figure 3A). The top three dominant genera in non-rhizosphere soil samples were *Cryptococcus* (18.53%), *Clavispora* (11.14%), and *Pichia* (10.44%) in that order; and *Cryptococcus* (24.27%), *Pichia* (8.787%), and *Clavispora* (7.358%) were found in the rhizosphere soil samples (Figure 3B). Further analysis showed that the top three dominant genera in the soil samples of S3B group were *Pichia* (20.23%), *Clavispora* (19.17%), and *Cryptococcus* (15.29%), in S3R group were *Cryptococcus* (28.25%), *Clavispora* (11.77%), and *Tausonia* (8.206%), in S8B group were *Cryptococcus* (28.68%), *Zygosaccharomyces* (13.97%), and *Cyniclomyces* (8.667%), in S8R group were *Cryptococcus* (27.12%), *Pichia* (14.85%), and *Zygosaccharomyces* (12.00%), S15B soils were *Cryptococcus* (11.62%), *Saturnispora* (10.38%), and *Clavispora* (8.991%), and the top three dominant genera in S15R soils were *Cryptococcus* (17.45%), *Trigonopsis* (7.058%), and *Tausonia* (6.946%), respectively (Figure 3C). And the relative abundances of 7 of the 19 dominant genera differed significantly among the S3B, S3R, S8B, S8R, S15B, and S15R groups, namely *Tausonia*, *Zygosaccharomyces*, *Udeniomyces*,

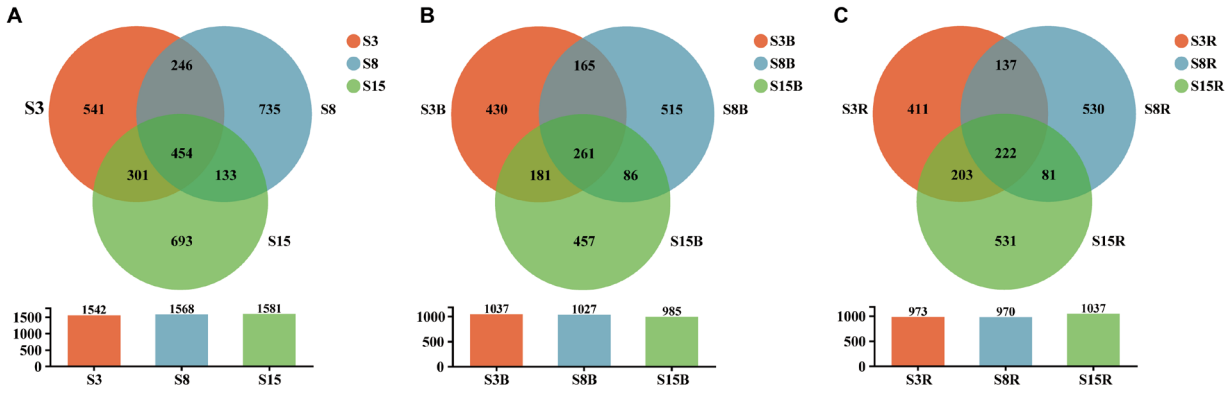

FIGURE 2
Venn diagram at the OTU level of soil samples from **(A)** non-rhizosphere and rhizosphere of 3-year-old (S3), 8-year-old (S8), and 15-year-old (S15) peach trees, **(B)** non-rhizosphere of 3-year-old (S3B), 8-year-old (S8B), and 15-year-old (S15B) peach trees and **(C)** rhizosphere of 3-year-old (S3R), 8-year-old (S8R), and 15-year-old (S15R) peach trees, respectively. Each circle with different colors in the diagram represents a group; middle core numbers represent the number of OTUs common to all groups. The shared and unique yeast OTUs were shown at a 0.03 dissimilarity distance after removing singletons.

Aureobasidium, *Papiliotrema*, *Cyniclomyces*, and *Naganishia* ($p < 0.05$). *Tausonia* and *Udeniomyces* were mainly present in S3R, S15B and S15R, *Zygosaccharomyces* was mainly present in S8B and S8R, *Aureobasidium* was mainly found in S15B and S15R, *Papiliotrema* and *Cyniclomyces* were mainly detected in S8B and *Cyniclomyces* could not be detected in S15R, and *Naganishia* was mainly found in S3R and S15R (Figure 4; Tables 3, 4). In addition, the heat map results largely show that soil samples from the same tree age are clustered together (Figure 4).

3.3. Relationship between yeast communities in soil samples of different ages

We further evaluated the similarity of the yeast community composition of 18 soil samples based on PCoA (Figure 5). The results showed that the variance explained by the first principal axis (PCoA1) alone was 43.92%, and the variance explained by the second principal axis (PCoA2) alone was 14.16%. In general, the 18 samples were first clustered together according to tree age, followed by clustering according to rhizosphere or non-rhizosphere criteria, only with an overlapping between the samples from the S3 and S15 groups on the score plots, indicating significant differences in community composition between groups, and this result can also be proved by both R-value (0.4315) and p-value ($p = 0.001$). S3 and S15 were more similar in community composition for intergroups, and there were significant differences in community composition between rhizosphere or non-rhizosphere samples at the same tree age.

3.4. Relationship among soil samples, yeast community structure, and soil factors

In order to clarify the relationship between soil sample similarity, yeast community structure and soil factors, we first examined the soil physical and chemical properties that including soil pH, conductivity (CO), soil water content (SWC), organic matter (OM), total nitrogen (TN), total phosphorus (TP) and total potassium (TK). The analysis of soil physical and chemical properties showed that the pH values were significantly higher in S3B and S8R and significantly lower in S15R than in the rest of the samples; SWC values were significantly higher in S3B and significantly lower in S8R and S15B than in other samples; while the OM, TN and TK contents were significantly higher in S15R than in other samples ($p < 0.05$); the CO and TK levels were not significantly different in all samples ($p > 0.05$; Table 5).

Moving on, redundancy analysis (RDA) based on yeast genera and soil physical and chemical properties in non-rhizosphere soil samples showed that the first and second RDA components explained 36.1% and 20.3% of the variation, respectively, for a total of 56.4% of the total variation (Figure 6A). The degree of influence of soil factors on yeast communities in non-rhizosphere soils was in the following order: CO (F-ratio: 2.06, p values: 0.04) > TK (F-ratio: 1.90, p-values: 0.086) > SWC (F-ratio: 1.18, p-values: 0.348) > pH (F-ratio: 1.08, p-values: 0.40) > TP (F-ratio: 1.08, p-values: 0.42) > TN (F-ratio: 0.33, p-values: 0.826) > OM (F-ratio: 1.29, p-values: 0.454). Among them, CO was significantly associated with the yeast communities in non-rhizosphere soils ($p < 0.05$). CO was positively correlated with *Pichia* but negatively correlated with *Cyniclomyces*, *Cryptococcus*, *Filobasidium*, and *Papiliotrema*.

Immediately after, we performed a RDA of the correlation between the yeast genera and soil physical and chemical properties in rhizosphere soil samples. The results show that the first and second RDA components explained 39.3% and 21.2% of the variation, respectively, for a total of 60.5% of the total variation (Figure 6B). The degree of influence of soil factors on yeast communities in rhizosphere soils was in the following order: pH (F-ratio: 1.97, p-values: 0.036) > TN (F-ratio: 1.54, p-values: 0.224) > CO (F-ratio: 1.27, p-values: 0.260) > TK (F-ratio: 1.70, p-values: 0.178) > SWC (F-ratio: 1.20, p-values: 0.344) > TP (F-ratio: 0.80, p-values: 0.548) > OM (F-ratio: 0.56, p-values: 0.650). pH was the soil factors that has significant effects on the distribution of yeast communities in rhizosphere soils ($p < 0.05$).

TABLE 3 The percentage and frequency of occurrence of Ascomycetous yeasts (accounted for 44.78%) in all samples.

No.	Genus	Sample name						Total[a] (%)	Occurrence frequency (%)
		S3B (%)	S3R (%)	S8B (%)	S8R (%)	S15B (%)	S15R (%)		
1	*Pichia*	20.23 ± 0.167a	6.310 ± 0.018a	4.539 ± 0.026a	14.85 ± 0.116a	6.559 ± 0.029a	5.200 ± 0.038a	9.615	100
2	*Clavispora*	19.17 ± 0.103a	11.77 ± 0.017a	5.263 ± 0.011a	5.300 ± 0.004a	8.991 ± 0.020a	5.000 ± 0.006a	9.249	100
3[c]	*Zygosaccharomyces*	2.569 ± 0.024b	0.062 ± 0.001b	13.97 ± 0.015a	12.00 ± 0.001a	0.212 ± 0.001b	0.287 ± 0.001b	4.849	100
4	*Candida*	2.419 ± 0.004a	1.546 ± 0.004a	2.008 ± 0.002a	2.993 ± 0.004a	7.333 ± 0.047a	3.467 ± 0.011a	3.294	100
5	*Trigonopsis*	2.818 ± 0.007a	1.746 ± 0.001a	2.581 ± 0.013a	1.460 ± 0.007a	3.080 ± 0.005a	7.058 ± 0.049a	3.124	100
6[c]	*Aureobasidium*	2.058 ± 0.005b	2.020 ± 0.004b	2.270 ± 0.003b	2.245 ± 0.004b	5.487 ± 0.002a	4.065 ± 0.018ab	3.024	100
7	*Saturnispora*	0.399 ± 0.002a	1.434 ± 0.009a	1.609 ± 0.009a	0.873 ± 0.004a	10.38 ± 0.016a	1.821 ± 0.016a	2.752	100
8[c]	*Cyniclomyces*	0.037 ± 0.001b	0.200 ± 0.002b	8.667 ± 0.043a	0.486 ± 0.002b	0.012 ± 0.001b	-	1.567	50
9	*Cyberlindnera*	0.075 ± 0.001a	0.224 ± 0.001a	-	0.025 ± 0.001a	0.137 ± 0.001a	6.273 ± 0.062a	1.122	66.7
10	*Hyphopichia*	0.860 ± 0.007a	0.761 ± 0.005a	0.611 ± 0.003a	1.322 ± 0.002a	0.200 ± 0.001a	0.661 ± 0.005a	0.736	100
11	*Meyerozyma*	1.097 ± 0.005a	0.299 ± 0.001a	0.324 ± 0.001a	0.362 ± 0.001a	0.449 ± 0.001a	1.434 ± 0.009a	0.661	100
12[c]	*Metschnikowia*	0.274 ± 0.001b	0.200 ± 0.001b	0.362 ± 0.001b	0.200 ± 0.001b	0.237 ± 0.013b	2.21 ± 0.003a	0.580	100
13[c]	*Yamadazyma*	0.549 ± 0.003b	0.175 ± 0.001b	0.112 ± 0.001b	0.237 ± 0.001b	1.372 ± 0.002a	0.337 ± 0.001b	0.463	100
14	*Blastobotrys*	0.524 ± 0.002a	0.536 ± 0.002a	0.108 ± 0.001a	0.150 ± 0.001a	0.287 ± 0.001a	0.811 ± 0.004a	0.401	94.4
15[c]	*Geotrichum*	0.125 ± 0.001b	0.274 ± 0.001b	0.010 ± 0.001b	0.150 ± 0.001b	0.412 ± 0.002b	0.935 ± 0.002a	0.333	94.4
16	*Collophora*	0.187 ± 0.001a	0.274 ± 0.002a	0.187 ± 0.001a	0.461 ± 0.002a	0.374 ± 0.001a	0.461 ± 0.001a	0.324	100
17[c]	*Wickerhamomyces*	0.187 ± 0.001b	0.112 ± 0.001b	0.050 ± 0.001b	0.212 ± 0.002b	0.187 ± 0.001b	1.110 ± 0.005a	0.310	94.4
18	*Eremothecium*	0.412 ± 0.001a	0.349 ± 0.001a	0.299 ± 0.002a	0.287 ± 0.001a	0.287 ± 0.001a	0.187 ± 0.001a	0.303	100
19	*Galactomyces*	0.137 ± 0.001a	0.125 ± 0.001a	-	0.112 ± 0.001a	0.112 ± 0.001a	1.097 ± 0.010a	0.264	55.6
20	*Kazachstania*	0.200 ± 0.001a	0.101 ± 0.001a	0.212 ± 0.001a	0.012 ± 0.001a	0.599 ± 0.006a	0.150 ± 0.001a	0.212	83.3
21	*Tetrapisispora*	0.025 ± 0.001a	0.012 ± 0.001a	0.175 ± 0.001a	0.960 ± 0.008a	0.050 ± 0.001a	0.025 ± 0.001a	0.208	61.1
22[c]	*Lachancea*	0.037 ± 0.001b	0.137 ± 0.001ab	0.050 ± 0.001b	0.200 ± 0.001ab	0.474 ± 0.002a	0.050 ± 0.001b	0.158	77.8
23	*Schizosaccharomyces*	0.162 ± 0.001a	0.100 ± 0.001a	0.212 ± 0.001a	0.037 ± 0.001a	0.010 ± 0.002a	0.249 ± 0.002a	0.143	88.9
24	*Nakaseomyces*	0.324 ± 0.003a	0.012 ± 0.001a	0.112 ± 0.000a	0.112 ± 0.001a	-	0.050 ± 0.002a	0.102	55.6
25[c]	*Issatchenkia*	0.087 ± 0.001b	0.037 ± 0.001b	0.012 ± 0.000b	0.025 ± 0.001b	0.387 ± 0.001a	0.025 ± 0.001b	0.096	66.7
26	*Starmerella*	0.012 ± 0.001a	0.237 ± 0.002a	0.012 ± 0.001a	0.025 ± 0.001a	0.050 ± 0.001a	0.150 ± 0.001a	0.081	61.1
27[c]	*Danielozyma*	-	0.050 ± 0.001b	0.037 ± 0.001b	0.125 ± 0.001ab	0.212 ± 0.001a	0.037 ± 0.001b	0.077	66.7
28[c]	*Millerozyma*	0.162 ± 0.001a	0.087 ± 0.001ab	0.037 ± 0.001b	-	0.012 ± 0.001b	0.150 ± 0.001a	0.075	66.7
29	*Hanseniaspora*	0.087 ± 0.001a	0.087 ± 0.001a	0.101 ± 0.001a	0.037 ± 0.001a	0.075 ± 0.001a	0.012 ± 0.001a	0.067	55.6
30	*Wickerhamiella*	0.062 ± 0.001a	0.012 ± 0.001a	0.050 ± 0.001a	0.012 ± 0.001a	0.012 ± 0.001a	0.150 ± 0.001a	0.050	55.6
31	*Ogataea*	0.025 ± 0.001a	0.162 ± 0.001a	0.037 ± 0.001a	0.012 ± 0.001a	0.037 ± 0.001a	0.012 ± 0.001a	0.048	50

10.3389/fmicb.2023.1226142

TABLE 3 (Continued)

No.	Genus	Sample name						Total[a] (%)	Occurrence frequency (%)
		S3B (%)	S3R (%)	S8B (%)	S8R (%)	S15B (%)	S15R (%)		
32	*Magnusiomyces*	0.150 ± 0.001a	-	0.062 ± 0.001a	-	-	0.050 ± 0.001a	0.044	22.2
33	*Zygoascus*	0.037 ± 0.001ab	0.012 ± 0.001ab	-	-	0.012 ± 0.001ab	0.187 ± 0.001a	0.042	38.9
34[c]	*Saccharomyces*	-	0.050 ± 0.001b	-	0.150 ± 0.001a	0.012 ± 0.001b	0.037 ± 0.001b	0.042	44.4
35	*Kluyveromyces*	0.062 ± 0.001a	-	0.037 ± 0.001a	0.025 ± 0.001a	0.075 ± 0.001a	0.050 ± 0.001a	0.042	50
36	*Sugiyamaella*	0.012 ± 0.001a	0.012 ± 0.001a	0.025 ± 0.001a	0.075 ± 0.001a	-	0.075 ± 0.001a	0.033	38.9
37	*Middelhovenomyces*	0.037 ± 0.001a	0.025 ± 0.001a	0.062 ± 0.001a	0.012 ± 0.001a	0.012 ± 0.001a	0.025 ± 0.001a	0.029	50
38	*Schwanniomyces*	0.012 ± 0.001a	0.012 ± 0.001a	0.062 ± 0.001a	0.037 ± 0.001a	0.037 ± 0.001a	-	0.027	38.9
39	*Torulaspora*	0.025 ± 0.001ab	-	-	0.012 ± 0.001ab	-	0.101 ± 0.001a	0.023	22.2
40	*Vanderwaltozyma*	0.037 ± 0.001a	-	0.050 ± 0.001a	-	0.050 ± 0.001a	-	0.023	27.8
41	*Debaryomyces*	-	0.050 ± 0.001a	0.050 ± 0.001a	-	0.012 ± 0.001a	0.012 ± 0.001a	0.021	33.3
42	*Trichomonascus*	0.062 ± 0.001a	0.025 ± 0.001a	0.012 ± 0.001a	0.012 ± 0.001a	0.012 ± 0.001a	-	0.021	33.3
43	*Spencermartinsiella*	0.050 ± 0.001a	0.037 ± 0.001a	-	0.012 ± 0.001a	-	0.012 ± 0.001a	0.019	27.8
44	*Zygotorulaspora*	0.012 ± 0.001a	0.012 ± 0.001a	0.037 ± 0.001a	0.025 ± 0.001a	-	0.012 ± 0.001a	0.017	38.9
45	*Kurtzmaniella*	-	0.025 ± 0.001a	0.025 ± 0.001a	0.025 ± 0.001a	-	0.012 ± 0.001a	0.015	27.8
46	*Saccharomycodes*	-	0.012 ± 0.001a	-	0.025 ± 0.001a	0.037 ± 0.001a	0.012 ± 0.001a	0.015	33.3
47	*Naumovozyma*	-	0.012 ± 0.001ab	-	-	0.012 ± 0.001ab	0.062 ± 0.001a	0.015	22.2
48	*Kodamaea*	0.012 ± 0.001a	-	-	-	0.037 ± 0.001a	0.012 ± 0.001a	0.010	16.7
49	*Scheffersomyces*	0.012 ± 0.001a	0.037 ± 0.001a	-	-	0.012 ± 0.001a	-	0.010	16.7
50	*Tortispora*	-	-	0.012 ± 0.001a	-	0.012 ± 0.001a	0.025 ± 0.001a	0.008	22.2
51	*Barnettozyma*	-	-	-	0.012 ± 0.001a	0.012 ± 0.001a	0.012 ± 0.001a	0.006	16.7
52[b]	*Spathaspora*	-	-	0.025 ± 0.001a	-	-	-	0.004	5.56
53[b]	*Lipomyces*	0.025 ± 0.001a	-	-	-	-	-	0.004	5.56
54[b]	*Sporopachydermia*	-	0.012 ± 0.001a	-	-	0.012 ± 0.001a	-	0.004	5.56
55[b]	*Citeromyces*	0.012 ± 0.001a	0.012 ± 0.001a	-	-	-	-	0.004	11.1
56[b]	*Macrorhabdus*	-	-	-	-	-	0.025 ± 0.001a	0.004	5.56
57[b]	*Nielozyma*	-	-	-	0.025 ± 0.001a	-	-	0.004	5.56
58[b]	*Myxozyma*	0.012 ± 0.001a	-	-	-	-	-	0.002	5.56
59[b]	*Nakazawaea*	-	-	-	-	0.012 ± 0.001a	-	0.002	5.56
60[b]	*Nadsonia*	-	-	-	0.012 ± 0.001a	-	-	0.002	5.56

"-" indicates a value of 0. [a]Percentage of sequence reads for the yeast genus in all samples, [b]rare yeasts of the genera (genus with an occurrence frequency of less than 10% in all samples), [c]Yeast genera with significantly different proportions in the different samples. Different lowercase letters indicate a significant difference between groups, while the same lowercase letter indicates no significant difference between groups (Kruskal-Wallis test, $P < 0.05$).

10.3389/fmicb.2023.1226142

TABLE 4 The percentage and frequency of occurrence of Basidiomycetes yeasts (accounted for 55.22%) in all samples.

No.	Genus	Sample name						Total[a] (%)	Occurrence Frequency (%)
		S3B (%)	S3R (%)	S8B (%)	S8R (%)	S15B (%)	S15R (%)		
1	*Cryptococcus*	15.29 ± 0.026a	28.25 ± 0.022a	28.68 ± 0.085a	27.12 ± 0.080a	11.62 ± 0.005a	17.45 ± 0.027a	21.40	100
2[c]	*Tausonia*	3.467 ± 0.010b	8.206 ± 0.149a	3.629 ± 0.001b	3.542 ± 0.015b	7.158 ± 0.009a	6.946 ± 0.002a	5.491	100
3	*Solicoccozyma*	6.934 ± 0.049a	2.968 ± 0.004a	2.095 ± 0.003a	3.217 ± 0.015a	5.711 ± 0.016a	6.235 ± 0.003a	4.527	100
4[c]	*Udeniomyces*	2.943 ± 0.008b	4.651 ± 0.005ab	3.367 ± 0.005ab	3.192 ± 0.006ab	4.377 ± 0.005ab	4.938 ± 0.004a	3.912	100
5	*Filobasidium*	2.407 ± 0.005a	1.596 ± 0.003a	5.026 ± 0.003a	4.427 ± 0.005a	5.163 ± 0.040a	1.085 ± 0.001a	3.284	100
6[c]	*Papiliotrema*	1.733 ± 0.004ab	3.093 ± 0.003ab	4.015 ± 0.012a	3.143 ± 0.006ab	3.729 ± 0.011ab	1.222 ± 0.005b	2.822	100
7	*Rhodotorula*	0.536 ± 0.001a	7.956 ± 0.063a	0.387 ± 0.001a	0.249 ± 0.001a	2.170 ± 0.010a	1.060 ± 0.003a	2.060	100
8	*Saitozyma*	1.334 ± 0.004a	3.292 ± 0.012a	1.322 ± 0.001a	1.895 ± 0.003a	2.594 ± 0.008a	1.908 ± 0.006a	2.058	100
9	*Goffeauzyma*	1.958 ± 0.007a	1.858 ± 0.003a	1.671 ± 0.003a	1.197 ± 0.004a	1.496 ± 0.004a	2.706 ± 0.008a	1.814	100
10[c]	*Naganishia*	1.122 ± 0.003b	1.858 ± 0.002ab	1.072 ± 0.001b	0.923 ± 0.001b	1.322 ± 0.001b	3.267 ± 0.013a	1.594	100
11	*Mrakia*	0.910 ± 0.003a	1.085 ± 0.001a	0.436 ± 0.001a	0.848 ± 0.002a	0.748 ± 0.001a	1.584 ± 0.010a	0.935	100
12[c]	*Cystofilobasidium*	0.823 ± 0.003ab	1.110 ± 0.003ab	0.486 ± 0.002b	0.549 ± 0.002ab	0.611 ± 0.002ab	1.496 ± 0.005a	0.846	100
13[c]	*Cystobasidium*	0.910 ± 0.005ab	0.723 ± 0.002ab	0.137 ± 0.001c	0.661 ± 0.002ab	1.122 ± 0.002a	0.224 ± 0.001bc	0.630	100
14	*Trichosporon*	0.349 ± 0.001a	0.436 ± 0.001a	0.120 ± 0.001a	0.262 ± 0.001a	0.486 ± 0.002a	1.684 ± 0.012a	0.569	100
15[c]	*Apiotrichum*	0.673 ± 0.001a	0.137 ± 0.001b	0.436 ± 0.002ab	0.474 ± 0.001ab	0.175 ± 0.001bc	0.120 ± 0.001bc	0.349	100
16	*Derxomyces*	0.387 ± 0.001a	0.324 ± 0.001a	0.474 ± 0.001a	0.412 ± 0.001a	0.212 ± 0.001a	0.262 ± 0.001a	0.345	100
17	*Vishniacozyma*	0.362 ± 0.002a	0.212 ± 0.002a	0.362 ± 0.001a	0.349 ± 0.002a	0.399 ± 0.002a	0.162 ± 0.001a	0.308	94.4
18[c]	*Kwoniella*	0.162 ± 0.001b	0.412 ± 0.002ab	0.262 ± 0.001ab	0.150 ± 0.001b	0.524 ± 0.001a	0.324 ± 0.002ab	0.306	100
19	*Piskurozyma*	0.249 ± 0.001a	0.262 ± 0.001a	0.162 ± 0.001a	0.137 ± 0.001a	0.125 ± 0.001a	0.524 ± 0.003a	0.243	88.9
20	*Xanthophyllomyces*	0.224 ± 0.001a	0.262 ± 0.001a	0.162 ± 0.001a	0.137 ± 0.001a	0.262 ± 0.001a	0.125 ± 0.001a	0.195	100
21	*Carlosrosaea*	0.120 ± 0.001a	0.162 ± 0.001a	0.112 ± 0.001a	0.175 ± 0.001a	0.212 ± 0.001a	0.237 ± 0.001a	0.183	100
22	*Heterocephalacria*	0.162 ± 0.001a	0.162 ± 0.001a	0.112 ± 0.001a	0.112 ± 0.001a	0.120 ± 0.001a	0.324 ± 0.002a	0.179	100
23	*Cutaneotrichosporon*	0.012 ± 0.001a	0.137 ± 0.001a	0.037 ± 0.000a	0.012 ± 0.001a	0.374 ± 0.003a	0.412 ± 0.003a	0.164	61.1
24	*Sporobolomyces*	0.137 ± 0.001a	0.436 ± 0.003a	0.037 ± 0.001a	0.062 ± 0.001a	0.125 ± 0.001a	0.075 ± 0.001a	0.145	77.8
25	*Malassezia*	0.324 ± 0.002a	0.010 ± 0.001a	0.010 ± 0.001a	0.062 ± 0.001a	0.062 ± 0.001a	0.212 ± 0.001a	0.143	83.3
26	*Kurtzmanomyces*	0.037 ± 0.001a	0.087 ± 0.001a	0.112 ± 0.001a	0.287 ± 0.002a	0.062 ± 0.001a	0.062 ± 0.001a	0.108	72.2
27[c]	*Sterigmatomyces*	0.050 ± 0.001b	-	0.187 ± 0.001a	0.224 ± 0.001a	0.012 ± 0.001b	0.125 ± 0.001ab	0.100	61.1
28	*Bullera*	0.062 ± 0.001a	0.062 ± 0.001a	0.062 ± 0.001a	0.050 ± 0.001a	0.062 ± 0.001a	0.137 ± 0.001a	0.073	94.4
29	*Sympodiomycopsis*	0.012 ± 0.001a	0.087 ± 0.001a	0.012 ± 0.001a	0.012 ± 0.001a	0.050 ± 0.001a	0.010 ± 0.001a	0.046	44.4
30	*Erythrobasidium*	0.012 ± 0.001a	0.050 ± 0.001a	0.025 ± 0.001a	0.050 ± 0.001a	0.050 ± 0.001a	0.075 ± 0.001a	0.044	38.9
31[c]	*Cystobasidiomycetes*	0.012 ± 0.001b	0.025 ± 0.001ab	0.075 ± 0.000ab	0.025 ± 0.001ab	0.012 ± 0.001b	0.087 ± 0.001a	0.039	66.7

10.3389/fmicb.2023.1226142

TABLE 4 (Continued)

No.	Genus	Sample name						Total[a] (%)	Occurrence Frequency (%)
		S3B (%)	S3R (%)	S8B (%)	S8R (%)	S15B (%)	S15R (%)		
32	*Fereydounia*	0.012 ± 0.001ab	0.025 ± 0.001ab	-	0.012 ± 0.001ab	0.050 ± 0.001ab	0.137 ± 0.001a	0.039	50
33[c]	*Bannoa*	0.012 ± 0.001b	-	0.012 ± 0.001b	0.025 ± 0.001b	-	0.162 ± 0.001a	0.035	33.3
34	*Curvibasidium*	-	-	0.075 ± 0.001a	0.075 ± 0.001a	-	-	0.025	27.8
35	*Tsuchiyaea*	-	0.050 ± 0.001a	0.025 ± 0.001a	0.062 ± 0.001a	-	0.012 ± 0.001a	0.025	38.9
36	*Vanrija*	0.087 ± 0.001a	-	0.012 ± 0.001a	0.025 ± 0.001a	-	0.012 ± 0.001a	0.023	27.8
37[c]	*Hannaella*	0.012 ± 0.001b	0.025 ± 0.001ab	-	0.012 ± 0.001b	0.075 ± 0.001a	0.012 ± 0.001b	0.023	38.9
38	*Trichosporonoides*	0.062 ± 0.001a	0.025 ± 0.001ab	0.025 ± 0.001ab	-	-	-	0.019	33.3
39	*Occultifur*	-	-	-	0.012 ± 0.001a	0.025 ± 0.001a	0.062 ± 0.001a	0.017	22.2
40	*Dioszegia*	0.037 ± 0.001a	-	0.012 ± 0.001a	0.012 ± 0.001a	-	0.025 ± 0.001a	0.015	22.2
41	*Sakaguchia*	-	-	0.012 ± 0.001a	-	0.037 ± 0.001a	0.037 ± 0.001a	0.015	22.2
42	*Cystobasidiopsis*	0.012 ± 0.001a	0.037 ± 0.001a	-	-	0.012 ± 0.001a	0.012 ± 0.001a	0.012	27.8
43	*Sterigmatosporidium*	-	-	-	-	-	0.075 ± 0.001a	0.012	5.56
44	*Acaromyces*	0.025 ± 0.001a	-	-	-	0.037 ± 0.001a	-	0.010	16.7
45	*Microbotryozyma*	-	0.037 ± 0.001a	-	-	0.012 ± 0.001a	-	-	11.1
46	*Ballistosporomyces*	0.037 ± 0.001a	-	-	-	-	-	0.006	5.56
47	*Symmetrospora*	0.012 ± 0.001a	-	-	-	0.025 ± 0.001a	-	0.006	11.1
48	*Kondoa*	-	-	-	0.012 ± 0.001a	0.012 ± 0.001a	-	0.004	11.1
49[b]	*Chionosphaera*	-	-	-	0.025 ± 0.001a	-	-	0.004	5.56
50[b]	*Rhodosporidiobolus*	-	-	0.012 ± 0.001a	-	-	-	0.002	5.56
51[b]	*Meira*	0.012 ± 0.001a	-	-	-	-	-	0.002	5.56
52[b]	*Buckleyzyma*	-	-	-	0.012 ± 0.001a	-	-	0.002	5.56
53[b]	*Langdonia*	-	-	-	-	-	0.012 ± 0.001a	0.002	5.56
54[b]	*Leucosporidium*	-	-	-	0.012 ± 0.001a	-	-	0.002	5.56

"-" indicates a value of 0. [a]Percentage of sequence reads for the yeast genus in all samples, [b]rare yeasts of the genera (genus with an occurrence frequency of less than 10% in all samples), [c]Yeast genera with significantly different proportions in the different samples. Different lowercase letters indicate a significant difference between groups, while the same lowercase letter indicates no significant difference between groups (Kruskal-Wallis test, $P < 0.05$).

10.3389/fmicb.2023.1226142

pH was positively correlated with *Zygosaccharomyces*, *Filobasidium*, *Cyniclomyces,* and *Papiliotrema* but negatively correlated with *Clavispora*, *Trigonopsis*, *Tausonia*, *Solicoccozyma*, *Udeniomyces*, *Goffeauzyma*, and *Naganishia*.

The above results indicate there is a correlation between the yeast communities and soil physical and chemical properties, particularly CO and pH levels in the soil, and that soil chemical properties are important factors influencing the appearance of differences in yeast community structure in non-rhizosphere and rhizosphere soil samples.

3.5. Analysis of yeast co-occurrence networks and topological properties

To investigate the potential interactions of yeast communities and changes in co-occurrence networks at temporal and spatial scales, we constructed yeast co-occurrence networks based on random matrix theory in all samples, in samples of each tree age, and in non-rhizosphere and rhizosphere samples, respectively (Figure 7). The topological properties of the network indicate that the ALL co-occurrence network consists of 126 nodes and 153 edges with an average degree of 2.429, implying that each node is directly connected to approximately two other nodes. The average degree reveals the degree of connectivity of the components in the yeast network, and the higher the average degree, the higher the degree of network interactions. Secondly, the network average clustering coefficient (ACC), average path length (APL), and density of the ALL co-occurrence network are 0.644, 3.769, and 0.019, respectively. These three together reveal the tightness of each component of the network, where the smaller the APL is, the higher the network tightness. The modularity of the network was 0.809 (Values > 0.4 indicate that the network have modular structures), indicating a high degree of modularity and representing a high degree of classification of the community structure and function of yeast. Overall, complex relationships existed in the soil yeast community of the peach orchard (Table 6).

On the time scale, the degree of interactions and tightness of connections among components in the S15 yeast network were significantly higher than those in S3 and S8. In the case that the network average clustering coefficients (ACC) and the average path lengths (APL) of the three network graphs were consistent, the S15 network had the highest number of nodes (731) and edges (11679) and the highest average degree (31.95), density (0.44), and modularity (0.845). The next highest degree and tightness of network interactions was S3, and S8 was the lowest. At the spatial scale, the average degree (4.944), APL (1.506), and density (0.014) of the yeast co-occurrence network of rhizosphere soils were slightly higher, and the ACC (0.886) and modularity (0.842) were slightly lower than those of the non-rhizosphere, indicating a slightly higher degree of interactions and a slightly lower degree of tightness and modularity in the rhizosphere soil network compared to the non-rhizosphere soil. The number of positively correlated edges in the network was greater than the number of negatively correlated edges, both at the overall level and at the temporal and spatial scales, indicating greater synergy and less antagonism among yeast communities. The largest synergistic effect of yeast network was found in the S15 on the time scale, with more than 99.78% of the positive correlation edges, and in the rhizosphere network on the spatial scale, with 100% of the positive correlation edges.

The nodes in the yeast co-occurrence network were divided by genus level, and to explore the variation of core species in the peach orchard soil yeast co-occurrence network, we counted the degree of all genera in each network (Supplementary Tables S14–S19) and enumerated the top five ranked hub genera (Table 7). The analysis showed that nodes in the ALL, S3, S8, S15, non-rhizosphere, and rhizosphere networks belonged to 40, 74, 74, 82, 62, and 68 genera, respectively. Hub genera in the ALL yeast network were, in order, *Zygosaccharomyces* (39.87%), *Cryptococcus* (9.80%), *Pichia* (9.15%), *Udeniomyces* (6.54%), and *Clavispora* (5.88%). The composition and proportion of hub genera in each network changed with spatial and temporal changes. For example, *Pichia* accounted for 11.55% and 15.03% in the S3 and S8 networks, respectively, and only 6.92% in S15. The unique hub genera in the S3 and S15 networks were *Clavispora* and *Filobasidium*, respectively, and the unique hub genera in S8 were *Zygosaccharomyces* and *Trigonopsis*. The non-rhizosphere compared with the rhizosphere network each had two unique hub genera, *Pichia* and *Cyniclomyces* for the non-rhizosphere and *Goffeauzyma* and *Filobasidium* for the rhizosphere.

4. Discussion

4.1. Yeast diversity and community composition of peach orchard

Based on high-throughput sequencing technology we obtained a total of 3,103 yeast OTUs from peach orchard soil, identified as 114 genera belonging to Ascomycota and Basidiomycota (Tables 3, 4). The species richness and species diversity of the soil samples in this study (Table 2) were at a high level compared to other soil types (Yurkov et al., 2016; Vadkertiová et al., 2019). This suggests that peach orchard soils are rich in yeast resources, which is consistent with previous studies obtained using culturable methods (Wang et al., 2019). But compared to traditional culture methods, high-throughput sequencing technology is significantly more advantageous and can provide more comprehensive detection of species composition in habitats (Zebin et al., 2016). Also, the results of the Alpha diversity index among groups showed no significant differences in yeast community diversity between non-rhizosphere and rhizosphere soils at ages 3, 8, and 15 years (Table 2), which indicated that the overall yeast distribution in the peach orchard soil was relatively stable. It validates the conclusions obtained by previous studies that the composition of the soil microbial community under fruit trees is generally more stable than that of annual crops, as it is less likely to be disturbed by management practices (Vadkertiová et al., 2017; Mercado-Blanco et al., 2018).

In our study, Ascomycetous yeast genera were more numerous than Basidiomycetes yeast genera, which further validates the idea that Ascomycetous yeasts are usually more frequent and abundant in agricultural soils, orchards, and grasslands (Slávikova and Vadkertiová, 2003; Yurkov et al., 2012). In addition, we found that 33 yeast genera were detected in both non-rhizosphere and rhizosphere soils of 3-, 8-, and 15-year-old peach trees in the peach

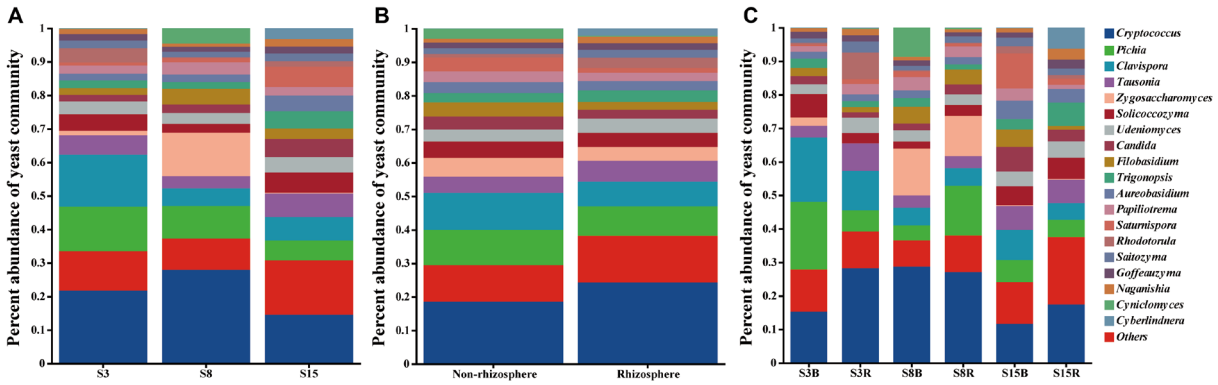

FIGURE 3
Proportion of dominant yeast genera in **(A)** peach trees of different ages soil samples, **(B)** non-rhizosphere and rhizosphere soil samples, and **(C)** non-rhizosphere and rhizosphere soil samples from peach trees of different ages. Others indicated that yeast genera accounted for less than 1%. Each sample had three replicates (Replicates are not specifically shown in the legend, but have been involved in the analysis). Sample abbreviations are same as presented in Figures 1, 2.

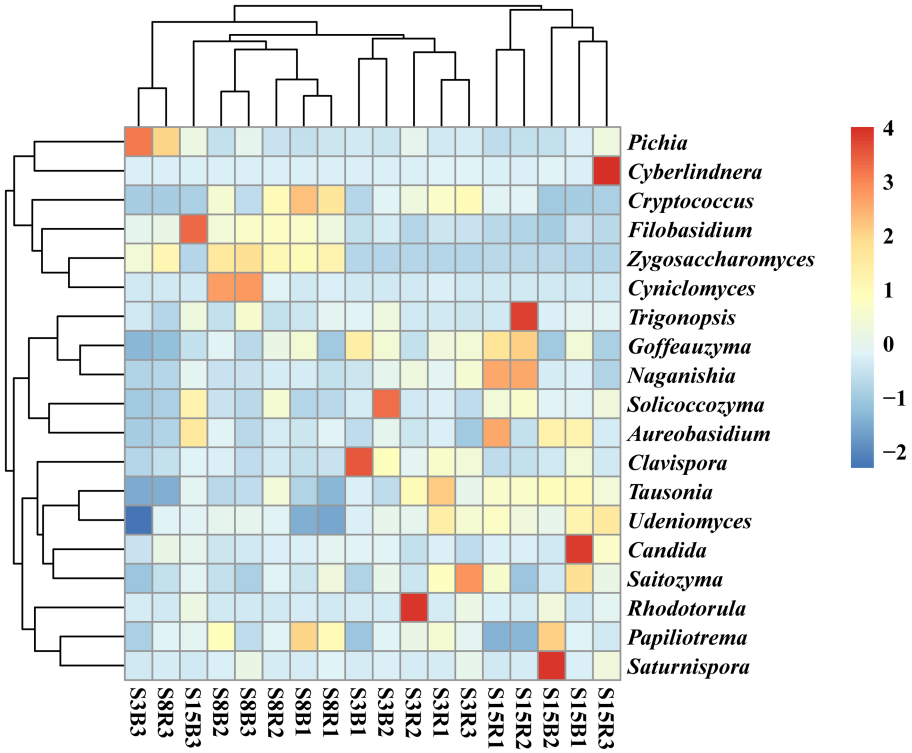

FIGURE 4
Heatmap of the distribution of the top 19 dominant yeast genera among the different soil samples. The normalized relative abundance of each genus is indicated by a gradient of color from blue (low abundance) to red (high abundance). Sample abbreviations are same as presented in Figure 1.

orchard, suggesting that these genera may be resident yeasts in peach orchard soils (Tables 3, 4). Among them, *Cryptococcus*, *Pichia*, *Candia*, *Rhodotorula*, and *Hanseniaspora* can be found in most soil types, but their diversity and abundance of these species vary from one habitat to another (Poliakova et al., 2001; Wang, 2007; Xu, 2009), this is supported by our findings. Apart from that, *Saitozyma*, *Solicoccozyma*, and *Goffeauzyma* are dominant yeasts in our study and are reported to be equally dominant in other soil types (França et al., 2016; Groenewald et al., 2018; Yurkov, 2018). In fact, not every yeast isolated from soil is a native soil dweller but may come from sources other than soil (Phaff et al., 1978; Phaff and Starmer, 1987). For example, some species of the Ascomycetous genera *Aureobasidium*, *Hanseniaspora*, *Metschnikowia*, *Saccharomyces*, and *Pichia*, as well as the Basidiomycetes genera *Rhodotorula*, *Cystobasidium*, *Vishniacozyma*, and *Sporobolomyces* that were detected in this study, are usually dominant species isolated from the above-ground vegetative organs (leaves, flowers, and fruits) of the plant (SlÁviková et al., 2009; Sipiczki, 2016;

Yurkov, 2018). This may be due to the fact that our sampling time was at the peak of the peach tree's fruiting season, and there would be epiphytic yeast entering the soil with the fallen peaches or leaves. Furthermore, the rare yeast genera discovered in this study accounted for approximately 13.16% of the yeast genera in all soil samples (Tables 3, 4), which is significantly lower than the proportion of rare yeasts found in other orchards (Vadkertiová et al., 2019), forest (França et al., 2016), grassland, and shrub soils (Yurkov et al., 2016). Previous studies have shown that reduced precipitation leads to increased populations of rare species in soil habitats (Yurkov et al., 2016). In contrast, the field management pattern of the peach orchard in this study provided sufficient water, so this may be more favorable for yeast survival.

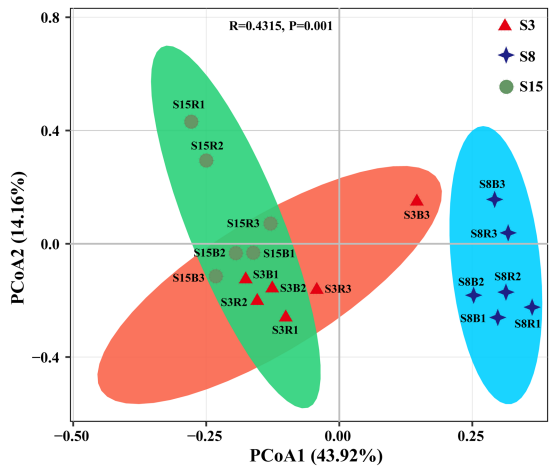

FIGURE 5
Principal Coordinates analysis (PCoA) based on Bray-Curtis distance method at the OTU level. Red triangles, blue diamonds and green circles represent samples from non-rhizosphere and rhizosphere of 3-year-old (S3), 8-year-old (S8), and 15-year-old (S15) peach trees, respectively. Sample abbreviations are same as presented in Figures 1, 2.

4.2. Spatial and temporal characteristics of soil yeast communities In peach orchard

Although there were no significant differences in yeast diversity among the groups, their community structure showed significant variation at temporal and spatial scales, particularly at the temporal scale (Figure 5). The yeast community was most evenly distributed at 15 years compared to the soil yeast community composition at 3 and 8 years (Figure 3; Tables 3, 4). This indicates that the soil yeast community was already more stable at 15 years. Previous studies have shown that an increase in shared species diversity can improve the stability of microbial communities (Wang et al., 2013). The variation in the number of shared yeast OTUs among the three ages in this study also proved this (Figure 2A). And, the stability of the yeast community also contributes to the resistance of peach trees. In addition, the abundance of the shared dominant genera *Zygosaccharomyces* and *Aureobasidium* increased significantly in 8- and 15-year-old peach soils, respectively. *Zygosaccharomyces* has been reported to be involved in the solubilization of soil insoluble phosphate, which may be related to the high phosphorus demand of 8-year-old peach trees (Gizaw et al., 2017; Petkova et al., 2022). Moreover, 8-year-old peach trees may accumulate pathogenic fungi with increasing age, and *Zygosaccharomyces* also has the ability to produce siderophore compounds (iron (III) ion compounds) that inhibit the growth of fungal phytopathogens (Hider and Kong, 2010; Petkova et al., 2022). *Aureobasidium* has been shown to be effective against postharvest fruit pathogens (Di Francesco et al., 2020; Podgórska-Kryszczuk, 2023).

In terms of spatial scale, we found that the total number of yeast OTUs in peach rhizosphere soil was higher than that in non-rhizosphere soil. In agreement with a previous study, rhizosphere microorganisms have better abundance and diversity than non-rhizosphere microorganisms (Yue et al., 2018). In addition, the number of shared OTUs in non-rhizosphere soil samples among different tree ages was higher than the number of shared OTUs in their rhizosphere samples (Figure 2). This indicates that the yeast community is more specific in the rhizosphere soil of different tree ages, possibly influenced by factors such as the rhizosphere secretion of peach trees. It has been reported that root secretions have a selective role in shaping the rhizosphere microbial community structure, which is unique of different plants (Paterson et al., 2007). For example, *Candida*, *Geotrichum*, *Rhodotorula*, and

TABLE 5 The soil physical and chemical properties of soil samples in peach orchard.

Sample name	pH	CO (mS/cm)	SWC (%)	OM (g/kg)	TN (g/kg)	TP (g/kg)	TK (g/kg)
S3B	8.02 ± 0.066ab	0.147 ± 0.018a	0.110 ± 0.017a	17.09 ± 2.356b	0.503 ± 0.058b	0.973 ± 0.082b	77.26 ± 19.55a
S3R	8.04 ± 0.029ab	0.163 ± 0.027a	0.071 ± 0.004ab	16.69 ± 2.783b	0.480 ± 0.049b	0.843 ± 0.032b	46.79 ± 18.19a
S8B	8.33 ± 0.204a	0.127 ± 0.009a	0.079 ± 0.016ab	17.32 ± 3.204b	0.507 ± 0.093b	1.750 ± 0.730b	50.03 ± 2.932a
S8R	8.41 ± 0.119a	0.143 ± 0.033a	0.048 ± 0.004b	15.13 ± 0.494b	0.450 ± 0.006b	0.983 ± 0.112b	46.22 ± 13.28a
S15B	7.93 ± 0.052ab	0.140 ± 0.015a	0.040 ± 0.008b	16.35 ± 0.530b	0.497 ± 0.024b	1.013 ± 0.058b	90.48 ± 23.74a
S15R	7.76 ± 0.042b	0.160 ± 0.010a	0.071 ± 0.025ab	31.20 ± 3.533a	1.037 ± 0.097a	3.573 ± 0.543a	53.79 ± 8.837a

Sample abbreviations are as in Figure 1. Each sample had three replicates. Soil physicochemical properties: pH, Conductivity (CO), Soil water content (SWC), Organic matter (OM), Total nitrogen (TN), Total phosphorus (TP), Total potassium (TK). The values of mean ± SE (standard error) of three samples are shown in the table. Different lowercase letters indicate a significant difference between groups, while the same lowercase letter indicates no significant difference between groups (Kruskal-Wallis test, $p < 0.05$).

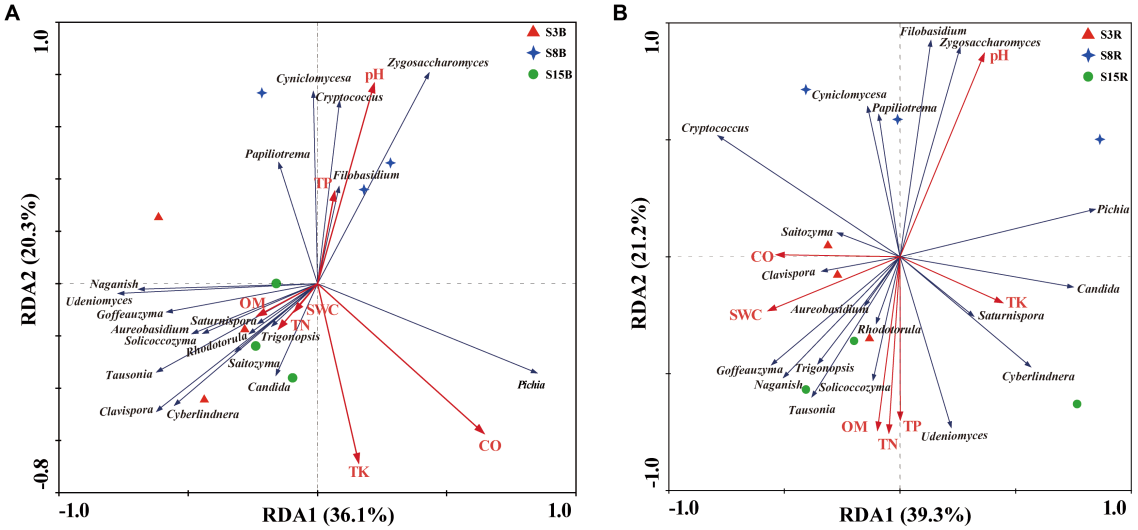

FIGURE 6
Redundancy analysis (RDA) of the correlation between the dominant yeast genera and soil physicochemical properties in **(A)** non-rhizosphere and **(B)** rhizosphere soil samples from peach trees of different ages. Red, blue, and green symbols in **(A)** and **(B)** represent non-rhizosphere and rhizosphere soil samples from 3-year-old (S3), 8-year-old (S8), and 15-year-old (S15) peach trees, respectively. Red and blue arrows represent the soil physical and chemical properties and genera, respectively. Soil physicochemical properties: pH, Conductivity (CO), Soil water content (SWC), Organic matter (OM), Total nitrogen (TN), Total phosphorus (TP), Total potassium (TK). Sample abbreviations are same as presented in Figure 1.

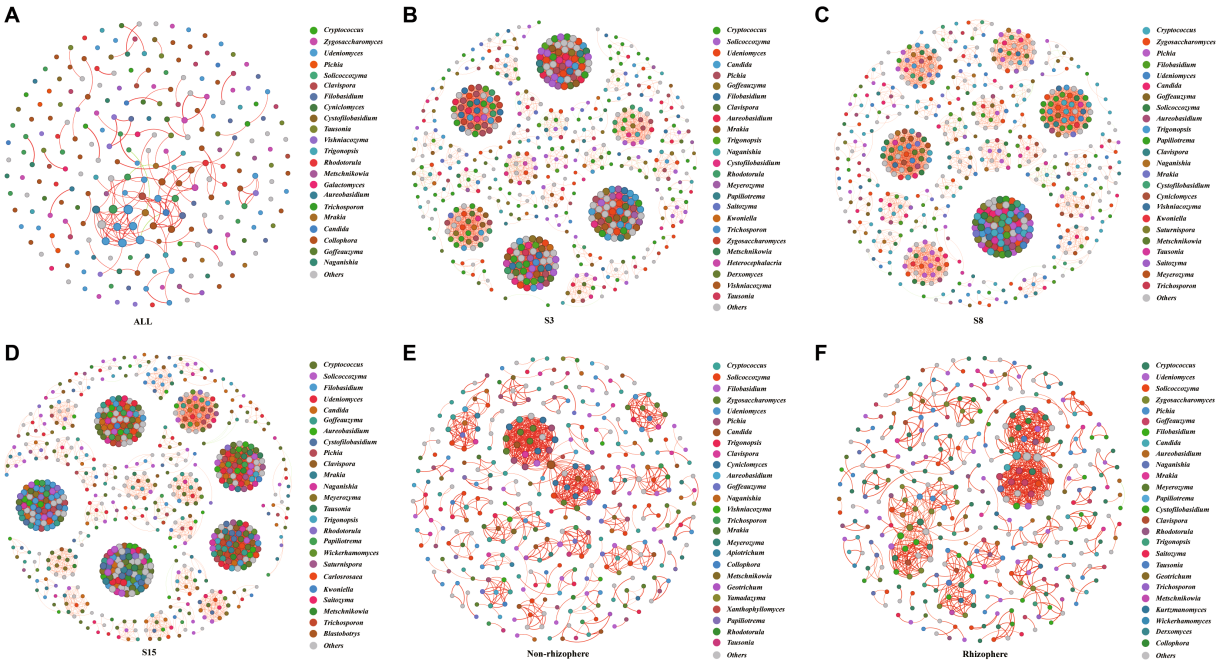

FIGURE 7
Network of co-occurring 90% cutoff OTUs based on correlation analysis. A connection stands for a strong (Spearman's |r|>0.6) and significant (*p*-value <0.01) correlation. Nodes in the network represent different genera (OTUs belonging to the same genera are grouped into the same color); the size of each node is proportional to the number of connections (that is, degree). A red edge represents a positive interaction, and a green edge represents a negative interaction. The thickness of the line is proportional to the correlation coefficient between OTUs. The greater the number of lines indicates the more closely related that OTU is to the others. Others indicated that yeast genera accounted for less than 1%. **(A)** ALL: All soil samples in this study. The remaining sample abbreviations **(B)** S3, **(C)** S8 **(D)** S15 **(E)** Non-rhizosphere **(F)** Rhizosphere are same as presented in Figures 1, 2.

Meyerozyma were all detected in all rhizosphere samples in this study, and their representative species are thought to be associated with nitrification in the soil, where nitrite and phosphate are solubilized *in vitro* to nitrate (Chen et al., 2012; Nakayan et al., 2013). It is worth noting that the abundance of the yeast genera *Metschnikowia*, *Wickerhamomyces*, *Geotrichum*, and *Torulaspora*

TABLE 6 Key topological features of yeast co-occurrence networks in each sample group.

Group	Nodes	Edges	Average degree	ACC	APL	Density	Positive edges	Negative edges	Modularity
ALL	126	153	2.429	0.644	3.769	0.019	150	3	0.809
S3	624	6,834	21.90	1	1	0.035	6,730	104	0.841
S8	599	6,595	22.02	1	1	0.037	6,495	100	0.754
S15	731	11,679	31.95	1	1	0.044	11,653	26	0.845
Non-rhizosphere	361	836	4.632	0.928	1.362	0.013	836	0	0.895
Rhizosphere	360	890	4.944	0.886	1.506	0.014	889	1	0.842

Sample abbreviations are as in Figures 1, 2. ACC, average clustering coefficient; and APL, average path length.

TABLE 7 The top five hub genera in co-occurrence networks for each sample group.

Sample groups	Genus				
ALL	*Zygosaccharomyces*	*Cryptococcus*	*Pichia*	*Udeniomyces*	*Clavispora*
S3	*Candida*	*Pichia*	*Clavispora*	*Cryptococcus*	*Aureobasidium*
S8	*Pichia*	*Zygosaccharomyces*	*Candida*	*Trigonopsis*	*Cryptococcus*
S15	*Candida*	*Filobasidium*	*Aureobasidium*	*Cryptococcus*	*Pichia*
Non-rhizosphere	*Zygosaccharomyces*	*Pichia*	*Candida*	*Cyniclomyces*	*Cryptococcus*
Rhizosphere	*Zygosaccharomyces*	*Cryptococcus*	*Candida*	*Goffeauzyma*	*Filobasidium*

Sample abbreviations are as in Figures 1, 2.

was significantly increased in the 15-year peach rhizosphere soil samples compared to the 3- and 8-year samples. The results of the present study suggest that the increase in abundance of the first three may be caused by the accumulation of a large number of pathogens due to the increase in the number of years of colonization of peach trees. Some representative species of *Metschnikowia* (Sipiczki, 2020; Wang et al., 2021), *Wickerhamomyces* (Lanhuang et al., 2022), and *Geotrichum* (Kawtharani et al., 2022) have been shown to be antagonistic to various pathogens and can be widely used as biocontrol agents in organic agriculture. *T. delbrueckii* in the genus *Torulaspora* has been reported to be able to produce phytase under certain conditions, increasing the nutritional content of peach and improving the absorption of trace elements in peach by humans (Kaur et al., 2007). All these results indicate that the rhizosphere microbial community and plant growth and development are mutually influential. In summary, the changes in yeast community structure in the soil of the peach orchard in this study were consistent with previous findings that soil microbial diversity has certain spatial and temporal characteristics (Kowalchuk et al., 2002; Yue et al., 2018).

4.3. The relationship between yeast community structure and soil factors in peach orchard

The drivers of yeast community assembly in soils are more complex and mainly include the effects of environmental conditions and vegetation (Mašínová et al., 2017), among which soil physicochemical properties are the key factors. Because the soil physical and chemical properties reflect both the growth state of plants and the survival conditions of yeast in the soil. In this study, there were significant differences in soil physicochemical properties among the samples, especially in pH, organic matter (OM), total nitrogen (TN), and total phosphorus (TP; Table 5). The results of the RDA analysis clearly revealed that conductivity (CO) and pH were the main factors influencing the structure of the yeast community (Figure 6). The same conclusion was reached in a previous study of the diversity of soil yeasts isolated from South Victoria Land, Antarctica (Connell et al., 2008). The soil conductivity CO reflects the amount of salt in the soil water solution. Generally speaking, the higher the CO value of the soil within a suitable range, the more fast-acting nutrients are available to the plant (Zhang et al., 2009). We found a significant positive correlation between *pichia* and CO, suggesting that *pichia* may be beneficial to plant growth. In addition, soil pH is also one of the main factors influencing the composition of the soil yeast community. It has been described as the "master soil variable" that influences a myriad of soil biological, chemical, and physical properties and processes and affects plant growth and biomass production (Minasny et al., 2016). The pH of the soil samples collected for this study ranged from 7.76 to 8.41, with an overall weak alkalinity. We found a negative correlation with pH for most of the yeast genera, indicating that overall the yeast community still prefers an acidic environment, which is a common characteristic of yeasts (Chen, 2012). In contrast, the genera *Zygosaccharomyces*, *Filobasidium*, *Cyniclomyces*, and *Papiliotrema* in this study showed a positive correlation with pH, indicating that these three yeast genera prefer alkaline environments for survival.

In this study, we found that 15-year-old peach inter-root soils had the lowest pH but significantly higher levels of OM, TN, and TP than the other samples ($p < 0.05$; Table 5). This indicates that the 15-year rhizosphere soil fertility was higher. Because pH can affect soil function and plant nutrition effectiveness by influencing the chemical solubility and availability of essential plant nutrients, pesticide performance, and organic matter decomposition

(McCauley et al., 2009). Furthermore, *Tausonia*, *Solicoccozyma*, *Trigonopsis*, and *Goffeauzyma* in this study showed positive correlations with OM, TN, and TP, indicating that they grow in abundance in nutrient-rich environments and can be used to indicate soil fertility. In summary, soil CO and pH play an important role in coordinating crop growth and soil yeast community structure. Tracing the factors that contribute to differences in the structure of soil yeast communities helps us better provide solutions to improve soil ecology and thus contribute to the sustainable development of fruit trees.

4.4. Co-occurrence patterns of soil yeasts in peach orchard

To further understand the survival mechanisms of yeast communities in peach orchard soils, we conducted a co-occurrence network analysis of yeast communities in soils in multiple dimensions: overall, temporal, and spatial (Figure 7). Co-occurrence network analysis has now been widely used in the field of microbiology. It measures the interactions between different microbial taxa by correlating the abundance of microbial taxa across multiple soil samples and extracting simple patterns from complex interactions to identify cooperative or competitive relationships between species and further infer community assembly and evolutionary mechanisms (Goberna and Verdú, 2022; Guseva et al., 2022). By calculating the degree of the network nodes, the central node microorganisms of the network can be screened for microorganisms with potential ecological functions (Shetty et al., 2017). The results of this study show that there is significant spatial and temporal specificity in soil yeast community interactions in the peach orchard, with particularly pronounced variation on the temporal scale. This is consistent with the changes in yeast community structure. The degree of interactions and connection tightness of the 15-year-old yeast community were higher than those of the 3-year-old and 8-year-old ones, while there were obvious yeast network modularity, core yeast genera, and network connection nodes, indicating the reliability of the interactions among the 15-year-old soil yeasts. This indicates that the yeast community has acquired certain structural and functional stability in its long-term evolution with increasing age. In addition, there were more positive connections than negative connections in the peach orchard soil yeast network, indicating that yeasts in peach orchard soil prefer to coexist in a synergistic mutualistic manner, and the strongest synergistic effect among the three tree-aged soil yeast networks was found among 15-year-old soil yeasts, which further supports the strong stability of their network structure and function.

Comparatively, although the rhizosphere network was more interactions than the non-rhizosphere, the degree of connectivity tightness and modularity were lower than the non-rhizosphere. It indicates that the interactions between rhizosphere soil yeasts are more random and do not have stability and reliability. And the fact that yeast synergistic effect is lower in the rhizosphere network than in the non-rhizosphere network also illustrates the same issue. Unlike the previous conclusions obtained that a more stable microbial network exists in rhizosphere soils compared to non-rhizosphere soils of wheat (Fan et al., 2018). This may be due to the fact that yeast is more sensitive to environmental changes in soil only as a taxon of fungi, while yeast in inter-rhizosphere soil is more susceptible to the influence of plant roots compared to non-rhizosphere yeast, in addition to the influence of the environment (Paterson et al., 2007; Fan et al., 2018).

At the same time, our observation of each network graph revealed that OTU nodes in low-abundance yeast genera are also likely to have a high degree (Figure 7), which reaffirms the important role of low-abundance microbial genera in maintaining the stability and function of microbial communities (Guo et al., 2022). Furthermore, we found that each network differed in the composition of the hub yeast genera, which may also be a response of the peach orchard soil yeast community to temporal and spatial changes. Hubs in the network are usually defined as keystone species because if these taxa are removed, the network may also split; thus, they play a crucial role in the network structure and can be identified as targets for microbial regulation to improve crop productivity (Olesen et al., 2007). In this study, we can take the hub yeast genera in the network as a reference and then use its related soil factor as a condition for the improvement of peach orchard soil to improve the quality of soil microbiology and finally achieve the purpose of maintaining the health of peach trees and promoting the quality growth of peach trees.

5. Conclusion

In this study, we found for the first time the living strategies of soil yeasts at the spatial and temporal scales of perennial peach trees. Unlike soil yeast diversity in the peach orchard, yeast community structure varies significantly on spatial and temporal scales. Soil factors such as CO and pH were the main factors influencing the differences in yeast community structure. This study reveals the changes in the diversity and community structure of non-rhizosphere and rhizosphere soil yeast at different ages in the peach orchard and the factors affecting them, as well as the spatio-temporal response of the soil yeast network in peach orchards, providing new insights into the role of soil yeast resources in achieving sustainable agricultural development in peach orchards and its spatio-temporal adaptation mechanisms.

Data availability statement

The data of high throughput sequencing in this project has been deposited in the Sequence Read Archive (SRA) of the National Center for Biotechnology Information (NCBI) under the accession number PRJNA992790 (https://www.ncbi.nlm.nih.gov/sra/?term=PRJNA992790).

Ethics statement

Ethical approval is not applicable in the case of the study. However, the collection of the soil samples from the peach orchard was verbally permitted by the farm owner.

Author contributions

SSZ designed and performed the experiments, analyzed the data, and drafted the manuscript. YLC helped design experiments, analyzed the data, and drafted the manuscript. YL performed sample collection, DNA extraction, PCR amplification and analyzed part of the data. JX performed sample collection and soil chemical property analysis. YHL performed sample collection, DNA extraction, and PCR amplification. YFS designed and performed the experiments and analyzed data. All authors contributed to the article and approved the submitted version.

Funding

The work was funded by the National Natural Science Foundation of China (project number: 31860003).

Acknowledgments

The authors would like to thank all the reviewers who participated in the review.

Conflict of interest

The authors declare that the research was conducted in the absence of any commercial or financial relationships that could be construed as a potential conflict of interest.

Publisher's note

All claims expressed in this article are solely those of the authors and do not necessarily represent those of their affiliated organizations, or those of the publisher, the editors and the reviewers. Any product that may be evaluated in this article, or claim that may be made by its manufacturer, is not guaranteed or endorsed by the publisher.

Supplementary material

The Supplementary material for this article can be found online at: https://www.frontiersin.org/articles/10.3389/fmicb.2023.1226142/full#supplementary-material

References

Bao, S. (2007). *Soil agro-chemistrical analysis*, vol. 268–270. Beijing: China Agriculture Press.

Barberán, A., Scott, T., Bates-Casamayor, K., and Fierer, N. (2012). Using network analysis to explore co-occurrence patterns in soil microbial communities. *ISME J.* 6, 343–351. doi: 10.1038/ismej.2011.119

Boby, V., Balakrishna, A., and Bagyaraj, D. (2008). Interaction between Glomus mosseae and soil yeasts on growth and nutrition of cowpea. *Microbiol. Res.* 163, 693–700. doi: 10.1016/j.micres.2006.10.004

Bokulich, N. A., Subramanian, S., Faith, J. J., Gevers, D., Gordon, J. I., Knight, R., et al. (2013). Quality-filtering vastly improves diversity estimates from Illumina amplicon sequencing. *Nat. Methods* 10, 57–59. doi: 10.1038/nmeth.2276

Botha, A. (2011). The importance and ecology of yeasts in soil. *Soil Biol. Biochem.* 43, 1–8. doi: 10.1016/j.soilbio.2010.10.001

Bunge, J., Epstein, S. S., and Peterson, D. G. (2006). Comment on "computational improvements reveal great bacterial diversity and high metal toxicity in soil". *Science* 313:918. doi: 10.1126/science.1126593

Caporaso, J. G., Kuczynski, J., Stombaugh, J., Bittinger, K., Bushman, F. D., Costello, E. K., et al. (2010). QIIME allows analysis of high-throughput community sequencing data. *Nat. Methods* 7, 335–336. doi: 10.1038/nmeth.f.303

Chen, R. (2012) Study on soil microbial diversity and new species of yeasts in apple orchards. Ph.D. thesis. Shandong Agricultural University.

Chen, R., Jiang, Y.-M., Wei, S.-C., and Wang, Q.-M. (2012). *Kwoniella shandongensis* sp. nov., a basidiomycetous yeast isolated from soil and bark from an apple orchard. *Int. J. Syst. Evol. Microbiol.* 62, 2774–2777. doi: 10.1099/ijs.0.039172-0

Chen, R., Wei, S.-C., Jiang, Y.-M., Wang, Q.-M., and Bai, F.-Y. (2010). *Kazachstania taianensis* sp. nov., a novel ascomycetous yeast species from orchard soil. *Int. J. Syst. Evol. Microbiol.* 60, 1473–1476. doi: 10.1099/ijs.0.016501-0

Chen, Z. J., Yang, X. C., Zhao, J., Hu, J. X., and Yuan, W. Y. (2018). Breeding of *Saccharomyces cerevisiae* with high ethanol tolerance and its application in kiwi wine. *Sci. Technol. Food Ind.* 39, 141–145,151. doi: 10.13386/j.issn1002-0306.2018.02.027

Cloete, K. J., Valentine, A. J., Stander, M. A., Blomerus, L. M., and Botha, A. (2009). Evidence of symbiosis between the soil yeast *Cryptococcus laurentii* and a sclerophyllous medicinal shrub, *Agathosma betulina* (berg.) Pillans. *Microb. Ecol.* 57, 624–632. doi: 10.1007/s00248-008-9457-9

Connell, L., Redman, R., Craig, S., Scorzetti, G., Iszard, M., and Rodriguez, R. (2008). Diversity of soil yeasts isolated from South Victoria land, Antarctica. *Microb. Ecol.* 56, 448–459. doi: 10.1007/s00248-008-9363-1

Di Francesco, A., Di Foggia, M., and Baraldi, E. (2020). *Aureobasidium pullulans* volatile organic compounds as alternative postharvest method to control brown rot of stone fruits. *Food Microbiol.* 87:103395. doi: 10.1016/j.fm.2019.103395

Edgar, R. C. (2013). UPARSE: highly accurate OTU sequences from microbial amplicon reads. *Nat. Methods* 10, 996–998. doi: 10.1038/nmeth.2604

El-Tarabily, K. A., and Sivasithamparam, K. (2006). Potential of yeasts as biocontrol agents of soil-borne fungal plant pathogens and as plant growth promoters. *Mycoscience* 47, 25–35. doi: 10.1007/s10267-005-0268-2

Fan, L. H., Cui, Y. J., He, Q., and Pan, X. L. (2006). Analysis on the climate change characteristics in the Shihezi region, Xinjiang in recent 40 years. *Arid Zone Res.* 23, 334–338. doi: 10.13866/j.azr.2006.02.024

Fan, K., Gilbert, P., Jack, A., and Chu, H. (2018). Wheat rhizosphere harbors a less complex and more stable microbial co-occurrence pattern than bulk soil. *Soil Biol. Biochem.* 125, 251–260. doi: 10.1016/j.soilbio.2018.07.022

Ferraz, P., Cássio, F., and Lucas, C. (2019). Potential of yeasts as biocontrol agents of the phytopathogen causing cacao witches' broom disease: is microbial warfare a solution? *Front. Microbiol.* 10:1766. doi: 10.3389/fmicb.2019.01766

França, L., Sannino, C., Turchetti, B., Buzzini, P., and Margesin, R. (2016). Seasonal and altitudinal changes of culturable bacterial and yeast diversity in alpine forest soils. *Extremophiles* 20, 855–873. doi: 10.1007/s00792-016-0874-2

Gizaw, B., Tsegay, Z., Tefera, G., and Aynalem, E. (2017). Phosphate solubilizing yeast isolated and characterized from teff rhizosphere soil collected from gojam; Ethiopia. *J. Bacteriol. Mycol.* 5, 218–223. doi: 10.15406/jbmoa.2017.05.00120

Goberna, M., and Verdú, M. (2022). Cautionary notes on the use of co-occurrence networks in soil ecology. *Soil Biol. Biochem.* 166:108534. doi: 10.1016/j.soilbio.2021.108534

Groenewald, M., Lombard, L., de Vries, M., Lopez, A. G., Smith, M., and Crous, P. W. (2018). Diversity of yeast species from Dutch garden soil and the description of six novel Ascomycetes. *FEMS Yeast Res.* 18:7. doi: 10.1093/femsyr/foy076

Guo, B., Zhang, L., Sun, H., Gao, M., Yu, N., Zhang, Q., et al. (2022). Microbial co-occurrence network topological properties link with reactor parameters and reveal importance of low-abundance genera. *NPJ Biofilms Microbiomes* 8:3. doi: 10.1038/s41522-021-00263-y

Guseva, K., Darcy, S., Simon, E., Alteio, L. V., Montesinos-Navarro, A., and Kaiser, C. (2022). From diversity to complexity: microbial networks in soils. *Soil Biol. Biochem.* 169:108604. doi: 10.1016/j.soilbio.2022.108604

Han, C. G., Ding, J. L., Pu, Y. J., Liu, H. T., and Wei, J. B. (2008). The change characteristics of the temperatures and precipitation in Shihezi, Xinjiang in the recent 41 years. *J Arid Land Resourc Environ* 22, 50–54.

He, M., Xu, Y., Qiao, Y., Zhang, Z., Liang, J., Peng, Y., et al. (2022). A novel yeast strain *Geotrichum* sp. CS-67 capable of accumulating heavy metal ions. *Ecotoxicol. Environ. Saf.* 236:113497. doi: 10.1016/j.ecoenv.2022.113497

Hernández-Fernández, M., Cordero-Bueso, G., Ruiz-Muñoz, M., and Cantoral, J. M. (2021). Culturable yeasts as biofertilizers and biopesticides for a sustainable agriculture: a comprehensive review. *Plan. Theory* 10:822. doi: 10.3390/plants10050822

Hider, R. C., and Kong, X. (2010). Chemistry and biology of siderophores. *Nat. Prod. Rep.* 27, 637–657. doi: 10.1039/b906679a

Igwegbe, C. A., Obiora-Okafo, I. A., Iwuozor, K. O., Ghosh, S., Kurniawan, S. B., Rangabhashiyam, S., et al. (2022). Treatment technologies for bakers' yeast production wastewater. *Environ. Sci. Pollut. Res. Int.* 29, 11004–11026. doi: 10.1007/s11356-021-17992-4

Ito, E., and Ito, N. (2001). Soil conditioner and soil-ameliorating method. Google Patents.

Kaur, P., Kunze, G., and Satyanarayana, T. (2007). Yeast phytases: present scenario and future perspectives. *Crit. Rev. Biotechnol.* 27, 93–109. doi: 10.1080/07388550701334519

Kawtharani, H., Beaufort, S., Anson, P., Taillandier, P., Mathieu, F., and Snini, S. P. (2022). Impact of the inoculation method of *Geotrichum candidum*, used as biocontrol agent, on T-2 toxin produced by fusarium sporotrichioides and F. langsethiae during the malting process. *Toxins* 14:239. doi: 10.3390/toxins14040239

Kowalchuk, G. A., Buma, D. S., De Boer, W., Klinkhamer, P. G., and Van Veen, J. A. (2002). Effects of above-ground plant species composition and diversity on the diversity of soil-borne microorganisms. *Antonie Van Leeuwenhoek* 81, 509–520. doi: 10.1023/a:1020565523615

Kumla, J., Nundaeng, S., Suwannarach, N., and Lumyong, S. (2020). Evaluation of multifarious plant growth promoting trials of yeast isolated from the soil of Assam tea (*Camellia sinensis var. assamica*) plantations in northern Thailand. *Microorganisms* 8:1168. doi: 10.3390/microorganisms8081168

Lanhuang, B., Yang, Q., Godana, E. A., and Zhang, H. (2022). Efficacy of the yeast *wickerhamomyces anomalus* in biocontrol of gray mold decay of tomatoes and study of the mechanisms involved. *Foods* 11:720. doi: 10.3390/foods11050720

Liu, K. P., Wei, Y. M., Xiong, J., Sun, Y. F., and Lei, Y. H. (2018). Analysis of diversity of endobiotic yeasts isolated from *Locusta migratoria manilensis* and *Ischiodon scutellaris* Fabricius. *Guangdong Agric Sci* 9, 90–95. doi: 10.16768/j.issn.1004-874X.2018.09.015

Liu, H., Zhang, Y., Wang, C., Sun, Y. F., and Lei, Y. H. (2019). Community structure analysis of yeast attached to flat peach leaves in Xinjiang. *Ecol Sci* 38, 29–34. doi: 10.14108/j.cnki.1008-8873.2019.04.005

Magoč, T., and Salzberg, S. L. (2011). FLASH: fast length adjustment of short reads to improve genome assemblies. *Bioinformatics* 27, 2957–2963. doi: 10.1093/bioinformatics/btr507

Marques, A. R., Resende, A. A., Gomes, F. C., Santos, A. R. O., Rosa, C. A., Duarte, A. A., et al. (2021). Plant growth–promoting traits of yeasts isolated from the tank bromeliad *Vriesea minarum* LB Smith and the effectiveness of *Carlosrosaea vrieseae* for promoting bromeliad growth. *Braz. J. Microbiol.* 52, 1417–1429. doi: 10.1007/s42770-021-00496-1

Mašínová, T., Bahnmann, B. D., Větrovský, T., Tomšovský, M., Merunková, K., and Baldrian, P. (2017). Drivers of yeast community composition in the litter and soil of a temperate forest. *FEMS Microbiol. Ecol.* 93:223. doi: 10.1093/femsec/fiw223

McCauley, A., Jones, C., and Jacobsen, J. (2009). Soil pH and organic matter. *Nutr Manage Module* 8, 1–12.

Meng, L., Xu, C., Wu, F., and Huhe, S. (2022). Microbial co-occurrence networks driven by low-abundance microbial taxa during composting dominate lignocellulose degradation. *Sci. Total Environ.* 845:157197. doi: 10.1016/j.scitotenv.2022.157197

Mercado-Blanco, J., Abrantes, I., Barra Caracciolo, A., Bevivino, A., Ciancio, A., Grenni, P., et al. (2018). Belowground microbiota and the health of tree crops. *Front. Microbiol.* 9:1006. doi: 10.3389/fmicb.2018.01006

Minasny, B., Hong, S. Y., Hartemink, A. E., Kim, Y. H., and Kang, S. S. (2016). Soil pH increase under paddy in South Korea between 2000 and 2012. *Agr Ecosyst Environ* 221, 205–213. doi: 10.1016/j.agee.2016.01.042

Mirabal Alonso, L., Kleiner, D., and Ortega, E. (2008). Spores of the mycorrhizal fungus *Glomus mosseae* host yeasts that solubilize phosphate and accumulate polyphosphates. *Mycorrhiza* 18, 197–204. doi: 10.1007/s00572-008-0172-7

Nakayan, P., Hameed, A., Singh, S., Young, L.-S., Hung, M.-H., and Young, C.-C. (2013). Phosphate-solubilizing soil yeast *Meyerozyma guilliermondii* CC1 improves maize (*Zea mays* L.) productivity and minimizes requisite chemical fertilization. *Plant and Soil* 373, 301–315. doi: 10.1007/s11104-013-1792-z

Nassar, A. H., El-Tarabily, K. A., and Sivasithamparam, K. (2005). Promotion of plant growth by an auxin-producing isolate of the yeast *Williopsis saturnus* endophytic in maize (*Zea mays* L.) roots. *Biol. Fertil. Soils* 42, 97–108. doi: 10.1007/s00374-005-0008-y

Olesen, J. M., Bascompte, J., Dupont, Y. L., and Jordano, P. (2007). The modularity of pollination networks. *Proc. Natl. Acad. Sci. U. S. A.* 104, 19891–19896. doi: 10.1073/pnas.0706375104

Paterson, E., Gebbing, T., Abel, C., Sim, A., and Telfer, G. (2007). Rhizodeposition shapes rhizosphere microbial community structure in organic soil. *New Phytol.* 173, 600–610. doi: 10.1111/j.1469-8137.2006.01931.x

Petkova, M., Petrova, S., Spasova-Apostolova, V., and Naydenov, M. (2022). Tobacco plant growth-promoting and antifungal activities of three endophytic yeast strains. *Plan. Theory* 11:751. doi: 10.3390/plants11060751

Phaff, H. J., Miller, M. W., and Mrak, E. M. (1978). *The life of yeasts*, vol. *59*. Cambridge, Mass: Harvard University Press, 553.

Phaff, H. J., and Starmer, W. (1987). *Yeasts associated with plants, insects and soil*. London: Academic Press, 123–179.

Podgórska-Kryszczuk, I. (2023). Biological control of aspergillus flavus by the yeast *Aureobasidium pullulans* in vitro and on tomato fruit. *Plan. Theory* 12:236. doi: 10.3390/plants12020236

Poliakova, A., Chernov, I., and Panikov, N. S. (2001). Yeast biodiversity in hydromorphic soils with reference to grass-Sphagnum swamp in Western Siberia and the hammocky tundra region (Barrow, Alaska). *Mikrobiologiia* 70, 714–720.

Shetty, S. A., Hugenholtz, F., Lahti, L., Smidt, H., and de Vos, W. M. (2017). Intestinal microbiome landscaping: insight in community assemblage and implications for microbial modulation strategies. *FEMS Microbiol. Rev.* 41, 182–199. doi: 10.1093/femsre/fuw045

Sipiczki, M. (2016). Overwintering of vineyard yeasts: survival of interacting yeast communities in grapes mummified on vines. *Front. Microbiol.* 7:212. doi: 10.3389/fmicb.2016.00212

Sipiczki, M. (2020). *Metschnikowia pulcherrima* and related pulcherrimin-producing yeasts: fuzzy species boundaries and complex antimicrobial antagonism. *Microorganisms* 8:1029. doi: 10.3390/microorganisms8071029

Sláviková, E., and Vadkertiová, R. (2003). The diversity of yeasts in the agricultural soil. *J. Basic Microbiol.* 43, 430–436. doi: 10.1002/jobm.200310277

SlÁviková, E., Vadkertiová, R., and Vránová, D. (2009). Yeasts colonizing the leaves of fruit trees. *Ann. Microbiol.* 59, 419–424. doi: 10.1007/BF03175125

Starmer, W., and Lachance, M.-A. (2011). *Yeast ecology* Elsevier, 65–83. doi: 10.1002/yea.320050708

Vadkertiová, R., Dudášová, H., and Balaščáková, M. (2017). "Yeasts in agricultural and managed soils," in *Yeasts in Natural Ecosystems: Diversity*, eds. P. Buzzini, M. A. Lachance, and A. M. Yurkov (Switzerland: Springer) 117–144.

Vadkertiová, R., Dudášová, H., Stratilová, E., and Balaščáková, M. (2019). Diversity of yeasts in the soil adjacent to fruit trees of the Rosaceae family. *Yeast* 36, 617–631. doi: 10.1002/yea.3430

Wang, Q. G. (2007). Studies on species diversity and application of wild yeast in Xinjiang. M.D. thesis. Shangdong Institute of Light Industry, Jinan, China.

Wang, Q., Garrity, G. M., Tiedje, J. M., and Cole, J. R. (2007). Naive Bayesian classifier for rapid assignment of rRNA sequences into the new bacterial taxonomy. *Appl. Environ. Microbiol.* 73, 5261–5267. doi: 10.1128/AEM.00062-07

Wang, R., Jing, M., Zhao, H., Xu, X., and Shao, Y. (2016). Isolation and screening of antagonism yeast against postharvest mango anthracnose. *Food Res Dev* 37, 180–183. doi: 10.3969/j.issn.1005-6521.2016.07.044

Wang, X., Wang, Z., and Feng, T. (2022). Screening of yeast in various vineyard soil and study on its flavor compounds from brewing grape wine. *Molecules* 27:512. doi: 10.3390/molecules27020512

Wang, Q. Q., Zhang, Y., Lei, Y. H., Feng, L., Xiong, J., and Sun, Y. F. (2019). Diversity of culturable yeast and screening of functional yeast in soils of flat peach trees of different ages in Shihezi. *Biotic Resourc* 9, 44–52. doi: 10.14188/j.ajsh.2019.01.007

Wang, S., Zhang, H., Ruan, C., Yi, L., Deng, L., and Zeng, K. (2021). *Metschnikowia citriensis* FL01 antagonize *Geotrichum citri-aurantii* in citrus fruit through key action of iron depletion. *Int. J. Food Microbiol.* 357:109384. doi: 10.1016/j.ijfoodmicro.2021

Wang, H.-D., Zhang, L.-L., and Zhu, Z.-H. (2013). Effects of clipping and fertilizing on the relationships between species diversity and ecosystem functioning and mechanisms of community stability in alpine meadow. *Chin J Plant Ecol* 37, 279–295. doi: 10.3724/SP.J.1258.2013.00028

Xu, M. X. (2009). Species diversity of wild yeast collected in the east part of Qinhai Province of China. M.D. thesis. Shangdong Institute of Light Industry, Jinan, China.

Xu, Y. N., Li, Q., Liu, Q. P., Xiao, J., Zheng, X. J., and Shi, X. W. (2015). Research Progress of non-saccharomyces yeasts in Xinjian. *Food Ind.* 36, 266–270. doi: 10.13414/j.cnki.zwpp.2019.01.012

Yang, Q., and Wang, Z. (2009). Distribution and function of yeast in eco-environments. *Environ. Sci. Technol.* 32, 86–91. doi: 10.3969/j.issn.1003-6504.2009.04.021

Yin, X. H., Wang, Q. G., Zhang, C., and Shi, J. Y. (2017). Isolation and identification of antagonistic bacteria against peach brown rot and its antibacterial activity. *Sci. Technol. Food Ind.* 38, 128–132. doi: 10.13386/j.issn1002-0306.2017.09.016

Yue, C., Guanghui, L., and Yan, L. (2018). Soil microbial functional diversity of rhizosphere and non-rhizosphere of three dominant herbaceous plants in the Dushanzi District. *Acta Ecol. Sin.* 38, 3110–3117. doi: 10.5846/stxb201703070382

Yurkov, A. (2018). Yeasts of the soil—obscure but precious. *Yeast* 35, 369–378. doi: 10.1002/yea.3310

Yurkov, A., Kemler, M., and Begerow, D. (2012). Assessment of yeast diversity in soils under different management regimes. *Fungal Ecol.* 5, 24–35. doi: 10.1016/j.funeco.2011.07.004

Yurkov, A. M., Röhl, O., Pontes, A., Carvalho, C., Maldonado, C., and Sampaio, J. P. (2016). Local climatic conditions constrain soil yeast diversity patterns in Mediterranean forests, woodlands and scrub biome. *FEMS Yeast Res.* 16:fov103. doi: 10.1093/femsyr/fov103

Zebin, C., Tiyuan, X., Dingkang, W., Guoxing, W., Jiani, L., Zhang, Y., et al. (2016). Diversity analysis of endophytic Fungi in Mentha using Illumina MiSeq high-throughput sequencing technology. *Medicinal Plant* 7. 412:127042. doi: 10.1016/j.surfcoat.2021.127042

Zhang, J. E., Gao, A. X., Xu, H. Q., and Luo, M. Z. (2009). Effects of maize/peanut in tercropping on rhizosphere soil microbes and nutrient contents. *Chin. J. Appl. Ecol.* 20, 1597–1602. doi: 10.13287/j.1001-9332.2009.0253

Zhang, H., Wang, Y., Chen, S., Zhao, Z., Feng, J., Zhang, Z., et al. (2018). Water bacterial and fungal community compositions associated with urban lakes, Xi'an, China. *Int. J. Environ. Res. Public Health* 15:469. doi: 10.3390/ijerph15030469

Zhang, J. J., Yang, X., Guo, C., Li, K., Zhang, W. Y., and Liu, C. H. (2017). The composition and differences of yeasts from the soils cultivating different grape varieties. *Liquor Making* 44, 76–81. doi: 10.3969/j.issn.1002-8110.2017.01.018

Zhao, L. F., Xu, Y. J., and Zhou, H. J. (2004). Study progress on comprehensive utilization of yeast. *Food Res Dev* 25, 29–32. doi: 10.3969/j.issn.1005-6521.2004.04.009

Zhou, C. Y., and Zhang, H. L. (2009) *Peach fruit processing technology. Nongcun Xinjishu Processed Version 2*. doi: 10.3969/j.issn.1002-3542.2009.12.047

frontiers | Frontiers in Microbiology

TYPE Original Research
PUBLISHED 06 October 2023
DOI 10.3389/fmicb.2023.1251698

OPEN ACCESS

EDITED BY
Jian-Wei Guo,
Kunming University, China

REVIEWED BY
Gaurav Raikhy,
Louisiana State University Health Shreveport, United States
Liying Sun,
Northwest A&F University, China

*CORRESPONDENCE
Hangxian Lai
✉ laihangxian@163.com

†These authors have contributed equally to this work and share first authorship

RECEIVED 02 July 2023
ACCEPTED 18 September 2023
PUBLISHED 06 October 2023

CITATION
Guo Q, Sun Y, Ji C, Kong Z, Liu Z, Li Y, Li Y and Lai H (2023) Plant resistance to tomato yellow leaf curl virus is enhanced by *Bacillus amyloliquefaciens* Ba13 through modulation of RNA interference.
Front. Microbiol. 14:1251698.
doi: 10.3389/fmicb.2023.1251698

Plant resistance to tomato yellow leaf curl virus is enhanced by *Bacillus amyloliquefaciens* Ba13 through modulation of RNA interference

Qiao Guo[1†], Yifan Sun[1†], Chenglong Ji[1], Zirong Kong[1], Zhe Liu[1], Yulong Li[1], Yunzhou Li[2] and Hangxian Lai[1*]

[1]College of Natural Resources and Environment, Northwest A&F University, Xianyang, China, [2]College of Agriculture, Guizhou University, Guiyang, China

Introduction: Tomato yellow leaf curl virus (TYLCV), which is a typical member of the genus *Begomovirus*, causes severe crop yield losses worldwide. RNA interference (RNAi) is an important antiviral defense mechanism in plants, but whether plant beneficial microbes used as biocontrol agents would modulate RNAi in defense against TYLCV remains unclear.

Methods: Here, we employed whole-transcriptome, bisulfite, and small RNA sequencing to decipher the possible role of *Bacillus amyloliquefaciens* Ba13 as a bacterial biocontrol agent against TYLCV in RNAi modulation.

Results: Potted tomato plants were exposed to whiteflies for natural viral infection 14 days after bacterial inoculation. Compared with non-inoculated controls, the abundance of TYLCV gene in the leaves of inoculated plants decreased by 70.1% at 28 days post-infection, which mirrored the pattern observed for plant disease index. The expression of the ARGONAUTE family genes (e.g., *AGO3, AGO4, AGO5*, and *AGO7*) involved in antiviral defense markedly increased by 2.44–6.73-fold following bacterial inoculation. The methylation level at CpG site 228 (in the open reading frame region of the RNA interference suppressing gene AV2) and site 461 (in the open reading frame regions of *AV1* and *AV2*) was 183.1 and 63.0% higher in inoculated plants than in non-inoculated controls, respectively. The abundances of 10 small interfering RNAs matched to the TYLCV genome were all reduced in inoculated plants, accompanied by enhancement of photosystem and auxin response pathways.

Discussion: The results indicate that the application of *Ba. amyloliquefaciens* Ba13 enhances plant resistance to TYLCV through RNAi modulation by upregulating RNAi-related gene expression and enhancing viral genome methylation.

KEYWORDS

***Bacillus amyloliquefaciens*, RNA interference, ARGONAUTE family, plant viral disease, antiviral defense**

Introduction

Tomato yellow leaf curl virus (TYLCV) is a single-stranded circular DNA virus of the genus *Begomovirus* (family Geminiviridae). Since it was first discovered in Israel, TYLCV has spread to many other places, including the Middle East, Mediterranean coast, Africa, and Asia (Lu et al., 2023). TYLCV is one of the most detrimental viruses to tomato cultivation and it causes severe crop yield losses in tropical and subtropical regions. Because TYLCV is transmitted through whiteflies (*Bemisia tabaci*) (Gafni, 2003), chemical pesticides are often used to control this virus disease (Palumbo et al., 2001). However, the long-term use of pesticides is harmful to the environment and easily induces resistance in *B. tabaci* (Cahill et al., 1996). Given its advantages such as low cost and environmental friendliness, the use of beneficial microbes as biocontrol strains has attracted increasing interest in the control of TYLCV disease.

Members of *Bacillus* (Kumar et al., 2016), *Pseudomonas* (Shen et al., 2014), and *Trichoderma* (Elsharkawy et al., 2013; Vitti et al., 2015) have been used to control plant diseases by improving plant systemic resistance. There are two main pathways of systemic resistance in plants (Wang et al., 2009). Systemic acquired resistance (SAR) is dependent on salicylic acid and the regulatory protein NPR1 (Mou et al., 2003), whereas induced systemic resistance (ISR) is modulated by hormones such as jasmonic acid and ethylene. It has been shown that plant beneficial microbes can activate disease resistance pathways by regulating the expression of resistance-related genes (Elsharkawy et al., 2012) and the biosynthesis of hormones (Niu et al., 2011), ultimately enhancing plant resistance to the virus.

In addition to systemic resistance, RNA interference (RNAi) is recognized as an important defense mechanism in plants against viral infection (Kanakala and Ghanim, 2016). RNAi can be divided into small interfering RNA (siRNA)-mediated post-transcriptional gene silencing (PTGS) and transcriptional gene silencing (TGS), depending on the site and mechanism of action (Arif et al., 2013). PTGS occurs in the cytoplasm to precisely target and degrade mRNA transcripts of specific genes, which has been widely demonstrated to play an essential role in plant resistance against viral infection (El-Sappah et al., 2021). This process is mainly mediated by 21–24 nt virus-derived siRNA cut by Dicer-like (DCL) nucleases (Zheng et al., 2019). RNA-directed DNA methylation (RdDM)-mediated TGS is another important mechanism of plant defense against geminiviral infection, and it inhibits virus replication by increasing the methylation level of cytosine on the viral genome (Raja et al., 2008). Among them, methylation of CpG sites is crucial for plant defense against virus invasion, and viruses even evade plant defense by reducing the frequency of CpG sites in the genome (de Pradena et al., 2020; Loew et al., 2020).

The occurrence of PTGS and TGS involves the ARGONAUTE (AGO) family proteins, which are effectors of RNAi in plants (Li Z. C. et al., 2019). A growing number of AGO proteins have been identified to participate in the antiviral defense processes in plants. In particular, AGO4 is a major component of TGS that has been widely studied. In the classical RNA polymerase IV-RdDM pathway, the siRNA binds to AGO4 to form an AGO4-siRNA complex. This complex then binds to polymerase IV to take part in methylation of virus genomic sequences that are homologous to the siRNA under the action of domains-rearranged methyltransferase 2 (Matzke et al., 2015). Additionally, AGO3 has been reported to play a vital role in abscisic acid (ABA)-mediated antiviral defense (Alazem et al., 2014). Evidence suggests that both AGO3 and AGO7 play antiviral roles during TCV infection (Zheng et al., 2019). However, it is still unclear whether inoculation with biocontrol strains could modulate AGOs to enhance plant antiviral defense.

A previous study has demonstrated the robust effects of a bacterial strain, *Bacillus amyloliquefaciens* Ba13, for plant growth promotion and TYLCV disease control in tomato (Guo et al., 2019). How the presence of *Ba. amyloliquefaciens* Ba13 modulates the RNAi-based antiviral system in the host plant remains unclear. Here we verified the biocontrol effects of *Ba. amyloliquefaciens* Ba13 against TYLCV and explored the underlying mechanisms from the RNAi perspective. We analyzed the changes in RNAi-related gene expression in TYLCV-infected tomato leaves, as well as the methylation rate of TYLCV genome and the abundance of antiviral siRNAs in plant cells, after bacterial inoculation. The aim of this study was to decipher the possible role of *Ba. amyloliquefaciens* Ba13 in the antiviral RNAi system against TYLCV. The results could provide new evidence for microbial control of viral plant diseases.

Materials and methods

Experimental materials

The biocontrol strain, *Ba. amyloliquefaciens* Ba13 (SUB3558699; GenBank: MG846076), was isolated from a stratified old manured loessial soil under a corn-wheat rotation system in Yangling, Shaanxi Province, China. The strain was preserved by the Resource and Environmental Biology Laboratory in the College of Resources & Environment, Northwest A&F University (Yangling, Shaanxi Province, China). Seeds of tomato (*Solanum lycopersicum* L.) cultivar "Jinpeng 1" were purchased from Xi'an Jinpeng Seedling Co., Ltd. (Xi'an, Shaanxi Province, China). To mimic natural viral infection, the TYLCV pathogen was sourced from viruliferous whiteflies (*B. tabaci*) collected in the field in Yangling.

Seedling cultivation, bacterial inoculation, and viral infection

The pot experiment was carried out in a greenhouse on campus of Northwest A&F University. Plump tomato seeds were selected and surface sterilized with 75% ethanol for 30 s, followed by at least five washes with sterile distilled water. The sterilized seeds were placed evenly onto a filter paper in sterile Petri dishes (~50 seeds per dish). To each dish, 2 mL of sterile water was added and the seeds were incubated in the dark at 26°C until germination. The germinated seeds were evenly sown into potted trays (50 holes per tray) containing seedling substrate and cultivated for 21 days. When true leaves formed, tomato seedlings with uniform growth were selected and transplanted into 60 pots with a diameter of 18.3 cm and a height of 12 cm (one seedling per pot).

Each pot contained fertile field soil collected from a wheat-maize rotation system in Yangling. The soil was classified as Eum-Orthic Anthrosols (Staff, 2010). The soil was passed through a 2-mm sieve before use. The experimental used a randomized complete block design with three blocks, and each block contained 20 pots. The pots in each block were randomly and equally divided into two groups. One group was inoculated with *Ba. amyloliquefaciens* Ba13 (treatment group), while the other group was not inoculated (control group).

Ba. amyloliquefaciens Ba13 was cultured in beef extract–peptone broth at 37°C for 48 h with a shaking frequency of 180 rpm. The bacterial culture was diluted to 1×10^8 colony-forming units (CFU) mL^{-1} with sterile phosphate-buffered saline. For the treatment group, 100 mL of diluted cell culture per pot was applied to the seedlings 7 days post-transplantation. The control group received 100 mL of sterile phosphate-buffered saline per pot. Natural viral infection was performed 14 days after bacterial inoculation. To do this, both non-inoculated controls and *Ba. amyloliquefaciens* Ba13-inoculated plants were placed in a greenhouse with whiteflies. Each block was covered with a 150-mesh high-quality nylon net of 1.2 m × 1.2 m × 1.5 m (length × width × height), and 1000 whiteflies were released under the net for infection over 4 weeks. The average temperature of the greenhouse was 28°C and the average light period per day was 12 h.

Disease severity evaluation, growth measurement, and leaf sampling

The infection rate and disease severity of tomato plants in each group were determined at 14 and 28 days post-viral infection (dpvi). The disease severity was scored as follows (Sun et al., 2016): 0 = healthy plant without with curling yellow leaves; 1 = mild dwarfing (~4/5 height of healthy plant) with curling yellow leaves (<20% on the top); 2 = dwarfing (~2/3 height of healthy plant) with leaf curling and yellowing (<40% on the top); 3 = obvious dwarfing (~1/2 to 2/3 height of healthy plant) with typical curling yellow leaves (60%); and 4 = severe dwarfing (<1/2 height of healthy plant) with typical curling yellow leaves (60% to all), or early withering. The disease index and control rate were calculated as follows.

$$\text{Disease index (\%)} = \frac{\sum(\text{Disease severity} \times \text{corresponding plant number})}{4 \times \text{Total number of plants}} \times 100$$

$$\text{Control rate (\%)} = \frac{\text{Disease index of control group} - \text{disease index of treatment group}}{\text{Disease index of control group}} \times 100$$

Plant height was measured 28 dpvi and leaf samples were taken for subsequent analyses. Three biological samples (repetitions) were collected from each group, and each biological repetition was a mixture of three leaf samples collected from the same part of three random plants in each block. The sample consisting of the first and second leaves from the apical growing point was used for virus quantification; the third leaf was used for whole-transcriptome RNA sequencing (RNA-seq), bisulfite sequencing, and small RNA-seq, as well as for quantitative validation of functional genes; and the fourth leaf was used for the analysis of plant hormone contents. The leaf samples destined for virus quantification and sequencing analyses were rinsed with distilled water and blotted dry, then immediately wrapped with tin foil and placed in liquid nitrogen. The samples for hormone analysis were weighed and then placed into liquid nitrogen. All samples were brought to the laboratory where they were kept at −80°C until used.

Virus genotyping and quantification

Total DNA was extracted from tomato plants using a modified hexadecyltrimethylammonium bromide (CTAB) method. PCR amplification was performed as described in the **Supplementary Note 1**, with previously reported primers for the full-length sequence of the complete TYLCV genome (**Supplementary Table 1**). The amplified products were sequenced to obtain the complete genome sequence. Then we determined the virus type by comparing the obtained sequence with available virus genotypes in the NCBI database. Gene sequence similarity analysis was performed using the MegAlign program in DNAstar (DNASTAR, Inc., Madison, WI, USA). The MEGA-X software (Kumar et al., 2018) and MUSCLE algorithm were used to align the nucleic acid sequences of multiple sequences, while the neighbor joining algorithm was applied to build phylogenetic trees for taxonomic analysis of the virus. There were 23 different TYLCV genotypes in the evolutionary tree (including the virus genotypes identified in this study). Their accession numbers in the NCBI database, origins, and the similarities to the genotype of the virus used in this study are listed in **Supplementary Table 2**. The search of virus open reading frame (ORF) was performed using the NCBI Open Reading Frame Finder.[1]

Quantification of TYLCV in tomato leaves was performed using the method of Sade et al. (2014). Total DNA was extracted from leaf samples using the M5 Plant Genomic DNA Kit (Mei5 Biotech Co., Ltd., Beijing, China). The concentration and purity of extracted DNA were measured using spectrophotometry with an ultra microplate (Epoch, BioTek, Winooski, VT, USA). The DNA integrity was detected using agarose gel electrophoresis. The DNA samples were subjected to real-time fluorescent quantitative PCR on an iQ5 PCR system (Bio-Rad, Hercules, CA, USA) as described in the **Supplementary Note 1**. The PCR amplification was performed using TYLCV-V1 as the primer (**Supplementary Table 1**) and the *EF1* gene as the internal reference. There were three technical replicates for each sample. Data collection and analysis were performed using the Bio-Rad iQ5 software (v2.1.97). The relative expression level of the viral gene was calculated using the $2^{-\Delta\Delta CT}$ method (Schmittgen and Livak, 2008).

Whole-transcriptome RNA-seq and gene functional analysis

Frozen leaf samples were sent to BGI Biotech Co., Ltd. (Shenzhen, China) for transcriptome sequencing using the BGISEQ-500 platform (BGI Biotech). Total RNA was isolated from the leaf samples using Trizol reagent (Invitrogen, Carlsbad, CA,

1 http://www.ncbi.nlm.nih.gov/gorf/gorf.html

USA) according to the manufacturer's instructions. Then mRNA libraries were constructed. Whole-transcriptome RNA-seq data processing was performed as described in **Supplementary Note 2**. The detection of significantly differentially expressed genes (DEGs) was performed following the method described by Wang et al. (2010). Genes with a | fold-change| > 2 and p-value ≤ 0.001 were defined as DEGs.

The DEGs were subjected to Gene Ontology (GO) and pathway enrichment analysis using the PANTHER classification system[2] (Mi et al., 2005) and the Kyoto Encyclopedia of Genes and Genomes (KEGG),[3] respectively (Kanehisa et al., 2008). The basic local alignment search tool (BLASTn) was adopted to identify homologous genes in the tomato genome.[4] The raw sequences were deposited at the Sequence Read Archive in the National Center for Biotechnology Information (NCBI)[5] under BioProject accession number: PRJNA553064.

Quantitative PCR validation

The validation of functional genes was performed by reverse transcription quantitative real-time PCR (RT-qPCR) using six genes involved in gene silencing, plant growth, and disease resistance. The PCR protocols are provided in **Supplementary Note 3**. There were three technical replicates for each sample, and the primer sequences used are provided in **Supplementary Table 1**. The relative expression levels of the selected genes and small RNAs were calculated as described for virus quantification.

ABA analysis

The content of ABA in tomato leaves was measured using a previously reported method (Pan et al., 2010) as described in **Supplementary Data** (**Note S4**). Briefly, the ABA was extracted from leaf samples with 80% methanol/water (v/v) followed by a mixture of 5% acetic acid/ethyl acetate and water (1:1, v/v). The levels of ABA in the extracts were measured using gas chromatography coupled to triple quadrupole mass spectrometry (Agilent, Santa Clara, CA, USA).

Viral genome methylation analysis by bisulfite sequencing

Gene-specific DNA methylation was assessed by a next generation sequencing-based BSP, according to previously published method (Gao et al., 2014). In brief, BSP primers were designed using the online MethPrimer software and listed in **Supplementary Table 1**. A total of 1 μg of genomic DNA was converted using the ZYMO EZ DNA Methylation-Gold Kit (Zymo Research, Irvine, CA, USA) and one twentieth of the elution products were used as templates for PCR amplification with 35 cycles using KAPA 2G Robust HotStart PCR Kit (Kapa Biosystems, Wilmington, MA, USA). For each sample, BSP products of multiple genes were pooled equally, 5′-phosphorylated, 3′-dA-tailed and ligated to barcoded adapter using T4 DNA ligase (NEB). Barcoded libraries from all samples were sequenced on Illumina platform. For the bisulfite sequencing reads of each sample, firstly, adapters and low-quality reads were removed using software Trimmomatic-0.36. After removing the adapter sequences and filtering out the low-quality reads, the clean sequencing reads were directly aligned to the target sequences using software Bsmap (v2.73) with the default parameters which combines genome hashing and bitwise masking to achieve fast and accurate bisulfite mapping. Methylation level of C base in TYLCV genome was calculated as follows.

$$\textit{Methylation rate of C site}\ (\%) = \frac{\text{methylated sequences}}{\text{methylated sequences} + \text{demethylated sequences}} \times 100$$

Small RNA-seq and identification of virus-derived siRNA

Small RNA-seq was used to detected the changes in the types and abundances of siRNA in tomato leaves, which have lengths mainly concentrated in the range of 19–24 nt (Seo et al., 2013). For the sample preparation and library construction, small RNA-seq was performed using the BGISEQ-500 platform (BGI Biotech). Sample selection and total RNA extraction followed the same methods that were used for the whole-transcriptome RNA-seq. Small RNA libraries were then constructed and small RNA-seq data were processed as described in **Supplementary Note 5**. The siRNAs with a p-value ≤ 0.05 were considered significantly differentially expressed. The raw sequences were deposited at the Sequence Read Archive in the NCBI (see text footnote 5) under BioProject accession number: PRJNA553309.

Given that siRNAs can bind to viral mRNA for transcriptional and post-transcriptional inhibition of viral replication, we aligned all the differentially expressed ($p < 0.05$) siRNAs against the genome of the TYLCV-SJ which identified in this study. The alignment of sequences was performed using the SOAP2.22 short-read alignment software package (Li et al., 2009), with no mismatches allowed. For siRNAs that completely matched to the viral genome sequence, their name, sequence, matched site, abundance in the two treatment groups (*Ba. amyloliquefaciens* Ba13 and control), and corresponding viral genotype were recorded.

Statistical analysis

Data were statistically analyzed using DPS 4.0.[6] The comparison of group means was performed using the Student's t-test, except that the disease index values obtained at two time points were compared using the least-significant difference (LSD)

2 http://www.pantherdb.org/data/
3 http://www.kegg.jp/
4 https://solgenomics.net/
5 https://www.ncbi.nlm.nih.gov/sra
6 http://www.dpsw.cn

test. A p-value of less than 0.05 was considered significant. The relative expression levels (fold-changes) of genes and small RNAs were plotted using Excel 2010 (Microsoft Corp., Redmond, WA, USA), and the relative quantities (chromatographic peaks) of plant hormones were drawn using Origin 2022b (OriginLab Corp., Northampton, MA, USA). The enrichment of DEGs in the biotic stress pathway was analyzed using Mapman (Thimm et al., 2004).

Results

TYLCV genotype

Based on PCR amplification and sequencing analysis, the genotype of the virus present in the tomato leaves was identified to be TYLCV virion DNA TYLCV-SJ (GenBank accession number: MN910280.1). The PCR results (**Supplementary Figure 1**) showed that the total length of the viral genome was 2781 nt, which encoded eleven ORFs (>150 bp). The starting and ending sites and coding proteins of corresponding genes and their functions are listed in **Table 1**. According to the phylogenetic tree (**Supplementary Figure 2**) and the comparison of virus genotypes, TYLCV-SJ (MN910280.1) had the closest genetic relationship with TYLCV-JSYC (MF590740) and TYLCV-FJFZ (KX885028). The sequence of TYLCV-SJ was 98.1% similar to that of the Israeli virus genotype TYLCV-IS (X15656), and therefore was deemed to be a relative of the Israeli virus in China.

TYLCV disease control and plant growth promotion

In the pot experiment, the tomato plants presented typical symptoms of TYLCV disease such as leaf curling and yellowing after viral infection. Compared with the control group, the plant height of the group treated with *Ba. amyloliquefaciens* Ba13 increased by 15.4% ($p < 0.05$; **Figure 1A**), while the relative abundance of the TYLCV gene in tomato leaves decreased by 70.1% at 28 dpvi ($p < 0.01$; **Figure 1B**). Additionally, the disease index of the treatment group was significantly lower than that of the control group at 28 dpvi ($p < 0.05$). The corresponding control rates in the treatment group were 38.7 and 32.1% at 14 and 28 dpvi, respectively (**Table 2**).

Modulation of the leaf transcriptome

General data of the transcriptome

Six leaf samples (three from each group) were analyzed using whole-transcriptome RNA-seq, which yielded 10.92 Gb of raw reads per sample. A total of 24,466 genes were detected, among which 1,897 genes (7.8%) were identified as DEGs with a $|$ fold-change$|$ > 2 and $p < 0.001$. There were 1352 DEGs upregulated and 545 DEGs downregulated in the group treated with *Ba. amyloliquefaciens* Ba13 relative to the control group. GO analysis showed that the DEGs were enriched in 2484 GO terms, 433 of which showed significant differences in expression. The 100 most significantly enriched GO terms, and the number of DEGs enriched in these terms, are provided in **Supplementary Table 3**. KEGG analysis revealed that a total of 126 pathways were enriched in the treatment group relative to the control group. Significant differences were found in 12 pathways including photosynthesis-antenna proteins, plant hormone signal transduction, and phenylpropanoid biosynthesis ($p < 0.05$; **Figure 2**).

Differential expression of functional genes

We specifically analyzed gene silencing-related genes after treatment with *Ba. amyloliquefaciens* Ba13. GO analysis showed that a total of eight DEGs including *AGO3*, *AGO4*, *AGO5*, and *AGO7* were enriched in the term gene silencing (GO: 0016458; **Table 3**). Multiple genes of the AGO family were upregulated in the RNAi system after treatment, with the fold-changes ranging from 2.03 to 6.73. The most pronounced upregulation was found in *AGO4*.

In addition to the silencing-related genes, a number of the identified DEGs were found to be involved in disease resistance pathways. *ABF*, a key gene involved in ABA biosynthesis, was upregulated 2.40-fold. Regarding salicylic acid biosynthesis, *NPR1*, an important defense signal regulatory gene downstream of salicylic acid was upregulated 4.58-fold. For mitogen-activated protein kinase (MAPK), eight DEGs related to serine/threonine-protein kinase OXI1 (OX1), mitogen-activated protein kinase kinase kinase (MAPKKK) ANP1, and mitogen-activated protein kinase kinase 4/5 (MKK4/5) were all upregulated between 2.06- and 4.72-fold.

Some DEGs were also found to be involved in growth regulation pathways. Regarding photosynthesis-antenna proteins, 14 DEGs involved in the biosynthesis of four light-harvesting complex II (LHCII) proteins including Lhca4 and Lhcb1 were upregulated between 2.03- and 3.07-fold (**Supplementary Figure 3**). For plant hormone signal transduction, there were 16 DEGs related to early auxin-responsive proteins including auxin-responsive protein/indoleacetic acid (AUX/IAA), small auxin-up RNA (SAUR), and Gretchen Hagen 3 (GH3). Of these 16 DEGs, 15 were upregulated between 2.01- and 236.14-fold. Additionally, three DEGs related to the auxin response factor (ARF) were upregulated, with a maximum fold-change of 3.81. Moreover, the physiological functions of brassinosteroids are similar to those of auxin; in relation to brassinosteroid biosynthesis, 12 DEGs participating in the biosynthesis of the proteins brassinosteroid insensitive 1 (BRI1), brassinosteroid resistant 1/2 (BZR1/2), and BRI1 kinase inhibitor 1 (BKI1), were upregulated. **Supplementary Table 4** summarizes the details (name, involved pathway, and expression change) of the above-mentioned genes.

The DEGs identified by whole-transcriptome RNA-seq were introduced into the corresponding biotic stress pathway in Mapman. Among the 1897 DEGs, 549 were enriched in this pathway. Following treatment with *Ba. amyloliquefaciens* Ba13, 97 of the 119 genes related to pathogenesis-related protein, auxin, and cell wall, were upregulated. Additionally, 67 of the 94 genes related to signaling and MAPK were upregulated (**Figure 3**). These results were consistent with the KEGG enrichment analysis of disease resistance-related genes.

10.3389/fmicb.2023.1251698

TABLE 1 Eight open reading frames corresponding to virus isolates used in this study.

	Gene	Position (nt)	Length (aa)	Encoded protein	Protein functions
Virus chain	*AV1*	308–1084	258	Coat protein	Unique known structural unit of virus particle; related to the packaging movement of virus; the main determinant of infection pathway of whitefly (Yaakov et al., 2011)
	AV2	148–498	116	AV2 protein	Participating in viral infection and suppressing RNA silencing (Wu et al., 2010)
	AV3	2350–2583	77	AV3 protein	Suppressing PTGS and TGS (Gong et al., 2021)
Complementary chain	*C1*	2615–1542	357	Virus replication-related protein	Initiating the rolling circle replication; its silencing impedes the growth and spread of TYLCV (Ramesh et al., 2007)
	C2	1633–1226	135	Transcription activator	Suppressing PTGS and TGS (van Wezel et al., 2002)
	C3	1485–1081	134	Reproduction enhancer	A replication accessory factor that enhances viral DNA accumulation (Sun et al., 2014)
	C4	2464–2171	97	C4 protein	Determining the disease phenotype (Padmanabhan et al., 2017)
	C5	862–655	67	C5 protein	Suppressing PTGS and TGS (Zhao et al., 2022)

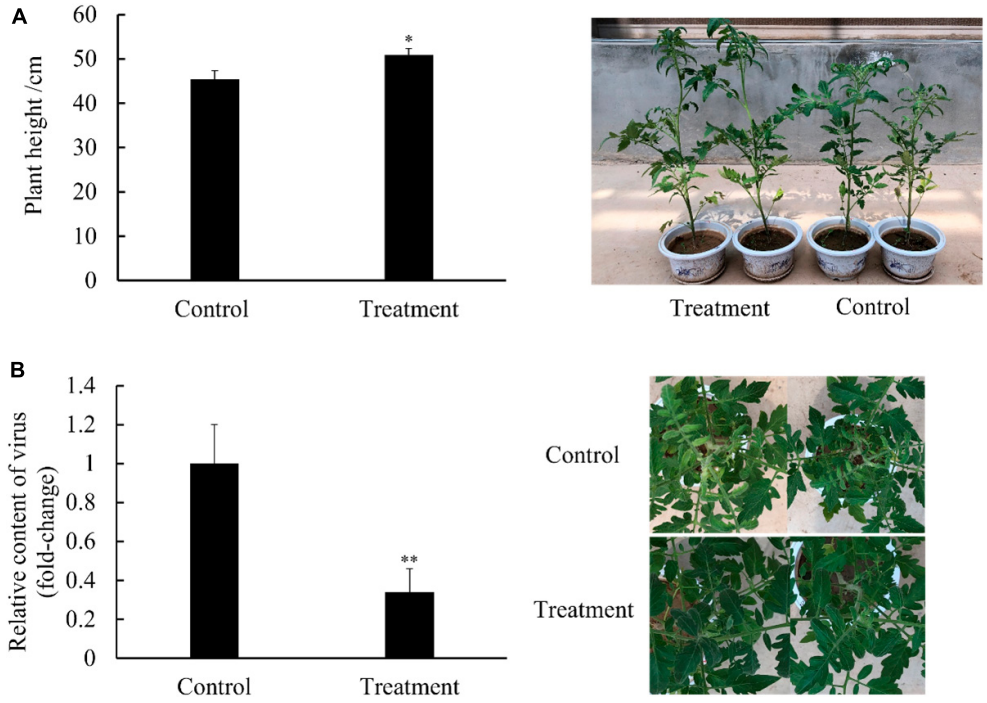

FIGURE 1
Effects of *Bacillus amyloliquefaciens* Ba13 in the promotion of tomato plant growth [**(A)**; $n = 30$, error bars = standard deviation] and defense against tomato yellow leaf curl virus disease [**(B)**; $n = 3$, error bars = standard deviation] at 28 days post-viral infection. $^{**}p < 0.01$; $^{*}p < 0.05$.

PCR validation of functional gene expression

The whole-transcriptome RNA-seq data were validated using RT-qPCR with six functional genes that were upregulated in the treatment group, with fold-changes of between 1.21 and 6.73. The PCR analysis revealed that all six genes increased their expression levels (between 1.61- and 4.34-fold) in the treatment group compared with the control group (Figure 4). The PCR results were generally consistent with the RNA-seq data. For example, according to the whole-transcriptome RNA-seq data, expression levels of *AGO4* (an important component of TGS), *FLS2* (a plant receptor kinase gene), and *NPR1* (a regulatory gene in the resistance system) increased 6. 73-, 2. 13-, and 4.58-fold, respectively; their expression changes were 4. 34-, 1. 77-, and 4.55-fold based on the RT-qPCR analysis. These results demonstrated the reliability of the whole-transcriptome RNA-seq data.

ABA content

The mean ABA content of tomato leaves in the treatment group was 693.3 ng/g at 28 dpvi, which was 15% higher compared with that of the control group ($p < 0.05$). The retention time and content of ABA after *Ba. amyloliquefaciens* Ba13 treatment are shown in Figure 5.

10.3389/fmicb.2023.1251698

TABLE 2 The effect of *Bacillus amyloliquefaciens* Ba13 against tomato yellow leaf curl virus (TYLCV) disease.

Time (dpvi)	Group	Total number of plants	Disease index (%)	Control rate (%)
14	Control	30	21.7 ± 3.8bc	–
	Treatment	30	13.3 ± 5.2c	38.7
28	Control	30	41.7 ± 6.3a	–
	Treatment	30	28.3 ± 1.4b	32.1

dpvi: days post-viral inoculation. Disease index values are means of 30 replicates ± standard error. Different lowercase letters indicate significant differences between the control (TYLCV) and treatment (*Ba. amyloliquefaciens* Ba13+TYLCV) groups (Fisher's LSD test; $p < 0.05$).

Modulation of viral genome methylation

Bisulfite sequencing detected methylation on 69 of 81 CpG sites in the TYLCV-SJ genome. The methylation level of sites 54, 228, 461, and 1244 ranged from 13.3 to 38.4%, which was significantly higher than that of other CpG sites (0.3%–1.8%; Figure 6). Among them, site 228 was located in the ORF region of *AV1* and 461 sites were located in the ORF region of *AV1* and *AV2*. After *Ba. amyloliquefaciens* Ba13 inoculation, the methylation level of sites 228 and 461 was 183.1% and 63.0% higher than that of the control group, respectively ($p < 0.01$). However, the methylation level of sites 54 and 1244 did not significantly differ between the two groups.

Virus-derived siRNA abundances

In total, 15,448 siRNA sequences were obtained by small RNA-seq, 8480 of which had significant differences in their expression ($p < 0.05$). There were 4578 siRNA upregulated and 3902 siRNA downregulated in the treatment group compared with the control group. Ten siRNAs completely matched to the genome of the TYLCV genotype used in this study (MN910280.1), and their virus binding sites and sequences are provided in Table 4. All the 10 siRNAs were downregulated in the *Ba. amyloliquefaciens* Ba13 treatment group compared with the control group, with 21–22 nt possibly participating in RNAi. For example, siRNA5429 was matched to the ORF region of *AV1*, and siRNA5327, siRNA12690, siRNA16430, and siRNA15617 were matched to the ORF region of *C1*. Their abundances in the treatment group were reduced by 47.9, 39.7, 60.3, 99.7, and 62.7%, respectively.

Discussion

RNAi is an antiviral system which allow plants to directly act on viruses. The application of *Ba. amyloliquefaciens* Ba13

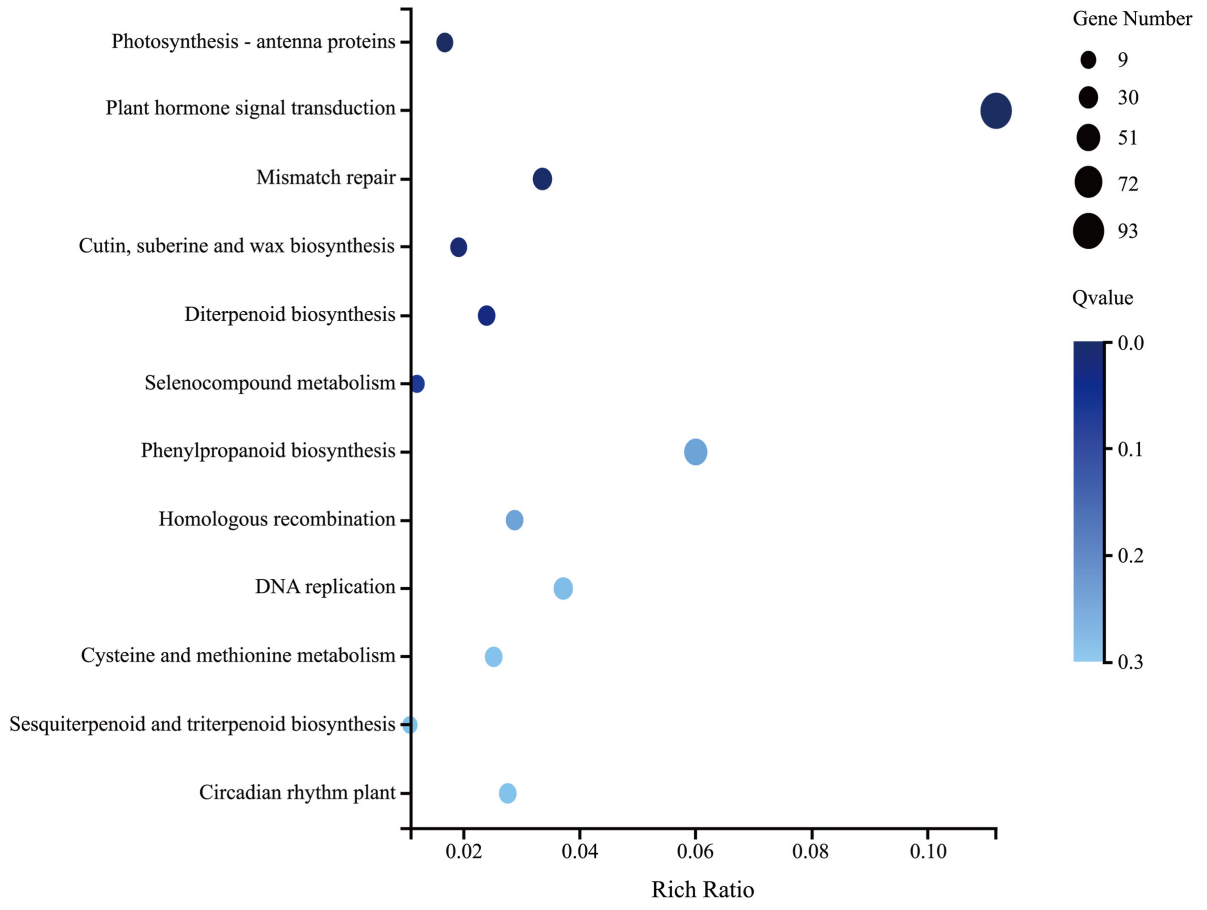

FIGURE 2
The 12 significantly enriched Kyoto Encyclopedia of Genes and Genomes (KEGG) pathways in tomato plants after treatment with *Bacillus amyloliquefaciens* Ba13.

10.3389/fmicb.2023.1251698

TABLE 3 Gene Ontology (GO) analysis of differentially expressed genes involved in gene silencing in tomato plants after treatment with *Bacillus amyloliquefaciens* Ba13.

Gene	Fold-change (Treatment vs. control)	*p*-value	Definition
AGO3	2.44	0.00029	ARGONAUTE RISC catalytic component 3
AGO4	6.73	1.90E-109	ARGONAUTE RISC component 4
AGO5	2.03	1.12E-105	ARGONAUTE family protein
AGO7	2.71	7.95E-69	ARGONAUTE family protein
AGO10	2.07	3.38E-128	Stabilizer of iron transporter SufD/Polynucleotide transferase
LOC101261608	6.89	9.99E-17	ARGONAUTE 4A-like protein
RPA32a	2.47	2.10E-187	Replication protein A
LOC101255202	2.72	5.29E-06	Protein INVOLVED IN DE NOVO 2-like

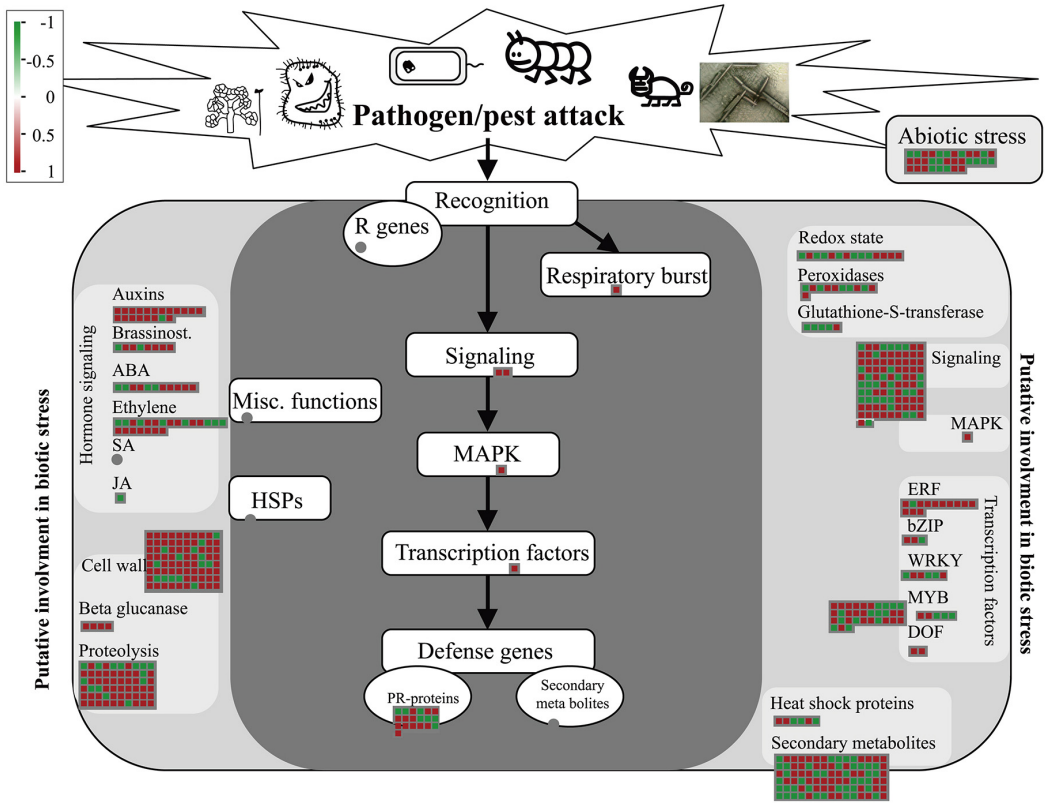

FIGURE 3
Gene expression changes of the biotic stress pathway in tomato plants after treatment with *Bacillus amyloliquefaciens* Ba13. Mapman was used to analyze the distribution of differentially expressed genes in the biotic stress pathway in the treatment group compared with the control group. Red squares indicate upregulated genes and green squares indicate downregulated genes.

as a biocontrol strain against TYLCV necessitates a holistic understanding of how this strain modulates the RNAi-based antiviral system in its host plants. In the present study, we found that inoculation with *Ba. amyloliquefaciens* Ba13 increased the expression of RNAi-related genes (e.g., *AGO3*, *AGO4*, *AGO5*, *AGO7*) in tomato leaves, with improved levels of viral genome methylation and ABA content. These results indicate that the tomato plants might have initiated RNAi-related pathways after TYLCV invasion, whereas the application of *Ba. amyloliquefaciens* Ba13 could improve plant resistance by enhancing RNAi.

As an integral part of RNAi, DNA methylation-mediated TGS is considered to be an important pathway for plant defense against infection by geminiviruses (Mei et al., 2020). For DNA viruses, AGO4 is the main effector protein in the antiviral silencing machinery. Based on the whole-transcriptome RNA-seq data, we observed upregulation of *AGO4* expression in tomato leaves upon *Ba. amyloliquefaciens* Ba13 inoculation. Taking into account the role of AGO4–siRNA complex in viral genome methylation, we expected that *Ba. amyloliquefaciens* Ba13 mediated increased methylation level of the TYLCV genome. This hypothesis was supported by the higher methylation levels at CpG sites in *AV1* and

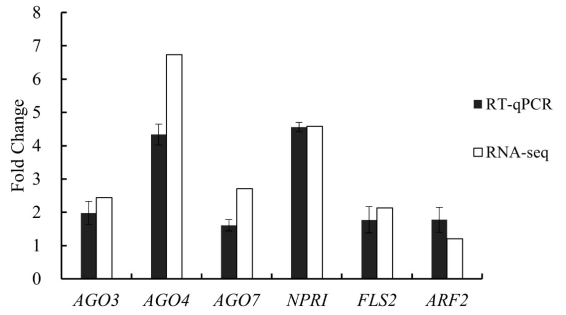

FIGURE 4
Expression changes of six genes involved in gene silencing, growth regulation, and disease resistance in tomato plants after treatment with *Bacillus amyloliquefaciens* Ba13 for validation of whole-transcriptome RNA sequencing (RNA-seq) data by reverse transcription quantitative real-time PCR (RT-qPCR).

AV2 following *Ba. amyloliquefaciens* Ba13 inoculation. Previous study has found that after infection with the tomato leaf curl New Delhi virus, the methylation level of the viral intergenic spacer in a resistant cultivar was substantially higher than in a sensitive cultivar after infection. Additionally, Brough et al. (1992) introduced the cytosine methylated DNA of tomato golden mosaic virus into tobacco protoplasts, leading to a reduction in viral replication to 1/20–1/5 of the original level. These observations indicate that *Ba. amyloliquefaciens* Ba13 inoculation increased the methylation level of viral DNA through upregulation of *AGO4* expression, which in turn inhibited *AV1* and *AV2* expression and enhanced plant resistance to TYLCV. It has been shown that the methylation frequency of CpG sites in the plant genome markedly increases during virus invasion. CpG methylation frequency is a key factor in inhibiting geminivirus replication and reducing plant symptoms (Rodriguez-Negrete et al., 2013). Further study is needed to ascertain whether inoculation with *Ba. amyloliquefaciens* Ba13 can affect the frequency of plant genome methylation, thereby improving tomato resistance to TYLCV.

In addition to AGO4, other AGO family members (e.g., AGO3, AGO5, AGO7) play non-negligible roles in plant antiviral defense. AGO3 has been reported to take part in ABA-mediated antiviral defense processes (Alazem et al., 2014). Promoters of *AGO* genes contain several ABA responsive elements, and their expression levels are affected by exogenous ABA (Alazem et al., 2017). Therefore, ABA can enhance the expression of *AGO3*—which is necessary for plants to resist *Bamboo mosaic virus* (Alazem et al., 2017). In the case of TYLCV infection, *Ba. amyloliquefaciens* Ba13 inoculation increased *AGO3* expression in tomato plants. To clarify whether the upregulation of AGO3 expression is related to ABA, we looked at ABA biosynthesis related genes and ABA content in tomato leaves. We observed a remarkable upregulation in the expression of *ABF* upon *Ba. amyloliquefaciens* Ba13 inoculation, along with an increase in the ABA content. These results provide strong evidence that the application of *Ba. amyloliquefaciens* Ba13 improved ABA biosynthesis and enhanced the expression of AGO3, thereby facilitating plant defense against TYLCV.

With regard to *AGO5* and *AGO7* expression, we observed a distinct upregulation in tomato leaves upon *Ba. amyloliquefaciens* Ba13 inoculation. AGO5 can bind to small RNAs derived from viruses or viroids. Potato virus X (PVX) infection induces *AGO5* expression, which is essential for *Arabidopsis* to limit PVX infection (Brosseau and Moffett, 2015). AGO7 is also involved in PTGS and thus plays a role in plant defense against viruses (Garcia-Ruiz et al., 2015). For example, AGO7 has been shown to collaborate with AGO1 in clearing viral RNA with different levels of secondary structure (Qu et al., 2008). AGO7 additionally participates in plant defense against *Turnip crinkle virus*, and together with AGO3, it becomes the major contributor to virus clearance in the leaves

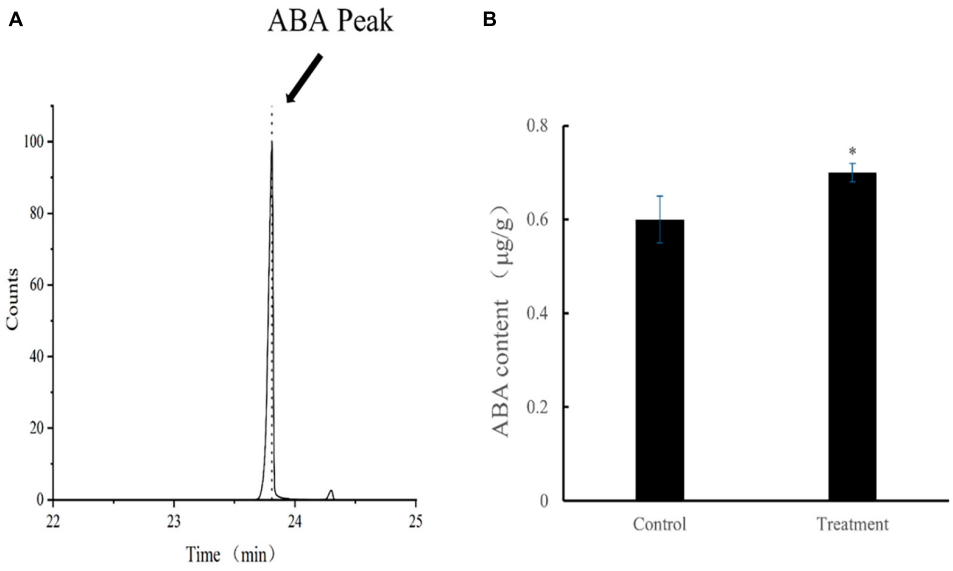

FIGURE 5
The content of abscisic acid (ABA) in leaves of tomato plants. **(A)** ABA standard retention time (23.787 min). **(B)** Changes in ABA content after *Bacillus amyloliquefaciens* Ba13 treatment compared with the control group. $n = 3$, error bar = standard deviation of ABA content in tomato leaves at 28 days post-viral infection. *$p < 0.05$.

10.3389/fmicb.2023.1251698

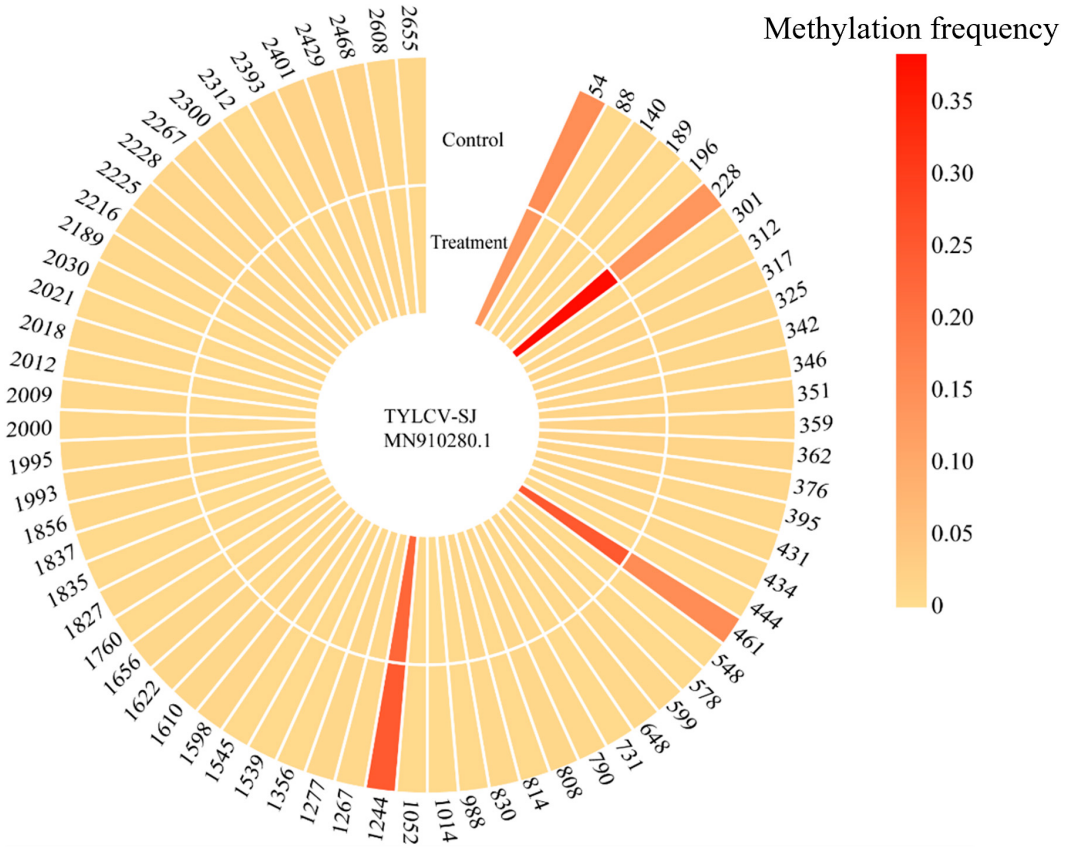

FIGURE 6
Changes in CpG methylation frequency of TYLCV genome after *Bacillus amyloliquefaciens* Ba13 treatment.

TABLE 4 Changes in the abundance of 10 virus-derived small interfering RNAs (siRNAs) in the leaves of tomato plants after treatment with *Bacillus amyloliquefaciens* Ba13.

Name	Sequence (5′–3′)/Size	Log2 fold-change (Treatment vs. control)	*p*-value	Binding site (virus chain: +, complementary chain: –)	Corresponding gene
siRNA5327	CTCCATTTCTTTCTTCTTCTT/21 nt	−0.78	4.39E-5	–, 2077–2057	*C1*
siRNA5429	CGCATCTATTTCTATGATTCAA/22 nt	−0.98	4.97E-11	+, 1052–1073	*AV1*
siRNA12690	AAGCACTTCAAGGAATTCATG/21 nt	−1.43	1.99E-09	–, 1817–1797	*C1*
siRNA15142	AAATTCGGAAGTTGAGAAAA/20 nt	−5.65	2.52E-07	+, 1272–1291	–
siRNA15143	CAAATTCGGAAGTTGAGAAAA/21 nt	−4.39	0.0012	+, 1271–1291	–
siRNA15613	CAACACAAGATAGCCAAGA/19 nt	−0.64	7.49E-05	–, 1580–1562	*C1*, *C2*
siRNA15615	CCAACACAAGATAGCCAAGA/20 nt	−0.92	1.83E-14	–, 1579–1562	*C1*, *C2*
siRNA15617	TCCAACACAAGATAGCCAAGA/21 nt	−1.39	0.0068	–, 1561–1581	*C1*, *C2*
siRNA16430	ATTTAAAATATATGCCAAAAA/21 nt	−5.71	1.41E-07	–, 2604–2584	*C1*
siRNA16557	ATCTGGAACTTGATTAAAAGA/21 nt	−0.40	0.0094	+, 2040–2060	–

(Zheng et al., 2019). The collective results allow us to conclude that the application of *Ba. amyloliquefaciens* Ba13 upregulated the expression of *AGO5* and *AGO7*, which synergistically acted to improve the efficiency of clearing viral RNAs in tomato plants.

While the expression levels of multiple *AGO* genes were upregulated in tomato plants inoculated with *Ba. amyloliquefaciens* Ba13, plant resistance to TYLCV was enhanced. It has been reported that an increase in *AGO* gene expression enhances plant resistance to different viruses such as *Bamboo mosaic virus*, Potato virus X, *Turnip crinkle virus* (Qu et al., 2008; Brosseau and Moffett, 2015; Alazem et al., 2017). This leads us to posit that *Ba. amyloliquefaciens* Ba13 is likely to regulate plant defense against other viruses by upregulating *AGO* expression. We additionally found that *Streptomyces pactum* Act12 can increase

tomato resistance to TYLCV by upregulating *AGO* gene expression (Li Y. L. et al., 2019). This suggests that other biocontrol bacteria may perform similar functions as observed in *Ba. amyloliquefaciens* Ba13. More experiments are required to verify whether the effects and mechanisms of *Ba. amyloliquefaciens* Ba13 are universal for other viruses and biocontrol strains.

RNAi plays a role in disease control via siRNAs, which target viral mRNAs with corresponding sequences at specific sites for degradation. We compared the obtained siRNA sequences against the TYLCV genotype (MN910280.1) and found 10 siRNAs completely matched to our obtained viral sequence. The siRNA matcher site in the ORF were corresponding to *AV1*, *C1*, and *C2*. *AV1* and *C1* are, respectively, involved in coding virus coat protein and replication-related proteins, which help TYLCV growth and spread. *C2* can revert TGS and decrease DNA methylation in plants by interfering with the methyl cycle (Buchmann et al., 2009). The complete matching of these siRNAs to the functional gene regions of TYLCV indicates that the siRNAs may interfere with viral protein synthesis by complementary binding and degrading mRNA of gene transcription. This result illustrates that RNAi-related pathways were initiated in tomato plants in response to TYLCV infection.

We observed *Ba. amyloliquefaciens* Ba13-mediated downregulation of all 10 siRNAs matched to the TYLCV genotype in tomato leaves, consistent with the pattern observed in a previous study. Rodriguez-Negrete et al. (2009) investigated the recovery of plants (with less susceptible symptoms) after infection with pepper golden mosaic virus. They found a lower total abundance of virus-derived siRNAs but a higher DNA methylation level of the viral genome in the recovered tissue than in the diseased tissue of pepper plants. Additionally, we found that the disease symptoms of *Ba. amyloliquefaciens* Ba13-inoculated tomato plants were alleviated compared with those of non-inoculated controls. The decrease in siRNA abundances could be related to the decrease in virus quantity in tomato plants treated with *Ba. amyloliquefaciens* Ba13. *Ba. amyloliquefaciens* Ba13 inoculation enhanced plant defense against TYLCV, allowing faster recovery from viral infection.

Our results indicated that the expression levels of genes related to SA, ABA, and RNAi pathways were upregulated in tomato leaves after inoculation with *Ba. amyloliquefaciens* Ba13. In fact, the defense processes of plants against viruses involve the participation and collaboration of multiple mechanisms, such as RNAi, dominant resistance, and SAR (Nicaise, 2014). Thus, inoculation with *Ba. amyloliquefaciens* Ba13 is likely to induce multifaceted plant response through various defense systems. Although both SAR and RNAi play a role in plant defense against viruses, RNAi has higher specificity for viruses compared with the broad-spectrum resistance mechanism of SAR and can target degradation of viruses. While this study has focused on RNAi modulation by *Ba. amyloliquefaciens* Ba13, the relationship between RNAi and other defense mechanisms in inoculated plants should be clarified by further studies.

Furthermore, we found that the application of *Ba. amyloliquefaciens* Ba13 strongly affected the expression of genes related to photosystem and auxin response pathways. A total of 12 DEGs related to the biosynthesis of LHCII chlorophyll a/b binding protein 1 (LHCb1), LHCb3, and LHCb7 in the LHCII pathway (the most abundant light harvester in plants) were upregulated in tomato leaves upon *Ba. amyloliquefaciens* Ba13 inoculation. Additionally, 13 of the 14 DEGs related to auxin/indoleacetic acid and small auxin-up RNA, as well as two DEGs related to GH3, were upregulated in tomato leaves of inoculated plants. Montasser et al. (2012) found that the content of photosynthesis related chemical components (e.g., chlorophyll a, b) decreased in tomato leaves infected with TYLCV compared with normal leaves. Wu et al. (2012) showed that auxin/indoleacetic acid proteins were significantly expressed in tomato plants during root and stem development. Small auxin-up RNA plays a major role in modulating cell elongation and positively regulates cell expansion by modulating the transport of auxin (Chae et al., 2012). Furthermore, *GH*-like genes mediate the interaction between auxin and salicylic acid signaling pathways. Overexpression of *GH3* can enhance the systemic disease resistance in plants (Zhang et al., 2007). Taken together, these results indicate that the presence of *Ba. amyloliquefaciens* Ba13 could attenuate the negative effects of viral infection on leaf photosynthetic efficiency, promote plant growth, and as such, enhance plant defense against TYLCV.

Data availability statement

The datasets presented in this study can be found in online repositories. The names of the repository/repositories and accession number(s) can be found below: https://www.ncbi.nlm.nih.gov/, MN910280.1, https://www.ncbi.nlm.nih.gov/, PRJNA553064, https://www.ncbi.nlm.nih.gov/, PRJNA553309.

Author contributions

HL conceived the study and proposed the experimental approaches. QG, YS, and CJ conducted the experiments. QG, YS, ZK, ZL, and YZL contributed to data processing and analysis. QG, YS, and YLL wrote the manuscript. All authors read, commented on, and approved the final version of the manuscript.

Funding

This research was financially supported by the Qinchuangyuan Scientific and Technological Innovation Funds (No. 2021ZDZXNY-0005), the Science and Technology Major Project of Ordos (2022EEDSKJZDZX019), the Science and Technology Planning Project of Inner Mongolia Autonomous Region (2022YFHH0114), the Natural Science Foundation of Shaanxi Province (No. 2021JQ-151), and the Youth Project of National Natural Science Foundation of China (31600407).

Acknowledgments

We thank Chaofeng Lin (Transcend Envirotech Consulting Co., Ltd.) for improving the English and Lu Wang (Plant Science Facility of the Institute of Botany, Chinese Academy of Sciences) for technical assistance with GC-MS analysis.

Conflict of interest

The authors declare that the research was conducted in the absence of any commercial or financial relationships that could be construed as a potential conflict of interest.

Publisher's note

All claims expressed in this article are solely those of the authors and do not necessarily represent those of their affiliated organizations, or those of the publisher, the editors and the reviewers. Any product that may be evaluated in this article, or claim that may be made by its manufacturer, is not guaranteed or endorsed by the publisher.

Supplementary material

The Supplementary Material for this article can be found online at: https://www.frontiersin.org/articles/10.3389/fmicb.2023.1251698/full#supplementary-material

References

Alazem, M., He, M., Moffett, P., and Lin, N. (2017). Abscisic acid induces resistance against bamboo mosaic virus through Argonaute 2 and 3. *Plant Physiol.* 174, 339–355. doi: 10.1104/pp.16.00015

Alazem, M., Lin, K., and Lin, N. (2014). The abscisic acid pathway has multifaceted effects on the accumulation of Bamboo mosaic virus. *Mol. Plant Microbe. Interact.* 27, 177–189. doi: 10.1094/MPMI-08-13-0216-R

Arif, M. A., Frank, W., and Khraiwesh, B. (2013). Role of RNA interference (RNAi) in the Moss Physcomitrella patens. *Int. J. Mol. Sci.* 14, 1516–1540. doi: 10.3390/ijms14011516

Brosseau, C., and Moffett, P. (2015). Functional and genetic analysis identify a role for *Arabidopsis* ARGONAUTE5 in antiviral RNA silencing. *Plant Cell* 27, 1742–1754. doi: 10.1105/tpc.15.00264

Brough, C. L., Gardiner, W. E., Inamdar, N. M., Zhang, X. Y., Ehrlich, M., and Bisaro, D. M. (1992). DNA methylation inhibits propagation of tomato golden mosaic virus DNA in transfected protoplasts. *Plant Mol. Biol.* 18, 703–712. doi: 10.1007/BF00020012

Buchmann, R. C., Asad, S., Wolf, J. N., Mohannath, G., and Bisaro, D. M. (2009). Geminivirus AL2 and L2 proteins suppress transcriptional gene silencing and cause genome-wide reductions in cytosine methylation. *J. Virol.* 83, 5005–5013. doi: 10.1128/JVI.01771-08

Cahill, M., Jarvis, W., Gorman, K., and Denholm, I. (1996). Resolution of baseline responses and documentation of resistance to buprofezin in *Bemisia tabaci* (Homoptera: Aleyrodidae). *Bull. Entomol. Res.* 86, 117–122. doi: 10.1017/s0007485300052342

Chae, K., Isaacs, C. G., Reeves, P. H., Maloney, G. S., Muday, G. K., Nagpal, P., et al. (2012). *Arabidopsis* small auxin up RNA63 promotes hypocotyl and stamen filament elongation. *Plant J.* 71, 684–697. doi: 10.1111/j.1365-313X.2012 05024.x

de Pradena, A., Jimenez, A., San Leon, D., Simmonds, P., Garcia, J., and Valli, A. (2020). Plant virus genome is shaped by specific dinucleotide restrictions that influence viral infection. *Mbio* 11, e2818–e2819. doi: 10.1128/mBio.02818-19

El-Sappah, A. H., Yan, K., Huang, Q. L., Islam, M. M., Li, Q. Z., Wang, Y., et al. (2021). Comprehensive mechanism of gene silencing and its role in plant growth and development. *Front. Plant. Sci.* 12:705249. doi: 10.3389/fpls.2021.705249

Elsharkawy, M. M., Shimizu, M., Takahashi, H., and Hyakumachi, M. (2012). Induction of systemic resistance against cucumber mosaic virus by *Penicillium simplicissimum* GP17-2 in *Arabidopsis* and tobacco. *Plant Pathol.* 61, 964–976. doi: 10.1111/j.1365-3059.2011 02573.x

Elsharkawy, M. M., Shimizu, M., Takahashi, H., Ozaki, K., and Hyakumachi, M. (2013). Induction of systemic resistance against cucumber mosaic virus in *Arabidopsis thaliana* by *trichoderma asperellum* SKT-1. *Plant Pathol. J.* 29, 193–200. doi: 10.5423/ppj.si.07.2012.0117

Gafni, Y. (2003). Tomato yellow leaf curl virus, the intracellular dynamics of a plant DNA virus. *Mol. Plant Pathol.* 4, 9–15. doi: 10.1046/j.1364-3703.2003.00147.x

Gao, F., Zhang, J. Y., Jiang, P. P., Gong, D. S., Wang, J. W., Xia, Y. D., et al. (2014). Marked methylation changes in intestinal genes during the perinatal period of preterm neonates. *BMC Genomics* 15:716. doi: 10.1186/1471-2164-15-716

Garcia-Ruiz, H., Carbonell, A., Hoyer, J. S., Fahlgren, N., Gilbert, K. B., Takeda, A., et al. (2015). Roles and programming of *Arabidopsis* ARGONAUTE proteins during Turnip Mosaic Virus infection. *Plos Pathog.* 11:e1004755. doi: 10.1371/journal.ppat.1004755

Gong, P., Tan, H., Zhao, S. W., Li, H., Liu, H., Ma, Y., et al. (2021). Geminiviruses encode additional small proteins with specific subcellular localizations and virulence function. *Nat. Commun.* 12:4278. doi: 10.1038/s41467-021-24617-4

Guo, Q., Li, Y. L., Lou, Y., Shi, M. D., Jiang, Y., Zhou, J., et al. (2019). *Bacillus amyloliquefaciens* Ba13 induces plant systemic resistance and improves rhizosphere microecology against tomato yellow leaf curl virus disease. *Appl. Soil Ecol.* 137, 154–166. doi: 10.1016/j.apsoil.2019.01.015

Kanakala, S., and Ghanim, M. (2016). RNA interference in insect vectors for plant viruses. *Viruses Basel* 8:329. doi: 10.3390/v8120329

Kanehisa, M., Araki, M., Goto, S., Hattori, M., Hirakawa, M., Itoh, M., et al. (2008). KEGG for linking genomes to life and the environment. *Nucleic Acids Res.* 36, 480–484. doi: 10.1093/nar/gkm882

Kumar, S., Chauhan, P. S., Agrawal, L., Raj, R., Srivastava, A., Gupta, S., et al. (2016). *Paenibacillus lentimorbus* inoculation enhances tobacco growth and extenuates the virulence of cucumber mosaic virus. *PLoS ONE* 11:e0149980. doi: 10.1371/journal.pone.0149980

Kumar, S., Stecher, G., Li, M., Knyaz, C., and Tamura, K. (2018). MEGA X: Molecular evolutionary genetics analysis across computing platforms. *Mol. Biol. Evol.* 35, 1547–1549. doi: 10.1093/molbev/msy096

Li, R. Q., Yu, C., Li, Y. R., Lam, T. W., Yiu, S. M., Kristiansen, K., et al. (2009). SOAP2: An improved ultrafast tool for short read alignment. *Bioinformatics* 25, 1966–1967. doi: 10.1093/bioinformatics/btp336

Li, Y. L., Guo, Q., Li, Y. Z., Sun, Y. F., Xue, Q. H., and Lai, H. X. (2019). *Streptomyces pactum* Act12 controls tomato yellow leaf curl virus disease and alters rhizosphere microbial communities. *Biol. Fertil. Soils* 55, 149–169. doi: 10.1007/s00374-019-01339-w

Li, Z. C., Li, W. Q., Guo, M. X., Liu, S. M., Liu, L., Yu, Y., et al. (2019). Origin, evolution and diversification of plant ARGONAUTE proteins. *Plant J.* 109, 1086–1097. doi: 10.1111/tpj.15615

Loew, L., Goonawardane, N., Ratcliff, J., Nguyen, D., and Simmonds, P. (2020). Use of a small DNA virus model to investigate mechanisms of CpG dinucleotide-induced attenuation of virus replication. *J. Gen. Virol.* 101, 1202–1218. doi: 10.1099/jgv.0.001477

Lu, D. Y. H., Liao, J. Y., Fajar, A., Chen, J. B., Wei, Y., Zhang, Z. H., et al. (2023). Co-infection of TYLCV and ToCV increases cathepsin B and promotes ToCV transmission by *Bemisia tabaci* MED. *Front. Microbiol.* 14:1107038. doi: 10.3389/fmicb.2023.1107038

Matzke, M. A., Kanno, T., and Matzke, A. J. M. (2015). RNA-directed DNA methylation: The evolution of a complex epigenetic pathway in flowering plants. In: Merchant SS ed. *Annu. Rev. Plant Biol.* 66, 243–267. doi: 10.1146/annurev-arplant-043014-114633

Mei, Y., Wang, Y., Li, F., and Zhou, X. (2020). The C4 protein encoded by tomato leaf curl Yunnan virus reverses transcriptional gene silencing by interacting with NbDRM2 and impairing its DNA-binding ability. *PLoS Pathol.* 16:1008829. doi: 10.1371/journal.ppat.1008829

Mi, H. Y., Lazareva-Ulitsky, B., Loo, R., Kejariwal, A., Vandergriff, J., Rabkin, S., et al. (2005). The panther database of protein families, subfamilies, functions and pathways. *Nucleic Acids Res.* 33, D284–D288. doi: 10.1093/nar/gki078

Montasser, M. S., Al-Own, F. D., Haneif, A. M., and Afzal, M. (2012). Effect of Tomato yellow leaf curl bigeminivirus (TYLCV) infection on tomato cell ultrastructure and physiology. *Can. J. Plant Pathol.* 34, 114–125. doi: 10.1080/07060661.2012.661767

Mou, Z., Fan, W. H., and Dong, X. N. (2003). Inducers of plant systemic acquired resistance regulate NPR1 function through redox changes. *Cell* 113, 935–944. doi: 10.1016/s0092-8674(03)00429-x

Nicaise, V. (2014). Crop immunity against viruses: Outcomes and future challenges. *Front. Plant Sci.* 21:660. doi: 10.3389/fpls.2014.00660

Niu, D. D., Liu, H. X., Jiang, C. H., Wang, Y. P., Wang, Q. Y., Jin, H. L., et al. (2011). The plant growth-promoting rhizobacterium *Bacillus cereus* AR156 induces systemic resistance in *Arabidopsis thaliana* by simultaneously activating salicylate- and jasmonate/ethylene-dependent signaling pathways. *Mol. Plant Microbe Interact.* 24, 533–542. doi: 10.1094/MPMI-09-10-0213

Padmanabhan, C., Zheng, Y., Shamimuzzaman, M., Fei, Z., and Ling, K. S. (2017). Tomato yellow leaf curl virus C4 protein is a determinant of disease phenotype in tomato. *Phytopathology* 107, 91–91.

Palumbo, J. C., Horowitz, A. R., and Prabhaker, N. (2001). Insecticidal control and resistance management for *Bemisia tabaci*. *Crop Prot*. 20, 739–765. doi: 10.1016/s0261-2194(01)00117-x

Pan, X. Q., Welti, R., and Wang, X. M. (2010). Quantitative analysis of major plant hormones in crude plant extracts by high-performance liquid chromatography-mass spectrometry. *Nat. Protoc.* 5, 986–992. doi: 10.1038/nprot.2010.37

Qu, F., Ye, X. H., and Morris, T. J. (2008). *Arabidopsis* DRB4, AGO1, AGO7, and RDR6 participate in a DCL4-initiated antiviral RNA silencing pathway negatively regulated by DCL1. *Proc. Natl. Acad. Sci. U.S.A.* 105, 14732–14737. doi: 10.1073/pnas.0805760105

Raja, P., Sanville, B. C., Buchmann, R. C., and Bisaro, D. M. (2008). Viral genome methylation as an epigenetic defense against geminiviruses. *J. Virol* 82, 8997–9007. doi: 10.1128/JVI.00719-08

Ramesh, S. V., Mishra, A. K., and Praveen, S. (2007). Hairpin RNA-Mediated strategies for silencing of Tomato leaf curl virus *AC1* and *AC4* genes for effective resistance in plants. *Oligonucleotides* 17, 251–257. doi: 10.1089/oli.2006.0063

Rodriguez-Negrete, E., Carrillo-Tripp, J., and Rivera-Bustamante, R. F. (2009). RNA silencing against geminivirus: Complementary action of posttranscriptional gene silencing and transcriptional gene silencing in host recovery. *J. Virol.* 83, 1332–1340. doi: 10.1128/jvi.01474-08

Rodriguez-Negrete, E., Lozano-Duran, R., Piedra-Aguilera, A., Cruzado, L., Bejarano, E. R., and Castillo, A. G. (2013). Geminivirus Rep protein interferes with the plant DNA methylation machinery and suppresses transcriptional gene silencing. *New Phytol.* 199, 464–475. doi: 10.1111/nph.12286

Sade, D., Sade, N., Shriki, O., Lerner, S., Gebremedhin, A., Karavani, A., et al. (2014). Water balance, hormone homeostasis, and sugar signaling are all involved in tomato resistance to tomato yellow leaf curl virus. *Plant Physiol.* 165, 1684–1697. doi: 10.1104/pp.114.243402

Schmittgen, T. D., and Livak, K. J. (2008). Analyzing real-time PCR data by the comparative C-T method. *Nat. Protoc.* 3, 1101–1108. doi: 10.1038/nprot.2008.73

Seo, J. K., Wu, J. G., Lii, Y. F., Li, Y., and Jin, H. L. (2013). Contribution of small RNA pathway components in plant immunity. *Mol. Plant Microbe Interact.* 26, 617–625. doi: 10.1094/mpmi-10-12-0255-ia

Shen, L. L., Wang, F. L., Yang, J. G., Qian, Y. M., Dong, X. W., and Zhan, H. X. (2014). Control of tobacco mosaic virus by *Pseudomonas fluorescens* CZ powder in greenhouses and the field. *Crop Prot*. 56, 87–90. doi: 10.1016/j.cropro.2013.11.020

Staff, S. S. (2010). *Keys to Soil Taxonomy*, 11th Edn. Washington, DC: USDA-Natural Resources Conservation Service.

Sun, S., Kang, X. P., Xing, X. J., Chen, Z. F., Zheng, S. W., and Xing, G. M. (2014). Transient expression of siRNA targeted against the TYLCV *AV1*, *AC1* and *AC3* genes for high resistance in tomato. *Sci. Hortic.* 179, 321–327. doi: 10.1016/j.scienta.2014.10.002

Sun, W. J., Lv, W. J., Li, L. N., Yin, G., Hang, X. F., Xue, Y. F., et al. (2016). Eugenol confers resistance to tomato yellow leaf curl virus (TYLCV) by regulating the expression of *SlPer1* in tomato plants. *Nat. Biotechnol.* 33, 345–354. doi: 10.1016/j.nbt.2016.01.001

Thimm, O., Blasing, O., Gibon, Y., Nagel, A., Meyer, S., Kruger, P., et al. (2004). MAPMAN: A user-driven tool to display genomics data sets onto diagrams of metabolic pathways and other biological processes. *Plant J.* 37, 914–939. doi: 10.1111/j.1365-313X.2004 02016.x

van Wezel, R., Dong, X. L., Liu, H. T., Tien, P., Stanley, J., and Hong, Y. G. (2002). Mutation of three cysteine residues in Tomato yellow leaf curl virus-China C2 protein causes dysfunction in pathogenesis and posttranscriptional gene-silencing suppression. *Mol. Plant Microbe Interact.* 15, 203–208. doi: 10.1094/MPMI.2002.15.3.203

Vitti, A., La Monaca, E., Sofo, A., Scopa, A., Cuypers, A., and Nuzzaci, M. (2015). Beneficial effects of *Trichoderma harzianum* T-22 in tomato seedlings infected by cucumber mosaic virus (CMV). *Biocontrol* 60, 135–147. doi: 10.1007/s10526-014-9626-3

Wang, L. K., Feng, Z. X., Wang, X., Wang, X. W., and Zhang, X. G. (2010). DEGseq: An R package for identifying differentially expressed genes from RNA-seq data. *Bioinformatics* 26, 136–138. doi: 10.1093/bioinformatics/btp612

Wang, S. A., Wu, H. J., Qiao, J. Q., Ma, L. L., Liu, J., Xia, Y. F., et al. (2009). Molecular mechanism of plant growth promotion and induced systemic resistance to tobacco mosaic virus by *Bacillus* spp. *J. Microbiol. Biotechnol.* 19, 1250–1258. doi: 10.4014/jmb.0901.008

Wu, J., Peng, Z., Liu, S. Y., He, Y. J., Cheng, L., Kong, F. L., et al. (2012). Genome-wide analysis of *Aux/IAA* gene family in Solanaceae species using tomato as a model. *Mol. Genet. Genomics* 287, 295–311. doi: 10.1007/s00438-012-0675-y

Wu, J., Zhang, J., and Zhou, X. (2010). AV2 protein encoded by tomato yellow leaf curl China virus is an RNA silencing suppressor. *Phytopathology* 100, S139–S139.

Yaakov, N., Levy, Y., Belausov, E., Gaba, V., Lapidot, M., and Gafni, Y. (2011). Effect of a single amino acid substitution in the NLS domain of tomato yellow leaf curl virus-Israel (TYLCV-IL) capsid protein (CP) on its activity and on the virus life cycle. *Virus Res.* 158, 8–11. doi: 10.1016/j.virusres.2011.02.016

Zhang, Z. Q., Li, Q., Li, Z. M., Staswick, P. E., Wang, M. Y., Zhu, Y., et al. (2007). Dual regulation role of GH3.5 in salicylic acid and auxin signaling during *Arabidopsis-Pseudomonas syringae* interaction. *Plant Physiol.* 145, 450–464. doi: 10.1104/pp.107.106021

Zhao, S., Gong, P., Ren, Y., Liu, H., Li, H., Li, F., et al. (2022). The novel C5 protein from tomato yellow leaf curl virus is a virulence factor and suppressor of gene silencing. *Stress Biol.* 2:19. doi: 10.1007/s44154-022-00044-3

Zheng, X., Fahlgren, N., Abbasi, A., Berry, J. C., and Carrington, J. C. (2019). Antiviral ARGONAUTEs against turnip crinkle virus revealed by image-based trait analysis. *Plant Physiol.* 180, 1418–1435. doi: 10.1104/pp.19.00121

frontiers | Frontiers in Microbiology

TYPE Review
PUBLISHED 09 October 2023
DOI 10.3389/fmicb.2023.1252039

OPEN ACCESS

EDITED BY
Jian-Wei Guo,
Kunming University, China

REVIEWED BY
Satyabrata Nanda,
Centurion University of Technology and Management, India
Baoyu Tian,
Fujian Normal University, China

*CORRESPONDENCE
Guoying Zhou
✉ zgyingqq@163.com
Junang Liu
✉ kjc9620@163.com

RECEIVED 03 July 2023
ACCEPTED 20 September 2023
PUBLISHED 09 October 2023

CITATION
Zhou D, Chen X, Chen X, Xia Y, Liu J and Zhou G (2023) Plant immune receptors interact with hemibiotrophic pathogens to activate plant immunity.
Front. Microbiol. 14:1252039.
doi: 10.3389/fmicb.2023.1252039

Plant immune receptors interact with hemibiotrophic pathogens to activate plant immunity

Diao Zhou[1,2,3], Xingzhou Chen[1,2,3], Xinggang Chen[1,2,3], Yandong Xia[1,2,3], Junang Liu[1,2,3]* and Guoying Zhou[1,2,3]*

[1]Key Laboratory of National Forestry and Grassland Administration on Control of Artificial Forest Diseases and Pests in South China, Central South University of Forestry and Technology, Changsha, China, [2]Hunan Provincial Key Laboratory for Control of Forest Diseases and Pests, Central South University of Forestry and Technology, Changsha, China, [3]Key Laboratory of Cultivation and Protection for Non-Wood Forest Trees, Ministry of Education, Central South University of Forestry and Technology, Changsha, China

Phytopathogens pose a devastating threat to the productivity and yield of crops by causing destructive plant diseases in natural and agricultural environments. Hemibiotrophic pathogens have a variable-length biotrophic phase before turning to necrosis and are among the most invasive plant pathogens. Plant resistance to hemibiotrophic pathogens relies mainly on the activation of innate immune responses. These responses are typically initiated after the plant plasma membrane and various plant immune receptors detect immunogenic signals associated with pathogen infection. Hemibiotrophic pathogens evade pathogen-triggered immunity by masking themselves in an arms race while also enhancing or manipulating other receptors to promote virulence. However, our understanding of plant immune defenses against hemibiotrophic pathogens is highly limited due to the intricate infection mechanisms. In this review, we summarize the strategies that different hemibiotrophic pathogens interact with host immune receptors to activate plant immunity. We also discuss the significant role of the plasma membrane in plant immune responses, as well as the current obstacles and potential future research directions in this field. This will enable a more comprehensive understanding of the pathogenicity of hemibiotrophic pathogens and how distinct plant immune receptors oppose them, delivering valuable data for the prevention and management of plant diseases.

KEYWORDS

hemibiotrophic pathogen, cell surface pattern recognition receptor, intracellular immune receptor, effector, plant immunity

1. Introduction

Plant diseases have been a devastating threat throughout the history of agriculture. In addition to causing significant losses in global crop yields, plant diseases present major challenges to natural and agricultural systems. Phytopathogens cause devastating plant diseases by deploying infection strategies (Fisher et al., 2018). They can be classified into three main groups based on their infection strategies to extract plant nutrients: biotrophs, hemibiotrophs, and necrotrophs. Biotrophs extract nutrients from living cells and sustain host viability, whereas necrotrophs rapidly kill host cells to extract nutrients (Rajarammohan, 2021). Intermediate lifestyle hemibiotrophs begin in the biotrophic phase and subsequently transition to the necrotrophic phase (Damm et al., 2014). Hemibiotrophic pathogens (HPs) are prevalent and

highly destructive phytopathogens that cause significant losses in crop quality and yield in key agricultural crops. The duration of each phase in HPs varies depending on factors such as the pathogen, host plant, temperature, secreted protein effectors, etc. (Qiu et al., 2022). For example, *Phytophthora infestans* has a shorter biotrophic phase than *Magnaporthe oryzae*, which has a shorter necrotrophic phase. Studies have also shown that hemibiotrophs utilize distinct effectors to adapt to various biotrophic/necrotic patterns. AVR3a stabilizes and targets the plant E3 ligase CMPG1 during the early stages of biotrophic infection by *P. infestans* to manipulate host immunity. AVR3a is subsequently downregulated, while the induction of other effectors INF1 and nep1-like proteins may facilitate the host transition to necrotrophic infection (Yaeno et al., 2011; Pirc et al., 2021). Although the term hemibiotroph was developed for pathogenic fungi, it is also sometimes used to describe the lifestyle of bacteria, oomycetes (Kraepiel and Barny, 2016; Panthapulakkal Narayanan et al., 2020). Different HPs differ in their pathogenic strategies, target hosts, etc. To induce disease in plants, HPs deploy various virulence factors to promote infection under defined environmental conditions.

Plants have evolved a sophisticated surveillance system to protect themselves from HPs. It devotes resources and energy to growth and development without threat. However, when threatened by virulence factors secreted by phytopathogens, including toxins, phytohormones, and enzymes, plants rapidly regulate gene expression to protect the host from pathogens (Jones et al., 2016). The plant surveillance system mainly relies on two classes of immune receptors to detect pathogens: membrane-anchored pattern recognition receptors (PRRs) and intracellular nucleotide-binding and leucine-rich repeat receptors (NLRs; Dangl, 2013; Van de Weyer et al., 2019). In the classical zig-zag pattern, these two classes of receptor proteins correspond to the two layers of the plant immune system (Ngou et al., 2022). In the first layer of immune surveillance, PRRs recognize pathogen- or microbe-associated molecules (PAMPs or MAMPs, respectively) present in the extracellular space, which results in PAMP-triggered immunity (PTI) or MAMP-triggered immunity (MTI; Macho and Zipfel, 2014; Wang and Chai, 2020). However, many phytopathogens can manipulate host targets to inhibit PTI signaling and successfully deliver effectors to plant cells. In the second layer of host immune surveillance, intracellular NLRs activate effector-triggered immunity (ETI) by specifically recognizing intracellular pathogen effectors (Chen et al., 2012; Kourelis and van der Hoorn, 2018). The distinction between PTI and ETI is an excellent framework for explaining the plant immune system. ETIs enhance PTI-induced defense responses by altering the expression of key genes involved in PRR signaling elements transcription and translation. Conversely, PTI also enhances ETI-triggered defense responses. PTI and ETI work together to provide robust immunity to pathogens (Ngou et al., 2021; Yuan et al., 2021b). Over the past few decades, researchers have made significant progress in studying plant immune signaling controlled by PRRs and NLRs against necrotrophic and biotrophic pathogens. In this review, we summarize the strategies by which various HPs interact with host immune receptors to activate plant immunity (Figure 1). We focus on how various immune receptors perceive characteristic molecules from different HPs. We also discuss the commonalities and differences in the pathogenicity of different HPs. This may be crucial in explaining the potential threat of pathogens attack on the host for effective defense, it can also guide the improvement and breeding of genetically diseased crops.

2. Plasma membrane participates in plant immunity

The plasma membrane (PM) serves as the frontline of defense against pathogens in plants and is essential for pathogen detection, signal transduction, and cellular homeostasis maintenance. Several PRRs are present in plant PMs that detect PAMPs, DAMPs, or effector proteins that induces PTI response. In the zig-zag immune model, the PTI response prevents most HPs from invasion and reproduction. Adapted pathogens secrete large amounts of effectors to evade or inhibit PTI. Correspondingly, plants have also evolved intracellular NLR receptors that directly or indirectly recognize effectors and trigger a robust ETI response. This ultimately leads to localized plant cell death (Ngou et al., 2022). The co-resistance of PTI and ETI determines many plant defense responses to pathogen infection, such as protein phosphorylation, changes in ion flux, generation of reactive oxygen species (ROS), activation of mitogen-activated protein kinases (MAPK), and pathogenesis associated with cell wall strengthening (Tsuda and Katagiri, 2010). The activation of the MAPK signaling pathway by PRR at the PM results in the phosphorylation of target proteins in plant immunity. In *Arabidopsis*, the HP effector protein AvrRpt2 specifically inhibits the phosphorylation of MPK4 and MPK11 induced by the PM-localized receptor FLAGELLIN-SENSITIVE 2 (FLS2; Tsuda et al., 2013; Eschen-Lippold et al., 2016). It has also been shown that MPK3 and MPK6 can regulate malate metabolism to promote PM-mediated stomatal immunity during pathogen infection (Su et al., 2017).

Although HPs primarily activate the PM-anchored protein PRR, plants can also utilize lipids on the PM to sense HPs. These lipids trigger immune signals independent of PRR interactions. For example, the effector NLP of HPs is sensed by glycosphingolipids (GIPCs) on the PM, and it is speculated that a conformational changes in the GIPC-NLP complex induces pore formation in the PM and thus cell death (Mamode Cassim et al., 2018). In the basic defense process, recognition of PAMP or DAMP by the PRR of the PM induces cell wall modification that activates endocytosis of PRR and PAMP/DAMP, followed by degradation in the vacuole. This process initiates and amplifies immune signaling (Mbengue et al., 2016). For example, *Arabidopsis* RLCK BIK1, BSK1 interacts with FLS2 and is rapidly phosphorylated in an FLS2-dependent manner upon recognition of the bacterial flagellin peptide flg22. FLS2's sustained anchoring to the PM is mediated *via* the BFA-sensitive endocytotic pathway under steady-state conditions (Beck et al., 2012). These findings contribute to a comprehensive understanding of the vital role of plant immunity in HP interference. Collectively, plant PM regulates immune responses by detecting HPs, activating signaling cascades, controlling the cellular entry and exit of molecules, and enabling PM endocytosis.

3. Plant surface immune receptors

Pattern recognition receptors (PRRs) play an important role in plant growth, development, reproduction, abiotic stress, and disease resistance, and many of them exhibit lineage-specific expansion to adapt to different pathogens within the innate immune system (Schellenberger et al., 2019; Ngou et al., 2022). Several plant PRRs have already been identified, such as FLS2, ELONGATION FACTOR-Tu RECEPTOR (EFR), ELICITOR

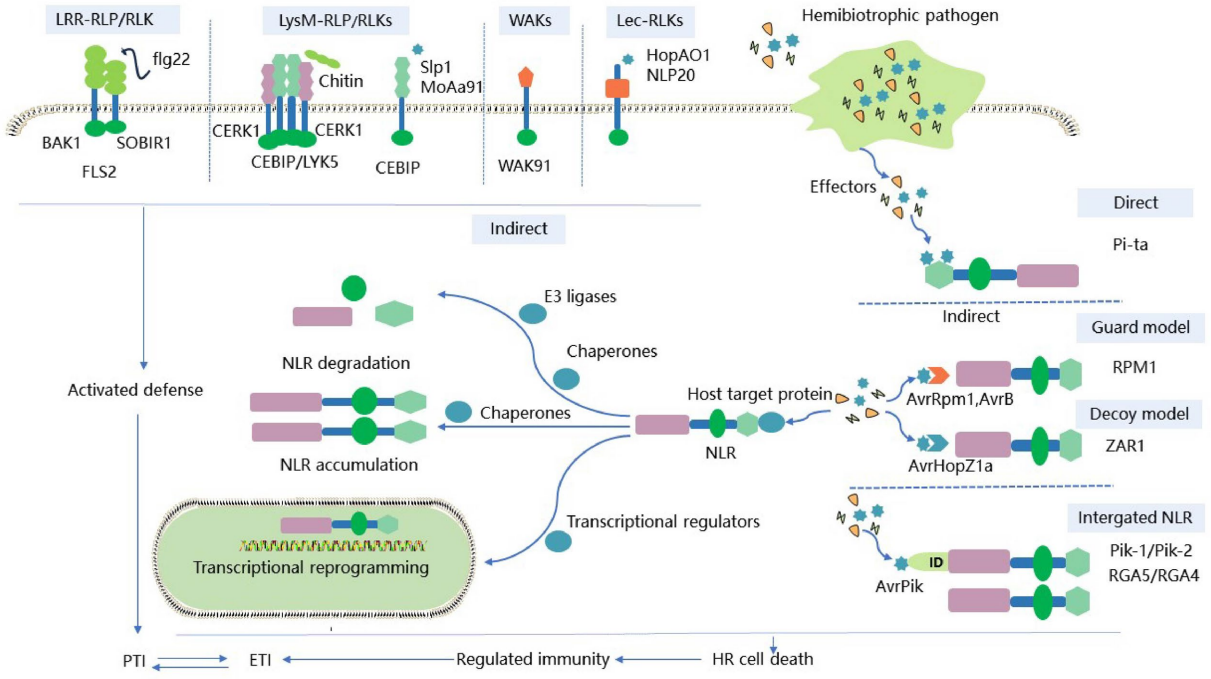

FIGURE 1
Schematic diagram of the two-layer immune system of plant immune receptors against HPs. Plant PRRs recognize PAMPs (e.g., bacterial flagellin , fungal chitin) or DAMPs (e.g., secretory minipeptides) to induce PTI. Adaptive HPs successfully translocate effectors into plant cells, thereby initiating a second round of plant immunity. Intracellular NLR immune receptors induce ETIs to trigger immune-related gene expression and local cell death through direct or indirect specific recognition of effector proteins. Activated PTIs enhance the defense response triggered by ETIs. While ETIs upregulate related genes that control signaling to PRRs, PTIs and ETIs together provide plants with strong immunity against HPs. ID, Integrated domain; PTI, PAMP-triggered immunity. ETI, Effector-triggered immunity; PRR, Pattern recognition receptor; HP, Hemibiotrophic pathogen; FLS2, Flagellin-sensitive 2; EFR, Elongation factor-Tu receptor; CERK1, Elicitor receptor kinase 1; CEBiP, Chitin elicitor binding protein; WAK, Wall-associated kinase; LRR, Leucine-rich repeat domain; LysM, Lysin motif domains; Lec, Lectin domain.

RECEPTOR KINASE 1 (CERK1), and CHITIN ELICITOR BINDING PROTEIN (CEBiP; Tang et al., 2017). They recognize the bacterial flagellin epitope flg22, the EF-Tu epitope elf18, the plant elicitor polypeptide, and chitin released during pathogen infection, respectively (Chen et al., 2020). These PRRs form complexes with their corresponding ligands. These complexes activate downstream immune signals such as calcium influx, ROS production, MAPK signaling cascade, and defense responses (Couto and Zipfel, 2016; Zhou and Zhang, 2020). Based on the presence or absence of intracellular kinase domains, the PRR family is classified into receptor-like kinases (RLKs) and receptor-like proteins (RLPs), which act on the first layer of the plant immune system. RLKs consist of a variable N-terminal extracellular domain (ECD), a transmembrane region (TM), and a conserved cytoplasmic kinase domain (KD; Wang and Chai, 2020); In contrast, RLPs have only short domains and lack distinct kinase domains that require interaction with other kinase domain-containing proteins such as BAK1 and SOBIR1 to activate downstream signaling (Gust and Felix, 2014; Liebrand et al., 2014). RLKs and RLPs are classified into several subfamilies based on their ECDs, which include leucine-rich repeat (LRR) domains, lysin motif (LysM) domains, lectin (Lec) domains, and epidermal growth factor-like (EGF) repeat domains (Macho and Zipfel, 2014). Various subfamilies of PRRs exhibit commonalities and differences in detecting diverse HPs (Table 1; Figure 1).

3.1. LRR receptors sense HPs to confer plant immunity

Leucine-rich repeat-containing PRRs are the largest subfamily, including LRR-RLP and LRR-RLK family members. LRR-RLP/RLKs detect HPs by interacting with shorter ECD co-receptors of the same family to enhance immune signaling (Smakowska-Luzan et al., 2018). BRASSINOSTEROID INSENSITIVE 1 (BRI1)-ASSOCIATED RECEPTOR KINASE 1 (BAK1) is one of the most versatile co-receptors, also known as SOMATIC EMBRYOGENESIS RECEPTOR KINASES 3 (SERK3). It has only five LRRs in its ECD, which are centrally involved in various PTI signaling pathways (Wu et al., 2020). When hemibiotrophic bacteria interact with plants, a well-studied PRR is the LRR-RK FLS2 in most higher plants, which detects a 22-amino acid peptide derived from the N-terminus of bacterial flg22 (Lee et al., 2021). Recognition of flg22 by FLS2 and its co-receptor BAK1 is accompanied by rapid heterodimerization and phosphorylation, which activate plant immunity. To prevent the host immune responses, *P. syringae* secrete effectors to interfere with immune signals, such as AvrPto, AvrPtoB, HopB1, etc. AvrPto and AvrPtoB interact with FLS2 to prevent the formation of the FLS2-BAK1 complex and the phosphorylation of BIK1 (Gravino et al., 2017; Lei et al., 2020). HopB1 constitutively interacts with FLS2 prior to the activation of flg22. Upon activation, BAK1 is recruited to the FLS2-HopB1 complex. HopB1 cleaves BAK1 and its analogs via genetic

10.3389/fmicb.2023.1252039

TABLE 1 Overview of PRRs and the outcome of interactions with typical HPs to mediate plant immunity.

Plant receptor	Organism	Co-receptor	Pathogen	Effector	Outcome (Enhance or suppress the host defense response)
LRR					
FLS2	*Arabidopsis*	BAK1/BIK1	*P. syringae*	AvrPto	Suppress
FLS2	*Arabidopsis*	BAK1	*P. syringae*	HopB1	Suppress
FLS2	*Arabidopsis*	BAK1	*P. syringae*	HopQ1	Suppress
EFR	*Arabidopsis*	BAK1/SOBIR1	*P. syringae*	elf18	Enhance
RLP23	*Arabidopsis*	BAK1/SOBIR1	*P. syringae*	NLP20	Enhance
FLS2	*Arabidopsis*	BAK1	*P. syringae*	AvrPtoB	Suppress
LysM					
LYK5	*Arabidopsis*	CERK1	All	Chitin oligomers	Enhance
AtCERK1	*Arabidopsis*	LYK4/LYK5	All	Chitin oligomers	Enhance
CEBiP	rice	CERK1	All	Chitin oligomers	Enhance
CEBiP	rice	None	*M. oryzae*	Slp1	Suppress
CEBiP	rice	None	*M. oryzae*	MoAa91	Suppress
WAK					
OsWAK14/	Rice	None	*M. oryzae*	None	Enhance
OsWAK91	Rice	None	*M. oryzae*	None	Enhance
OsWAK92	Rice	None	*M. oryzae*	None	Enhance
OsWAK112d	Rice	None	*M. oryzae*	None	Suppress
OsWAK1	Rice	None	*M. oryzae*	None	Enhance
OsWAK25	Rice	None	*M. oryzae*	None	Enhance
AtWAKL10	Rice	None	*P. syringae*	None	Enhance
GmWAK1	Soybean	None	*P. infestans*	None	Enhance
SlWAK1	Tomato	None	*P. syringae*	None	Enhance
AtWAKL10	Tomato	None	*P. syringae*	None	Enhance
Lec					
FaMBL1	Strawberry	None	*C. fioriniae*	None	Enhance
OsLecRK	rice	None	*M. grisea*	None	Enhance
Pi-d2	rice	None	*M. grisea*	None	Enhance
LORE	*Arabidopsis*	None	*P. syringae*	HopAO1	Suppress
LecRK-IX.2	*Arabidopsis*	None	*P. syringae*	None	Enhance
LecRK-I.9	*Arabidopsis*	None	*P. syringae* / *P. infestans*	None	Enhance
SBP1/SBP2	*Arabidopsis*	BAK1/SOBIR2	*P. syringae*	NLP20	Suppress

[a]PRR, Pattern recognition receptor; HP, Hemibiotrophic pathogen; FLS2, Flagellin-sensitive 2, EFR, Elongation factor-Tu receptor; CERK1, Elicitor receptor kinase 1; CEBiP, Chitin elicitor binding protein; WAK, Wall-associated kinase; LRR, Leucine-rich repeat domain; LysM, Lysin motif domains; Lec, Lectin domain; *P. syringae*, *Pseudomonas syringae*; *M. oryzae*, *Magnaporthe oryzae*; *M. grisea*, *Magnaporthe grisea*; *C. fioriniae*, *Colletotrichum fioriniae*. [b]None indicates that no data are available. [C]This table is not a detailed list of all plant receptors for detecting hemibiotrophic pathogens (HPs).

transformation or bacterial delivery to inhibit FLS2 signaling and enhance pathogen virulence (Li et al., 2016; Wu et al., 2020). Like FLS2, another extensively studied LRR is the *Arabidopsis* EFR, which recognizes the N-terminal N-acetylated elongation factor Tu (EF-Tu) peptide of hemibiotrophic bacteria. Upon ligand binding, BAK1 is also recruited by EFR to participate in host immune signaling. Resistance to the hemibiotrophic bacteria *P. syringae* is activated by recognition of elf18C by EFR-*Cf*-9 in conjunction with SOBIR1 and BAK (Wu et al., 2019). In addition, rice LRR-RK XA21 can sense tyrosine sulfonate proteins derived from *Xanthomonas oryzae* to induce effective resistance to Xoo (Wei et al., 2016). These results suggest that under hemibiotrophic bacterial attack, plant LRR-RLKs participate in immune defense and self-development by phosphorylation upon binding to the corresponding co-receptors. Plant RLKs such as FLS2, EFR, and XA21 all belong to the LRR-XII subfamily, which suggests that RLKs of this subfamily may induce immunity by recognizing various protein ligands of hemibiotrophic bacteria. Similar to RLKs, BAK1 is also recruited to the two-component

RLP or SOBIR1 complex by ligand recognition by RLP. BAK1 and SOBIR1 can transphosphorylate each other to activate immune signaling pathways. The *Arabidopsis* RLP23 forms a receptor complex by interacting with SOBIR1. Upon recognizing NLP20, it recruits the co-receptor BAK1 to the complex to enhance the LRR-mediated plant immune response to HPs (Albert et al., 2015; van der Burgh et al., 2019). Several effectors of hemibiotrophic bacteria, fungi, and oomycetes can prevent host LRR-RLP resistance to pathogens by inhibiting NLP-induced cell death, such as suppressor of necrosis 1 (SNE1) from *P. infestans* (Kelley et al., 2010), *Colletotrichum higginsianum* effector candidate (ChECs) from *C.higginsianum* (Kleemann et al., 2012), and MoNLP 1 (Chen et al., 2021), *M. oryzae* hypothetical effector gene 13 (MoHEG13; Mogga et al., 2016), and suppressors of plant cell death (SPDs) from *M. oryzae* (Sharpee et al., 2017). Regardless of whether hemibiotrophic bacteria, fungi, or oomycetes infect plants, although the immune response outcomes are different, FLS, EFR, and RLP23 all rely on kinase domain-containing proteins such as BAK1 or SOBIR1 receptor complexes for immune signaling. Different receptor complexes may elicit diverse immune responses by influencing intracellular structural domain phosphorylation and downstream immune signaling. Further studies of the phosphorylation properties of the different receptor complexes may reveal how these receptors are effective against localized HP infection.

3.2. LysM receptors sense HPs to confer plant immunity

During the game between HPs and plants, plant LysM ectodomains induce immune responses by recognizing N-acetylglucosamine molecules, such as fungal chitin oligomers and bacterial peptidoglycan (PGN; McCombe et al., 2022). The LysM family consists of LysM-RLK and LysM-RLP. LysM-RLKs have a LysM outer domain, a single channel transmembrane domain and a cytoplasmic kinase domain. LysM-RLP has only one outer domain connected to the outer membrane by GPI anchors (Buendia et al., 2018). CERK1 is a typical member of the LysM-RLK family consisting of three LysM structural domains. In rice and *Arabidopsis*, autophosphorylation of specific amino acids in CERK1 regulates chitin-induced immune signals secreted by HPs (Fliegmann et al., 2011; Suzuki et al., 2016; Yu et al., 2021). CERK1 not only recognizes hemibiotrophic fungal chitin, but is also a crucial co-receptor for bacterial PGN. CERK1, together with lysin motif receptor kinase 1 (LYM1) and LYM3, is required for the perception of bacterial PGN and for the development of basal resistance to *P. syringae*. Studies have also shown that deletion of CERK1 increases susceptibility to hemibiotrophic fungi and bacteria (Giovannoni et al., 2021). In *Arabidopsis*, LYK5 exhibits a greater affinity for chitin than CERK1. Once LYK5 externally detects chitin, CERK1 forms a dimer and transmits chitin signals to LYK5. Afterward, CERK1 phosphorylates LYK5 and itself in vesicles, which are then internalized (Erwig et al., 2017). LYK4 and AtCERK1 can form a complete complex with LYK5. LYK4 serves as a scaffolding protein or a co-receptor for LYK5, whereas AtCERK1 senses chitin and mediates homodimerization and phosphorylation, all of which promotes chitin triggering signaling (Wan et al., 2012; Cao et al., 2014; Xue et al., 2019). Unlike the chitin-sensing mechanism in *Arabidopsis*, the rice LysM-RLP CEBiP recognizes chitin and forms a dimer with OsCERK1 to activate plant disease resistance to HP and initiates downstream immune signaling pathways (Hayafune et al., 2014; Desaki et al., 2018; Hu et al., 2021). The results suggest that dimerization of the LysM receptor plays a vital role in ligand detecting, receptor activation, and immune signal transduction during HP infection. Aggregated PGN from hemibiotrophic bacteria is recognized as PAMP by the LysM receptor in *Arabidopsis* and activates immunity against hemibiotrophic bacteria in plants. Chitin is a major component of fungal cell walls. It plays a crucial molecular role in LysM-mediated host defense responses. Recognition and immune stimulation of chitin secreted by hemibiotrophic fungi in rice or *Arabidopsis* depend on the LysM-type PRRs OsCEBiP/OsCERK1, LYK4/LYK5, or AtCERK1, respectively. While plants use different sensing systems for bacterial-secreted PGN and fungal-secreted chitin, the chitin sensing system employed by fungi is structurally similar to the carbohydrate portion of bacterial-secreted PGN.

Plant LysM proteins recognize HPs to induce immune responses. HPs have evolved multiple mechanisms to evade plant immune recognition (Wang et al., 2022; Zhao L. et al., 2023). HPs secrete effectors with LysM domains that compete with high affinity for plant LysM receptors. Alternatively, HPs secrete effectors that modify plant LysM receptors to sequester, mask, alter, or prevent the host from degrading pathogen cell walls. These behaviors would regulate plant cytoplasmic signaling, suppress plant immunity, and regulate the transition of HPs from the biotrophic to the necrotrophic stage (Hu et al., 2021; Tian et al., 2022b). The secreted effector protein Slp1 of *M. oryzae* contains a LysM domain that accumulates at the early stage of infection between fungi and rice cells. This protein disrupts host chitin-triggered immunity by utilizing the LysM structural domain to competitively bind chitin oligosaccharides with CEBiP (Sanchez-Vallet et al., 2013). Similarly, *M. oryzae* depends not only on LysM Slp1 but also on MoAa91 of *M. oryzae*. This protein is vital for surface recognition and inhibition of chitin-induced plant immune responses. Further studies shown that MoAa91 competitively binds chitin to the rice immune receptor CEBiP to inhibit chitin-induced plant immune responses (Li et al., 2020). Many HPs-secreted LysM effectors remove chitin oligomers from the host infection site by intermolecular LysM dimerization, or prevent host recognition of chitin by the formation of polymeric precipitates, such as *C.higginsianum* ChElp1 and ChElp2 (Takahara et al., 2016; Sanchez-Vallet et al., 2020; Tian et al., 2022a). Intermolecular interactions such as homodimerization and phosphorylation demonstrate the significant implications of precisely management of host-pathogen processes, which are also essential for enhancing disease resistance in crops. However, it is unclear whether there are secreted proteins in HPs that more broadly regulate plant defense responses and cell death, potentially mediating the transition from biotrophy to necrotrophy.

3.3. Other PRR receptors sense HPs to confer plant immunity

Besides PRRs with LRR structures and LysM structures, there is increasing evidence that WAK receptors and lectin receptors play a significant role in plant-microbe interactions. A number of many immune-related WAKs have also been cloned recently. WAKs, a receptor-like kinase required for recognizing oligogalacturonides

(OGs), often possess an extracellular EGF-like domain, and are found in both dicots and monocots (Stephens et al., 2022). They can identify pathogens with different lifestyles and regulate HP resistance by modifying host cell walls and regulating hormone fluctuations within host cells. WAKs play a crucial role in plant signaling pathways for immune and abiotic stress responses (Yue et al., 2022). OsWAKs in rice have been discovered to regulate the basic defense against *M. oryzae* either positively or negatively. Quantitative resistance has been positively affected by OsWAK14, OsWAK91, and OsWAK92, whereas resistance to rice blast has been negatively affected by OsWAK112d. OsWAK91 participates in intercellular signal transduction by generating ROS with possess antibacterial properties (Delteil et al., 2016). AtWAKL10 is thought to enhance plant resistance against *P. syringae*. Transgenic *Arabidopsis* lacking *WAK* exhibits increased susceptibility to *P. syringae* compared to the wild type (Bot et al., 2019). WAK receptors may regulate host immune resistance by modulating hormone fluctuations during HP infection of different host plants. Overexpression of *OsWAK1* and *OsWAK25* can enhance host resistance to *M. oryzae,* and salicylic acid (SA) treatment can up-regulate the expression of *OsWAK1* and *OsWAK25* genes (Li et al., 2009; Harkenrider et al., 2016). Recently, it was discovered that GmWAK1 relies on the SA pathway to alleviate oxidative stress-induced damage in soybeans resistant to *P. infestans* (Zhao M. et al., 2023). Immune-related WAK also prevents pathogen penetration during HP attack by altering cell wall composition to enhance cell wall strength. Upon infection of tomato by *P. syringae*, SlWAK1 strengthens the cell wall through callose deposition to restrict pathogen penetration and spread (Zhang et al., 2020). This ability of WAKs to regulate the cell wall indicates their potential role in plant growth, development, and response to abiotic stresses. OsWAK91/OsDees1 knockout rice has increased susceptibility to *M. oryzae* and inhibited growth (Delteil et al., 2016). In tomato, AtWAKL10 exhibits resistance to *P. syringae* while also upregulated when treated with the abiotic stress signaling factor S-nitroso-L-cysteine. Additionally, its knockout gene mutant displays increased tolerance to drought stress, but lower tolerance to salt stress (Bot et al., 2019). The WAK receptors not only enhance or inhibit host resistance when different HPs infect various hosts, but also affect plant growth and development. The mechanisms by which WAK receptors recognize or transduce pathogen signals and their impact on the transition of HPs from the biotrophic to necrotrophic stage remain unclear.

Lectin receptor-like kinases (LecRKs) are unique PRRs that specifically recognize carbohydrates such as mannose induced by elicitors or pathogens (De Coninck and Van Damme, 2022). LecRKs appear to constitute a vital recognition system on the surface of plant cells during plant-microbe interactions, and may play a vital role in plant immunity or stress responses (Wang and Gou, 2022). Furthermore, LecRKs are classified into L-type, C-type, and G-type. G-type and L-type LecRKs are activated by PAMP signaling perception, which triggers PTI to HPs. G-type LecRKs Pi-d2 and OsLecRK have been found to trigger plant defense against rice blast and leaf blight, as well as activate various signal responses in plant innate immunity (Li et al., 2015). Among them, the OsLecRK mutant is more susceptible to *Magnaporthe grisea* infection than the wild type, with a reduction in mRNA levels of *PR1*, *LOX2*, and *CHS* defense-related genes (Cheng et al., 2013). Similar to LRR receptors, G-type SBP1 and SBP2 can specifically activate immunity by positively regulating the interaction between RLP23 receptors and BAK1 co-receptors (Bao et al., 2023). G-type LecRK LORE was identified as a target site for the effector HopAO1 of *P. syringae*. During the initial stages of infection, LORE detects bacterial lipopolysaccharides and triggers autophosphorylation to activate the immune response. In the advanced stage of infection, HopAO1 interacts with LORE within host cells, leading to the dephosphorylation of LORE. This effectively suppresses the immune response and makes the host more susceptible to the infection (Chen et al., 2017; Luo et al., 2020). HPs that secrete various molecules recognized by the same host PRR receptors lead to diverse plant immune reactions. Phytohormones play a vital role in plant-pathogen interactions, such as JA, which activate plant defense responses against pathogens. The G-type Lec-RLK FaMBL1 from strawberry can bind to mannose from the cell wall of *Colletotrichum fioriniae*. Overexpression of FaMBL1 leads to a reduction in JA content (Ma et al., 2023). The L-types of LecRK-IX.1, LecRK-IX.2, and LecRK-I.9 in *Arabidopsis* are considered to have defense responses against *Phytophthora*. Overexpression of LecRK-IX.2 phosphorylates RBOHD to enhance ROS production and SA accumulation in PTI response (Wang Y. et al., 2015; Wang Y. et al., 2016; Luo et al., 2017). Similar to LecRK-IX.2, LecRK-I.9 is another L-type LecRK in *Arabidopsis*, known as DORN1, which also confers plant resistance to *P. syringae* DC3000 and *Phytophthor*a resistance (Balague et al., 2017; Sun Y. L. et al., 2020). DORN1 recognizes extracellular ATP signals and directly phosphorylates RBOHD. This induces $Ca2^{+}$ influx, MAPK activation, ROS accumulation, and defense gene expression, and host stomatal closure to restrict HPs invasion (Luo et al., 2017; Wang et al., 2018). These studies indicate that LecRLKs are involved in PTI, ETI, SA, and JA signaling pathways and could enhance plant defense against HPs. In molecular breeding, manipulation of one pathway may impact other signaling responses, due to the interconnected nature of these pathways.

4. Intracellular recognition receptors

The NLRs perceive effector proteins in host cells to activate an ETI immune response against these pathogens (Barragan and Weigel, 2021). It is a significant member of the plant resistance R protein family with a conserved modular structure consisting of a central NB-ARC domain (nucleotide-binding adapter, APAF-1, R protein, and CED-4), a C-terminal leucine-rich repeat (LRR) domain, and a unique N-terminal domain (Duxbury et al., 2021). Based on their variable N-terminal structure, it is predominantly categorized as either the coil-coil (CC) type or Toll/interleukin-1 receptor type (TIR), known as CNLs and TNLs (Monteiro and Nishimura, 2018; Yuan et al., 2021a; Maruta et al., 2022). Typically, the CC or TIR in the N-terminal domain is considered the signaling domain. The central NB-ARC domain acts as a molecular switch that regulates the binding or hydrolysis of ADP or ATP to determine the signaling state of NLR. LRR domains may play a significant role in ligand recognition and regulatory activity (Jubic et al., 2019; Ma et al., 2020). NLRs often exist in an inactive state when not infected by pathogens due to various intramolecular and intermolecular interactions. Upon recognition of hemibiotrophic effectors, these interactions are disrupted, which activates the NLR to trigger programmed cell death (Sun Y. et al., 2020).

Nucleotide-binding and leucine-rich repeat receptors recognize pathogen effectors through various strategies, including direct

recognition, indirect recognition, and paired NLR recognition (Kroj et al., 2016). Some NLRs recognize effector protein patterns directly, which are extensively characterized. HPs are mainly recognized by NLR receptors indirectly. The indirect interaction between ligands and receptors is well-described in the "guard" and "decoy" recognition models (van der Hoorn and Kamoun, 2008). Other effector targets, including transcriptional regulators, molecular chaperones, and ubiquitin ligases, could serve as potential "guards" or "decoys." These effector targets regulate transcriptional reprogramming and host protein stability, respectively (Sun Y. et al., 2020; Duxbury et al., 2021). There is also a small portion of plant NLR that includes an additional "integrated" domain (ID). This ID recognizes HPs through integrated decoy patterns and activates downstream immune responses (Sarris et al., 2016). The strategies used to activate immunity by various interactions between NLRs and different HPs are discussed in detail below (Figure 1; Table 2).

4.1. NLR directly senses HPs to confer plant immunity

Most of the proteins encoded by R genes in each plant genome are NLRs. NLRs directly or indirectly recognize effectors secreted by HPs and activate ETI response (Barragan and Weigel, 2021). Direct interaction between hemibiotrophic effectors and plant NLRs is the most intuitive and simple method. Most CNLs act as effector receptors, called sensor CNL. For example, plant CNLs detect their cognate effectors via direct interactions. Rice NLR Pi-ta binds to the *M. oryzae* effector AVR-Pita (Jia et al., 2000). Intriguingly, the CNL protein encoded by the *Pik* allele in rice can also perceive multiple AVR-Pik effectors of *M. oryzae* via physical interaction. Pikm can recognize three AvrPik effectors of *M. oryzae*, while Pikp can recognize only one (De la Concepcion et al., 2018).

4.2. NLRs indirectly sense HPs to confer plant immunity

Hemibiotrophic pathogens are mainly recognized by NLR receptors indirectly. Two recognition models can well describe the indirect interaction between ligands and receptors, namely the "guard" model and the "decoy" model (van der Hoorn and Kamoun, 2008). Modification of guards or decoys by effectors may cause changes in the conformation of NLRs, which leads to the activation of ETI (Schreiber et al., 2016). Since many effectors targeted by NLRs are unknown, and it is often unclear whether these effector targets are guardees or decoys (Kapos et al., 2019). The "guard" model suggests that NLR proteins monitor the integrity of target proteins in plant cells and activate immune responses upon perturbation or modification by pathogen effectors. For example, *P. syringae* effectors AvrRpm1, AvrB, and AvrRpt2 specifically target the guardee protein RPM1-interacting 4 (RIN4), while CNLs RPM1 and RPS2 monitor RIN4 steric hindrance or post-translational modification to exert disease resistance (Day et al., 2005; El Kasmi et al., 2017). In soybean, CNL RPG1-B monitors the homolog RIN4 in a comparable way (Selote and Kachroo, 2010). Another well-studied example is that of the guardee CNL RPS5 monitors the host target kinase PBS1, where the *P. syringae* effector protease AvrPphB cleaves PBS1 to activate RPS5-mediated immunity (Ade et al., 2007). It is generally established that all kinases and pseudokinases serve as "guards" or "decoys," and interact with CNLs, but not with TNLs. Decoy proteins have no defined biological, cellular, or physiological role in host defense. Instead, they imitate toxic targets to activate the host surveillance system and detect effector molecules. Decoys probably evolved by duplicating ancestral guardians (van Wersch et al., 2020). As a decoy protein, the pseudokinase RLCK XII family ZED1 interacts with the acetyltransferase HopZ1a effector secreted by *P. syringae*. ZED1 is acetylated to activate CNL ZAR1 (Wang G. X. et al., 2015). Recent research revealed that ZED1 forms a complex with ZAR1 after acetylation by HopZ1a, triggering the assembly of higher-order complexes in plants that form a resistosome similar to the ZAR1-RKS1-PBL2^{UMP} complex (Hu et al., 2020). Other RLCKs are targeted by HopZ1a and are recognized by the ZAR1-ZED1 complex. RKS1 performs an adapter function similar to ZED1 (Bastedo et al., 2019). The pseudokinase ZRK3 and the RLCK family SZE1 and SZE2 also bind to ZAR1 (Liu et al., 2019). It appears that indirect interactions may expand the capacity of certain plant immune receptors to detect additional pathogen effectors. Furthermore, indirect interactions may offer more avenues to enhance pathogen control by regulating receptors.

Plant NLRs' assembly, activity, and stability are tightly regulated to ensure appropriate host defense responses against HPs. Studies have shown that molecular chaperones and ubiquitin ligases are essential for NLRs' assembly, activity, and stability (Duxbury et al., 2021; Huang et al., 2021). There are several chaperones in the HSP90 family that play a role in NLR-mediated defenses in *Arabidopsis*. HSP90.2 interacts with CNL RPM1 to strengthen RPM1 protein stability. HSP90.3 interacts with TNL SNC1 to negatively regulate SNC1 accumulation (Hubert et al., 2003; Huang S. et al., 2014). Recent studies have shown that the *P. syringae* effector HopBF1 phosphorylates HSP90 to trigger hypersensitivity in plants. This finding uncovers a previously unidentified mechanism by which hemibiotrophic bacteria regulate host immunity (Lopez et al., 2019). And HSP90 may assist the suppressor of G-two allele of SKP1 (SGT1) in forming the Skp1-Cul1-F-box (SCF) E3 ubiquitin ligase complex, which targets immune receptors for degradation. This process is critical for maintaining appropriate levels of immune receptor proteins to avoid autoimmunity. Similarly, ubiquitin ligases interact with NLRs to help regulate their levels without pathogen infection. Upon *P. syringae* infection, the proteasome effector destroys the E3 ligase F-box protein CPR1, interacts with *Arabidopsis* TNL SNC1 and CNL RPS2, and reduces their protein accumulation, thus inducing a defense response (Gou et al., 2012). Knocking down the E4 ligase MUSE3 in *Arabidopsis* causes increased levels of TNL SNC1 and CNL RPS2. Overexpression of MUSE3 and CPR1 enhanced polyubiquitination and protein degradation of these immune receptors (Huang Y. et al., 2014). Host molecular chaperones and ubiquitin indirectly control NLR activity and stability to modulate immune responses when various HP infect the host. This suggests that NLR activity and homeostasis are critical for plant disease resistance.

Transcriptional reprogramming is a frequent occurrence in plant immunity that involves numerous transcriptional regulators. The coordination and nuclear localization of NLRs and immune transcription factors in the transcriptional machinery is crucial to selectively activate plant defense genes during HPs infection. The transcription factor RRM shows CNL-dependent nuclear localization and is unaffected by HPs. RRM binds to the CNL

10.3389/fmicb.2023.1252039

TABLE 2 Overview of intracellular recognition receptors and the outcome of interactions with typical HPs to mediate immune results.

Organism	NLR	Type	Pathogen	Effector	Effector target protein	Recognition domain	Evidence	Outcome
Rice	Pi-ta	CNL	*M. oryzae*	AvrPi-ta	None	None	Y2H	Resistance
Rice	Pikp	CNL	*M. oryzae*	AVR-PikD	None	CC	Y2H, BiFC, pull-down	Resistance
Rice	Pikm	CNL	*M. oryzae*	AVR-PikD, AVR-PikE, AVR-PikA	None	CC	Y2H, co-IP	Resistance
Arabidopsis	RPM1	CNL	*P. syringae*	AvrRpm1, AvrB	RIN4	CC, FL	Y2H, co-IP	Resistance
Arabidopsis	RPS2	CNL	*P. syringae*	AvrRpt2	RIN4	CC, FL	Co-IP	Resistance
Arabidopsis	RPS5	CNL	*P. syringae*	AvrPphB	PBS1	CC, FL	Co-IP	Resistance
Arabidopsis	ZAR1	CNL	*P. syringae*	AvrHopZ1a	ZED1	CC, CC-NB, FL	Y2H, BiFC	Resistance
Arabidopsis	ZAR1	CNL	*P. syringae*	HopF2a	ZRK3	FL	Co-IP	Resistance
Arabidopsis	ZAR1	CNL	*P. syringae*	AvrHopZ1a	SZE1, 2	FL	BiFC, co-IP, pull-down	Resistance
Arabidopsis	RPM1	CNL	*P. syringae*	AvrRpm1, AvrB	HSP90.2	FL	Co-IP	Resistance
Arabidopsis	SNC1	TNL	*P. syringae*	None	HSP90.3	FL	Co-IP	Resistance
Arabidopsis	None	CNL	*P. syringae*	HopBF1	HSP90	NB	IP-MS	Susceptibility
Arabidopsis	SNC1	TNL	*P. syringae*	None	CPR1	FL	Co-IP, pull-down	Susceptibility
Arabidopsis	RPS2	CNL	*P. syringae*	None	CPR1	FL	Co-IP, pull-down	Susceptibility
Arabidopsis	SNC1	TNL	*P. syringae*	None	MUSE3	FL	Co-IP	Resistance
Rice	PigmR	CNL	*M. oryzae*	None	PIBP1	CC, FL	Y2H, SLC, BiFC, co-IP, pull-down	Resistance
Rice	Pi9	CNL	*M. oryzae*	None	PIBP2	CC	Y2H, SLC	Resistance
Rice	Piz-t	CNL	*M. oryzae*	None	PIBP1	CC	Y2H, SLC	Resistance
Rice	Piz-t	CNL	*M. oryzae*	AvrPiz-t	APIP5	NT, FL	SLC, pull-down	Resistance
Rice	Pb1	CNL	*M. oryzae*	None	WRKY45	CC, FL	Y2H, SLC, co-IP, pull-down	Resistance
Arabidopsis	RPS4	TNL	*P. syringae*	AvrRps4	bHLH84	FL	Co-IP	Resistance
Rice	Piz-t	CNL	*M. oryzae*	AvrPiz-t	APIP5	None	Co-IP, pull-down, BiFC, Y2H	Resistance
Arabidopsis	RPS4	CNL	*P. syringae*	AvrRps4	EDS1	FL	BiFC, co-IP	Resistance
Arabidopsis	RPS4	TNL	*P. syringae*	AvrRps4	RRS1	TIR, FL	Y2H, co-IP, pull-down	Resistance
Rice	RGA4	CNL	*M. oryzae*	AVR1-CO39, AVR-Pia	RGA5	CC, FL	Y2H, co-IP	Resistance
Rice	Pik-2	CNL	*M. oryzae*	AvrPik	Pik-1	CC	Y2H, BiFC, pull-down	Resistance

[a]HP, Hemibiotrophic pathogen; CNL, CC-NLR; TNL, TIR-NLR; CC, Coiled-coil; NB, Nucleotide binding; NT, N-terminus; FL, Full length; TIR, Toll/interleukin 1 receptor (TIR) domain; Y2H, Yeast two-hybrid; BiFC, Bimolecular fluorescence complementation; Co-IP, Coimmunoprecipitation; SLC, Split luciferase complementation; IP-MS, Immunoprecipitation, and mass spectrometry; *P. syringae*, *Pseudomonas syringae*; and *M. oryzae*, *Magnaporthe oryzae*. [b]None indicates that no data are available. [c]This table is not a detailed list of all plant receptors for detecting HPs.

encoded by the resistance genes *PigmR*, *Pi9*, and *Piz-t*, and establishes a direct link between transcriptional activation of the immune response and NLR-mediated pathogen perception by directly binding to the A/T-rich cis-element DNA in the target gene (Zhai et al., 2019). This is in contrast to the nuclear localization of the constitutive transcription factor WRKY45. This transcription factor induces resistance through the SA signaling pathway regulated by the ubiquitin-proteasome system. The CNL protein encoded by the rice blast resistance gene *Pb1* interacts with WRKY45 in the nucleus to regulate broad-spectrum resistance to *M. oryzae* (Inoue

et al., 2013). EDS1 regulates the defense signaling pathway. The interactions between *Arabidopsis* NLR RSP4 and EDS1 result in similar but distinct nuclear NLR-dependent translocations. The RPS4 and EDS1 complex is predominantly located in the cytoplasm, but can also be observed in the nucleus during homeostasis or upon AvrRPS4 infection. Additionally, RPS4 binds to EDS1 in the cytoplasm without relying on another NLR RRS1. Instead, when RRS1 is present, an RPS4-EDS1 complex is observed in the nucleus. This suggests the existence of pre- and post-activation states for the nuclear localization of RPS4, RRS1 and EDS1 complexes. The RPS4-EDS1 binding in the nucleus may be unaffected by HP effectors such as AvrRps4 in the presence of RRS1 (Wang R. Y. et al., 2016). It has also been shown that the effector Avrpiz-t from *M. oryzae* interacts with the bzip-type transcription factor APIP5 in the cytoplasm, inhibiting its transcriptional activity and protein accumulation during the necrotic stage. Additionally, the rice NLR Piz-t inhibits plant ETI necrosis by interacting with APIP5 (Wang R. Y. et al., 2016). These showing how the host utilizes transcription factors as imitation substances for effectors to prevent host immune responses induced by various HPs.

4.3. Paired NLRs sense HPs to confer plant immunity

Many NLRs paired with additional domains or motifs are also critical for plant protection against HPs compared to regular NLRs. The paired NLR contains one NLR with an ID at its C-terminus that mimics the virulence target of an effector protein, and thus acts as a sensor for detecting effector proteins. Another NLR acts as a classical executive NLR that performs signal transduction functions (Grund et al., 2019). Some NLR gene pairs are frequently close in the same locus on the chromosome. These pairs share a promoter. The two genes that encode RPS4 and RRS1 are located adjacent to each other and are arranged in opposite directions. This suggests they may co-regulate transcription, with an interval of approximately 300 bp between them (Narusaka et al., 2009). RRS1 has an extra structural domain called WRKY at the C-terminus. RPS4 and RRSI together form a heterodimeric complex that recognizes the effector AvrRps4 and confers resistance to *P. syringae* (Guo et al., 2020). In rice, the C-terminus of the NLR-paired RGA5 contains an HMA structural domain that acts as an ID that interacts with the effectors AVR1-CO39 and AVR-Pia in *M. oryzae*. The NLR-paired RGA4 acts as an NLR executor that induces robust HR in tobacco leaves (Cesari et al., 2013; De la Concepcion et al., 2021). The co-expression of Pikp-1, Pikp-2, and *M. oryzae* effector AVR-PikD, where Pikp-1 possesses an HMA, and Pikp-2 conducts signal transduction, induces a significant HR in tobacco (Maqbool et al., 2015; Cesari et al., 2022). Guardees or decoys allows plants to detect a wide range of pathogen effectors with a relatively small repertoire of NLRs (Frailie and Innes, 2021; Liu et al., 2021). In the RPS4/RRS1 and RGA4/RGA5 heterodimers, one NLR is involved in effector identification while the other is involved in defense signaling. Understanding the extent of heterodimerization in plant NLRs is crucial in gaining insights into plant NLR evolution and diversity. Moreover, pairing NLR sensors and actuators in plant design could improve effector recognition specificity and resistance profiles.

5. Conclusion and perspective

Plant diseases caused by phytopathogens are a major threat to global food security and can lead to significant economic losses, such as HPs. Notably, *M. oryzae*, *Colletotrichum* spp., and *P. syringae* are considered important HPs due to their ease of cultivation, genetic modification, and typical hemibiotrophic characteristics (Doehlemann et al., 2017). Therefore, they are commonly utilized as models for studying plant immunity activation by HPs. Several other species from broad genera are also classified as HPs, including significant plant pathogens like *Fusarium* (Ma et al., 2013), *Verticillium* (Fradin and Thomma, 2006), *Mycosphaerella* (Churchill, 2011), and others. All of these species have an asymptomatic stage of varying lengths. In most cases, they do not develop into typical biotrophic specialized organs and do not make close contact with the host cells. Therefore, the pathogenic lifestyle of HPs comprises asymptomatic, quiescent, latent or endogenous stages and requires different forms of control. To effectively manage plant diseases caused by HPs, it is essential to understand the interaction between HPs and host plants, as well as their strategies for activating plant immunity. Currently, genetic control of plant diseases aims to improve plant resistance. This is achieved through techniques like genome editing, which targets specific genes, and resistance gene enrichment sequencing. Plant disease resistance is mostly determined by genes that have receptors detect when pathogens enter the plant and trigger immune responses. In this review, we discuss plant cell surface PRR and intracellular NLR immunoreceptors that detect various HP and initiate appropriate immune responses. Furthermore, we discuss effector target proteins, including transcription factors, ubiquitin ligases, and molecular chaperones. These proteins could potentially function as models of "guards" and "decoys" for the indirect molecular immunity against HP in the ongoing arms race between plants and pathogens. Over time, a complex recognition system has developed between the immune receptors and HP. By summarizing the interaction between HPs and plant immune receptors that trigger host immune responses, it was found that PAMPs may be conserved and prevalent in various microorganisms, and the cell-surface PRR complexes have similar co-receptors, including BAK1, SOBIR1, or CERK1. By combining genomics, transcriptomics, effectomics, and high-throughput phenotypic analysis, it is anticipated that that crops will achieve better and sustainable protection against various diseases through the utilization of stacked plant immune receptors. For example, multiple plant immune receptors may be designed to recognize the same type of pathogen, or they may be designed for different types of pathogens, such as oomycetes and fungi. We may discover novel defense mechanisms and corresponding pathogen factors. This results in improved disease management and control.

However, it is unclear how these simple conceptual models allow PRRs and NLRs to adapt to the virtually unlimited of immune signaling space. Moreover, the *Agrobacterium* transient assay is useful for enhancing analysis of plant receptor function in solanaceous hosts. However, it might not work well for studying receptor function in soybean or other monocotyledonous plants. This difficulty has also been a major constraint in finding different pathogen effector proteins. Plant PTI and ETI signaling systems may appear simple, but they are rather complex. One immune receptor like EDSI could regulate a single target protein of the host and may be targeted by multiple effectors like RIN4 (Sun Y. L. et al., 2020). Each signal directly or indirectly coordinates with each other to jointly regulate plant

immunity, growth and development. Elimination of host susceptibility to HPs through gene editing techniques poses potential risks. New susceptibility genes may be introduced while the desired traits are being engineered for transfer to other species. A recent study of cell trajectory analysis of based on single-cell omics technology found that, at the early stages of immune cell trajectory, the progression of disease from the immune state to the susceptible state is a continuous process (Zhu et al., 2023). In the future, advancements in spatial omics with high resolution, next-generation sequencing technology, and new bioinformatics algorithms and pipelines will provide new genome-wide data for HPs. This will enable researchers to gain greater insight into intricate plant immune responses and their dynamic interactions with pathogens in specific spatial contexts. However, with so many candidate effector genes or genomes, it is unclear how HP effectors shift from biotrophy to necrotrophy, manipulate host targets, and interfere with plant immune activation.

Author contributions

DZ, GZ, and JL contributed to the conception of the manuscript. DZ wrote the original draft. XZC, XGC, and YX provided editing assistance. All authors contributed to the article and approved the submitted version.

Funding

This research was supported by grants from the National Natural Science Foundation of China (32271900), the National Natural Science Foundation of China (31971661), the Hunan Provincial Innovation Foundation for Postgraduate (CX20230748), and the Scientific Innovation Fund for Postgraduates of Central South University of Forestry and Technology (2023CX01002).

Conflict of interest

The authors declare that the research was conducted in the absence of any commercial or financial relationships that could be construed as a potential conflict of interest.

Publisher's note

References

Ade, J., DeYoung, B. J., Golstein, C., and Innes, R. W. (2007). Indirect activation of a plant nucleotide binding site-leucine-rich repeat protein by a bacterial protease. *Proc. Natl. Acad. Sci. U. S. A.* 104, 2531–2536. doi: 10.1073/pnas.0608779104

Albert, I., Bohm, H., Albert, M., Feiler, C. E., Imkampe, J., Wallmeroth, N., et al. (2015). An RLP23-SOBIR1-BAK1 complex mediates NLP-triggered immunity. *Nat Plants* 1:15140. doi: 10.1038/nplants.2015.140

Balague, C., Gouget, A., Bouchez, O., Souriac, C., Haget, N., Boutet-Mercey, S., et al. (2017). The *Arabidopsis thaliana* lectin receptor kinase LecRK-I.9 is required for full resistance to Pseudomonas syringae and affects jasmonate signalling. *Mol. Plant Pathol.* 18, 937–948. doi: 10.1111/mpp.12457

Bao, Y., Li, Y., Chang, Q., Chen, R., Wang, W., Zhang, Q., et al. (2023). A pair of G-type lectin receptor-like kinases modulates nlp20-mediated immune responses by coupling to the RLP23 receptor complex. *J. Integr. Plant Biol.* 65, 1312–1327. doi: 10.1111/jipb.13449

Barragan, A. C., and Weigel, D. (2021). Plant NLR diversity: the known unknowns of pan-NLRomes. *Plant Cell* 33, 814–831. doi: 10.1093/plcell/koaa002

Bastedo, D. P., Khan, M., Martel, A., Seto, D., Kireeva, I., Zhang, J. F., et al. (2019). Perturbations of the ZED1 pseudokinase activate plant immunity. *PLoS Pathog.* 15:e1007900. doi: 10.1371/journal.ppat.1007900

Beck, M., Zhou, J., Faulkner, C., MacLean, D., Robatzek, S., and Zhou, J. (2012). Spatio-temporal cellular dynamics of the *Arabidopsis* flagellin receptor reveal activation status-dependent endosomal sorting. *Plant Cell* 24, 4205–4219. doi: 10.1105/tpc.112.100263

Bot, P., Mun, B. G., Imran, Q. M., Hussain, A., Lee, S. U., Loake, G., et al. (2019). Differential expression of AtWAKL10 in response to nitric oxide suggests a putative role in biotic and abiotic stress responses. *PeerJ* 7:e7383. doi: 10.7717/peerj.7383

Buendia, L., Girardin, A., Wang, T. M., Cottret, L., and Lefebvre, B. (2018). LysM receptor-like kinase and LysM receptor-like protein families: an update on phylogeny and functional characterization. *Front. Plant Sci.* 9:1531. doi: 10.3389/fpls.2018.01531

Cao, Y. R., Liang, Y., Tanaka, K., Nguyen, C. T., Jedrzejczak, R. P., Joachimiak, A., et al. (2014). The kinase LYK5 is a major chitin receptor in *Arabidopsis* and forms a chitin-induced complex with related kinase CERK1. *Elife* 3:e03766. doi: 10.7554/eLife.03766

Cesari, S., Thilliez, G., Ribot, C., Chalvon, V., Michel, C., Jauneau, A., et al. (2013). The Rice resistance protein pair RGA4/RGA5 recognizes the *Magnaporthe oryzae* effectors AVR-pia and AVR1-CO39 by direct binding. *Plant Cell* 25, 1463–1481. doi: 10.1105/tpc.112.107201

Cesari, S., Xi, Y. X., Declerck, N., Chalvon, V., Mammri, L., Pugniere, M., et al. (2022). New recognition specificity in a plant immune receptor by molecular engineering of its integrated domain. *Nat. Commun.* 13:1524. doi: 10.1038/s41467-022-29196-6

Chen, J. B., Bao, S. W., Fang, Y. L., Wei, L. Y., Zhu, W. S., Peng, Y. L., et al. (2021). An LRR-only protein promotes NLP-triggered cell death and disease susceptibility by facilitating oligomerization of NLP in *Arabidopsis*. *New Phytol.* 232, 1808–1822. doi: 10.1111/nph.17680

Chen, D., Cao, Y., Li, H., Kim, D., Ahsan, N., Thelen, J., et al. (2017). Extracellular ATP elicits DORN1-mediated RBOHD phosphorylation to regulate stomatal aperture. *Nat. Commun.* 8:2265. doi: 10.1038/s41467-017-02340-3

Chen, Q., Dong, C., Sun, X., Zhang, Y., Dai, H., and Bai, S. (2020). Overexpression of an apple LysM-containing protein gene, MdCERK1-2, confers improved resistance to the pathogenic fungus, *Alternaria alternata*, in Nicotiana benthamiana. *BMC Plant Biol.* 20:146. doi: 10.1186/s12870-020-02361-z

Chen, Y., Liu, Z. Y., and Halterman, D. A. (2012). Molecular determinants of resistance activation and suppression by *Phytophthora infestans* effector IPI-O. *PLoS Pathog.* 8:e1002595. doi: 10.1371/journal.ppat.1002595

Cheng, X. Y., Wu, Y., Guo, J. P., Du, B., Chen, R. Z., Zhu, L. L., et al. (2013). A rice lectin receptor-like kinase that is involved in innate immune responses also contributes to seed germination. *Plant J.* 76, 687–698. doi: 10.1111/tpj.12328

Churchill, A. C. (2011). Mycosphaerella fijiensis, the black leaf streak pathogen of banana: progress towards understanding pathogen biology and detection, disease development, and the challenges of control. *Mol. Plant Pathol.* 12, 307–328. doi: 10.1111/j.1364-3703.2010.00672.x

Couto, D., and Zipfel, C. (2016). Regulation of pattern recognition receptor signalling in plants. *Nat. Rev. Immunol.* 16, 537–552. doi: 10.1038/nri.2016.77

Damm, U., O'Connell, R. J., Groenewald, J. Z., and Crous, P. W. (2014). The Colletotrichum destructivum species complex—hemibiotrophic pathogens of forage and field crops. *Stud. Mycol.* 79, 49–84. doi: 10.1016/j.simyco.2014.09.003

Dangl, J. L. (2013). Pivoting the plant immune system from dissection to deployment (vol 341, pg 746, 2013). *Science* 341:1175. doi: 10.1126/science.123601

Day, B., Dahlbeck, D., Huang, J., Chisholm, S. T., Li, D., and Staskawicz, B. J. (2005). Molecular basis for the RIN4 negative regulation of RPS2 disease resistance. *Plant Cell* 17, 1292–1305. doi: 10.1105/tpc.104.030163

De Coninck, T., and Van Damme, E. J. M. (2022). Plant lectins: Handymen at the cell surface. *Cell Surf.* 8:100091. doi: 10.1016/j.tcsw.2022.100091

De la Concepcion, J. C., Franceschetti, M., Maqbool, A., Saitoh, H., Terauchi, R., Kamoun, S., et al. (2018). Polymorphic residues in rice NLRs expand binding and response to effectors of the blast pathogen (vol 4, pg 576, 2018). *Nat. Plants* 4:734. doi: 10.1038/s41477-018-0248-0

De la Concepcion, J. C., Maidment, J. H. R., Longya, A., Xiao, G., Franceschetti, M., and Banfield, M. J. (2021). The allelic rice immune receptor Pikh confers extended resistance to strains of the blast fungus through a single polymorphism in the effector binding interface. *PLoS Pathog.* 17:e1009368. doi: 10.1371/journal.ppat.1009368

Delteil, A., Gobbato, E., Cayrol, B., Estevan, J., Michel-Romiti, C., Dievart, A., et al. (2016). Several wall-associated kinases participate positively and negatively in basal defense against rice blast fungus. *BMC Plant Biol.* 16:17. doi: 10.1186/s12870-016-0711-x

Desaki, Y., Miyata, K., Suzuki, M., Shibuya, N., and Kaku, H. (2018). Plant immunity and symbiosis signaling mediated by LysM receptors. *Innate Immun.* 24, 92–100. doi: 10.1177/1753425917738885

Doehlemann, G., Okmen, B., Zhu, W., and Sharon, A. (2017). Plant pathogenic fungi. *Microbiol. Spectr.* 5. doi: 10.1128/microbiolspec.FUNK-0023-2016

Duxbury, Z., Wu, C. H., and Ding, P. (2021). A comparative overview of the intracellular guardians of plants and animals: NLRs in innate immunity and beyond. *Annu. Rev. Plant Biol.* 72, 155–184. doi: 10.1146/annurev-arplant-080620-104948

El Kasmi, F., Chung, E. H., Anderson, R. G., Li, J., Wan, L., Eitas, T. K., et al. (2017). Signaling from the plasma-membrane localized plant immune receptor RPM1 requires self-association of the full-length protein. *Proc. Natl. Acad. Sci. U. S. A.* 114, E7385–E7394. doi: 10.1073/pnas.1708288114

Erwig, J., Ghareeb, H., Kopischke, M., Hacke, R., Matei, A., Petutschnig, E., et al. (2017). Chitin-induced and CHITIN ELICITOR RECEPTOR KINASE1 (CERK1) phosphorylation-dependent endocytosis of *Arabidopsis thaliana* LYSIN MOTIF-CONTAINING RECEPTOR-LIKE KINASE5 (LYK5). *New Phytol.* 215, 382–396. doi: 10.1111/nph.14592

Eschen-Lippold, L., Jiang, X., Elmore, J. M., Mackey, D., Shan, L., Coaker, G., et al. (2016). Bacterial AvrRpt2-like cysteine proteases block activation of the *Arabidopsis* mitogen-activated protein kinases, MPK4 and MPK11. *Plant Physiol.* 171, 2223–2238. doi: 10.1104/pp.16.00336

Fisher, M. C., Hawkins, N. J., Sanglard, D., and Gurr, S. J. (2018). Worldwide emergence of resistance to antifungal drugs challenges human health and food security. *Science* 360, 739–742. doi: 10.1126/science.aap7999

Fliegmann, J., Uhlenbroich, S., Shinya, T., Martinez, Y., Lefebvre, B., Shibuya, N., et al. (2011). Biochemical and phylogenetic analysis of CEBiP-like LysM domain-containing extracellular proteins in higher plants. *Plant Physiol. Biochem.* 49, 709–720. doi: 10.1016/j.plaphy.2011.04.004

Fradin, E. F., and Thomma, B. P. (2006). Physiology and molecular aspects of Verticillium wilt diseases caused by V. dahliae and V. albo-atrum. *Mol. Plant Pathol.* 7, 71–86. doi: 10.1111/j.1364-3703.2006.00323.x

Frailie, T. B., and Innes, R. W. (2021). Engineering healthy crops: molecular strategies for enhancing the plant immune system. *Curr. Opin. Biotechnol.* 70, 151–157. doi: 10.1016/j.copbio.2021.04.006

Giovannoni, M. A.-O., Lironi, D., Marti, L., Paparella, C., Vecchi, V., Gust, A. A.-O., et al. (2021). The *Arabidopsis thaliana* LysM-containing receptor-like kinase 2 is required for elicitor-induced resistance to pathogens. *Plant Cell Environ.* 44, 3545–3562. doi: 10.1111/pce.14192

Gou, M. Y., Shi, Z. Y., Zhu, Y., Bao, Z. L., Wang, G. Y., and Hua, J. (2012). The F-box protein CPR1/CPR30 negatively regulates R protein SNC1 accumulation. *Plant J.* 69, 411–420. doi: 10.1111/j.1365-313X.2011.04799.x

Gravino, M., Locci, F., Tundo, S., Cervone, F., Savatin, D. V., and De Lorenzo, G. (2017). Immune responses induced by oligogalacturonides are differentially affected by AvrPto and loss of BAK1/BKK1 and PEPR1/PEPR2. *Mol. Plant Pathol.* 18, 582–595. doi: 10.1111/mpp.12419

Grund, E., Tremousaygue, D., and Deslandes, L. (2019). Plant NLRs with integrated domains: Unity makes strength. *Plant Physiol.* 179, 1227–1235. doi: 10.1104/pp.18.01134

Guo, H., Ahn, H. K., Sklenar, J., Huang, J., Ma, Y., Ding, P., et al. (2020). Phosphorylation-regulated activation of the *Arabidopsis* RRS1-R/RPS4 immune receptor complex reveals two distinct effector recognition mechanisms. *Cell Host Microbe* 27, 769–781 e766. doi: 10.1016/j.chom.2020.03.008

Gust, A. A., and Felix, G. (2014). Receptor like proteins associate with SOBIR1-type of adaptors to form bimolecular receptor kinases. *Curr. Opin. Plant Biol.* 21, 104–111. doi: 10.1016/j.pbi.2014.07.007

Harkenrider, M., Sharma, R., De Vleesschauwer, D., Tsao, L., Zhang, X. T., Chern, M., et al. (2016). Overexpression of rice wall-associated kinase 25 (OsWAK25) alters resistance to bacterial and fungal pathogens. *PLoS One* 11:e0147310. doi: 10.1371/journal.pone.0147310

Hayafune, M., Berisio, R., Marchetti, R., Silipo, A., Kayama, M., Desaki, Y., et al. (2014). Chitin-induced activation of immune signaling by the rice receptor CEBiP relies on a unique sandwich-type dimerization. *Proc. Natl. Acad. Sci. U. S. A.* 111, E404–E413. doi: 10.1073/pnas.1312099111

Hu, S. P., Li, J. J., Dhar, N., Li, J. P., Chen, J. Y., Jian, W., et al. (2021). Lysin motif (LysM) proteins: interlinking manipulation of plant immunity and fungi. *Int. J. Mol. Sci.* 22:3114. doi: 10.3390/ijms22063114

Hu, M. J., Qi, J. F., Bi, G. Z., and Zhou, J. M. (2020). Bacterial effectors induce oligomerization of immune receptor ZAR1 in vivo. *Mol. Plant* 13, 793–801. doi: 10.1016/j.molp.2020.03.004

Huang, Y., Minaker, S., Roth, C., Huang, S., Hieter, P., Lipka, V., et al. (2014). An E4 ligase facilitates Polyubiquitination of plant immune receptor resistance proteins in *Arabidopsis*. *Plant Cell* 26, 485–496. doi: 10.1105/tpc.113.119057

Huang, S., Monaghan, J., Zhong, X., Lin, L., Sun, T., Dong, O. X., et al. (2014). HSP90s are required for NLR immune receptor accumulation in *Arabidopsis*. *Plant J.* 79, 427–439. doi: 10.1111/tpj.12573

Huang, J., Wu, X., and Gao, Z. (2021). A nucleocytoplasmic-localized E3 ligase affects the NLR receptor stability. *Biochem. Biophys. Res. Commun.* 583, 1–6. doi: 10.1016/j.bbrc.2021.10.052

Hubert, D. A., Tornero, P., Belkhadir, Y., Krishna, P., Takahashi, A., Shirasu, K., et al. (2003). Cytosolic HSP90 associates with and modulates the *Arabidopsis* RPM1 disease resistance protein. *EMBO J.* 22, 5679–5689. doi: 10.1093/emboj/cdg547

Inoue, H., Hayashi, N., Matsushita, A., Liu, X. Q., Nakayama, A., Sugano, S., et al. (2013). Blast resistance of CC-NB-LRR protein Pb1 is mediated by WRKY45 through protein-protein interaction. *Proc. Natl. Acad. Sci. U. S. A.* 110, 9577–9582. doi: 10.1073/pnas.1222155110

Jia, Y., McAdams, S. A., Bryan, G. T., Hershey, H. P., and Valent, B. (2000). Direct interaction of resistance gene and avirulence gene products confers rice blast resistance. *EMBO J.* 19, 4004–4014. doi: 10.1093/emboj/19.15.4004

Jones, J. D. G., Vance, R. E., and Dangl, J. L. (2016). Intracellular innate immune surveillance devices in plants and animals. *Science* 354:aaf6395. doi: 10.1126/science.aaf6395

Jubic, L. M., Saile, S., Furzer, O. J., El Kasmi, F., and Dangl, J. L. (2019). Help wanted: helper NLRs and plant immune responses. *Curr. Opin. Plant Biol.* 50, 82–94. doi: 10.1016/j.pbi.2019.03.013

Kapos, P., Devendrakumar, K. T., and Li, X. (2019). Plant NLRs: from discovery to application. *Plant Sci.* 279, 3–18. doi: 10.1016/j.plantsci.2018.03.010

Kelley, B. S., Lee, S. J., Damasceno, C. M. B., Chakravarthy, S., Kim, B. D., Martin, G. B., et al. (2010). A secreted effector protein (SNE1) from *Phytophthora infestans* is a broadly acting suppressor of programmed cell death. *Plant J.* 62, 357–366. doi: 10.1111/j.1365-313X.2010.04160.x

Kleemann, J., Rincon-Rivera, L. J., Takahara, H., Neumann, U., van Themaat, E. V. L., van der Does, H. C., et al. (2012). Sequential delivery of host-induced virulence effectors by Appressoria and intracellular hyphae of the Phytopathogen *Colletotrichum higginsianum*. *PLoS Pathog.* 8:e1002643. doi: 10.1371/journal.ppat.1002643

Kourelis, J., and van der Hoorn, R. A. L. (2018). Defended to the nines: 25 years of resistance gene cloning identifies nine mechanisms for R protein function. *Plant Cell* 30, 285–299. doi: 10.1105/tpc.17.00579

Kraepiel, Y., and Barny, M. A. (2016). Gram-negative phytopathogenic bacteria, all hemibiotrophs after all? *Mol. Plant Pathol.* 17, 313–316. doi: 10.1111/mpp.12345

Kroj, T., Chanclud, E., Michel-Romiti, C., Grand, X., and Morel, J. B. (2016). Integration of decoy domains derived from protein targets of pathogen effectors into plant immune receptors is widespread. *New Phytol.* 210, 618–626. doi: 10.1111/nph.13869

Lee, D. H., Lee, H. S., and Belkhadir, Y. (2021). Coding of plant immune signals by surface receptors. *Curr. Opin. Plant Biol.* 62:102044. doi: 10.1016/j.pbi.2021.102044

Lei, L., Stevens, D. M., and Coaker, G. (2020). Phosphorylation of the Pseudomonas effector AvrPtoB by *Arabidopsis* SnRK2.8 is required for bacterial virulence. *Mol. Plant* 13, 1513–1522. doi: 10.1016/j.molp.2020.08.018

Li, L., Kim, P., Yu, L., Cai, G., Chen, S., Alfano, J. R., et al. (2016). Activation-dependent destruction of a co-receptor by a *Pseudomonas syringae* effector dampens plant immunity. *Cell Host Microbe* 20, 504–514. doi: 10.1016/j.chom.2016.09.007

Li, Y., Liu, X., Liu, M., Wang, Y., Zou, Y., You, Y., et al. (2020). *Magnaporthe oryzae* auxiliary activity protein MoAa91 functions as chitin-binding protein to induce Appressorium formation on artificial inductive surfaces and suppress plant immunity. *mBio* 11, e03304–19. doi: 10.1128/mbio.03304-03319

Li, J. B., Sun, Y. D., Liu, H., Wang, Y. Y., Jia, Y. L., and Xu, M. H. (2015). Natural variation of rice blast resistance gene pi-d2. *Genet. Mol. Res.* 14, 1235–1249. doi: 10.4238/2015.February.13.2

Li, H., Zhou, S. Y., Zhao, W. S., Su, S. C., and Peng, Y. L. (2009). A novel wall-associated receptor-like protein kinase gene, OsWAK1, plays important roles in rice blast disease resistance. *Plant Mol. Biol.* 69, 337–346. doi: 10.1007/s11103-008-9430-5

Liebrand, T. W. H., van den Burg, H. A., and Joosten, M. H. A. J. (2014). Two for all: receptor-associated kinases SOBIR1 and BAK1. *Trends Plant Sci.* 19, 123–132. doi: 10.1016/j.tplants.2013.10.003

Liu, X. R., Ao, K., Yao, J., Zhang, Y. L., and Li, X. (2021). Engineering plant disease resistance against biotrophic pathogens. *Curr. Opin. Plant Biol.* 60:101987. doi: 10.1016/j.pbi.2020.101987

Liu, C., Cui, D. Y., Zhao, J. B., Liu, N., Wang, B., Liu, J., et al. (2019). Two *Arabidopsis* receptor-like cytoplasmic kinases SZE1 and SZE2 associate with the ZAR1-ZED1 complex and are required for effector-triggered immunity. *Mol. Plant* 12, 967–983. doi: 10.1016/j.molp.2019.03.012

Lopez, V. A., Park, B. C., Nowak, D., Sreelatha, A., Zembek, P., Fernandez, J., et al. (2019). A bacterial effector mimics a host HSP90 client to undermine immunity. *Cells* 179:205. doi: 10.1016/j.cell.2019.08.020

Luo, X., Wu, W., Liang, Y., Xu, N., Wang, Z., Zou, H., et al. (2020). Tyrosine phosphorylation of the lectin receptor-like kinase LORE regulates plant immunity. *EMBO J.* 39:e102856. doi: 10.15252/embj.2019102856

Luo, X. M., Xu, N., Huang, J. K., Gao, F., Zou, H. S., Boudsocq, M., et al. (2017). A lectin receptor-like kinase mediates pattern-triggered salicylic acid signaling. *Plant Physiol.* 174, 2501–2514. doi: 10.1104/pp.17.00404

Ma, L. J., Geiser, D. M., Proctor, R. H., Rooney, A. P., O'Donnell, K., Trail, F., et al. (2013). Fusarium pathogenomics. *Annu. Rev. Microbiol.* 67, 399–416. doi: 10.1146/annurev-micro-092412-155650

Ma, L., Haile, Z. M., Sabbadini, S., Mezzetti, B., Negrini, F., and Baraldi, E. (2023). Functional characterization of MANNOSE-BINDING LECTIN 1, a G-type lectin gene family member, in response to fungal pathogens of strawberry. *J. Exp. Bot.* 74, 149–161. doi: 10.1093/jxb/erac396

Ma, S., Lapin, D., Liu, L., Sun, Y., Song, W., Zhang, X., et al. (2020). Direct pathogen-induced assembly of an NLR immune receptor complex to form a holoenzyme. *Science* 370:eabe3069. doi: 10.1126/science.abe3069

Macho, A. P., and Zipfel, C. (2014). Plant PRRs and the activation of innate immune signaling. *Mol. Cell* 54, 263–272. doi: 10.1016/j.molcel.2014.03.028

Mamode Cassim, A., Gouguet, P., Gronnier, J., Laurent, N., Germain, V., Grison, M., et al. (2018). Plant lipids: key players of plasma membrane organization and function. *Prog. Lipid Res.* 73, 1–27. doi: 10.1016/j.plipres.2018.11.002

Maqbool, A., Saitoh, H., Franceschetti, M., Stevenson, C. E. M., Uemura, A., Kanzaki, H., et al. (2015). Structural basis of pathogen recognition by an integrated HMA domain in a plant NLR immune receptor. *Elife* 4:e08709. doi: 10.7554/eLife.08709

Maruta, N., Burdett, H., Lim, B. Y. J., Hu, X., Desa, S., Manik, M. K., et al. (2022). Structural basis of NLR activation and innate immune signalling in plants. *Immunogenetics* 74, 5–26. doi: 10.1007/s00251-021-01242-5

Mbengue, M., Bourdais, G., Gervasi, F., Beck, M., Zhou, J., Spallek, T., et al. (2016). Clathrin-dependent endocytosis is required for immunity mediated by pattern recognition receptor kinases. *Proc. Natl. Acad. Sci. U. S. A.* 113, 11034–11039. doi: 10.1073/pnas.1606004113

McCombe, C. L., Greenwood, J. R., Solomon, P. S., and Williams, S. J. (2022). Molecular plant immunity against biotrophic, hemibiotrophic, and necrotrophic fungi. *Essays Biochem.* 66, 581–593. doi: 10.1042/Ebc20210073

Mogga, V., Delventhal, R., Weidenbach, D., Langer, S., Bertram, P. M., Andresen, K., et al. (2016). Magnaporthe oryzae effectors MoHEG13 and MoHEG16 interfere with host infection and MoHEG13 counteracts cell death caused by *Magnaporthe*-NLPs in tobacco (vol 35, pg 1169, 2016). *Plant Cell Rep.* 35:1187. doi: 10.1007/s00299-016-1968-0

Monteiro, F., and Nishimura, M. T. (2018). Structural, functional, and genomic diversity of plant NLR proteins: An evolved resource for rational engineering of plant immunity. *Annu. Rev. Phytopathol.* 56, 243–267. doi: 10.1146/annurev-phyto-080417-045817

Narusaka, M., Shirasu, K., Noutoshi, Y., Kubo, Y., Shiraishi, T., Iwabuchi, M., et al. (2009). RRS1 and RPS4 provide a dual resistance-gene system against fungal and bacterial pathogens. *Plant J.* 60, 218–226. doi: 10.1111/j.1365-313X.2009.03949.x

Ngou, B. P. M., Ahn, H. K., Ding, P. T., and Jones, J. D. G. (2021). Mutual potentiation of plant immunity by cell-surface and intracellular receptors. *Nature* 592:110. doi: 10.1038/s41586-021-03315-7

Ngou, B. P. M., Ding, P. T., and Jones, J. D. G. (2022). Thirty years of resistance: zig-Zag through the plant immune system. *Plant Cell* 34, 1447–1478. doi: 10.1093/plcell/koac041

Panthapulakkal Narayanan, S., Lung, S. C., Liao, P., Lo, C., and Chye, M. L. (2020). The overexpression of OsACBP5 protects transgenic rice against necrotrophic, hemibiotrophic and biotrophic pathogens. *Sci. Rep.* 10:14918. doi: 10.1038/s41598-020-71851-9

Pirc, K., Hodnik, V., Snoj, T., Caserman, S., Podobnik, M., Bohm, H., et al. (2021). Nep1-like proteins as a target for plant pathogen control. *PLoS Pathog.* 17:e1009477. doi: 10.1371/journal.ppat.1009477

Qiu, J. H., Xie, J. H., Chen, Y., Shen, Z. N., Shi, H. B., Naqvi, N. I., et al. (2022). Warm temperature compromises JA-regulated basal resistance to enhance *Magnaporthe oryzae* infection in rice. *Mol. Plant* 15, 723–739. doi: 10.1016/j.molp.2022.02.014

Rajarammohan, S. (2021). Redefining plant-Necrotroph interactions: the thin line between Hemibiotrophs and Necrotrophs. *Front. Microbiol.* 12:673518. doi: 10.3389/fmicb.2021.673518

Sanchez-Vallet, A., Saleem-Batcha, R., Kombrink, A., Hansen, G., Valkenburg, D. J., Thomma, B. P. H. J., et al. (2013). Fungal effector Ecp6 outcompetes host immune receptor for chitin binding through intrachain LysM dimerization. *Elife* 2:e00790. doi: 10.7554/eLife.00790

Sanchez-Vallet, A., Tian, H., Rodriguez-Moreno, L., Valkenburg, D. J., Saleem-Batcha, R., Wawra, S., et al. (2020). A secreted LysM effector protects fungal hyphae through chitin-dependent homodimer polymerization. *PLoS Pathog.* 16:e1008652. doi: 10.1371/journal.ppat.1008652

Sarris, P. F., Cevik, V., Dagdas, G., Jones, J. D. G., and Krasileva, K. V. (2016). Comparative analysis of plant immune receptor architectures uncovers host proteins likely targeted by pathogens. *BMC Biol.* 14:8. doi: 10.1186/s12915-016-0228-7

Schellenberger, R., Touchard, M., Clement, C., Baillieul, F., Cordelier, S., Crouzet, J., et al. (2019). Apoplastic invasion patterns triggering plant immunity: plasma membrane sensing at the frontline. *Mol. Plant Pathol.* 20, 1602–1616. doi: 10.1111/mpp.12857

Schreiber, K. J., Baudin, M., Hassan, J. A., and Lewis, J. D. (2016). Die another day: molecular mechanisms of effector-triggered immunity elicited by type III secreted effector proteins. *Semin. Cell Dev. Biol.* 56, 124–133. doi: 10.1016/j.semcdb.2016.05.001

Selote, D., and Kachroo, A. (2010). RPG1-B-derived resistance to AvrB-expressing *Pseudomonas syringae* requires RIN4-like proteins in soybean. *Plant Physiol.* 153, 1199–1211. doi: 10.1104/pp.110.158147

Sharpee, W., Oh, Y., Yi, M., Franck, W., Eyre, A., Okagaki, L. H., et al. (2017). Identification and characterization of suppressors of plant cell death (SPD) effectors from *Magnaporthe oryzae*. *Mol. Plant Pathol.* 18, 850–863. doi: 10.1111/mpp.12449

Smakowska-Luzan, E., Mott, G. A., Parys, K., Stegmann, M., Howton, T. C., Layeghifard, M., et al. (2018). An extracellular network of *Arabidopsis* leucine-rich repeat receptor kinases. *Nature* 553, 342–346. doi: 10.1038/nature25184

Stephens, C., Hammond-Kosack, K. E., and Kanyuka, K. (2022). WAKsing plant immunity, waning diseases. *J. Exp. Bot.* 73, 22–37. doi: 10.1093/jxb/erab422

Su, J. A.-O., Zhang, M. A.-O. X., Zhang, L., Sun, T., Liu, Y. A.-O., Lukowitz, W. A.-O., et al. (2017). Regulation of stomatal immunity by interdependent functions of a pathogen-responsive MPK3/MPK6 Cascade and abscisic acid. *Plant Cell* 29, 526–542. doi: 10.1105/tpc.16.00577

Sun, Y. L., Qiao, Z. Z., Muchero, W., and Chen, J. G. (2020). Lectin receptor-like kinases: the sensor and mediator at the plant cell surface. *Front. Plant Sci.* 11:596301. doi: 10.3389/fpls.2020.596301

Sun, Y., Zhu, Y. X., Balint-Kurti, P. J., and Wang, G. F. (2020). Fine-tuning immunity: players and regulators for plant NLRs. *Trends Plant Sci.* 25, 695–713. doi: 10.1016/j.tplants.2020.02.008

Suzuki, M., Shibuya, M., Shimada, H., Motoyama, N., Nakashima, M., Takahashi, S., et al. (2016). Autophosphorylation of specific threonine and tyrosine residues in *Arabidopsis* CERK1 is essential for the activation of chitin-induced immune signaling. *Plant Cell Physiol.* 57, 2312–2322. doi: 10.1093/pcp/pcw150

Takahara, H., Hacquard, S., Kombrink, A., Hughes, H. B., Halder, V., Robin, G. P., et al. (2016). *Colletotrichum higginsianum* extracellular LysM proteins play dual roles in appressorial function and suppression of chitin-triggered plant immunity. *New Phytol.* 211, 1323–1337. doi: 10.1111/nph.13994

Tang, D. Z., Wang, G. X., and Zhou, J. M. (2017). Receptor kinases in plant-pathogen interactions: more than pattern recognition. *Plant Cell* 29, 618–637. doi: 10.1105/tpc.16.00891

Tian, H., Fiorin, G. L., Kombrink, A., Mesters, J. R., and Thomma, B. (2022a). Fungal dual-domain LysM effectors undergo chitin-induced intermolecular, and not intramolecular, dimerization. *Plant Physiol.* 190, 2033–2044. doi: 10.1093/plphys/kiac391

Tian, H., MacKenzie, C. I., and Rodriguez-Moreno, L. (2022b). Three LysM effectors of *Zymoseptoria tritici* collectively disarm chitin-triggered plant immunity (vol 22, pg 683, 2021). *Mol. Plant Pathol.* 23:1830. doi: 10.1111/mpp.13271

Tsuda, K., and Katagiri, F. (2010). Comparing signaling mechanisms engaged in pattern-triggered and effector-triggered immunity. *Curr. Opin. Plant Biol.* 13, 459–465. doi: 10.1016/j.pbi.2010.04.006

Tsuda, K., Mine, A., Bethke, G., Igarashi, D., Botanga, C. J., Tsuda, Y., et al. (2013). Dual regulation of gene expression mediated by extended MAPK activation and salicylic acid contributes to robust innate immunity in *Arabidopsis thaliana*. *PLoS Genet.* 9:e1004015. doi: 10.1371/journal.pgen.1004015

Van de Weyer, A. L., Monteiro, F., Furzer, O. J., Nishimura, M. T., Cevik, V., Witek, K., et al. (2019). A species-wide inventory of NLR genes and alleles in *Arabidopsis thaliana*. *Cells* 178:1260-+. doi: 10.1016/j.cell.2019.07.038

van der Burgh, A. M., Postma, J., Robatzek, S., and Joosten, M. H. A. J. (2019). Kinase activity of SOBIR1 and BAK1 is required for immune signalling. *Mol. Plant Pathol.* 20, 410–422. doi: 10.1111/mpp.12767

van der Hoorn, R. A., and Kamoun, S. (2008). From guard to decoy: a new model for perception of plant pathogen effectors. *Plant Cell* 20, 2009–2017. doi: 10.1105/tpc.108.060194

van Wersch, S., Tian, L., Hoy, R., and Li, X. (2020). Plant NLRs: the whistleblowers of plant immunity. *Plant Commun.* 1:100016. doi: 10.1016/j.xplc.2019.100016

Wan, J. R., Tanaka, K., Zhang, X. C., Son, G. H., Brechenmacher, L., Tran, H. N. N., et al. (2012). LYK4, a Lysin motif receptor-like kinase, is important for chitin signaling and plant innate immunity in *Arabidopsis*. *Plant Physiol.* 160, 396–406. doi: 10.1104/pp.112.201699

Wang, J. Z., and Chai, J. J. (2020). Structural insights into the plant immune receptors PRRs and NLRs(1)([OPEN]). *Plant Physiol.* 182, 1566–1581. doi: 10.1104/pp.19.01252

Wang, Y., Cordewener, J. H. G., America, A. H. P., Shan, W. X., Bouwmeester, K., and Govers, F. (2015). *Arabidopsis* lectin receptor kinases LecRK-IX.1 and LecRK-IX.2 are functional analogs in regulating Phytophthora resistance and plant cell death. *Mol. Plant-Microbe Interact.* 28, 1032–1048. doi: 10.1094/Mpmi-02-15-0025-R

Wang, Z., and Gou, X. P. (2022). The first line of defense: receptor-like protein kinase-mediated stomatal immunity. *Int. J. Mol. Sci.* 23:343. doi: 10.3390/ijms23010343

Wang, R. Y., Ning, Y. S., Shi, X. T., He, F., Zhang, C. Y., Fan, J. B., et al. (2016). Immunity to Rice blast disease by suppression of effector-triggered necrosis. *Curr. Biol.* 26, 2399–2411. doi: 10.1016/j.cub.2016.06.072

Wang, Y., Nsibo, D. L., Juhar, H. M., Govers, F., and Bouwmeester, K. (2016). Ectopic expression of *Arabidopsis* L-type lectin receptor kinase genes LecRK-I.9 and LecRK-IX.1 in Nicotiana benthamiana confers Phytophthora resistance. *Plant Cell Rep.* 35, 845–855. doi: 10.1007/s00299-015-1926-2

Wang, Y., Pruitt, R. N., Nurnberger, T., and Wang, Y. C. (2022). Evasion of plant immunity by microbial pathogens. *Nat. Rev. Microbiol.* 20, 449–464. doi: 10.1038/s41579-022-00710-3

Wang, G. X., Roux, B., Feng, F., Guy, E., Li, L., Li, N. N., et al. (2015). The decoy substrate of a pathogen effector and a Pseudokinase specify pathogen-induced modified-self recognition and immunity in plants. *Cell Host Microbe* 18, 285–295. doi: 10.1016/j.chom.2015.08.004

Wang, L. M., Wilkins, K. A., and Davies, J. M. (2018). Arabidopsis DORN1 extracellular ATP receptor; activation of plasma membrane K+-and Ca2+−permeable conductances. *New Phytol.* 218, 1301–1304. doi: 10.1111/nph.15111

Wei, T., Chern, M., Liu, F., and Ronald, P. C. (2016). Suppression of bacterial infection in rice by treatment with a sulfated peptide. *Mol. Plant Pathol.* 17, 1493–1498. doi: 10.1111/mpp.12368

Wu, Y., Gao, Y., Zhan, Y., Kui, H., Liu, H., Yan, L., et al. (2020). Loss of the common immune coreceptor BAK1 leads to NLR-dependent cell death. *Proc. Natl. Acad. Sci. U. S. A.* 117, 27044–27053. doi: 10.1073/pnas.1915339117

Wu, J., Reca, I. B., Spinelli, F., Lironi, D., De Lorenzo, G., Poltronieri, P., et al. (2019). An EFR-Cf-9 chimera confers enhanced resistance to bacterial pathogens by SOBIR1- and BAK1-dependent recognition of elf18. *Mol. Plant Pathol.* 20, 751–764. doi: 10.1111/mpp.12789

Xue, D. X., Li, C. L., Xie, Z. P., and Staehelin, C. (2019). LYK4 is a component of a tripartite chitin receptor complex in *Arabidopsis thaliana*. *J. Exp. Bot.* 70, 5507–5516. doi: 10.1093/jxb/erz313

Yaeno, T., Li, H., Chaparro-Garcia, A., Schornack, S., Koshiba, S., Watanabe, S., et al. (2011). Phosphatidylinositol monophosphate-binding interface in the oomycete RXLR effector AVR3a is required for its stability in host cells to modulate plant immunity. *Proc. Natl. Acad. Sci. U. S. A.* 108, 14682–14687. doi: 10.1073/pnas.1106002108

Yu, T. Y., Sun, M. K., and Liang, L. K. (2021). Receptors in the induction of the plant innate immunity. *Mol. Plant-Microbe Interact.* 34, 587–601. doi: 10.1094/Mpmi-07-20-0173-Cr

Yuan, M., Jiang, Z., Bi, G., Nomura, K., Liu, M., Wang, Y., et al. (2021a). Pattern-recognition receptors are required for NLR-mediated plant immunity. *Nature* 592, 105–109. doi: 10.1038/s41586-021-03316-6

Yuan, M., Ngou, B. P. M., Ding, P., and Xin, X. F. (2021b). PTI-ETI crosstalk: an integrative view of plant immunity. *Curr. Opin. Plant Biol.* 62:102030. doi: 10.1016/j.pbi.2021.102030

Yue, Z. L., Liu, N., Deng, Z. P., Zhang, Y., Wu, Z. M., Zhao, J. L., et al. (2022). The receptor kinase OsWAK11 monitors cell wall pectin changes to fine-tune brassinosteroid signaling and regulate cell elongation in rice. *Curr. Biol.* 32, 2454–2466.e2457. doi: 10.1016/j.cub.2022.04.028

Zhai, K. R., Deng, Y. W., Liang, D., Tang, J., Liu, J., Yan, B. X., et al. (2019). RRM transcription factors interact with NLRs and regulate broad-Spectrum blast resistance in Rice. *Mol. Cell* 74:996. doi: 10.1016/j.molcel.2019.03.013

Zhang, N., Pombo, M. A., Rosli, H. G., and Martin, G. B. (2020). Tomato Wall-associated kinase SlWak1 depends on Fls2/Fls3 to promote Apoplastic immune responses to *Pseudomonas syringae*. *Plant Physiol.* 183, 1869–1882. doi: 10.1104/pp.20.00144

Zhao, M., Li, N. H., Chen, S. M., Wu, J. J., He, S. F., Zhao, Y. X., et al. (2023). GmWAK1, Novel Wall-associated protein kinase, positively regulates response of soybean to Phytophthora sojae infection. *Int. J. Mol. Sci.* 24:798. doi: 10.3390/ijms24010798

Zhao, L., Liao, Z. W., Feng, L. P., An, B., He, C. Z., Wang, Q. N., et al. (2023). Colletotrichum gloeosporioides Cg2LysM contributed to virulence toward rubber tree through affecting invasive structure and inhibiting chitin-triggered plant immunity. *Front. Microbiol.* 14:1129101. doi: 10.3389/fmicb.2023.1129101

Zhou, J. M., and Zhang, Y. (2020). Plant immunity: danger perception and signaling. *Cells* 181, 978–989. doi: 10.1016/j.cell.2020.04.028

Zhu, J., Lolle, S., Tang, A., Guel, B., Kvitko, B., Cole, B., et al. (2023). Single-cell profiling of Arabidopsis leaves to Pseudomonas syringae infection. *Cell Rep.* 42:112676. doi: 10.1016/j.celrep.2023.112676

frontiers | Frontiers in Microbiology

TYPE Original Research
PUBLISHED 16 November 2023
DOI 10.3389/fmicb.2023.1286740

OPEN ACCESS

EDITED BY
Jian-Wei Guo,
Kunming University, China

REVIEWED BY
Manik Prabhu Narsing Rao,
Sun Yat-sen University, China
Eduardo Valencia-Cantero,
Michoacana University of San Nicolás de Hidalgo, Mexico

*CORRESPONDENCE
Qiao Guo
✉ shuiyiwei83@163.com

RECEIVED 31 August 2023
ACCEPTED 24 October 2023
PUBLISHED 16 November 2023

CITATION
Zhang M, Kong Z, Fu H, Shu X, Xue Q, Lai H and Guo Q (2023) Rhizosphere microbial ecological characteristics of strawberry root rot. *Front. Microbiol.* 14:1286740. doi: 10.3389/fmicb.2023.1286740

Rhizosphere microbial ecological characteristics of strawberry root rot

Meilin Zhang, Zirong Kong, Huijing Fu, Xiaolong Shu, Quanhong Xue, Hangxian Lai and Qiao Guo*

College of Natural Resources and Environment, Northwest A&F University, Yangling, China

Introduction: Strawberry (*Fragaria* × ananassa Duch.) holds a preeminent position among small fruits globally due to its delectable fruits and significant economic value. However, strawberry cultivation is hampered by various plant diseases, hindering the sustainable development of the strawberry industry. The occurrence of plant diseases is closely linked to imbalance in rhizosphere microbial community structure.

Methods: In the present study, a systematic analysis of the differences and correlations among non-culturable microorganisms, cultivable microbial communities, and soil nutrients in rhizosphere soil, root surface soil, and non-rhizosphere soil of healthy and diseased strawberry plants affected by root rot was conducted. The goal was to explore the relationship between strawberry root rot occurrence and rhizosphere microbial community structure.

Results: According to the results, strawberry root rot altered microbial community diversity, influenced fungal community composition in strawberry roots, reduced microbial interaction network stability, and enriched more endophytic-phytopathogenic bacteria and saprophytic bacteria. In addition, the number of bacteria isolated from the root surface soil of diseased plants was significantly higher than that of healthy plants.

Discussion: In summary, the diseased strawberry plants changed microbial community diversity, fungal species composition, and enriched functional microorganisms significantly, in addition to reshaping the microbial co-occurrence network. The results provide a theoretical basis for revealing the microecological mechanism of strawberry root rot and the ecological prevention and control of strawberry root rot from a microbial ecology perspective.

KEYWORDS

***Fragaria* × *ananassa* Duch., root rot, culturable microorganisms, high-throughput sequencing, microbial network**

1. Introduction

Strawberry (*Fragaria* × *ananassa* Duch.), a herbaceous plant belonging to the family Rosaceae and the genus *Fragaria*, has gained prominence globally as a cultivated fruit due to its short growth cycle, delightful taste, substantial consumer demand, and high economic returns. In fact, strawberries are one of the most extensively cultivated fruit crops globally (Whitaker et al., 2020). As the strawberry industry advances, the cultivation area of strawberry has expanded, accompanied by prolonged planting durations. Consequently, challenges associated with strawberry crop rotation have intensified, leading to the prevalence of various diseases.

Strawberry root rot is one of the major diseases encountered in strawberry production. Strawberry root rot is caused by *Phytophthora fragariae* and various soil-borne pathogens,

including *Fusarium oxysporum* and *Rhizoctonia solani* (Fang et al., 2013; Juber et al., 2014; Chen et al., 2017b). When the disease is severe, the entire strawberry garden is infected and the harvest is destroyed. Strawberry root rot disease occurs rapidly, and the symptoms of the diseased plants are not obvious in the early stages. In the middle and late stages of the disease, the plants wither and wilt quickly, especially after rain (Sánchez et al., 2013; Dinler et al., 2016). Preventative measures constitute the primary approach of managing strawberry root rot. The etiology behind the malady is multifaceted, encompassing factors such as inadequate seedbed drainage, soil compaction and salinization resulting from excessive fertilization, the accumulation of harmful substances due to successive planting, and disruption of soil microbial communities. Such factors collectively decrease plant resilience, in turn triggering root rot occurrence (Osman and Osman, 2013; Shankar et al., 2014; Abbas et al., 2022).

Soil has an intimately intertwined relationship with plant health, with its physical, chemical, and biological properties directly influencing plant growth and development (Timmis and Ramos, 2021). Within such a context, soil microorganisms have a pivotal role as decomposers within the soil ecosystem. Soil microbes play vital roles in plant growth, development, and stress resistance (Sun et al., 2017). Philippot et al. (2013) defined the rhizosphere as an ecological system comprised of the interactions among plant roots, rhizosphere soil, and rhizosphere microbes. This triad forms a dynamically balanced ecosystem that influences plant growth and health profoundly. Monocropping disrupts the equilibrium through plant–soil negative feedback, altering the soil environment and fostering plant disease (van der Putten et al., 2013). Imbalance and reduced adaptability within the plant-root-microbiota-soil system underlies the continuous cropping obstacle phenomenon (Cook and Baker, 1983; Weller et al., 2002). Consequently, soil microbial community structure represents a key indicator of soil health (Nannipieri et al., 2003).

Beneficial rhizosphere microbes establish symbiotic relationships with plants in the roots. They participate in functions such as nutrient absorption, immune defense, disease resistance, and growth regulation in plants (Bulgarelli et al., 2013). Harmful microorganisms, conversely, such as soil-borne plant pathogens, can adversely affect crops (Pieterse et al., 2014), by causing root infections and subsequently diminishing crop yield and quality. Hence, understanding the microbial ecological mechanisms underlying their occurrence is essential for effective biological control of strawberry root diseases. Current research on plant disease management mainly focuses on the suppressive effects of chemical and biological control methods on pathogens (Anandhakumar and Zeller, 2008; Parikka et al., 2017); however, investigations on the mechanistic aspects of strawberry disease from healthy and diseased root ecosystem perspectives are scarce. Therefore, studying root ecosystem dynamics in the context of strawberry continuous cropping and soil-borne disease carries significant implications for biocontrol strategies.

The present study investigated differences in soil nutrients and non-culturable and culturable microbial communities in rhizosphere soil and root surface soil between healthy and diseased strawberries. The aim was to shed light on the microbial ecological mechanisms behind strawberry root rot occurrence and provide insights that could facilitate their biocontrol. Furthermore, the bacteria isolated and identified from the root surface and rhizosphere soil could provide valuable resources for biocontrol and pave the way for further research and development.

2. Materials and methods

2.1. Soil sample collection and preparation

The soil samples from both diseased and healthy strawberry plants were collected at the Strawberry Experimental Base in Huyi District, Xi'an City, Shaanxi Province, China (latitude 34°6′5″ N, longitude 108°31′49″ E, elevation 430 m, and an average annual temperature of 14.3°C). The strawberry variety used in the present study was "Hongyan." The progression of strawberry disease is illustrated in Supplementary Figure 1. Field observations indicated that the roots of diseased plants turned black, with reduced lateral root numbers. Upon dissection, the central column of the infected plants exhibited a distinct reddish-brown color, whereas in healthy plants, the central column appeared yellowish-white (Supplementary Figure 2). Diseased plants were selected based on clear strawberry root rot symptoms, including wilting of the aboveground parts and reddening of the core in the underground roots. Healthy plants were selected around the diseased ones (within <1 m) and were characterized by robust growth. There were six replicates for the diseased and healthy plants.

The strawberry root system was shaken to shake off the soil not closely attached to the root system, and the rhizosphere soil closely attached to the root system was collected as the rhizosphere soil. As for the root surface soil, visible soil was removed, and the roots were suspended in sterile distilled water. The mixture was subjected to ultrasonic cleaning for 10 min (160 W, 30/30s). The resulting soil solution was centrifuged at 12,000 g for 10 min to remove the supernatant, leaving behind the tightly adhered root surface soil (Edwards et al., 2015; Khan et al., 2019). Non-rhizosphere soil was collected randomly from six points within the 5–20 cm plow layer that was not influenced by root presence. Rhizosphere, root surface, and non-rhizosphere soil samples were stored at 4°C and −80°C for subsequent soil microbial analyses. Additionally, some soil samples were air-dried, ground, and sieved for use in soil nutrient and enzyme activity analyses. Hereafter, the rhizosphere soil of healthy plants is referred to as "HR," the root surface soil of healthy plants as "HS," the rhizosphere soil of diseased plants as "DR," the root surface soil of diseased plants as "DS," and the non-rhizosphere soil as "NR."

2.2. Soil physicochemical property analysis

Following the collection described in section 2.1, the HR, DR and NR soil sample were air-dried and ground, sieved through a 2-mm and 0.25-mm sieve. The meticulously prepared soil samples were then used for the determination of soil physicochemical indicators. Organic matter content was determined using the potassium dichromate volumetric method (Inclán et al., 2007). Total nitrogen content was determined using the Kjeldahl method. Similarly, total phosphorus content was assessed using the $HClO_4$-H_2SO_4 digestion method followed by molybdenum antimony colorimetry. Total potassium content was determined using the NaOH fusion-flame atomic absorption spectrometry technique. Alkali hydrolyzable nitrogen was quantified using the diffusion method (Restrepo et al., 2016). The evaluation of rapidly available phosphorus was accomplished using the sulfuric acid-molybdenum antimony colorimetric procedure. Available potassium content was assessed using flame photometry.

Finally, the pH of the soil samples was measured using the potentiometric method (Read et al., 2003; Shrestha and Lal, 2011).

2.3. Determination of culturable soil microbial abundance

The quantification of cultivable bacterial populations in the soil was achieved using the plate dilution spread method. Bacteria were cultivated on LB agar medium at 30°C for 72 h. Subsequently, bacterial colony-forming units (CFUs) that developed on the counting plates were converted into CFUs per gram of dry soil (CFU/g) to represent microbial abundance. After enumeration, individual bacterial colonies were carefully selected from the bacterial plates cultured from the rhizosphere, root surface soil, and non-rhizosphere soil samples of both diseased and healthy plants. The selected colonies were subjected to purification and isolation, followed by thorough identification.

Bacterial Molecular Identification: Bacteria were inoculated into liquid LB medium and placed in a constant temperature oscillating incubator (30°C, 150 rpm) for 48 h until the culture medium became turbid. DNA was extracted using the freeze–thaw method to obtain DNA templates (Cullen and Hirsch, 1998). After extracting bacterial DNA and conducting quality assessment using NanoDrop 2000 (Thermo Fisher Scientific, Wilmington, DE, USA), the extracted bacterial genomes were used as templates for PCR amplification using specific primers 27F/1492R targeting the bacterial 16S rDNA gene (Lane, 1991). Amplification reactions (25-μL volume) consisted of 2 × T5 Super PCR Mix (Basic) 12.5 μL, forward primer (10 μM) 1 μL, reverse primer (10 μM) 1 μL, template DNA (100 ng)1 μL and DNase-free water 9.5 μL. The PCR amplification was performed as follows: initial denaturation at 94°C for 3 min, followed by 30 cycles of denaturing at 95°C for 30 s, annealing at 58°C for 30 s and extension at 72°Cfor 45 s, and single extension at 72°C for 10 min, and end at 4°C. The obtained 16S rDNA sequences of the bacteria were aligned with the NCBI nucleotide database through online BLAST comparison (Zhang et al., 2010; BLAST: Basic Local Alignment Search Tool[1]), providing insights into the genetic relationships among different bacterial strains.

2.4. Soil DNA extraction and third-generation long amplicon sequencing

Each of the 24 samples, including "HS," "DS," "HR," and "DR" had 6 replicates each were stored at −80°C. Microbial community DNA was extracted according to the instructions of the E.Z.N.A.® Soil DNA kit (Omega Bio-tek, Norcross, GA, United States). The extracted DNA served as the template for the amplification of both the full-length 16S rRNA gene and the full-length ITS region through PCR. After PCR purification, the purified products were quantified using a Quantus™ Fluorometer (Promega, United States). Subsequently, adhering to the sequencing requirements of each sample, the products were mixed at corresponding proportions. Library preparation was conducted using the SMRTbell® Express Template Prep Kit 2.0 (PacBio, Menlo Park, CA, United States), involving steps such as (1) DNA damage repair, (2) end repair, and (3) adapter ligation. Sequencing was performed using the Pacbio Sequel II System (Shanghai Meiji Biopharmaceutical Technology Co., Ltd.). The resulting PacBio raw data were subreads, and the Circular Consensus Sequence (CCS) sequences were obtained using the SMRTLink 8.0 (PacBio) with parameters set as minfullpass =3 and minPredictedAccuracy = 0.99. To distinguish data from different samples, barcode sequences were employed, followed by length filtering to retain sequences ranging from 1,000 to 1,800 bp for bacteria and 300 to 900 bp for fungi.

2.5. Data processing

The soil physicochemical properties and counts of cultivable microorganisms indicators were analyzed for significant differences among different soil samples using IBM SPSS Statistics 25 (IBM Corp., Armonk, NY, United States) using the Duncan's test ($p < 0.05$). Analysis of high-throughput sequencing data was conducted on the Majorbio Cloud Platform[2] using the following comprehensive procedures:

Sequence quality control: Using UPARSE 7.1 (http://drive5.com/uparse/version 7.1; Stackebrandt and Goebel, 1994; Edgar, 2013), sequences were clustered into Operational Taxonomic Units (OTUs) based on a 97% similarity threshold, with meticulous removal of chimeric sequences. Moreover, the sequences annotated as chloroplasts and mitochondria across all samples were systematically excluded, followed by subsampling to ensure consistency in sample sequence numbers.

Species annotation: Using the Silva138.1/16s_bacteria[3] (Dueholm et al., 2020) and unite8.0/its_fungi (Release 8.0 http://unite.ut.ee/index.php; Nilsson et al., 2019). the sequences contained in each sample were meticulously aligned to determine the diversity of species present, accomplished thorough species annotation.

Diversity analysis: Leveraging the MOTHUR software,[4] a comprehensive suite of alpha diversity indices was computed for each sample, including Shannon Wiener, Chao1, and Gini-Simpson indices. For beta diversity analysis, the Bray-Curtis distance-based Principal Coordinates Analysis (PCoA) was performed, yielding graphical representations.

Microbial correlation network construction: Through amalgamation of bacterial and fungal species annotation data tables, a curated set of species that exhibited presence in over 50% of all samples was retained. The data were subjected to comprehensive microbial correlation network analysis at the genus level, using the Hmisc package in R-4.3.1 (R Foundation for Statistical Computing, Vienna, Austria; Chen et al., 2017a). The evaluation entailed computation of Spearman correlation coefficients, thereby generating matrices containing correlation values (r) and significance levels (p). Further refinement involved the inclusion of species data that satisfied criteria with $|r| > 0.90$ and $p < 0.05$, followed by importing the data into

1 https://blast.ncbi.nlm.nih.gov/Blast.cgi

2 https://cloud.majorbio.com

3 http://www.arb-silva.de

4 http://www.mothur.org/wiki/Calculators

10.3389/fmicb.2023.1286740

the Gephi software (version 0.10.1) for the construction of correlation network graphs and the calculation of their topological properties.

Network natural connectivity assessment: Assessment of network natural connectivity was performed using fastnc[5] (Peng and Wu, 2016; Wu et al., 2021). This involved rigorously testing the network's resilience by randomly eliminating nodes within the network, ranging from 1% to 99%, through an iterative simulation process conducted 1,000 times. The resulting averaged values were then utilized for the calculation and evaluation of the network's natural connectivity and overall stability.

Functional prediction: The FAPROTAX database was used for comprehensive 16S functional analysis to predict functional attributes (Sansupa et al., 2021). Additionally, the FUNGuild database was harnessed for the systematic prediction of ITS functional attributes (Nguyen et al., 2016).

3. Results

3.1. Soil physicochemical properties

The various physicochemical properties of strawberry root rot-diseased plant rhizosphere soil, healthy plant rhizosphere soil, and non-rhizosphere soil are presented in Table 1. As shown in the table, significant differences were observed in TN (total nitrogen) and AN (available nitrogen) between HR and DR ($p < 0.05$), while other physicochemical indicators showed minimal differences and were not statistically significant. HR and DR exhibited higher TN, SOM (Soil Organic Matter), and OP (Olsen Phosphorus) values than NR. The pH of HR and DR was significantly higher than that of NR ($p < 0.05$). However, AK (available potassium) content was higher in NR than in both HR and DR.

TABLE 1 Physical and chemical properties of rhizosphere soil of healthy plants, rhizosphere soil of diseased plants, and non-rhizosphere soil of strawberry.

Treatment	HR	DR	NR
TN (g/kg)	1.06 ± 0.08a	1.02 ± 0.04ab	0.96 ± 0.01c
SOM (g/kg)	19.15 ± 2.15a	19.07 ± 0.85a	17.50 ± 0.34a
AN (mg/kg)	72.93 ± 4.75a	68.99 ± 4.26a	72.93 ± 3.51a
OP (mg/kg)	26.58 ± 2.66a	26.63 ± 7.91a	20.96 ± 1.46a
AK (mg/kg)	123.83 ± 11.88a	123.83 ± 7.20a	131.17 ± 5.61a
pH	6.59 ± 0.21a	6.54 ± 0.20a	6.25 ± 0.04b

Values followed by different letters within the columns are significantly different according to Duncan's Test ($p < 0.05$), HR, DR and NR are healthy rhizosphere soil, diseased rhizosphere soil, and non-rhizosphere soil, respectively.

3.2. Soil microbial diversity

Using high-throughput sequencing technology, a total of 1,348,655 fungal sequences with 849,575,807 bases and an average sequence length of 629 bp, as well as 890,840 optimized bacterial sequences with 1,286,151,991 bases and an average sequence length of 1,443 bp, were obtained from 24 samples of healthy strawberry rhizosphere soil, healthy plant root surface soil, diseased plant rhizosphere soil, and diseased plant root surface soil. A total of 19,851 fungal OTUs and 4,728 bacterial OTUs were generated from the 24 soil samples.

Soil microbial community diversity in different ecological niches of healthy strawberry plants and those affected by root rot are illustrated in Figure 1. The results reveal diversity variations in fungal and bacterial communities among different soil samples. The alpha diversity of fungal communities in both Ds and DR was higher than those in HS and HR; however, there were no significant differences in alpha diversity among different ecological niches (root surface soil and rhizosphere soil) for either healthy or diseased plants (Figure 1A). The alpha diversity of bacterial communities exhibited distinct trends when compared with those in fungal communities. In the root surface soil, the alpha diversity of bacterial communities showed no significant difference between healthy and diseased plants. However, in rhizosphere soil, the alpha diversity of HR bacterial communities was significantly higher than that of DR bacterial communities ($p < 0.05$; Figure 1B).

Principal coordinates analysis (PCoA) results based on Bray-Curtis distance are illustrated in Figure 1C for fungal communities, revealing no significant differences among soil samples. In contrast, for bacterial communities (Figure 1D), there were no significant differences in beta diversity among bacterial colonies in root surface soil between healthy and diseased plants ($p > 0.05$). However, significant differences were observed in bacterial community beta diversity between healthy and diseased plants in rhizosphere soil ($p = 0.041$, Adonis test).

3.3. Soil microbial species composition

In the fungal community, Basidiomycota (50.05%–71.13%) and Ascomycota (25.05%–42.17%) were dominant phyla across all soil samples. Additionally, the top 10 genera in terms of species abundance are listed (Supplementary Figure 3). Dominant genera included *Clitopilus* (32.20%–47.75%), *Solicoccozyma* (5.94%–16.42%), *unclassified_c_Agaricomycetes* (6.89%–13.72%), *Trichoderma* (2.95%–4.99%), and *Colletotrichum* (0%–6.01%), as shown in Figure 2A.

There were pronounced differences in fungal community structure between healthy and diseased plants. Conversely, fungal community structures in different ecological niches of strawberry soil exhibited similarity. In diseased strawberry plants, the relative abundances of Basidiomycota, *Clitopilus*, *unclassified_c_Agaricomycetes*, and *Pilidium* decreased, while the relative abundances of Ascomycota, Rozellomycota, *Trichoderma*, and *Colletotrichum* increased when compared with those in healthy plants. Notably, the relative abundances of the genus *Colletotrichum* in DR and DS were 6.96 and 6.01%, respectively, whereas it was less than 1% in HR and HS. The observation might be linked to the occurrence of strawberry root rot.

In the case of bacterial community (Figure 2B), Proteobacteria (31.43%–51.13%), Firmicutes (9.41%–27.31%), Acidobacteriota (8.59%–14.05%), Actinobacteriota (5.81%–6.74%), Planctomycetes (3.33%–5.94%), and Bacteroidota (2.54%–5.58%) were the dominant phyla across all soil samples. Additionally, the top 10 genera in terms

5 https://github.com/wqssf102/fastnc

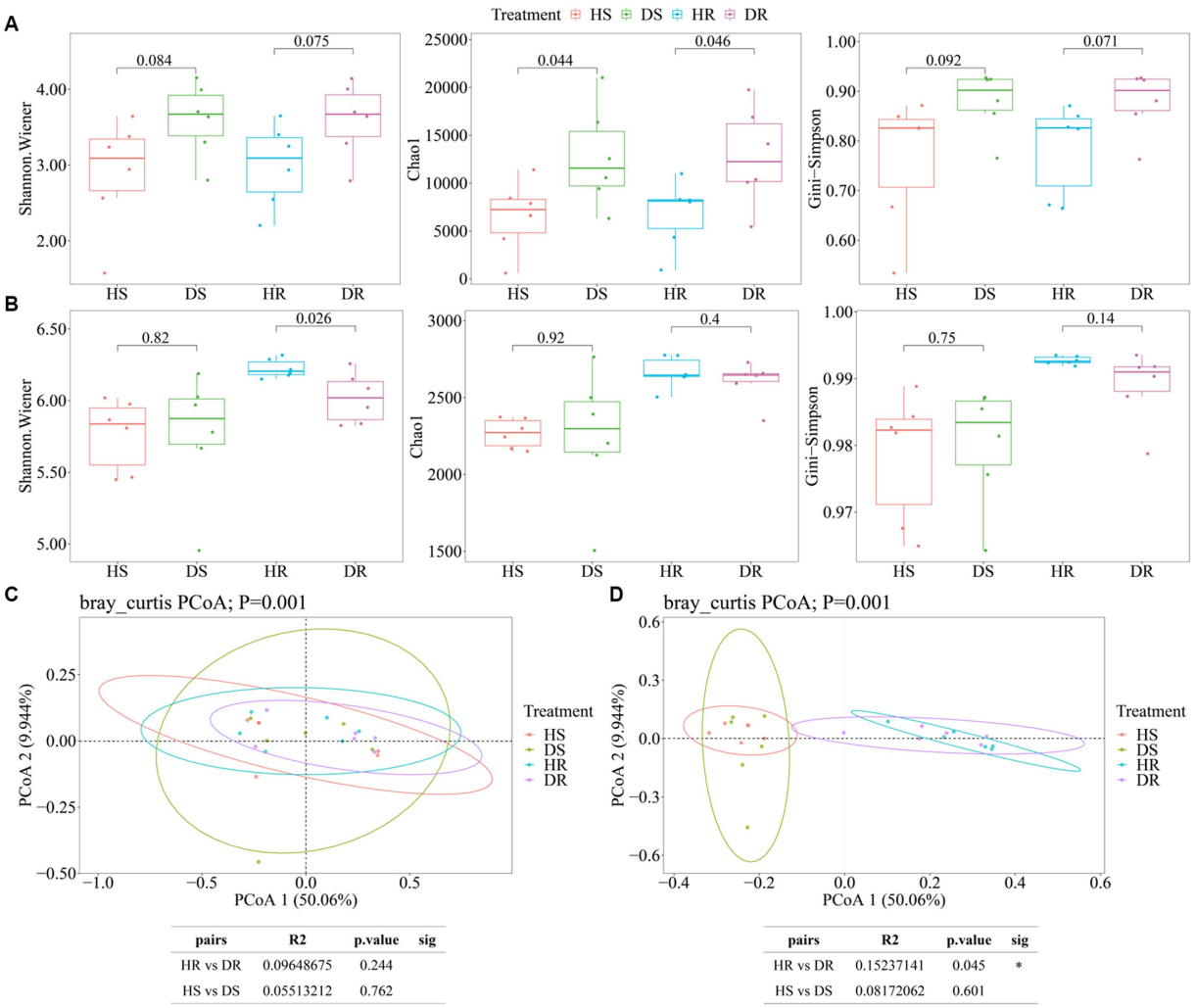

FIGURE 1
Microbial alpha diversity. The α-diversity indices of soil fungal **(A)** and bacterial **(B)** communities in the root surface soil and rhizosphere soil of healthy and diseased strawberry plants. **(C,D)** Comparison of beta diversity related to root surface soil and rhizosphere soil between healthy and diseased strawberry plants, **(C)** fungal beta diversity; **(D)** Bacterial beta diversity. Alpha diversity: The horizontal bars within boxes represent medians. The tops and bottoms of boxes represent the 75th percentiles and 25th percentiles, respectively. The asterisk above the horizontal line represents a significant difference between the two groups, $*p < 0.05$, $**p < 0.01$, and $***p < 0.001$. Beta diversity: Different color points represent the samples in each group, and the circle in the figure is a confidence ellipse at a confidence level of 95%.

of species abundance are listed (Supplementary Figure 3). Dominant genera included *Bacillus* (5.00%–20.80%), *Sphingomonas* (2.22%–5.64%), *uncultured_f_Gemmatimonadaceae* (1.92%–4.67%), and *Novosphingobium* (0.40%–5.35%) at the genus level.

In the comparison between diseased and healthy strawberry plants, there was a decrease in the relative abundance of Firmicutes in the root surface soil of diseased plants (Figure 2B). Although the species composition of most bacteria showed no significant differences between diseased and healthy plants, bacterial community structure exhibited significant differences among the different ecological niches within healthy or diseased plants, indicating that different ecological niches of strawberry roots have specific effects on bacterial taxa selection. In other words, bacterial community assembly in strawberry roots is primarily driven by organ-specific ecological niches. The occurrence of strawberry disease has minimal impact on root bacterial community structure.

3.4. Soil microbial co-occurrence networks

To delve into the interconnectivity within the root-associated microbial communities of healthy and diseased soils, a comprehensive co-occurrence network analysis was conducted. Within the networks, the fungal nodes predominantly stem from eight distinct phyla, among which Basidiomycota, Ascomycota, and Rozellomycota exhibit widespread distribution. With regard to bacteria, nodes predominantly hail from 11 diverse phyla, with Proteobacteria, Firmicutes, Acidobacteriota, and Actinobacteriota displaying high prevalence (Figure 3). Additionally, the topological properties of the microbial co-occurrence networks in the rhizosphere soil of healthy and diseased strawberry plants were computed separately (Supplementary Table 1). The microbial interaction network in the diseased plants had higher node and edge numbers than those in the healthy plants, indicating a more intricate network. However, the

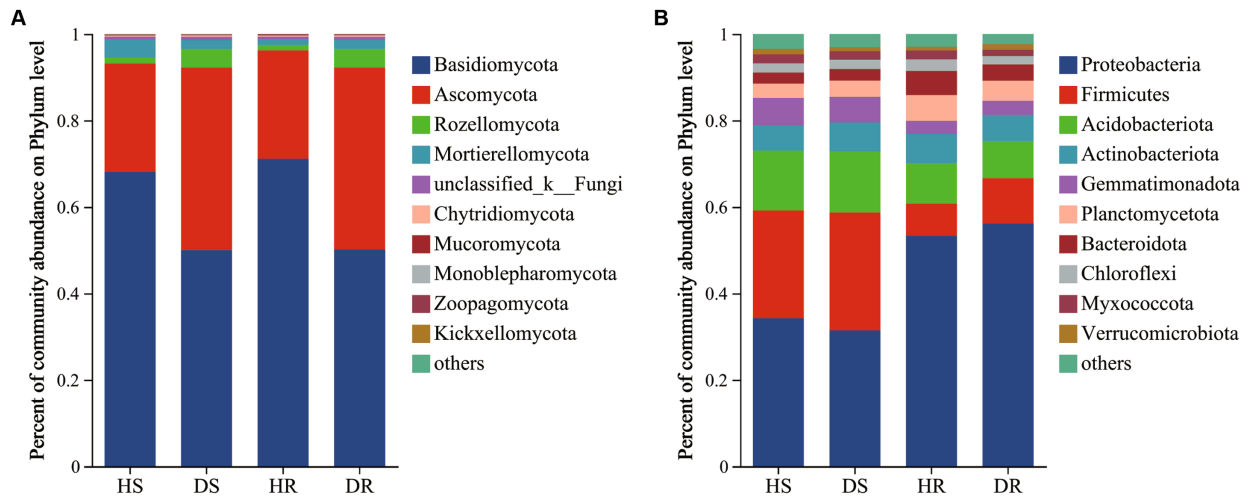

FIGURE 2
Microbial community composition of the root surface soil and rhizosphere soil of healthy and diseased strawberry at the phylum level, **(A)** fungal community composition; **(B)** Bacterial community composition.

diseased plant network had lower modularity and higher average path length.

The keystone species were evaluated by calculating the intra-module connectivity (Zi) and inter-module connectivity (Pi) of nodes in the network. The proportions of module hubs in the co-occurrence networks of HS and HR were 1.63% and 2.61%, respectively, which were higher than those in the co-occurrence network of DS and DR (1.56% and 1.42%, respectively). The proportions of connecting nodes (Connectors) of HS and HR were 53.67% and 52.54%, respectively, which were also higher than those of DS (53.13% and 49.36%, respectively; Figure 4A). The results show that the connectivity within and between modules of healthy plant soil co-occurrence network were higher.

The resistance of the microbial interaction network to plant infection and network structure stability were tested by removing nodes to alter the natural connectivity of the network. The results showed that by removing the same proportion of nodes, the natural connectivity of the microbial interaction network of the healthy plant had a gentler downward trend than the natural connectivity of the diseased plant (the slope of the fitting curve was lower; Figure 4B), indicating that the microbial interaction networks in HS and HR had higher network stability and higher resistance to adversity than those of DS and DR.

3.5. Soil microbial functional prediction

By employing FAPROTAX, a comprehensive functional prediction was conducted on the bacterial communities within the root systems of both healthy and diseased strawberry plants. A total of 60 functional categories were anticipated across all soil samples, among which a plethora of bacterial functional types exhibited significant enrichment, including chemoheterotrophy, aerobic chemoheterotrophy, nitrogen fixation, ureolysis, nitrate reduction, plant pathogen, and chitinolysis. Analysis of functional classification discrepancies between the root-associated bacteria of healthy and diseased strawberry plants was performed using the Kruskal-Wallis rank-sum test, subsequently revealing distinctly altered bacterial functional assemblages in root surface soils ($p < 0.05$; refer to Figure 5A). The findings unveiled prominent differences in bacterial functional pathways across different soil samples. Notably, the relative abundance of aromatic hydrocarbon degradation bacteria was significantly higher in the root surface soil of diseased plants than in soils of healthy plants. Furthermore, in the rhizosphere soil of diseased plants, there was a significant reduction ($p < 0.05$) in the relative abundance of photoautotrophy and predatory or exoparasitic bacteria, while the relative abundance of the plant pathogen type displayed a notable increase when compared with that in healthy plants ($p < 0.05$).

Utilizing FUNGuild for functional prediction analysis of fungi within the rhizosphere and root surface soils of both healthy and diseased strawberry plants, a total of 17,574 OTUs were annotated into seven nutritional guilds, including Pathotroph, Symbiotroph, Pathotroph-saprotroph-Symbiotroph, Pathotroph-Saprotroph, Pathotroph-Symbiotroph, Soprotroph, and Soprotroph-Symbiotroph. Using the Kruskal-Wallis rank-sum test for prediction of functional subcategories of soil fungi, notable differences were observed between diseased and healthy plants at the root surface soil level (Figure 5B). Specifically, the Leaf Saprotroph guild in the root surface soil of diseased plants surpassed that of healthy plants at a highly significant level ($p < 0.01$). In the rhizosphere soil, the relative abundance of Leaf Saprotroph guild was also significantly higher in diseased plants. In addition, notably, the relative abundance of Endophyte-Plant Pathogen in diseased plants was significantly higher ($p < 0.01$), suggesting a direct correlation with the onset of strawberry plant disease.

3.6. Isolation and identification of cultivable soil microorganisms

The number of bacterial taxa in diseased plants was higher than that in in healthy plants. Additionally, the number of isolated bacteria in different ecological niches of strawberry roots had the following

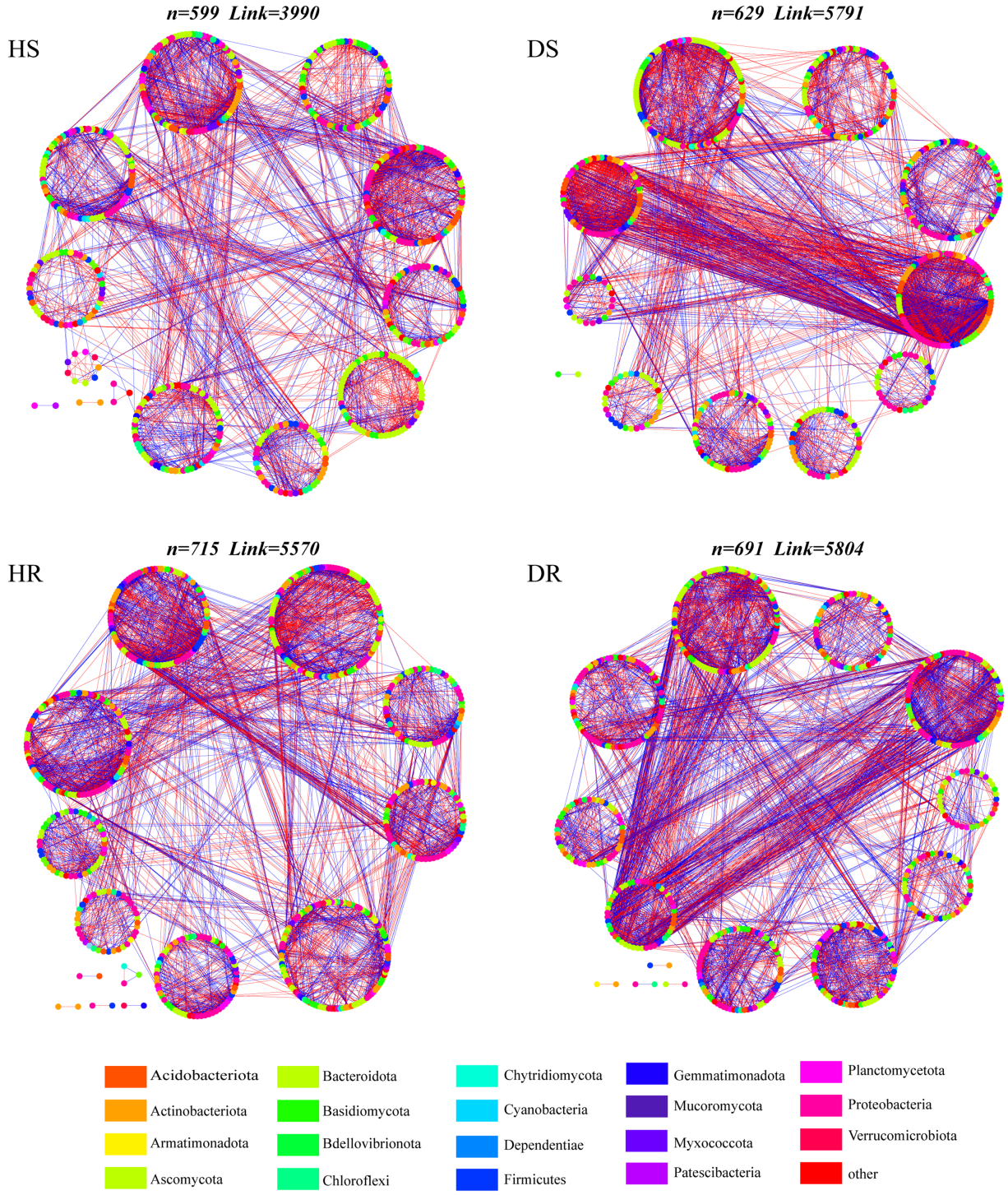

FIGURE 3
Visualizations of microbial co-occurrence networks in different soil samples. The nodes are colored according to bacterial phylum and fungal phylum. The circle surrounded by nodes represents the module. Edge color represents positive (green) and negative (red) correlations.

order: root surface > rhizosphere > non rhizosphere ($p < 0.05$). The quantity of bacteria in the root surface of diseased plants was significantly higher than that in healthy plants, as depicted in Figure 6A ($p < 0.05$). In the present study, further isolation and purification were carried out on the dilution plate-isolated bacteria, resulting in a total of 912 strains. After removing redundancy through analysis of 16S rDNA gene similarity, 192 bacterial species were identified. The 192 strains were distributed across four phyla, six classes, 20 orders, 41 families, and 75 genera.

Culturable bacteria in strawberry root surface soil belonged primarily to the phyla Actinobacteria, Bacteroidetes, Proteobacteria, and Firmicutes, with Actinobacteria being more prevalent in the HR

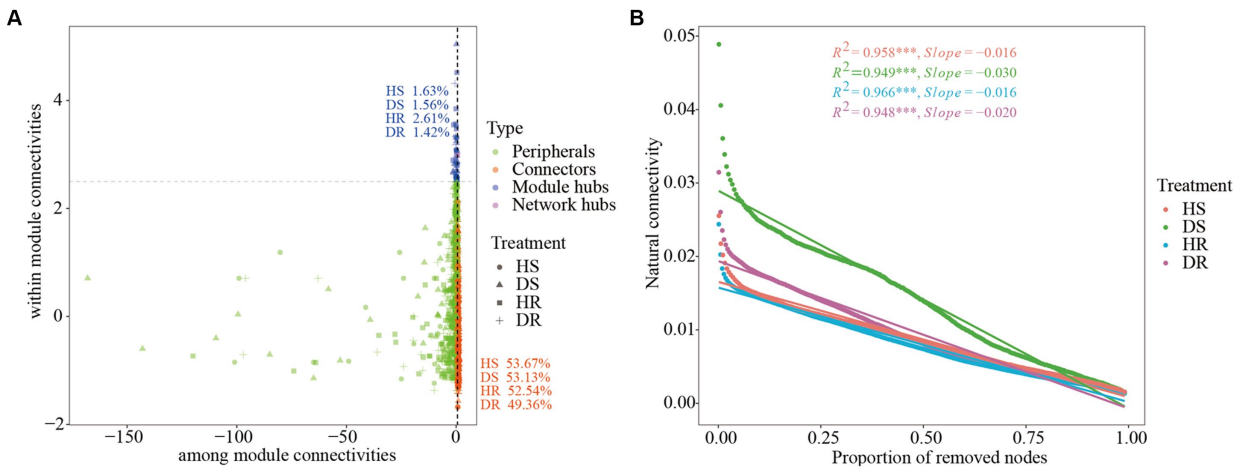

FIGURE 4
(A) Zi–Pi plot shows the distribution of OTUs based on their topological roles with different soil samples. **(B)** Changes in the natural connectivity of different soil samples.

(Figure 6B). Furthermore, species-level richness Venn diagram and species abundance pie chart were generated (Supplementary Figure 4). Among the microbial isolates from DR, the greatest diversity was observed in prokaryotic microorganisms. Notably, certain species, such as *Pseudomonas alcaligenes* (3%), *Pseudomonas aeruginosa* (2%), and *Chryseobacterium cucumeris* (2%), were isolated exclusively from the DR. *Luteimonas panaciterrae,* a ginseng-associated bacterium, was detected at a proportion of 4% in the root surface of healthy plants but was absent from other soil samples.

4. Discussion

Soil physicochemical characteristics are crucial indicators of soil quality. In the present study, there were no significant differences in most physical and chemical indexes between HR rand DR; however, there were significant differences in TN (total nitrogen), SOM (soil organic matter), OP (Olsen phosphorus), and AK (available potassium) between HR and DR, and NR. The variations in soil physicochemical properties across different root ecological niches were much more substantial than the differences between healthy and diseased plants. Notably, the pH values of both HR and DR were significantly higher than that of NR ($p < 0.05$), Soil pH can directly reflect soil acidity and alkalinity, and rhizosphere soil has a certain buffering capacity for pH changes. Roots can compensate for unbalanced cation-anion absorption at the soil-root interface by releasing H^+ or OH^-, thereby significantly changing rhizosphere pH (Riley and Barber, 1969). Youssef and Chino (1989) found that the difference in rhizosphere and non-rhizosphere soil pH was more dependent on plant species and initial non-rhizosphere soil pH, rather than nitrogen source or nitrogen application level. Root-mediated pH changes involve many basic processes and a variety of environmental factors (Hinsinger et al., 2003). The interaction between soil pH and strawberry roots needs further study. A deficiency in soil elements such as N, P, and K increases plant disease risk significantly (Walters and Bingham, 2007). Significant differences in TN and AN (available nitrogen) were observed between HR and DR, which is consistent with the findings of Liao et al. (2022) in their study on root rot disease in Sichuan pepper plants, where they observed significant reductions in TN and AN levels in the rhizosphere soil of diseased plants when compared with healthy ones. The trends suggest correlation between soil TN and AN and the occurrence of strawberry plant disease. However, further experimental validation is required to definitively establish and explain the relationship.

The intricate interplay of root-associated microbial communities has a pivotal role in host plant immunogenic defense (Stringlis et al., 2018). Such communities not only suppress disease (Carrión et al., 2019) but also provide essential nourishment (Zhang et al., 2019) and safeguard against both biotic and abiotic stresses. Therefore, alterations in soil microbiota can serve as indicators of plant growth conditions and serve as a crucial metric for gauging soil health (Lehmann et al., 2020). High-throughput sequencing revealed notable discrepancies in fungal species composition between diseased and healthy strawberry plants. Conversely, within the diverse ecological niches of the strawberry root system, the variance in fungal species composition remained modest. Among diseased plants, the relative abundances of dominant phyla such as Basidiomycota and *Clitopilus* were markedly lower when compared with those in healthy plants. Conversely, the relative abundances of phyla such as Ascomycota, Rozellomycota, and genus *Trichoderma* were elevated significantly in diseased plants. This is similar to Yang et al. (2020) who found that the relative abundance of Ascomycota in strawberry plants increased by 20% after infection with powdery mildew, while the relative abundance of Basidiomycota decreased by 20%. The trends are consistent with the findings of Zheng et al. (2022) who reported reduced abundance of Basidiomycota in healthy tobacco roots when compared with that in tobacco afflicted by Rhizoctonia root rot. Moreover, the congruence with the findings of Gu et al. (2020) on tomato plants underscores the interconnectedness between decreased Basidiomycota and increased Ascomycota abundances in DR. The results indicate that the decrease and increase in relative abundance of Ascomycota and Basidiomycota were closely related to plant disease. However, whether the relationship between Basidiomycetes and Ascomycota is nutritional, attributable to niche competition, or antagonistic needs to be verified further. Notably, at

10.3389/fmicb.2023.1286740

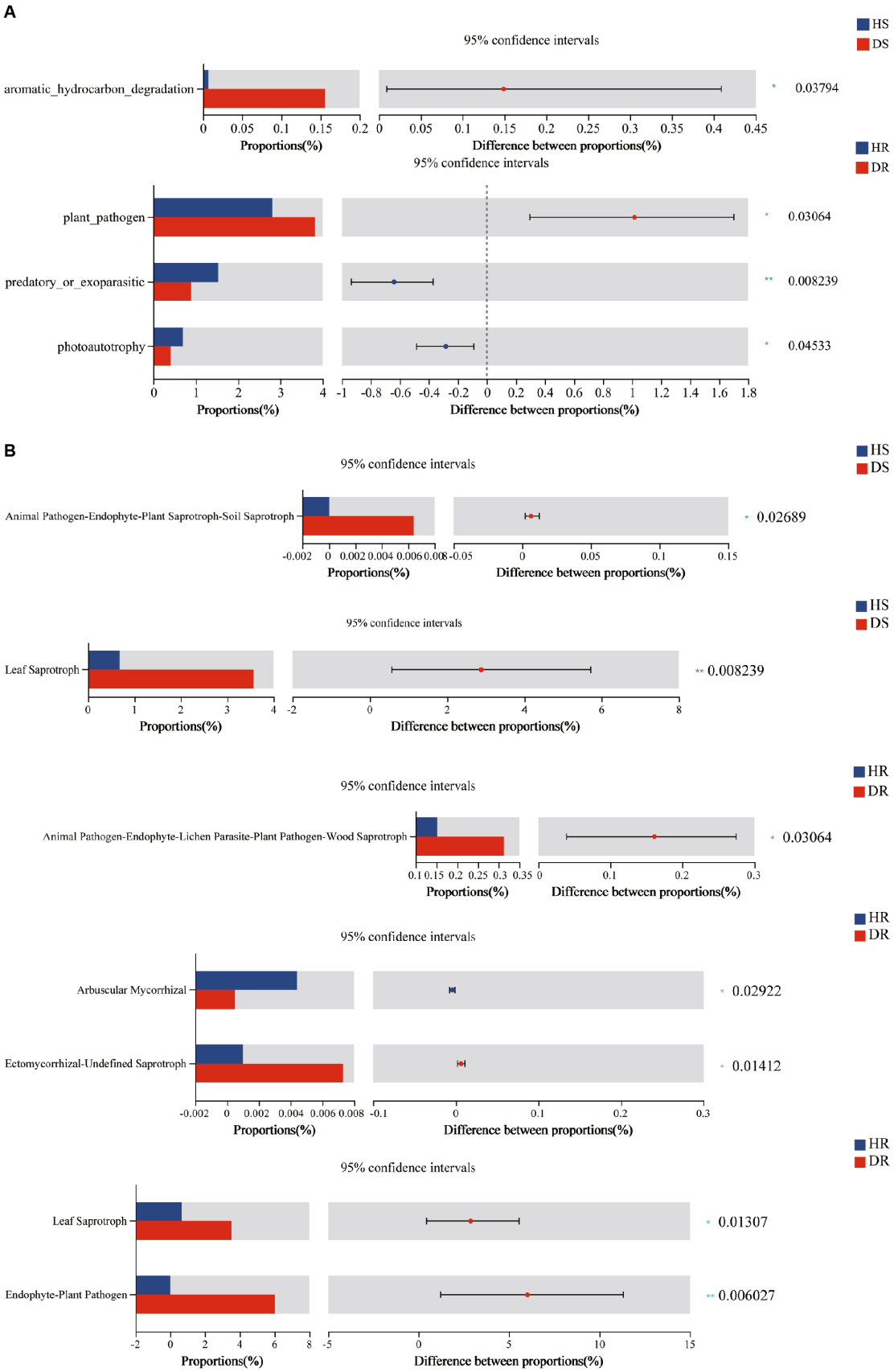

FIGURE 5
(A) Prediction results of root surface soil and rhizosphere soil FAPROTAX function of healthy and diseased strawberry plants, **(B)** Prediction results of root surface soil and rhizosphere soil FUNGuild function of healthy and diseased strawberry plants. The abscissa of the left histogram represents the average relative abundance of a feature in different groups. The ordinate represents the grouping category of different features or pairwise comparison in the task group. Different colors represent different groupings. The rightmost is *p*-value, *0.01 < *p* < 0.05, **0.001 < *p* < 0.01, ***$p < 0.001$.

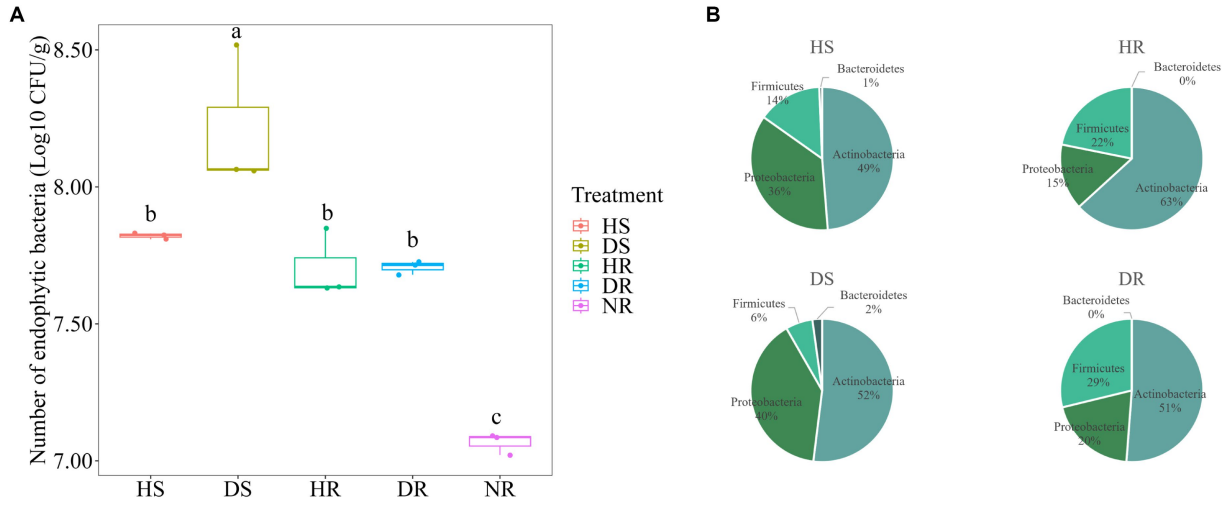

FIGURE 6
(A) Isolation frequency of the bacteria with different soil samples. **(B)** Community composition of culturable bacteria at phylum level in different soil samples.

the genus level, the relative abundance of *Clitopilus* decreased by 15.39% in DR, while the relative abundance of *Colletotrichum* increased by 6.01%, when compared with HR. The increased presence of *Colletotrichum* could potentially be a direct cause of strawberry disease. *Colletotrichum* spp., causing anthracnose, poses a devastating threat to various crops globally, and extensive research indicates that *Colletotrichum* is a major pathogen in strawberry fields. Anthracnose is likely to occur throughout the growth cycle of strawberries (Curry et al., 2002; Rahman and Louws, 2017). The increased *Colletotrichum* relative abundance could be a significant factor triggering strawberry disease. Bacterial species composition varies significantly across different ecological niches within the strawberry root system. However, the differences between diseased and healthy plants are minimal, with only Firmicutes exhibiting lower relative abundance in the rhizosphere and root surface soils of diseased plants when compared with those of healthy plants.

The alpha diversity of fungal communities in diseased plants surpassed that in healthy plants. Simultaneously, differences in alpha diversity indices among various ecological niches within the strawberry root system are less conspicuous. The beta diversity of root surface soil and rhizosphere soil from diseased plants clusters within a shared confidence interval, implying high fungal similarity within the diseased plant rhizosphere. Previous studies suggest a negative correlation between fungal quantity/diversity and soil health, as certain fungi can hamper plant growth by disrupting root systems, thereby impacting plant vitality (Yim et al., 2013; Emmett et al., 2014). Siegieda et al. (2023) found that the alpha diversity index of strawberry fungal community in non-rhizosphere and rhizosphere soil was higher than that of healthy plants. At the same time, Su et al. (2022) found that the rhizosphere soil microbial community diversity and richness of strawberry anthracnose plants were higher than those of healthy strawberry rhizosphere soil, which was consistent with the results of this study. Conversely, bacterial community alpha diversity follows a distinct trend when compared with fungal communities. No marked distinction is evident between the root surface soils of diseased and healthy plants. However, significant differences are observed in the bacterial alpha diversity indices across distinct ecological niches within the strawberry root system under similar treatment. There are few studies on the microorganisms of different niches of strawberry roots, and the research on different niches of other plant roots is referred to. The finding is consistent with Wang et al. (2023), who noted that changes in hydrodynamics and physicochemical properties can alter microbial diversity in aquatic environments significantly, but it does not change the alpha diversity of rhizosphere and endophytic bacteria significantly.

Research has indicated significant variations in bacterial communities across different ecological niches in tomatoes (Han et al., 2020). Gdanetz and Trail (2017) affirmed that wheat microbial community establishment is influenced predominantly by location-based ecological niches and host species, with minimal impact from soil, climate factors, or fertilization practices. The alpha diversity of bacteria in the rhizosphere of diseased plants was lower than that of healthy plants, but it did not reach a significant level, which was contrary to fungal diversity. In summary, in comparison to healthy plants, diseased plants display elevated fungal diversity and decreased = bacterial diversity. Furthermore, fungal communities exhibit consistent patterns in both species composition and diversity across different ecological niches within the root system. In contrast, bacterial communities display significant variations among the niches, demonstrating a gradient within the root environment, indicative of regional stability. This might reflect bacterial adaptation to long-term environmental change (Gibbons et al., 2014; Liu et al., 2018).

Using co-occurrence networks to depict the intricate interrelationships among microorganisms, we employed perturbation of natural network connectivity through random node removal to evaluate network structural stability. The results revealed a stability ranking for microbial interaction networks across the treatments as follows: HR > HS > DR > DS. The results show that the microbial interaction network has large difference in community stability between diseased plants and healthy plants, and there are differences

in different niches of strawberry roots. Fungal community diversity of the diseased plants increased, and the microbial interaction network was more complex than that of the healthy plants; however, microbial interaction network stability was reduced and the degree of modularization was low. The higher the degree of network modularity, the greater the number of modules in the network. When the interactive network is subject to external interference, the existence of such modules can control the interference within one module and avoid its spread to other modules (Wang et al., 2016). Such findings underscore that the rhizosphere microbial community of healthy strawberry plants possesses a certain degree of structural and functional stability. However, mere diversity and richness are insufficient to ensure the stability of microbial community structure and function. Therefore, the microbial community in the rhizosphere of healthy plants exhibits greater resilience and stability when confronted with pathogenic interference.

Significant enrichment was in the Endophyte-Plant Pathogen, Leaf Saprotroph, and other Saprotroph guilds in diseased plants was observed following FUNGuild prediction analysis. The observations are likely associated with the decomposition of root tissues following plant infection. In addition, functional prediction analysis of bacterial communities within the root surface soils of healthy and diseased strawberry plants using PAFPROTAX revealed marked enrichment in aromatic hydrocarbon degradation and plant pathogenic functional categories in the diseased plants. Notably, previous studies have shown that *Pseudomonas* species possess aromatic compound-degradation capacity (Lunt and Evans, 1970; Ahmed and Focht, 1973). Additionally, earlier cultivation-based investigations have reported notable presence of *Pseudomonas* in the root surface soil of diseased plants, encompassing species such as *Pseudomonas putida*, *Pseudomonas alcaligenes*, and *Pseudomonas umsongensis*. *Pseudomonas putida*, in particular, has found extensive applications in industrial pollution mitigation (Henríquez et al., 2023) and serves as a biological control agent against pathogens (Ashajyothi et al., 2023). Furthermore, a recent study (Yi et al., 2022) revealed that benzo[a] pyrene (BaP) addition enriched microbes associated with aromatic compound degradation (Sphingomonas, Bacilli, Fusarium). Overall, the findings suggest that upon exposure to pathogens, strawberry plants might secrete specific root exudates, consequently fostering the enrichment of aromatic hydrocarbon-degrading bacteria. Conversely, in the rhizosphere of healthy plants, substantial enrichment of predatory or exoparasitic and photoautotrophic guilds was observed. Notably, following plant infection, root-associated bacterial communities shifted from autotrophic to saprotrophic guilds.

In the present study, bacterial groups were isolated and the number of microorganisms in the rhizosphere and root surface of both healthy and diseased plants was much greater than that in the non-rhizosphere. This is because the secretions produced by the root system can be used as a nutrient source by microbes for growth and reproduction (Bais et al., 2006). Consequently, due to root exudates, microbial abundance exhibited the following pattern: root surface microbes > rhizosphere microbes > non-rhizosphere microbes, suggesting a higher level of connection between plants and root surface microbes than with rhizosphere and non-rhizosphere microbes. Moreover, the quantity of root surface microbes in diseased plants exceeded that in healthy plants significantly. This might be linked to the degree of disease progression, as during the middle to later stages of disease, root rot releases organic substances that provide nutrients, resulting in substantial bacterial reproduction. Furthermore, there was a substantial increase in Actinobacteria in the rhizosphere of healthy plants. Considering soil Actinobacteria often produce antibiotics and promote plant growth (Zhao et al., 2023), they play a crucial role in generation of soil-borne antimicrobial substances. The decrease in the proportion of soil Actinobacteria can lead to weakened soil disease resistance and influence the regulation of soil microbial ecology (Doumbou et al., 2001). Further isolation and identification of bacteria showed that the relative abundance of *Pseudomonas alcaligenes*, *Pseudomonas aeruginosa*, and *Pseudomonas putida* in the root surface of the diseased plants was relatively high, and *Pseudomonas putida* could easily degrade and utilize aromatic compounds and other substances (Furuno et al., 2010). In addition, Li et al. (2019) observed that 1-aminocyclopropane-1-carboxylate (ACC) is a major component of plant rhizosphere secretions and can be chemotactic for *Pseudomonas putida*. Therefore, when strawberry is attacked by pathogens, some root exudates will be secreted to attract *Pseudomonas putida* to colonize roots, and the key substances need to be explored further. In such a context, various indicators suggest that saprotrophic bacteria increase substantially in the rhizosphere soil of diseased plants, while a decrease in Actinobacteria implies weakened soil disease resistance, enhanced pathogenicity, microbial community imbalance, and degraded soil microbial ecosystem.

5. Conclusion

In the present study, the relationship between strawberry root rot occurrence and rhizosphere microbial community structure was explored across different rhizosphere soil and root surface soil niches in healthy and diseased strawberry. According to the results, incidence of strawberry root rot influenced microbial community diversity and drove fungal community composition in strawberry roots. However, the different niches selected specific bacterial groups, while the incidence of strawberry root rot had minimal effect on the bacterial community structure of strawberry roots. After strawberry was infected with pathogens, microbial interaction network stability also decreased, and more endophytic-plant pathogen groups and saprophytic functional groups were enriched, which led imbalance in soil microbial community structure. In addition, the number of culturable bacteria in the root surface soil of diseased plants was significantly higher than that in healthy plants. In summary, the present study provides a comprehensive analysis of rhizosphere microecology and root microbial community composition in healthy and diseased strawberry plants, offering a theoretical basis for the prevention and control of strawberry root rot from a microbial ecology perspective.

Data availability statement

The datasets presented in this study can be found in online repositories. The names of the repository/repositories and accession number(s) can be found at: the Picbio single reads for bacterial 16s

rRNA gene and fungal ITS regions have been deposited in NCBI SRA database using accession code PRJNA1011218.

Author contributions

MZ: Data curation, Formal analysis, Methodology, Writing – original draft. ZK: Data curation, Formal analysis, Methodology, Writing – original draft. HF: Formal analysis, Methodology, Writing – review & editing. XS: Methodology, Project administration, Writing – review & editing. QX: Methodology, Resources, Writing – review & editing. HL: Conceptualization, Writing – review & editing, Supervision. QG: Conceptualization, Writing – review & editing, Methodology, Visualization.

Funding

The author(s) declare financial support was received for the research, authorship, and/or publication of this article. This research was financially supported by the Qinchuangyuan Scientific and Technological Innovation Funds (no. 2021ZDZXNY-0005), the Science and Technology Major Project of Ordos (2022EEDSKJZDZX019), the Science and Technology Planning Project of Inner Mongolia Autonomous Region (2022YFHH0114), the Natural Science Foundation of Shaanxi Province (no. 2021JQ-151), and the Youth Project of National Natural Science Foundation of China (31600407).

Acknowledgments

The authors thank Transystom Editing and Translation Services for improving the English.

Conflict of interest

The authors declare that the research was conducted in the absence of any commercial or financial relationships that could be construed as a potential conflict of interest.

Publisher's note

All claims expressed in this article are solely those of the authors and do not necessarily represent those of their affiliated organizations, or those of the publisher, the editors and the reviewers. Any product that may be evaluated in this article, or claim that may be made by its manufacturer, is not guaranteed or endorsed by the publisher.

Supplementary material

The Supplementary material for this article can be found online at: https://www.frontiersin.org/articles/10.3389/fmicb.2023.1286740/full#supplementary-material

References

Abbas, A., Mubeen, M., Sohail, M. A., Solanki, M. K., Hussain, B., Nosheen, S., et al. (2022). Root rot a silent alfalfa killer in China: distribution, fungal, and oomycete pathogens, impact of climatic factors and its management. *Front. Microbiol.* 13:961794. doi: 10.3389/fmicb.2022.961794

Ahmed, M., and Focht, D. (1973). Degradation of polychlorinated biphenyls by two species of Achromobacter. *Can. J. Microbiol.* 19, 47–52. doi: 10.1139/m73-007

Anandhakumar, J., and Zeller, W. (2008). Biological control of red stele (Phytophthora fragariae var. fragariae) and crown rot (P. cactorum) disease of strawberry with rhizobacteria/Untersuchungen zur biologischen Bekämpfung der Roten Wurzelfäule und Rhizomfäule der Erdbeere (Phytophthora fragariae var. fragariae und F. cactorum) mit Rhizosphärebakterien. *J. Plant Dis. Protect.* 49–56.

Ashajyothi, M., Balamurugan, A., Patel, A., Krishnappa, C., Kumar, R., and Kumar, A. (2023). Cell wall polysaccharides of endophytic *Pseudomonas putida* elicit defense against rice blast disease. *J. Appl. Microbiol.* 134:lxac042. doi: 10.1093/jambio/lxac042

Bais, H. P., Weir, T. L., Perry, L. G., Gilroy, S., and Vivanco, J. M. (2006). The role of root exudates in rhizosphere interactions with plants and other organisms. *Annu. Rev. Plant Biol.* 57, 233–266. doi: 10.1146/annurev.arplant.57.032905.105159

Bulgarelli, D., Schlaeppi, K., Spaepen, S., Van Themaat, E. V. L., and Schulze-Lefert, P. (2013). Structure and functions of the bacterial microbiota of plants. *Annu. Rev. Plant Biol.* 64, 807–838. doi: 10.1146/annurev-arplant-050312-120106

Carrión, V. J., Perez-Jaramillo, J., Cordovez, V., Tracanna, V., De Hollander, M., Ruiz-Buck, D., et al. (2019). Pathogen-induced activation of disease-suppressive functions in the endophytic root microbiome. *Science* 366, 606–612. doi: 10.1126/science.aaw9285

Chen, D.-G. D., Peace, K. E., and Zhang, P. (2017a). *Clinical trial data analysis using R and SAS*. United Kingdom: CRC Press.

Chen, Z., Huang, J., Zhao, J., and Liang, H. (2017b). Research advance on the red stele root rot of strawberry. *Biotechnol. Bull.* 33:37. doi: 10.13560/j.cnki.biotech.bull.1985.2017.03.006

Cook, R. J., and Baker, K. F. (1983). *The nature and practice of biological control of plant pathogens*. American: Phytopathological Society.

Cullen, D., and Hirsch, P. R. (1998). Simple and rapid method fordirect extraction of microbial DNA fromsoil for PCR. *Soil Biol. Biochem.* 30, 983–993. doi: 10.1016/S0038-0717(98)00001-7

Curry, K. J., Abril, M., Avant, J. B., and Smith, B. J. (2002). Strawberry anthracnose: histopathology of *Colletotrichum* acutatum and *C. fragariae*. *Phytopathology* 92, 1055–1063. doi: 10.1094/PHYTO.2002.92.10.1055

Dinler, H., Benlioglu, S., and Benlioglu, K. (2016). Occurrence of fusarium wilt caused by *fusarium oxysporum* on strawberry transplants in Aydın Province in Turkey. *Aust Plant Dis Notes* 11, 1–3. doi: 10.1007/s13314-016-0196-3

Doumbou, C. L., Hamby Salove, M., Crawford, D. L., and Beaulieu, C. (2001). Actinomycetes, promising tools to control plant diseases and to promote plant growth. *Phytoprotection* 82, 85–102. doi: 10.7202/706219ar

Dueholm, M. S., Andersen, K. S., McIlroy, S. J., Kristensen, J. M., Yashiro, E., Karst, S. M., et al. (2020). Generation of comprehensive ecosystem-specific reference databases with species-level resolution by high-throughput full-length 16S rRNA gene sequencing and automated taxonomy assignment (AutoTax). *MBio* 11:1520. doi: 10.1128/mbio.01557-01520

Edgar, R. C. (2013). UPARSE: highly accurate OTU sequences from microbial amplicon reads. *Nat. Methods* 10, 996–998. doi: 10.1038/nmeth.2604

Edwards, J., Johnson, C., Santos-Medellín, C., Lurie, E., Podishetty, N. K., Bhatnagar, S., et al. (2015). Structure, variation, and assembly of the root-associated microbiomes of rice. *Proc. Natl. Acad. Sci.* 112, E911–E920. doi: 10.1073/pnas.1414592112

Emmett, B., Nelson, E. B., Kessler, A., and Bauerle, T. L. (2014). Fine-root system development and susceptibility to pathogen colonization. *Planta* 239, 325–340. doi: 10.1007/s00425-013-1989-7

Fang, X., Finnegan, P. M., and Barbetti, M. J. (2013). Wide variation in virulence and genetic diversity of binucleate Rhizoctonia isolates associated with root rot of strawberry in Western Australia. *PloS One* 8:e55877. doi: 10.1371/journal.pone.0055877

Furuno, S., Päzolt, K., Rabe, C., Neu, T. R., Harms, H., and Wick, L. Y. (2010). Fungal mycelia allow chemotactic dispersal of polycyclic aromatic hydrocarbon-degrading bacteria in water-unsaturated systems. *Environ. Microbiol.* 12, 1391–1398. doi: 10.1111/j.1462-2920.2009.02022.x

Gdanetz, K., and Trail, F. (2017). The wheat microbiome under four management strategies, and potential for endophytes in disease protection. *Phytobiomes* 1, 158–168. doi: 10.1094/PBIOMES-05-17-0023-R

Gibbons, S. M., Jones, E., Bearquiver, A., Blackwolf, F., Roundstone, W., Scott, N., et al. (2014). Human and environmental impacts on river sediment microbial communities. *PloS One* 9:e97435. doi: 10.1371/journal.pone.0097435

Gu, Z., Wang, M., Wang, Y., Zhu, L., Mur, L. A. J., Hu, J., et al. (2020). Nitrate stabilizes the rhizosphere fungal community to suppress fusarium wilt disease in cucumber. *Mol. Plant Microbe Interact.* 33, 590–599. doi: 10.1094/MPMI-07-19-0198-R

Han, Q., Ma, Q., Chen, Y., Tian, B., Xu, L., Bai, Y., et al. (2020). Variation in rhizosphere microbial communities and its association with the symbiotic efficiency of rhizobia in soybean. *ISME J.* 14, 1915–1928. doi: 10.1038/s41396-020-0648-9

Henríquez, T., Hsu, J.-S., Hernandez, J. S., Kuppermann, S., Eder, M., and Jung, H. (2023). Contribution of uncharacterized target genes of MxtR/ErdR to carbon source utilization by *Pseudomonas putida* KT2440. *Microbiol Spectr* 11, e02923–e02922. doi: 10.1128/spectrum.02923-22

Hinsinger, P., Plassard, C., Tang, C., and Jaillard, B. (2003). Origins of root-mediated pH changes in the rhizosphere and their responses to environmental constraints: a review. *Plant and Soil* 248, 43–59. doi: 10.1023/A:1022371130939

Inclán, R., De la Torre, D., Benito, M., and Rubio, A. (2007). Soil CO 2 efflux in a mixed pine-oak forest in Valsaín (Central Spain). *Sci. World J.* 7, 166–174. doi: 10.1100/tsw.2007.7

Juber, K. S., Al-Juboory, H. H., and Al-Juboory, S. B. (2014). Fusarium wilt disease of strawberry caused by *Fusarium oxysporum* f. sp. Fragariae in Iraq and its control. *J. Exp. Biol. Agric. Sci.* 2, 419–427. doi: 10.13140/RG.2.2.35459.14889

Khan, M. U., Li, P., Amjad, H., Khan, A. Q., Arafat, Y., Waqas, M., et al. (2019). Exploring the potential of overexpressed OsCIPK2 rice as a nitrogen utilization efficient crop and analysis of its associated rhizo-compartmental microbial communities. *Int. J. Mol. Sci.* 20:3636. doi: 10.3390/ijms20153636

Lane, D. (1991). *16S/23S rRNA sequencing. Nucleic acid techniques in bacterial systematics*. United Kingdom: Wiley.

Lehmann, J., Bossio, D. A., Kögel-Knabner, I., and Rillig, M. C. (2020). The concept and future prospects of soil health. *Nat Rev Earth Environ* 1, 544–553. doi: 10.1038/s43017-020-0080-8

Li, T., Zhang, J., Shen, C., Li, H., and Qiu, L. (2019). 1-Aminocyclopropane-1-carboxylate: a novel and strong chemoattractant for the plant beneficial rhizobacterium *Pseudomonas putida* UW4. *Mol. Plant Microbe Interact.* 32, 750–759. doi: 10.1094/MPMI-11-18-0317-R

Liao, L. B., Chen, X. X., Xiang, J., Zhang, N. N., Wang, E. T., and Shi, F. S. (2022). Zanthoxylum bungeanum root-rot associated shifts in microbiomes of root endosphere, rhizosphere, and soil. *PeerJ* 10:e13808. doi: 10.7717/peerj.13808

Liu, J., Li, C., Jing, J., Zhao, P., Luo, Z., Cao, M., et al. (2018). Ecological patterns and adaptability of bacterial communities in alkaline copper mine drainage. *Water Res.* 133, 99–109. doi: 10.1016/j.watres.2018.01.014

Lunt, D., and Evans, W. (1970). The microbial metabolism of biphenyl. *Biochem. J.* 118, 54P–55P. doi: 10.1042/bj1180054Pb

Nannipieri, P., Ascher, J., Ceccherini, M., Landi, L., Pietramellara, G., and Renella, G. (2003). Microbial diversity and soil functions. *Eur. J. Soil Sci.* 54, 655–670. doi: 10.1046/j.1351-0754.2003.0556.x

Nguyen, N. H., Song, Z., Bates, S. T., Branco, S., Tedersoo, L., Menke, J., et al. (2016). FUNGuild: an open annotation tool for parsing fungal community datasets by ecological guild. *Fungal Ecol.* 20, 241–248. doi: 10.1016/j.funeco.2015.06.006

Nilsson, R. H., Larsson, K.-H., Taylor, A. F. S., Bengtsson-Palme, J., Jeppesen, T. S., Schigel, D., et al. (2019). The UNITE database for molecular identification of fungi: handling dark taxa and parallel taxonomic classifications. *Nucleic Acids Res.* 47, D259–D264. doi: 10.1093/nar/gky1022

Osman, K. T., and Osman, K. T. (2013). Soil resources and soil degradation. *Soils: principles, properties and management*. Netherlands: Springer Netherlands. 175–213.

Parikka, P., Vestberg, M., Karhu, S., Haikonen, T., and Hautsalo, J. (2017). "Possibilities for biological control of red core (Phytophthora fragariae)", in: *VIII international strawberry symposium* 1156), 751–756.

Peng, G.-S., and Wu, J. (2016). Optimal network topology for structural robustness based on natural connectivity. *Physica A Stat Mechan Appl* 443, 212–220. doi: 10.1016/j.physa.2015.09.023

Philippot, L., Raaijmakers, J. M., Lemanceau, P., and Van Der Putten, W. H. (2013). Going back to the roots: the microbial ecology of the rhizosphere. *Nat. Rev. Microbiol.* 11, 789–799. doi: 10.1038/nrmicro3109

Pieterse, C. M., Zamioudis, C., Berendsen, R. L., Weller, D. M., Van Wees, S. C., and Bakker, P. A. (2014). Induced systemic resistance by beneficial microbes. *Annu. Rev. Phytopathol.* 52, 347–375. doi: 10.1146/annurev-phyto-082712-102340

Rahman, M., and Louws, F. J. (2017). Epidemiological significance of crown rot in the fruiting field in relation to *Colletotrichum* gloeosporioides infection of strawberry nursery plants. *Plant Dis.* 101, 907–915. doi: 10.1094/PDIS-06-16-0802-RE

Read, D. B., Bengough, A. G., Gregory, P. J., Crawford, J. W., Robinson, D., Scrimgeour, C., et al. (2003). Plant roots release phospholipid surfactants that modify the physical and chemical properties of soil. *New Phytol.* 157, 315–326. doi: 10.1046/j.1469-8137.2003.00665.x

Restrepo, O. M. D., Flores, J. C. M., and Arboleda, F. M. (2016). Influence of management systems on the nitrogen mineralization and fertilization of sugarcane. *Revista Facultad Nacional de Agronomía Medellín* 69, 7755–7762. doi: 10.15446/rfna.v69n1.54742

Riley, D., and Barber, S. (1969). Bicarbonate accumulation and pH changes at the soybean (*Glycine max* (L.) Merr.) root-soil interface. *Soil Sci. Soc. Am. J.* 33, 905–908. doi: 10.2136/sssaj1969.03615995003300060031x

Sánchez, S., Gambardella, M., Henríquez, J., and Díaz, I. (2013). First report of crown rot of strawberry caused by Macrophomina phaseolina in Chile. *Plant Dis.* 97:996. doi: 10.1094/PDIS-12-12-1121-PDN

Sansupa, C., Wahdan, S. F. M., Hossen, S., Disayathanoowat, T., Wubet, T., and Purahong, W. (2021). Can we use functional annotation of prokaryotic taxa (FAPROTAX) to assign the ecological functions of soil bacteria? *Appl. Sci.* 11:688. doi: 10.3390/app11020688

Shankar, R., Harsha, S., and Bhandary, R. (2014). *A practical guide to identification and control of tomato diseases*. India: Tropica Seeds PVT Ltd.

Shrestha, R. K., and Lal, R. (2011). Changes in physical and chemical properties of soil after surface mining and reclamation. *Geoderma* 161, 168–176. doi: 10.1016/j.geoderma.2010.12.015

Siegieda, D., Panek, J., and Frąc, M. (2023). Plant and soil health in organic strawberry farms–greater importance of fungal trophic modes and networks than α-diversity of the mycobiome. *Appl. Soil Ecol.* 188:104925. doi: 10.1016/j.apsoil.2023.104925

Stackebrandt, E., and Goebel, B. M. (1994). Taxonomic note: a place for DNA-DNA reassociation and 16S rRNA sequence analysis in the present species definition in bacteriology. *Int. J. Syst. Evol. Microbiol.* 44, 846–849. doi: 10.1099/00207713-44-4-846

Stringlis, I. A., Yu, K., Feussner, K., de Jonge, R., Van Bentum, S., Van Verk, M. C., et al. (2018). MYB72-dependent coumarin exudation shapes root microbiome assembly to promote plant health. *Proc. Natl. Acad. Sci.* 115, E5213–E5222. doi: 10.1073/pnas.1722335115

Su, D., Chen, S., Zhou, W., Yang, J., Luo, Z., Zhang, Z., et al. (2022). Comparative analysis of the microbial community structures between healthy and anthracnose-infected strawberry rhizosphere soils using Illumina sequencing Technology in Yunnan Province, Southwest of China. *Front. Microbiol.* 13:881450. doi: 10.3389/fmicb.2022.881450

Sun, S., Li, S., Avera, B. N., Strahm, B. D., and Badgley, B. D. (2017). Soil bacterial and fungal communities show distinct recovery patterns during forest ecosystem restoration. *Appl. Environ. Microbiol.* 83, e00966–e00917. doi: 10.1128/AEM.00966-17

Timmis, K., and Ramos, J. L. (2021). The soil crisis: The need to treat as a global health problem and the pivotal role of microbes in prophylaxis and therapy. *J. Microbial. Biotechnol.* 14, 769–797. doi: 10.1111/1751-7915.13771

Van der Putten, W. H., Bardgett, R. D., Bever, J. D., Bezemer, T. M., Casper, B. B., Fukami, T., et al. (2013). Plant–soil feedbacks: the past, the present and future challenges. *J. Ecol.* 101, 265–276. doi: 10.1111/1365-2745.12054

Walters, D., and Bingham, I. (2007). Influence of nutrition on disease development caused by fungal pathogens: implications for plant disease control. *Ann. Appl. Biol.* 151, 307–324. doi: 10.1111/j.1744-7348.2007.00176.x

Wang, L., Liu, J., Zhang, M., Wu, T., and Chai, B. (2023). Ecological processes of bacterial and fungal communities associated with Typha orientalis roots in wetlands were distinct during plant development. *Microbiol Spectr* 11, e05051–e05022. doi: 10.1128/spectrum.05051-22

Wang, Y., Zhang, R., Zheng, Q., Deng, Y., Van Nostrand, J. D., Zhou, J., et al. (2016). Bacterioplankton community resilience to ocean acidification: evidence from microbial network analysis. *ICES J. Mar. Sci.* 73, 865–875. doi: 10.1093/icesjms/fsv187

Weller, D. M., Raaijmakers, J. M., Gardener, B. B. M., and Thomashow, L. S. (2002). Microbial populations responsible for specific soil suppressiveness to plant pathogens. *Annu. Rev. Phytopathol.* 40, 309–348. doi: 10.1146/annurev.phyto.40.030402.110010

Whitaker, V. M., Knapp, S. J., Hardigan, M. A., Edger, P. P., Slovin, J. P., Bassil, V. N., et al. (2020). A roadmap for research in octoploid strawberry. *Horticult Res* 7:33. doi: 10.1038/s41438-020-0252-1

Wu, M.-H., Chen, S.-Y., Chen, J.-W., Xue, K., Chen, S.-L., Wang, X.-M., et al. (2021). Reduced microbial stability in the active layer is associated with carbon loss under alpine permafrost degradation. *Proc. Natl. Acad. Sci.* 118:e2025321118. doi: 10.1073/pnas.2025321118

Yang, J., Wei, S., Su, D., Zhang, Z., Chen, S., Luo, Z., et al. (2020). Comparison of the rhizosphere soil microbial community structure and diversity between powdery mildew-infected and noninfected strawberry plants in a greenhouse by high-throughput sequencing technology. *Curr. Microbiol.* 77, 1724–1736. doi: 10.1007/s00284-020-01948-x

Yi, M., Zhang, L., Li, Y., and Qian, Y. (2022). Structural, metabolic, and functional characteristics of soil microbial communities in response to benzo [a] pyrene stress. *J. Hazard. Mater.* 431:128632. doi: 10.1016/j.jhazmat.2022.128632

Yim, B., Smalla, K., and Winkelmann, T. (2013). Evaluation of apple replant problems based on different soil disinfection treatments—links to soil microbial community structure? *Plant and Soil* 366, 617–631. doi: 10.1007/s11104-012-1454-6

Youssef, R. A., and Chino, M. (1989). Root-induced changes in the rhizosphere of plants. I. pH changes in relation to the bulk soil. *Soil Sci. Plant Nutr.* 35, 461–468. doi: 10.1080/00380768.1989.10434779

Zhang, Z., Gai, L., Hou, Z., Yang, C., Ma, C., Wang, Z., et al. (2010). Characterization and biotechnological potential of petroleum-degrading bacteria isolated from oil-contaminated soils. *Bioresour. Technol.* 101, 8452–8456. doi: 10.1016/j.biortech.2010.05.060

Zhang, J., Liu, Y.-X., Zhang, N., Hu, B., Jin, T., Xu, H., et al. (2019). NRT1. 1B is associated with root microbiota composition and nitrogen use in field-grown rice. *Nat. Biotechnol.* 37, 676–684. doi: 10.1038/s41587-019-0104-4

Zhao, Y., Sun, C., Wang, S., Zhang, M., Li, Y., Xue, Q., et al. (2023). Widely targeted metabolomic, transcriptomic, and metagenomic profiling reveal microbe–plant–metabolic reprogramming patterns mediated by *Streptomyces pactum* Act12 enhance the fruit quality of *Capsicum annuum* L. *Food Res. Int.* 166:112587. doi: 10.1016/j.foodres.2023.112587

Zheng, Y., Wang, J., Zhao, W., Cai, X., Xu, Y., Chen, X., et al. (2022). Effect of bacterial wilt on fungal community composition in rhizosphere soil of tobaccos in tropical Yunnan. *Plant Pathol J* 38, 203–211. doi: 10.5423/PPJ.OA.03.2022.0035

frontiers | Frontiers in Microbiology

TYPE Original Research
PUBLISHED 20 November 2023
DOI 10.3389/fmicb.2023.1295722

OPEN ACCESS

EDITED BY
Jian-Wei Guo,
Kunming University, China

REVIEWED BY
Nagaraju Yalavarthi,
National Bureau of Agriculturally Important Microorganisms (ICAR), India
Wei Jiang,
Western Sydney University, Australia

*CORRESPONDENCE
XingWang Ma
✉ maxw2001@163.com

†These authors have contributed equally to this work

RECEIVED 17 September 2023
ACCEPTED 19 October 2023
PUBLISHED 20 November 2023

CITATION
Shi Y, Niu X, Chen B, Pu S, Ma H, Li P, Feng G and Ma X (2023) Chemical fertilizer reduction combined with organic fertilizer affects the soil microbial community and diversity and yield of cotton. *Front. Microbiol.* 14:1295722. doi: 10.3389/fmicb.2023.1295722

Chemical fertilizer reduction combined with organic fertilizer affects the soil microbial community and diversity and yield of cotton

YingWu Shi[1,2,3†], XinXiang Niu[2,4†], BaoZhu Chen[2,4], ShengHai Pu[2,4], HongHong Ma[2,4], Pan Li[2,4], GuangPing Feng[2,4] and XingWang Ma[2,4*]

[1]Institute of Microbiology, Xinjiang Academy of Agricultural Sciences, Urumqi, Xinjiang, China, [2]Key Laboratory of Agricultural Environment in Northwest Oasis of Ministry of Agriculture and Countryside, Urumqi, Xinjiang, China, [3]Xinjiang Laboratory of Special Environmental Microbiology, Urumqi, Xinjiang, China, [4]Institute of Soil, Fertilizer and Agricultural Water Conservation, Xinjiang Academy of Agricultural Sciences, Urumqi, Xinjiang, China

Introduction: The soil microbial community plays an important role in modulating cotton soil fertility. However, the effects of chemical fertilizer combined with organic fertilizer on soil chemical properties, microbial community structure, and crop yield and quality in arid areas are still unclear. This study aimed to explore the effects of different organic fertilizers on soil microbial community structure and diversity and cotton growth and yield.

Methods: High-throughput sequencing was used to study the soil bacteria and fungi in different growth stages of cotton. The field fertilization experiment had five treatments.

Results: The results indicated that the treatments of chemical fertilizer reduction combined with organic fertilizer significantly increased soil available nitrogen and phosphorus in cotton field. There were significant differences in the abundance of the bacterial and fungal communities in the dominant phyla among the treatments. At the phyla level, there were not significantly different in the diversity of bacteria and fungi among treatments. There were significant differences in the composition and diversity of bacterial and fungal communities during the entire cotton growth period ($p = 0.001$). The rhizosphere bacterial and fungal community structure was significantly affected by soil TK, NH_4^+, AK, TP, AN, and NO_3^-. The different fertilization treatments strongly influenced the modular structure of the soil bacterial and fungal community co-occurrence network. A reduction in chemical fertilizer combined with organic fertilizer significantly improved cotton stem diameter and seed yield, and the effect of the biological organic fertilizer on plant growth and yield formation was greater than that of ordinary organic fertilizer.

Discussion: This study provide a scientific and technical basis for the establishment of environmentally friendly green fertilization technology for cotton in arid areas and the promotion of sustainable development of cotton industry.

KEYWORDS

cotton, Illumina MiSeq, organic fertilizer, reduced chemical fertilizer, soil microbial community, yield

1 Introduction

Xinjiang is the largest commodity cotton base in China (Niu et al., 2021). Applying chemical fertilizer increases the number of bolls per plant, reduces the bud and boll abscission rate, and increases cotton yields (Zheng et al., 2015). However, the long-term use of chemical fertilizers can lead to a deterioration in soil physicochemical properties, resulting in agricultural non-point source pollution, which can lead to sustained increases in fertilizer use and water, air, and soil pollution (Zhou et al., 2011). Excessive nitrogen fertilizer inputs not only waste resources, but also lead to environmental pollution and soil degradation (Chen J. S. et al., 2021).

It has become an urgent challenge in agricultural production to identify reasonable fertilization measures that reduce the harm caused by excessive soil fertilizer applications. Chemical fertilizer reduction combined with organic fertilizer is an environmental protection fertilization technology (Ye et al., 2020). Appropriate organic fertilizer substitution promotes crop yield, improves soil nutrients and protects soil ecology (Ding et al., 2021; Li et al., 2021a,b; Xiao et al., 2022).

Organic fertilizer combined with chemical fertilizer can reduce nutrient losses in cotton fields (Adeli et al., 2008), improve the fertilizer utilization rate, and increase soil organic matter content (Mensik et al., 2018; Wang et al., 2022). This fertilization method activate soil nutrients, improve soil microbial community structure and diversity (Guo et al., 2019; Zhang et al., 2019; Dong et al., 2020), and change rhizosphere soil enzyme activity. It enhance soil microbial activity, improve soil fertility, and reduce soil salinization and soil-borne diseases (Halihashi et al., 2020; Zhang et al., 2021). Then it improve crop root activity (Wang et al., 2022), antioxidant enzyme activity (Tang et al., 2018), and leaf pigment content (Wang N. et al., 2020; Wang Y. et al., 2020; Wang Q. Q. et al., 2020). It also increases water and fertilizer conservation and ultimately improves crop yield and stress resistance.

One study reported that 80% conventional fertilization combined with moderate amino acid, fulvic acid, and biogas slurry inputs produced the highest cotton yield and benefit (Li et al., 2019), and was significantly higher than that produced by conventional fertilization (Li et al., 2019). Previous studies have shown that when the amount of organic fertilizer was the same, and there was no significant difference in cotton yield between different types of organic fertilizer treatments (Tao et al., 2017; Li et al., 2019; Sun et al., 2020). The application of 70% chemical fertilizer combined with green manure did not reduce the nutrient accumulation, seed cotton yield and fertilizer utilization rate of cotton plant (Li et al., 2019). Furthermore, the agronomic efficiency of chemical fertilizer was significantly higher than that for the 100 and 85% chemical fertilizer treatments, and the seed cotton yield increased by nearly 30% (Sun et al., 2015; Li et al., 2021a,b). The improvement in phosphorus use efficiency after applying biological organic fertilizer is better than that achieved by applying ordinary organic fertilizer. The replacement of 40% chemical fertilizer with bio-organic fertilizer significantly increased cashmere length and yield (Sun et al., 2020). Chemical fertilizer combined with organic fertilizer also significantly increased the number of bacteria and actinomycetes, decreased the number of fungi, and increased urease, catalase, sucrose, and alkaline phosphatase activities (Wang N. et al., 2020; Wang Y. et al., 2020; Wang Q. Q. et al., 2020). Reducing nitrogen fertilization by 30% can reduce soil electrical conductivity and improve soil nutrient content, which will ultimately increase cotton yield and quality (Zhu et al., 2020). It can be seen that chemical fertilizer reduction combined with organic fertilizer is economically feasible. Few studies have investigated the effect of replacing chemical fertilizer with organic fertilizer on microorganisms and cotton growth traits and yield.

In this study, ordinary organic fertilizer, humic acid urea, biological bacterial fertilizer substitution, and conventional fertilization were taken as the research objects. Field experiments were used to investigate the effects of different fertilization regimes on cotton yield, soil nutrients, and the microbial community. In addition, the scientific and economic efficiency of combining chemical fertilizer reduction and organic fertilizer applications was also evaluated. The underlying hypotheses are that (I) the reduction of chemical fertilizer combined with organic fertilizer increases the content of soil nutrient in cotton fields; and (II) affects the community structures of soil microorganism over the whole cotton growth period.

2 Materials and methods

2.1 Field site and experimental design

The experiment was conducted at Xinjiang Academy of Agricultural Sciences in Korla City, Xinjiang, in 2020. The experimental area was located on Baotouhu Farm, Xinjiang Academy of Agricultural Sciences, Korla City, southern Xinjiang (E 85°52′, N 41°41′). The experimental area has a typical arid climate, the average annual rainfall is 56.20 mm. The tested soil was a medium fertility sandy loam soil, the soil organic matter in the 0–30 cm of soil above the plow layer was 10.24 g/kg, available nitrogen was 48.78 mg/kg, available phosphorus was 20.36 mg/kg, available potassium was 139.00 mg/kg, and the pH was 8.20.

The experiment consisted of five treatments (Supplementary Table S1): T1: no fertilizer application; T2: conventional fertilization (*CF*; NPK dosage: 714 kg/ha: 357 kg N/ha, 207 kg P/ha, and 150 kg K/ha); T3: 60% *CF* + 12,000 kg/ha organic fertilizer; T4: 46% *CF* + 428.4 kg/ha humic acid urea; and T5: 73% *CF* + 225 kg/ha bio-organic fertilizer. Each treatment was replicated three times and the area of each experimental plot was 40.5 m^2. Organic fertilizer refers to sheep manure. The nutrient contents of sheep manure were N 0.192%, P2O5 1.16%, K2O 0.82%, humic acid 19.04%, organic matter 56.05%, water content 51.50%. Humic acid urea is a urea containing 0.12% humic acid. The nutrient contents of *Bacillus velezensis* were N 0.357%, P2O5 0.09%, K2O 0.04%, humic acid 2.00%, organic matter 1.94%. The bio-organic fertilizer is a bacterial fertilizer produced by fermentation of *Bacillus velezensis* BHZ-29, which we isolated from cotton fields (Zhang et al., 2018).

The cotton variety was Xinluzhong 66. The common organic fertilizer was used as a base fertilizer and applied to the 0–20 cm soil layer before sowing. The chemical fertilizers, humic acid urea, and bio-organic fertilizer were drip applied with water six times throughout the cotton growing season according to their fertilizer requirements (Niu et al., 2021).

2.2 Soil sampling and analysis of physicochemical properties

Soil samples from the 0–20 cm soil layer were collected by soil drilling at the cotton seedling stage (B), bud stage (M), flowering

stage (H), boll opening stage (T) in 2020. There were three replicates per treatment, a five-spot sampling method for each treatment. Each replicate collected 500 g soil samples. Plant residues and stones were removed from the soil samples using a 2 mm mesh sieve. Some of the samples were placed in a 4°C refrigerator for the determination of soil microbial diversity, whereas the others were stored under natural air drying to determine the soil physicochemical properties. The SPAD (Soil and Plant Analyzer Development) value of cotton leaves was measured at bud stage, flowering stage and boll stage (Chen et al., 2011). The agronomic traits, yield, and yield related factors were measured at the cotton boll opening stage and the harvest stage. Ten cotton plants were randomly selected from each plot before boll opening. The number of fruit branches per plant, plant height, and boll number per plant were measured. The yield was measured after drying and the seed cotton yield for the plot was calculated. The lint yield and lint percentage were calculated after rolling and the cotton quality index was determined by the Cotton Quality Supervision and Testing Center of the Ministry of Agriculture and Rural Areas (Wan et al., 2018; Chen et al., 2020).

Soil moisture content (WCR) was determined by the drying method. Soil organic matter (OM) was determined using potassium dichromate dilution heat method, total nitrogen (TN) was quantified by a Kjeldahl nitrogen analyzer (multi N/C 2100 S, Analytik Jena, Jena, Germany), alkaline nitrogen (AN) was measured using the diffusion method, soil ammonium nitrogen (NH4+) and nitrate (NO3-) was determined by flow analyzer, total phosphorus (TP) was determined by the acid-soluble-molybdenum-antimony colorimetric method, effective phosphorus (AP) was determined using sodium bicarbonate extraction-molybdenum antimony antispectrophotometry, total potassium (TK) was measured using an NaOH alkali fusion-flame photometer, and available potassium (AK) was determined using the ammonium acetate extraction-flame photometric method (Ma et al., 2022). Each analysis was repeated three times.

2.3 Extraction and sequencing of soil microbial DNA

The soil microbial DNA was extracted according to the Power Soil DNA Isolation Kit instructions (MoBio Laboratories, Carlsbad, CA, United States). The extracted DNA was detected by 1% agarose gel electrophoresis and spectrophotometry, and the qualified samples were stored at −20°C until needed. Primers 338F (5'-ACTCCTAC GGGAGGCAGCAG-3′) and 806R (5'-GGACTACHVGGGTWT CTAAT-3′) were used to amplify the V3–V4 region of bacterial 16S rRNA gene (Jones et al., 2021) and the primers for ITS gene sequencing of the fungi were ITS1F (5'-CTTGGTCATTT AGAGAAGTAA-3′) and ITS2 (5'-TGCGTTCTTCATCGATGC-3′) (Li S. et al., 2020; Li Y. et al., 2020). The above primers with barcode sequences were synthesized for the PCR amplification procedure. The PCR products were detected by 1.5% agarose gel electrophoresis, purified using a TIANgel nucleic acid purification kit (Tiangen, Beijing, China) and then used to construct a microbial diversity sequencing library. Paired-end sequencing was performed using the Illumina MiSeq high-throughput sequencing platform by Shanghai Majorbio Bio-pharm Technology Co., Ltd. (Shanghai, China).

2.4 Analysis method for the sequencing data

To improve the accuracy and reliability of the information analysis, the offline data were split into samples according to their Barcode sequence by QIIME1 (v 1.8.0) software. The data were filtered and spliced by Pear (v 0.9.6) software and the chimera sequences are removed using the Uchime method according to the Gold Database. Finally, the Vsearch (v 2.7.1) software UPARSE algorithm was used to cluster the high-quality sequences based on 97% consistency and the Silva128 database was used to annotate the OTUs (Operational Taxonomic Units) using the RDP Classifier algorithm. Then, the community composition of each sample was analyzed at the phylum, class, order, family, genus, and species levels to obtain the species composition and relative abundance at each taxonomic level (Shi et al., 2022). The α-diversity of each sample was calculated using Mothur 1.45.3 (Barouillet et al., 2022) and Excel 2007 (Microsoft, Redmond, WA, United States) software and included the Chao1 value, the Shannon index, and the Simpson index. Rarefaction curves were obtained from the ratio of the number of OTUs in the sample to the effective reads.

2.5 Data processing

Microsoft Excel 2007 was used for data pre-processing and presentation, and SPSS 20.0 (IBM Corp, Armonk, NY, United States) software was used for the one-way analysis of variance (ANOVA) and the Duncan method ($\alpha = 0.05$) for multiple comparisons and difference testing. The data are shown as the mean ± standard error. A principal coordinate analysis (PCoA) and a permutation multi-factor analysis of variance (Adonis) based on the sample Bray-Curtis distance (OTU level) were performed by R Studio (version 4.0.3), and a dominant OTU heat map and a correlation heat map were constructed. Canoco 5.1 was used to draw a redundancy analysis diagram (redundancy analysis, RDA) (Dalu et al., 2021). Finally, the Spearman's correlation coefficient was used to calculate the correlations among OTUs (relative abundance ≥0.1%) and OTUs with correlation coefficients of $r \geq 0.6$ and $p < 0.01$ were selected as data sources to construct the co-occurrence network for soil bacteria using Gephi (version 9.2) (Tang et al., 2018).

3 Results

3.1 Soil properties in response to chemical fertilizer reduction combined with organic fertilizer

It can be seen from Supplementary Table S2 that the treatments of chemical fertilizer reduction combined with organic fertilizer increased the contents of soil organic matter (OM), total nitrogen (TN), total phosphorus (TP), total potassium (TK), available nitrogen (AN), available phosphorus (AP) and available potassium (AK) in cotton field. Compared with T1, T3, T4 and T5 treatments significantly increased the content of soil available nitrogen and available phosphorus in cotton fields. The content of soil available nitrogen and available phosphorus in T3 treatment was the highest, reaching

32.33 mg / kg and 32.35 mg/kg. The trend of soil TN, TP, AN and AK in different fertilization treatments was T3 > T5 > T2 > T4 > T1. The content of SOM in each growth period of T3, T4 and T5 treatments showed an increasing trend. Except for T5, the total nitrogen of each treatment increased first and then decreased, and the total nitrogen of each treatment at flowering stage was the highest. Total phosphorus changed little in each period, and total potassium showed an increasing trend. Available nitrogen, phosphorus and potassium showed a downward trend.

3.2 Soil microbial alpha diversity

The 16S rRNA gene and ITS sequencing results showed that 2,616,391 and 3,812,536 original sequences were obtained from 60 samples. The samples contained 34,107–73,318 bacterial and 38,032–74,915 fungal sequences. The minimum numbers of sequences (34,107 and 38,032, respectively) were used as the sampling depth for the bacteria and fungi. The number of OTUs after flattening was 2,685–3,576 and 183–372 for bacteria and fungi, respectively (Table 1). There was no significant difference in the Chao1 indexes, Shannon indexes, and Simpson indexes for the rhizosphere bacterial and fungal communities among treatments (Table 2), indicating that chemical fertilizer reduction combined with organic fertilizer did not significantly change soil microbial α-diversity. The ACE, Chao and Shannon indexes of soil bacteria in the boll opening stage decreased significantly, and the ACE, Chao and Simpson indexes of soil fungi in the flowering and boll opening stages increased significantly.

3.3 Soil microbial community composition and structure

Among the five fertilization treatments, organic fertilizer combined with chemical fertilizer treatments (T3, T5) did not change the community structure of soil bacteria and fungi, but affected the bacterial abundance at different species classification levels (Figure 1). Among the five fertilization treatments, Proteobacteria, Actinobacteriota, Chloroflexi, Acidobacteriota, Gemmatimonadota, Firmicutes, Bacteroidota, and Ascomycota, Mortierellomycota, Basidiomycota, and Chytridiomycota were the dominant phyla in the bacterial and fungal communities, respectively (Figures 1A,D). Alphaproteobacteria, Actinobacteria, Gammaproteobacteria, Acidimicrobiia, Anaerolineae, Vicinamibacteria, Chloroflexia, Gemmatimonadetes, Bacilli, Dehalococcoidia, Thermoleophilia, Bacteroidia. KD4-96 was the dominant class of bacterial community (Figures 1B,E). The class with relative abundances greater than 2% in the T1, T2, T3, T4, and T5 treatments accounted for 73.11, 74.62, 73.11, 74.48, 73.76, 96.19, 95.91, 97.02, 96.69, and 92.94% of the total bacterial and fungal class, respectively (Figures 1B,E). With regards to the dominant genera of the bacterial and fungal community (relative abundance >1%), the T3 and T5 treatments increased the relative abundance of norank_f__norank_o__Vicinamibacterales, norank_f__Vicinamibacteraceae, norank_f__norank_o__norank_c__MB-A2-108 and Preussia compared to T1 and T2, but the norank_f__Gemmatimonadaceae and *Mortierella* relative abundances decreased (Figures 1C,F).

TABLE 1 Statistics of sample sequence of soil bacteria and funge under different treatments.

Treatment	Bacterial		Fungal	
	Sequences	OTUs	Sequences	OTUs
T1	540,418	6,731	769,780	770
T2	530,104	6,503	776,576	738
T3	511,787	6,645	744,029	746
T4	516,572	6,487	758,039	709
T5	517,510	6,660	764,112	774
Total	2,616,391	7,802	3,812,536	1,180

T1: no fertilizer application (CK); T2: Conventional fertilization (CF; NPK dosage: 714 kg ha−1: 357 kg N ha−1, 207 kg P ha−1, and 150 kg K ha−1); T3: 60% CF + 12,000 kg ha organic fertilizer (CFO; NPK dosage: 428.4 kg ha−1: 214.2 kg N ha−1, 124.2 kg P ha−1, and 90 kg K ha−1); T4: 46% CF + 428.4 kg ha humic acid urea (CFO; NPK dosage: 714 kg ha−1: 357 kg N ha−1, 207 kg P ha−1, and 150 kg K ha−1); T5: 73% CF + 225 kg ha bio-organic fertilizer (CFB; NPK dosage: 617.55 kg ha−1: 260.55 kg N ha−1, 207 kg P ha−1, and 150 kg K ha−1).

3.4 Dynamics of the soil microbial communities

The PCoA analysis showed that there are seasonal differences in the bacterial and fungal community structure among the samples (Figures 2A,B). The PC1 axis for bacteria and fungi explained 23.97 and 28.26% of the difference, respectively, and the PC2 axis explained 19.34 and 17.95%, respectively. Together, they explained 43.31 and 46.21% of the variability, respectively (Figures 2A,B). Figure 2 also showed that the dispersion degree of the samples at the bud, flowering, and boll stages was low. However, the dispersion degree was high for the samples at the seedling stage. There were significant differences in the community structures of the bacteria and fungi over the whole cotton growth period. The bacteria samples were highly clustered on the PC1 axis, which showed that the rhizosphere bacteria were highly similar in the samples, but the fungi were very different at the flowering stage.

The cluster analysis (Supplementary Figure S1) showed that there were significant differences in bacterial and fungal community composition among the samples at the bud, flowering, and boll stages, while the samples at the seedling stage were clustered on the same branch. The growth period had significant effects on the bacterial floras Actinobacteria, Gammaproteobacteria, Acidimicrobiia, Chloroflexia, Gemmatimonadetes, Dehalococcoidia, and Bacteroidia, and the fungal floras Leotiomycetes, Sordariomycetes, Mortierellomycetes, Eurotiomycetes, and Pezizomycetes were dominant in the five treatments (Supplementary Figure S2).

3.5 Correlation between bacterial and fungal abundance and soil properties

The Spearman's correlation heatmap analysis indicated that the soil physicochemical factors affecting the soil bacterial and fungal communities were TK, NH4, AK, TP, and AN and TP, AN, NO3, and TK, respectively (Supplementary Figure S3). The effect of soil physicochemical factors on *Bacillus* was weak and only TK, NH4, TP, and AN were significant factors. *Pseudounas* was sensitive to most soil physicochemical factors, except for NH4+ and NO3-. The physical and chemical factors OM and NH4+ had significant

10.3389/fmicb.2023.1295722

TABLE 2 Soil microbial diversity index of different treatment and different growth stages.

Microbe	Sampling time	Treatment	Ace	Chao	Shannon	Simpson	Coverage
Bacteria	B	T1	4536.67 ± 386.62[a]	4348.68 ± 71.06[a]	6.60 ± 0.04[a]	0.0046 ± 0.0009[a]	0.9683 ± 0.0038[a]
		T2	4117.57 ± 89.06[a]	4158.72 ± 110.67[a]	6.57 ± 0.06[a]	0.0052 ± 0.0012[a]	0.9680 ± 0.0016[a]
		T3	4358.96 ± 410.72[a]	4179.94 ± 203.59[a]	6.63 ± 0.02[a]	0.0041 ± 0.0005[a]	0.9688 ± 0.0025[a]
		T4	4596.39 ± 378.84[a]	4218.28 ± 62.83[a]	6.58 ± 0.10[a]	0.0059 ± 0.0025[a]	0.9694 ± 0.0039[a]
		T5	4376.90 ± 190.53[a]	4201.28 ± 147.43[a]	6.58 ± 0.04[a]	0.0048 ± 0.0005[a]	0.9655 ± 0.0005[a]
	M	T1	4489.46 ± 202.27[a]	4491.07 ± 241.34[a]	6.60 ± 0.03[a]	0.0041 ± 0.0006[a]	0.9806 ± 0.0023[a]
		T2	4380.59 ± 183.77[a]	4338.51 ± 201.31[a]	6.56 ± 0.06[a]	0.0044 ± 0.0002[a]	0.9803 ± 0.0016[a]
		T3	4234.93 ± 54.27[a]	4227.17 ± 95.44[a]	6.51 ± 0.04[a]	0.0056 ± 0.0013[a]	0.9799 ± 0.0005[a]
		T4	4504.83 ± 288.02[a]	4326.57 ± 131.56[a]	6.52 ± 0.07[a]	0.0044 ± 0.0007[a]	0.9788 ± 0.007[a]
		T5	4540.26 ± 87.55[a]	4506.48 ± 43.22[a]	6.63 ± 0.05[a]	0.0041 ± 0.0006[a]	0.9787 ± 0.0008[a]
	H	T1	4736.61 ± 342.15[a]	4482.58 ± 140.08[a]	6.59 ± 0.04[a]	0.0041 ± 0.0001[a]	0.9749 ± 0.0011[a]
		T2	4483.86 ± 181.42[a]	4534.25 ± 192.78[a]	6.60 ± 0.02[a]	0.0042 ± 0.0004[a]	0.9743 ± 0.0029[a]
		T3	4466.28 ± 152.33[a]	4444.78 ± 168.34[a]	6.62 ± 0.05[a]	0.0037 ± 0.0002[a]	0.9758 ± 0.0031[a]
		T4	4299.29 ± 157.52[a]	4325.31 ± 167.40[a]	6.54 ± 0.06[a]	0.0048 ± 0.0006[a]	0.9763 ± 0.0014[a]
		T5	4594.59 ± 117.60[a]	4445.61 ± 278.72[a]	6.58 ± 0.07[a]	0.0039 ± 0.0003[a]	0.9746 ± 0.0019[a]
	T	T1	4224.49 ± 94.45[a]	4183.12 ± 92.73[a]	6.46 ± 0.07[a]	0.0057 ± 0.0013[a]	0.9774 ± 0.0008[a]
		T2	4369.93 ± 353.65[a]	4106.09 ± 36.31[a]	6.40 ± 0.02[a]	0.0058 ± 0.0008[a]	0.9786 ± 0.0019[a]
		T3	4170.23 ± 300.76[a]	4135.48 ± 279.01[a]	6.47 ± 0.07[a]	0.0056 ± 0.0005[a]	0.9754 ± 0.0014[a]
		T4	4285.48 ± 348.73[a]	4081.21 ± 240.30[a]	6.42 ± 0.06[a]	0.0057 ± 0.0008[a]	0.9771 ± 0.0012[a]
		T5	4124.10 ± 75.04[a]	4092.05 ± 135.40[a]	6.46 ± 0.03[a]	0.0051 ± 0.0003[a]	0.9789 ± 0.0020[a]
Fungi	B	T1	282.49 ± 27.84[a]	289.42 ± 19.71[a]	2.93 ± 0.37[a]	0.1320 ± 0.0467[a]	0.9993 ± 0.0002[a]
		T2	248.09 ± 2.23[a]	246.76 ± 4.61[a]	2.54 ± 0.22[a]	0.2085 ± 0.0249[a]	0.9994 ± 0.0001[a]
		T3	240.42 ± 13.30[a]	238.33 ± 8.38[a]	2.22 ± 0.49[a]	0.3180 ± 0.1499[a]	0.9991 ± 0.0002[a]
		T4	254.79 ± 37.75[a]	252.25 ± 36.41[a]	2.64 ± 0.39[a]	0.2158 ± 0.0887[a]	0.9994 ± 0.0001[a]
		T5	264.64 ± 46.87[a]	265.95 ± 50.00[a]	2.94 ± 0.09[a]	0.1298 ± 0.0155[a]	0.9994 ± 0.0002[a]
	M	T1	265.26 ± 31.31[a]	274.97 ± 34.69[a]	2.37 ± 0.19[a]	0.2754 ± 0.0731[a]	0.9994 ± 0.0002[a]
		T2	290.41 ± 37.62[a]	288.43 ± 39.52[a]	2.67 ± 0.16[a]	0.2232 ± 0.0620[a]	0.9993 ± 0.0003[a]
		T3	275.90 ± 46.58[a]	278.92 ± 50.87[a]	3.08 ± 0.37[a]	0.1331 ± 0.0414[a]	0.9994 ± 0.0003[a]
		T4	265.84 ± 28.97[a]	268.43 ± 27.74[a]	2.67 ± 0.12[a]	0.1787 ± 0.0169[a]	0.9994 ± 0.0002[a]
		T5	293.79 ± 16.28[a]	294.81 ± 16.68[a]	2.78 ± 0.19[a]	0.1807 ± 0.0217[a]	0.9993 ± 0.0001[a]
	H	T1	309.92 ± 25.09[a]	314.01 ± 23.06[a]	2.27 ± 0.15[a]	0.3362 ± 0.0416[a]	0.9993 ± 0.0001[a]
		T2	341.50 ± 71.90[a]	340.29 ± 75.35[a]	2.30 ± 0.79[a]	0.3279 ± 0.1976[a]	0.9992 ± 0.0003[a]
		T3	341.95 ± 5.16[a]	337.49 ± 3.27[a]	2.34 ± 0.30[a]	0.3209 ± 0.0807[a]	0.9993 ± 0.0001[a]
		T4	335.95 ± 23.39[a]	340.77 ± 25.87[a]	2.37 ± 0.25[a]	0.3122 ± 0.0796[a]	0.9993 ± 0.0001[a]
		T5	332.84 ± 15.08[a]	326.19 ± 7.73[a]	2.34 ± 0.13[a]	0.2885 ± 0.0301[a]	0.9992 ± 0.0001[a]
	T	T1	352.05 ± 36.79[a]	360.53 ± 30.73[a]	2.44 ± 0.20[a]	0.3012 ± 0.0423[a]	0.9992 ± 0.0002[a]
		T2	349.80 ± 26.72[a]	341.89 ± 28.35[a]	2.35 ± 0.46[a]	0.2709 ± 0.1266[a]	0.9992 ± 0.0001[a]
		T3	341.93 ± 23.17[a]	342.91 ± 27.11[a]	2.47 ± 0.52[a]	0.2547 ± 0.0914[a]	0.9992 ± 0.0001[a]
		T4	336.92 ± 27.30[a]	339.55 ± 34.77[a]	2.13 ± 0.14[a]	0.3555 ± 0.0366[a]	0.9991 ± 0.0002[a]
		T5	293.64 ± 55.99[a]	313.67 ± 63.39[a]	2.30 ± 0.01[a]	0.2917 ± 0.0349[a]	0.9993 ± 0.0002[a]

Values indicate mean ± SE ($n = 3$). Different superscript letters in the columns represent significant differences among fertilizer treatments according to one-way ANOVA (Duncan's test, $p < 0.05$). The abbreviations T1, T2, T3, T4, and T5 are as defined in the footnote to Table 1. B: seedling stage; M: bud stage; H: flowering stage; T: boll opening stage.

effects on *Microascus*, and WCR and NO3 had significant effects on *Fusarium*, and NO3-had significant effects on *Tricharina* (Supplementary Figures S3A,B).

The RDA analysis showed that soil physicochemical factors explained 35.50% of the differences in the community structure of the dominant bacteria and fungi, and that RDA1 and RDA2 explained

10.3389/fmicb.2023.1295722

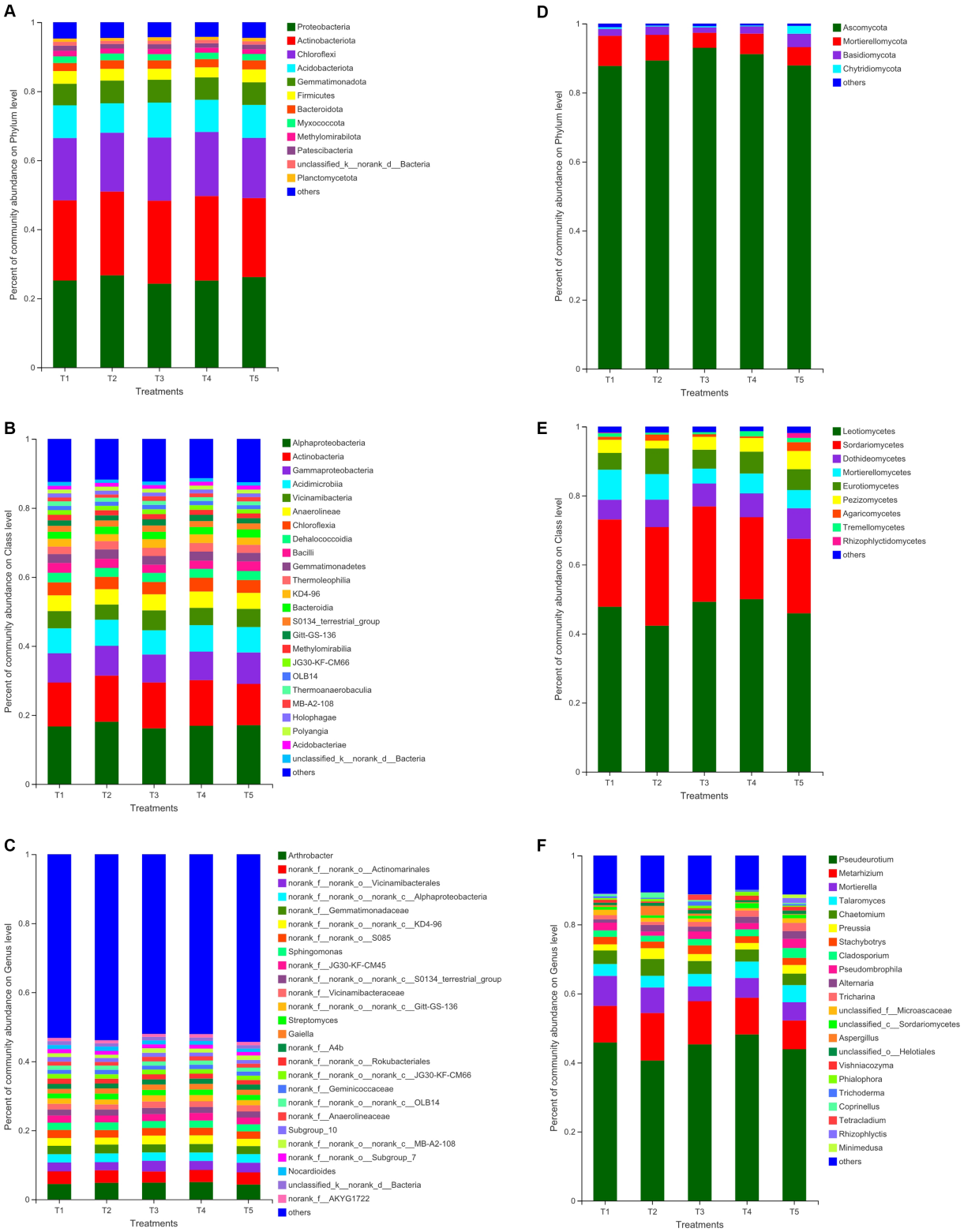

FIGURE 1
Relative abundances of bacterial **(A–C)** and fungal **(D–F)** taxa at the phylum, class, genus level, respectively. T1: no fertilizer application (CK); T2: Conventional fertilization (CF; NPK dosage: 714 kg ha-1: 357 kg N ha-1, 207 kg P ha-1, and 150 kg K ha-1); T3: 60% CF + 12,000 kg ha organic fertilizer (CFO; NPK dosage: 428.4 kg ha-1: 214.2 kg N ha-1, 124.2 kg P ha-1, and 90 kg K ha-1); T4: 46% CF + 428.4 kg ha humic acid urea (CFH; NPK dosage: 714 kg ha-1: 357 kg N ha-1, 207 kg P ha-1, and 150 kg K ha-1); T5: 73% CF + 225 kg ha bio-organic fertilizer (CFB; NPK dosage: 617.55 kg ha-1: 260.55 kg N ha-1, 207 kg P ha-1, and 150 kg K ha-1).

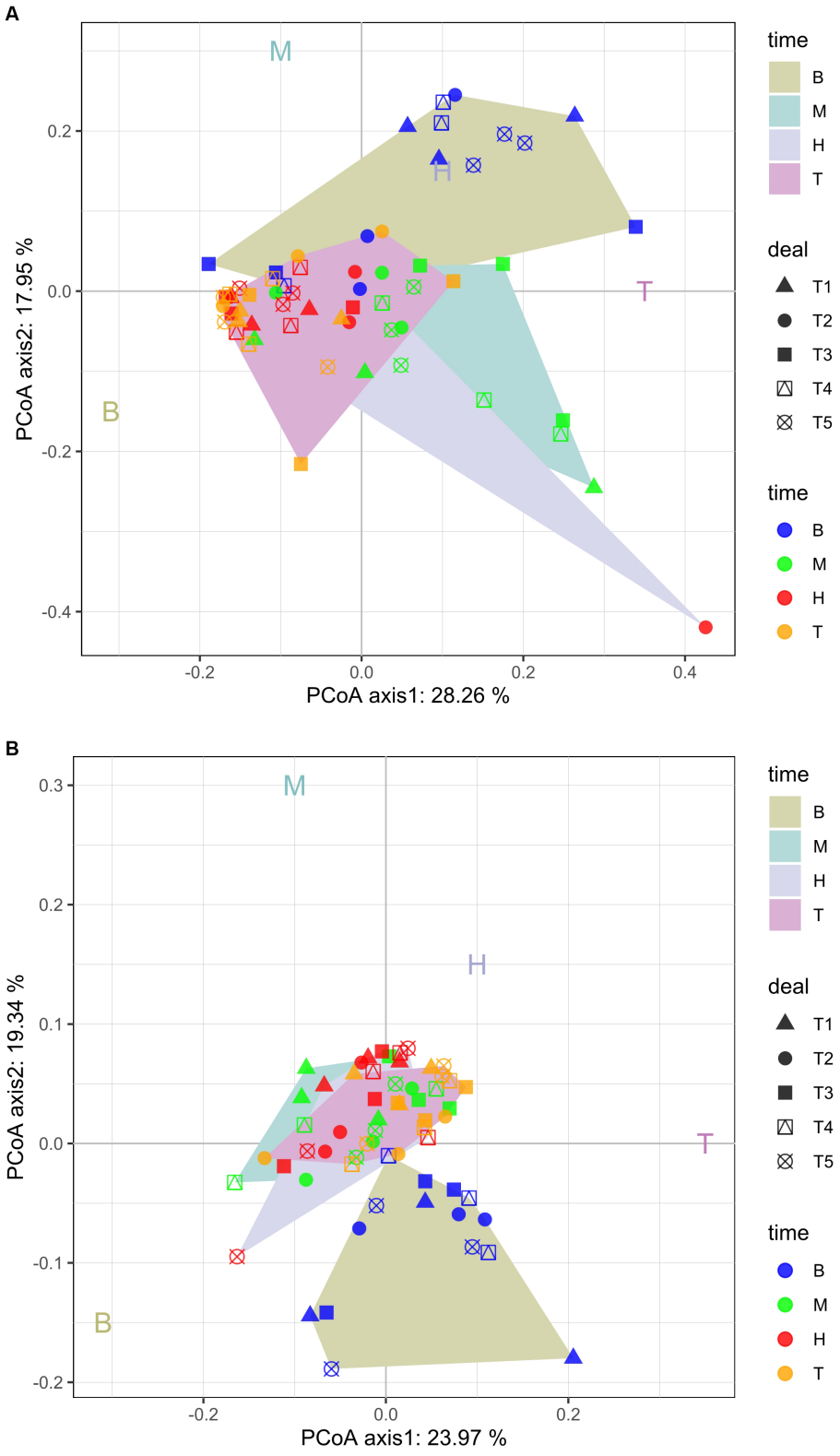

FIGURE 2
Principal coordinate analysis (PCoA) plots of bacterial **(A)** and fungal **(B)** community composition at the OTU level. T1, T2, T3, T4, and T5 are as defined in the Figure 1 legend. B: seedling stage: M: bud stage: H: flowering stage: T: boll opening stage.

29.09, 21.97 and 6.41%, 9.77% of the bacterial and fungal differences, respectively (Figure 3). Total phosphate ($R^2 = 0.75$, $p = 0.0000$), TK ($R^2 = 0.47$, $p = 0.0000$), and AN ($R^2 = 0.59$, $p = 0.0000$) for the bacterial community and TP ($R^2 = 0.17$, $p = 0.0012$), TK ($R^2 = 0.10$, $p = 0.0139$), and AN ($R^2 = 0.15$, $p = 0.0022$) for the fungal community reached significant levels (Figures 3A,B).

3.6 Soil microbial network structure and composition analysis

The soil bacterial and fungal co-occurrence networks under the T1, T2, T3, T4, and T5 treatments were composed of 251, 253, 247, 254, 361, and 84, 85, 87, 79, 84 nodes, respectively, and 3,698, 3,403, 3,071, 3,776, and 4,291, 308, 337, 332, 305, 297 had highly significantly positively correlated edges, with average degrees of 28.337, 26.901, 24.866, 29.732, 32.881, and 7.333, 7.929, 7.632, 7.722, 7.071, respectively (Figures 4A,B). The modular indexes were 3.249, 5.458, 2.793, 3.498, 2.955, and 1.798, 0.638, 0.757, 0.316, 1.965, respectively. A modularity index >0.4 indicates that the co-occurrence network has a modular structure.

Figure 4A also indicated that the bacterial co-occurrence networks for T1, T2, and T4 were similar, whereas the bacterial co-occurrence networks for T5 were relatively complex. The fungal co-occurrence networks for T1, T4, and T5 were similar, as were the fungal co-occurrence networks for T2 and T3 (Figure 4B).

Supplementary Table S3 showed that the proportions of the bacterial and fungal groups in the co-occurrence network were different in each treatment. The Proteobacteria and Actinobacteriota proportions were the largest in the bacterial co-occurrence network and the Ascomycota and Basidiomycota proportions were largest in the fungal co-occurrence network. The bacterial groups in each treatment were basically the same, but the number of fungal groups was lower in T3. In addition. Proteobacteria, Actinobacteriota, Chloroflexi, Bacteroidota, Acidobacteriota, Firmicutes, and Myxococcota were the dominant genera in the soil bacterial co-occurrence network and Pseudeurotium, Metarhizium, Talaromyces, Trichoderma, Preussia, Chaetomium, and Mortierella were the dominant genera in the soil fungal co-occurrence network.

3.7 Cotton agronomic traits, quality and yield

The T5 treatment produced the highest yield (Table 3). The four fertilization treatments significantly increased the boll number per plant and the seed cotton yield compared to T1 (Table 3). Compared to T2, the stem diameter and seed cotton yield significantly increased under the chemical fertilizer reduction combined with organic fertilizer treatments, but there was no significant difference in plant height, leaf number, SPAD, single boll weight, and lint percentage. This showed that organic fertilizer promoted cotton plant growth and boll formation, but had no significant effect on cotton yield per plant. The raw cotton yields of the chemical fertilizer reduction combined with organic fertilizer treatments were in the order T5 > T4 > T3 and the differences among the three treatments were significant. The raw cotton yields of T4 and T5 were 5.27 and 12.10% higher than those of T2, respectively, when T2 was reduced by 50 and 54%, combined with 428.4 kg hm^{-2} humic acid urea (T4) and 225 L hm-2 *Bacillus velezensis* fertilizer (T5), respectively, and there was no significant effect on cotton quality.

4 Discussion

4.1 Effects of fertilization on soil physicochemical properties

The proportion of soil available nutrients compared to the total soil nutrients is one of the important indicators used to evaluate the effectiveness of soil nutrients (Zhao and Huang, 2022). Reasonable combinations of organic and inorganic fertilizers can improve the soil physicochemical properties. In this study, we have demonstrated that reductions in chemical fertilizer combined with organic fertilizer could increase soil nutrients, such as AP, SOM and TN, which was consistent with previous studies on agricultural soils (Lu et al., 2009; Hossain et al., 2021; Yang W. N. et al., 2022). The increase in AP content by the fertilizer combined with organic fertilizer suggests that the organic fertilizer provided a large amount of soil organic matter (SOM), and then, organic matter decomposes under the action of microorganisms to produce a large number of organic acids, which can activate soil phosphorus, thereby increasing the soil AP content (Alori et al., 2017).

4.2 Effects of fertilization on the diversity and composition of soil microbial community

In microbial diversity studies, the greater the Shannon index, the higher the microbial community evenness; the higher the Chao1 and Ace indices, the higher the richness of the microbial communities (Hartmann et al., 2006). We also found that chemical fertilizer reduction combined with organic fertilizer increased soil bacterial richness and diversity, and reduced fungal richness and diversity (Table 2), which was consistent with previous studies that showed increased richness and diversity of the bacterial community, and decreased richness and diversity of the fungal community (Liu et al., 2021; Jin et al., 2022).

Microorganisms are an important part of the soil ecosystem. Their community composition and diversity show certain dynamic changes at different growth stages and under different nutritional statuses, fertilization measures, and tillage modes (Yang and Crowley, 2000; Wang et al., 2016; Liu et al., 2020; Iqbal et al., 2022). They are important indicators for evaluating soil fertility and are related to the occurrence of plant soil-borne diseases, continuous cropping obstacles, and soil acidification and salinization (Yao and Wu, 2010; Shen et al., 2016; Gao et al., 2021; Song et al., 2022). We found that there was little differentiation in the composition of bacterial or fungal communities among different fertilization treatments (Figures 2A,B). The reason might be that the soil organic matter content and microbial community diversity of long-term continuous cropping cotton field were low, and the organic matter content in fertilization treatment was not high.

4.3 Correlation between microorganism and soil physicochemical properties

Soil can directly provide the necessary environmental conditions for the survival of microorganisms (Santoyo et al., 2017). Organic fertilizer application can not only increase the total amount of soil nutrients such as soil total organic carbon, total nitrogen, and total phosphorus but can also increase the content of available soil nutrients (alkali nitrogen, available phosphorus, available potassium) (Liu et al., 2014; Qaswar et al., 2020). TP, TK, AN is significantly associated with the bacterial and fungal communities and is one of the main factors promoting changes in the soil microbial community (Dong et al.,

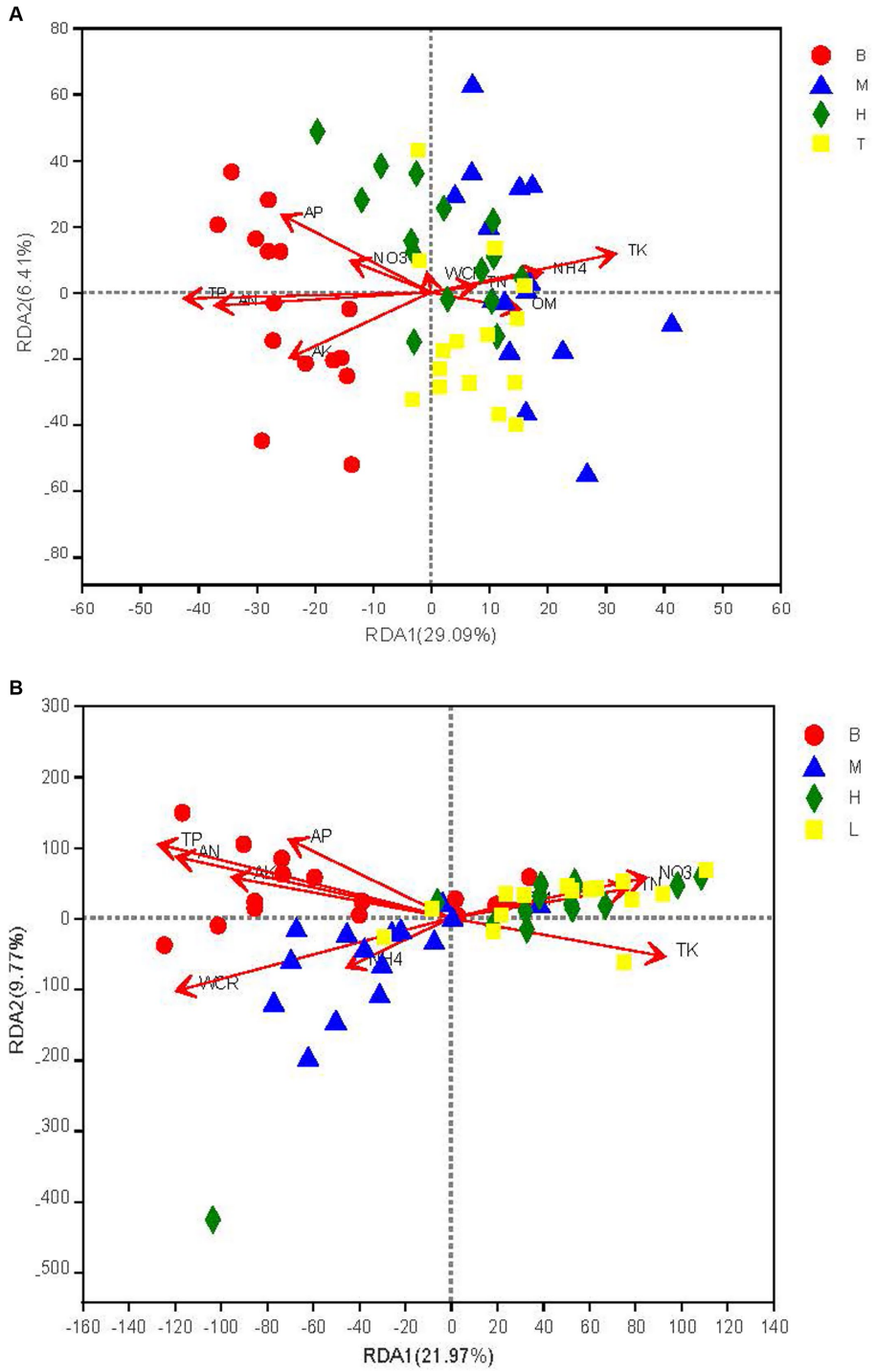

FIGURE 3
Redundancy analysis (RDA) of bacterial **(A)** and fungal **(B)** communities with soil chemical properties. WCR, electrical conductivity; OM, soil organic matter, NO3, electrical conductivity, NH4, soil organic matter.TN. total nitrogen: TP. total phosphorus: TK, total potassium; AN, total nitrogen, AP. total phosphorus: AK, total potassium. T1, T2, T3, T4, and T5 are as defined in the Figure 1 legend. B: seedling stage; M: bud stage, H: flowering stage. T. boll opening stage.

2014; Hu et al., 2019; Chen Y. et al., 2021; Li et al., 2021a,b; Zhao et al., 2021). Proteobacteria and Ascomycota is a dominant taxon in the bacterial and fungal community, separately and is positively correlated with the soil nitrogen, phosphorus and potassium pool; therefore, TP, TK, AN has been proven to drive changes in the soil bacterial and fungal community (Landesman and Dighton, 2010; Zhong et al., 2010; Ducousso-Détrez et al., 2022). In the present study, TP, TK, and AN were found to be the key determinants driving changes in the bacterial and fungal community in this study (Figures 3A,B; Supplementary Figures S3A,B), which was consistent with previous studies on soils (Landesman and Dighton, 2010; Zhong et al., 2010; Ducousso-Détrez et al., 2022).

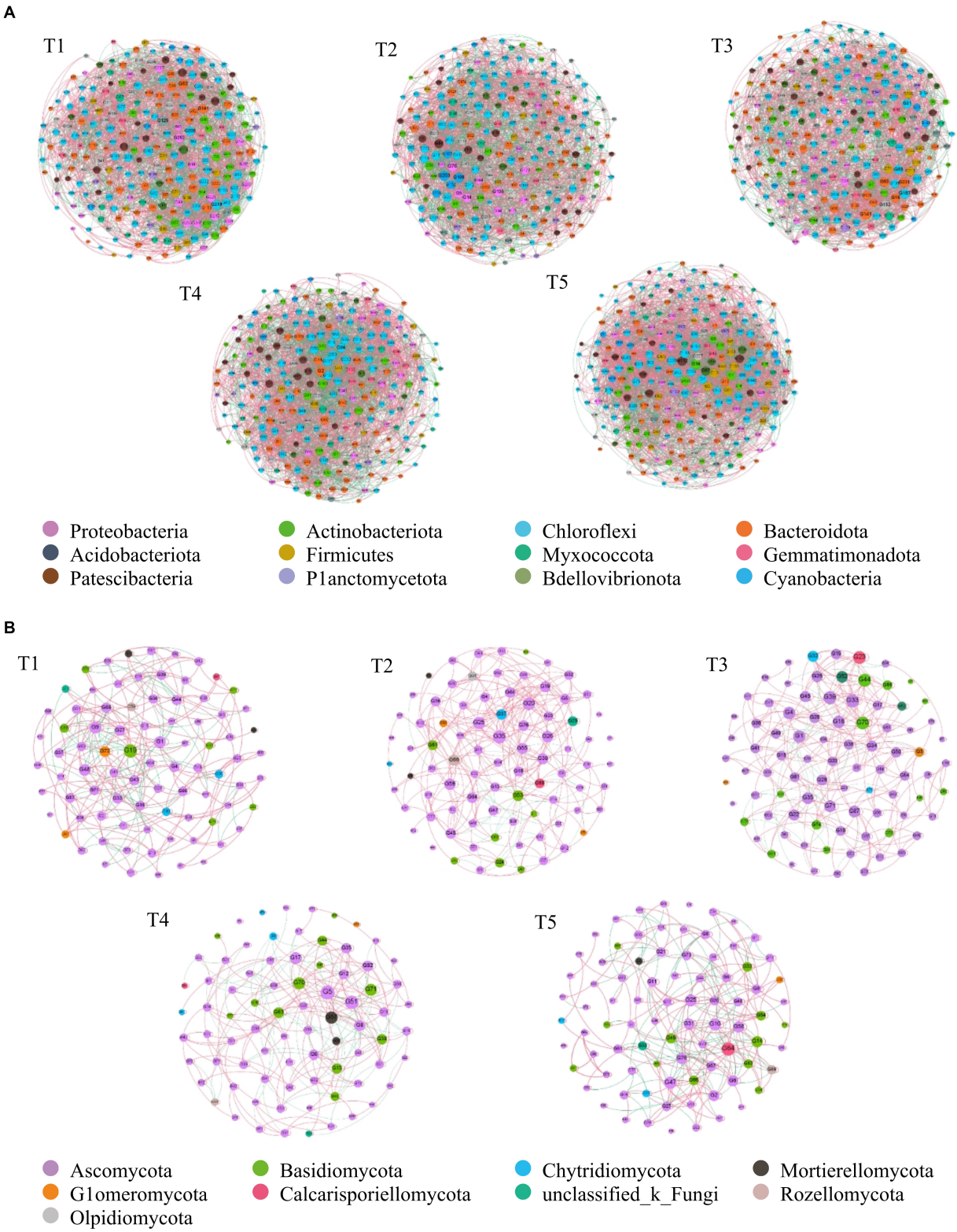

FIGURE 4
The co-occurrence network of soil bacterial and fungal community composition in a cotton field with different fertilization treatments on the phylum level. **(A)** bacterial community, **(B)** fungal community. Each node denotes a bacterial or a fungal OTU (defined at a 97% similarity level); each edge linking two nodes represents a positive (pink line) or negative (black line) relationship. OTUS are colored by different phylum. The size of each node is proportional to the number of connections. A connection between two nodes is a statistically significant ($p < 0.01$) and strong ($r > 0.60$) correlation. The percentage of positive links in every network: A 90.08%, B 73.87%.

TABLE 3 Effects of different fertilizer treatments on agronomic characters, quality and yield of cotton.

Parameters	Treatments				
	T1	T2	T3	T4	T5
Plant height	63.57 ± 12.28[a]	60.93 ± 8.04[a]	66.00 ± 9.46[a]	67.07 ± 10.97[a]	66.40 ± 6.49[a]
Number of blades	12.87 ± 1.46[b]	13.07 ± 1.80[a]	14.00 ± 1.65[a]	14.07 ± 1.28[a]	13.93 ± 1.91[a]
Stem diameter	9.14 ± 0.88[a]	8.91 ± 1.11[b]	9.65 ± 1.33a	9.71 ± 1.15[a]	9.87 ± 1.51[a]
SPAD	51.0 ± 9.64a	54.39 ± 12.09[a]	49.81 ± 11.95[a]	50.95 ± 14.44[a]	53.78 ± 14.22[a]
Boll number per plant	5.55 ± 1.35[b]	9.89 ± 0.70[a]	9.33 ± 0.67[a]	10.45 ± 3.24[a]	10.11 ± 2.37[a]
Boll weight	5.42 ± 0.27[a]	5.77 ± 0.20[a]	5.68 ± 0.11[a]	5.80 ± 0.18[a]	5.70 ± 0.35[a]
Lint percent	44.64 ± 0.38[a]	44.39 ± 0.54[a]	44.11 ± 0.16[a]	44.52 ± 0.43[a]	44.12 ± 0.53[a]
Raw cotton yield	309.47 ± 3.30[d]	427.68 ± 8.83[c]	418.43 ± 5.44[c]	450.2 ± .83[b]	479.43 ± 9.48[a]

Values indicate mean ± SE ($n = 3$). Different superscript letters in the columns represent significant differences among fertilizer treatments according to one-way ANOVA (Duncan's test, $p < 0.05$). The abbreviations T1, T2, T3, T4, and T5 are as defined in the footnote to Table 1.

Another study reported that SOM were the major driver on structuring soil microbial communities across land uses, while soil bacterial communities were more sensitive to variations in SOM and geochemical characteristics compared with fungi (Bahadori et al., 2022). This is inconsistent with our results and suggests that the effect of chemical fertilizer reduction combined with organic fertilizer on microbial community structure is not the only factor. This makes it difficult to assess the full effect of their nutritional potential on the soil microbial community in a short-term study period (Zhang et al., 2021). Therefore, the short-term effect of chemical fertilizer reduction combined with organic fertilizer on soil microbial community may be smaller than chemical fertilizer.

4.4 Co-occurrence networks for soil microorganisms in cotton fields

The network complexity became gradually more complicated as soil nutrient levels increased (Liao et al., 2020; Wang et al., 2021; Ye et al., 2021), indicating that the increase in the co-occurrence network complexity in the T5 treatment was closely related to the increases in SOM, TN, TP, and AP contents (Supplementary Table S2). The proportion of Proteobacteria in the T5 co-occurrence network was higher than that for the other treatments, but the Patescibacteria, Chloroflexi, and Planctomycetota proportions were lower than in the other treatments in our study (Supplementary Table S3). Proteobacteria are mainly distributed in the upper humus layer of farmland soil or the rhizosphere and are enriched in environments with high levels of active organic carbon (Pinhassi and Berman, 2003; Sagova-Mareckova et al., 2016). In contrast, Chloroflexi are oligotrophic bacteria with slow growth characteristics (Feng et al., 2022) and are ubiquitous in nutrient-poor soils (Wang N. et al., 2020; Wang Y. et al., 2020; Wang Q. Q. et al., 2020). When the substrate concentration of the microbial environment increased, the nutrient-rich bacteria replaced the oligotrophic bacteria and colonize the nutrient-rich environment, which strongly suggested that the T5 treatment improved the growth of nutrient-rich bacteria and restricted the growth of oligotrophic bacteria (Wang N. et al., 2020; Wang Y. et al., 2020; Wang Q. Q. et al., 2020).

The dominant groups are considered to be important drivers of microbial community structure and function (Banerjee et al., 2018). Zhang et al. (2017) found that Acinetobacter and Pseudomonas were the core functional bacteria in acid red soil paddy fields and that their relative abundances increased by 5.7–10 times over 31 years, indicating that bacterial communities experienced ecological succession, and that dominant bacteria occupied specific niches and had specific functions. In this study, Proteobacteria, Actinobacteriota, Chloroflexi, and Pseudeurotium, and Metarhizium and Talaromyces were the core genera of soil bacteria and fungi in the co-occurrence networks.

4.5 Effects of fertilization on agronomic traits and cotton yield

Combined applications of chemical fertilizer and organic fertilizer can regulate the release and intensity of soil and fertilizer nutrients, which means that crops can obtain stable and balanced amounts of nutrients at all growth stages (Zhao et al., 2016; Muhammad et al., 2020). This study showed that the chemical fertilizer reduction combined with organic fertilizer treatments increased cotton yields by different degrees, which is consistent with previous studies on cotton field soils (Bai et al., 2014). Previous studies have shown that the ratio of chemical fertilizer to organic fertilizer is related to soil fertility and climatic conditions (Ye et al., 2020). When soil fertility is high, increasing the proportion of organic fertilizer can promote reproduction by microorganisms, improve soil structure, and increase crop yields (Ye et al., 2020). Bioorganic fertilizers can replace 23–52% of nitrogen fertilizers without causing a loss of yield (Rose et al., 2014).

In this study, the effect of fertilizer reduction combined with bacterial fertilizer on yield increase was clear, indicating that the nutrient release law for organic fertilizer was consistent with the nutrient demand law for cotton growth. At the same time, crop yield was significantly correlated with soil nutrients, microorganisms, and related enzyme activities (Jiang et al., 2017). Therefore, reductions in chemical fertilizer and reasonable applications of organic fertilizer could effectively control the number of soil microorganisms, improved soil enzyme activity and soil fertility. At present, soil nutrient imbalances in cotton fields caused by unreasonable fertilization is common in Xinjiang (Gong et al., 2012; Yang J. Y. et al., 2022). The fertilization structure can be adjusted and optimized to reduce chemical fertilizer application rates through the combined use of chemical fertilizer and organic fertilizer. In this study, reducing chemical fertilizer by 30% combined with 12,000 kg·hm^{-2} common organic fertilizer or 225 kg·hm^{-2} bio-organic fertilizer produced the

highest yields, but the continuous application of organic fertilizer changed soil fertility. Therefore, future research should investigate the most appropriate proportion of organic fertilizer to apply to a field when combined with a chemical fertilizer application.

5 Conclusion

This study indicated that the reduction of chemical fertilizer combined with organic fertilizer significantly increased the content of soil available nitrogen and phosphorus in cotton fields, and that total and available nitrogen, phosphorus and potassium contents in the chemical fertilizer reduction combined with organic fertilizer treatments were basically stable in the cotton fields. The application of chemical fertilizer reduction combined with organic fertilizer significantly affected the community structures of the bacteria and fungi over the whole cotton growth period, without significantly changing the soil microbial alpha diversity. The different fertilization treatments strongly influenced the modular structure of the soil bacterial and fungal community co-occurrence network. A reduction in chemical fertilizer combined with organic fertilizer significantly improved cotton stem diameter and seed yield, and the effect of the biological organic fertilizer on plant growth and yield formation was greater than that of ordinary organic fertilizer.

Data availability statement

The datasets presented in this study can be found in online repositories. The sequences from rhizosphere bacterial samples are available at NCBI SRA: BioProject PRJNA876230.

Author contributions

YS: Formal analysis, Investigation, Writing – original draft. XN: Funding acquisition, Investigation, Resources, Writing – original draft, Writing – review & editing. BC: Investigation, Resources, Writing – original draft. SP: Investigation, Resources, Writing – review & editing. HM: Data curation, Formal analysis, Investigation, Writing – original draft. PL: Data curation, Resources, Writing – review & editing. GF: Formal analysis, Investigation, Writing – review & editing. XM: Formal analysis, Software, Supervision, Writing – review & editing.

Funding

The author(s) declare financial support was received for the research, authorship, and/or publication of this article. This work was supported by the Open Fund Project of Key Laboratory of Agricultural Environment of Northwest Oasis, Ministry of Agriculture and rural Affairs (XBLZ-20205), the National Nature Science Foundation of China (31860024), the Project of Renovation Capacity Building for the Young Sci-Tech Talents Sponsored by Xinjiang Academy of Agricultural Sciences (xjnkq-2019014), the Major Scientific and Technological Project of Xinjiang Uygur Autonomous Region of China (2020A01002), the National Key Research and Development Program of China (2017YFD0201903, 2018YFD0800804).

Conflict of interest

The authors declare that the research was conducted in the absence of any commercial or financial relationships that could be construed as a potential conflict of interest.

Publisher's note

All claims expressed in this article are solely those of the authors and do not necessarily represent those of their affiliated organizations, or those of the publisher, the editors and the reviewers. Any product that may be evaluated in this article, or claim that may be made by its manufacturer, is not guaranteed or endorsed by the publisher.

Supplementary material

The Supplementary material for this article can be found online at: https://www.frontiersin.org/articles/10.3389/fmicb.2023.1295722/full#supplementary-material

References

Adeli, A., Shankle, M. W., Tewolde, H., Sistani, K. R., and Rowe, D. E. (2008). Nutrient dynamics from broiler litter applied to no-till cotton in an upland soil. *Agron. J.* 100, 564–570. doi: 10.2134/agronj2007.0224

Alori, E. T., Glick, B. R., and Babalola, O. O. (2017). Microbial phosphorus solubilization and its potential for use in sustainable agriculture. *Front. Microbiol.* 8:971. doi: 10.3389/fmicb.2017.00971

Bahadori, M., Wang, J. T., Shen, J. P., Lewis, S., Rezaei Rashti, M., and Chen, C. (2022). Soil organic matter and geochemical characteristics shape microbial community composition and structure across different land uses in an Australian wet tropical catchment. *Land Degrad. Dev.* 33, 817–831. doi: 10.1002/ldr.4174

Bai, L., Li, J. H., Chu, G. X., and Hua, R. (2014). Effects of organic manure application combined with chemical fertilizers on nutrients absorption and nitrogen efficiency of cotton in Xinjiang China. *Agric. Res. Arid Areas* 32, 143–148.

Banerjee, S., Schlaeppi, K., and Van Der Heijden, M. G. A. (2018). Keystone taxa as drivers of microbiome structure and functioning. *Nat. Rev. Microbiol.* 16, 567–576. doi: 10.1038/s41579-018-0024-1

Barouillet, C., Vasselon, V., Keck, F., Millet, L., Etienne, D., Galop, D., et al. (2022). Paleoreconstructions of ciliate communities reveal long-term ecological changes in temperate lakes. *Sci. Rep.* 12, 1–12. doi: 10.1038/s41598-022-12041-7

Chen, Y., Li, S., Liu, N., He, H., Cao, X., Lv, C., et al. (2021). Effects of different types of microbial inoculants on available nitrogen and phosphorus, soil microbial community, and wheat growth in high-P soil. *Environ. Sci. Pollut. Res.* 28, 23036–23047. doi: 10.1007/s11356-020-12203-y

Chen, B. Y., Ma, X. W., Yang, T., Yao, Q. Q., Xue, X. R., Wang, B., et al. (2011). Research on the relationship between the accuracy of SPAD value and sample number in growing period of cotton. *Sci. Agric. Sin.* 44, 4748–4755. doi: 10.3864/j.issn.0578-1752.2011.22.024

Chen, J. S., Sun, W. H., Wang, G. S., Abubakar, S. A., and Gao, Y. (2021). Effects of different nitrogen application rates on soil water stable aggregates and N(2)O emission in winter wheat field. *Chin. J. Appl. Ecol.* 32, 3961–3968. doi: 10.13287/j.1001-9332.202111.024

Chen, L. Y., Zhang, L. F., Lu, Z. Y., Xian, F., Zhang, J. Z., and Zhang, X. Q. (2020). Effect of pipeline buried depth and water amount of trace irrigation on cotton quality and yield. *Water Saving Irrigation* 3, 7–11. doi: 10.3969/j.issn.1007-4929.2020.03.002

Dalu, T., Dlamini, P., Wasserman, R. J., Mokgoebo, M. J., Mutshekwa, T., Dondofema, F., et al. (2021). Effects of environmental variables on littoral macroinvertebrate community assemblages in subtropical reservoirs. *Chem. Ecol.* 37, 419–436.

Ding, W. T., Fang, J. J., Wu, X. P., Zhang, J. Z., Zhang, J. M., Zhang, J. Z., et al. (2021). Effects of different ratios of organic fertilizers instead of chemical fertilizers on black soil microbiological properties and spring wheat yield and quality. *Soil Fert. Sci. China* 2, 44–52. doi: 10.11838/sfsc.1673-6257.20452

Dong, W. Y., Zhang, X. Y., Dai, X. Q., Fu, X. L., Yang, F. T., Liu, X. Y., et al. (2014). Changes in soil microbial community composition in response to fertilization of paddy soils in subtropical China. *Appl. Soil Ecol.* 84, 140–147. doi: 10.1016/j.apsoil.2014.06.007

Dong, W., Zhang, Q., Luo, T., and Wang, H. P. (2020). Effects of continuous application of different organic fertilizers on soil quality. *Chin. Agric. Sci. Bull.* 36, 106–110.

Ducousso-Détrez, A., Fontaine, J., Lounes-Hadj Sahraoui, A., and Hijri, M. (2022). Diversity of phosphate chemical forms in soils and their contributions on soil microbial community structure changes. *Microorganisms* 10:609. doi: 10.3390/microorganisms10030609

Feng, H., Pan, H., Li, C., and Zhuge, Y. (2022). Microscale heterogeneity of soil bacterial communities under long-term fertilizations in fluvo-aquic soils. *Soil Ecol. Lett.* 4, 337–347. doi: 10.1007/s42832-021-0121-3

Gao, Z., Hu, Y., Han, M., Xu, J., Wang, X., Liu, L., et al. (2021). Effects of continuous cropping of sweet potatoes on the bacterial community structure in rhizospheric soil. *BMC microbiol.* 21, 1–13.

Gong, L., Ran, Q. Y., and Han, L. (2012). Enzymatic activities and related physicochemical properties in soils of continuous cropping cotton fields within a typical oasis in upper reaches of Tarim River. *Bull. Soil Water Conserv.* 32, 36–42.

Guo, Z., Han, J., Li, J., Xu, Y., and Wang, X. (2019). Effects of long-term fertilization on soil organic carbon mineralization and microbial community structure. *PLoS One* 14:e0211163. doi: 10.1371/journal.pone.0211163

Halihashi, Y. B. T., Li, Q. J., and Zhang, Y. (2020). Effects of cheimcal feritilzers appilcaiton combined with manure on yield and nutrient absorption in cotton field. *Xinjiang Agric. Sci.* 57, 1049–1056. doi: 10.6048/j.issn.1001-4330.2020.06.008

Hartmann, M., Hartmann, M., and Widmer, F. (2006). Community structure analyses are more sensitive to differences in soil bacterial communities than anonymous diversity indices. *Appl. Environ. Microbiol.* 72, 7804–7812. doi: 10.1128/AEM.01464-06

Hossain, M. E., Mei, X., Zhang, W., Dong, W., Yan, Z., Liu, X., et al. (2021). Substitution of chemical fertilizer with organic fertilizer affects soil Total nitrogen and its fractions in northern China. *Int. J. Environ. Res. Public Health* 18:12848. doi: 10.3390/ijerph182312848

Hu, L., Zi, H., Wu, P., Wang, Y., Lerdau, M., Wu, X., et al. (2019). Soil bacterial communities in grasslands revegetated using Elymus nutans are largely influenced by soil pH and total phosphorus across restoration time. *Land Degrad. Dev.* 30, 2243–2256. doi: 10.1002/ldr.3414

Iqbal, A., Ali, I., Yuan, P., Khan, R., Liang, H., Wei, S., et al. (2022). Combined application of manure and chemical fertilizers alters soil environmental variables and improves soil fungal community composition and Rice grain yield. *Front. Microbiol.* 13:856355. doi: 10.3389/fmicb.2022.856355

Jiang, R., Tang, L., Li, M., and Xu, Z. (2017). Response of greenhouse soil microbial community and enzyme activities to combined application of chemical fertilizer reduction with organic fertilizer. *Chin. J. Soil Sci.* 48, 639–646. doi: 10.19336/j.cnki.trtb.2017.03.19

Jin, N., Jin, L., Wang, S., Li, J., Liu, F., Liu, Z., et al. (2022). Reduced chemical fertilizer combined with bioorganic fertilizer affects the soil microbial community and yield and quality of lettuce. *Front. Microbiol.* 13:863325. doi: 10.3389/fmicb.2022.863325

Jones, B., Goodall, T., George, P. B., Gweon, H. S., Puissant, J., Read, D. S., et al. (2021). Beyond taxonomic identification: integration of ecological responses to a soil bacterial 16S rRNA gene database. *Front. Microbiol.* 12:682886. doi: 10.3389/fmicb.2021.682886

Landesman, W. J., and Dighton, J. (2010). Response of soil microbial communities and the production of plant-available nitrogen to a two-year rainfall manipulation in the New Jersey pinelands. *Soil Biol. Biochem.* 42, 1751–1758. doi: 10.1016/j.soilbio.2010.06.012

Li, S., Deng, Y., Wang, Z., Zhang, Z., Kong, X., Zhou, W., et al. (2020). Exploring the accuracy of amplicon-based internal transcribed spacer markers for a fungal community. *Mol. Ecol. Resour.* 20, 170–184. doi: 10.1111/1755-0998.13097

Li, Y., Li, Q. J., Zhang, Y., Halihashi, Y. B. T., and Wang, A. L. (2020). Effects of liquid organic fertilizers with reduced N and P fertilizer application on soil nutrient of drip irrigated cotton field under plastic film mulching. *Agric. Res. Arid Areas.* 38, 99–104. doi: 10.7606/j.issn.1000-7601.2020.02.14

Li, H., Qiu, Y., Yao, T., Han, D., Gao, Y., Zhang, J., et al. (2021a). Nutrients available in the soil regulate the changes of soil microbial community alongside degradation of alpine meadows in the northeast of the Qinghai-Tibet plateau. *Sci. Total Environ.* 792:148363. doi: 10.1016/j.scitotenv.2021.148363

Li, H., Yang, S., Semenov, M. V., Yao, F., Ye, J., Bu, R., et al. (2021b). Temperature sensitivity of SOM decomposition is linked with a K-selected microbial community. *Glob. Chang. Biol.* 27, 2763–2779. doi: 10.1111/gcb.15593

Li, Y., Zhang, Y., Halihashi, Y. B. T., and Li, Q. J. (2019). Effects of chemical fertilizer reduction application combined with liquid organic fertilizer on nutrient absorption and yield of cotton (*Gossypium hirsutum* L.). *Xinjiang Agric. Sci.* 56, 137–145. doi: 10.6048/j.issn.1001-4330.2019.01.017

Liao, H., Zhang, Y., Wang, K., Hao, X., Chen, W., and Huang, Q. (2020). Complexity of bacterial and fungal network increases with soil aggregate size in an agricultural Inceptisol. *Appl. Soil Ecol.* 154:103640. doi: 10.1016/j.apsoil.2020.103640

Liu, Z., Liu, J., Yu, Z., Yao, Q., Li, Y., Liang, A., et al. (2020). Long-term continuous cropping of soybean is comparable to crop rotation in mediating microbial abundance, diversity and community composition. *Soil Tillage Res.* 197:104503. doi: 10.1016/j.still.2019.104503

Liu, K., Yang, Y. L., Yang, J. Z., Wang, Z. X., Tian, Y. Y., Yang, B. K., et al. (2021). Effects of reduced chemical fertilizer combined with organic fertilizer on bacterial community diversity of Tobacco rhizosphere soil in field. *Southwest China J. Agri. Sci.* 34, 2191–2196. doi: 10.16213/j.cnki.scjas.2021.10.018

Liu, P. P., Zhou, Y., Fu, G. X., Gao, X., Zhang, P., Zhang, L., et al. (2014). Effects of fertilization on crop yield and soil phosphorus availablity based on the returning straw. *Nanjing Nongye Daxue Xuebao* 37, 27–33. doi: 10.7685/j.issn.1000-2030.2014.05.005

Lu, S. J., Han, X. Z., Zhag, D., Wang, F. J., and Zhu, W. W. (2009). Effect of long-term fertilization on microbial biomass C and N in soybean rhizosphere. *Soybean Sci.* 28, 495–498.

Ma, L., Song, D., Liu, M., Li, Y., and Li, Y. (2022). Effects of earthworm activities on soil nutrients and microbial diversity under different tillage measures. *Soil Tillage Res.* 222:105441. doi: 10.1016/j.still.2022.105441

Mensik, L., Hlisnikovsky, L., Pospisilova, L., and Kunzova, E. (2018). The effect of application of organic manures and mineral fertilizers on the state of soil organic matter and nutrients in the long-term field experiment. *J. Soils Sediments* 18, 2813–2822. doi: 10.1007/s11368-018-1933-3

Muhammad, Q., Huang, J., Waqas, A., Li, D., Liu, S., Zhang, L., et al. (2020). Yield sustainability, soil organic carbon sequestration and nutrients balance under long-term combined application of manure and inorganic fertilizers in acidic paddy soil. *Soil Tillage Res.* 198:104569. doi: 10.1016/j.still.2019.104569

Niu, X. X., Pu, S., Wu, X. L., Li, P., Yang, T., Ma, H. H., et al. (2021). Effects of the substitution for chemical fertilizer with organic manure on the cotton growth character and yield. *Xinjiang Agric. Sci.* 58, 2043–2048. doi: 10.6048/j.issn.1001-4330.2021.11.009

Pinhassi, J., and Berman, T. (2003). Differential growth response of colony-forming α-and γ-proteobacteria in dilution culture and nutrient addition experiments from Lake Kinneret (Israel), the eastern Mediterranean Sea, and the Gulf of Eilat. *Appl. Environ. Microbiol.* 69, 199–211. doi: 10.1128/AEM.69.1.199-211.2003

Qaswar, M., Chai, R., Ahmed, W., Jing, H., Han, T., Liu, K., et al. (2020). Partial substitution of chemical fertilizers with organic amendments increased rice yield by changing phosphorus fractions and improving phosphatase activities in fluvo-aquic soil. *J. Soils Sediments* 20, 1285–1296. doi: 10.1007/s11368-019-02476-3

Rose, M. T., Phuong, T. L., Nhan, D. K., Cong, P. T., Hien, N. T., and Kennedy, I. R. (2014). Up to 52% N fertilizer replaced by biofertilizer in lowland rice via farmer participatory research. *Agron. Sustain. Dev.* 34, 857–868. doi: 10.1007/s13593-014-0210-0

Sagova-Mareckova, M., Zadorova, T., Penizek, V., Omelka, M., Tejnecky, V., Pruchova, P., et al. (2016). The structure of bacterial communities along two vertical profiles of a deep colluvial soil. *Soil Biol. Biochem.* 101, 65–73. doi: 10.1016/j.soilbio.2016.06.026

Santoyo, G., Pacheco, C. H., Salmeron, J. H., and Leon, R. H. (2017). The role of abiotic factors modulating the plant-microbe-soil interactions: toward sustainable agriculture. A review. Span. *J. Agric. Res.* 15:e03R01. doi: 10.5424/SJAR/2017151-9990

Shen, W., Ni, Y., Gao, N., Bian, B., Zheng, S., Lin, X., et al. (2016). Bacterial community composition is shaped by soil secondary salinization and acidification brought on by high nitrogen fertilization rates. *Appl. Soil Ecol.* 108, 76–83.

Shi, K., Shao, H., Han, C. X., and Toshmatov, Z. (2022). Diversity of the rhizosphere soil Fungi of the invasive plant (*Solanum rostratum* Dunal) and the Allelopathic potential of their secondary metabolites. *Chin. J. Soil Sci.* 53, 548–557. doi: 10.19336/j.cnki.trtb.2021090202

Song, L., Wang, J., Pan, J., Yan, Y., and Niu, S. (2022). Chronic nitrogen enrichment decreases soil gross nitrogen mineralization by acidification in topsoil but by carbon limitation in subsoil. *Geoderma* 428:116159.

Sun, G. L., Feng, K. Y., Zhao, X. X., Wang, Z. B., and Li, Y. B. (2020). Effects of organic manure replacing chemical fertilizer on cotton growth, development and yield. *Xinjiang Agric. Sci.* 57, 762–769. doi: 10.6048/j.issn.1001-4330.2020.04.023

Sun, W. Y., Yin, H. J., Xu, J. X., Li, Z. J., Tian, C. Y., and Tang, J. W. (2015). The study of winter green manure on cotton production and soil fertility. *Acta Agric. Boreali-Sin.* 30, 129–132. doi: 10.7668/hbnxb.2015.S1.023

Tang, H. M., Xiao, X. P., Li, C., Tang, W. G., Guo, L. J., Wang, K., et al. (2018). Effects of different long-term fertilization managements on the physiological characteristics of leaves and yield of rice in double cropping paddy field. *J. China Agric. Univ.* 23, 60–71. doi: 10.11841/j.issn.1007-4333.2018.11.06

Tao, R., Wakelin, S. A., Liang, Y., and Chu, G. (2017). Organic fertilization enhances cotton productivity, nitrogen use efficiency, and soil nitrogen fertility under drip irrigated field. *Agron. J.* 109, 2889–2897. doi: 10.2134/agronj2017.01.0054

Wan, H. L., Liu, P. C., Liu, L. T., Zhang, Y. J., Liu, Y. C., Bai, Z. Y., et al. (2018). Effect of moderate drought in the early stage on cotton yield, Fiber quality and water use efficiency. *Cotton Sci.* 30, 464–472. doi: 10.11963/1002-7807.whlshc.20181113

Wang, N., Feng, K. Y., Nan, H. Y., and Zhang, T. H. (2022). Effects of combined application of organic fertilizer and chemical fertilizer on root characteristics and yield of cotton under different water conditions. *Chin. Agric. Sci.* 55, 2187–2201. doi: 10.3864/j.issn.0578-1752.2022.11.009

Wang, E., Lin, X., Tian, L., Wang, X., Ji, L., Jin, F., et al. (2021). Effects of short-term rice straw return on the soil microbial community. *Agriculture* 11:561. doi: 10.3390/agriculture11060561

Wang, N., Nan, H. Y., and Feng, K. Y. (2020). Effects of reduced chemical fertilizer with organic fertilizer application on soil microbial biomass, enzyme activity and cotton yield. *Chin. J. Appl. Ecol.* 31, 173–181. doi: 10.13287/j.1001-9332.202001.022

Wang, Y., Osman, J. R., and DuBow, M. S. (2020). Bacterial communities on the surface of the mineral sandy soil from the desert of Maine (USA). *Curr. Microbiol.* 77, 1429–1437. doi: 10.1007/s00284-020-01946-z

Wang, J., Xue, C., Song, Y., Wang, L., Huang, Q., and Shen, Q. (2016). Wheat and rice growth stages and fertilization regimes alter soil bacterial community structure, but not diversity. *Front. Microbiol.* 7:1207. doi: 10.3389/fmicb.2016.01207

Wang, Q. Q., Zhu, D. Q., Wang, C., Niu, T. H., Mao, Z. Y., and Xie, J. M. (2020). Effects of chemical fertilizer reduction and bio-organic fertilizer on photosynthesis, yield and quality of garlic seedlings. *Gansu Nongye Daxue Xuebao* 55, 69–75. doi: 10.13432/j.cnki.jgsau.2020.04.010

Xiao, X., Li, J., Lyu, J., Feng, Z., Zhang, G., Yang, H., et al. (2022). Chemical fertilizer reduction combined with bio-organic fertilizers increases cauliflower yield via regulation of soil biochemical properties and bacterial communities in Northwest China. *Front. Microbiol.* 13:922149. doi: 10.3389/fmicb.2022.922149

Yang, C. H., and Crowley, D. E. (2000). Rhizosphere microbial community structure in relation to root location and plant iron nutritional status. *Appl. Environ. Microb.* 66, 345–351. doi: 10.1128/AEM.66.1.345-351.2000

Yang, J. Y., Xu, Y. M., and Sun, J. S. (2022). Effects of long-term fertilization on nutrients in Irrigated Desert soil of eastern Xinjiang. *Xinjiang Agric. Sci.* 59, 433–440. doi: 10.6048/j.issn.1001-4330.2022.02.021

Yang, W. N., Yu, L., Luo, D. H., Xiong, Z. Y., Wang, Y. Y., Xu, M., et al. (2022). Effect of combined application of biochar with chemical fertilizer and organic fertilizer on soil phosphatase activity and microbial community. *Environ. Sci.* 43, 540–549. doi: 10.13227/j.hjkx.202105279

Yao, H., and Wu, F. (2010). Soil microbial community structure in cucumber rhizosphere of different resistance cultivars to fusarium wilt. *FEMS Microbiol. Ecol.* 72, 456–463. doi: 10.1111/j.1574-6941.2010.00859.x

Ye, Z., Li, J., Wang, J., Zhang, C., Liu, G., and Dong, Q. G. (2021). Diversity and co-occurrence network modularization of bacterial communities determine soil fertility and crop yields in arid fertigation agroecosystems. *Biol. Fert. Soils* 57, 809–824. doi: 10.1007/s00374-021-01571-3

Ye, L., Zhao, X., Bao, E., Li, J., Zou, Z., and Cao, K. (2020). Bio-organic fertilizer with reduced rates of chemical fertilization improves soil fertility and enhances tomato yield and quality. *Sci. Rep.* 10:177. doi: 10.1038/s41598-019-56954-2

Zhang, T., Kong, Y., Xiu, W. M., Li, G., Zhao, J. N., Yang, D. L., et al. (2019). Effects of fertilization treatments on soil microbial community characteristics under the wheat-maize rotation system in fluvo-aquic soil region in North China. *Ecol. Environ. Sci.* 28, 1159–1167. doi: 10.16258/j.cnki.1674-5906.2019.06.011

Zhang, T., Li, X. Y., Yang, H. M., Chu, M., and Shi, Y. W. (2018). Isolation, screening and identification of antagonistic bacteria against Verticillium dahliae Kleb. *Xinjiang* 45, 2418–2428. doi: 10.13344/j.microbiol.china.180003

Zhang, X., Zhang, R., Gao, J., Wang, X., Fan, F., Ma, X., et al. (2017). Thirty-one years of rice-rice-green manure rotations shape the rhizosphere microbial community and enrich beneficial bacteria. *Soil Biol. Biochem.* 104, 208–217. doi: 10.1016/j.soilbio.2016.10.023

Zhang, M., Zhang, X., Zhang, L., Zeng, L., Liu, Y., Wang, X., et al. (2021). The stronger impact of inorganic nitrogen fertilization on soil bacterial community than organic fertilization in short-term condition. *Geoderma* 382:114752. doi: 10.1016/j.geoderma.2020.114752

Zhao, W., and Huang, L. M. (2022). Stoichiometric characteristics and influencing factors of soil nutrients under different land use types in an alpine mountain region. *Acta Ecol. Sin.* 42, 4415–4427. doi: 10.5846/stxb202105061179

Zhao, J., Li, Y., Ran, W., Zhang, R. F., Shen, B., and Shen, Q. R. (2016). Effects of organic manure partial substitution for chemical fertilizer on crop yield and soil microbiome in a rice-wheat cropping system. *Nanjing Nongye Daxue Xuebao* 39, 594–602. doi: 10.7685/jnau.201603016

Zhao, Y., Mao, X., Zhang, M., Yang, W., Di, H. J., Ma, L., et al. (2021). The application of *Bacillus Megaterium* alters soil microbial community composition, bioavailability of soil phosphorus and potassium, and cucumber growth in the plastic shed system of North China. *Agric. Ecosyst. Environ.* 307:107236. doi: 10.1016/j.agee.2020.107236

Zheng, J. C., Yan, M. M., Zhang, J. S., Shi, H. L., and Wang, J. (2015). Effects of nitrogen fertilizer top dressed earlier under the shade on the yield and the fiber quality of cotton. *Xinjiang Agric. Sci.* 52, 1982–1988. doi: 10.6048/j.issn.1001-4330.2015.11.004

Zhong, W., Gu, T., Wang, W., Zhang, B., Lin, X., Huang, Q., et al. (2010). The effects of mineral fertilizer and organic manure on soil microbial community and diversity. *Plant Soil* 326, 511–522. doi: 10.1007/s11104-009-9988-y

Zhou, J., Gao, Z., Ma, H., and Chen, W. (2011). "Prevention and study on agricultural non-point source pollution in China" in *Advances in electrical engineering and electrical machines* (Berlin, Heidelberg: Springer), 565–569.

Zhu, Q. Q., Wu, X. P., Zhang, S. X., Xu, Y. M., Ji, L. L., Zhao, L. M., et al. (2020). Effects of reducing chemical fertilizer and organic fertilizer supplement on the yield and soil nutrient of drip Irrigationcotton in Xinjiang. *Xinjiang Agric. Sci.* 57, 2135–2143.

frontiers | Frontiers in Microbiology

TYPE Mini Review
PUBLISHED 23 November 2023
DOI 10.3389/fmicb.2023.1215024

OPEN ACCESS

EDITED BY
Jian-Wei Guo,
Kunming University, China

REVIEWED BY
Abhay K. Pandey,
Tea Research Association, North Bengal Regional R&D Centre, India

*CORRESPONDENCE
Guoying Zhou
zgyingqq@163.com
Junang Liu
kjc9620@163.com

RECEIVED 01 May 2023
ACCEPTED 30 October 2023
PUBLISHED 23 November 2023

CITATION
Chen X, He Y, Wang Z, Niu A, Xue Y, Zhou D, Zhou G and Liu J (2023) Research progress and management strategies of fungal diseases in *Camellia oleifera*. *Front. Microbiol.* 14:1215024. doi: 10.3389/fmicb.2023.1215024

Research progress and management strategies of fungal diseases in *Camellia oleifera*

Xingzhou Chen[1,2,3], Yuan He[1,2,3], Zhikai Wang[1,2,3], Anqi Niu[1,2,3], Yi Xue[1,2,3], Diao Zhou[1,2,3], Guoying Zhou[1,2,3]* and Junang Liu[1,2,3]*

[1]Key Laboratory of Cultivation and Protection for Non-Wood Forest Trees, Central South University of Forestry and Technology, Changsha, China, [2]Key Laboratory of National Forestry and Grassland Administration on Control of Artificial Forest Diseases and Pests in South China, Central South University of Forestry and Technology, Changsha, China, [3]Hunan Provincial Key Laboratory for Control of Forest Diseases and Pests, Central South University of Forestry and Technology, Changsha, China

Camellia oleifera Abel, a woody oil plant, that is endemic to China. Tea oil, also referred to as "oriental olive oil," is a superior quality plant-based cooking oil. The production of tea oil accounts for 8% of the total edible vegetable oil production in the country. Since 2022, the annual output value of *C. oleifera* industry has exceeded 100 billion yuan, making it one of the major economic contributors to China's rural revitalization development strategy. In recent years, demand and production have grown in parallel. However, this has led to an increase in the incidence levels of pest and diseases. Pests and diseases significantly reduce the quality and yield of *C. oleifera*. *C. oleifera* diseases are mainly caused by pathogenic fungi. *C. oleifera* anthracnose, soft rot, leaf spot, coal stain, leaf gall disease, and root rot are the most important fungal diseases affecting the *C. oleifera* industry. However, the same disease may be caused by different pathogenic fungi. *C. oleifera* can be found in half of China and is found in several climatic zones. The geographical distribution of woody plant diseases is consistent with the distribution of the tree species and the ecology of the range, which also results in a highly complex distribution of fungal diseases of *C. oleifera*. The management of fungal diseases in *C. oleifera* is extremely challenging due to the variety of pathogenic fungal species, multiple routes of transmission, the lack of resistant plants, and the environmental safety of chemical measures. The optimal strategy for addressing fungal diseases in *C. oleifera* is to develop and apply an integrated disease management plan. This review provides a brief overview of the pathogenic species, pathogenesis, pathogenesis, geographical distribution, current management strategies, and potentially new methods of *C. oleifera* fungal diseases, to provide direction for the development of comprehensive management measures for *C. oleifera* fungal diseases in the future.

KEYWORDS

***Camellia oleifera*, fungal pathogens, plant diseases, management strategies, geographical distribution**

1 Introduction

Camellia oleifera Abel has been cultivated for more than 2,000 years in China, and the domestic cultivation area is the largest in the world (He and He, 2002). In addition, it is minor planting in Japan, South Korea, India, Southeast Asia, and certain Western countries (Aukkanimart et al., 2013; Suealek et al., 2018; He et al., 2021; Teixeira and Sousa, 2021). *C. oleifera* is a leading industry in China's rural areas, promoting it enriching the people, and serving as a livelihood industry to combat poverty. Since 2022, the national *C. oleifera* planting area reached 467 million hectares, with a total output of tea oil of 1 million tons, and a total output value of the industry exceeding 1,160 billion yuan (The Central People's Government of the People's Republic of China, 2020; National Forestry and Grassland Administration, 2023). Tea oil boasts high nutritional value and an array of healthcare benefits (Hong et al., 2019; Du et al., 2020), including aging inhibiting, assistance to pregnant women during lactation and postpartum recovery (Zhang et al., 2019), antioxidant (Zhong et al., 2019), anti-cancer properties (Zong et al., 2016; Zheng et al., 2019), among others. In recent years, the Chinese government has strongly supported the expansion of the *C. oleifera* plantation area to foster the development of the advantageous *C. oleifera* industry (National Forestry and Grassland Administration, 2021; Central People's Government of the People's Republic of China, 2022). However, as the cultivation area of *C. oleifera* continues to increase, the occurrence of diverse diseases is increasing daily. During previous investigations, it was discovered that plant pathogenic fungi were the primary causes of diseases in *C. oleifera*. This causes the flower and fruit drop rates of *C. oleifera* to increase up to 70–80% in certain regions. The traditional diagnosis of diseases in *C. oleifera* often depends on the practitioner's experience, with symptoms serving as the sole basis for deducing the disease type. However, the symptoms vary due to different pathogenic fungi in various environments, different stages of infection, and different plant tissues, resulting in confusion in the classification of *C. oleifera* disease. Researchers were not able to develop the fact that there is a wide range of pathogenic fungi causing *C. oleifera* disease and that the same disease can be caused by multiple pathogenic fungi until the advent of molecular tools (Zhu and He, 2023). The natural geographic distribution of woody plant diseases is closely linked to the distribution of tree species, pest biota, and ecological environment. *C. oleifera* is widely grown and can survive in complex environments, therefore, analyzing the distribution of fungal diseases in *C. oleifera* will aid in the implementation of integrated disease management strategies. Targeted and precise prevention and management of plant diseases is a hot topic of discussion in the academic community, which cannot be achieved without an in-depth investigation into the pathogenic mechanisms of pathogenic fungi. Emerging research findings on the causal fungi of *C. oleifera* fungal diseases are emerging, which providing a strong basis for new integrated management strategies. The majority of reviews pertaining to fungal diseases in *C. oleifera* merely provide a brief summary of the conditions under which they occur and the pathogenic fungal species involved, lacking detailed descriptions of their geographical distribution, pathogenic fungi, and the mechanisms of their pathogenicity. Furthermore, as more and more novel pathogenic fungi are identified, it is crucial to promptly summarize these details. The purpose of this review is to provide summary of the present condition of the primary fungal diseases affecting *C. oleifera* (pathogenic species, geographical distribution, pathogenic mechanisms). Also, discuss potential integrated management strategies for *C. oleifera* disease in the context of existing research.

2 Current occurrence of major fungal diseases of *Camellia oleifera*

Common fungal diseases of *C. oleifera* include anthracnose, soft rot, leaf spot, coal stain, leaf gall, and root rot. These diseases spread rapidly and can cause significant harm, often resulting in the widespread death of *C. oleifera* in severe cases. Rarely have white rot, scab disease, and algal spot disease of *C. oleifera* been reported, and systematic studies are lacking. Hence, solely the corresponding pathogenic fungal species are presented in this paper (**Table 1**).

C. oleifera anthracnose has been the primary disease. It can cause severe fruit drop, fall buds, branch tip dieback, and even whole plant decline. Due to this disease, *C. oleifera* yields are frequently reduced by 10–30% in all provinces (districts), and by up to 40–80% in heavily affected regions (Zhou, 2023). The fungus of the genus *Colletotrichum* is the primary cause of *C. oleifera* anthracnose, with 12 identified species of *Colletotrichum* (Teleomorph: *Glomerella cingulata*) capable of infecting *C. oleifera* (**Table 1**). *Colletotrichum fructicola* is the predominant pathogenic fungus that cause anthracnose in *C. oleifera*, which is widely distributed across all *C. oleifera* growing areas in China (Li, 2018). *Colletotrichum* spp typically invades *C. oleifera* tissues in two forms, one by producing infestation pegs that can directly penetrate the cuticle of *C. oleifera*, and the other way is by producing bud tubes from conidia or invading stomata with their mycelium (Li, 2021). *Colletotrichum* spp as a typical semi-living trophic fungus with both living and dead trophic phases. During the live nutrient stage, the structural or functional integrity of the pathogenic fungal infestation is critical in determining it's to successfully invade plant tissues. However, certain mutants can lose their pathogenicity due to conidia not properly germinating (Liang et al., 2021; Lee et al., 2022). In addition, the formation of the appressorium of plant pathogenic fungi and the strong turgor pressure within it determine the host penetration mediated by compression. Studies have shown that the deletion of autophagy-related proteins CfAtg8 and CfAtg9 leads to a reduction in the melanin layer of the appressorium of *C. fructicola*, accompanied by cytorrhysis and plasmolysis, ultimately affecting the pathogenicity of the pathogenic fungi (Zhang S. et al., 2022). Necrotrophic stage pathogenic fungi are more likely to interfere with plant immunity or induce plant cell death, which consequently fosters further infestation activity. If important PAMPs (es) or DAMPs (Damage associated molecular patterns) are absent, the causative agent cannot suppress the immune responses to ROS, callose, and hormone accumulation in plant tissues, leading to decreased virulence (Balmer et al., 2013; Sun et al., 2016). Anthracnose follows a distinct seasonal pattern, with the average daily temperature beginning to rise from early April, and the minimum dew-point temperature reaching approximately 24°C, moisture condenses on the leaves, and the pathogen begins to infect the young leaf and tip tissues (**Figure 1A**;

TABLE 1 Statistics on the names of essential fungal diseases and the types of pathogens in *Camellia oleifera*.

Name	Another name	Pathogens
Camellia oleifera anthracnose	/	*Colletotrichum fructicola* (Li et al., 2016), *C. gloeosporioides* (Li H. et al., 2017), *C. camalliae* (Wang Y. et al., 2020), *C. siamense* (Li et al., 2015), *C. aenigma* (Wang Y. et al., 2020), *C. karstii* (Jiang and Li, 2018), *C. nymphaeae* (Li and Li, 2020), *Colletotrichum kahawae* (Sun W. et al., 2022), *C. boninense* (Tang et al., 2015), *C. horii* (Sun W. et al., 2022), *C. fioriniae* (Qin et al., 2019a), *Glomerella cingulata* (Li H. et al., 2017)
Camellia oleifera soft rot	"Deciduous disease," "Leaf blight"	*Agaricodochium camelliae* Liu Wei ei Fan (Liu et al., 1981; Song et al., 2021)
Camellia oleifera leaf spot	"Red leaf spot" "Gray spot disease," "Purple spot disease," "Frogeye leaf spot"	*Phyllosticta theicola* Petch (He, 2016), *Neopestalotiopsis longiappendiculata* (Wang Q. T. et al., 2022), *Cercosporella theae* (Huang and Meng, 1986), *Phyllosticta theaefolia* Hara (Liu, 1964), *Pestalozzia Palmarm* Cooke (Liu, 1964), *Leptosphaeria* sp (Kirk et al., 2008), *Mycosphaerella* sp (Kirk et al., 2008), *Macrophoma* sp (Kirk et al., 2008), *Ascochyta* sp (He, 2016), *Lasiodiplodia theobromae* (Liu et al., 2019), *Epicoccum layuense* (Xie et al., 2022), *Haradamyces foliicola* (Lu et al., 2019), *Neofusicoccum parvum* (Yu et al., 2022), *Botryosphaeria dothidea* (Hao et al., 2022), *Nigrospora sphaerica* (Qin et al., 2021), *Nigrospora chinensis* (Liu et al., 2020), *Pestalotiopsis microspora* (*Li et al., 2011*), *N. cubana*, *N. iberica*, *N. camelliae-oleiferae*, *N.* sp.1, *P. camelliae-oleiferae*, *P. hunanensis*, *P. nanjingensis*, *P. naningensis* (Li et al., 2021), *P. cocculin* (Qin et al., 2019b), *Pestalozzia theae* Saw, *Athelia scutellare* (Xie et al., 2022), *Alternaria alternata* (Shi et al., 2015)
Camellia oleifera coal stain	"Coal disease"	*Capnodium theae* Hara, *Meliola camelliae* (Catt) Sacc (Liu, 1964; Chinese Academy of Forestry, 1984; Yang, 1996; Zhuang, 2008)
Camellia oleifera leaf gall	"Tea blister blight," "Tea bud disease," "Tea peach," "Cha Pao," "Cha Pian"	*Exobasidium gracile* (Shi-rai) Syd (Lee et al., 2015; Zhang T. T. et al., 2022)
Camellia oleifera algal spot	/	*Cephaleuros virescens* Kunze (Su and Zhang, 2009)
Camellia oleifera scab disease	/	*Monochaetia* sp (Liu, 1964; Zhao and Qin, 2015)
Camellia oleifera white rot	"Ban bianfeng," "Bai xiu disease," "Foot rot," "Plaster tree," "White dry rot"	*Corticium scutellare* Brek. et Cur (Yuan et al., 1997)
Camellia oleifera root rot	"Athelia rolfsii," "Mycorrhizal disease," "Mycorrhizal root rot"	*Sclerotium rolfsii* (Liu, 1964), *Athelia rolfsii* (Li et al., 2009), *Fusarium oxysporum* (Zhao et al., 2020), *Fusarium proliferatum* (Li et al., 2008), *Cylindrocarpon destructans* (Zins.) Scholten (Cao et al., 1993)

Noriega Cantú et al., 2017). The peak was reached in August, and along with the phenology changes in *C. oleifera,* a large number of fruits were infected (**Figure 1B**). As temperatures and air humidity decrease at the end of October, the disease tends to slow down (Jing et al., 2009; Liu, 2012). The mycelia or conidia of the pathogen overwinter in the tissue of the spot, young fruit, or receptacle, serving as the origin of the initial infestation the following year (Liu, 2012; Wang et al., 2013).

In recent years, the occurrence of *C. oleifera* soft rot has been frequent and severe. In 1981, *Agaricodochium camelliae* Liu Wei ei Fan as the causal fungus responsible for causing *C. oleifera* soft rot (Liu et al., 1981). Later, the morphology of its conidiophores and conidia led to it also being referred to as *Myrothecium camelliae* (Liu Wei ei Fan) P. K. Chi, Wu ex Lin (Qi and Wei, 1983). In 2013, *A. camelliae* was included in the *National List of Hazardous Pests in Forestry* (National Forestry and Grassland Administration, 2013). *A. camelliae* differs from the majority of plant pathogenic fungi in that its invasion is directly achieved by sporodochium rather than conidia. During an infestation, sporodochium grows parallel brush-like mycelial tufts, invading the plant cells through the stomata or penetrating the epidermis. As the invasion process progresses, the sporodochium gradually shrinks (Wei and Qi, 1982). It mainly impacts the leaves and fruits of *C. oleifera*. In severe cases, up to 95% of the plants and 50% of the fruits can be affected by the disease (**Figures 1C, D**; Jiang, 2007; Wang Y. C. et al., 2020). The principal characteristic of the disease is the development of waterlogged state spots that are yellowish-brown or brownish-yellow, mushroom-like sporodochium. During the late period, the spots are scattered with earthy-yellow mushroom-like sporodochium, and the spots rot, causing the diseased fruit to split (Qi and Wei, 1983; Wei and Ma, 2010). The onset of *C. oleifera* soft rot is affected by the ambient temperature and humidity, with two peak development periods occurring from April to June and October to November each year, when temperatures average between 15–25°C. Temperatures that are too high or too low can hinder the progress of the disease (Lin et al., 1981; Wang Y. C. et al., 2020; Lu, 2021).

Capnodium theae Hara and *Meliola camelliae* (Catt) Sacc are recognized as the pathogenic fungi that cause *C. oleifera* coal stain. According to the nutritional mode, some scholars believe that bituminous coal pathogens can be classified into parasitic and saprophytic types (Yamamoto, 1955). As saprophytic type fungi, *Ca. theae* mainly derives nutrients from nectar secreted by insects. Spore germination and shoot tube elongation occur only in the presence of honeydew from insects or secretions of plants. Stimulation of germination and growth is not achieved through ordinary sugar water or nutrient solutions (Yamamoto, 1952). This type of fungus does not cause direct harm to plant tissues, instead, it covers the surface of branches and leaves, influencing photosynthesis and gas exchange, thus causing plant damage indirectly (Reynolds, 1999). Disease outbreaks caused by this pathogenic fungus are usually accompanied by severe insect infestations (Chomnunti et al., 2014; Khalkho et al., 2021). In contrast, *M. camelliae*, as a parasitic type, typically infects the

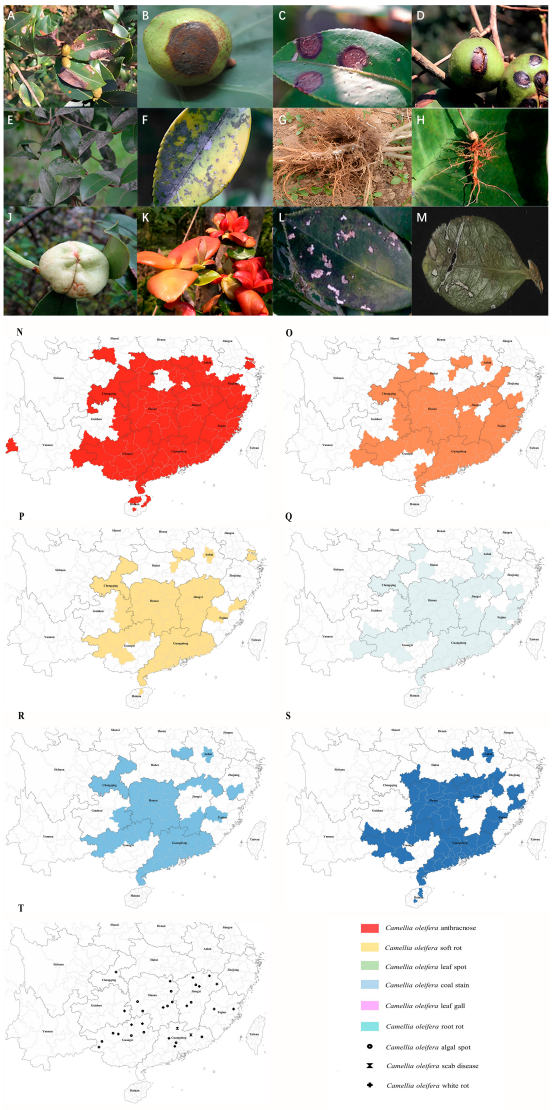

FIGURE 1
Images showing symptoms of major diseases of *Camellia oleifera* and geographical distribution of the main fungal diseases. **(A)** Anthracnose (leaf), **(B)** Anthracnose (fruit), **(C)** Soft rot (leaf), **(D)** Soft rot (fruit), **(E,F)** Coal stain (leaf), **(G,H)** Root rot, **(J)** Leaf gall (fruit), **(K)** Leaf gall (leaf), **(L)** Leaf spot (caused by *Pestalotiopsis theae*), **(M)** Leaf spot (caused by *Neopestalotiopsis longiappendiculata*), **(N)** Distribution of *C. oleifera* anthracnose, **(O)** Distribution of *C. oleifera* soft rot, **(P)** Distribution of *C. oleifera* leaf spot, **(Q)** Distribution of *C. oleifera* coal stain, **(R)** Distribution of *C. oleifera* leaf gall, **(S)** Distribution of *C. oleifera* root rot. **(T)** Distribution of *C. oleifera* algal spot, white rot and scab disease. Geographical distribution statistical criteria: the disease is mainly controlled or severely damaged in the area. See **Supplementary material** for reference.

extrafloral nectaries region of plant leaves and stems, drawing nutrients from plant tissues to fuel its growth (Mesquita et al., 2022). Severe cases of *C. oleifera* coal stain have been documented to cause a reduction in yields by 60–70%, which can persist for years to come, ultimately leading to no harvest (Chen, 1980). The key characteristics of *C. oleifera* coal stain are the presence of black sooty spots on branches and leaves during the initial stages, and black mycelium covering the entire leaf in the later stages (**Figures 1E, F**). The pathogenic fungi have a preference for cool, highly humid conditions, with the highest prevalence of the disease occurring during the months of March to May and September to November (Yu, 2019).

Camellia oleifera root rot can be subdivided into two categories (**Figures 1G, H**). Initially, it was believed that *Sclerotium rolfsii* (Teleomorph: *Athelia rolfsii*) was the causal agent of *C. oleifera* root rot (**Table 1**). The study discovered that *S. rolfsii* tends to infect the stems of plants close to the soil, but it can also damage various tissues, including shoots, buds, and petioles (Xu et al., 2008; Balamurugan et al., 2022; Thomas and Saravanakumar, 2023). Plant diseases caused by *S. rolfsii* are therefore also referred to as stem rot or blight. *S. rolfsii* can be found in soil or soil surface residues in the form of mycelia and sclerotia, utilizing two infection modes to fully colonize, including invading from damaged plant tissues and directly infecting the plant's soft tissues (Bhuiyan et al., 2019). The pathogenic fungus produces the virulence factor oxalic acid, which inhibits the host's defenses and causes stomatal opening, ultimately leading to increases transpiration rates and reduced biomass, resulting in wilting (Guimarães and Stotz, 2004; Kabbage et al., 2015). Infected plants of *S. rolfsii* produce white mycelial mats on the surface of the lesion, which are followed by the formation of globular nuclei either at the infection site or in the surrounding soil (Han et al., 2012; Amaradasa et al., 2020). *C. oleifera* is predominantly a seedling disease, and infection with *S. rolfsii* causes lesions to appear near the ground at the base of the stem or at the root base, which indicates a covering of white mycelium and dark-colored pycnidia. The affected seedlings grow poorly, their stem rots, their leaves turn yellow and wilt, and they can be easily pulled up (Huang and Xiao, 2015). Thus far, there have been no reports indicating that *S. rolfsii* causes harm to the buds, fruits, and other tissues of *C. oleifera*. In recent years, more *Fusarium* spp have been isolated and identified from diseased *C. oleifera* (**Table 1**). As weak parasites, they specialize in infesting plants that are poorly grown or have a lower resistant. Normally, they are harbored in the soil as saprophytic nutrients or spores that sprout and grow upon stimulated by plant root secretions (Ding et al., 2020). *Fusarium* spp tends to invade from the root tips of the plant, resulting in symptoms like yellowing of the leaves, reduced leaf size, and plant dwarfism. Some pathogenic fungi enter the vascular bundles and secrete pectinase and cellulase enzymes that degrade cells, and block the transport of water and nutrients. As a result, the plants exhibit symptoms of water loss and wilt (Garcia-Maceira et al., 2001). In addition to this, *Fusarium* spp secretes toxins, including monocotyledons and fusaric acid, that aid in the rapid colonization of disease-causing fungi by inhibiting protein synthesis, altering plant cell growth, mitochondrial activity, membrane permeability, or inducing programmed cell death in plant cells (Bouizgarne et al., 2006; Jiao et al., 2013). It's worth noting that the toxin produced by *Fusarium* spp maintains a high degree of toxicity to humans and animals as well. Accidental ingestion of infected fruits or seeds may pose a life-threatening risk (Qiu et al., 2019). According to survey statistics, the incidence of *C. oleifera* root rot in seedlings is as high as 50%, and in severe cases, it can reach 30% or more in young stands (Zhao et al., 2020). *Sclerotia* spp is maintained at 15–25°C for 27–34 days to initiate germination, and higher soil moisture accelerates this process (Clarkson et al., 2004). Similarly, *Fusarium* spp demonstrated increased pathogenicity at around 25°C, with increased humidity accelerating the development of the disease

(Marin et al., 1995; Lui and Kushalappa, 2002). The incidence of both types of root rot peaks during July to August (Li et al., 2008; He, 2016; Ma and Luo, 2019).

Camellia oleifera leaf gall drew attention in the 1940s (Yang, 1941). The pathogenic fungus causing the lesions is *Exobasidium gracile* (Shi-rai) Syd. Over 170 species of *Exobasidium* spp are plant pathogens, all of which share the common trait of infecting young, tender plant tissues, leading to the formation of leaf and flower galls (**Figures 1J, K**; Weille, 1960; Nickerson and Kloet, 1997). Currently only *E. gracile* is found in *C. oleifera* (Dong et al., 2019). After infecting the young flower and leaf buds of *C. oleifera*, the pathogen stimulates tissue proliferation and cell expansion, resulting in the formation of gall bodies (Liu et al., 2012; Huang et al., 2017). Once the flower buds proliferate, they do not produce fruit and seeds, resulting in reduced yields. The proliferation of leaves disrupts the usual process of photosynthesis, consequently leading to reduced yields. Documented that the average incidence of *C. oleifera* leaf swelling is around 39%, with a maximum of 80% or more causing serious damage (Qiu et al., 2011; Jia et al., 2017). Most *Exobasidium* spp produce both basidiospores and conidia, although both types of spores are capable of infection. However, conidia are more resilient, and the causal fungus often attaches itself to the tissue, surviving through winter or summer as the initial. The basidiospore is constrained by its structural specificity and serves primarily for dissemination (Ingram et al., 2019). The basidiospores are often present following the onset of disease, thus challenging the prediction of disease occurrence by detecting spores in the air. *C. oleifera* leaf gall often occurs in early spring, and a warm and humid environment is favorable for the disease. However, when the temperature exceeds 29°C, the growth of the pathogenic fungi is restricted, and the disease occurrence is slowed down (Ingram et al., 2019). Interestingly, *C. oleifera* leaf gall can reduce yields and affect the plant's health. However, the galls are edible and have a fresh and sweet taste. In addition, it is rich in nutrients and has been found to have hypoglycemic and anticancer effects (Zhu et al., 2007a,b; Huang et al., 2018).

Camellia oleifera leaf spot generally refers to a disease that cause leaf damage and form "leaf spots," including anthracnose and soft rot disease. Many different pathogenic fungi can cause these diseases (He, 2016). Leaf spots often lead to the destruction of over 50% of the infected leaves, resulting in serious economic losses (Lu et al., 2019; Qin et al., 2021; Hao et al., 2022; Yu et al., 2022). So far, we have identified 28 pathogenic fungi (excluding anthracnose and soft rot) that can cause *C. oleifera* leaf spot (**Table 1**). *Pestalotiopsis* spp and *Neopestalotiopsis* spp are the primary pathogenic fungi that cause *C. oleifera* leaf spot (**Figures 1L, M**). It is noteworthy that *Neopestalotiopsis* spp is a novel genus isolated from *Pestalotiopsis* spp, distinguished by analyses of systematics, sporulation structure, and conidial characteristics (Maharachchikumbura et al., 2014). *Pestalotiopsis* spp is a common pathogenic fungus, endophyte, and saprophyte. It is interesting to note that certain endophytic *Pestalotiopsis* spp can transform into a pathogenic phenotype, which can cause harm to the plant under specific conditions (Song, 2016). Conversely, when acting as an endophyte, it not only remains harmless but also produces a diverse array of compounds that assist the plant in resisting other pathogens (Rehman et al., 2022). Similar to other pathogenic fungi, the conidia of *Pestalotiopsis* spp have a crucial role in their pathogenicity, and any reduction in conidial numbers or functional deficiencies can significantly impact their ability to cause disease (Zhou et al., 2021; Yan et al., 2023). The pathogenic fungus overwinters in the form of mycelia or conidia in diseased leaf tissue and explodes in warm and humid conditions the following year, commonly in June and September, respectively (Liu et al., 2019; Lu et al., 2019). Some pathogenic fungi are more conducive to infestation during low temperatures and rainy weather (Kirk et al., 2008).

3 Geographical distribution of major fungal diseases of *C. oleifera*

Currently, there are 15 provinces (autonomous regions and municipalities directly under the central government) suitable for the cultivation of *C. oleifera* (National Forestry and Grassland Administration, 2023), primarily covering tropical monsoon, subtropical monsoon, and temperate monsoon climatic regions (Liu, 2019), all of which are characteristics by high temperature and rainy summer. It is highly conducive to the growth and spread of many pathogenic fungi. At present, *C. oleifera* anthracnose is currently the most serious disease, covering almost all the suitable areas for *C. oleifera* (**Figure 1N**). This is followed by soft rot, coal stain leaf gall, leaf spot, and root rot, which are also widespread (**Figures 1O–S**). There are only sporadic reports of white rot, scab disease, and algal spot (**Figure 1T**). *C. oleifera* leaf spot is difficult to distinguish because of the many different pathogenic fungi and the disease is likely to be confused with other foliar diseases. The actual extent of the real occurrence might be much larger than the areas depicted on the map, and we speculate that similar to anthracnose, it is present in all crucial production regions of *C. oleifera* in China. Due to global warming, the average temperature has increased, providing more opportunities for pathogens to thrive in the future (Roos et al., 2011). This means that more *C. oleifera* producing areas in China will be affected by more diseases in the future. *C. oleifera* plantation area in China is rapidly expanding, which also poses unprecedented challenges for disease management. According to the present statistical results, there are no significant geographical variations in the distribution of pathogenic fungi. Moreover, multiple pathogenic fungi can often be identified in *C. oleifera* stands, leading to the concurrence of several simultaneous diseases.

4 Management of fungal diseases in *Camellia oleifera*

Currently, the demand for tea oil and the associated quality requirements are on the rise in the international market, and there is also growing concern over domestic food safety. The development of the *C. oleifera* industry needs to maintain the excellent quality of tea oil while addressing the need to increase production significantly. To ensure the long-term health of *C. oleifera* forests, guarantee the high quality of tea oil, and prevent environmental pollution. It is necessary to establish a pollution-free management technology system that is founded on ecological management technology. Taking into account the entire ecosystem of the *C. oleifera* forest, we should establish

an accurate monitoring and forecasting system, select and breed disease-resistant varieties, develop biological control techniques, and utilize chemical pesticides rationally to carry out integrated management. Both to management diseases in *C. oleifera* below the permissible economic threshold and to ensure the high and stable production of pollution-free tea oil. Currently, the management of *C. oleifera* diseases is primarily conducted through traditional chemical methods. The use of broad-spectrum fungicides increases both the cost of production and the risk of disease-causing fungal resistance. Although there are numerous methods for the prevention and control of plant diseases, each one possesses advantages, disadvantages, and limitations. Practice has demonstrated that no single control measure for any disease can entirely and efficiently address the issue of damage. Only by adapting measures to local conditions and implementing integrated disease management (IDM) can we achieve the best control effect by leveraging the strengths of various measures and addressing their shortcomings. However, the development of new methods and technologies for managing *C. oleifera* fungal disease is seriously lagging, which is not conducive to the sustainable development of the industry. In the context of *C. oleifera* fungal disease patterns and the pathogenic mechanisms of the causal fungi, we will discuss several potential management strategies.

4.1 Selection and breeding of disease-resistant varieties

Cultivating varieties that are resistant to diseases is considered the best way to manage plant diseases in the long term (de Resende et al., 2021). Crossbreeding and systematic selection are frequently employed in the selection of new *C. oleifera* varieties, while traditional selection methods, which are labor-intensive, time-consuming, and highly dependent on environmental conditions, have demonstrated limitations in the development of broad-spectrum disease-resistant varieties. Indeed, newly improved varieties are often unable to adapt to the frequent emergence of new virulent microspecies of pathogens. With the development of biotechnology and molecular biology, the use of molecular breeding can overcome the limitations imposed by traditional breeding. The technique of molecular marker-assisted selection (MAS) has found extensive application in variety selection. Molecular markers can improve the efficiency and precision of genetic analyses, particularly in cases where multiple resistance genes are present in a single variety (Paterson et al., 1991). The disease resistance (R) gene is characteristics by specific evolution, enables plants to recognize pathogen-specific Avr genes, initiate signal transduction to activate defense capabilities, and naturally become an ideal target. The causal fungi that cause *C. oleifera* disease typically complete the infestation through mechanical invasion, toxin production, or induction of cell death. However, R genes can prevent the invasion of pathogenic fungi by regulating the strength of structures such as the plant cell wall and callose in a relative manner (Bacete et al., 2020); Altering the target or direct detoxification of toxins secreted by pathogenic fungi (Wang et al., 2021); Scavenging excessively accumulated ROS while inhibiting cell death (Navarrete et al., 2022). R genes improve disease resistance in plants in various ways. Moreover, the proteins encoded by disease-resistance genes have much in common, which opens up the possibility of selecting broad-spectrum disease-resistant varieties. The mining of R genes within the *C. oleifera* genome is bound to significantly assist in the identification of *C. oleifera* varieties that possess broad-spectrum disease resistance. Naturally, the publication of genome-wide data for *C. oleifera* will make this task much easier (Lin et al., 2022). In addition to mining disease-resistance genes, another future task that needs to be completed is the construction of a mature *C. oleifera* tissue culture system. This will significantly shorten the selection cycle and minimize the impact on the environment. It has been reported that treating healing tissues with pathogenic fungal toxins can also induce plants to develop corresponding resistance under selection pressure (Hui et al., 2003). Furthermore, another method to obtain precisely resistant varieties is by utilizing tissue culture technology and gene editing technology to introduce genes encoding antimicrobial proteins into *C. oleifera,* resulting in the construction of disease-resistant transgenic plants. However, some legal, ethical, and experimental issues continue to hinder the commercial utilization of transgenic plants (Fritsche et al., 2018). However, few key disease resistance genes have been identified in *C. oleifera*, and there is a lack of a mature genetic transformation system. Currently, precise cultivation of plants with targeted resistance poses a challenge.

4.2 Establishing an accurate monitoring and forecasting system

Fungal diseases of *C. oleifera* can be said to be an important reason for the loss of *C. oleifera* yield. Therefore, accurate modeling and prediction of such diseases can facilitate advance understanding of the time and severity of disease outbreaks. The majority of pathogenic fungi, that cause *C. oleifera* diseases, are disseminated through the medium of spores. Pathogenic fungi produce a significant quantity of spores on affected tissues, including diseased branches, leaves, and fruits, which can then spread via air currents or animals or human activities, frequently leading to widespread disease outbreaks. As a result, the presence and variety of spores in the air are strongly linked to the incidence of diseases (Volz, 1997; Suffert et al., 2011; Mukherjee et al., 2021). The spore capture technology can collect and detect spores of pathogenic fungi in the air of a given area, and simultaneously integrate them with the phenological phase of *C. oleifera* and the corresponding meteorological factors. It can accurately predict and analyze the period and degree of occurrence of disease, as well as their spatial and temporal variations, in *C. oleifera* forest regions (Redondo et al., 2020; Galagedara et al., 2021; Miller et al., 2022). Initially, spore trapping techniques were frequently employed in conjunction with microscopic examination to identify and quantify spores, but the method entails a high degree of detection error, such that even seasoned professionals cannot ensure a high degree of accuracy. Moreover, the form and size of the spores of certain pathogenic fungi may vary over time. The qPCR technique is deemed to be the most dependable technique for measuring the relative levels of genes in various samples simultaneously, thanks to its high efficiency and sensitivity (Galli et al., 2015; Machado et al., 2015). Several studies have successfully combined

spore-trapping techniques with qPCR to analyze the environmental spore densities of various plant pathogens (Dvořák et al., 2017; Quesada et al., 2018). It is noteworthy that a diverse array of fungal spores coexist in the air, encompassing non-pathogenic spores, and in addition, spore densities are lower in the air. Therefore, the specificity and sensitivity of qPCR protocols for the detection and quantification of *C. oleifera* pathogenic fungi spores are critical. The fungal ITS sequence is a suitable choice for the specificity requirement as it experiences minimal natural selection pressure during evolution and can accommodate greater variation. To achieve the best possible detection, the sensitivity can be optimized by optimizing primer sequences, DNA extraction techniques, and other factors. At present, there have been studies on high-precision detection technology for some *C. oleifera* diseases (Song, 2012), which provides support for improving the monitoring and prediction system for *C. oleifera* diseases. As a soil-borne disease, *C. oleifera* root rot is caused by a fungus that does not rely on conidia as its primary mode of transmission, making it unpredictable through the methods described above. Root rot is a so insidious disease, causing symptoms to go unnoticed in its early stages, and once the typical symptoms surface, they are often irreversible. Although the initial symptoms of root rot are not obvious, subtle changes in tissue metabolic pathways occur when plant tissues are attacked by the causal fungus. The NIR broad-spectrum method can rapidly identify this nuanced difference to diagnose the health status of the plant, making it effective for the early detection of plant root rot (Calamita et al., 2021). However, little research has been conducted on the differential changes in tissue metabolic pathways following infection by pathogenic fungi in *C. oleifera*, hindering the promotion and application of this technology in monitoring fungal diseases in this plant.

4.3 Use of biological control technology

Biological control is one of the practices of integrated plant disease management that uses biological agents to suppress the growth of pathogens, thereby preventing the development of plant disease (O'Brien, 2017; Kohl et al., 2019). These include the utilization of microbial antagonists like bacteria, fungi, viruses, or nematodes for disease suppression (Heydari and Pessarakli, 2010). Multiple studies have indicated that microorganisms isolated from the surface or inner part of plant tissues, as well as inter-root soil, can inhibit the growth of pathogenic bacteria, compete for colonization, or improve plant resistance (Dong et al., 2022; Kong et al., 2022; Sun Z. Z. et al., 2022; Zhou et al., 2022). Against *Colletotrichum* spp, a multitude of antagonistic microorganisms secrete extracellular enzymes, antibiotics, or volatile compounds that trigger mycelial disintegration, shrinkage, or abnormal conidial development of the pathogenic fungus, thus preventing its infestation (Bonatelli et al., 2016; Won et al., 2019). Furthermore, some antagonistic microorganisms can prevent disease by disrupting the cell wall structure of the parasitic mycelia (Alvindia, 2018). When selecting antagonistic microorganisms, it is important to consider the ability to colonize as well. The working principle of such antagonistic microorganisms is rapid dominance in plant tissues, access to more nutrients, and the simultaneous synthesis of more inhibitory substances. Moreover, possessing greater athleticism and the capability to ability to adapt to harsh environmental conditions is a necessary prerequisite for achieving success (Carvajal et al., 2002; Capdevila et al., 2004). Improving the plant's resistance can better handle diverse disease-causing fungi. Undoubtedly, using beneficial microorganisms to indirectly improve the resistance of *C. oleifera* is an effective method in the practical setting of lacking highly resistant *C. oleifera* varieties. *Trichoderma* fungi and *Bacillus* bacteria are often applied for biological control. They can enhance plant growth by improving the soil environment or producing a range of secondary metabolites to stimulate the plant's defense mechanism, thereby improving the plant's resistance to diseases (Perelló and Bello, 2011; Miljakovic et al., 2020; Asad, 2022). In addition, the application of fungus-feeding nematodes has been found to effectively decrease the progression of soil-borne diseases (Hasna et al., 2008), and mycoviruses to control the incidence of sclerotinia blight (Jiang et al., 2013). The control techniques presented hold immense potential for managing fungal diseases of *C. oleifera*. The key to the effectiveness of microbial antagonists lies in obtaining high-quality microbial that have strong environmental adaptability and athletics, while maintaining good antibacterial activity. This results in an extremely high cost for the preparation and development of microbial agents. At the same time, the use of pharmaceuticals necessitates professional training. Therefore, high human and economic costs are one of the key constraints to the diffusion of microbial antagonists. In addition to microbial antagonists, plant-derived fungicides are also highly sought after by people. Many phytochemicals have the potential to suppress the progression of plant fungal diseases (Cho et al., 2007; Gahukar, 2018). Plant-derived fungicides have the characteristics of low toxicity to humans and can be rapidly degraded into non-toxic substances under natural conditions. The study discovered that aldehydes, phenols, alkaloids, and other substances derived from plants can impact the development of numerous plant pathogenic fungi, including *Fusarium* spp, *Colletotrichum* spp, and *Sclerotinia* spp (Cho et al., 2007). For example, cinnamaldehyde can inhibit the synthesis of chitin in fungal cell walls and inhibit the infection activity of *F. solani* (Wang J. et al., 2022); Berberine has the ability to suppress the growth of various pathogenic fungi, including *C. capsici* and *Pyricularia oryzae* Cav. by inhibiting the growth of fungal hyphae and the germination of spores (Singh et al., 2001; Kokkrua et al., 2019). Despite the fact that botanical fungicides have been used in production, their development has been hindered by factors such as unstable properties, susceptibility to degradation, and slow efficacy.

4.4 Reasonable use of chemical pesticides

In production practice, Fungicides such as carbendazim, Bordeaux mixture and thiophanate methyl are frequently employed to manage fungal diseases of *C. oleifera*. The indiscriminate use of these chemicals poses risks, including chemical residue transfer (Li Y. H. et al., 2017; Zhou et al., 2018) and severe plant toxicity (Gaikwad and Nimbalkar, 2005). They remain toxic to animals, animal embryos, and even humans (Fimognari et al., 1999;

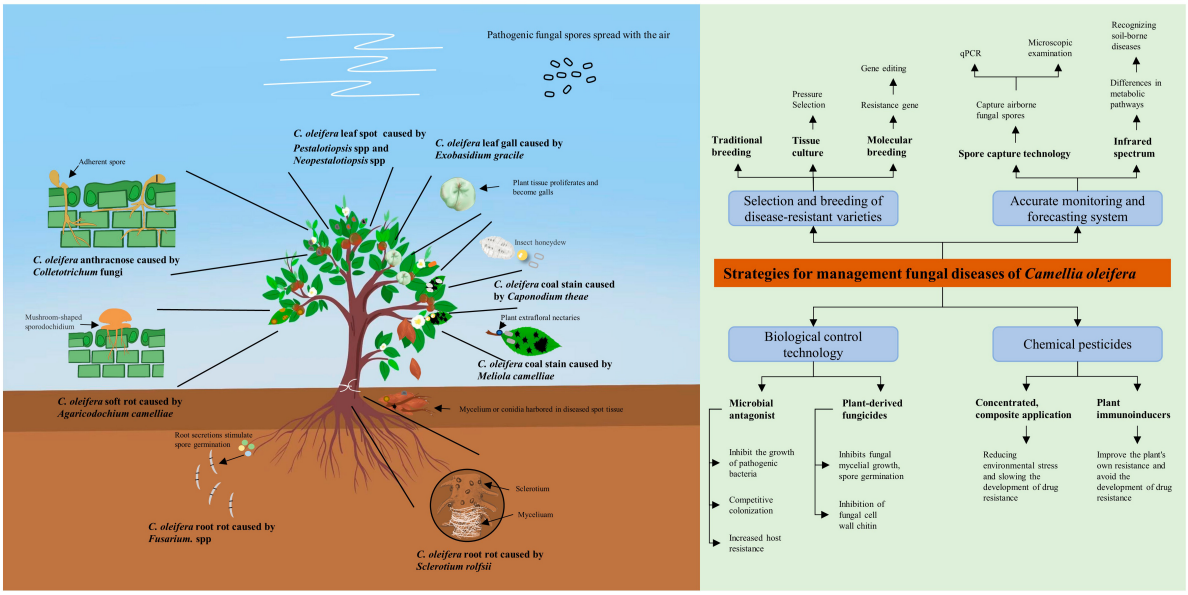

FIGURE 2
Schematic diagram of pathogenic bacteria infesting *Camellia oleifera* and integrated disease management strategies. This figure serves as an image summary outlining the basic elements of the literature review.

Ellis et al., 2010; Baurand et al., 2016). Apart from the safety issue, drug resistance is also a problem that cannot be disregarded. One of the key factors in the emergence of resistance is the reduction in protein affinity that is targeted by fungicides, resulting from a single target of drug action and a single gene mutation (e.g., carbendazim, thiophanate-methyl). Current chemical management methods, often in the disease-prone period of centralized application, and with a variety of agents used in combination, not only improve the efficiency of the use of chemical pesticides but also reduce the risk of drug resistance (Mueller et al., 2004). Fungicide resistance management is essential to slowing the emergence and spread of resistance for as long as possible while maintaining the necessary level of disease management. Developing a scientific pesticide application plan for the daily management of *C. oleifera* disease to reduce various risks is urgently needed in this regard. During the development of new chemical agents, the captivation of plant resistance using plant immune inducers can effectively achieve disease resistance (Caffi and Rossi, 2018). Immune inducers are mostly plant hormones or active small molecules produced during the interaction between pathogens and their hosts (Bektas and Eulgem, 2014), which do not induce resistance in disease-causing fungi as they do not significantly inhibit the pathogenic fungi themselves. They are also environmentally friendly with low toxicity to humans and animals, and can be used at low concentrations with a wide range of effects. The comprehensive and flexible application of plant immune inducers will facilitate the discovery of potential solutions to challenges related to food safety and agrochemicals (Guo et al., 2021). As a "vaccine" for plants, the development of drugs for immune inducers requires the search for corresponding "antigens," which cannot be separated from the study of pathogenic mechanisms of pathogenic fungi. At present, the research on the pathogenic mechanism of pathogenic fungi in *C. oleifera* is still in its infancy, and the development of corresponding immune inducers is still very difficult.

5 Conclusion and outlook

This review provides a more detailed understanding of *C. oleifera* diseases by describing the species, geographic distribution, and pathogenesis of the major fungal diseases (**Figure 2**). Among the numerous fungal diseases of *C. oleifera*, anthracnose caused by *Colletotrichum* spp has the widest distribution range. Moreover, *Colletotrichum* spp possesses numerous hosts and exhibits robust destructive power, often leading to cross-infection of different plants in the same forest (Eaton et al., 2021; Sharma et al., 2022). Therefore, *Camellia* anthracnose is the key object of prevention in daily production. The causal fungi responsible for fungal diseases of *C. oleifera* are diverse, with multiple diseases co-occurring, but there is no evidence of significant geographic variation in them. Therefore, the management of *C. oleifera* fungal diseases in all regions needs to maintain a high level of attention to multiple diseases at the same time. A comprehensive examination of the pathogenesis of each disease can facilitate the development of more effective targeted prevention and management strategies. As an example, *C. oleifera* root rot, as a soil-borne disease, is greatly limited in its ability to spread by the soil environment, with the causal fungus tending to only attack poorly healthy and young *C. oleifera* plants. Therefore, by implementing effective fertilizer management strategies to maintain seedlings healthy, along with regular disinfecting the of soil in the seedbed, *C. oleifera* root rot can be effectively management.

The management of fungal diseases in *C. oleifera* needs to combine a variety of measures. A single chemical management

measure is often ineffective in suppressing the disease and plants are subjected to combined attacks by multiple pathogenic fungi (Yimer et al., 2018). The traditional methods of prevention and management have limitations. For example, an integrated management strategy that prioritizes selects of resistant varieties and combines them with rational chemical methods and cultivation measures can be more effective in minimizing losses caused by plant spotted wilt diseases (Culbreath et al., 2003). However, the present strategies for managing *C. oleifera* fungal disease remains relatively homogenous, and the advancement of new management strategies is inseparable from fundamental research on *C. oleifera* and the fungi responsible for causing the disease. Recent research should therefore focus on, but not be limited to, the following two areas. Firstly, the selection of resistant varieties is the best option to maximize the benefits of production. Not only is it environmentally friendly, but it's also long-lasting. Therefore, it is worth identifying disease-resistance genes in *C. oleifera*. Secondly, a comprehensive understanding of the epidemiology and pathogenesis of various diseases, along with targeted early administration of drugs and the use of compound agents, would significantly reduce production costs and environmental hazards. This would also facilitate the establishment of accurate monitoring and prediction systems. Similarly, developing "specific drugs" for different diseases also requires a sufficient understanding of the pathogenic mechanisms of fungi. In addition, an in-depth understanding of the interactions between *C. oleifera* and pathogenic fungi will facilitate the development of highly effective targeting agents. For example, the development of plant immune inducers requires understanding the immune response mechanisms of *C. oleifera* in response to different pathogenic fungi, targeted stimulation of key gene regulation, and can effectively improve the overall disease resistance of *C. oleifera* without the risk of drug resistance. Furthermore, continuously screening high-quality microbial resources with the potential to develop microbial antagonists, establishing a database of plant-derived fungicide resources, and enhancing and optimizing extraction processes are directions of research that demand ongoing attention.

Author contributions

XC, GZ, and JL contributed to the conception of the manuscript. ZW, YH, AN, YX, and DZ contributed to the data analysis. All authors have read and agreed to the published version of the manuscript.

Funding

This research was funded by the National Natural Science Foundation of China (32271900) and the Hunan Provincial Innovation Foundation for Postgraduate (CX20230748).

Conflict of interest

The authors declare that the research was conducted in the absence of any commercial or financial relationships that could be construed as a potential conflict of interest.

Publisher's note

Supplementary material

The Supplementary Material for this article can be found online at: https://www.frontiersin.org/articles/10.3389/fmicb.2023.1215024/full#supplementary-material

References

Alvindia, D. G. (2018). The antagonistic action of *Trichoderma harzianumstrain* DGA01 against anthracnose-causing pathogen in mango cv. 'Carabao'. *Biocontrol Sci. Technol.* 28, 591–602. doi: 10.1080/09583157.2018.1468998

Amaradasa, B. S., Turner, A., Lowman, S., and Mei, C. (2020). First report of southern blight caused by *Sclerotium rolfsii* in industrial hemp in southern virginia. *Plant Dis.* 104, 1563–1563. doi: 10.1094/pdis-10-19-2157-pdn

Asad, S. A. (2022). Mechanisms of action and biocontrol potential of *Trichoderma* against fungal plant diseases - A review. *Ecol. Complexity* 49:100978. doi: 10.1016/j.ecocom.2021.100978

Aukkanimart, R., Boonmars, T., Pinlaor, S., Tesana, S., Aunpromma, S., Booyarat, C., et al. (2013). Histopathological changes in tissues of *Bithynia siamensis goniomphalos* incubated in crude extracts of camellia seed and mangosteen pericarp. *Korean J. Parasitol.* 51, 537–544. doi: 10.3347/kjp.2013.51.5.537

Bacete, L., Melida, H., Lopez, G., Dabos, P., Tremousaygue, D., Denance, N., et al. (2020). *Arabidopsis* response regulator 6 (ARR6) modulates plant cell-wall composition and disease resistance. *Mol. Plant Microbe Interact.* 33, 767–780. doi: 10.1094/MPMI-12-19-0341-R

Balamurugan, A., Ashajyothi, M., Charishma, K., Prakash, G., and Kumar, A. (2022). Athelia rolfsii causing sprout and shoot rot of sugarcane in India. *Aust. Plant Pathol.* 51, 597–600. doi: 10.1007/s13313-022-00887-4

Balmer, D., de Papajewski, D. V., Planchamp, C., Glauser, G., and Mauch-Mani, B. (2013). Induced resistance in maize is based on organ-specific defence responses. *Plant J.* 74, 213–225. doi: 10.1111/tpj.12114

Baurand, P. E., Dallinger, R., Capelli, N., and de Vaufleury, A. (2016). Metallothionein gene expression in embryos of the terrestrial snail (*Cantareus aspersus*) exposed to cadmium and copper in the Bordeaux mixture. *Environ. Sci. Pollut. Res.* 23, 3068–3072. doi: 10.1007/s11356-015-5649-2

Bektas, Y., and Eulgem, T. (2014). Synthetic plant defense elicitors. *Front. Plant Sci.* 5:804. doi: 10.3389/fpls.2014.00804

Bhuiyan, S. A., Wickramasinghe, P., Mudge, S. R., Adhikari, P., and Magarey, R. C. (2019). *Athelia rolfsii* causes sett rots and germination failure in sugarcane (*Saccharum* hybrid): Pathogenicity and symptomatology. *Australas. Plant Pathol.* 48, 473–483. doi: 10.1007/s13313-019-00648-w

Bonatelli, M. L., Tsui, S., Marcon, J., Batista, B. D., Kitajima, E. W., Pereira, J. O., et al. (2016). Antagonistic activity of fungi from anthracnose lesions on paullinia cupana aganist *Colletotrichum* sp. *J. Plant Pathol.* 98, 197–205. doi: 10.4454/Jpp.V98i2.029

Bouizgarne, B., El-Maarouf-Bouteau, H., Frankart, C., Reboutier, D., Madiona, K., Pennarun, A. M., et al. (2006). Early physiological responses of *Arabidopsis thaliana* cells to fusaric acid: Toxic and signalling effects. *New Phytol.* 169, 209–218. doi: 10.1111/j.1469-8137.2005.01561.x

Caffi, T., and Rossi, V. (2018). Fungicide models are key components of multiple modelling approaches for decision-making in crop protection. *Phytopathol. Mediterr.* 57, 153–169. doi: 10.14601/Phytopathol_Mediterr-22471

Calamita, F., Imran, H. A., Vescovo, L., Mekhalfi, M. L., and La Porta, N. (2021). Early identification of root rot disease by using hyperspectral reflectance: The case of pathosystem Grapevine/Armillaria. *Remote Sensing* 13:2436 doi: 10.3390/rs13132436

Camacho Carvajal, M. M., Wijfjes, A. H., Mulders, I. H., Lugtenberg, B. J., and Bloemberg, G. V. (2002). Characterization of NADH dehydrogenases of *Pseudomonas fluorescens* WCS365 and their role in competitive root colonization. *Mol. Plant Microbe Interact.* 15, 662–671. doi: 10.1094/MPMI.2002.15.7.662

Cao, F. X., Wu, G. J., Tian, Z. R., Hu, Q. F., Zhang, C. X., and Jiang, G. B. (1993). Research on the pathogenesis of root rot of non-wood forest research. *Non-wood Forest Res.* S1, 323–326. doi: 10.14067/j.cnki.1003-8981.1993.s1.080

Capdevila, S., Martinez-Granero, F. M., Sanchez-Contreras, M., Rivilla, R., and Martin, M. (2004). Analysis of *Pseudomonas fluorescens* F113 genes implicated in flagellar filament synthesis and their role in competitive root colonization. *Microbiology* 150(Pt 11), 3889–3897. doi: 10.1099/mic.0.27362-0

Central People's Government of the People's Republic of China (2022). *2022 Central Document No. 1 [Online]*. Bejing: Central People's Government of the People's Republic of China.

Chen, H. L. (1980). Preliminary report of a trial on the control of coal stain on oil tea by dried lego coating. *J. Zhejiang For. Sci. Technol.* 18, 2–4.

Chinese Academy of Forestry (1984). *China Forest Diseases*. Beijing: China Forestry Publishing House.

Cho, J. Y., Choi, G. J., Son, S. W., Jang, K. S., Lim, H. K., Lee, S. O., et al. (2007). Isolation and antifungal activity of lignans from *Myristica fragrans* against various plant pathogenic fungi. *Pest Manage. Sci.* 63, 935–940. doi: 10.1002/ps.1420

Chomnunti, P., Hongsanan, S., Aguirre-Hudson, B., Tian, Q., Persoh, D., Dhami, M. K., et al. (2014). The sooty moulds. *Fungal Divers.* 66, 1–36. doi: 10.1007/s13225-014-0278-5

Clarkson, J. P., Phelps, K., Whipps, J. M., Young, C. S., Smith, J. A., and Watling, M. (2004). Forecasting sclerotinia disease on lettuce: Toward developing a prediction model for carpogenic germination of sclerotia. *Phytopathology* 94, 268–279. doi: 10.1094/phyto.2004.94.3.268

Culbreath, A. K., Todd, J. W., and Brown, S. L. (2003). Epidemiology and management of tomato spotted wilt in peanut. *Annu. Rev. Phytopathol.* 41, 53–75. doi: 10.1146/annurev.phyto.41.052002.095522

de Resende, M. L. V., Pozza, E. A., Reichel, T., and Botelho, D. M. S. (2021). Strategies for coffee leaf rust management in organic crop systems. *Agronomy-Basel* 11:14. doi: 10.3390/agronomy11091865

Weille, A. G. (1960). Blister blight (*Exobasidium vexans*) in tea and its relationship with environmental conditions. *Neth. J. Agric. Sci.* 8, 183–210.

Khalkho, A., Nand Rai, A., and Bhardwaj, S. (2021). Capnodium variegatum – a new foliicolous species of sooty mould infecting *Bauhinia Variegata* L. from chhattisgarh, India. *Plant Arch.* 21, 218–225. doi: 10.51470/PLANTARCHIVES.2021.v21.no1.250

Ding, Y., Gardiner, D. M., Xiao, D., and Kazan, K. (2020). Regulators of nitric oxide signaling triggered by host perception in a plant pathogen. *Proc. Natl. Acad.* 117, 11147–11157. doi: 10.1073/pnas.1918977117

Dong, Y. J., Tang, B. B., He, M. M., Wang, L. L., Wu, K., Yang, S. X., et al. (2022). High concentrations of antagonistic bacterial strains from diseased sanqi ginseng rhizosphere suppressed *Fusarium* root rot. *Eur. J. Plant Pathol.* 163, 143–153. doi: 10.1007/s10658-022-02463-4

Dong, Z., Liu, W., Zhou, D., Li, P., Wang, T., Sun, K., et al. (2019). Bioactive exopolysaccharides reveal *Camellia oleifera* infected by the fungus exobasidium gracile could have a functional use. *Molecules* 24:2048. doi: 10.3390/molecules24112048

Du, M., Hu, L., Fang, X., and Zhang, J. (2020). Anti-hypertensive effects of blended *Camellia oleifera* Abel oil and eucommia extract on SHR mice. *Open J. For.* 10, 1–6. doi: 10.4236/ojf.2020.101001

Dvořák, M., Janoš, P., Botella, L., Rotková, G., and Zas, R. (2017). Spore dispersal patterns of *Fusarium circinatum* on an infested monterey pine forest in North-western Spain. *Forests* 8:432. doi: 10.3390/f8110432

Eaton, M. J., Edwards, S., Inocencio, H. A., Machado, F. J., Nuckles, E. M., Farman, M., et al. (2021). Diversity and cross-infection potential of *Colletotrichum causing* fruit rots in mixed-fruit orchards in kentucky. *Plant Dis.* 105, 1115–1128. doi: 10.1094/pdis-06-20-1273-re

Ellis, S. R., Hodson, M. E., and Wege, P. (2010). Determining the influence of rainfall patterns and carbendazim on the surface activity of the earthworm *Lumbricus terrestris*. *Environ. Toxicol. Chem.* 29, 1821–1827. doi: 10.1002/etc.219

Fimognari, C., Nusse, M., and Hrelia, P. (1999). Flow cytometric analysis of genetic damage, effect on cell cycle progression, and apoptosis by thiophanate-methyl in human lymphocytes. *Environ. Mol. Mutagen.* 33, 173–176.

Fritsche, S., Poovaiah, C., MacRae, E., and Thorlby, G. (2018). A new zealand perspective on the application and regulation of gene editing. *Front. Plant Sci.* 9:1323. doi: 10.3389/fpls.2018.01323

Gahukar, R. T. (2018). Management of pests and diseases of important tropical/subtropical medicinal and aromatic plants: A review. *J. Appl. Res. Med. Aromat. Plants.* 9, 1–18. doi: 10.1016/j.jarmap.2018.03.002

Gaikwad, A. P., and Nimbalkar, C. A. (2005). Phytotoxicity of copper fungicides to guava fruits. *J. Environ. Biol.* 26, 155–156.

Galagedara, N., Doyle, V., Price, P., Robertson, C. L., and Thomas-Sharma, S. (2021). Comparing the efficiency of spore traps to capture airborne inoculum of *Cercospora* spp. on soybean. *Phytopathology* 111, 29–29.

Galli, V., Borowski, J. M., Perin, E. C., Messias, R. D., Labonde, J., Pereira, I. D., et al. (2015). Validation of reference genes for accurate normalization of gene expression for real time-quantitative PCR in strawberry fruits using different cultivars and osmotic stresses. *Gene* 554, 205–214. doi: 10.1016/j.gene.2014.10.049

Garcia-Maceira, F. I., Di Pietro, A., Huertas-Gonzalez, M. D., Ruiz-Roldan, M. C., and Roncero, M. I. (2001). Molecular characterization of an endopolygalacturonase from *Fusarium oxysporum* expressed during early stages of infection. *Appl. Environ. Microbiol.* 67, 2191–2196. doi: 10.1128/AEM.67.5.2191-2196.2001

Guimarães, R. L., and Stotz, H. U. (2004). Oxalate production by sclerotinia sclerotiorum deregulates guard cells during infection. *Plant Physiol.* 136, 3703–3711. doi: 10.1104/pp.104.049650

Guo, S. X., He, F., Song, B. A., and Wu, J. (2021). Future direction of agrochemical development for plant disease in China. *Food Energy Secur.* 10:e293. doi: 10.1002/fes3.293

Han, K. S., Lee, S. C., Lee, J. S., Soh, J. W., and Kim, S. (2012). First report of sclerotium rot on cymbidium orchids caused by *Sclerotium rolfsii* in Korea. *Mycobiology* 40, 263–264. doi: 10.5941/MYCO.2012.40.4.263

Hao, Y., Liao, K., Guo, J., Jin, C., Guo, K., and Chen, M. (2022). First report of *Botryosphaeria dothidea* causing leaf spot of *Camellia oleifera* in China. *Plant Dis.* [Online ahead of print]. doi: 10.1094/PDIS-06-22-1452-PDN

Hasna, M. K., Lagerlöf, J., and Rämert, B. (2008). Effects of fungivorous nematodes on corky root disease of tomato grown in compost-amended soil. *Acta Agric. Scand., Sect. B.* 58, 145–153. doi: 10.1080/09064710701412767

He, F., and He, B. (2002). Cultural distribution and site classification for *Camellia oleifera*. *Sci. Silvae Sin.* 38, 64–72.

He, X. Y. (2016). *The Illustrated Handbook of Diseases and Insects of Oil-tea Camellia*. Beijing: Science Press.

He, Y.-C., Wu, M.-J., Lei, X.-L., Yang, J.-F., Gao, W., Soo, B. Y., et al. (2021). Gallotannins from nut shell extractives of *Camellia oleifera*. *J. Korean Wood Sci. Technol.* 49, 267–273.

Heydari, A., and Pessarakli, M. (2010). A review on biological control of fungal plant pathogens using microbial antagonists. *J. Biol. Sci.* 10, 273–290. doi: 10.3923/jbs.2010.273.290

Hong, C., Chang, C., Zhang, H., Jin, Q., Wu, G., and Wang, X. (2019). Identification and characterization of polyphenols in different varieties of *Camellia oleifera* seed cakes by UPLC-QTOF-MS. *Food Res. Int.* 126:108614. doi: 10.1016/j.foodres.2019.108614

Huang, C. W., and Xiao, C. Y. (2015). Characteristics of the occurrence and control trials of root rot of oil tea in Enshi. *Hubei Plant Protect.* 152, 9–10.

Huang, F. L., and Meng, M. Q. (1986). Preliminary report of purple spot disease of *Camellia oleifena* in Guangxi Province. *For. Sci. Technol.* 09, 29–30. doi: 10.13456/j.cnki.lykt.1986.09.017

Huang, R. J., Wang, Z. Q., Yang, Y., and Li, J. (2017). Observation on morphological traits and ultrastructure of abnormal leaf induced by *Exobasidium gracile* in *Camellia oleifera*. *Acta Bot. Boreali-Occidentalia Sin.* 37, 8–13.

Huang, Y. P., Huang, G., Liu, S. B., and Peng, X. L. (2018). Nutrient composition analysis of *Camellia oleifera* leaf swelling gall body tea buds and tea flakes. *Jiangxi Agric.* 145, 36–37. doi: 10.19394/j.cnki.issn1674-4179.2018.20.028

Hui, X. M., Yun, L. C., Bin, L. J., Tan, X. L., Tian, W. Z., and Tang, Z. S. (2003). Analysis of resistant spectrum to rice blast in transgenic rice lines introduced lysozyme gene from T4 Phage. *Sci. Agric. Sin* 2, 273–279.

Ingram, R. J., Ludwig, H. D., and Scherm, H. (2019). Epidemiology of Exobasidium leaf and fruit spot of rabbiteye blueberry: Pathogen overwintering, primary infection, and disease progression on leaves and fruit. *Plant Dis.* 103, 1293–1301. doi: 10.1094/PDIS-09-18-1534-RE

Jia, D. S., Mao, J. H., Chen, F., Mao, M. H., and Liao, Y. J. (2017). Occurrence and control of *Camellia oleifera* gall disease induced by *Exobasidium gracile* in highland areas. *J. West China For. Sci.* 46, 29–34. doi: 10.16473/j.cnki.xblykx1972.2017.05.006

Jiang, D. H., Fu, Y. P., Li, G. Q., and Ghabrial, S. A. (2013). *Viruses of the Plant Pathogenic Fungus Sclerotinia Sclerotiorum*. San Diego: Elsevier Academic Press Inc.

Jiang, S. Q., and Li, H. (2018). First report of leaf anthracnose caused by *Colletotrichum karstii* on tea-oil trees (*Camellia oleifera*) in China. *Plant Dis.* 102, 674–675. doi: 10.1094/PDIS-08-17-1195-PDN

Jiang, X. P. (2007). Control of soft rot of oil tea. *For. Ecol.* 599:29.

Jiao, J., Zhou, B., Zhu, X., Gao, Z., and Liang, Y. (2013). Fusaric acid induction of programmed cell death modulated through nitric oxide signalling in tobacco suspension cells. *Planta* 238, 727–737. doi: 10.1007/s00425-013-1928-7

Jing, A., Zhou, G., and Li, H. (2009). Recent advances in tea-oil tree anthracnose research. *Chin. For. Pathol.* 28, 27–31.

Kabbage, M., Yarden, O., and Dickman, M. B. (2015). Pathogenic attributes of *Sclerotinia sclerotiorum*: Switching from a biotrophic to necrotrophic lifestyle. *Plant Sci.* 233, 53–60. doi: 10.1016/j.plantsci.2014.12.018

Kirk, P. M., Cannon, P. F., David, J. C., and Stalpers, J. A. (2008). *Ainsworth and Bisby's Dictionary of the Fungi*, 10th Edn. Wallingford: CAB international.

Kohl, J., Kolnaar, R., and Ravensberg, W. J. (2019). Mode of action of microbial biological control agents against plant diseases: Relevance beyond efficacy. *Front. Plant Sci.* 10:19. doi: 10.3389/fpls.2019.00845

Kokkrua, S., Ismail, S. I., Mazlan, N., and Dethoup, T. (2019). Efficacy of berberine in controlling foliar rice diseases. *Eur. J. Plant Pathol.* 156, 147–158. doi: 10.1007/s10658-019-01871-3

Kong, W. L., Chen, X., Sun, H., Sun, X. R., and Wu, X. Q. (2022). Identification of two fungal pathogens responsible for *Liriodendron chinense x tulipifera* black spot and screening of Trichoderma sp. for disease control. *Plant Dis.* 106, 2172–2181. doi: 10.1094/pdis-06-21-1266-re

Lee, C. K., Lee, S. H., Shin, H. D., Park, J. H., and Sieber, T. (2015). First report of *Exobasidium gracile* causing hypertrophied leaves of *Camellia sasanquain* South Korea. *For. Pathol.* 45, 258–261. doi: 10.1111/efp.12184

Lee, K. H., Gumilang, A., Fu, T., Kang, S. W., and Kim, K. S. (2022). The autophagy protein CsATG8 is involved in asexual development and virulence in the Pepper anthracnose fungus *Colletotrichum scovillei*. *Mycobiology* 50, 467–474. doi: 10.1080/12298093.2022.2148393

Li, H. (2018). *Population Genetic Analyses of the Fungal Pathogen Colletotrichum on Tea-Oil Trees in China and Characterization of MAPK gene CfPMK1 in the Pathogen*. Changsha: Central South University of Forestry and Technology.

Li, H., Li, Y., Jiang, S. Q., Liu, J. A., and Zhou, G. Y. (2017). Pathogen of oil-tea anthracnose caused by *Colletotrichum* spp. in Hunan Province. *Sci. Silvae Sin.* 53, 43–53. doi: 10.11707/j.1001-7488.20170806

Li, Y. H., Zhou, B. L., Qian, M. R., Wang, Q., and Zhang, H. (2017). Transfer assessment of carbendazim residues from rape flowers to apicultural products. *J. Anal. Methods Chem.* 2017:7. doi: 10.1155/2017/6075405

Li, H., Song, G. T., Zhou, G. Y., and Liu, J. A. (2009). Molecular detection of *Athelia rolfsii* of *Camellia oleifera* by PCR. *Biotechnology* 19, 40–41. doi: 10.16519/j.cnki.1004-311x.2009.05.030

Li, H., Zhou, G. Y., and He, M. J. (2008). Study on biological characteristics and molecular identification of pathogens causing root rot of *Camellia oleifera*. *J. Southw. For. Univ.* 4:56.

Li, H., Zhou, G. Y., Liu, J. A., and Xu, J. P. (2016). Population genetic analyses of the fungal pathogen *Colletotrichum fructicola* on tea-oil trees in China. *PLoS One* 11:e0156841. doi: 10.1371/journal.pone.0156841

Li, H., Zhou, G. Y., and Xu, J. P. (2015). Pathogen identification of a new anthracnose of *Camellia oleifera*in China based on multiple-gene sequences. *Plant Protect.* 41, 92–96.

Li, H., Zhou, G. Y., Zhang, H. Y., Song, G. T., and Liu, J. N. (2011). Study on isolated pathogen of leaf blight and screening antagonistic bacteria from healthy leaves of *Camellia oleifera*. *Afr. J. Agric. Res.* 6, 4560–4566. doi: 10.5897/AJAR09.099

Li, L., Yang, Q., and Li, H. (2021). Morphology, phylogeny, and pathogenicity of *Pestalotioid* species on *Camellia oleifera* in China. *J. Fungi* 7:1080. doi: 10.3390/jof7121080

Li, M. (2021). *Studies on Leaf Cytology and Immunity of Colletotrichum fructicola-Camellia oleifera Interaction at Early Stage*. Changsha: Central South University of Forestry and Technology.

Li, S. Z., and Li, H. (2020). First report of *Colletotrichum nymphaeae* causing anthracnose on *Camellia oleifera* in China. *Plant Dis.* 104, 1860–1861. doi: 10.1094/PDIS-09-19-2016-PDN

Liang, C., Zhang, B., Zhou, Y., Yin, H., An, B., Lin, D., et al. (2021). CgNPG1 as a novel pathogenic gene of *Colletotrichum gloeosporioides* from *Hevea brasiliensis* in mycelial growth, conidiation, and the invasive structures development. *Front. Microbiol.* 12:629387. doi: 10.3389/fmicb.2021.629387

Lin, P., Wang, K., Wang, Y., Hu, Z., Yan, C., Huang, H., et al. (2022). The genome of oil-Camellia and population genomics analysis provide insights into seed oil domestication. *Genome Biol.* 23, 14. doi: 10.1186/s13059-021-02599-2

Lin, X. J., Wu, G. J., and Wang, J. X. (1981). Study of the disease pattern of soft rot of *Camellia oleifera*. *J. Central South Univ. For. Technol.* 1, 78–84. doi: 10.14067/j.cnki.1673-923x.1981.01.007

Liu, H. L. (2019). *Identification of the Anthraconse of Camellia oleifera Pathogen in Different Climate Zones and Cene Differential Expression*. Changsha: Central South University of Forestry and Technology.

Liu, S. B., Li, Y., Long, H., and Zhou, T. T. (2012). Observation on morphological and structural characteristics of ovary gall and leaf gall induced by *Exobasidium gracile* in *Camellia oleifera*. *Acta Bot. Boreali-Occidentalia Sin.* 32, 1752–1757.

Liu, S. Q. (1964). *Camellia oleifera* disease survey report in Anhui province. *J. Anhui Agric. Univ.* 75–86. doi: 10.13610/j.cnki.1672-352x.1964.00.006

Liu, W. (2012). *Studies on Etiology,Occurrence and Control of Camellia oleifera Anthracnose*. Wuhan: Huazhong Agricultural University.

Liu, X. J., Wei, A. J., Fan, S. R., Yang, W. A., Li, H. Z., and Zhou, S. L. (1981). Studies on the pathogenic fungus of the soft-rot of tea-oil trees. *Acta Microbiol. Sin.* 2, 132–133.

Liu, X. Y., Yu, F. Y., Fu, D. Q., Yang, W. B., Jia, X. C., and Chen, L. Q. (2019). Identification and characterization of *Camellia oleifera* leaf spot disease pathogen. *China Trop. Agric.* 1, 38–42.

Liu, Y. J., Hu, F., Chen, L. S., and Xu, S. W. (2020). First report of *Nigrospora sphaerica* causing leaf blight on oil tea (*Camellia oleifera*) in China. *Plant Dis.* 104, 3252–3252. doi: 10.1094/pdis-03-20-0563-pdn

Lu, P. K., Hsieh, W. T., Pan, H. R., and Ou, J. H. (2019). First report of *Haradamyces foliicola* causing leaf blight on oil tea (*Camellia oleifera*) in Taiwan. *Plant Dis.* 103, 1027–1028. doi: 10.1094/pdis-07-18-1175-pdn

Lu, X. F. (2021). Survey on the occurrence of soft rot of oil tea and integrated control technology. *Rural Sci. Technol.* 12, 70–71. doi: 10.19345/j.cnki.1674-7909.2021.01.037

Lui, L. H., and Kushalappa, A. C. (2002). Response surface models to predict potato tuber infection by *Fusarium sambucinum* from duration of wetness and temperature, and dry rot lesion expansion from storage time and temperature. *Int. J. Food Microbiol.* 76, 19–25. doi: 10.1016/s0168-1605(01)00752-8

Ma, Y. L., and Luo, L. C. (2019). Isolation, detection and screening of control agents on pathogenic bacteria of *Camellia oleifer* root rot. *J. Anhui Agric. Sci.* 47, 154–156.

Machado, R. D., Christoff, A. P., Loss-Morais, G., Margis-Pinheiro, M., Margis, R., and Korbes, A. P. (2015). Comprehensive selection of reference genes for quantitative gene expression analysis during seed development in *Brassica napus*. *Plant Cell Rep.* 34, 1139–1149. doi: 10.1007/s00299-015-1773-1

Maharachchikumbura, S. S., Hyde, K. D., Groenewald, J. Z., Xu, J., and Crous, P. W. (2014). Pestalotiopsis revisited. *Stud Mycol.* 79, 121–186. doi: 10.1016/j.simyco.2014.09.005

Marin, S., Sanchis, V., and Magan, N. (1995). Water activity, temperature, and pH effects on growth of *Fusarium moniliforme* and *Fusarium proliferatum* isolates from maize. *Can. J. Microbiol.* 41, 1063–1070. doi: 10.1139/m95-149

Mesquita, N. L. S., Santos, A., de Oliveira, R. J. V., Soares, P. P. D., de Novaes, Q. S., and Bezerra, J. L. (2022). Sooty mould caused by *Capnodium alfenasii* on *Azadirachta indica* Key-words. *J. Phytopathol.* 170, 574–578. doi: 10.1111/jph.13120

Miljakovic, D., Marinkovic, J., and Balesevic-Tubic, S. (2020). The significance of *Bacillus* spp. in disease suppression and growth promotion of cield and vegetable crops. *Microorganisms* 8:1037 doi: 10.3390/microorganisms8071037

Miller, I. F., Jiranek, J., Brownell, M., Coffey, S., Gray, B., Stahl, M., et al. (2022). Predicting the effects of climate change on the cross-scale epidemiological dynamics of a fungal plant pathogen. *Sci Rep.* 12:14823. doi: 10.1038/s41598-022-18851-z

Mueller, D. S., Bradley, C. A., Grau, C. R., Gaska, J. M., Kurle, J. E., and Pedersen, W. L. (2004). Application of thiophanate-methyl at different host growth stages for management of sclerotinia stem rot in soybean. *Crop Protect.* 23, 983–988. doi: 10.1016/j.cropro.2004.02.013

Mukherjee, R., Gruszewski, H. A., Bilyeu, L. T., Schmale, D. G., and Boreyko, J. B. (2021). Synergistic dispersal of plant pathogen spores by jumping-droplet condensation and wind. *Proc. Natl. Acad. Sci. U. S. A.* 118:e2106938118. doi: 10.1073/pnas.2106938118

National Forestry and Grassland Administration (2013). *National List of Dangerous Pests in Forestry*. Available online at: http://www.forestry.gov.cn/portal/main/govfile/13/govfile_1983.htm (accessed January 12, 2013).

National Forestry and Grassland Administration (2021). *Fourteen Five" Forestry and Grassland Protection and Development Plan Outline*. Available online at: http://www.forestry.gov.cn/main/5461/20210819/091113145233764.html (accessed December 14, 2021).

National Forestry and Grassland Administration (2023). *Three-Year Action Plan to Accelerate the Development of Oil Tea Industry (2023-2025)*. Available online at: http://www.forestry.gov.cn/main/6222/20230110/202930861565261.html (accessed December 22, 2022).

Navarrete, F., Gallei, M., Kornienko, A. E., Saado, I., Khan, M., Chia, K. S., et al. (2022). TOPLESS promotes plant immunity by repressing auxin signaling and is targeted by the fungal effector Naked1. *Plant Commun.* 3:100269. doi: 10.1016/j.xplc.2021.100269

Nickerson, N. L., and Vander Kloet, S. P. (1997). Exobasidium leaf spot of lowbush blueberry. *Can. J. Plant Pathol.* 19, 66–68. doi: 10.1080/07060669709500575

Noriega Cantú, D. H., Pereyda Hernández, J., and Garrido Ramírez, E. R. (2017). Efecto de factores climatológicos sobre la fluctuación de esporas en árboles de mango cv. Ataulfo en Guerrero, México. *Rev. Mex. Fitopatol.* 35, 227–241. doi: 10.18781/r.Mex.Fit.1610-1

O'Brien, P. A. (2017). Biological control of plant diseases. *Austral. Plant Pathol.* 46, 293–304. doi: 10.1007/s13313-017-0481-4

Paterson, A. H., Damon, S., Hewitt, J. D., Zamir, D., Rabinowitch, H. D., Lincoln, S. E., et al. (1991). Mendelian factors underlying quantitative traits in tomato: Comparison across species, generations, and environments. *Genetics* 127, 181–197. doi: 10.1093/genetics/127.1.181

Perelló, A. E., and Dal Bello, G. M. (2011). Suppression of tan spot and plant growth promotion of wheat by synthetic and biological inducers under field conditions. *Ann. Appl. Biol.* 158, 267–274. doi: 10.1111/j.1744-7348.2011.00460.x

Qi, Y. H., and Wei, A. J. (1983). Observation and study on the sporodochium receptacle of the pathogen of *Camellia oleifera* soft rot. *J. South China Agric. Coll.* 4, 16-22.

Qin, S. Z., Chen, X. Y. L., Zhou, X. H., Zhao, J., Baccelli, I., and Cernava, T. (2021). First report of *Camellia oleifera* leaf blight caused by *Nigrospora chinensis*. *J. Plant Pathol.* 103, 711–712. doi: 10.1007/s42161-021-00793-6

Qin, S. Z., Hong, Z. G., and Wang, Z. W. (2019a). Study on the identification of the pathogen of *Colletotrichum fioriniae* in *Camellia oleifera* in Guizhou province. *Tea Fujian* 41:3.

Qin, S. Z., Wang, J. W., and Zhang, Z. T. (2019b). Identification of the pathogen of oil tea leaf blight in Guizhou. *South China Agric.* 13, 134–135. doi: 10.19415/j.cnki.1673-890x.2019.26.067

Qiu, J., Xu, J., and Shi, J. (2019). Fusarium toxins in Chinese wheat since the 1980s. *Toxins* 11:248. doi: 10.3390/toxins11050248

Qiu, J. S., Yu, J. Y., Wu, Y. K., Zhu, X. E., Wang, J., Xu, J., et al. (2011). Preliminary report on the *Exobasidium gracile*(Shirai)Syd. of *Camellia oleifera* in Guizhou Province. *Guizhou For. Sci. Technol.* 39, 19–22.

Quesada, T., Hughes, J., Smith, K., Shin, K., James, P., and Smith, J. (2018). A low-cost spore trap allows collection and real-time PCR quantification of airborne *Fusarium circinatum* spores. *Forests* 9:586. doi: 10.3390/f9100586

Redondo, M. A., Berlin, A., Boberg, J., and Oliva, J. (2020). Vegetation type determines spore deposition within a forest-agricultural mosaic landscape. *FEMS Microbiol. Ecol.* 96:fiaa082. doi: 10.1093/femsec/fiaa082

Rehman, B., Khan, S. A., Hamayun, M., Iqbal, A., and Lee, I. J. (2022). Potent bioactivity of endophytic fungi isolated from *Moringa oleifera* leaves. *Biomed. Res. Int.* 2022:2461021. doi: 10.1155/2022/2461021

Reynolds, D. R. (1999). *Capnodium citri*: The sooty mold fungi comprising the taxon concept. *Mycopathologia* 148, 141–147. doi: 10.1023/a:1007170504903

Roos, J., Hopkins, R., Kvarnheden, A., and Dixelius, C. (2011). The impact of global warming on plant diseases and insect vectors in Sweden. *Eur. J. Plant Pathol.* 129, 9–19. doi: 10.1007/s10658-010-9692-z

Sharma, G., Maymon, M., Meshram, V., and Freeman, S. (2022). Characterization of *Colletotrichum* isolates from strawberry and other hosts with reference to cross-inoculation potential. *Plants-Basel* 11:16. doi: 10.3390/plants11182373

Shi, H. A., Fu, B. Z., Zhang, Z. L., Li, G. Y., and Wang, L. H. (2015). The study of two *Camellia* pathogens isolation, identification and biological characteristics. *Hubei Agric. Sci.* 54, 5908–5911. doi: 10.14088/j.cnki.issn0439-8114.2015.23.028

Singh, B., Srivastava, J. S., Khosa, R. L., and Singh, U. P. (2001). Individual and combined effects of berberine and santonin on spore germination of some fungi. *Folia Microbiol.* 46, 137–142. doi: 10.1007/bf02873592

Song, G. T. (2012). *The Study on Detection and Biological Control to the Main Pathogens of Camellia oleifera*. Changsha: Central South University of Forestry and Technology.

Song, L. S. (2016). *Research on Taxonomy, Molecular Systematics and DNA Barcoding of Pestalotiopsis*. Nanning: Guangxi University.

Song, Y. P., Wang, P., and Zhou, H. W. (2021). Detection and controlmeasures on *Agaricodochium camellia*. *J. Jiujiang Univ.* 36:56. doi: 10.19717/j.cnki.jjun.2021.02.001

Su, Q. L., and Zhang, L. F. (2009). *Oil-tea Cultivation and Pest Control in China*. Beijing: China Forestry Publishing House.

Suealek, N., Yokoyama, W. H., Rojpibulstit, P., Holt, R. R., and Hackman, R. M. (2018). Thai tea seed (*Camellia oleifera*) oil favorably affects plasma lipid responses in hamsters fed high-fat diets. *Eur. J. Lipid Sci. Technol.* 121:1800024. doi: 10.1002/ejlt.201800024

Suffert, F., Sache, I., and Lannou, C. (2011). Early stages of *Septoria tritici* blotch epidemics of winter wheat: Build-up, overseasoning, and release of primary inoculum. *Plant Pathol.* 60, 166–177. doi: 10.1111/j.1365-3059.2010.02369.x

Sun, W., Lei, T., Yuan, H., and Chen, S. (2022). First report of anthracnose caused by *Colletotrichum kahawae* and *Colletotrichum horri* on tea-oil tree in China. *Plant Dis.* 107:1944. doi: 10.1094/PDIS-06-22-1312-PDN

Sun, Z. Z., Liu, T. T., Liu, Z., Zeng, C. Z., and Liu, Z. X. (2022). Screening of antagonistic bacteria against the blue mold of citrus fruit from soil by a new parallel screening method without prior isolation of single strains. *Biol. Control.* 176:105066. doi: 10.1016/j.biocontrol.2022.105066

Sun, Y., Wang, Y., and Tian, C. (2016). bZIP transcription factor CgAP1 is essential for oxidative stress tolerance and full virulence of the poplar anthracnose fungus *Colletotrichum gloeosporioides*. *Fungal Genet. Biol.* 95, 58–66. doi: 10.1016/j.fgb.2016.08.006

Tang, Y. L., Zhou, G. Y., Li, H., Zhong, W. B., Long, H. E., and Wang, L. Y. (2015). Identification of a new anthracnose of *Camellia oleifera* based on multiple-gene phylogeny. *Chin. J. Trop. Crops* 36, 972–977.

Teixeira, A. M., and Sousa, C. (2021). A review on the biological activity of *Camellia* species. *Molecules* 26:2178 doi: 10.3390/molecules26082178

The Central People's Government of the People's Republic of China (2020). *The Planting Area of Camellia oleifera in China Reaches 68 million mu*. Available online at: http://www.gov.cn/xinwen/2020-11/17/content_5562082.htm (accessed November 17, 2020).

Thomas, A., and Saravanakumar, D. (2023). First report of *Sclerotium rolfsii* (*Athelia rolfsii*) causing basal rot in lettuce in Trinidad. *J. Plant Pathol.* 105, 611–611. doi: 10.1007/s42161-023-01319-y

Volz, P. A. (1997). Transmission of fungal spores in space and their conditions for survival: A review. *Microbios* 91, 145–151.

Wang, F., Li, X., Li, Y., Han, J., Chen, Y., Zeng, J., et al. (2021). Arabidopsis P4 ATPase-mediated cell detoxification confers resistance to *Fusarium graminearum* and *Verticillium dahliae*. *Nat. Commun.* 12:6426. doi: 10.1038/s41467-021-26727-5

Wang, J., Zhang, J., Ma, J., Liu, L., Li, J., Shen, T., et al. (2022). The major component of cinnamon oil as a natural substitute against *Fusarium solani* on *Astragalus membranaceus*. *J. Appl. Microbiol.* 132, 3125–3141. doi: 10.1111/jam.15458

Wang, Q. T., Cheng, Y. H., Zhuo, L., Wang, Y., Zhou, H., and Hou, C. L. (2022). *Neopestalotiopsis longiappendiculata* as the agent of grey blight disease of *Camellia* spp. *J. Phytopathol.* 170, 770–777. doi: 10.1111/jph.13139

Wang, Y., Chen, J. Y., Xu, X., Cheng, J., Zheng, L., Huang, J., et al. (2020). Identification and characterization of *Colletotrichum* species associated with anthracnose disease of *Camellia oleifera* in China. *Plant Dis.* 104, 474–482. doi: 10.1094/PDIS-11-18-1955-RE

Wang, Y. C., Yang, H., Deng, L. Q., and Yang, C. X. (2020). Survey on the occurrence of soft rot of oil tea and integrated control technology. *Mod. Agric. Sci. Technol.* 779, 145–153.

Wang, Y. X., Liu, W., Chen, J. Y., Liu, Y. J., and Huang, J. B. (2013). Overwintering sites, various stages and amount of *Colletotrichum gloeosporioides* on *Camellia oleifera*. *Hubei For. Sci. Technol.* 179, 32–46.

Wei, A. J., and Qi, Y. H. (1982). Preliminary studies on the mechanism of infestation by the causal agent of soft rot of *Camellia oleifera*. *For. Sci. Technol.* 3, 26–28. doi: 10.13456/j.cnki.lykt.1982.03.014

Wei, C. Y., and Ma, Y. L. (2010). Risk analysis and control technology of *Myrothecium camelliae* in China. *J. Anhui Agric. Sci.* 38, 18187–18189. doi: 10.13989/j.cnki.0517-6611.2010.32.163

Won, S. J., Kwon, J. H., Kim, D. H., and Ahn, Y. S. (2019). The effect of *Bacillus licheniformis* MH48 on control of foliar fungal diseases and growth promotion of *Camellia oleifera* seedlings in the coastal reclaimed land of Korea. *Pathogens* 8:6. doi: 10.3390/pathogens8010006

Xie, X., Zhang, S., Yu, Q., Li, X., Liu, Y., and Wang, L. (2022). First report of *Epicoccum layuense* causing leaf brown spot on *Camellia oleifera* in Hefei, China. *Plant Dis.* [Online ahead of print]. doi: 10.1094/PDIS-08-21-1726-PDN

Xu, Z., Gleason, M. L., Mueller, D. S., Esker, P. D., Bradley, C. A., Buck, J. W., et al. (2008). Overwintering of *Sclerotium rolfsii* and S. rolfsii var. delphinii in different latitudes of the United States. *Plant Dis.* 92, 719–724. doi: 10.1094/PDIS-92-5-0719

Yamamoto, W. (1952). The germination of spores of the sooty mould fungus, and the growth of their germ tubes, with special reference to the honeydews secreted by insects. *Jpn. J. Phytopathol.* 16, 49–53. doi: 10.3186/jjphytopath.16.49

Yamamoto, W. (1955). On the so-called host range of sooty mould fungi. *Jpn. J. Phytopathol.* 19, 97–103. doi: 10.3186/jjphytopath.19.97

Yan, X., Zhang, S., Yu, Z., Sun, L., Sohail, M. A., Ye, Z., et al. (2023). The MAP kinase PvMK1 regulates hyphal development, autophagy, and pathogenesis in the bayberry twig blight fungus *Pestalotiopsis versicolor*. *J. Fungi* 9:606 doi: 10.3390/jof9060606

Yang, W. (1996). *Forest Pathology*. Beijing: China Forestry Publishing House.

Yang, X. M. (1941). Meitan's oil Tea ovary gall. *Knowl. Pests Dis.* 1, 31–35.

Yimer, S. M., Ahmed, S., Fininsa, C., Tadesse, N., Hamwieh, A., and Cook, D. R. (2018). Distribution and factors influencing chickpea wilt and root rot epidemics in Ethiopia. *Crop Protect.* 106, 150–155. doi: 10.1016/j.cropro.2017.12.027

Yu, F. Y., Liu, X. Y., Jia, X. C., Fu, D. Q., Song, W. W., and Niu, X. Q. (2022). First report of *Neofusicoccum parvum* causing leaf spot of *Camellia drupifera* in China. *J. Plant Pathol.* 104, 431–431. doi: 10.1007/s42161-021-00992-1

Yu, Y. C. (2019). Occurrence and control of oil tea sooty mold in susong area. *J. Agric. Catastrophol.* 9, 17–18. doi: 10.19383/j.cnki.nyzhyj.2019.02.008

Yuan, S. L., Sao, L. P., and Li, C. D. (1997). *Diseases of Trees and Shrubs in China*. Beijing: China Science Publishing.

Zhang, J., Ying, Y., and Yao, X. (2019). Effects of turning frequency on the nutrients of *Camellia oleifera* shell co-compost with goat dung and evaluation of co-compost maturity. *PLoS One* 14:e0222841. doi: 10.1371/journal.pone.0222841

Zhang, S., Guo, Y., Li, S., Li, H., and Di Pietro, A. (2022). Histone acetyltransferase CfGcn5-mediated autophagy governs the pathogenicity of *Colletotrichum fructicola*. *mBio* 13:e01956-22. doi: 10.1128/mbio.01956-22.

Zhang, T. T., Cai, X. Y., Teng, L., Li, X., Zhong, N. F., and Liu, H. M. (2022). Molecular characterization of three novel mycoviruses in the plant pathogenic fungus *Exobasidium*. *Virus Res.* 307:198608. doi: 10.1016/j.virusres.2021.198608

Zhao, D. Y., and Qin, C. S. (2015). *Original Color Ecological Atlas for Diagnosis and Control of Oil-Tea Pests and Diseases*. Guangzhou: Guangdong Science and Technology Press.

Zhao, Z. X., Yan, W. R., Xiao, M., Xiao, D. B., and Lei, F. (2020). Molecular identification of pathogens causing root rot of *Camellia oleifera* in tropical. *Mol. Plant Breed.* 18, 6433–6440. doi: 10.13271/j.mpb.018.006433

Zheng, L. F., Chen, L., Li, J., Liang, L., Fan, Y. W., Qiu, L. Y., et al. (2019). Two kaempferol glycosides separated from *Camellia oleifera* meal by high-speed countercurrent chromatography and their possible application for antioxidation. *J. Food Sci.* 84, 2805–2811. doi: 10.1111/1750-3841.14765

Zhong, W. Q., Shen, J. L., Liao, X. D., Liu, X. L., Zhang, J., Zhou, C. H., et al. (2019). *Camellia* (*Camellia oleifera* Abel.) seed oil promotes milk fat and protein synthesis-related gene expression in bovine mammary epithelial cells. *Food Sci. Nutr.* 8, 419–427. doi: 10.1002/fsn3.1326

Zhou, G. Y. (2023). Green control techniques for oil tea diseases (I). *For. Ecol.* 808, 36–38. doi: 10.13552/j.cnki.lyyst.2023.01.014

Zhou, J. P., Xie, Y. Q., Liao, Y. H., Li, X. Y., Li, Y. M., Li, S. P., et al. (2022). Characterization of a *Bacillus velezensis* strain isolated from *Bolbostemmatis rhizoma* displaying strong antagonistic activities against a variety of rice pathogens. *Front. Microbiol.* 13:983781. doi: 10.3389/fmicb.2022.983781

Zhou, L., Jiang, Y. P., Lin, Q., Wang, X., Zhang, X. Z., Xu, J., et al. (2018). Residue transfer and risk assessment of carbendazim in tea. *J. Sci. Food Agric.* 98, 5329–5334. doi: 10.1002/jsfa.9072

Zhou, M., Li, Z., Liu, Y., Zhang, P., Hao, X., and Zhu, X. (2021). Transcription factors Pmr1 and Pmr2 cooperatively regulate melanin biosynthesis, conidia development and secondary metabolism in *Pestalotiopsis microspora*. *J. Fungi* 8:38. doi: 10.3390/jof8010038

Zhu, B. F., Peng, L., and Luo, L. F. (2007a). Study on health care functions of extract from fleshy fruit and fleshy leaf of *Camellia oleifera* Abel. *J. Food Sci. Biotechnol.* 26, 46–50.

Zhu, B. F., Peng, L., Luo, L. F., Liu, J. H., and He, Q. D. (2007b). The analysis of exploitive value and edible security in fleshy fruit and fleshy leaf of *Camellia oleifera* Abel. *J. Food Sci. Biotechnol.* 26, 1–6.

Zhu, H., and He, C. (2023). Identification and characterization of *Colletotrichum* Species causing tea-Oil Camellia (*Camellia oleifera* C.Abel) anthracnose in Hainan, China. *Forests* 14:1030. doi: 10.3390/f14051030

Zhuang, R. L. (2008). *China Oil-Tea*. Beijing: China Forestry Publishing House.

Zong, J. F., Peng, Y. R., Bao, G. H., Hou, R. Y., and Wan, X. C. (2016). Two new oleanane-type saponins with anti-proliferative activity from *Camellia oleifera* Abel. seed cake. *Molecules* 21:188. doi: 10.3390/molecules21020188

frontiers | Frontiers in Microbiology

TYPE Original Research
PUBLISHED 01 December 2023
DOI 10.3389/fmicb.2023.1282609

OPEN ACCESS

EDITED BY
Osama Abdalla Abdelshafy Mohamad,
Chinese Academy of Sciences (CAS), China

REVIEWED BY
Ahmed A. A. Aioub,
Zagazig University, Egypt
Deepanshu Jayaswal,
Indian Institute of Seed Science, India

*CORRESPONDENCE
Yi Cao
✉ yicao1001@163.com

RECEIVED 24 August 2023
ACCEPTED 23 October 2023
PUBLISHED 01 December 2023

CITATION
Cao Y, Lu N, Yang D, Mo M, Zhang K-Q, Li C and Shang S (2023) Root-knot nematode infections and soil characteristics significantly affected microbial community composition and assembly of tobacco soil microbiota: a large-scale comparison in tobacco-growing areas.
Front. Microbiol. 14:1282609.
doi: 10.3389/fmicb.2023.1282609

Root-knot nematode infections and soil characteristics significantly affected microbial community composition and assembly of tobacco soil microbiota: a large-scale comparison in tobacco-growing areas

Yi Cao[1]*, Ning Lu[1], Dongmei Yang[1], Minghe Mo[2], Ke-Qin Zhang[2], Caibin Li[3] and Shenghua Shang[1]

[1]Guizhou Academy of Tobacco Science, Guiyang, Guizhou, China, [2]State Key Laboratory for Conservation and Utilization of Bio-Resources in Yunnan, Yunnan University, Kunming, Yunnan, China, [3]Bijie Tobacco Company of Guizhou Province, Bijie, Guizhou, China

Introduction: Tobacco root-knot nematode (RKN) is a highly destructive soil-borne disease worldwide. However, there is a lack of research on the relationship between RKN and tobacco root microbial community composition under large-scale geographical conditions in China.

Methods: In this study, we collected 65 samples from 28 main tobacco-growing areas across 10 provinces in China and conducted 16S rDNA sequencing to investigate the dynamic microbial changes in tobacco soil infected by RKN compared to healthy tobacco soil. Based on the analysis of rhizosphere soil bacterial communities, changes after RKN infection, and soil environmental factors.

Results: We found the 28 tobacco-growing areas could be divided into two distinct groups with different microbial compositions and varying responses to RKN infection. In group1 of the provinces of Anhui, Henan, Shanxi, and Heilongjiang, Vicinamibacteria dominated the bacterial community, while Acidobacteriae was present in low abundance. In contrast, group2 of the other six provinces (Yunnan, Guizhou, Chongqing, Guangxi, Hubei, and Shandong) exhibited an opposite pattern. After infected by RKN, the genera *Chitinophaga* increased significant in group 1, while the genera *Rhodococcus* in group 2 exhibited a substantial increase. Alpha-diversity analysis revealed that RKN-infected tobacco exhibited a richer and more diverse rhizosphere soil bacterial community compared to healthy tobacco in most growing areas. A total of 12 kinds of soil environmental factors were measured in healthy and RKN-infected tobacco soil, and based on the co-occurrence and correlation analysis between environmental factors and microbial species, the pH level, calcium (Ca), magnesium (Mg), phosphorus (P), iron (Fe), and sodium (Na) were identified as key environmental factors influencing the population composition of rhizosphere microorganisms during RKN infection. We observed that RKN infection further increased the pH in weakly alkaline group 1 soil, while weakly acidic group 2 soil experienced a further decrease in pH. Furthermore, we identified three genera as potential biocontrol or plant growth-promoting bacteria for tobacco.

Discussion: These findings provide valuable reference data for managing RKN disease in different tobacco-growing areas and contribute to the exploration of new and effective biological control methods.

KEYWORDS

root-knot nematode, rhizosphere microorganisms, bacterial community, soil physical and chemical factors, large-scale geographical condition

Introduction

Root-knot nematodes (RKN; *Meloidogyne* spp.) are soil-borne pathogens that can infect a wide range of crops and cause significant damage (Jeger et al., 2018; Hemmati and Saeedizadeh, 2020). Various plants can be susceptible to infection by RKN, such as tobaccos (Barker and Weeks, 1991), tomatoes (Liu et al., 2020; El-Ashry et al., 2021), cucumbers (Yin et al., 2021), peppers (Eldeeb et al., 2022), and eggplants (Sharma et al., 2021). These nematodes are highly pathogenic and can destroy host resistance. According to the Food and Agriculture Organization of the United Nations (FAO), plant parasitic nematode infection has been considered the fourth invasive type of disease to affect plants, with an annual loss of more than 157 billion dollars worldwide (Huang et al., 2020). In China, the problem of tobacco suffering from RKN disease and other soil-borne diseases has become increasingly severe, leading to yield losses ranging from 30 to 50% (Huang et al., 2020).

Over 100 RKN species have been reported worldwide (Jones et al., 2013), with *Meloidogyne incognita*, *M. hapla*, *M. arenaria*, and *M. javanica* being the major pathogens in China. Among them, *M. incognita* is the dominant species causing the most damage to tobacco (Cui et al., 2021). By penetrating the root tips of tobacco and moving to the vascular cylinder, RKNs can induce the formation of specialized feeding sites called "giant cells" (Kyndt et al., 2013; Bartlem et al., 2014; Escobar et al., 2015). As the proliferation of tissues surrounds the nematode feeding site, the root system is disrupted, and general metabolic functions such as the absorption and transportation of water and minerals are hindered, leading to wilting and withering (Cao et al., 2022). Moreover, RKN infection can also drive pathogen infections that may cause fusarium wilt, root rot, and bacterial diseases (Khan and Ahamad, 2020; Leonetti and Molinari, 2020).

To protect tobacco from soil-borne diseases such as RKN disease, farmers have adopted various practices, including crop rotation, soil fumigation, and pesticide application. However, these methods are only temporarily effective and have led to increasingly serious resistance. Scientists have conducted many studies to control RKN disease in tobacco, including identifying resistance genes to RKN (Filho et al., 2016; Banakar et al., 2020), developing efficient biocontrol agents against RKNs (Cao et al., 2022), studying interactions between plant-parasitic RKNs and their hosts (Walsh et al., 2017; Qin et al., 2022), and investigating microbial community changes in rhizosphere soil (Huang et al., 2020). Of all types of plant-parasitic nematode management strategies, biocontrol methods are considered safer and more practical options (Aioub et al., 2022). For example, co-fertilization with animal manure and rhizobacteria can suppress phytonematodes and enhance the production of cucumbers and tomatoes (Ali et al., 2022). The combination of abamectin and/or emamectin benzoate with *Purpureocillium lilacinum* and rhizobacteria has been proven to be effective against *Meloidogyne incognita* on tomatoes (El-Ashry et al., 2021).

The rhizosphere is a tiny area of 1–2 mm outside the root of plants (Philippot et al., 2013). It is an interface where plant–soil ecosystems frequently exchange energy and nutrients, and it contains a huge number of microorganisms (Ding et al., 2021). Some species may be beneficial to plant growth and health in rhizosphere soil, such as nitrogen-fixing bacteria, photosynthetic bacteria, and biocontrol microorganisms (Ding et al., 2021), while others may be harmful and lead to plant diseases, including *Rhizoctonia solani*, *Ralstonia solanacearum*, and *Fusarium oxysporum* (Navarrete et al., 2013). Plant root exudates serve as the primary food sources for microbes, which can "shape" a unique rhizosphere microbial community around plants and significantly impact the composition of the rhizosphere microbiome (Zhang et al., 2020; Liang et al., 2021). The "plant–soil-microorganism" ecosystem is a complex "holobiont." Due to nematode infection, tobacco can regulate the plasticity of its root morphology and architecture in order to adapt to the new rhizosphere environment (Zeng et al., 2022). Simultaneously, this adaptation can modify the structure and function of soil microbial communities by affecting the availability of soil organic matter and nutrients (Wan et al., 2021). Numerous studies have demonstrated an intimate relationship between root-knot nematodes (RKN) and the diverse and abundant plant-associated microbiota. Several investigations have found that nematode infections often lead to an enrichment of beneficial bacteria for plants, which has been considered a plant-healing mechanism (Li et al., 2023). However, the most common consequence is complex diseases caused by bacterial pathogens resulting from microbial imbalances.

The main hypothesis of this study is that there may be specific patterns in the changes of rhizosphere microbial communities before and after RKN infection in different tobacco-growing areas in China. Moreover, certain microorganisms with biocontrol functions might play a role in resisting nematode infection. Our aim is to identify key factors that influence the occurrence of tobacco RKN disease by examining the relationship between RKN infections, bacterial communities, and soil environmental factors in various tobacco-growing regions. This research will be valuable in exploring new and effective biological control methods. To investigate this, we collected samples from 28 tobacco-growing areas across 10 provinces in China. We utilized 16S rDNA sequencing to explore microbial communities and conducted a detailed examination of the composition of rhizosphere bacteria in both healthy and infected plants.

Materials and methods

Sample collection

Soil samples were collected during the tobacco growing season, approximately 90–120 days after transplantation, from 28 major tobacco-growing areas in 10 provinces in China (namely, Yunnan, Guizhou, Chongqing, Guangxi, Anhui, Henan, Hubei, Shandong, Shanxi, and Heilongjiang). All tobacco farms used traditional cultivation methods, including seedling production, fertilization, pest control, and other field management practices. Soil samples were collected from healthy plants and plants infected with root-knot nematodes. In summary, five plots were randomly selected from each farm for field sample collection, and roots of 3–5 random plants were sampled from the middle of each plot. Finally, 15–25 roots of plants were collected and mixed in one sterile sampling bag. For each plant, a root segment of 5 cm length and 0.5–3 mm diameter was collected from near the base of the plant, along with any adhering soil particles. The root segments were mixed and placed in sterile sampling bags. One portion of the samples was frozen at −80°C for DNA extraction, while the other portion was used for soil physicochemical analysis. Detailed information for each sample is presented in Supplementary Table S1.

DAN extraction, 16S rDNA amplification, and sequencing

Microbial DNA was extracted from the soil using the Power Soil DNA Isolation Kit (MoBio Laboratories, Carlsbad, CA, United States), following the standard protocol. The final concentration and purity of the genomic DNA were measured using NanoDrop 2000 (NanoDrop Technologies, Wilmington, DE, United States), and DNA quality was assessed by 1% agarose gel electrophoresis. Primers 27F (5′-AGAGTTTGATCC TGGCTCAG-3′) and 533R (5′-TTACCGCGGCTGCTGGCAC-3′) were used to amplify the V1-V3 variable region of the 16S rRNA gene. High-quality PCR products were extracted and purified from a 2% agarose gel. The purified PCR products were sequenced on the 454 GS FLX platform. Detailed sequence information for each sample is presented in Supplementary Table S2. All the sequenced data and the names of the accession numbers can be found at https://www.ncbi.nlm.nih.gov/bioproject/PRJNA971867.

Bioinformatics and statistical analyses

The raw data were trimmed and filtered to obtain high-quality reads, which were clustered into operational taxonomic units (OTUs) with a similarity threshold of 97% using USEARCH v11.0.667 (Edgar, 2018) in the QIIME v1.7.0 pipeline (Caporaso et al., 2010). Taxonomic classification was assigned to representative sequences of each OTU using the QIIME pipeline based on the SILVA database (release 138). OTUs identified as chloroplasts or mitochondria were removed, and the filtered OTU table was normalized by the minimum number of reads across all samples. Chao1 and Shannon indices were calculated to measure alpha diversity and determine community richness and diversity. For beta diversity, Bray–Curtis distance metrics were calculated using QIIME. Principal coordinate analysis (PCoA) using Bray–Curtis distances was performed with the "Vegan" package in R v4.2.2 (Oksanen et al., 2019). Pearson correlation coefficients were computed using the "corrplot" R package. Co-occurrence networks were visualized using Gephi 0.9.5 software and Cytoscape 3.8.0.

Determination of physical and chemical parameters of soil samples

A mixture of 10 g of soil with 50 mL of sterile water was prepared, and the pH was measured using a digital pH meter. The concentration of soil organic matter (OM) was determined by the potassium dichromate oxidation-sulfuric acid titration method using 5 g of dried soil (Jankauskas et al., 2006). Available phosphorus and potassium in the soil were measured using the methods described by Lin et al. (2021) and Bray (1945). Ammonium nitrogen ($NH4^+$-N) was measured using a continuous flow analyzer (Tan et al., 2021). The concentrations of sodium (Na), zinc (Zn), iron (Fe), calcium (Ca), magnesium (Mg), manganese (Mn), and copper (Cu) were measured using a standard elemental analyzer, with methods referenced from Bao (2000). Detailed information on the chemical parameters of each sample is presented in Supplementary Table S3.

Results

The composition and structure of bacterial communities in the rhizosphere of 28 main tobacco-growing areas

We sequenced the 16S rDNA amplifications of 65 samples collected from 28 main tobacco-growing areas in 10 provinces in China. However, the library construction failed for three samples, namely, YN-5 from Yunnan province and SD-3 and SD-4 from Shandong province. In addition, three other samples (R56 from Henan province and R51 and R58 from Yunnan province) were removed from subsequent analysis due to insufficient sequence reads. As a result, we used 59 good quality samples for operational taxonomic unit annotation. These samples included 25 healthy samples, 24 diseased samples, and 10 samples from other plants. We identified 31,828 OTUs, which were assigned to 1,330 genera belonging to 47 phyla. Among all the bacterial OTUs, 18,101 were associated with healthy tobacco, assigned to 1,094 genera and 45 phyla, while 18,843 were associated with diseased tobacco, assigned to 1,099 genera and 42 phyla. Acidobacteriota was the dominant bacterial phylum in all soil samples from different areas, followed by Proteobacteria, Chloroflexi, Actinobacteriota, and Planctomycetota, accounting for approximately 80% and even more than 90% in some samples.

Composition of microbial communities in the rhizosphere of samples collected from other plants (healthy forest, maize, vegetable, and fruit) in Yunnan and Guizhou provinces was almost the same as those from tobacco plants at the phylum, class, and genus levels (Figure 1; Supplementary Figure S1). The rhizosphere bacterial communities of healthy tobacco and RKN-infected tobacco were similar, especially in

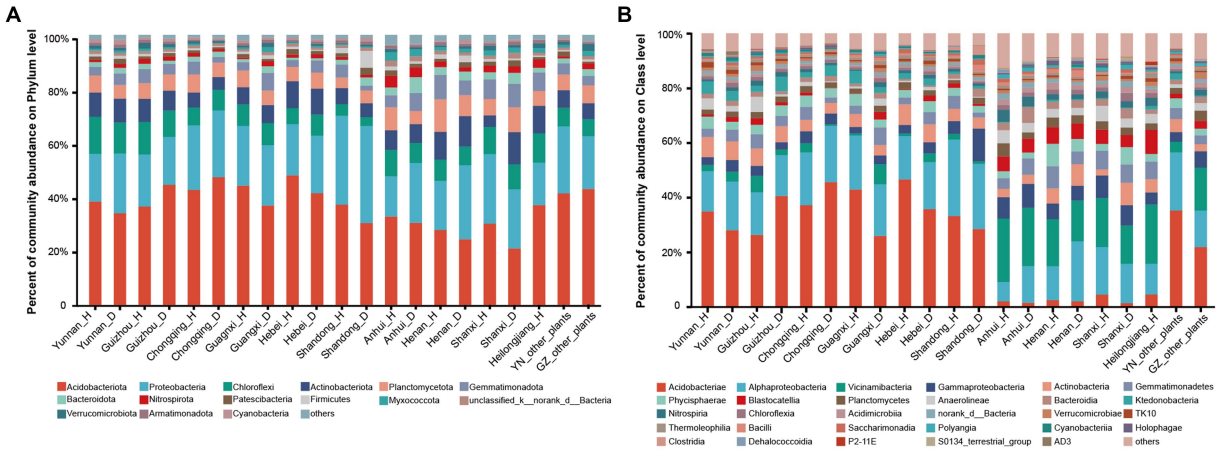

FIGURE 1
Composition of microorganisms in healthy and RKN-infected tobacco from different provinces. **(A)** Composition of microorganisms at the phylum level. **(B)** Composition of microorganisms at the class level.

terms of the dominant taxa across all samples. However, there were differences between the percentage of exact species and the composition of some endemic species, most of which accounted for a low percentage. Detailed information is presented in Supplementary Table S4.

Based on the analysis of microbial communities, we discovered distinct microbial composition patterns at the class level between samples collected from Anhui, Henan, Shanxi, and Heilongjiang provinces and samples collected from the other six provinces (Yunnan, Guizhou, Chongqing, Guangxi, Hubei, and Shandong). Samples collected from the four former provinces tended to be dominated by bacteria in the Alphaproteobacteria and Vicinamibacteria taxa, followed by the Gammaproteobacteria and Actinobacteria classes, while the class Acidobacteria accounted for a low percentage, even less than 2%. In contrast, the latter six provinces exhibited a diametrically opposed situation. For instance, the taxon Vicinamibacteria was a minority class, and the class Acidobacteria predominated the community (more than 40%, Supplementary Table S4) of soil samples from these provinces (Figure 1B). To further characterize these patterns, we assigned the four provinces to group 1 and categorized the remaining six provinces as group 2.

RKN infection drove the establishment of rhizosphere bacterial communities

The Venn diagram revealed that 884 genera, classified into 38 phyla, were shared by both healthy and RKN-infected tobacco, while 197 unique genera belonging to eight phyla were only found in the soil of healthy tobacco. On the other hand, 187 unique genera, all belonging to the phylum Halanaerobiaeota, were only found after RKN infection (Supplementary Table S5). This finding provides a clue for further research on biomarkers in microbial community diversity induced by RKN infection.

Alpha diversity analysis was conducted to examine the species diversity between and among samples from different tobacco-growing provinces. No significant differences were observed within each province before and after RKN infection at the phylum, genus, and OTU levels (data not shown). However, when comparing group 1 samples (from the four provinces) with group 2 samples (from the other six provinces), we found that the rhizosphere soil of group 1 samples exhibited higher richness and diversity of bacteria based on the Chao1 index and the Shannon index results (Figure 2). Although there was no statistically significant difference between the rhizosphere soil microbiota of healthy tobacco and nematode-parasitized tobacco in both group 1 and group 2 samples, RKN-infected tobacco tended to exhibit greater richness and diversity of bacterial species in the rhizosphere soil compared with healthy tobacco.

It is worth noting that the rhizosphere soil of diseased tobacco had greater bacterial richness but lower evenness. For example, samples from Guizhou province (Supplementary Figure S2) indicated that disease occurrence led to the recruitment of more types of microbes with low abundance around the roots, resulting in a decline in overall evenness and a subsequent reduction in the value of the Shannon index. In contrast to the samples from other regions, samples from Chongqing exhibited an opposing result, where the rhizosphere soil of healthy tobacco had higher bacterial richness and greater bacterial diversity compared with the diseased samples (Supplementary Figure S2).

Comparison of root microbial composition after RKN infection in different tobacco-growing areas

Principal coordinate analysis (PCoA) of Bary–Curtis distances revealed that all samples could be significantly separated into two groups, closely corresponding to group 1 and group 2 (Figure 3B). The PC1 component, which contributed the most to the differentiation, explained 19.29% of the total variance. This result indicated a significant differentiation of bacterial communities across latitudes (all provinces in group 1 are located north of the Yangtze River, while provinces in group 2 except Shandong are located south of the Yangtze River).

Further comparisons of changed microorganisms between healthy and infected tobacco showed significant differences between group 1 and group 2. RKN infection resulted in a marked change in bacterial abundance, with nine genera in group 1 and 17 genera in group 2, showing a sharp increase after infection, while only three genera declined (Figures 3C,D). Interestingly, none of the significantly changed bacteria belonged to the same genus. After infected by RKN,

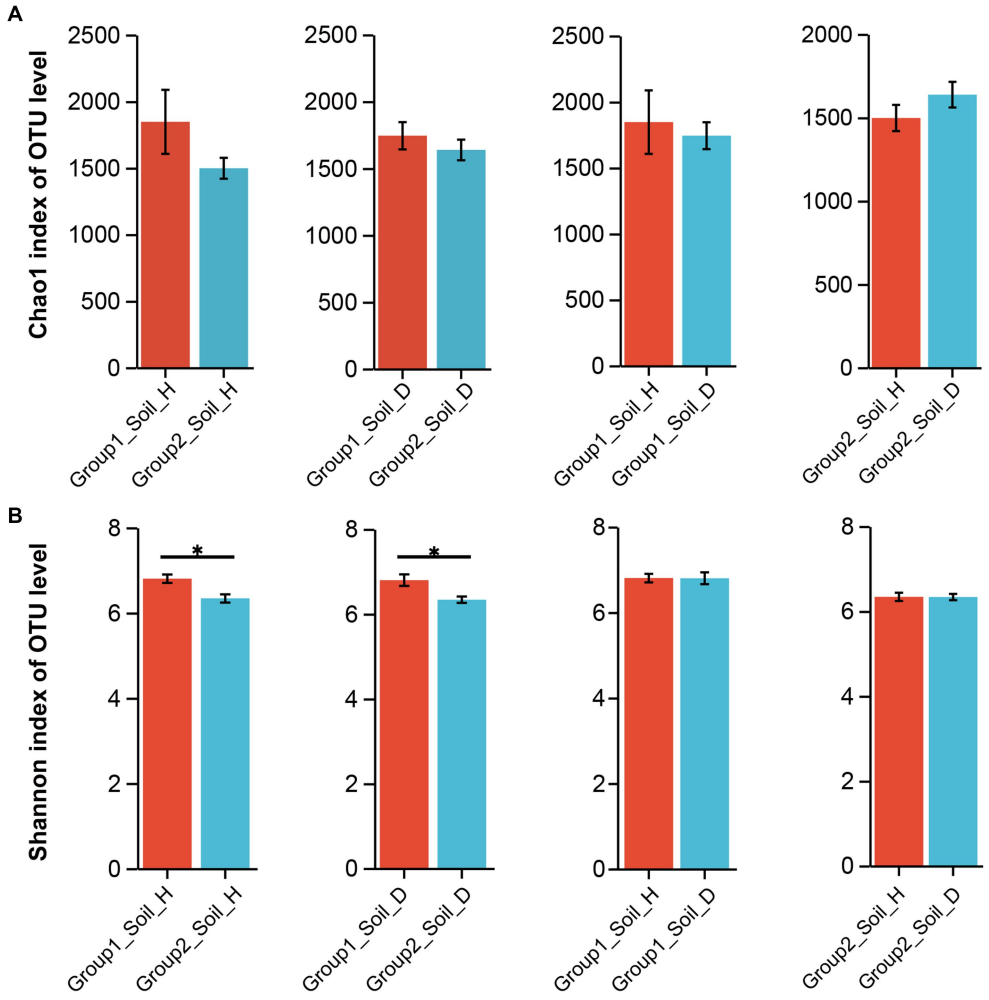

FIGURE 2
Changes in richness and diversity of rhizosphere soil microorganisms of healthy and RKN-infected tobacco on OTU level. **(A)** Statistics of microorganisms between group1 and group2 rhizosphere soil based on Chao1 index. **(B)** Statistics of microorganisms between group1 and group2 rhizosphere soil based on Shannon index.

genera *Allorhizobium-Neorhizobium-Pararhizobium-Rhizobium* and *Chitinophaga* increased by 4.35 and 38.16 times, respectively, in group 1, while the genera *Burkholderia-Caballeronia-Paraburkholderia*, *Rhodococcus*, and *norank_f__Solirubrobacteraceae* in group 2 exhibited a substantial increase of more than 2- and even 10-fold in some cases. However, the genus *Chryseolinea* in group 1 and genus *Rhizomicrobium* in group 2 decreased to a very low level. Notably, the proportion of all significantly changed bacteria in the abundance was very low, indicating that they may play a critical role as a keystone species in RKN infection or defending against further damage to tobacco.

Probiotic flora suggesting potential biocontrol bacteria

Biological control is considered a very promising approach for preventing or weakening RKN infection and other microbial pathogens. 16S rRNA gene sequencing is considered to be an effective approach to identify microorganisms with biocontrol or growth-promoting properties. In our study, based on the 197 unique genera found in healthy tobacco, we conducted additional analyses to identify specific types of bacteria, ultimately selecting three genera as potential probiotic candidates. The genus *Rhizomicrobium* primarily exists in the rhizosphere soil of plants, forming a symbiotic relationship with plant roots and exerting a series of beneficial effects on plant growth and health. For example, *Rhizomicrobium* sp. can produce substances such as plant hormones and trace elements, thereby facilitating plant growth and development. It also possesses the ability to inhibit the growth of plant pathogens, aiding plants in defending against diseases. The gram-negative genus *Dinghuibacter* exhibits diverse metabolic abilities and ecological functions, playing a significant role in carbon cycling and organic matter degradation. Finally, the genus *Chitinimonas* is considered to have the ability to degrade chitin, providing essential nutrients and energy for other microbial communities and promoting the health and balance of plant rhizosphere microbiota.

Multiple soil environmental factors significantly correlated with RKN disease

In this study, 12 types of soil environmental factors were measured, and the detailed results are presented in Supplementary Table S3. Based

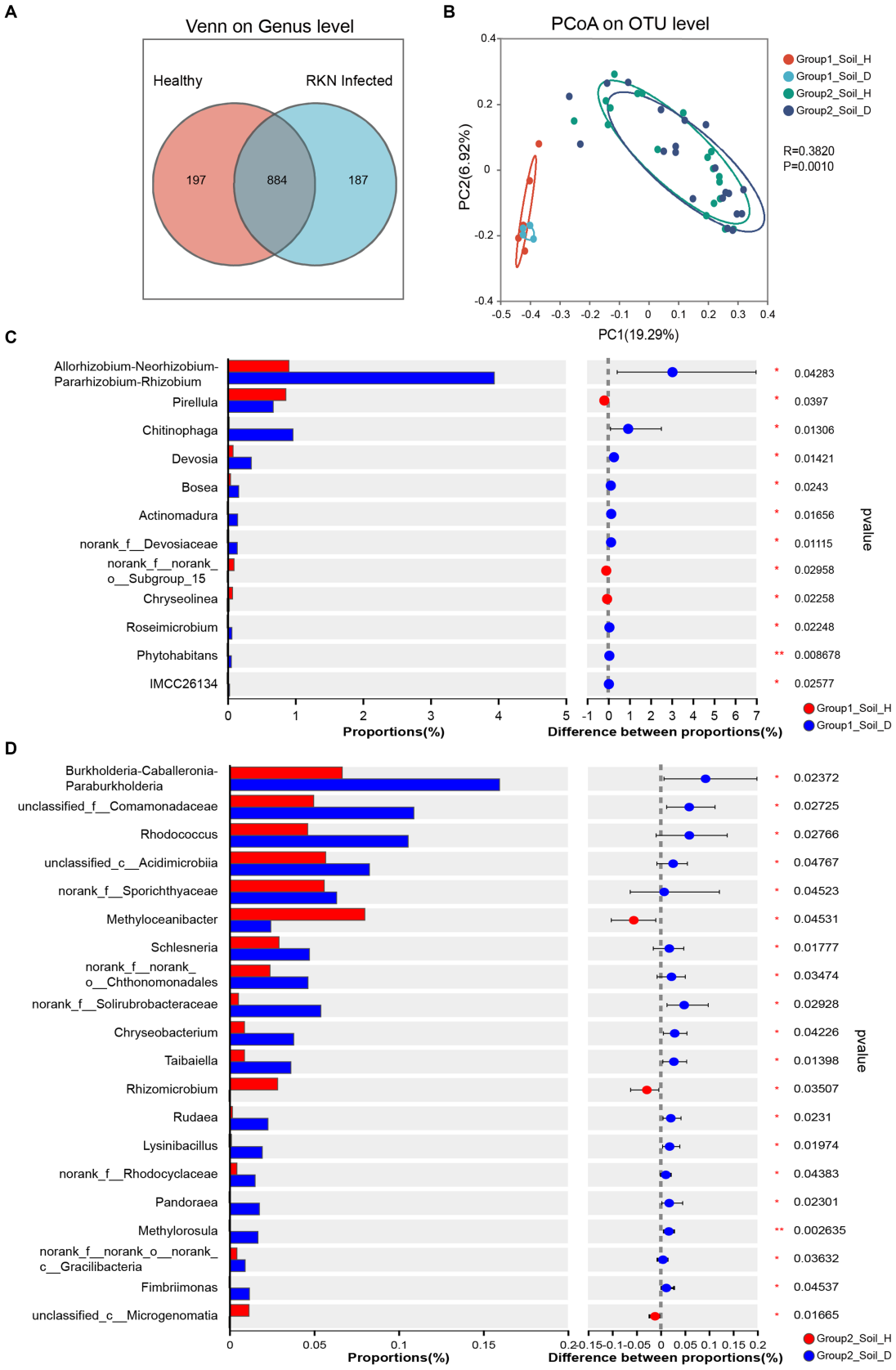

FIGURE 3
Community diversity measurements of microbial species in RKN-infected and healthy tobacco root rhizosphere. **(A)** Venn diagram showing the shared and unique genera between healthy and RKN-infected tobacco root soil. **(B)** PCoA analysis of bacterial communities in the rhizosphere based on Bray-Curtis distances at the OTU level among healthy and RKN-infected tobacco root soil in group1 and group2. **(C, D)** Enrichment of specific taxa at genus level in the rhizosphere of healthy tobacco plants against RKN-parasitized samples. Two-way ANOVA was conduced to determine the enriched species in healthy and infected plants (*$p < 0.05$, **$p < 0.01$, ***$p < 0.001$).

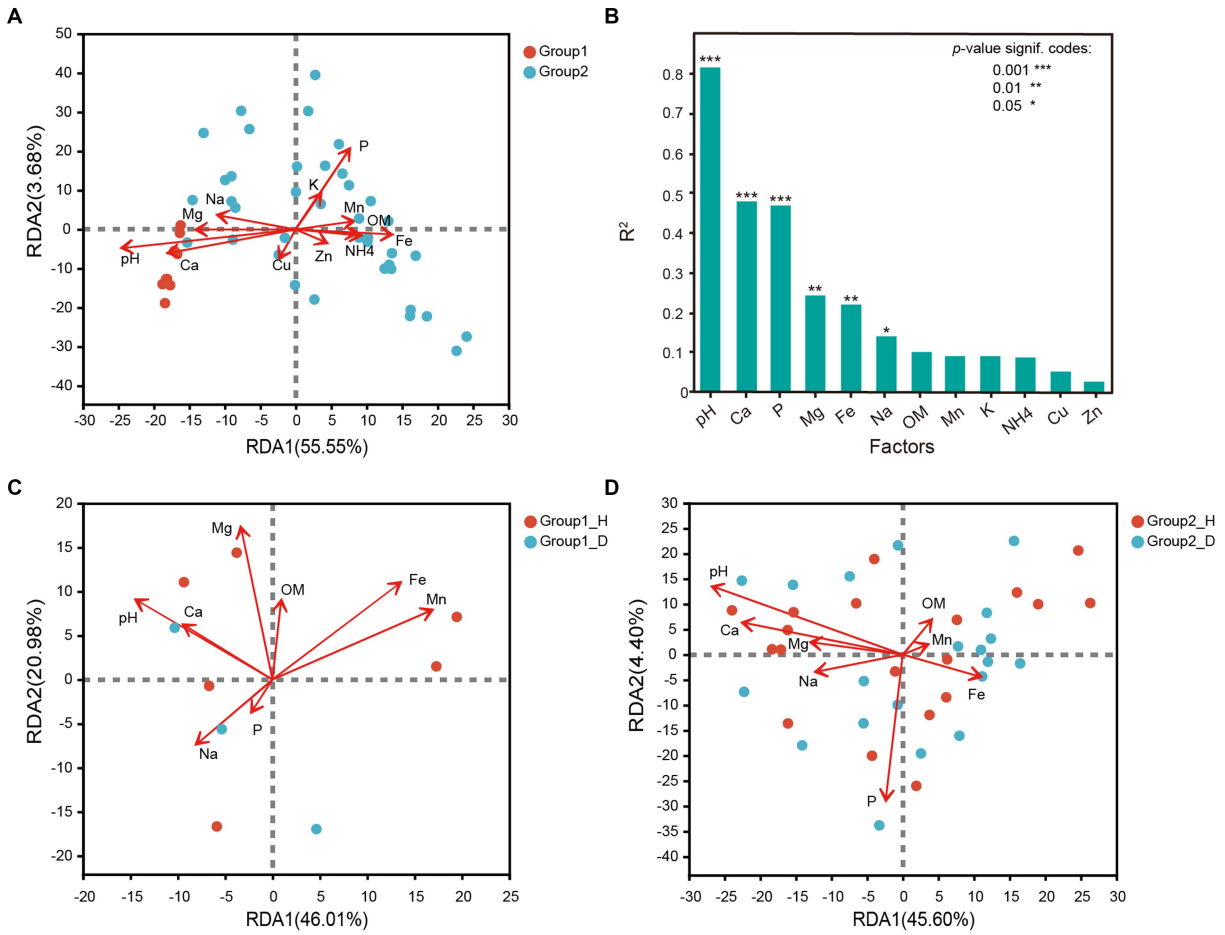

FIGURE 4
Correlation analysis between the bacterial community structure at genus level and soil environmental factors. **(A)** Redundancy analysis of soil environmental factors and all samples in group1 and group2. **(B)** Correlation analysis between chemical parameters of soil and the microbial community composition. **(C,D)** Redundancy analysis of soil environmental factors and samples with and without RKN disease in group1 and group2.

on variance inflation factor (VIF) selection and redundancy analysis, all the 12 chemical parameters exhibited some degree of correlation with the bacterial community structures at the OTU level. Redundancy analysis revealed that the bacterial community in group 1 and group 2 responded differently to these factors. Group 1 had weakly alkaline soil with higher calcium (Ca) and magnesium (Mg) contents, while group 2 had weakly acidic soil with lower phosphorus (P) and iron (Fe) contents. Soil pH and the metals Ca, Mg, and Na were identified as key parameters significantly correlated with rhizosphere microbial communities of tobacco root. On the other hand, P, Fe, and manganese (Mn) significantly but negatively affected bacterial community structures. Zinc (Zn), copper (Cu), potassium (K), and ammonium-N ($NH4^+$-N) were considered insignificant as they had less impact on microbial distribution (Figure 4B). Further analysis revealed that, Mn ($R^2=0.5087$, $p=0.020$) was the most important effector affecting microbial distribution between healthy and RKN-infected tobacco in group 1, followed by Mg ($R^2=0.4543$), Fe ($R^2=0.444$), and pH ($R^2=0.424$; Figure 4C). In group 2, pH ($R^2=0.6931$, $p=0.001$) had a significant influence on microbial distribution, while P ($R^2=0.5549$, $p=0.001$) and Ca ($R^2=0.4047$, $p=0.001$) were also key parameters (Figure 4D). Both in group 1 and group 2, pH and Ca had a consistent impact on bacterial distribution and had no correlation with parameter P. Interestingly, pH was found to change due to RKN infection, with an increase in alkaline soil and a decrease in acidic soil.

Co-occurrence networks for bacterial communities between healthy and RKN-infected plants

To investigate microbial co-occurrence and correlation between environmental factors and microbial species in soil bacteria from both healthy and RKN-infected tobacco plants, the study selected the top 400 genera in abundance from both group 1 and group 2 for further analysis. The network results showed that while there were a large number of bacteria sharing complex interaction relationships in group 1 between healthy plants and RKN-infected plants, there were few genera sharing interactions in group 2. Based on these interactions, all the taxa could be divided into more than eight different modules (Figure 5), with varying species and different connections. The network complexity could be evaluated by the number of nodes, edges, and average degrees in each group. Taken together, there was a more complex bacterial interaction in group 1 (up to 400 genera over 33 phyla) than in group 2 (only 242 genera from 19 phyla with interactions). Certain genera, such as *Ferruginibacter,*

Ramlibacter, Sumerlaea, Kribbella, norank_f__norank_o__norank_c__OM190, *norank_f__norank_o__11-24*, *unclassified_c__Gammaproteobacteria*, *norank_f__norank_o__norank_c__Subgroup_5*, *unclassified_o__Acidobacteriales,* and *norank_f__norank_o__SBR1031* tended to be more important as they had significantly positive or negative correlations with more than 70 types of other genera based on the changes in soil bacterial community structures of healthy and RKN-infected plants of group 1. In contrast, the top 10 genera having interactions with other bacteria in group 2 were *norank_f__Vicinamibacteraceae*, *UTCFX1*, *norank_f__A4b, norank_f__Roseiflexaceae*, *norank_f__norank_o__Vicinamibacterales*, *Pirellula*, *Ilumatobacter, Nordella*, *Steroidobacter,* and *Acidothermus*, and none of them were the same in group 1. Many genera were associated with different species, and their interactions with each other may be diverse. For instance, *Ferruginibacter* had a strong positive correlation with *Streptomyces*, *Ellin6055,* and *Kribbella* but negatively related to *Haliangium*, *Paludibaculum,* and *Nitrospira* in group 1 (Supplementary Table S7, Sheet 1), whereas in group 2, *Pirellula* was directly proportional to *UTCFX1* and *Tundrisphaera* and inversely correlated with *Acidothermus* and *Actinospica* (Supplementary Table S7, Sheet 2).

Our study also investigated the impact of six soil environmental factors (pH, Ca, P, Mg, Na, and Fe) on changes in microbial communities. The results showed distinct differences between group1 and group2 (Figure 6A). In group 1, every soil factor showed relationships with some exact species, and only a few species were affected by up to two environmental factors. However, there was a complex correlation between environmental factors and bacterial structures in group2. pH was the most critical factor (correlating with up to 119 genera), followed by Ca (correlating with 57 genera) and Mg (correlating with 30 genera). Species were significantly affected by Mg and also affected by pH and Ca at the same time. None of the genera except the unknown *g__norank_p__FCPU426* had a correlation with Na (Figure 6B). Five genera from the phylum Proteobacteria, three genera from phyla Bacteroidota, Acidobacteriota, and Planctomycetota, and another three genera belonging to other phyla showed high correlation with P, while only eight genera from phyla Planctomycetota, Actinobacteriota, and Acidobacteriota significantly correlated with Fe (Figure 6B).

Some genera, such as *Solirubrobacter*, were mainly positively correlated with Mg with a high level in group 1, whereas in group 2, not only Mg but also pH and Ca had a positive correlation with it, despite a low correlation degree. Other two genera, namely, *Sporosarcina* and *Marmoricola*, shared a significant correlation with Mg and Ca in group 1 but not with group 2. This phenomenon is not uncommon in other species–environment correlations, suggesting that differences in the composition of flora between group 1 and group 2 may account for the varying correlations between bacterial communities and environmental factors.

Discussion

Tobacco-growing areas can be divided into two groups based on key indicator differences

Based on the 16S rDNA sequencing results, the rhizosphere bacterial communities of different areas could be divided into two groups: group 1 (Anhui, Henan, Shanxi, and Heilongjiang) in the north and group 2 (Yunnan, Guizhou, Chongqing, Guangxi, Hubei, and Shandong) in the south. Notably, the Shandong Tobacco Farm, located in North China, had a highly similar rhizosphere microflora composition to those in South China and Southwest China. While there were large differences in the community structure and taxa composition at the genus and class levels, there was a high degree of consistency at the phylum level between group1 and group 2 (Figure 1; Supplementary Figure S1). Further analysis revealed that group 1 had weakly alkaline soil with higher Ca and Mg content, while group 2 had weakly acidic soil with higher P and Fe content. These differences in pH and nutrient levels likely account for the variation in flora between the two groups. Calcium and magnesium ions can react with water molecules to form hydroxide ions, thereby increasing the pH of the soil (Weil and Brady, 2017), while phosphorus may contribute to soil acidification by forming phosphate (Wang P. et al., 2022). In southern China, iron (Fe) often forms salts, leading to increased hydrogen ion concentration in the soil and subsequent pH decrease. In southern China, iron (Fe) often forms salts and promotes the increase of hydrogen ion concentration in soil, thus leading to the decrease in pH (Yan et al., 2020). Taken together, the difference of pH may be one of the major reasons for the variation in flora between the two groups.

Changes in species richness and composition of microorganisms after RKN infection

The alpha diversity results showed that the richness and diversity of microbial flora in weakly alkaline group 1 soil were higher than those in weakly acidic group 2 soil, irrespective of the presence of RKN infection (Figure 2). This suggests that acidic soil may inhibit the growth of many microbial species. Although there was no significant change in microbial community diversity after RKN infection in both group 1 and group 2, there was a significant change in species richness and composition of microorganisms, which was similar to our previous study (Cao et al., 2022). After infection, approximately 20% of the total genera in healthy and diseased tobacco plants exhibited unique rhizosphere bacterial composition (Figure 3A). Additionally, the species richness decreased in group 1 but increased in group 2 after infection (Figure 2A), although Chongqing showed a contrary trend (Supplementary Figure S2). Previous studies indicated that the RKN infection may lead to an increase in the diversity of microbial flora, which may be caused by changes in plant root phenotypic traits (Zeng et al., 2022) and increased root secretions such as organic acids to recruit more microbial flora with beneficial effect on plants (Wang H. et al., 2022). Another hypothesis suggests that parasitizing nematodes may introduce their own microbial flora to the root site, resulting in changes in rhizosphere bacterial population diversity (Li et al., 2023). However, based on our extensive research spanning different tobacco-growing areas, we found that the influence of RNK infection and the changes in rhizosphere microflora had various characteristics. This comprehensive result may be attributed to a variety of factors, including the local climate, tobacco varieties, and the interactions between soil and other environmental factors.

Impact of RKN infection on rhizosphere microbial community

Root-knot nematode infection resulted in changes in the relative abundance of rhizosphere microorganisms. For example, after RKN

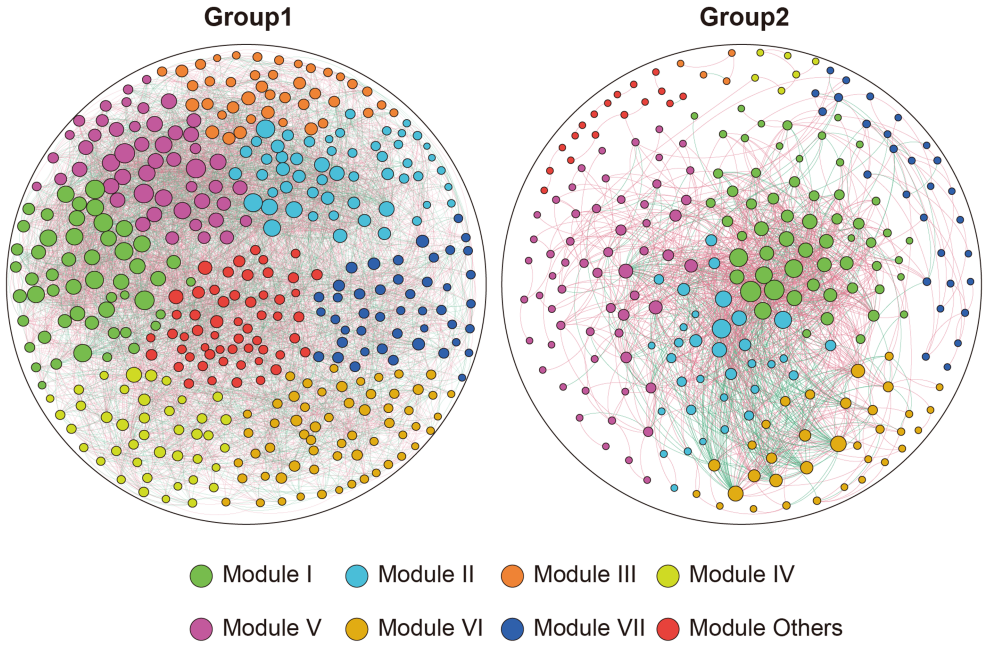

Network Properties

	Nodes	Edges	Ave. Degree	Clust. Coefficient	Ave. Path Length	Modularity
Group1	400	5805	29.025	0.357	2.397	0.357
Group2	242	1549	12.802	0.442	3.222	0.303

FIGURE 5
Networks of rhizosphere communities in soils of group1 and group2. The top 400 genera in abundance were selected for co-occurrence and correlation analysis. Genera with an absolute correlation value greater than 0.6 were selected for further analysis. Every node represents a different genus, and a large size of the node means a more complex correlation with other genera. Colours of each node represents eight modules with different co-occurrence. Edge with red colour means a positive correlation while green colour means a negative correlation. Thicker connections indicate higher correlation between genera.

infection, there was a significant increase in the phylum Bacteroidota in group 1 and a minimal increase in group 2. In both group 1 and group 2, more taxa were observed, such as phyla Proteobacteria, Actinobacteriota (Figure 1A), Patescibacteria, Firmicutes, and Cyanobacteria. Bacteroidota is known to play a crucial role in soil carbon and nitrogen cycle, plant–microbial interaction, and humus degradation (Larsbrink and McKee, 2020). Proteobacteria and Actinobacteriota, which are highly abundant in plant rhizospheres (Figure 1A), are essential for maintaining rhizosphere health, as reported in previous studies (Cao et al., 2022; Wang H. et al., 2022). However, the function of Patescibacteria remains unclear due to its challenging isolation and limited research. Acidobacteriota and Nitrospirota exhibited higher relative abundance in group 1 of healthy plant soil but increased in group 2 after infection. Acidobacteriota could produce hydrogen ions (H^+) or hydroxyl ions (OH^-) and interact with other bacterial communities, and the decrease in the relative abundance may also be related to the increase in pH (Nunes da Rocha et al., 2013).

The relationship between pH changes and RKN infection

Remarkably, we observed that RKN infection further increased the pH in weakly alkaline group 1 soil, while weakly acidic group 2 soil experienced a further decrease in pH. The results in group2 were consistent with other studies conducted in Hubei and Fujian provinces (Li et al., 2023; Lu et al., 2023). It is speculated that plants secrete organic acids and alter the microenvironment to inhibit nematode diseases and potential subsequent pathogen infections. Regarding the pH increase observed after RKN infection, it is possible that ammonium metabolism contributes to this phenomenon. When tobacco roots secrete a compound called "nodulin," it can initiate a symbiotic relationship with *Rhizobium* (Oldroyd, 2013), promoting the growth of nitrogen-fixing bacteria and converting nitrogen from the rhizosphere soil into fertilizer, which, in turn, provides nutrients for tobacco. Furthermore, the release of nodulin could also offset the acidic substances in the rhizosphere soil, leading to a rise in pH value. In our follow-up analysis, the genus *Nitrospira* in group 1 was also found to be associated with ammonium metabolism. The association between RKN infection and changes in rhizosphere pH is not fully understood. However, our hypothesis suggests that plants may preferentially adopt strategies that best suit their self-protection based on the original physicochemical properties of the rhizosphere soil, such as Ca and P concentrations, to mitigate or suppress the adverse effects of RKN infection.

Factors influencing the relationship between RKN infection and rhizosphere microflora changes

The interactions between microbiomes in the root rhizosphere soil play essential roles in maintaining a stable microbial community and

10.3389/fmicb.2023.1282609

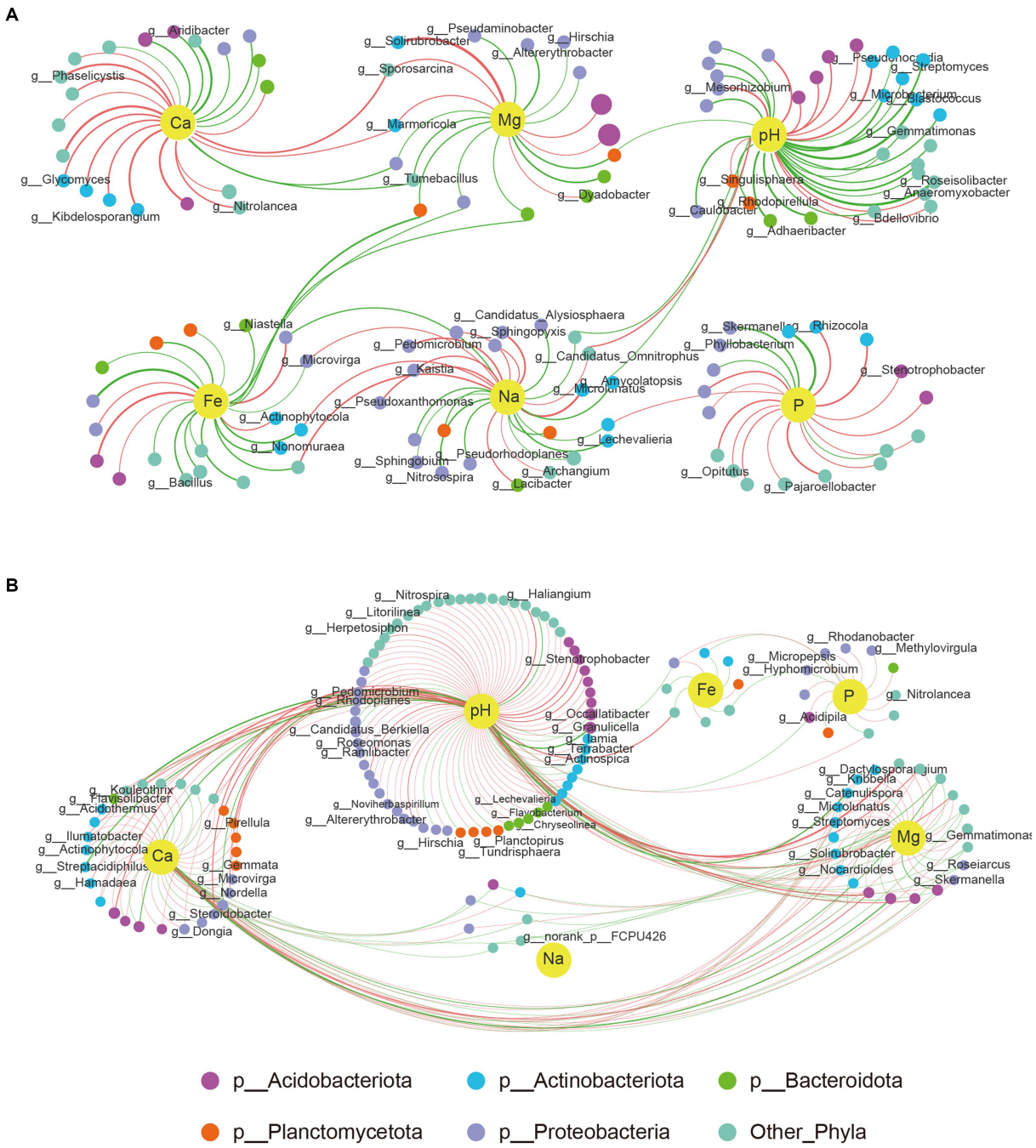

FIGURE 6
Networks of genera and chemical parameters of soil. **(A)** Correlations between genera with six soil environmental factors in group1. **(B)** Correlations between genera with six soil environmental factors in group 2. A big size of each node means a higher abundance at genus level. Colors of each genus represents six phyla. Edge with red color means a positive correlation while green color means a negative correlation. Thicker connections indicate higher correlation.

plant health (Chen et al., 2022). Co-occurrence patterns and microbial networks are effective ways to identify key and important species. In our study, we constructed microbial networks and microbe–soil environmental factor networks to depict the complex interactions. The results showed that there were much more complex microbial interactions in group 1 than in group 2 (Figure 5). In group1, the genus *Ferruginibacter*, classified as phylum Proteobacteria, increased in relative abundance after RKN infection and positively correlated with *Streptomyces* and *Kribbella*, both belonging to phylum Actinobacteria. It also shared a negative correlation with genera *Haliangium*, *Paludibaculum*, and *Nitrospira*. Another example is the increase in relative abundance of the genus *Ramlibacter* (p__Proteobacteria) in the diseased root soil, which is positively related to *Arthrobacter* (p__Actinobacteriota) and *Massilia* (p__Proteobacteria) and highly negatively correlated with *norank_f__Pirellulaceae*, *norank_f__Pirellulaceae*, and *Methyloceanibacter* (p__Proteobacteria; Supplementary Table S7). These findings illustrate that

these bacteria may be a keystone species in microbial community interactions and play an important role in defense against nematode infection and nutrient uptake. Many species of bacteria in group 2, such as *UTCFX1*, *Tundrisphaera*, *Acidothermus*, and *Actinospica*, changed in abundance due to the decreased relative abundance of the genus *Pirellula* (p__Planctomycetota). *Pirellula* has been reported to perform photosynthesis and is widely found in the ocean. Some reports have shown that *Pirellula* may be related to energy supply and substrate conversion in soil (Rabus et al., 2002). The results of correlation networks showed that six environmental factors, namely, pH, Ca, P, Mg, Fe, and Na, may be closely related to changes in the microbial flora (Figure 4), with pH being the most important factor. In group 2, only a few microorganisms were just correlated with Ca or Mg but were more closely correlated with pH changes at the same time (Figure 6). It indicated that bacterial communities under weakly acidic conditions may be more susceptible to pH changes, which is consistent with the significant influence of soil pH on microbial flora reported in other studies (Li et al., 2021; Tian et al., 2021).

Two interesting findings emerged from this study. First, there were still a large number of species with unclear taxa, many of which could not even be confirmed at the order or class level. Many unclassified species had significantly increased or decreased relative abundance (Figure 2). Additionally, numerous unclassified species were significantly correlated with multiple environmental factors (Figure 6). These results indicated that the presence of a large number of function-unknown species in the tobacco rhizosphere soil warrant further study. Second, there were many genera with abundances less than 1%, accounting for approximately 30% of the total, which was even higher than the abundance of the most abundant species (Supplementary Figure S1). This indicated that the composition of tobacco rhizosphere microorganisms was quite complex. Some reports have suggested that low-abundance species may also play specific biological roles in rhizosphere microecology (Ding et al., 2015; Leff et al., 2015; Jousset et al., 2017). We included the top 400 species in terms of relative abundance to construct different networks and found some key bacteria in low relative abundance, such as genera *Solirubrobacter* and *Phaselicystis*, although the underlying mechanism is still unknown.

Conclusion

In this study, we collected samples from 28 tobacco-growing areas in 10 provinces in China and examined the composition of rhizosphere bacteria in healthy and infected plants in detail. Significant differences were found in the microbial composition, especially the core bacteria at the class and genus levels, between the four Northern provinces and the other six provinces, indicating distinct regional characteristics. RKN-infected tobacco exhibited a richer and more diverse rhizosphere soil bacterial community compared with healthy tobacco in most growing areas. Environmental factors such as pH, calcium (Ca), magnesium (Mg), phosphorus (P), iron (Fe), and sodium (Na) may play key roles in changing the population composition of rhizosphere microorganisms during RKN infection. Three genera were identified as potential biocontrol or plant growth-promoting bacteria for tobacco. This research provides valuable reference data for RKN disease in different tobacco-growing areas and helps explore new and effective biological control methods.

Data availability statement

The data presented in this study is deposited in the NCBI database under BioProject accession number PRJNA971867 (https://www.ncbi.nlm.nih.gov/bioproject/PRJNA971867).

Author contributions

YC: Conceptualization, Supervision, Writing – original draft, Funding acquisition. NL: Data curation, Investigation, Visualization, Writing – original draft. DY: Investigation, Writing – original draft. MM: Investigation, Resources, Writing – review & editing. K-QZ: Supervision, Writing – review & editing. CL: Investigation, Resources, Writing – original draft. SS: Investigation, Resources, Writing – review & editing.

Funding

The author(s) declare financial support was received for the research, authorship, and/or publication of this article. This study was supported by grants from the National Basic Research Program of China (973) (2013CB127500), the National Natural Science Foundation of China (No. 31660544), the Major Science and Technology Program of China Tobacco Corporation [110202101055(LS-15)], and the Science and Technology Program of Guizhou Tobacco Company (2020XM12; 2023XM05). The funders were not involved in the study design, analysis, interpretation of data, the writing of this article or the decision to submit it for publication.

Acknowledgments

The authors thank the assistance of Xiangna Niu and Mei Wang from Shanghai Winnerbio Technology Co., Ltd. (Shanghai, China) for bioinformatics and statistical analyses. Wei Ding from Southwest University, Shujun Li from Henan Academy of Agricultural Sciences, Xihong Li from Hubei Academy of Tobacco Science, Yumei Qian from Tobacco Research Institute of Chinese Academy of Agricultural Sciences, and Benguo Zhou from Anhui Academy of Agricultural Sciences for their help in sampling and identifying RKN.

Conflict of interest

CL was employed by Bijie Tobacco Company of Guizhou Province.

The remaining authors declare that the research was conducted in the absence of any commercial or financial relationships that could be construed as a potential conflict of interest.

Publisher's note

Supplementary material

The Supplementary material for this article can be found online at: https://www.frontiersin.org/articles/10.3389/fmicb.2023.1282609/full#supplementary-material

SUPPLEMENTARY TABLE 1
Basic information of each sample.

SUPPLEMENTARY TABLE 2
Sequence results of each sample.

SUPPLEMENTARY TABLE 3
Physical and chemical parameters statistics of each sample.

SUPPLEMENTARY TABLE 4
Annotation at genus and phylum levels of all samples.

SUPPLEMENTARY TABLE 5
Shared and unique species at the genus and phylum levels between soil from healthy and RKN infected plants.

SUPPLEMENTARY FIGURE 1
Composition of microorganisms at the genus level in healthy and RKN-infected tobacco from different provinces.

SUPPLEMENTARY FIGURE 2
Changes in richness and diversity of rhizosphere soil microorganisms of healthy and RKN-infected tobacco on OTU level in Guizhou and Chongqing areas.

SUPPLEMENTARY FIGURE 3
Correlation analysis between the bacterial community structure at genus level and soil environmental factors of all samples without RKN disease.

References

Aioub, A. A. A., Elesawy, A. E., and Ammar, E. E. (2022). Plant growth promoting rhizobacteria (PGPR) and their role in plant-parasitic nematodes control: a fresh look at an old issue. *J. Plant Dis. Prot.* 129, 1305–1321. doi: 10.1007/s41348-022-00642-3

Ali, A. A., El-Ashry, R. M., and Aioub, A. A. (2022). Animal manure rhizobacteria co-fertilization suppresses phytonematodes and enhances plant production: evidence from field and greenhouse. *J. Plant Dis. Prot.* 129, 155–169. doi: 10.1007/s41348-021-00529-9

Banakar, P., Hada, A., Papolu, P. K., and Rao, U. (2020). Simultaneous RNAi knockdown of three FMRFamide-like peptide genes, mi-flp 1, mi-flp 12, and mi-flp18 provides resistance to root-knot nematode, meloidogyne incognita. *Front. Microbiol.* 11:573916. doi: 10.3389/fmicb.2020.573916

Bao, S. D. (2000). *Soil Agricultural Chemical Analysis 3rd Edn.* Beijing: China Agricultural Press

Barker, K. R., and Weeks, W. W. (1991). Relationships between soil and levels of meloidogyne incognita and tobacco yield and quality. *J. Nematol.* 23, 82–90.

Bartlem, D. G., Jones, M. G., and Hammes, U. Z. (2014). Vascularization and nutrient delivery at root-knot nematode feeding sites in host roots. *J. Exp. Bot.* 65, 1789–1798. doi: 10.1093/jxb/ert415

Bray, R. H. (1945). Soil-plant relations: II. Balanced fertilizer use through soil tests for potassium and phosphoru. *Soil Sci.* 60, 463–474. doi: 10.1097/00010694-194512000-00005

Cao, Y., Yang, Z. X., Yang, D. M., Lu, N., Yu, S. Z., Meng, J. Y., et al. (2022). Tobacco root microbial community composition significantly associated with root-knot nematode infections: dynamic changes in microbiota and growth stage. *Front. Microbiol.* 13:807057. doi: 10.3389/fmicb.2022.807057

Caporaso, J. G., Kuczynski, J., Stombaugh, J., Bittinger, K., Bushman, F. D., Costello, E. K., et al. (2010). QIIME allows analysis of high-throughput community sequencing data. *Nat. Methods* 7, 335–336. doi: 10.1038/nmeth.f.303

Chen, G., Wu, C., Wang, F., Lyu, H., Lu, Y., Yan, C., et al. (2022). Microbial community changes in different underground compartments of potato affected yield and quality. *3 Biotech.* 12:106. doi: 10.1007/s13205-022-03167-6

Cui, J. K., Ren, H. H., Meng, H. G., Chang, D., and Jiang, S. J. (2021). Research progress on the occurrence and control of tobacco root knot nematode in China. *Acta Phytopathol. Sin.* 51, 663–682. doi: 10.13926/j.cnki.apps.000487

Ding, Y., Chen, Y., Lin, Z., Tuo, Y., Li, H., and Wang, Y. (2021). Differences in soil microbial community composition between suppressive and root rot-conducive in tobacco fields. *Curr. Microbiol.* 78, 624–633. doi: 10.1007/s00284-020-02318-3

Ding, J., Zhang, Y., Wang, M., Sun, X., Cong, J., Deng, Y., et al. (2015). Soil organic matter quantity and quality shape microbial community compositions of subtropical broadleaved forests. *Mol. Ecol.* 24, 5175–5185. doi: 10.1111/mec.13384

Edgar, R. C. (2018). Updating the 97% identity threshold for 16S ribosomal RNA OTUs. *Bioinformatics* 34, 2371–2375. doi: 10.1093/bioinformatics/bty113

El-Ashry, R. M., Ali, M. A. S., Elsobki, A. E. A., and Aioub, A. A. A. (2021). Integrated management of Meloidogyne incognita on tomato using combinations of abamectin, Purpureocillium lilacinum, rhizobacteria, and botanicals compared with nematicide. *Egypt J. Biol. Pest Control.* 31, 1–10. doi: 10.1186/s41938-021-00438-x

Eldeeb, A. M., Farag, A. A. G., Al-Harbi, M. S., Kesba, H., Sayed, S., Elesawy, A. E., et al. (2022). Controlling of Meloidgyne incognita (Tylenchida: Heteroderidae) using nematicides, *Linum usitatissimum* extract and certain organic acids on four peppers cultivars under greenhouse conditions. *Saudi J. Biol. Sci.* 29, 3107–3113. doi: 10.1016/j.sjbs.2022.03.018

Escobar, C., Barcala, M., Cabrera, J., and Fenoll, C. (2015). Overview of root-knot nematodes and giant cells. In plant nematode interactions: a view on compatible interrelationships. *Adv. Bot. Res.* 73, 1–32. doi: 10.1016/bs.abr.2015.01.001

Filho, J. V. A., Machado, A. C. Z., Dallagnol, L. J., and Aranha Camargo, L. E. (2016). Root-knot nematodes (Meloidogyne spp.) parasitizing resistant tobacco cultivars in southern Brazil. *Plant Dis.* 100, 1222–1231. doi: 10.1094/PDIS-03-15-0341-RE

Hemmati, S., and Saeedizadeh, A. (2020). Root-knot nematode, Meloidogyne javanica, in response to soil fertilization. *Braz. J. Biol.* 80, 621–630. doi: 10.1590/1519-6984.218195

Huang, K., Jiang, Q., Liu, L., Zhang, S., Liu, C., Chen, H., et al. (2020). Exploring the key microbial changes in the rhizosphere that affect the occurrence of tobacco root-knot nematodes. *AMB Express* 10:72. doi: 10.1186/s13568-020-01006-6

Jankauskas, B., Slepetiene, A., Jankauskiene, G., Fullen, M., and Booth, C. (2006). A comparative study of analytical methodologies to determine the soil organic matter content of Lithuanian Eutric Albeluvisols. *Geoderma* 136, 763–773. doi: 10.1016/j.geoderma.2006.05.015

Jeger, M., Bragard, C., Caffier, D., Candresse, T., Chatzivassiliou, E., Dehnen-Schmutz, K., et al. (2018). Pest categorisation of *Nacobbus aberrans*. *EFSA J.* 16:e05249. doi: 10.2903/j.efsa.2018.5249

Jones, J. T., Haegeman, A., Danchin, E. G., Gaur, H. S., Helder, J., Jones, M. G., et al. (2013). Top 10 plant-parasitic nematodes in molecular plant pathology. *Mol. Plant Pathol.* 14, 946–961. doi: 10.1111/mpp.12057

Jousset, A., Bienhold, C., Chatzinotas, A., Gallien, L., Gobet, A., Kurm, V., et al. (2017). Where less may be more: how the rare biosphere pulls ecosystems strings. *ISME J.* 11, 853–862. doi: 10.1038/ismej.2016.174

Khan, M. R., and Ahamad, F. (2020). Incidence of root-knot nematode (Meloidogyne graminicola) and resulting crop losses in paddy rice in northern India. *Plant Dis.* 104, 186–193. doi: 10.1094/PDIS-12-18-2154-RE

Kyndt, T., Vieira, P., Gheysen, G., and de Almeida-Engler, J. (2013). Nematode feeding sites: unique organs in plant roots. *Planta* 238, 807–818. doi: 10.1007/s00425-013-1923-z

Larsbrink, J., and McKee, L. S. (2020). Bacteroidetes bacteria in the soil: glycan acquisition, enzyme secretion, and gliding motility. *Adv. Appl. Microbiol.* 110, 63–98. doi: 10.1016/bs.aambs.2019.11.001

Leff, J. W., Jones, S. E., Prober, S. M., Barberan, A., Borer, E. T., Firn, J. L., et al. (2015). Consistent responses of soil microbial communities to elevated nutrient inputs in grasslands across the globe. *Proc. Natl. Acad. Sci. U. S. A.* 112, 10967–10972. doi: 10.1073/pnas.1508382112

Leonetti, P., and Molinari, S. (2020). Epigenetic and metabolic changes in root-knot nematode-plant interactions. *Int. J. Mol. Sci.* 21:7759. doi: 10.3390/ijms21207759

Li, Y., Lei, S., Cheng, Z., Jin, L., Zhang, T., Liang, L. M., et al. (2023). Microbiota and functional analyses of nitrogen-fixing bacteria in root-knot nematode parasitism of plants. *Microbiome.* 11:48. doi: 10.1186/s40168-023-01484-3

Li, H. Q., Shen, Y. J., Wang, W. L., Wang, H. T., Li, H., and Su, J. Q. (2021). Soil pH has a stronger effect than arsenic content on shaping plastisphere bacterial communities in soil. *Environ. Pollut.* 287:117339. doi: 10.1016/j.envpol.2021.117339

Liang, J. F., Li, Q. W., Gao, J. Q., Feng, J. G., Zhang, X. Y., Wu, Y. Q., et al. (2021). Biochar rhizosphere addition promoted *Phragmites australis* growth and changed soil properties in the Yellow River Delta. *Sci. Total Environ.* 761:143291. doi: 10.1016/j.scitotenv.2020.143291

Lin, X., Zhang, J., Chen, H., and Han, L. (2021). Determination of available phosphorus in alkaline soil by molybdenum blue spectrophotometry. *IOP Conf Ser: Earth Environ Sci.* 781:052003. doi: 10.1088/1755-1315/781/5/052003

Liu, G., Lin, X., Xu, S., Liu, G., Liu, F., and Mu, W. (2020). Screening, identification and application of soil bacteria with nematicidal activity against root-knot nematode (Meloidogyne incognita) on tomato. *Pest Manag. Sci.* 76, 2217–2224. doi: 10.1002/ps.5759

Lu, P., Shi, H., Tao, J., Jin, J., Wang, S., Zheng, Q., et al. (2023). Metagenomic insights into the changes in the rhizosphere microbial community caused by the root-knot nematode Meloidogyne incognita in tobacco. *Environ. Res.* 216:114848. doi: 10.1016/j.envres.2022.114848

Navarrete, A. A., Kuramae, E. E., de Hollander, M., Pijl, A. S., van Veen, J. A., and Tsai, S. M. (2013). Acidobacterial community responses to agricultural management of soybean in Amazon forest soils. *FEMS Microbiol. Ecol.* 83, 607–621. doi: 10.1111/1574-6941.12018

Nunes da Rocha, U., Plugge, C. M., George, I., van Elsas, J. D., and van Overbeek, L. S. (2013). The rhizosphere selects for particular groups of acidobacteria and verrucomicrobia. *PLoS One* 8:e82443. doi: 10.1371/journal.pone.0082443

Oksanen, J., Blanchet, F. G., Friendly, M., Kindt, R., Legendre, P., McGlinn, D., et al. (2019). Vegan: community ecology package, R package version 2.5–6.

Oldroyd, G. E. (2013). Speak, friend, and enter: signalling systems that promote beneficial symbiotic associations in plants. *Nat. Rev. Microbiol.* 11, 252–263. doi: 10.1038/nrmicro2990

Philippot, L., Raaijmakers, J. M., Lemanceau, P., and van der Putten, W. H. (2013). Going back to the roots: the microbial ecology of the rhizosphere. *Nat. Rev. Microbiol.* 11, 789–799. doi: 10.1038/nrmicro3109

Qin, X., Xue, B., Tian, H., Fang, C., Yu, J., Chen, C., et al. (2022). An unconventionally secreted effector from the root knot nematode Meloidogyne incognita, mi-ISC-1, promotes parasitism by disrupting salicylic acid biosynthesis in host plants. *Mol. Plant Pathol.* 23, 516–529. doi: 10.1111/mpp.13175

Rabus, R., Gade, D., Helbig, R., Bauer, M., Glockner, F. O., Kube, M., et al. (2002). Analysis of N-acetylglucosamine metabolism in the marine bacterium Pirellula sp. strain 1 by a proteomic approach. *Proteomics* 2, 649–655. doi: 10.1002/1615-9861(200206)2:6<649::AID-PROT649>3.0.CO;2-R

Sharma, M., Saini, I., Kaushik, P., Aldawsari, M. M., Balawi, T. A., and Alam, P. (2021). Mycorrhizal fungi and *Pseudomonas fluorescens* application reduces root-knot nematode (Meloidogyne javanica) infestation in eggplant. *Saudi J. Biol. Sci.* 28, 3685–3691. doi: 10.1016/j.sjbs.2021.05.054

Tan, G., Liu, Y., Peng, S., Yin, H., Meng, D., Tao, J., et al. (2021). Soil potentials to resist continuous cropping obstacle: three field cases. *Environ. Res.* 200:111319. doi: 10.1016/j.envres.2021.111319

Tian, Q., Jiang, Y., Tang, Y., Wu, Y., Tang, Z., and Liu, F. (2021). Soil pH and organic carbon properties drive soil bacterial communities in surface and deep layers along an elevational gradient. *Front. Microbiol.* 12:646124. doi: 10.3389/fmicb.2021.646124

Walsh, E., Elmore, J. M., and Taylor, C. G. (2017). Root-knot nematode parasitism suppresses host RNA silencing. *Mol. Plant-Microbe Interact.* 30, 295–300. doi: 10.1094/MPMI-08-16-0160-R

Wan, X., Chen, X., Huang, Z., and Chen, H. Y. H. (2021). Contribution of root traits to variations in soil microbial biomass and community composition. *Plant Soil* 460, 483–495. doi: 10.1007/s11104-020-04788-7

Wang, P., Li, Q., Ge, F., Li, F., Liu, Y., Deng, S., et al. (2022). Correlation of bacterial community with phosphorus fraction drives discovery of Actinobacteria involved soil phosphorus transformation during the trichlorfon degradation. *Environ. Pollut.* 302:119043. doi: 10.1016/j.envpol.2022.119043

Wang, H., Wu, C., Zhang, H., Xiao, M., Ge, T., Zhou, Z., et al. (2022). Characterization of the belowground microbial community and co-occurrence networks of tobacco plants infected with bacterial wilt disease. *World J. Microbiol. Biotechnol.* 38:155. doi: 10.1007/s11274-022-03347-9

Weil, R. R., and Brady, N. C. (2017). *The Nature and Properties of Soils*, *15th Edn*. England: Pearson Education Ltd.

Yan, X., Yang, W., Chen, X., Wang, M., Wang, W., Ye, D., et al. (2020). Soil phosphorus pools, bioavailability and environmental risk in response to the phosphorus supply in the red soil of southern China. *Int. J. Environ. Res. Public Health* 17:7384. doi: 10.3390/ijerph17207384

Yin, N., Zhao, J. L., Liu, R., Li, Y., Ling, J., Yang, Y. H., et al. (2021). Biocontrol efficacy of *Bacillus cereus* strain Bc-cm 103 against meloidogyne incognita. *Plant Dis.* 105, 2061–2070. doi: 10.1094/PDIS-03-20-0648-RE

Zeng, W., Wang, Z., Xiao, Y., Teng, K., Cao, Z., Cai, H., et al. (2022). Insights into the interactions between root phenotypic traits and the rhizosphere bacterial community. *Curr. Microbiol.* 79:176. doi: 10.1007/s00284-022-02870-0

Zhang, Y., Tian, C., Xiao, J., Wei, L., Tian, Y., and Liang, Z. (2020). Soil inoculation of Trichoderma asperellum M45a regulates rhizosphere microbes and triggers watermelon resistance to fusarium wilt. *AMB Express* 10:189. doi: 10.1186/s13568-020-01126-z

frontiers | Frontiers in Microbiology

TYPE Original Research
PUBLISHED 04 January 2024
DOI 10.3389/fmicb.2023.1294616

OPEN ACCESS

EDITED BY
Jian-Wei Guo,
Kunming University, China

REVIEWED BY
Jinping Zhao,
Texas A & M University, United States
Zihao Xia,
Shenyang Agricultural University, China

*CORRESPONDENCE
Wanlong Ding
✉ wlding@implad.ac.cn
Yong Li
✉ liyong@implad.ac.cn

RECEIVED 15 September 2023
ACCEPTED 12 December 2023
PUBLISHED 04 January 2024

CITATION
Wang R, Liu S, Xu C, Yu J, Wei J, Ding W and Li Y (2024) Identification and characterization of a novel *Cytorhabdovirus* associated with goji berry (*Lycium barbarum* L.) crinkle disease.
Front. Microbiol. 14:1294616.
doi: 10.3389/fmicb.2023.1294616

Identification and characterization of a novel *Cytorhabdovirus* associated with goji berry (*Lycium barbarum* L.) crinkle disease

Rong Wang, Sai Liu, Changqing Xu, Jing Yu, Jianhe Wei, Wanlong Ding* and Yong Li*

Institute of Medicinal Plant Development, Chinese Academy of Medical Sciences and Peking Union Medical College, Beijing, China

Goji berry (*Lycium barbarum* L.) is a traditional Chinese herbal medicinal plant that is extensively cultivated in the arid and semiarid regions of northwest China. In this study, a novel cytorhabdovirus, tentatively named "goji cytorhabdovirus A (GCVA)," was identified from the goji berry plant exhibiting leaf crinkle symptoms through high-throughput sequencing (HTS). GCVA contains a linear, negative sense single-stranded RNA genome of 14,812 nucleotides and encodes six open reading frames in the order of 3′ leader-N-P-P4-M-G-L-5′ trailer. The genome of GCVA shares the highest nucleotide (nt) identity of 65.80% (16% query coverage) with yerba mate virus A (YmVA) (NC_076472). The N and L proteins also share low amino acid (aa) identities (<35.42 and < 41.23%, respectively) with known cytorhabdoviruses. Typical features of the viruses in the genus *Cytorhabdovirus* include a highly conserved consensus sequence in the intergenic regions and extensive complementation of the 5′ non-coding trailer and the 3′ leader. These features were also found in GCVA. These data in combination with a phylogenetic analysis that was based on the aa sequences of the N and L proteins support the proposal that GCVA is a new species in the genus *Cytorhabdovirus*.

KEYWORDS

Lycium barbarum*, virome, next-generation sequencing, novel virus, *Cytorhabdovirus

1 Introduction

Goji (*Lycium barbarum* L.), which is also known as goji berry or wolfberry, is a solanaceous shrub and is extensively cultivated in the arid and semiarid regions of northwest China, including the Ningxia Hui Autonomous Region, Qinghai Province, Gansu Province, Xinjiang Uygur Autonomous Region, and Inner Mongolia (Xin et al., 2013). It is a highly valuable crop. Its fruits (Gou-qi), and root bark (Di-gu-pi) have been used for centuries in traditional Chinese medicine to improve eyesight, liver and kidney function (Wang et al., 2010; Yao et al., 2011). It can also be used as food, and many people avidly use the berries in soups. To our knowledge, almost no viruses have been reported in goji, except for *goji berry chlorosis virus* (GBCV), which was chlorotic identified in

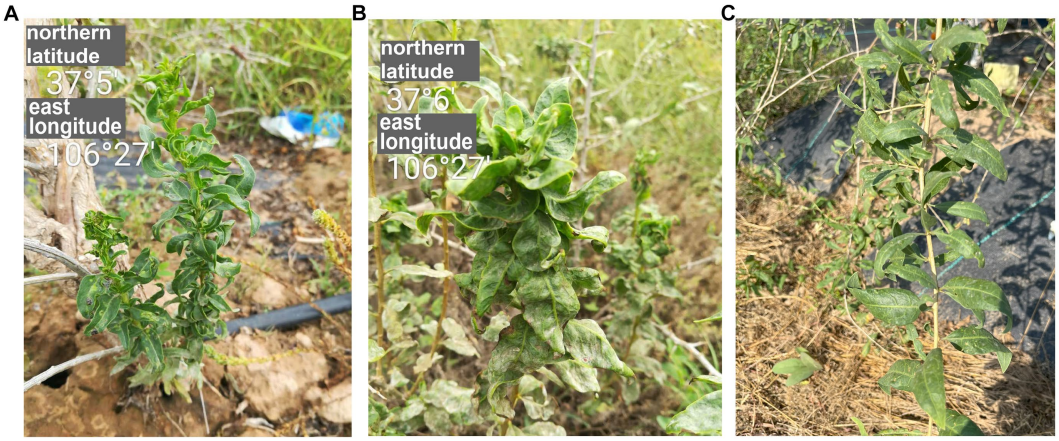

FIGURE 1
The symptoms of goji berry viral diseases. **(A)** and **(B)** Plants showing symptoms of GCVA infection. **(C)** Healthy plant.

another species of goji berry plant (*L. chinense* Miller) (Kwon et al., 2018).

The family *Rhabdoviridae* in the order *Mononegavirales* currently consists of three subfamilies and 46 genera (ICTV, https://ictv.global/taxonomy). Viruses that infect plant hosts and arthropod vectors are grouped in the subfamily of *Betarhabdovirinae*, which are classified into six genera (*Alphanucleorhabdovirus*, *Betanucleorhabdovirus*, *Cytorhabdovirus*, *Dichorhavirus*, *Gammanucleorhabdovirus*, and Var*icosavirus*) based on their replication sites (nucleus or cytoplasm), genome structures (monopartite or bipartite), and vector species (Jackson et al., 2005; Walker et al., 2022). Rhabdoviruses contain a linear, negative sense single-stranded RNA genome that is 11–16 kb long (Dietzgen et al., 2017) and includes five canonical genes in the order of 3′-nucleocapsid protein (N) - phosphoprotein (P) - matrix protein (M) - glycoprotein (G) - polymerase (L) - 5′ (Dietzgen et al., 2020; Walker et al., 2022). The genes are separated by conserved gene junctions, and the entire coding region is flanked by partly complementary 3′ leader and 5′ trailer sequences with transcription and replication initiation signals (Dietzgen et al., 2017). Arthropods, which include aphids (*Aphis fabae* and *A. ruborum*), leafhoppers (*Recilia dorsalis*), planthoppers (*Laodelphax striatellus*) and whiteflies (*Bemisia tabaci*), are common vectors that transmit cytorhabdoviruses in nature (Yang et al., 2017; Cao et al., 2018; Fránová et al., 2019; Dietzgen et al., 2020; Pinheiro-Lima et al., 2020).

In 2017, goji berry plants with crinkled leaves were found in the Ningxia Autonomous Region, China (Figures 1A,B). Because of their typical symptoms of viral diseases, we analyzed the virus species in the diseased leaves using high-throughput sequencing (HTS). This is a rapidly developing technique that is used to detect and diagnose viral infections, and it identified a novel rhabdovirus that infects plants. The genome of this virus was determined by Sanger sequencing. The virus has a genomic structure that is typical for viruses in the family of *Rhabdoviridae* and is phylogenetically related to cytorhabdoviruses. We proposed to name this virus goji cytorhabdovirus A (GCVA) and classify it as a new member of the genus *Cytorhabdovirus* of the family *Rhabdoviridae*.

2 Materials and methods

2.1 Plant samples

Goji plants with crinkle leaves (Figure 1A) were found at Tongxin County, Wuzhong City, Ningxia autonomy region, China, in 2017, and were transported to the laboratory for cultivation and preservation. Leaf samples were collected from this plant and were stored at -80°C for paired-end RNA-Seq.

2.2 RNA extraction, NGS, and data processing

Total RNA was extracted from the leaf sample from symptomatic goji using a mirVana™ microRNA (miRNA) Isolation kit (Ambion, Thermo Fisher Scientific, Waltham, MA, United States). After treatment with an RNA Clean XP Kit (Beckman Coulter, Brea, CA, United States) and an RNase-Free DNase Set (QIAGEN GmbH, Hilden, Germany), the quality and quantity of total RNA were measured using a NanoDrop spectrophotometer (Thermo Fisher Scientific) and Agilent2100 (Agilent Technologies, Santa Clara, CA, United States). After ribosomal RNA depletion using a Ribo-Zero Magnetic Kit (Epicentre, Lucigen, Middleton, WI, United States), an RNA library was built using a TruSeq RNA Sample Prep Kit (Illumina, San Diego, CA, United States), paired-end sequenced on an Illumina HiSeq X platform according to the manufacturer's instructions[1] (Li et al., 2022). Raw sequencing data for the goji library was processed to trim the adaptors and low-quality reads using the FASTX-Toolkit software.[2] Retained reads were assembled *de novo* using CLC Genomics Workbench 6.0.4 (Qiagen, Valencia, CA, United States) according to the scaffolding contig algorithm. The second assembly

1 www.illumina.com
2 http://hannonlab.cshl.edu/fastx_toolkit/index.html

was then conducted using CAP3 sequence assembly program.[3] The final contigs were compared against the NCBI non-redundant (Nr) database using BLASTX with an E-value<1e^{-5} (Li et al., 2022).

2.3 Recovery of viral genomes

Viral contigs of 14,839 bp covered most of the genome of the novel virus. The genome of the novel virus was also determined by overlapping reverse transcription (RT)-PCR with primers designed based on the viral contig sequences using Primer Premier 6 (PREMIER Biosoft, Palo Alto, CA, USA) (Supplementary Table S1). The 5′- and 3′-end sequences of viral genomic RNAs were determined by the rapid amplification of cDNA ends-PCR (RACE-PCR) using a SMARTer RACE 5′/3′ Kit (Clontech, Mountain View, CA, USA). For sequencing purposes, PCR amplicons were purified by a TIANgel Midi Purification Kit (TianGen, Beijing, China) and cloned into the pMD18 vector (TaKaRa, Dalian, China), which was used to transform competent *Escherichia coli* DH5α cell. More than five clones per amplicon were sequenced in both directions by the biotechnology company Tsingke (Beijing, China).

2.4 Sequence analysis and read assembly

The ORF finder program[4] was used to analyze viral genome organizations. The Conserved Domain Search Service on the NCBI website[5] was used to analyze conserved domains of ORFs. The multiple sequence alignment of conserved gene junctions of cytorhabdovirus were performed using CLC Genomics Workbench 21.0.5 (Qiagen). The molecular weight (MW) and isoelectric point (pI) of proteins were computed using Expasy[6] with default parameters. Signal peptide was predicted using SignalP 6.0 server[7] The potential transmembrane (TM) topology was predicted using TMHMM Server 2.0.[8] Pairwise comparisons between viruses were performed using MAFFT program[9] and displayed by Sequence Demarcation Tool (SDT) software using a color-coded matrix (Muhire et al., 2014).

2.5 Phylogenetic analysis

Phylogenetic trees were constructed based on the aa sequences of the L protein and N protein of GCVA, 10 most similar cytorhabdoviruses, two alphanucleorhabdoviruses, two betanucleorhabdoviruses, two dichorhavirus, one gammanucleorhabdovirus, and one varicosavirus. Phylogenetic analyses were performed using the maximum-likelihood method with 1,000 bootstrap replicates in MEGA X (Kumar et al., 2018).

2.6 Reverse transcription loop-mediated isothermal amplification (RT-LAMP)

For RT-LAMP, the total RNA of goji leaf was extracted using TRNzol universal reagent (TianGen, Beijing, China) according to the manufacturer's instructions. The RT-LAMP primers including two outer primers (forward primer F3 and backward primer B3), two inner primers (forward inner primer FIP and backward inner primer BIP), and two loop primers (forward loop primer LF and backward loop primer LB) were designed using the Primer Explorer version 5 software[10] (Eiken Chemical Co., Tokyo, Japan) (Supplementary Table S1). Before use in LAMP, all primers were assessed for specificity by performing a BLAST search. RT-LAMP was carried out using the Colorimetric pH-sensitive LAMP kit (TransGen Biotech, Beijing, China). The components and their concentrations of RT-LAMP reactions are as follows: FIP/BIP primers 1.6 μM each, F3/B3 primers 0.4 μM each, Loop F/B primers 0.8 μM each, 2.5× pH sensitive LAMP reaction mix 10 μL, N-red stain 1.3 μL, *Bst* II DNA polymerase 1 μL, reverse transcriptase (high temperature) 1 μL, total RNA 1 μL, The volume was refilled to 25 μL with RNase-free ddH_2O. The isothermal amplification procedure is 62°C for 30 min, 85°C for 10 min.

3 Results

3.1 Identification of potential viruses infecting the goji berry

In September 2017, goji plants that exhibited severe crinkle symptoms were found in a field (N 37°5′, E106°27′) in Tongxin County, Wuzhong City, Ningxia Autonomous Region, China (Figures 1A,B). No crinkle symptoms were observed on healthy plants (Figure 1C). To identify the viruses in the goji plant, a library was generated using symptomatic leaf sample for paired-end RNA-Seq. A total of 67,439,294 clean reads were obtained. Assembly of the clean reads generated 73,974 contigs that ranged from 200 to 14,839 nucleotides (nt). A BLASTx analysis of the contigs revealed that six contigs (ranged from 565 to 14,839 bp) that obtained from the assembly of 14,076 reads were similar to several viruses in the family of *Rhabdoviridae* (Supplementary Table S2).

3.2 Determination of the virus genome

To confirm the results of HTS and characterize the rhabdovirus in symptomatic goji plants, the viral genome was determined by amplifying overlapping and terminal cDNA fragments of the new rhabdovirus by reverse transcription PCR (RT-PCR) and rapid amplification of cDNA ends (RACE) PCR with specific primers based on the viral contig sequences (Figure 2A; Supplementary Table S1). The genomic sequence of the novel rhabdovirus was 14,812 nt (GenBank accession number OR489165). A BLASTN analysis with the nucleotide sequence of the genome revealed that this novel

3 http://doua.prabi.fr/software/cap3
4 https://www.ncbi.nlm.nih.gov/orffinder
5 www.ncbi.nlm.nih.gov/Structure/cdd/wrpsb.cgi
6 https://web.expasy.org/protparam/
7 https://services.healthtech.dtu.dk/services/SignalP-6.0/
8 https://services.healthtech.dtu.dk/services/TMHMM-2.0/
9 https://mafft.cbrc.jp/alignment/server/
10 http://primerexplorer.jp/lampv5e/index.html

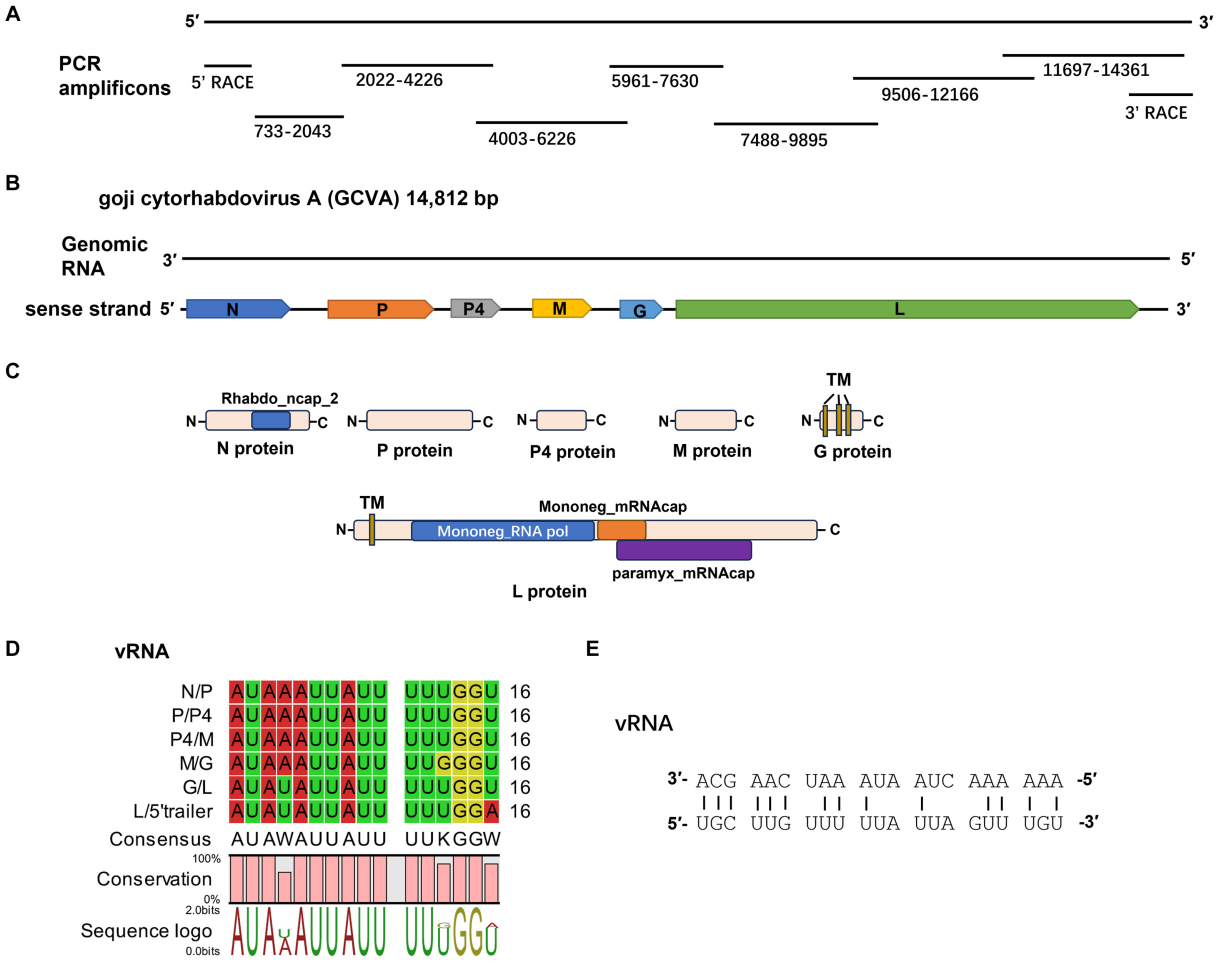

FIGURE 2
Characterization of a novel cytorhabdovirus, GCVA, isolated from goji berry in China. **(A)** Schematic diagram of genome amplification and sequencing strategy of GCVA. **(B)** Genomic organization of GCVA. N, nucleocapsid protein; P, phosphoprotein; M, matrix protein; G, glycoprotein; L, polymerase. **(C)** Conserved domains of GCVA-encoded proteins. TM, transmembrane topology. **(D)** Conserved gene junction regions of GCVA. **(E)** Complementary terminal nucleotides of GCVA.

rhabdovirus was the most similar to YmVA (NC_076472), which was isolated from yerba mate (*Ilex paraguariensis*) in Argentina with nt identities of 65.80% (16% query coverage). We tentatively named this novel rhabdovirus identified in goji berry as "goji cytorhabdovirus A (GCVA)."

3.3 Characterizations of the viral genome

Six open reading frames (ORFs) were identified in the sense strand of GCVA, which has a gene arrangement that is similar to that of most rhabdoviruses (Figure 2B) (Dietzgen et al., 2020).

ORF1 (436–1,950 nt), which follows a short 3′- untranslated region (UTR) of 435 nt, is 1,515 nt long and predicted to encode a 504 amino acid (aa) N protein with a predicted MW of 56.46 kDa and a pI of 7.06 (Table 1). Protein N contains one conserved domain, which was rhabdovirus nucleoprotein (Rhabdo_ncap_2, cl03939) at aa position 222–407 (Figure 2C).

ORF2 (2,499–4,046) is 1,548 nt long and predicted to encode a putative P protein of 515 aa with a predicted MW of 58.38 kDa and a pI of 7.11 (Table 1).

ORF3 (4,305–5,024) is 720 nt long and predicted to encode a putative P4 protein of 239 aa with a predicted MW of 26.86 kDa and a pI of 8.34 (Table 1).

ORF4 (5,480–6,340) is 861 nt long and predicted to encode a putative M protein of 286 aa with a predicted MW of 32.61 kDa and a pI of 5.68 (Table 1).

ORF5 (6,742–7,368) is 627 nt long and predicted to encode a putative G protein of 208 aa with a predicted MW of 24.35 kDa and a pI of 8.53 (Table 1). Three TM helices and topologies were predicted in the G protein at the 7–26, 67–89, 102–124 aa positions, respectively (Figure 2C; Table 1). A signal peptide was also predicted in the putative G protein, which appeared to have a cleavage site between aa 26 and 27 with a probability of 65.22% (Table 1).

ORF6 (7,562–14,344) is 6,783 nt long and predicted to encode an L protein of 2,260 aa. The L protein has three conserved domains, including mononegaviral RNA dependent RNA polymerase (Mononeg_RNA pol, cl15638; aa positions 283–1,173), mononegaviral mRNA-capping region V (Mononeg_mRNAcap, cl16796; aa positions 1,192–1,426), and mRNA capping enzyme (paramyx_mRNAcap, cl44358; aa positions 1,286–1,492) (Figure 2C). One TM topology was

TABLE 1 Features of proteins encoded in the positive-sense orientation by the goji cytorhabdovirus A (GCVA) anti-genome.

ORF	Position (nt)	Protein	Size (nt)	Size (aa)	MW (KDa)	pI[a]	BLASTp match in NCBI[b]	Identity (%)	TM[c]	Signal peptide (cleavage site, Probability)
ORF1	436–1,950	N	1,515	504	56.46	7.06	nucleocapsid (YmVA)	35.42	ND	ND
ORF2	2,499–4,046	P	1,548	515	58.38	7.11	phosphoprotein (YmVA)	26.96	ND	ND
ORF3	4,305–5,024	P4	720	239	26.86	8.34	P4 protein (YmVA)	34.50	ND	ND
ORF4	5,480–6,340	M	861	286	32.61	5.68	–	–	ND	ND
ORF5	6,742–7,368	G	627	208	24.35	8.53	–	–	aa 7–26, 67–89, 102–124	aa 26 and 27, 65.22%
ORF6	7,562–14,344	L	6,783	2,260	259.79	7.00	polymerase (YmVA)	41.23	aa 13–33	ND

[a]pI, Isoelectric point.
[b]–, no match.
[c]TM, transmembrane topology; ND, not detected.

predicted in the L protein at the 69–91 aa positions (Figure 2C; Table 1).

The 5′ UTR is 468 nt in size. The gene order 3′ N-P-P4-M-G-L 5′ is consistent with that of plant rhabdoviruses, whose genomes have five conserved canonical genes in the order 3′ N-P-M-G-L 5′ (Dietzgen et al., 2020). P4 is an accessory gene that is located between P and M.

A BLASTp analysis showed that the N, P, P4 and L proteins of GCVA were the most homologous to those of YmVA with 35.42, 26.96, 34.50, and 41.23% aa sequence identities, respectively (Table 1).

The intergenic regions contain the highly conserved consensus sequences "3′ AUAA(U)AUUAUUUUU(G)GGU(A) 5′" (Figure 2D). In addition, the 5′ non-coding trailer sequence had extensive complementarity to the 3′ leader with 14 out of 21 nt (Figure 2E), which is consistent with the characteristics of plant rhabdoviruses (Dietzgen et al., 2017).

Pairwise comparisons between GCVA and the 10 most similar cytorhabdoviruses were performed based on the nt and aa sequences of the *N* and *L* genes using the MAFFT program and SDT software, respectively. The *N* gene of GCVA shared 44.5–51.6% nt sequence identities and 9.0–31.7% aa sequence identities with *N* genes in the other aligned cytorhabdoviruses (Figures 3A,B; Supplementary Table S3). The *L* gene of GCVA shared 49.8–55.6% nt sequence identities and 20.2–37.4% aa sequence identities with the *L* genes in the other aligned cytorhabdoviruses (Figures 3C,D; Supplementary Table S3).

3.4 Phylogenetic analysis

A phylogenetic analysis of the L protein showed that GCVA grouped closely with the other cytorhabdoviruses, particularly *Cytorhabdovirus yerbamate* (Figure 4A). A similar result was obtained in a phylogenetic analysis of the N protein (Figure 4B). These results demonstrate that GCVA should be classified as a new species in the genus *Cytorhabdovirus* in the family of *Rhabdoviridae*.

3.5 RT-PCR detection of GCVA in goji berry

To identify the incidence of GCVA in goji berry, 22, 10 and 10 crinkle leaf samples of goji berry were collected from the cultivation area of goji berry in Beijing (BJ), Zhongwei city in Ningxia Hui Autonomous Region (NX), and Golmud city in Qinghai Province (QH), respectively, for RT-PCR detection. The samples were numbered BJ1–BJ22, NN1–NX10, and QH1–QH10, respectively. The specific primer pair (GQ-11380F and GQ-12178R) for GCVA detection and the general primer pair for GCVA and YmVA detection were designed and shown in Supplementary Table S1. The RT-PCR detection results showed that 4 of the 42 samples were positive for GCVA with a detection rate 9.5%, two of which were collected from Beijing, and the other two were collected from Qinghai province (Supplementary Figure S1).

Almost complete genome sequences (755–14,345 nt) of one GCVA BJ isolate (GCVA-BJ) were amplified and sequenced. The sequences have been uploaded to GenBank (GenBank accession number OR860428). The nucleotide sequences alignment revealed that GCVA-BJ isolate shared 98.93 and 45.14% identity with GCVA-NX and YmVA, respectively (Supplementary Figure S2 and Supplementary Table S4).

3.6 Development RT-LAMP as a visual diagnostic platform for the detection of GCVA

LAMP is a sensitive and rapid nucleic acid amplification method that is studied widely for the detection of many infectious diseases in the field (Soroka et al., 2021). LAMP allows biosensing of target DNA or RNA under isothermal conditions with high specificity in a short period (Notomi et al., 2000). In this study, we developed a RT-LAMP assay with a set of six primers, F3-176, B3-176, FIP-176, BIP-176, LF-176 and LB-176 (Supplementary Table S1), that specifically

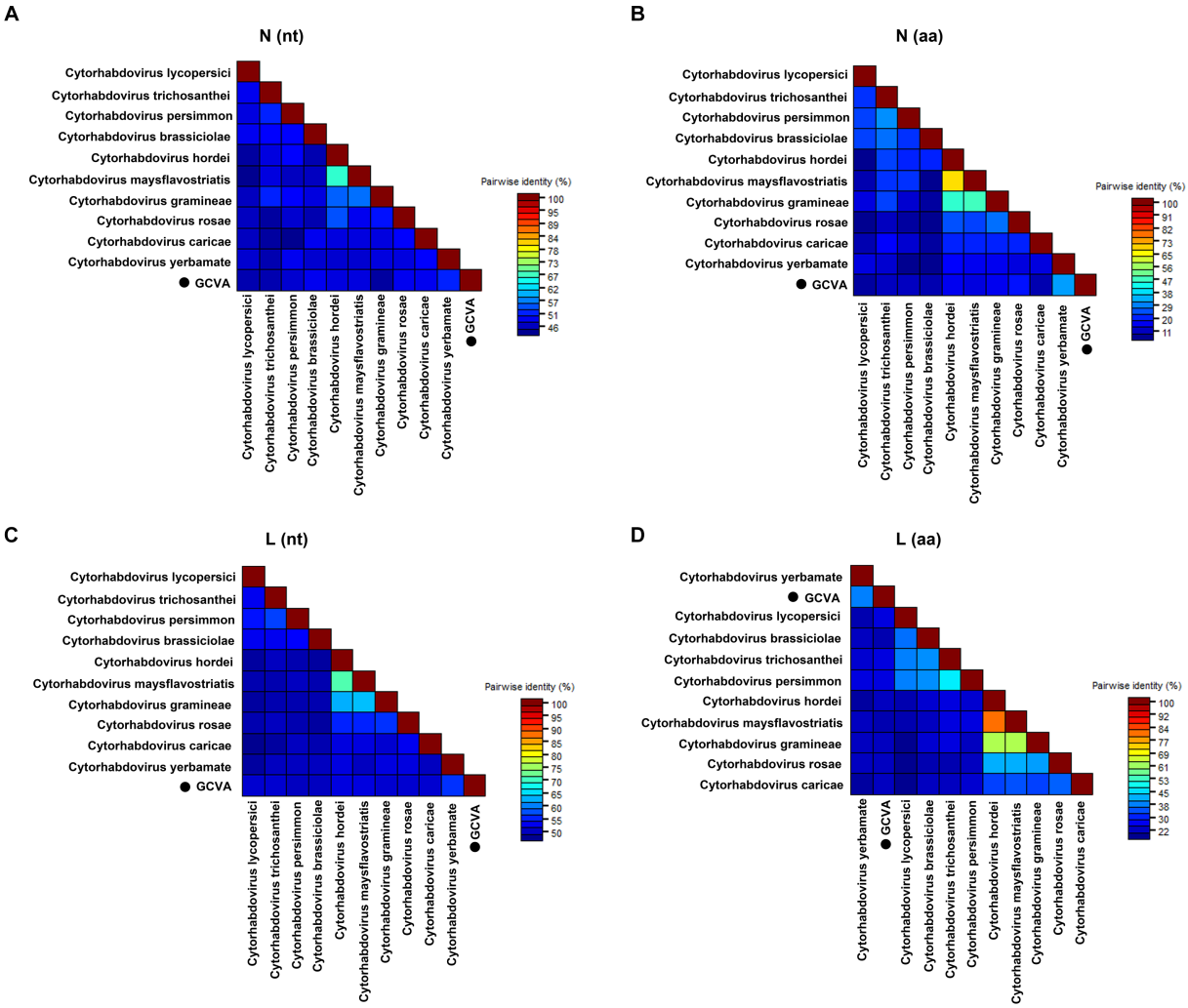

FIGURE 3
The pairwise identities plot of N and L protein of GCVA and 10 most similar cytorhabdoviruses based on nucleotide (nt) sequence **(A) (C)** and amino acid (aa) sequence **(B) (D)** aligned by MAFFT and displayed by SDT software. N, nucleocapsid protein; L, polymerase.

amplifies the N gene of GCVA. Since the N-red staining solution was added to the reaction solution, the results could be observed by the naked eye, and the positive samples were magenta, while the negative samples were orange-yellow. Twelve goji berry leaf samples (BJ1–BJ12) were detected using the established RT-LAMP assay, of which only one sample was positive, and the result was consistent with the RT-PCR detection (Figure 5 and Supplementary Figure S1).

4 Discussion

Goji berry is perennial solanaceous defoliated shrub, which is cultivated extensively in the arid and semiarid regions of northwest China. To our knowledge, apart from the goji berry chlorosis virus (GBCV), which is classified in an intermediate position between the families *Benyviridae* and *Virgaviridae* (Kwon et al., 2018), there are almost no reports of viral diseases on goji berry. In this study, HTS combined with conventional Sanger sequencing was used to identify a novel virus, GCVA, in a goji berry plant that exhibited typical virus symptoms (Figure 1). The genome of GCVA consists of 14,812 nt and is predicted to encode six ORFs in the order 3′ leader-N-P-P4-M-G-L 5′ trailer (Figure 2B), which conforms to the basic canonical organization (3′ leader-N-P-M-G-L 5′ trailer) described for plant rhabdoviruses (Dietzgen et al., 2020). GCVA shared the highest genomic sequence identity (65.80%) with YmVA (NC_076472), and its N and L proteins were 9.0–31.7% and 20.2–37.4% homologous at the aa level with the 10 most similar cytorhabdoviruses available in the GenBank database (Figures 3B,D; Supplementary Table S3), which met the criteria for species demarcation in the genus *Cytorhabdovirus* (Wang et al., 2021). In the phylogenetic analysis deduced from the aa sequences of proteins L and N, the novel virus clustered together with YmVA within the cytorhabdovirus group (Figures 4A,B). These results show that GCVA should be considered a new species in the genus *Cytorhabdovirus*.

N, P, M, G and L are the five conserved canonical genes in the genomes of plant rhabdoviruses (Walker et al., 2011). One or several accessory genes that may intersperse among or overprint with the canonical genes lead to diverse viral genome organizations containing

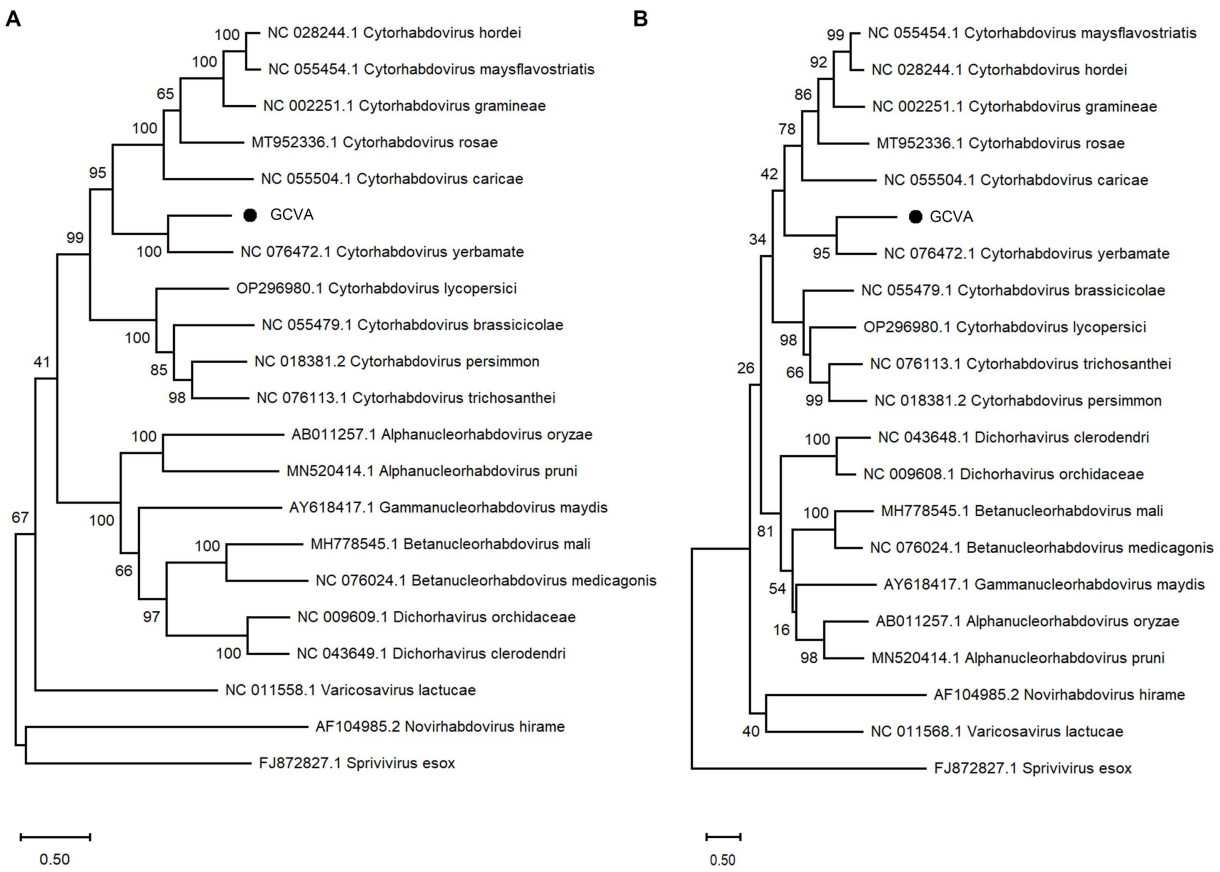

FIGURE 4
Phylogenetic analysis based on the amino acid sequences of the L **(A)** and N **(B)** of GCVA and 10 most similar cytorhabdoviruses, 2 alphanucleorhabdoviruses, 2 betanucleorhabdovirus, 2 dichorhaviruses, 1 gammanucleorhabdovirus, 1 varicosavirus, 1 novirhabdovirus and 1 sprivivirus, performed by the maximum-likelihood method in MEGA X software. Bootstrap values (1,000 replicates) are shown below the branches. The black triangles represent GCVA identified in this study.

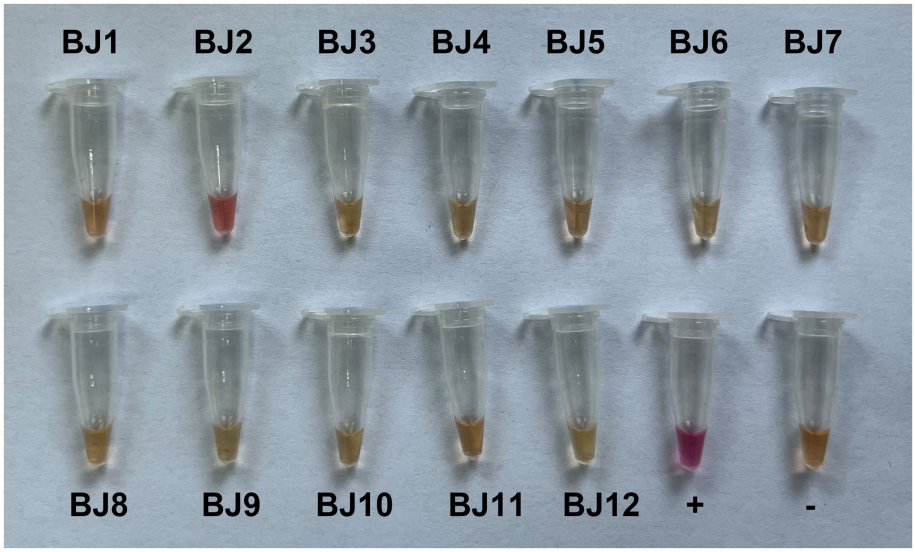

FIGURE 5
RT-LAMP assay detection of goji cytorhabdovirus A (GCVA) in goji berry.

up to 6–10 genes (Walker et al., 2011). An accessory gene, P4, is located between the P3 and M proteins in the genome of GCVA. A BLASTp analysis showed that P4 of GCVA shares the highest identity with that of YmVA with 34.50% aa sequence identities (Table 1). Unlike the P4 protein of YmVA, TM topology was not predicted on the P4 protein of GCVA (Bejerman et al., 2017).

ORF4 and ORF5 were hypothesized to encode the putative M and G proteins, respectively, based on their locations in the genome. However, the BLASTp analysis did not find any protein that was homologous to the putative M and G proteins (Table 1). Fortunately, three TM topologies were identified in the putative G protein in GCVA at the 7–26, 67–89, 102–124 aa positions (Figure 2C; Table 1), which is similar to the G proteins of the other plant rhabdoviruses and consistent with their membrane functions (Bejerman et al., 2017, 2020). A signal peptide was also predicted in the putative G protein (Table 1), which is similar to the G proteins in several cytorhabdoviruses (Bejerman et al., 2020). These results support the concept that ORF5 may encode a G protein. Since the M protein has no special structural features, we can only hypothesize that the protein encoded by ORF4 is an M protein based on its position in the genome. These may highlight the distinctiveness of GCVA to some extent.

The relative abundance of each viral mRNA is regulated by the transcription termination polyadenylation (TTP) signal at the end of each viral gene. Once the transcriptase reaches this signal, it dissociates from the RNA template (Abraham and Banerjee, 1976). Rhabdoviruses possess conserved TTP signal-like poly(U) tracts in their intergenic regions (Dietzgen et al., 2012). Several highly conserved sequences with a consensus of "3′-AUAA(U)AUUAUUUUU(G)GGU(A)-5′" were also found in the intergenic regions of GCVA RNA (Figure 2D). Although, to the best of our knowledge, this conserved sequence is not similar to those of other rhabdoviruses, they also contain poly(U) tracts that should be TTP signals. The extensive complementarity between the 5′ non-coding trailer and 3′ leader was also found in GCVA, which is consistent with the characteristics of plant rhabdoviruses (Dietzgen et al., 2017).

The occurrence of GCVA in goji berry was preliminarily identified, only 4 of 42 randomly selected leaf samples were positive for GCVA (Supplementary Figure S1), which indicate that GCVA is not popular in goji berry.

Cytorhabdoviruses have been reported to be transmitted by aphids (*Aphis fabae* and *A. ruborum*), leafhoppers (*Recilia dorsalis*), planthoppers (*Laodelphax striatellus*) and whiteflies (*Bemisia tabaci*) in nature (Yang et al., 2017; Cao et al., 2018; Fránová et al., 2019; Dietzgen et al., 2020; Pinheiro-Lima et al., 2020). Psyllid (*Bactericera gobica*), gall mite (*Aceria pallida*), aphids (*Aphis gossypii*), gall midge (*Jaapiella* sp.), and thrips (*Psilothrips indicus*) are five common pests in goji berry (Xu et al., 2014; Li et al., 2017). Further studies are needed to detect whether arthropods harbor GCVA and to determine whether these arthropods can transmit GCVA.

In conclusion, this study is the first to report the complete nucleotide sequences of GCVA that infects goji berry. This novel virus has a genomic organization that is similar to those of members in the genus *Cytorhabdovirus* and shows low levels of genomic homology with reported cytorhabdoviruses. Thus, it should be considered to be a new species in the genus *Cytorhabdovirus*.

Data availability statement

The datasets presented in this study can be found in online repositories. The names of the repository/repositories and accession number(s) can be found in the article/Supplementary material.

Author contributions

RW: Formal analysis, Funding acquisition, Investigation, Methodology, Writing – original draft. SL: Resources, Writing – review & editing. CX: Resources, Writing – review & editing. JY: Resources, Writing – review & editing. JW: Project administration, Supervision, Writing – review & editing. WD: Formal Analysis, Investigation, Writing – review & editing. YL: Formal analysis, Methodology, Writing – review & editing.

Funding

The author(s) declare financial support was received for the research, authorship, and/or publication of this article. This work was supported by the National Key Research and Development Program of China (2022YFC3501504), and CAMS Innovation Fund for Medical Sciences (CIFMS) (2021-I2M-1-032).

Conflict of interest

The authors declare that the research was conducted in the absence of any commercial or financial relationships that could be construed as a potential conflict of interest.

Publisher's note

Supplementary material

The Supplementary material for this article can be found online at: https://www.frontiersin.org/articles/10.3389/fmicb.2023.1294616/full#supplementary-material

References

Abraham, G., and Banerjee, A. K. (1976). Sequential transcription of the genes of vesicular stomatitis virus. *Proc. Natl. Acad. Sci. U. S. A.* 73, 1504–1508. doi: 10.1073/pnas.73.5.1504

Bejerman, N., Acevedo, R. M., de Breuil, S., Ruiz, O. A., Sansberro, P., Dietzgen, R. G., et al. (2020). Molecular characterization of a novel cytorhabdovirus with a unique genomic organization infecting yerba mate (*Ilex paraguariensis*) in Argentina. *Arch. Virol.* 165, 1475–1479. doi: 10.1007/s00705-020-04609-3

Bejerman, N., de Breuil, S., Debat, H., Miretti, M., Badaracco, A., and Nome, C. (2017). Molecular characterization of yerba mate chlorosis-associated virus, a putative cytorhabdovirus infecting yerba mate (*Ilex paraguariensis*). *Arch. Virol.* 162, 2481–2484. doi: 10.1007/s00705-017-3363-8

Cao, Q., Xu, W. Y., Gao, Q., Jiang, Z. H., Liu, S. Y., Fang, X. D., et al. (2018). Transmission characteristics of barley yellow striate mosaic virus in its planthopper vector *Laodelphax striatellus*. *Front. Microbiol.* 9:1419. doi: 10.3389/fmicb.2018.01419

Dietzgen, R. G., Bejerman, N. E., Goodin, M. M., Higgins, C. M., Huot, O. B., Kondo, H., et al. (2020). Diversity and epidemiology of plant rhabdoviruses. *Virus Res.* 281:197942. doi: 10.1016/j.virusres.2020.197942

Dietzgen, R. G., Calisher, C. H., Kurath, G., Kuzmin, I. V., Rodriguez, L. L., Stone, D. M., et al. (2012). "Family Rhabdovirus" in *Virus taxonomy: Ninth report of the international committee on taxonomy of viruses*. eds. A. M. Q. King, M. J. Adams, E. B. Carstens and E. J. Lefkowitz (London: Elsevier Academic Press), 686–713.

Dietzgen, R. G., Kondo, H., Goodin, M. M., Kurath, G., and Vasilakis, N. (2017). The family Rhabdoviridae: mono- and bipartite negative-sense RNA viruses with diverse genome organization and common evolutionary origins. *Virus Res.* 227, 158–170. doi: 10.1016/j.virusres.2016.10.010

Fránová, J., Přibylová, J., and Koloniuk, I. (2019). Molecular and biological characterization of a new strawberry cytorhabdovirus. *Viruses* 11:982. doi: 10.3390/v11110982

Jackson, A. O., Dietzgen, R. G., Goodin, M. M., Bragg, J. N., and Deng, M. (2005). Biology of plant rhabdoviruses. *Annu. Rev. Phytopathol.* 43, 623–660. doi: 10.1146/annurev.phyto.43.011205.141136

Kumar, S., Stecher, G., Li, M., Knyaz, C., and Tamura, K. (2018). MEGA X: molecular evolutionary genetics analysis across computing platforms. *Mol. Biol. Evol.* 35, 1547–1549. doi: 10.1093/molbev/msy096

Kwon, S. J., Choi, G. S., Choi, B., and Seo, J. K. (2018). Molecular characterization of an unusual new plant RNA virus reveals an evolutionary link between two different virus families. *PLoS One* 13:e0206382. doi: 10.1371/journal.pone.0206382

Li, Y., Liu, S., Guo, K., Ding, W., and Wang, R. (2022). Virome of Pseudostellaria heterophylla: identification and characterization of three novel carlaviruses and one novel amalgavirus associated with viral diseases of Pseudostellaria heterophylla. *Front. Microbiol.* 13:955089. doi: 10.3389/fmicb.2022.955089

Li, J., Liu, S., Xu, C., Zhu, X., Qiao, H., Guo, K., et al. (2017). Population dynamics and control strategies of major pests of wolfberry, *Lycium barbarum*. *Mod. Chin. Med.* 19, 1599–1604. doi: 10.13313/j.issn.1673-4890.2017.11.021

Muhire, B. M., Varsani, A., and Martin, D. P. (2014). SDT: a virus classification tool based on pairwise sequence alignment and identity calculation. *PLoS One* 9:e108277. doi: 10.1371/journal.pone.0108277

Notomi, T., Okayama, H., Masubuchi, H., Yonekawa, T., Watanabe, K., Amino, N., et al. (2000). Loop-mediated isothermal amplification of DNA. *Nucleic Acids Res.* 28, 63e–663e. doi: 10.1093/nar/28.12.e63

Pinheiro-Lima, B., Pereira-Carvalho, R. C., Alves-Freitas, D. M. T., Kitajima, E. W., Vidal, A. H., Lacorte, C., et al. (2020). Transmission of the bean-associated cytorhabdovirus by the whitefly *Bemisia tabaci* MEAM1. *Viruses* 12:1028. doi: 10.3390/v12091028

Soroka, M., Wasowicz, B., and Rymaszewska, A. (2021). Loop-mediated isothermal amplification (LAMP): the better sibling of PCR? *Cells* 10:1931. doi: 10.3390/cells10081931

Walker, P. J., Dietzgen, R. G., Joubert, D. A., and Blasdell, K. R. (2011). Rhabdovirus accessory genes. *Virus Res.* 162, 110–125. doi: 10.1016/j.virusres.2011.09.004

Walker, P. J., Freitas-Astúa, J., Bejerman, N., Blasdell, K. R., Breyta, R., Dietzgen, R. G., et al. (2022). ICTV virus taxonomy profile: Rhabdoviridae 2022. *J. Gen. Virol.* 103:001689. doi: 10.1099/jgv.0.001689

Wang, C., Chang, S., Inbaraj, B. S., and Chen, B. (2010). Isolation of carotenoids, flavonoids and polysaccharides from *Lycium barbarum* L. and evaluation of antioxidant activity. *Food Chem.* 120, 184–192. doi: 10.1016/j.foodchem.2009.10.005

Wang, Y., Wang, G., Bai, J., Zhang, Y., Wang, Y., Wen, S., et al. (2021). A novel Actinidia cytorhabdovirus characterized using genomic and viral protein interaction features. *Mol. Plant Pathol.* 22, 1271–1287. doi: 10.1111/mpp.13110

Xin, T. Y., Yao, H., Gao, H. H., Zhou, X. Z., Ma, X. C., Xu, C. Q., et al. (2013). Super food *Lycium barbarum* (Solanaceae) traceability via an internal transcribed spacer 2 barcode. *Food Res. Int.* 54, 1699–1704. doi: 10.1016/j.foodres.2013.10.007

Xu, C., Liu, S., Xu, R., Chen, J., Qiao, H., Jin, H., et al. (2014). Investigation of production status in major wolfberry producing areas of China and some suggestions. *China J. Chin. Materia Med.* 39, 1979–1984. doi: 10.4268/cjcmm.20141106

Yang, X., Huang, J., Liu, C., Chen, B., Zhang, T., and Zhou, G. (2017). Rice stripe mosaic virus, a novel cytorhabdovirus infecting rice via leafhopper transmission. *Front. Microbiol.* 7:2140. doi: 10.3389/fmicb.2016.02140

Yao, X., Peng, Y., Xu, L. J., Li, L., Wu, Q. L., and Xiao, P. G. (2011). Phytochemical and biological studies of Lycium medicinal plants. *Chem. Biodivers.* 8, 976–1010. doi: 10.1002/cbdv.201000018

frontiers | Frontiers in Microbiology

TYPE Original Research
PUBLISHED 16 January 2024
DOI 10.3389/fmicb.2023.1276656

OPEN ACCESS

EDITED BY
Jian-Wei Guo,
Kunming University, China

REVIEWED BY
YingWu Shi,
Xinjiang Academy of Agricultural Sciences, China
Zhanfeng Xia,
Tarim University, China

*CORRESPONDENCE
Yi Zheng
✉ eyizheng@fjnu.edu.cn

RECEIVED 12 August 2023
ACCEPTED 27 December 2023
PUBLISHED 16 January 2024

CITATION
Zheng Y, Yu C, Xiao Y, Ye T and Wang S (2024) The impact of utilizing oyster shell soil conditioner on the growth of tomato plants and the composition of inter-root soil bacterial communities in an acidic soil environment.
Front. Microbiol. 14:1276656.
doi: 10.3389/fmicb.2023.1276656

The impact of utilizing oyster shell soil conditioner on the growth of tomato plants and the composition of inter-root soil bacterial communities in an acidic soil environment

Yi Zheng[1,2]*, Chaofan Yu[1], Yujun Xiao[1], Tinge Ye[1] and Songgang Wang[1]

[1]College of Life Sciences, Fujian Normal University, Fuzhou, Fujian, China, [2]National Joint Engineering Research Center of Industrial Microbiology and Fermentation Technology, College of Life Sciences, Fujian Normal University, Fuzhou, Fujian, China

Introduction: The objective of this study is to examine the impact of various oyster shell soil conditioners, which are primarily composed of oyster shells, on the growth of tomatoes in acidic soil. Moreover, the aim of this investigation is to analyze the variety and structure of soil bacterial populations in close proximity to tomato roots while also contributing to the understanding of the physical, chemical, and biological mechanisms of oyster shell soil conditioners.

Methods: Tomato plants were grown in acidic red soil in three groups: a control group and a treatment group that used two types of oyster shell soil conditioners, OS (oyster shell powder) and OSF (oyster shell powder with organic microbial fertilizer). A range of soil physicochemical properties were measured to study differences in inter-soil physicochemical parameters and the growth of tomato plantings. In addition, this study utilized the CTAB (Cetyltrimethylammonium Bromide) technique to extract DNA from the soil in order to investigate the effects of oyster shell soil conditioner on the composition and diversity of bacterial populations. Utilizing high-throughput sequencing technologies and diversity index analysis, the composition and diversity of bacterial populations in the soil adjacent to plant roots were then evaluated. Ultimately, correlation analysis was used in this study to explore the relationship between environmental factors and the relative abundance of soil bacteria in the inter-root zone of tomato plants.

Results: The findings indicated that the oyster shell soil conditioners were capable of modifying the physicochemical characteristics of the soil. This was evidenced by significant increases in soil total nitrogen (16.2 and 59.9%), soil total carbon (25.8 and 27.7%), pH (56.9 and 55.8%), and electrical conductivity (377.5 and 311.7%) in the OS and OSF groups, respectively, compared to the control group ($p < 0.05$). Additionally, data pertaining to tomato seed germination and seedling growth biomass demonstrated that both oyster shell

soil conditioners facilitated the germination of tomato seeds and the growth of seedlings in an acidic red clay soil ($p < 0.05$). On the other hand, the application of two oyster shell soil conditioners resulted in a modest reduction in the diversity of inter-root soil bacteria in tomato plants. Specifically, the group treated with OSF exhibited the most substantial fall in the diversity index, which was 13.6% lower compared to the control group. The investigation carried out on the soil between tomato plant roots yielded findings about the identification of the ten most abundant phyla. These phyla together represented 91.00-97.64% of the overall abundance. In the inter-root soil of tomatoes, a study identified four major phyla, namely *Proteobacteria, Bacteroidetes, Acidobacteria*, and *Actinobacteria*, which collectively accounted for up to 85% of the total abundance. At the general level, the relative abundance of *Massilia* increased by 2.18 and 7.93%, *Brevundimonas* by 5.43 and 3.01%, and *Lysobacter* by 3.12 and 7.49% in the OS and OSF groups, respectively, compared to the control group. However, the pathogenic bacteria *unidentified_Burkholderiaceae* decreased by 5.76 and 5.05%, respectively. The correlation analysis yielded conclusive evidence indicating that, which involved the use of CCA (Canonical Correlation Analysis) graphs and Spearman correlation coefficients, pH exhibited a positive correlation ($p < 0.05$) with *Shewanella* and a negative correlation ($p < 0.05$) with *Bradyrhizobium*. The relative abundance of *Lysobacter* and *Massilia* exhibited a positive correlation with the levels of total soil nitrogen.

Discussion: The utilization of oyster shell soil conditioner on acidic red soil resulted in several positive effects. Firstly, it raised the pH level of the inter-root soil of tomato plants, which is typically acidic. This pH adjustment facilitated the germination of tomato seeds and promoted the growth of seedlings. In addition, the application of oyster shell soil conditioner resulted in changes in the structure of the bacterial community in the inter-root soil, leading to an increase in the relative abundance of *Proteobacteria* and *Bacteroidetes* and a decrease in the relative abundance of *Acidobacteria*. Furthermore, this treatment fostered the proliferation of genera of beneficial bacteria like *Massilia*, *Brevundimonas*, and *Lysobacter*, ultimately enhancing the fertility of the red soil.

KEYWORDS

oyster shell soil conditioner, acidic red loam soil, tomato, soil physicochemical, bacterial flora structure

1 Introduction

Soils exhibiting a pH level lower than 6.5 are categorized as acidic (Huang, 2000). In typical scenarios, the process of soil acidification occurs gradually over a span of around 100 years (Krug and Frink, 1983). In recent years, there has been a significant increase in the expansion of facility-based agriculture (Shen, 1999). The process of reducing soil acidity has been expedited by the expansion, in conjunction with factors such as limited precipitation and specific environmental conditions prevalent in protected areas. These circumstances include high indoor air temperatures, high humidity, inadequate aeration, and heavy irrigation (Li and Zhang, 2001). Consequently, this has led to the emergence of various soil-related issues (Jiang et al., 2005; Wang et al., 2005; Deng and Zhang, 2006). Each plant species has evolved to thrive within a specific soil pH range, which is considered best for their growth throughout a significant duration of evolutionary history (Gilroy et al., 1989). Soil acidification causes soil surface consolidation, which prevents the soil root system from extending, resulting in a number of phenomena such as a decrease in the number of roots, slow growth, and reduced plant growth (Zeng, 2018), as well as a large loss of effective soil nutrients, resulting in Al^{3+} enrichment and toxic effects, severely affecting crop yield in the region (Xie, 2019). According to research, soil pH influences the relative number and variety of microorganisms (Zhalnina et al., 2015). The inter-root soil is home to a plethora of microorganisms, including bacteria, fungus, actinomycetes, and protozoa, with bacteria playing an important role in soil fertility, plant growth and development, and nutrient absorption by plant roots (Dotaniya and Meena, 2015; Zhang W. et al., 2019). Inter-rhizosphere bacteria can affect the efficacy of nitrogen, phosphorus, and trace metals, including iron, manganese, zinc, and copper, for plants and soil

microbial communities, in addition to the geochemical cycling of these elements. By enhancing the nutritional content of plants, stimulating the production of growth hormones, or serving as a biological agent for disease control, it effectively enhances agricultural yields (Dotaniya and Meena, 2015).

Oysters serve as a crucial marine resource that is utilized by human populations (Southgate and Lucas, 2008; Zhou et al., 2014). Oysters are widely recognized as a highly valuable marine resource in terms of their suitability for human consumption. China is first in terms of oyster production among countries and areas engaged in oyster cultivation, with Korea, Japan, the United States, and France following suit (Zhang, 2014). Throughout an extended period of evolutionary time, each plant species has acquired a distinct and ideal soil pH for its growth. The oyster farming areas in China are all located along the coast, and the main production areas for Chinese oysters are in Fujian, Guangdong, and Shandong, with Fujian having the longest history of oyster farming and currently being the largest oyster farming area in China (Li et al., 2017; Lin et al., 2019). Currently, oysters are predominantly used for their edible component, while the shell, which accounts for 60% of their volume, is underutilized (Zhao et al., 2015). Recent research has demonstrated that oyster shells play a significant role in the improvement of acidic soils. Li (2019) observed that a homemade oyster shell soil conditioner could enhance the acidic soil of Guanxi honeydew, change the compacted soil into a crop-growing state, and raise soil nutrients from class IV to class III. Lee et al. (2008) applied oyster shell powder to the soil and planted cabbage seedlings to study the impact of oyster shell powder on enhancing the physicochemical qualities and crop yield in chalky loam (SiL, pH 6.2) and sandy loam (SL, pH 5.8) soils. They discovered that oyster shell significantly increased the soil pH to 6.9 and 7.4. Strictly established (Yan, 2019) by applying base fertilizer and oyster shell soil conditioner at 2250 and 1500 kg/hm^2 to peanuts grown in yellow clay fields, flower production increased by 16.8 and 10.1%, respectively. The soil pH also increased by 0.8 and 0.5, and the soil's organic, effective phosphorus, alkaline nitrogen, exchangeable calcium, and rapid-efficiency magnesium content were significantly increased. The oyster shell can boost soil organic, rapid phosphorus, and exchange ion concentrations, as well as significantly raise soil microbial carbon and nitrogen content, stimulate soil enzyme activity, and increase crop production (Lee et al., 2008).

In prior studies, our research team has successfully created two soil conditioner products derived from oyster shells. The first product, referred to as OS (Oyster shell powder), is produced by subjecting oyster shell powder to a thermal modification process at a temperature of 700°C and then sieving it through a 300-mesh screen. The second product, known as OSF (Oyster shell powder with organic microbial fertilizer), is a composite material consisting of OS combined with an organic microbial fertilizer.

This study aimed to examine the impact of oyster shell conditioner on tomato growth and the bacterial community in acidic inter-root soil. High-throughput sequencing was employed to analyze the red loam soil samples collected from Wenwu Xuefeng Farm in Minhou, Fujian Province, China. This study holds considerable importance in the comprehensive assessment of the impact of oyster shell conditioner on the bacterial community in acidic inter-root soil. This study provides theoretical support for the application of oyster shell conditioner as a means to improve acidic soil conditions, based on insights from microbiological viewpoints.

2 Research materials and methods

2.1 Overview of the study area

The soil used in this study was collected from Wenwu Xuefeng Farm, located in Minhou County, Fuzhou City, Fujian Province. The geographical coordinates of the farm are 118°51′ 119°25′ E and 25°47′ 26°37′ N. The climate in this region is characterized by a subtropical monsoon climate, with an annual precipitation of 1,673.9 mm and an average annual temperature ranging from 18 to 26°C. The topography exhibits a threshold characteristic, the climatic conditions are of a moderate nature, and the soil composition is notably characterized by a high level of acidity. The soil's pH level is approximately 4.8. The experimental site is situated within the Qishan campus of Fujian Normal University in Fuzhou City, Fujian Province. Geographically, it is positioned at coordinates 26°03′ N and 119°20′ E. The region has a subtropical monsoon climate characterized by an average annual temperature of 19.6°C and an annual precipitation of 1674 mm.

2.2 Applicators and application methods

The experiment utilized 200 g of red loam soil obtained from Wenwu Xuefeng Farm as the foundational soil. The control group CK did not receive any treatment, while the experimental groups I and II were treated with oyster shell soil conditioner products OS and OSF, respectively. The laboratory independently prepared OS products by subjecting oyster shells to thermal modification at a temperature of 700°C. The resulting shells were subsequently crushed to obtain pure oyster shell powder, which passed through a 300-mesh sieve. The primary constituents of this powder were found to be CaCO3 (90−95%) and CaO (3−5%). OSF products are based on OS products, added to Fujian Hengxiang Fisheries Company's commercialized organic microbial fertilizer products at 50:1 (w/w). The main components of organic microbial fertilizer are the mass fraction of total nutrients (N+P2O5+K2O) ≥ 4.0% and the number of effective live cells (cfu) ≥ 1 × 108/mL. Mix them thoroughly and place them in a 5 cm tall by 10 cm wide receptacle. Add deionized water to 60−70% of the soil's normal water content and compact the soil. Then, apply oyster shell soil conditioner at a rate of 1.5 percent of the soil's weight. Tomato seeds were submerged in water and grown for 24 h. The tomato seeds were immersed in water and cultivated for a duration of 24 h. The seeds were subsequently dispersed evenly across the surface of the soil. Each treatment consisted of 30 One Pine Red Israel Hard Fruited Tomato F1 (Green Bar Seedling Co., Guangzhou) seeds, with three replications being established. After sowing, a layer of dry soil measuring 0.5 cm was used to cover the seeds. Subsequently, a small amount of water was sprayed onto the soil using a watering can. Subsequently, the pots were placed within an incubator set at a temperature of 25°C, and a daily rehydration process was carried out. The experimental groups'

locations were randomly changed at various intervals during the course of the trial.

2.3 Measurement of tomato growth indicators

1. Determination of tomato germination potential, germination rate, and germination index The tomato germination cycle endured 8 days, and the number of seeds that germinated in each experimental group was measured daily, with day 5 being the day of germination potential measurement (Xu, 2019) and day 8 being the day of germination rate measurement; the germination potential, germination rate, and germination index were then calculated. Germination potential (%) = (Number of generates on a specified day/total number of seeds) × 100; Germination rate = (total number of germinations in the germination cycle/total number of seeds) × 100;

$$\text{germination index } (\%) = \sum \frac{G_t}{D_t}$$

In the equation, Gt is the number of germination days in the final period of the germination test, and Dt is the number of germination days.

2. determining the height, root length, plant fresh weight, root fresh weight, plant dry weight, and root dry weight of tomato vegetation: Five plants of uniform growth were taken from each treatment on the 30th day of incubation, and their plant height and root length were measured with a ruler; the fresh weight of the plants and the fresh weight of the roots were weighed on a one-in-ten-thousand balance; the plants were separated from the roots with scissors, sterilized at 105°C for 5 min, and then dried at 60°C to a constant weight before the dry weight of the plants and the dry weight of the roots.

2.4 Soil sample collection and processing

Upon the completion of the inquiry, namely on the 30 day, soil samples from the inter-root region were gathered from the OSF, OS, and CK experimental groups. The soil was carefully distributed in a controlled and sterile setting. The tomato seedlings were extracted using sterilized forceps, and the soil adhering to the tomato roots was delicately removed using a sterile soft-bristle brush, ensuring a distance of 1−2 mm from the root surface. Adequate amounts of soil located between the roots were collected into EP tubes. The dirt that remained was isolated from the roots and debris, transferred into a hermetically sealed container, and stored in a refrigeration unit at a temperature of roughly −20°C.

2.5 Soil physicochemical properties determination

In this phase of the investigation, the following experimental instruments were utilized: a portable pH meter (model PHS-3C), a portable conductivity meter (model 2265FS, manufactured in the United States), and a soil carbon and nitrogen analyzer (model Elementar Vario MAX CN, manufactured in Germany) for the determination of soil total nitrogen (TN) and total carbon (TC).

1. Soil water content (WC): a certain mass of fresh soil is weighed, desiccated to a constant weight at 105°C, and then the dry soil mass is weighed and calculated using the formula as follows:

$$WC\ (\%) = \frac{Mw - Mt}{Mw} \times 100$$

In the equation, Mw is the mass of fresh soil (g); Mt is the mass of dried soil (g); and WC is the water content of the soil (%).

2. Soil pH and electrical conductivity (EC): A sample of soil was removed from the self-sealing bag, air-dried at room temperature, passed through a 2 mm sieve, mixed with deionized water at a ratio of 1:2.5, and stirred for 30 min. After 10 min, the soil pH and EC were measured directly using a portable pH meter (pHS-3C) and conductivity meter (2265FS, USA).
3. Determination of mineral nitrogen: 10.0 g of fresh soil samples were weighed and passed through a 2 mm sieve in a 50 mL centrifuge tube. Revise Su Tao's literature (Su et al., 2005).
4. The carbon and nitrogen content of the soil was determined by adding a sample of air-dried soil that had been sieved through a 100 mesh sieve to a carbon and nitrogen analyzer. The analyzer was run following the provided instructions. Before determining the sample, it is necessary to make a subtraction of the blank value.

2.6 Analysis of rhizosphere soil bacterial community structure in tomato

2.6.1 Extraction of genomic DNA and PCR amplification

The soil DNA was extracted in accordance with the methodology described by Kamdem et al. (2023). The genomic DNA was isolated from soil samples using the CTAB method, followed by an assessment of its purity and concentration using agarose gel electrophoresis. The DNA extract was diluted to a concentration of 1 nanogram per microliter (ng/μL) and employed as a template for polymerase chain reaction (PCR) amplification. The PCR reaction utilized Phusion® High-Fidelity PCR Master Mix containing GC Buffer and high-performance, high-fidelity enzymes sourced from New England Biolabs. The study done by Zhang H. et al. (2019) examined the application of prokaryotic universal primers 341F and 806R. The primers and sequences utilized for PCR amplification were as described below:

341F(CCTAYGGGRBGCASCAG)

806R(GGACTACNNGGGTATCTAAT)

2.6.2 PCR product purification and mixing

Libraries were constructed using Thermofisher's Ion Plus Fragment Library Kit 48rxns library construction kit and

then sequenced using Thermofisher's Life Ion S5TM after completion of library construction, passing Qubit quantification, and library testing.

2.6.3 Library construction and high-throughput sequencing

This study analyzed the bacterial community composition of tomato inter-rhizosphere soil using high-throughput sequencing. The V3 ~ V4 regions in the 16S rDNA of the inter-root soil genome of tomatoes grown under CK, OS, and OSF treatments were sequenced and analyzed. In the reference study (Liu et al., 2022), Venn diagrams, PCA plots, Speraman correlation analysis heat maps, and CCA plots were developed based on high-throughput sequencing results to analyze the effects of oyster shell soil amendments on the community structure and diversity of rhizobacteria in acidic tomato soil.

2.7 Data processing and analysis

Using Excel 2016 and SPSS 24 statistical analysis software, the data were analyzed and assembled. To investigate the diversity of species composition in the various treatment groups, all effective tags were clustered into OTUs (operational taxonomic units) with 97% identity, and then the representative sequences of OTUs were annotated with species. The representative sequences for each OTU were then annotated. Spearman correlation was applied to examine the association between bacterial abundance and environmental factors.

3 Results and analysis

3.1 Effect of oyster shell soil conditioner on tomato cultivation

3.1.1 Effect of oyster shell soil conditioner on tomato seed germination

The formulas in the experimental method were used to calculate the germination potential, germination rate, and germination index of tomato seeds. Different oyster shell soil conditioners had varying effects on the germination of tomato seeds, as shown in **Table 1**. The order of germination potential was OSF > OS > CK, with significant improvements of 24.99% in the OS group and 41.65% in the OSF group over the CK group; the order of germination rate was OSF = OS > CK, with significant improvements of 17.34% in both the OS and OSF groups over the CK group. The order of germination rate was OSF = OS > CK, and the germination rate of both OS and OSF groups was significantly increased by 17.34% relative to the CK group; the order of germination index was OS > OSF > CK, and it was significantly increased by 39.17% in the OS group and 36.86% in the OSF group compared to the CK group. In conclusion, the oyster shell soil conditioner supplemented with oyster shell powder was effective in promoting tomato seed germination in acidic red loam soil, and the OSF group was more effective in promoting germination.

TABLE 1 Effects of different treatment groups on tomato seed germination.

Sample	Germination potential/%	Germination rate/%	Germination index/%
CK	66.67 ± 3.33c	83.33 ± 3.33c	28.11 ± 3.53c
OS	83.33 ± 3.33b	97.78 ± 1.92a	39.12 ± 1.45a
OSF	94.44 ± 1.92a	97.78 ± 3.85a	38.47 ± 0.95b

a, b, and c indicate significant differences between treatment groups $p < 0.05$.

3.1.2 Effect of oyster shell soil conditioner on the development of tomato seedlings

At the end of the 30th day of the experiment, plant height, root length, plant's fresh weight, root's fresh weight, plant's dry weight, and root's dry weight were measured for each treatment group; the results are shown in **Table 2**. The biomass data of the OS and OSF groups exhibited statistically significant improvements compared to the CK group, with a significant difference observed ($p < 0.05$). Moreover, there was no significant difference in biomass between the OSF and OS groups, suggesting that the primary constituent of calcium carbonate in both groups played a significant role in ameliorating soil acidity. Furthermore, the effectiveness of OS and OSF in improving soil conditions was found to be comparable.

3.2 Effect of oyster shell soil conditioner application on the physicochemical properties of tomato inter-root soil

Oyster shell powder is made by grinding the shells of the marine organism oyster, which is alkaline in nature. Oyster shell powder mostly consists of calcium carbonate, a compound known for its excellent adsorption capabilities and ability to raise the soil's pH level. Moreover, the rise in pH level creates the ideal physicochemical environment for acid-tolerant species to reproduce and metabolize soil organic components, resulting in an augmented biomass of microorganisms and soil respiration (Neale et al., 1997; Lee et al., 2008). Oyster shells are rich in minerals, proteoglycans, and various organic matter, such as sodium, barium, copper, iron, magnesium, manganese, nickel, and several trace elements. Incorporating oyster shell soil conditioner into the soil increases its content, thereby augmenting the availability of ionic minerals to plants. This enhancement facilitates plant growth and effectively improves the soil's electrical conductivity. Additionally, it has been shown that the application of oyster shell soil conditioner leads to an increase in soil organic matter, rapid phosphorus availability, and exchangeable cation concentrations. Moreover, it has been found to dramatically enhance the levels of soil microbial carbon and nitrogen content, stimulate soil enzyme activity, and ultimately result in higher crop yields.

As shown in **Table 3**, the different treatment groups had different amounts of total nitrogen (TN), total carbon (TC), pH, electrical conductivity (EC), and water content (WC) in the soil. In comparison to the control group, the implementation of OS and OSF resulted in a substantial increase in soil total nitrogen ($p < 0.05$), soil total carbon ($p < 0.05$), soil pH ($p < 0.05$), and soil electrical conductivity ($p < 0.05$). In the two treatment groups, the percentage increase in soil total nitrogen was 16.2 and 59.9%,

TABLE 2 Effects of different treatment groups on tomato growth.

Sample	Plant height/cm	Root length/cm	Plant's fresh weight/g	Root's fresh weight/g	Plant's dry weight/g	Root's dry weight/g
CK	3.21 ± 0.45c	2.5 ± 0.57c	0.0297 ± 0.0065c	0.0034 ± 0.0013b	0.0022 ± 0.0007b	0.0008 ± 0.0005b
OS	5.68 ± 0.36b	3.15 ± 1.07b	0.1003 ± 0.0147a	0.0173 ± 0.0028a	0.0062 ± 0.0012a	0.004 ± 0.0015a
OSF	6.31 ± 0.67a	3.46 ± 1.03a	0.0985 ± 0.0101a	0.0185 ± 0.0039a	0.0062 ± 0.001a	0.0029 ± 0.0008a

a, b, and c indicate significant differences between treatment groups $p < 0.05$.

TABLE 3 Effects of different treatment groups on the physical and chemical properties of red soil.

Sample	TN/(g·kg^{-1})	TC/(g·kg^{-1})	pH	EC/(us·cm^{-1})	WC/(%)
CK	1.42 ± 0.11c	11.21 ± 0.55b	4.8 ± 0.02b	120 ± 25c	15.88 ± 1.06a
OS	1.65 ± 0.24b	14.1 ± 1.73a	7.53 ± 0.02a	573 ± 52a	14.27 ± 0.76b
OSF	2.27 ± 0.34a	14.31 ± 1.25a	7.48 ± 0.04a	494 ± 20b	15.74 ± 0.87a

a, b, c indicate significant differences between different treatment groups $p < 0.05$.

soil total carbon was 25.8 and 27.7%, pH was 56.9 and 55.9%, and conductivity was 377.5 and 311.5%, while soil water content varied. Compared to the control group, the OS group reduced the amount of The OS group experienced a 10.1% decrease in soil water content compared to the control group ($p < 0.05$), while the OSF group experienced fluctuations compared to the control group that were not significant changes ($p > 0.05$).

3.3 Effect of oyster shell soil conditioner application on the bacterial diversity of tomato inter-rhizosphere soil

In the field of microbial diversity research, investigators utilize two distinct spatial scales for analysis, namely alpha and beta. Alpha diversity examines the abundance and diversity of microorganisms within a given community through the application of single-sample diversity analysis. The aforementioned investigations encompass a variety of statistically assessed indices that facilitate the assessment of species abundance and diversity within ecological groups. Beta diversity is a measure of the variation in species composition between communities that occupy different habitats along an environmental gradient.

3.3.1 The impact of oyster shell soil conditioner on the quantity and variety of bacteria in the inter-root soil of tomato plants

Table 4 displays the results of the alpha diversity analysis conducted on the bacterial diversity inside the soil next to the roots of tomato plants. The CK, OS, and OSF categories demonstrated a significant number of operational taxonomic units (OTUs), with counts of 1334, 1271, and 1153, respectively. The extent of library coverage for each of the three sample groups was found to be 99.5%. The extensive coverage seen in this study indicates a substantial likelihood of identifying gene sequences within the soil samples. This finding shows that the sequencing depth was adequate and that the resulting sequencing outcomes accurately represent the bacterial population present in the inter-rhizosphere soil of tomatoes.

TABLE 4 Bacterial diversity index of rhizosphere soil in different treatment groups.

Sample	Diversity analysis				
	OTUs	Shannon	Chao1	ACE	Coverage
CK	1334	7.761	1493.091	1503.759	99.5%
OS	1271	7.684	1384.282	1408.293	99.5%
OSF	1153	7.126	1293.671	1314.915	99.5%

Based on the findings presented in Table 4, it can be observed that the bacterial community's diversity experienced a decrease in both the OS and OSF groups when compared to the control group. Specifically, the OS group exhibited a reduction of 4.7%, while the OSF group saw a more substantial decrease of 13.6%. Employing the Chao1 and ACE indices, the number of OUTs in the bacterial community and the diversity of the microbial community in the samples were estimated. Based on the Chao1 and ACE indices, the administration of either OS or OSF decreased the bacterial community's abundance. OSF significantly reduced bacterial abundance compared to OS.

3.3.2 Effect of oyster shell soil conditioner application on the OTU distribution of inter-root soil bacteria in tomatoes

The utilization of Venn diagrams proves to be a valuable method for evaluating the similarities and distinctions in the composition of operational taxonomic units (OTUs) between the treatment group employing oyster shell soil conditioner and the control group. Additionally, it allows for the analysis of the number of OTUs that are unique to individual samples and those that are shared among numerous samples. The root soil bacteria operational taxonomic unit (OTU) distribution chart for various treatment groups (Figure 1) demonstrates that the CK, OS, and OSF groups harbored 250, 216, and 91 distinct OTUs, respectively. Additionally, it is noteworthy that 1228 OTUs were found to be common among all three groups. The utilization of OS or OSF resulted in the introduction of new species and modifications in the community structure of bacteria residing in the inter-rhizosphere soil of tomato plants, with a more pronounced effect observed in the OS group.

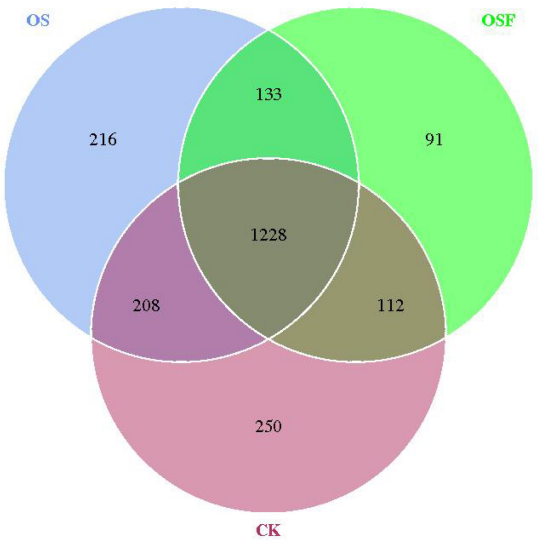

FIGURE 1
Venn of OTUs distribution of rhizosphere soil bacteria in different treatment groups.

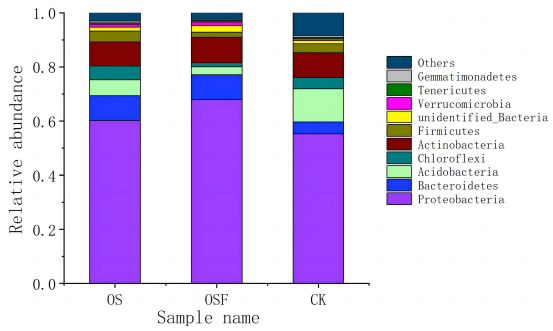

FIGURE 2
Community composition of bacterial phylum in rhizosphere soil of different treatment groups.

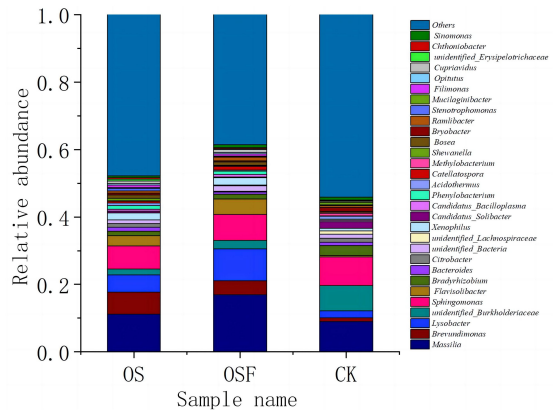

FIGURE 3
Community composition of bacterial genus in rhizosphere soil of different treatment groups.

3.3.3 Effect of oyster shell soil conditioner application on bacterial community composition of tomato inter-root soil

3.3.3.1 Soil bacterial colonies in the inter-root zone of tomato: composition analysis

Figure 2 presents the makeup of soil bacterial communities at the phylum level, specifically focusing on the inter-root region. This figure illustrates the variations in population composition across different treatment settings. The relative abundance of the top 10 phyla in soil samples from the CK, OS, and OSF groups varied between 91.00 and 97.64%. The relative abundances of these 10 phyla were: *Proteobacteria* 55.32 ~ 67.97%, *Bacteroidetes* 4.42~9.22%, *Acidobacteria* 2.87 ~ 12.18%, *Chloroflexi* 1.45 ~ 5.12%, *Actinobacteria* 8.92 ~ 9.46%, *Firmicutes* 1.98 ~ 4.03%, *unidentified Bacteria* 1.27 ~ 2.29%, *Verrucomicrobia* 0.67 ~ 1.35%, and *Tenericutes* 0.45~0.70%, and *Gemmatimonadetes* 0.39 ~ 0.76%. *Proteobacteria*, *Bacteroidetes*, *Acidobacteria*, and *Actinobacteria* constituted more than 85% of the total number of samples and were the primary phylum in the three sample categories.

Figure 3 illustrates the horizontal community composition of soil bacterial species across different treatment settings in the root soil. The relative abundance of the top 30 genera in each of the three categories ranged from 45.88 to 61.44% of the total genera. They are: *Massilia, Brevundimonas, Lysobacter, unidentified Burkholderiaceae, Sphingomonas, Flavisolibacter, Bradyrhizobium, Bacteroides, Citrobacter, unidentified_Bacteria, unidentified_Lachnospiraceae, Xenophilus, Candidatus_Solibacter, Candidatus_Bacilloplasma, phenylobacterium, Acidothermus, Catellatospora, Methylobacterium, Shewanella, Bosea, Bryobacter, Ramlibacter, Stenotrophomonas, Mucilaginibacter, Filimonas, Opitutus, Cupriavidus, unidentified_Erysipelotrichaceae, Chthoniobacter, Sinomonas*. Among them, *Massilia, Brevundimonas, Lysobacter, unidentified_Burkholderiaceae, Sphingomonas, Flavisolibacter, and Bradyrhizobium* were relatively abundant and were the dominant bacterial genera in tomato inter-rhizosphere soil.

3.3.3.2 Effect of application of oyster shell soil amendment on the structure of bacterial genera in the inter-root soil of tomato

At the phylum level, *Proteobacteria*, *Bacteroidetes*, and *Acidobacteria* exhibited greater variability in the OS and OSF groups compared to the control group. Specifically, the relative abundance of *Proteobacteria* and *Bacteroidetes* increased, while the relative abundances of *Acidobacteria* and other phyla decreased. In the OS and OSF groups, the relative abundance of *Proteobacteria* increased from 55.3 to 60.2 and 68.0%, respectively. Moreover, the relative abundance of *Bacteroidetes* increased from 4.4 to 9.2%. Conversely, the relative abundance of *Acidobacteria* decreased from 12.2 to 5.8 and 2.9%, respectively. Additionally, the relative abundance of other phyla decreased from 8.3 to 9.2% in the OS and OSF groups.

At the genus level, the utilization of different oyster shell soil conditioners (OS and OSF) led to a significant alteration in the relative abundance of several bacterial genera compared to the control group. Specifically, there was a marked increase in the relative abundances of the genera *Massilia*, *Brevundimonas*,

and *Lysobacter*, while a significant decrease was observed in the relative abundance of *unidentified_Burkholderiaceae*. The specific alterations were as follows: in the OS and OSF groups, the relative abundance of *Massilia* increased from 9.00 to 11.18 and 16.93%, respectively; the relative abundance of *Brevundimonas* increased from 1.13 to 6.56 and 4.14%, respectively; the relative abundance of *Lysobacter* increased from 2.00 to 5.12 and 9.49%; whereas the relative abundance of *unidentified_Burkholderiacea* decreased from 7.50 to 1.74 and 2.49%, respectively.

In order to examine the variations in the predominant genera of soil bacteria in the inter-rhizosphere of tomatoes across different treatment groups, we selected the top 35 genera with significant relative abundance. This selection was based on the species annotation and abundance data of all samples at the genus level. The chosen genera were then clustered according to their abundance information and visualized as a heat map (**Figure 4**). This approach aimed to facilitate the identification of the extent of aggregation among different genera within the distinct treatment groups.

As shown in the heat map (**Figure 4**), there are differences at the genus level among the three dominant groups, CK, OS, and OSF. *Mucilaginibacter*, *Candidatus_Solibacter*, *Bryobacter, Acidibacter*, *Bradyrhizobium*, and *Methylobacterium* are the dominant genera in the CK group; *Shewanella* and *Stenotrophomonas* are the dominant genera in the OS group; and *Gemmobacter*, *Ramlibacter*, *Massilia*, *Catellatospora*, *Candidatus_Solibacter*, *Intrasporangium*, and *Lysobacter* are the dominant genera in the OSF group. It can be observed that the relative abundance of various bacterial genera in distinct treatment groups varied slightly, as did their dominant genera.

The findings above suggest that the implementation of oyster shell soil conditioners, namely OS and OSF, had a considerable impact on the structure of the rhizosphere microbiome. This resulted in a modification of the microbial niche situated between plant roots, which varied in intensity and scope, thus indicating that the effects of OS and OSF on soil composition were distinguishable and independent of one another.

3.3.4 Principal component effects of the application of oyster shell soil conditioner to the inter-root soil bacterial communities of tomato

In order to analyze the differences caused by oyster shell soil amendments on the soil bacterial community structure in the tomato rhizosphere, we performed principal component analysis (PCA) on the soil bacterial community composition of the different treatment groups using PCA analysis in beta diversity analysis; the results of the PCA analysis are shown in the PCA analysis graph (**Figure 5**).

The first two principal components (PC1 and PC2) were selected for the analysis of the three groups of tomato inter-root soils. The first principal component made up 57.15% of the difference between samples, and the second principal component made up 17.1% of the difference between samples. This means that these two principal components were the main reasons why the bacterial community structure of tomato inter-root soils was different. The graph depicts the communities of three parallel samples from each treatment group, with the dots representing different colors to indicate the variation in bacterial community structure. Notably, the degree of separation between the dots corresponds to the level of significance of the observed changes. The observed spatial separation between the OS and OSF groups, as measured along the principal component 1 axis (PC1), was found to be larger than that observed for the CK group. Similarly, the spatial separation between the OS and OSF groups along the principal component 2 axis (PC2) was also larger than that observed for the CK group. These findings suggest that both the OS and OSF groups have significantly influenced the composition and structure of bacterial communities.

3.4 Analysis of the correlation between inter-root soil bacterial species diversity and environmental factors in various treatment groups

3.4.1 Spearman correlation analysis

As depicted in the Spearman correlation analysis thermogram (**Figure 6**), the water content (WC) was positively correlated with *unidentified_Alphaproteobacteria*, *Sinomonas*, and *Bradyrhizobium* ($p < 0.05$) and negatively correlated with *Filimonas* ($p < 0.05$). pH had a significant positive correlation with Shewanella ($p < 0.05$); a negative correlation with *Bradyrhizobium*, *unidentified_Alphaproteobacteria*, and *unidentified_Burkholderiaceae* ($p < 0.05$); and a highly significant negative correlation with *Methylobacterium* ($p < 0.01$). Electroconductivity (EC) is highly positively correlated with *Filimonas*, *Stenotrophomonas*, etc. ($p < 0.01$), positively correlated with *Bosea*, etc. ($p < 0.05$), highly negatively correlated with *Bryobacter*, etc. ($p < 0.01$), and negatively correlated with *Methylobacterium*, etc. ($p < 0.05$). And for TC and TN, there are also some bacterial properties that are positively (or negatively) related in a very significant way. The aforementioned results indicate that total carbon (TC), total soil nitrogen (TN), electrical impact on thermal conductivity, soil pH, and water content have a great abundance of interracial soil bacteria, with varying effects on distinct bacteria.

3.4.2 CCA analysis

The distance between the points of the CK, OS, and OSF groups was farther in the CCA (**Figure 7**), indicating that the differences in bacterial community composition among the three groups were obvious. The angles of the control group and WC were acute and obtuse with pH, EC, TN, and TC, indicating that the control group was positively correlated with WC and negatively correlated with pH, EC, TN, and TC; the distribution of the OS group was more dispersed and all were obtuse with WC, indicating that the OS group was negatively correlated with WC, while the angles of the OS group were different with pH, EC, TN, and TC, with large differences; the OSF group was at an obtuse angle to WC and at an acute angle with pH, EC, TN, and TC, indicating that the OSF group was negatively correlated with WC and positively correlated with pH, EC, TN, and TC. Therefore, variations in the structural composition of the inter-rhizosphere soil bacterial community may be related to changes in soil physicochemical factors.

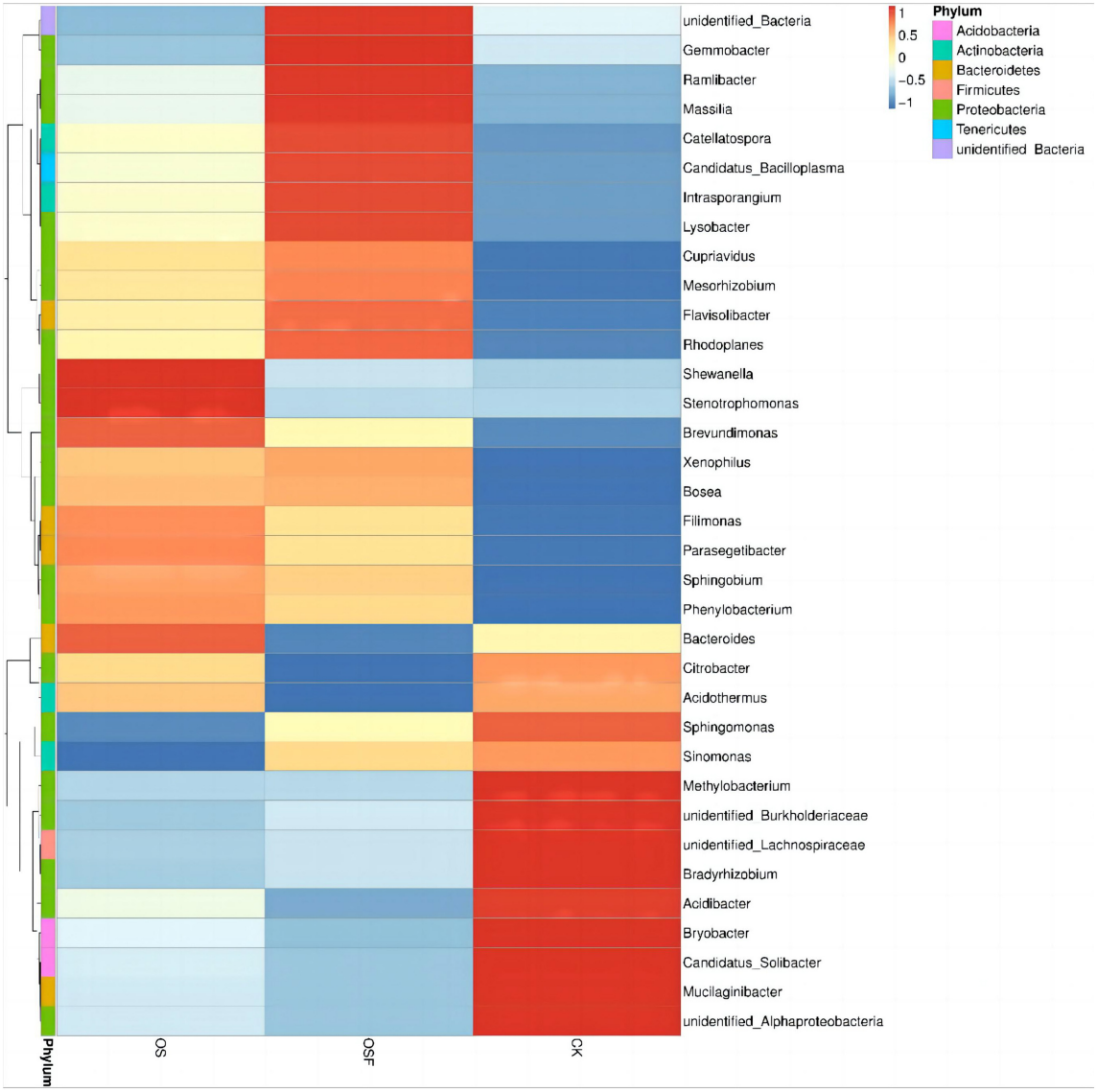

FIGURE 4
Cluster heat map of bacterial abundance in rhizosphere soil of different treatment groups.

4 Discussion

4.1 Effect of oyster shell soil conditioner application on tomato

In the tomato cultivation experiment, seed germination and seedling growth were enhanced in the OS and OSF groups relative to the CK group. It is possible that the Ca^{2+} contained in the OS and OSF groups improved the acidic soil environment and stimulated the growth of tomato seedlings. Based on empirical findings, it has been observed that when a tomato plant experiences stress due to adverse conditions, there is a notable elevation in the concentration of Ca^{2+}. This surge in Ca^{2+} concentration prompts the activation of calcium channels inside the plant, thereby exerting regulatory control over crucial physiological processes and augmenting the plant's resilience to adverse circumstances (Zhang, 2019). This study examines the impact of utilizing oyster shell soil conditioner on the growth of tomato seedlings in acidic soil. It is hypothesized that one potential mechanism behind this observed growth promotion is the facilitation of Ca^{2+} channel initiation in tomato plants. However, Ca^{2+} is an important structural and functional part of plant chloroplasts and is involved in photosynthesis. Adding calcium from outside the plant increases its ability to synthesize food when it is exposed to abiotic stress (Zhang et al., 2014). Therefore, in acidic soils, the application of oyster shell soil conditioner promoted photosynthesis in tomatoes, which in turn promoted the growth of tomatoes. In addition, Ca^{2+} in soil can interact with P^{5+} and K^{+} ions to significantly improve the biological condition and tomato fruit quality during the growth of tomatoes (Xu, 2003). The synergistic effect of Ca^{2+} and other inorganic salt ions on tomato growth may be another reason why oyster shell soil conditioner promotes tomato growth. Furthermore, a variety of physiological ailments, including navel

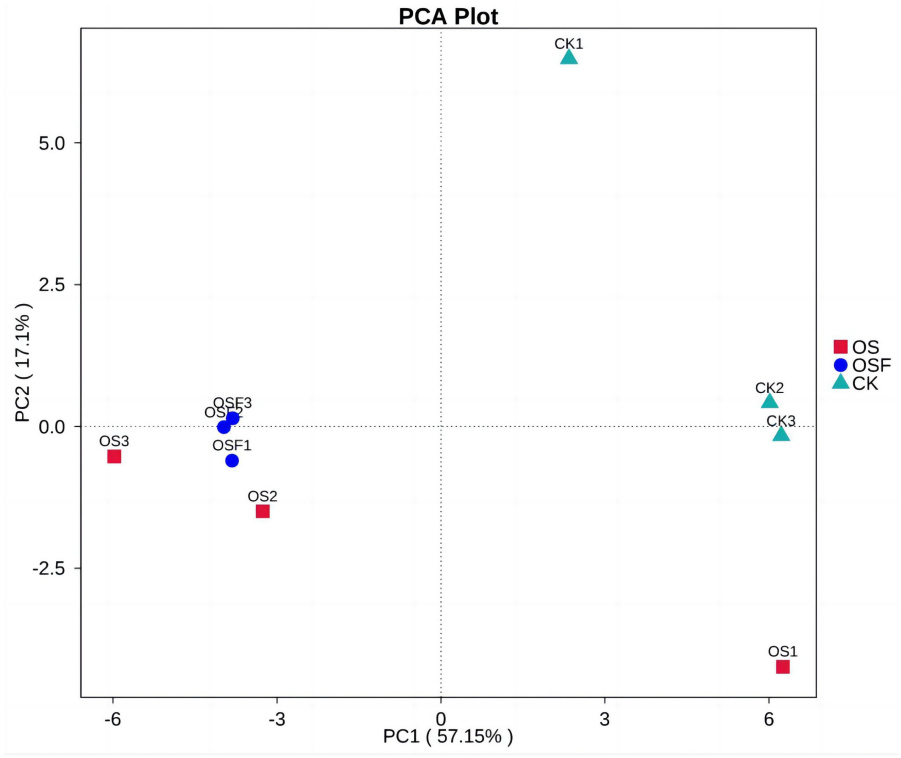

FIGURE 5
Principal component analysis (PCA) analysis of bacterial community composition in rhizosphere soil of different treatment groups.

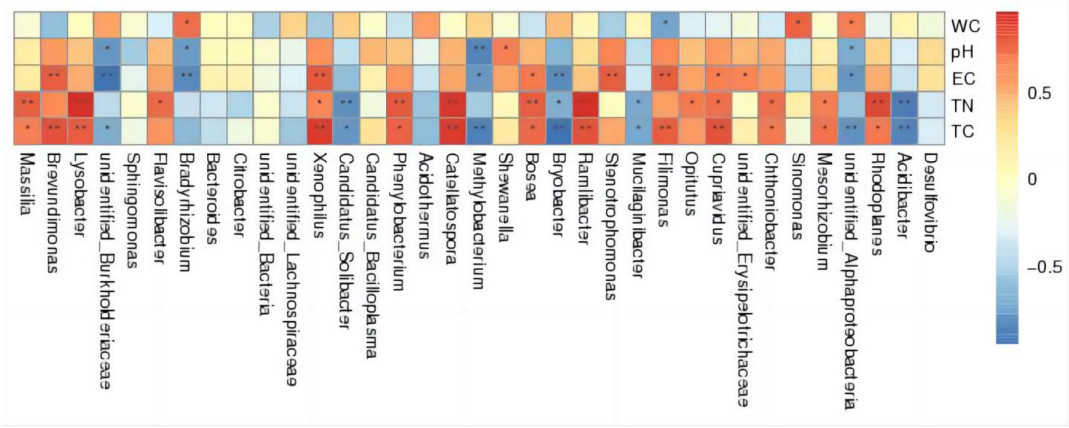

FIGURE 6
Spearman correlation analysis thermogram.

rot, fruit breaking, and poor coloring, may manifest during the growth of tomatoes in the absence of sufficient calcium (Li et al., 2019; Liu et al., 2019). However, the application of oyster shell soil conditioner can effectively ensure optimal growth conditions, facilitate successful blooming and fruiting, and enhance the overall quality of tomatoes. OS is solely calcium carbonate and contains a small amount of calcium oxide, which is too alkaline and may cause seedling burn if used improperly. OSF, on the other hand, is more suitable for very acidic soils, and the dosage must be calculated and rigorously controlled. When considering all factors, it can be concluded that the oyster shell soil conditioner developed by OSF demonstrated the highest level of effectiveness.

4.2 Effect of oyster shell soil conditioner application on bacterial diversity in acidic inter-root soil of tomato

The diversity of soil microorganisms has become an essential factor in maintaining soil function (Xu et al., 2010; Tan et al., 2014)

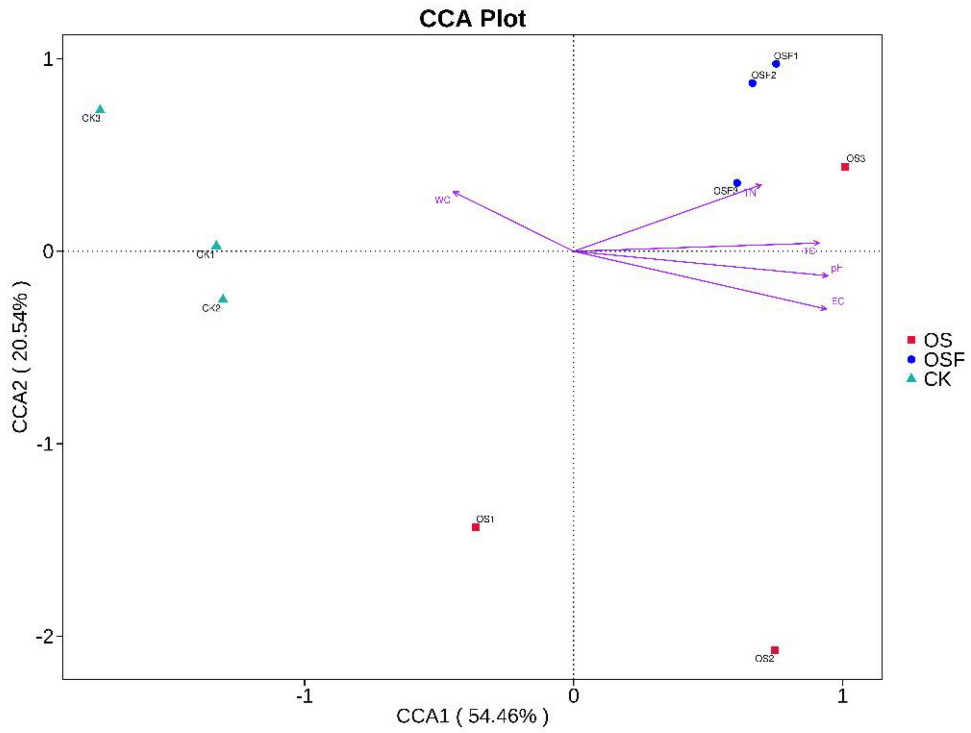

FIGURE 7
CCA analysis chart of different treatment group.

and an important index for managing and evaluating soil quality (Fernandez et al., 2016; Li, 2018). According to studies, oyster shell powder can modify bacterial abundance and diversity, leading to a rise in bacterial abundance and diversity (Zhang, 2018). In this study, however, OS and OSF altered the relative abundance, diversity, and community structure of tomato soil bacteria, resulting in a slight reduction in bacterial community diversity and a different effect for each. It is hypothesized that this difference is due to the fact that the structure of the tomato inter-rooted bacterial community has not yet reached a stable state during the 30-day cultivation period, and studies have shown that this structure stabilized gradually between 60 and 70 days (Cheng, 2018). It is also possible that OS and OSF altered the soil pH too drastically for too short a period of time, resulting in the mass extinction of the original acid-tolerant bacterial population in the inter-rooted soil, whereas the bacterial community that adapted to the new environment did not recover within a short period of time. Additionally, bacterial diversity and relative abundance were greater in the OSF group than in the OS group, most likely due to the presence of organic microbial fertilizer in the OSF group, which is consistent with previous research (Xiang et al., 2021).

4.3 Effect of oyster shell soil conditioner application on bacterial community structure of tomato acidic inter-root soil

The introduction of oyster shell soil conditioner into acidic soils has the potential to modify the structure of the soil microbial community and facilitate its evolutionary processes (Ji, 2020). Cheng (2018) employed high-throughput sequencing techniques to identify the predominant microbial communities present in the inter-rhizosphere soils of tomatoes. The results revealed that *Acidobacteria*, *Bacteroidetes*, *Gemmatimonadetes*, and *Proteobacteria* were the primary microbial taxa observed. *Proteobacteria* constituted the predominant species in the inter-rhizosphere soil of tomatoes, comprising approximately 34.15% of the bacterial population in this particular soil environment. Previous research has demonstrated the substantial contribution of *Proteobacteria* to soil remediation and the enhancement of nitrogen fertilizer utilization (Zhang et al., 2012; Xu et al., 2017). The phylum identified in this study included the above phylum after the application of oyster shell soil conditioner powder, and the relative abundance of *Proteobacteria* was the highest, consistent with previous discoveries. In addition, the relative abundance of *Bacteroidetes* increased significantly in the OS and OSF groups compared to the CK group, indicating that the relative abundance of *Bacteroidetes* was greater in healthy tomatoes than in diseased tomatoes (Shen et al., 2021), indicating that the application of oyster shell soil conditioner increased the number of dominant *Bacteroidetes* in tomato inter-root soil and promoted tomato growth. The impact of OSF was marginally more significant compared to OS, presumably due to the inclusion of organic microbial fertilizer in OSF. This component has the ability to assimilate a diverse range of advantageous bacteria, nutrients, and trace elements that facilitate the development of tomatoes. Consequently, this fosters the proliferation and reproductive capabilities of rhizosphere bacteria (Rousk et al., 2010; Wu et al., 2019).

At the taxonomic level of genus, the present study observed that the application of oyster shell soil conditioners OS and OSF resulted in an increase in the relative abundance of *Massilia* from 9 to 11.18 and 16.93%, respectively. Similarly, the relative abundance of *Brevundimonas* grew from 1.13 to 6.56 and 4.14% with the application of OS and OSF, respectively. Additionally, the relative abundance of *Lysobacter* increased from 2 to 5.12 and 9.49% with the application of OS and OSF, respectively.

The principal constituent of oyster shell powder, according to our previous analysis, is calcium carbonate, which alters the soil's pH when applied to the soil. According to previous studies, changes in soil pH have a cascading effect, i.e., fluctuations in soil pH may trigger changes in a range of soil nutrients, including, but not limited to, microbial-dominated soil nitrogen turnover, soil phosphorus solubility, soil fast-acting potassium content, and soil organic matter. In addition, the pH fluctuations also affect the microbial indicators in the soil (Wang et al., 2013; Reza et al., 2016; Penn and Camberato, 2019; Wu et al., 2023). Therefore, we suppose that the change in soil pH after the application of oyster shell soil conditioner was the main reason for the change in the occupancy structure of bacterial genera in the soil.

At the phylum level, the community structure of tomato inter-rhizosphere soil didn't change much. However, the genus distribution heat map of tomato inter-rhizosphere soil showed that the genus varied a lot between the applied treatments, and each sample treatment had its own dominant genus. Although the principal components of OS and OSF are identical, the principal dominant genera of the two are distinctive. It's possible that OSF absorbs related probiotics that have antagonistic or synergistic effects on inter-rhizosphere bacterial populations. It's also possible that other nutrients or trace elements that OSF absorbs have some effect on inter-rhizosphere bacterial growth that helps it grow. Finally, OSF may cause tomato roots to make more secretions that affect inter-rhizosphere bacterial growth (Zhalnina et al., 2015). When oyster shell soil conditioner was put on tomato inter-rhizosphere soil, it changed the soil's physical and chemical properties and acted on microorganisms. This caused changes in the species and relative abundance of dominant genera in the soil, which in turn changed the structure and distribution of soil bacterial communities.

4.4 Correlation between the application of oyster shell soil conditioner on microorganisms and environmental factors in acidic tomato inter-root soil

The soil's microbial activity, abundance, and community structure interact with plant growth and a variety of parameters like carbon and nitrogen content, pH, and electrical conductivity. The number, species, and composition of inter-rooted microorganisms can vary according to environmental factors (Andrew et al., 2012). The principal soil parameter that determines the diversity and biomass of soil microorganisms is pH, which influences the microbial community by modulating the efficacy of soil nutrients (Zhalnina et al., 2015). In this experiment, pH in the experimental group was positively correlated with *Shewanella* ($p < 0.05$) and negatively correlated with *Bradyrhizobium*, *unidentified_Alphaproteobacteria*, and *unidentified_Burkholderiaceae* ($p < 0.01$), showing a highly significant negative correlation with *Methylobacterium* ($p < 0.01$). All of the aforementioned genera belong to the *Proteobacteria*, and it is assumed that the bacteria of the *Proteobacteria* may be closely related to the regulation of soil pH. This is consistent with previous studies (Cheng, 2018).

4.5 Efficacy of oyster shell soil conditioner application for plant disease control

Previous studies (Ofek et al., 2012; Naqqash et al., 2020; Lin et al., 2021) have demonstrated that *Massilia*, *Lysobacter*, and *Brevundimonas* exhibit beneficial effects on plants, including the induction of resistance mechanisms and promotion of growth. These bacterial species can be classified as helpful bacteria. The *Burkholderiaceae*, conversely, represent a clearly delineated genus of pathogenic bacteria. Within this genus, many phytopathogenic bacteria are known to induce distinct manifestations of plant diseases, such as rot, wilt, and extensive necrosis.

In this study, the relative abundance of *Massilia*, *Brevundimonas*, and *Lysobacter* increased significantly after the application of oyster shell soil conditioner, while the relative abundance of *unidentified_Burkholderiaceae* decreased most significantly. As mentioned in the previous paper (Carrión et al., 2018; Gu et al., 2019), the addition of oyster shell soil conditioner to acidic soil will change the community structure of soil microorganisms, and the change in community structure is also important for the control of plant disease. According to previous studies, *Massilia* plays an important role in soil remediation and amelioration. Feng et al. (2016) found a new *Massilia* that can produce dimethyl disulfide (DMDS), which can be used as an alternative fumigant to control the high infection levels of soilborne pathogens, nematodes, and weeds. DMDS can also degrade PAH phenanthrene and chloroacetamide-based herbicides, produce heavy metal resistance, and have phosphorus solubilization (Islam et al., 2019; Yang et al., 2019) showed that isolates of *Brevundimonas* can promote the growth of tomato plants, act as an effective biocontrol agent against tomato wilt, and play an important role in soil toxicity removal (Gu et al., 2019). *Lysobacter* is not only able to colonize the inter-root zone of many plants but also secretes a variety of antibiotics, extracellular hydrolytic enzymes, and biosurfactants to inhibit the growth of pathogens, thus controlling plant diseases (Ji, 2011), and *Lysobacter* strains are able to produce a type of antibiotic that has a pronounced antagonistic effect on seedling blight (Hashidoko et al., 1999; Yu et al., 2007). Kobayashi and Yuen (2005) studied enzyme-producing lysogenic bacilli and found a new antibiotic substance with heat stability that altered the morphology of the mycelium by regulating the synthesis pathway of ceramidase to control the disease. In this study, *unidentified_Burkholderiaceae* showed the most significant decrease in relative abundance. Burkholderia is an important group of plant pathogenic bacteria, including eight different species of phytopathogenic bacteria, and varies according to the specific host plant as well as to a particular occasion and cultivar (Zhang, 2016). Individual species have also

been found to be closely related to plant roots (Urakami et al., 1994). After the introduction of oyster shell soil conditioner, we observed significant changes in the relative abundance of the four plant genera mentioned above. Based on examples from previous studies (Shen et al., 2018), microbial abundance and diversity were highly significant and negatively correlated with the incidence of siderophore diseases. Consequently, we deduce that the application of oyster shell soil conditioner led to a steady increase in the presence of beneficial genera, resulting in the suppression of detrimental genera. This was the underlying cause for the observed drop in the overall relative abundance. These data suggest that using oyster shell soil conditioner can improve the ability of tomato plants to fight diseases.

4.6 Main data analysis methods used in the article

The present study utilized various statistical techniques, such as the Shannon index, Spearman correlation, CCA chart, and PAC chart, to examine and interpret the experimental data. The Shannon index was utilized to estimate the diversity of the microbial population in the samples, where higher values corresponded to increased levels of diversity. In the figure depicting the Principal Component Analysis (PCA) analysis (**Figure 5**), The distance observed on the principal component axis 1 (PC1) between the OS group and the OSF group was significantly greater than that of the CK group. Similarly, the spatial distance between the two groups on the principal component axis 2 (PC2) was also significantly greater than that of the CK group. These findings suggest that both the OS group and the OSF group have altered the composition and structure of the bacterial community. However, the spatial distribution difference between the OS group and the OSF group on the two axes was relatively small, indicating a limited dissimilarity in community composition between these two groups. The disparity in structure is minimal. The observed phenomenon can be attributed to the predominant constituents of OS and OSF, namely calcium carbonate. These constituents primarily influence the structure and diversity of the bacterial population by modulating the pH levels of the soil. Spearman's correlation analysis was used to figure out how environmental factors, microbial species, and the number of them affected each other. The *p*-values typically showed the correlation and significance between the two. CCA plots can be used to detect relationships between environmental factors, between samples and colonies, or between two, and to identify the most influential environmental factors on the distribution of samples.

5 Conclusion

The utilization of oyster shell soil conditioner facilitated the germination and development of tomato seedlings, with oyster shell flour (OSF) demonstrating greater overall efficacy compared to oyster shell (OS).

The Shannon index showed that applying OS and OSF to soil decreased the variety of microbes compared to the control group. The OSF group had the biggest drop, at 13.6%.

Between 91.00 and 97.64% of the dirt around tomato plants belonged to the ten most common phyla. A total of 85% of the main groups in the inter-rhizosphere soil of tomatoes were *Proteobacteria*, *Bacteroidetes*, *Acidobacteria*, and *Actinobacteria*.

When oyster shell soil conditioner was added, the relative abundance of three helpful genera—*Massilia*, *Brevundimonas*, and *Lysobacter*—increased to varying degrees. On the other hand, the relative abundance of the disease-causing *Burkholderiaceae* dropped by a large amount.

Environmental factors were correlated with the relative abundance of soil bacteria in the inter-root zone of tomatoes. pH was positively correlated with *Shewanella* ($p < 0.05$), negatively correlated with *Bradyrhizobium*, *unidentified Alphaproteobacteria,* and *unidentified_Burkholderiaceae* ($p < 0.05$), and highly significantly negatively correlated with *Methylobacterium* ($p < 0.01$).

Data availability statement

The datasets presented in this study can be found in online repositories. The names of the repository/repositories and accession number(s) can be found in the article/supplementary material.

Author contributions

YZ: Writing – original draft, Writing – review & editing. CY: Writing – review & editing, Writing – original draft. YX: Writing – review & editing. TY: Writing – review & editing. SW: Writing – review & editing.

Funding

The author(s) declare financial support was received for the research, authorship, and/or publication of this article. This work was supported by grants from the National Natural Science Foundation of China (Nos. 31670125) and the Fujian Province regional development project (Nos. 2017N3015).

Conflict of interest

The authors declare that the research was conducted in the absence of any commercial or financial relationships that could be construed as a potential conflict of interest.

Publisher's note

References

Andrew, D. R., Fitak, R. R., Munguia-Vega, A., Racolta, A., Martinson, V. G., and Dontsova, K. (2012). Abiotic factors shape microbial diversity in Sonoran Desert soils. *Appl. Environ. Microbiol.* 78, 7527–7537. doi: 10.1128/aem.01459-12

Carrión, V. J., Cordovez, V., Tyc, O., Etalo, D. W., De Bruijn, I., De Jager, V. C., et al. (2018). Involvement of Burkholderiaceae and sulfurous volatiles in disease-suppressive soils. *ISME J.* 12, 2307–2321. doi: 10.1038/s41396-018-0186-x

Cheng, Z. Q. (2018). *Composition structural, diversity, succession and function of the tomato Rhizosphere and Endophytes*. Master's thesis. Fuzhou: Fujian Normal University.

Deng, Y. L., and Zhang, N. M. (2006). Soil pH and organic matter in greenhouse. *Ecol. Environ.* 15, 367–370. doi: 10.3969/j.issn.1674-5906.2006.02.035

Dotaniya, M., and Meena, V. (2015). Rhizosphere effect on nutrient availability in soil and its uptake by plants: a review. *Proc. Natl. Acad. Sci. India B* 85, 1–12. doi: 10.1007/s40011-013-0297-0

Feng, G. D., Yang, S. Z., Li, H. P., and Zhu, H. H. (2016). *Massilia putida* sp. nov., a dimethyl disulfide-producing bacterium isolated from wolfram mine tailing. *Int. J. Syst. Evol. Microbiol.* 66, 50–55. doi: 10.1099/ijsem.0.000670

Fernandez, A. L., Sheaffer, C. C., Wyse, D. L., Staley, C., Gould, T. J., and Sadowsky, M. J. (2016). Associations between soil bacterial community structure and nutrient cycling functions in long-term organic farm soils following cover crop and organic fertilizer amendment. *Sci. Total Environ.* 566, 949–959. doi: 10.1016/j.scitotenv.2016.05.073

Gilroy, S., Hughes, W. A., and Trewavas, A. J. (1989). A comparison between quin-2 and aequorin as indicators of cytoplasmic calcium levels in higher plant cell protoplasts. *Plant Physiol.* 90, 482–491. doi: 10.1104/pp.90.2.482

Gu, X., Liu, Y. W., Wang, X. P., Sun, Q., Wang, R., Hu, F. F., et al. (2019). Microbial remediation of chlorpyrifos by *Brevundimonas* sp. A1A18 in alkaline soil. *Ecol. Environ.* 28, 181–189. doi: 10.16258/j.cnki.1674-5906.2019.01.021

Hashidoko, Y., Nakayama, T., Homma, Y., and Tahara, S. (1999). Structure elucidation of xanthobaccin A, a new antibiotic produced from *Stenotrophomonas* sp. strain SB-K88. *Tetrahedron Lett.* 40, 2957–2960. doi: 10.1016/S0040-4039(99)00336-6

Huang, C. Y. (2000). *Facing the 21st century curriculum materials Edaphology*. Beijing: China Agricultre Press.

Islam, A., Kabir, M. S., and Khair, A. (2019). Molecular identification and evaluation of indigenous bacterial isolates for their plant growth promoting and biological control activities against Fusarium wilt pathogen of tomato. *Plant Pathol. J.* 35, 137–148. doi: 10.5423/PPJ.OA.06.2018.0104

Ji, G. H. (2011). Advances in the study on *Lysobacter* spp. bacteria and their effects on biological control of plant diseases. *J. Yunnan Agric. Univ.* 26, 124–130.

Ji, J. Q. (2020). *Effect of oyster shell powder on adjusting soil pH and controlling tobacco bacterial wilt*. Master's thesis. Chongqing: Southwest University.

Jiang, Y., Zhang, Y. G., and Liang, W. J. (2005). Influence of greenhouse vegetable cultivation on composition of soil exchangeable base cations. *J. Soil Water Conserv.* 19, 78–81. doi: 10.3321/j.issn:1009-2242.2005.06.020

Kamdem, C. N., Fogue, P. S., Tiofack, A. A. Z., Mewamba, E. M., Womeni, H. M., Koffi, M., et al. (2023). Assessment of cetyl-trimethyl-ammonium bromide (CTAB) based method for the extraction of soil-transmitted helminth DNAs from stools for molecular dagnostic of soil-transmitted helminthiasis. *J. Microbiol. Methods* 204:106661. doi: 10.1016/j.mimet.2022.106661

Kobayashi, D. Y., and Yuen, G. Y. (2005). The role of clp-regulated factors in antagonism against *Magnaporthe poae* and biological control of summer patch disease of *Kentucky bluegrass* by *Lysobacter enzymogenes* C3. *Can. J. Microbiol.* 51, 719–723. doi: 10.1139/w05-056

Krug, E. C., and Frink, C. R. (1983). Acid rain on acid soil: a new perspective. *Science* 221, 520–525. doi: 10.1126/science.221.4610.520

Lee, C. H., Lee, D. K., Ali, M. A., and Kim, P. J. (2008). Effects of oyster shell on soil chemical and biological properties and cabbage productivity as a liming materials. *Waste Manag.* 28, 2702–2708. doi: 10.1016/j.wasman.2007.12.005

Li, G. (2018). Application of soil microbial studies to farmland quality evaluation. *Acta Pedol. Sin.* 55, 543–556. doi: 10.11766/trxb201710310320

Li, H., Li, J., Qin, X., Zeng, Z., Lin, Z., and Li, Q. (2017). The status, problems, and countermeasure of oyster industry in China based on the empirical analyses of Shandong Fujian and Guangdong Guangxi provinces. *Mar. Sci.* 41, 125–129.

Li, W. Q., and Zhang, M. (2001). Salt contents in soils under plastic greenhouse gardening in China. *Pedosphere* 11, 359–367. doi: 10.1007/s11769-001-0054-9

Li, X. T., Yang, W. Y., Sun, S. S., Gong, B., and Shi, Q. H. (2019). Effect of exogenous melatonin on alleviating calcium deficiency stress in tomato. *Plant Physiol. Commun.* 55, 169–176. doi: 10.13592/j.cnki.ppj.2018.0517

Li, Y. Q. (2019). *Effect of oyster shell soil conditioner on the quality of Guanxi pomelo*. Master's thesis. Xiamen: Jimei University.

Lin, D., Sun, M. Q., Zhang, K. F., and Lin, R. X. (2019). Analysis on the development situation of Fujian oyster industry. *China Fish.* 53–57.

Lin, L., Xu, K., Shen, D., Chou, S. H., Gomelsky, M., and Qian, G. (2021). Antifungal weapons of *Lysobacter*, a mighty biocontrol agent. *Environ. Microbiol.* 23, 5704–5715. doi: 10.1111/1462-2920.15674

Liu, J. L., Bao, J., Li, J. S., and Gao, Y. M. (2019). Effects of different calcium application on tomato quality, yield and nutrients under roots restriction. *Southwest China J. Agric. Sci.* 32, 2403–2411. doi: 10.16213/j.cnki.scjas.2019.10.024

Liu, Y., Sun, M., Hou, P., Wang, W., Shen, X., Zhang, L., et al. (2022). Analysis of microbial community structure and volatile compounds in pit mud used for manufacturing Taorong-type Baijiu based on high-throughput sequencing. *Sci. Rep.* 12:7347. doi: 10.1038/s41598-022-10412-8

Naqqash, T., Imran, A., Hameed, S., Shahid, M., Majeed, A., Iqbal, J., et al. (2020). First report of diazotrophic *Brevundimonas* spp. as growth enhancer and root colonizer of potato. *Sci. Rep.* 10:12893. doi: 10.1038/s41598-020-69782-6

Neale, S. P., Shah, Z., and Adams, W. A. (1997). Changes in microbial biomass and nitrogen turnover in acidic organic soils following liming. *Soil Biol. Biochem.* 29, 1463–1474. doi: 10.1016/s0038-0717(97)00040-0

Ofek, M., Hadar, Y., and Minz, D. (2012). Ecology of root colonizing *Massilia* (Oxalobacteraceae). *PLoS One* 7:e40117. doi: 10.1371/journal.pone.0040117

Penn, C., and Camberato, J. (2019). A critical review on soil chemical processes that control how soil pH affects phosphorus availability to plants. *Agriculture* 9:120. doi: 10.3390/agriculture9060120

Reza, S. K., Baruah, U., Sarkar, D., and Singh, S. K. (2016). Spatial variability of soil properties using geostatistical method: a case study of lower Brahmaputra plains, India. *Arab. J. Geosci.* 9:446. doi: 10.1007/s12517-016-2474-y

Rousk, J., Bååth, E., Brookes, P. C., Lauber, C. L., Lozupone, C., Caporaso, J. G., et al. (2010). Soil bacterial and fungal communities across a pH gradient in an arable soil. *ISME J.* 4, 1340–1351. doi: 10.1038/ismej.2010.58

Shen, G., Zhang, S., Liu, X., Jiang, Q., and Ding, W. (2018). Soil acidification amendments change the rhizosphere bacterial community of tobacco in a bacterial wilt affected field. *Appl. Microbiol. Biotechnol.* 102, 9781–9791. doi: 10.1007/s00253-018-9347-0

Shen, T. X. (1999). Current situation of facility agricultue at home and abroad and development countermeasures of our province. *J. Agric. Mech. Res.* 5–10.

Shen, Z. Z., Huang, Y., Cao, Y. F., Wang, D. S., Liu, H. J., Li, R., et al. (2021). Comparison of bacterial communities in bulk and rhizosphere soils of healthy and diseased tomato infected by bacterial wilt. *Soils* 53, 5–12. doi: 10.13758/j.cnki.tr.2021.01.002

Southgate, P. C., and Lucas, J. S. (2008). *The pearl oyster*. Amsterdam: Elsevier Science.

Su, T., Si, M., Wang, Z., and Li, S. (2005). Effects of pretreatment, shaking and conserving method and extracting solution on results for soil mineral nitrogen. *J. Agro-Environ. Sci.* 24, 1238–1242.

Tan, Y., He, Y., and Guo, W. (2014). Research progress on soil microbial diversity based on molecular techniques. *J. Cent. South Univ. For. Technol.* 34, 1–9. doi: 10.3969/j.issn.1673-923X.2014.10.001

Urakami, T., Ito-Yoshida, C., Araki, H., Kijima, T., Suzuki, K. I., and Komagata, K. (1994). Transfer of *Pseudomonas plantarii* and *Pseudomonas* glumae to *Burkholderia* as *Burkholderia* spp. and description of *Burkholderia vandii* sp. nov. *Int. J. Syst. Evol. Microbiol.* 44, 235–245. doi: 10.1099/00207713-44-2-235

Wang, H., Dong, Y., An, Q., and Sun, H. (2005). Change in pH and salinity of vegetable soil under intensive cultivation—a case study of southern suburbs of Nanjing. *Soils* 37, 530–533. doi: 10.3321/j.issn:0253-9829.2005.05.011

Wang, L., Du, H., Han, Z., and Zhang, X. (2013). Nitrous oxide emissions from black soils with different pH. *J. Environ. Sci.* 25, 1071–1076. doi: 10.1016/s1001-0742(12)60129-6

Wu, H. N., Huang, Z. P., and Tang, X. M. (2019). Effects of nitrogen reduction on diversity of soil nitrogen-fixing microbes in peanut rhizosphere. *Jiangsu Agric. Sci.* 47, 93–97. doi: 10.15889/j.issn.1002-1302.2019.16.019

Wu, Y., Guo, J., Tang, Z., Wang, T., Li, W., Wang, X., et al. (2023). Moso bamboo (Phyllostachys edulis) expansion enhances soil pH and alters soil nutrients and microbial communities. *Sci. Total Environ.* 912:169346. doi: 10.1016/j.scitotenv.2023.169346

Xiang, F., Li, W., Liu, H., Yin, X., Zeng, Z., and Zhou, L. (2021). On the influence of nitrogen fertilizer reduction on the structure of bacterial community in tea plantation soil. *Biotechnol. Bull.* 37, 1–8. doi: 10.13560/j.cnki.biotech.bull.1985.2020-1287

Xie, J. W. (2019). Current situation and improvement measures of paddy soil acidification in Dongkou County. *China Agric. Technol. Ext.* 35, 50–52. doi: 10.3969/j.issn.1002-381X.2019.03.026

Xu, P. X., Han, L. L., He, J. Z., Luo, F., and Zhang, L. M. (2017). Research advance on molecular ecology of asymbiotic nitrogen fixation microbes. *J. Appl. Ecol.* 28, 3440–3450. doi: 10.13287/j.1001-9332.201710.035

Xu, X. J. (2003). *Effects of the phosphorus, Potassium cooperated with Calcium on Calcium Absorption of Tomasto in Greenhous*. Master's thesis. Shanxi: Shanxi Agricultural University.

Xu, X. Y. (2019). *Screening of combined initiators for tomato rootstock seeds and study on their effects*. Master's thesis. Nanjing Agricultural University.

Xu, Y., Yu, W., Ma, Q., and Zhou, H. (2010). Assessment of the impact of different fertilization systems on soil microbial ecology. *Chin. J. Soil Sci.* 41, 1262–1269. doi: 10.1080/00949651003724790

Yan, J. H. (2019). Oyster shell soil conditioner: effects on peanut yield and acidified soil amendment in yellow clayey field. *J. Agric. Sci.* 9, 17–20.

Yang, E. D., Cui, D. X., and Wang, W. Y. (2019). Research progress on the genus *Massilia*. *Microbiol. China* 46, 1537–1548. doi: 10.13344/j.microbiol.china.180573

Yu, F., Zaleta-Rivera, K., Zhu, X., Huffman, J., Millet, J. C., Harris, S. D., et al. (2007). Structure and biosynthesis of heat-stable antifungal factor (HSAF), a broad-spectrum antimycotic with a novel mode of action. *Antimicrob. Agents Chem.* 51, 64–72. doi: 10.1128/AAC.00931-06

Zeng, B. (2018). Research progress of acidified soil improvement technology. *Rural Sci. Technol.* 17, 110–111. doi: 10.3969/j.issn.1674-7909.2018.17.067

Zhalnina, K., Dias, R., De Quadros, P. D., Davis-Richardson, A., Camargo, F. A., Clark, I. M., et al. (2015). Soil pH determines microbial diversity and composition in the park grass experiment. *Microb. Ecol.* 69, 395–406. doi: 10.1007/s00248-014-0530-2

Zhang, G., Liu, Y., Ni, Y., Meng, Z., Lu, T., and Li, T. (2014). Exogenous calcium alleviates low night temperature stress on the photosynthetic apparatus of tomato leaves. *PLoS One* 9:e97322. doi: 10.1371/journal.pone.0097322

Zhang, H., Wang, L., Li, Y., Wang, P., and Wang, C. (2019). Background nutrients and bacterial community evolution determine 13C-17β-estradiol mineralization in lake sediment microcosms. *Sci. Total Environ.* 651, 2304–2311. doi: 10.1016/j.scitotenv.2018.10.098

Zhang, J., Lin, X., Liu, W., and Yin, R. (2012). Response of soil microbial community to the bioremediation of soil contaminated with PAHs. *Environ. Sci.* 33, 2825–2831.

Zhang, K. W. (2019). *Identification and stress response analysis of tomato calcium channel OSCA gene family*. Master's thesis. Harbin: Northeast Agricultural University.

Zhang, Q. M. (2016). *Study on the DNA barcode detection technology of Burkholderia spp. plant pathogens*. Master's thesis. Nanjing: Nanjing Agricultural University.

Zhang, R. (2014). *Public policy research of oyster industry in Guangdong Province*. Master's thesis. Zhanjiang: GuangdongOcean University.

Zhang, S. T. (2018). *Study on the mechanism of aluminum ions affecting the occurrence of tobacco bacterial wilt*. Master's thesis. Chongqing: Southwest University.

Zhang, W., Liu, S., Zhang, M., Li, Y., Sheng, K., and Xu, Z. (2019). *Phyllostachys edulis* (*Moso bamboo*) rhizosphere increasing soil microbial activity rather than biomass. *J. Soils Sediments* 19, 2913–2926. doi: 10.1007/s11368-019-02334-2

Zhao, J., Yang, N. D., and Zhou, L. (2015). Review on development and utilization of oyster shell resources. *Anhui Agric. Sci. Bull.* 21, 79–80. doi: 10.3969/j.issn.1007-7731.2015.21.036

Zhou, C. S., Xun, C. K., and Mu, Y. T. (2014). Research on oyster industry development strategy in the coastal area of the pearl river delta – based on the deep interview survey of farmers. *Enterprises Gov. Manag. Depart. Res. Agric. Modern.* 35, 757–762. doi: 10.13872/j.1000-0275.2014.0090

frontiers | Frontiers in Microbiology

TYPE Original Research
PUBLISHED 12 March 2024
DOI 10.3389/fmicb.2024.1280333

OPEN ACCESS

EDITED BY
Osama Abdalla Abdelshafy Mohamad,
Chinese Academy of Sciences (CAS), China

REVIEWED BY
Hai-Ming Zhao,
Jinan University, China
Kang Qiao,
Shandong Agricultural University, China
Javid A. Parray,
GDC Eidgah Srinagar, India

*CORRESPONDENCE
Xiumei Yu
✉ xiumeiyu@sicau.edu.cn
Guoshu Gong
✉ guoshugong@126.com

†These authors have contributed equally to this work

RECEIVED 25 August 2023
ACCEPTED 22 February 2024
PUBLISHED 12 March 2024

CITATION
Cui Y, Zhu Y, Dong G, Li Y, Xu J, Cheng Z, Li L, Gong G and Yu X (2024) Evaluation of the control efficacy of antagonistic bacteria from V-Ti magnetite mine tailings on kiwifruit brown spots in pot and field experiments. *Front. Microbiol.* 15:1280333. doi: 10.3389/fmicb.2024.1280333

Evaluation of the control efficacy of antagonistic bacteria from V-Ti magnetite mine tailings on kiwifruit brown spots in pot and field experiments

Yongliang Cui[1,2†], Yuhang Zhu[3†], Guanyong Dong[4], Yanmei Li[3], Jing Xu[3], Zuqiang Cheng[1,2], Lijun Li[1], Guoshu Gong[3*] and Xiumei Yu[3*]

[1]Sichuan Provincial Academy of Natural Resource Sciences, Chengdu, China, [2]Wild Plants Sharing and Service Platform of Sichuan Province, Chengdu, China, [3]College of Resources and College of Agronomy, Sichuan Agricultural University, Chengdu, China, [4]Kiwifruit Industry Development Bureau of Cangxi, Guangyuan, China

Seemingly barren heavy-metal-polluted vanadium (V) and titanium (Ti) magnetite mine tailings contain various functional microbes, yet it is unclear whether this includes microbial resources relevant to the biological control of plant diseases. Kiwifruit brown leaf spot disease, caused by *Corynespora cassiicola*, can seriously reduce kiwifruit yield. To discover effective control measures for kiwifruit leaf spot, 18 bacteria strains among 136 tailing-isolated bacteria from V-Ti magnetite mine tailings were identified as inhibiting *C. cassiicola* by the confrontation plate method, indicating that antagonistic bacteria surviving in the V-Ti magnetite mine tailings were present at a low level. The 18 antagonistic strains could be divided into two BOX-A1R clusters. The 13 representative strains that were selected for phylogenetic tree construction based on their 16S rRNA sequences belonged to the *Bacillus* genus. Five predominant strains exhibited different toxin-production times and intensities, with four of them initiating toxin production at 32 h. Among them, *Bacillus* sp. KT-10 displayed the highest bacteriostatic rate (100%), with a 37.5% growth inhibition rate and an antagonistic band of 3.2 cm against *C. cassiicola*. *Bacillus* sp. KT10 also showed a significant inhibitory effect against the expansion speed of kiwifruit brown spots in the pot. The relative control effect was 78.48 and 83.89% at 7 days after the first and last spraying of KT-10 dilution, respectively, confirming a good effect of KT-10 on kiwifruit brown leaf spots in the field. This study demonstrated for the first time that there are some antagonistic bacteria to pathogenic *C. cassiicola* in V-Ti magnetite mine tailings, and *Bacillus* sp. KT10 was found to have a good control effect on kiwifruit brown leaf spots in pots and fields, which provided an effective biological control measurement for kiwifruit brown leaf spots.

KEYWORDS

biological control, kiwifruit disease, *Bacillus*, inhibitory effect, field efficacy

Introduction

Kiwifruit (*Actinidia chinensis*) is a perennial deciduous vine in the family *Actinidiaceae* (Richardson et al., 2018). Kiwifruit is deeply loved by consumers and has broad market prospects, owing in part to its richness in vitamins A, C, E, B6, and B12 and its overall high nutritional value (Drummond, 2013). The wild resources and cultivated areas for kiwifruit in China are considerable, with the main production areas concentrated in Sichuan and Shaanxi Provinces. In Sichuan, kiwifruit is grown extensively around cities like Chengdu, Ya'an, and Guangyuan. In recent years, the cultivated areas have expanded in response to increasing market demand. The total kiwifruit cultivation area in China is 2.43×10^5 hm^2, yielding an annual harvest of 2.5×10^6 t (Wang et al., 2021). Furthermore, kiwifruit has played a positive role in helping farmers overcome poverty (Richardson et al., 2018).

However, kiwifruit diseases have become increasingly serious with the rapid growth of its cultivation, which is severely affecting kiwifruit yield and quality, leading to substantial economic losses and making the expansion of kiwifruit cultivation one of the main factors restricting the continued development of kiwifruit cultivation. More than 30 kinds of kiwifruit diseases exist, including bacterial canker disease, brown spot, root rot, flower rot, fruit soft rot, phytophthora, leaf blight, root-knot nematode disease, black spot, and other common and severe diseases (Jeong et al., 2008). Kiwifruit brown spot caused by the fungal pathogen *Corynespora cassiicola* is particularly problematic in Sichuan, China, occurring and spreading rapidly in July and August in particular (Cui et al., 2015). It leads to leaf desiccation and early leaf abscission, with high disease rates of 60%—100%, thus adversely affecting photosynthesis, causing branches to wither, fruit loss, and yield reductions of 30%—50%. Thus, the kiwifruit brown spot has become a significant obstacle to the kiwifruit industry's growth (Cui et al., 2015; Zhang et al., 2021).

Hence, there is an urgent need to find more effective biological control methods. Biological control often involves using antagonistic bacteria, metabolites of antagonistic bacteria, and/or plant extracts to control diseases. Many studies have shown that beneficial microbial preparations can indeed effectively control diseases and reduce or even eliminate pesticide residues (Ren et al., 2010). Biological management of kiwifruit postharvest diseases using antagonistic yeasts and bacteria has been demonstrated to be safe and effective (Li et al., 2022). *Candida oleophila*, originally isolated from the surface of tomato fruit, was shown to effectively inhibit gray mold and black rot in kiwifruit caused by *Botryis cinerea* and *Alternaria alternata*, as well as the incidence of natural decay (Wang Y. et al., 2018). Another antagonistic yeast *Meyerozyma caribbia* isolated from the surface of kiwifruit had antagonism to *Penicillium expansum*, resulting in kiwi fruit decay, so it can be used to control postharvest blue mold of kiwifruit (Qiu et al., 2022). Five endophytic bacteria from *Leptospermum scoparium* showed antagonism against *Pseudomonas syringae* pv. *actinidiae* (Psa), the causative agent of kiwifruit canker. Furthermore, three *Pseudomonas* sp. strains of these endophytic bacteria were transmissible to kiwifruit by wound inoculation, where they inhibited colonization by Psa and reduced canker disease severity (Wicaksono et al., 2018). However, there is limited research on the biological control of the kiwifruit brown spots. As such, the identification and development of biocontrol strains for kiwifruit brown spots are of great importance.

The vanadium (V) and titanium (Ti) magnetite mine tailings found at Panzhihua in Sichuan, China, contain various harmful components, including heavy metals, most notably. The harsh environment has fostered the presence of beneficial microorganisms, such as plant-growth-promoting bacteria and heavy-metal-resistant microbes (Yu et al., 2014; Shen et al., 2023). However, there is no research on whether microbial strains with antagonistic effects on pathogens like *C. cassiicola* can be identified from among such tailings. Accordingly, this study was aimed at isolating antagonistic bacteria and elucidating their control effects on the pathogen *C. cassiicola* from the V-Ti magnetite tailings, providing biological control bacterial resources for kiwifruit leaf brown spot disease.

Materials and methods

Screening for antagonistic bacteria

Corynespora cassiicola ACC10 (Cui et al., 2015), which was first identified as the pathogenic microorganism of the kiwifruit brown leaf spot, was used for confrontation culture. Additionally, a total of 136 bacteria (Yu et al., 2014) from V-Ti magnetite mine tailings at Panzhihua in Sichuan, China (26°36′59.8″N, 101°58′11.1″E) were used to preliminarily screen antagonistic strains by a confrontation culture method (Comby et al., 2017) on PDA medium (200 g/L potato, 10 g/L glucose, agar 18 g/L, and pH 7.4). Each PDA medium plate was divided into four equal sections (Figure 1A), and the isolated bacteria were streak inoculated with streak lengths of 2–3 cm. A 5-mm mycelial plug of *C. cassiicola* ACC10 was placed in the center of each PDA plate. Plates without streaked inoculation were used as blank controls. After incubation at 28°C for 5 days, the shapes of the pathogen colonies were observed, and the strains that significantly inhibited the growth of *C. cassiicola* ACC10 were identified as antagonistic.

Quantitative evaluation of antagonistic effects of bacteria

The antagonistic effects of the screened antagonistic bacteria were determined by previously described growth inhibitory rate (GIR), antagonistic band (AB), and bacteriostatic rate (RE) assays (Bu et al., 2021; Zhang et al., 2022), with some modifications.

For the GIR assay, a 5-mm mycelial plug of the pathogenic fungus *C. cassiicola* ACC10 was inoculated at the center of a PDA plate, and antagonistic bacteria were streak inoculated on both sides (Figure 1B). Streaks of antagonistic bacteria strains were replicated three times, and pathogenic fungi without any antagonistic bacteria inoculation under the same culture conditions served as the control. After incubation at 28°C for 5 days, the diameters of the pathogen colony in each treatment (PTR) and the control (CKR) were measured, and the growth inhibitory rate (GIR) was calculated using the formula GIR(%) = (CKR – PTR)/CKR. A higher GIR indicated a stronger antagonistic effect.

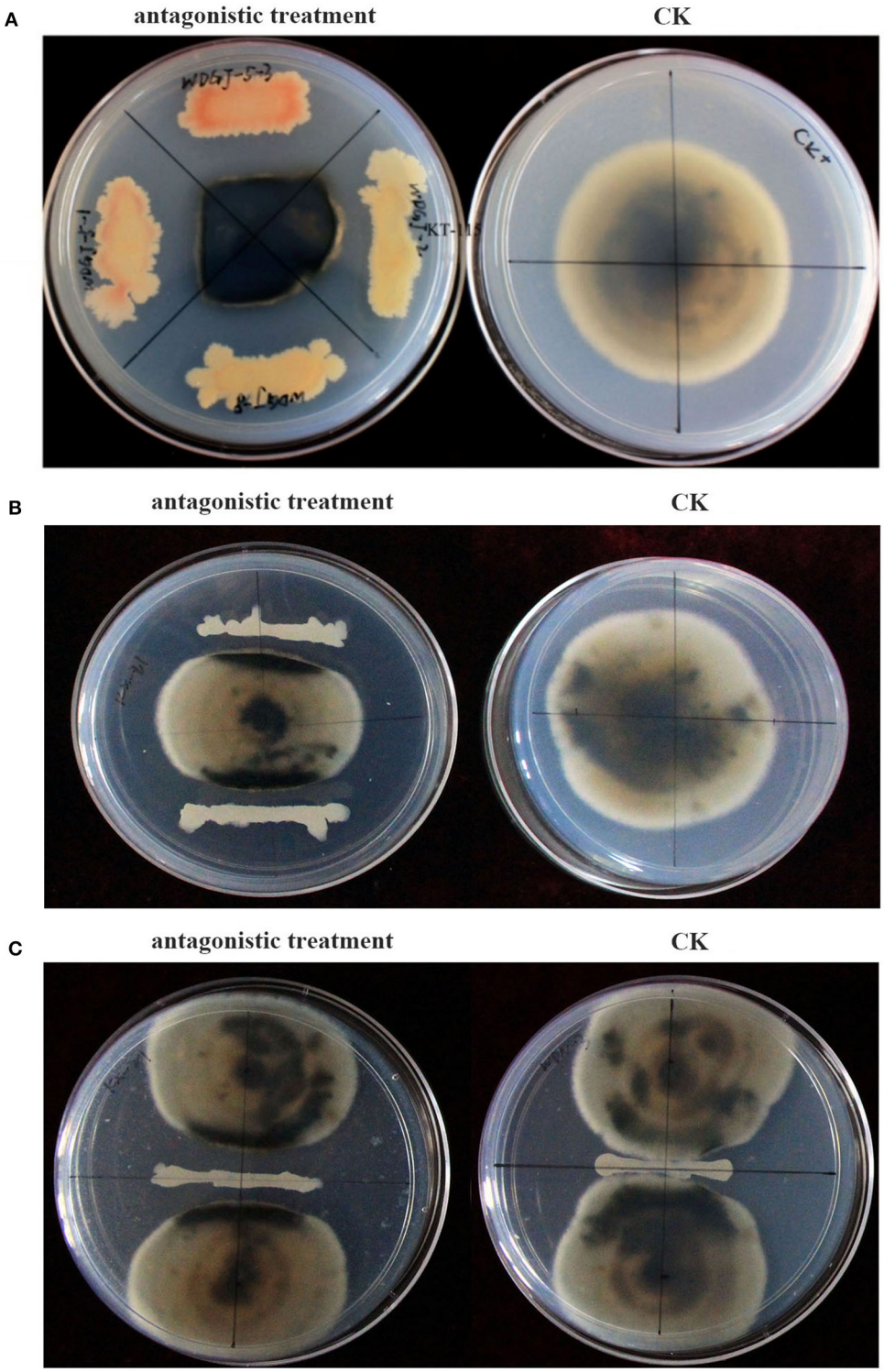

FIGURE 1
Antagonistic effects of the isolated bacterial strains against *Corynespora cassiicola* ACC10. **(A)** Screening method for antagonistic bacteria. **(B)** Determination of growth inhibitory rate (GIR). **(C)** Measurement of the antagonistic band (AB).

For the AB assay, 2–3 cm streaks of antagonistic bacteria were inoculated in the center of PDA plates, and *C. cassiicola* ACC10 was inoculated at the center of each of the two halves of each plate (Figure 1C). The antagonistic band (AB) was determined as the distance between the closest edges of the two pathogen colonies. A higher AB indicated a stronger antagonistic effect. The antagonistic effect of each antagonistic bacteria strain was assessed in triplicate.

For the RE assay, 20 *C. cassiicola* strains (Supplementary Table S1) that can cause kiwi brown spots and were obtained from various disease outbreak sites in Sichuan or Chongqing were randomly selected to determine the bacteriostatic rate (RE) of 18 isolated antagonistic bacterial strains. The pathogenicity of the 20 *C. cassiicola* strains had been confirmed in previous research (Xu et al., 2023). RE was determined using the confrontation culture method of the GIR assay after cultivating them at the same temperature simultaneously. RE was defined as the percentage of antagonistic bacteria effectively controlling the 20 pathogenic *C. cassiicola* strains. A higher RE indicated a better control effect against the pathogenic fungi responsible for the kiwifruit brown leaf spot in Sichuan.

Molecular identification of antagonistic bacteria

The total DNA of antagonistic bacteria was extracted by using the EZ-10 Spin Column Bacterial Genomic DNA Isolation Kit (Sangon Biotech, Shanghai, China), and stored at −20°C for molecular identification. All antagonistic bacteria were subjected to BOX-A1R clustering analysis, and then one representative strain per fingerprint type was chosen for 16S rRNA gene sequencing (Yu et al., 2014). The phylogenetic tree of the 16S rRNA sequences of antagonistic strains and reference strains was constructed using the neighbor-joining method with MEGA5.0 (Tamura et al., 2011). The 16S rRNA gene sequences of the representative strains were submitted to the GenBank database (accession numbers: KJ733949, KJ733981, KJ733954, KJ733993, KJ734012, KJ733995, KJ733985, KJ733947, KJ733955, KJ734004, KJ733963, KJ733996, and KJ733944).

Antagonistic toxin production time of bacteria

Bacterial strains with a highly antagonistic effect were cultured in an LB liquid medium, and fresh culture filtrate was collected using disposable filters at 8-h intervals for the Oxford cup experiment (Zhou et al., 2022). Two sterilized Oxford cups were placed vertically on culture plates of *C. cassiicola* ACC10, positioned 3 cm away from the center (Figure 4B). To analyze the toxin production time of antagonistic bacteria, 200 μl of fresh filtrate collected at different culture periods were added to each Oxford cup, followed by incubation at 28°C for 2 days before recording the antagonistic effect. The diameter of the pathogen colony in the treatment (PTR) and the control (CKR) conditions were measured to obtain the growth inhibitory rate (GIR) of the antagonistic toxin of bacteria at different culture times.

Control effect of antagonistic bacteria against kiwifruit brown spot in potted seedlings

The 2-year-old "Hongyang" kiwifruit seedlings were moved into a 25°C greenhouse. The control effect was determined after the seedlings had adapted to greenhouse conditions and their leaves had fully unfolded. Five-millimeter mycelial plugs of *C. cassiicola* ACC10 were placed on the leaves, with five mycelial plugs per leaf. After 40 h of culture, 50 ml culture broth diluent (10^7 CFU/ml) of the antagonistic bacteria strain *Bacillus* sp. KT-10 was sprayed onto five leaves, and the same nutrient solution without antagonistic bacteria was sprayed on five leaves as the negative control. The experimental treatment and control were each repeated on three seedlings. The diameter of the brown spots was measured after 5, 10, 15, 20, 25, and 30 days. The differences in spot sizes were tested using a one-tailed paired-samples *t*-test.

Control effect of antagonistic bacteria against kiwifruit brown spots in field conditions

An orchard with flat terrain, uniform fertility, and uniformly growing 8-year-old "Hongyang" kiwifruit vines was selected for the field experiment. *Bacillus subtilis* KT-10 fermentation broth (approximately 10^9 cells/ml) was diluted 400 times and sprayed on kiwifruit leaves, while the medium was used as a negative control. The experiment treatments and control each consisted of three replicates, with a row of three kiwifruit trees in each replicate. The trees were sprayed at the initial time of kiwifruit brown spot occurrence, followed by additional spraying 7, 14, and 21 days later. Disease severity was assessed before spraying, 7 days after the first spraying, and 7 days after the last spraying. For disease severity assessment, the trees were sampled at five points, and 20 leaves were investigated at each time point. Disease severity was rated using a classification standard scale from 0 to 9 (Xu et al., 2023). Disease index (DI) and control effect (CE) were calculated according to the following formulas (Zhang et al., 2020):

$$DI = \frac{\sum (\text{the leaves' number of every grade} \times \text{the value of disease grade})}{\text{the number of all leaves} \times \text{the value of highest grade}} \times 100,$$

$$CE\,(\%) = \left(1 - \frac{CK_0 \times PT_1}{CK_1 \times PT_0}\right) \times 100\%.$$

where CK_0 is the DI value of the control before spraying; CK_1 is the DI value of the control after spraying; PT_0 is the DI value of the treatment before spraying; and PT_1 is the DI value of the treatment after spraying.

Results

Antagonistic bacteria isolated from V-Ti magnetite mine tailings

A total of 136 bacterial strains with different colony characteristics, including variations in the size, color, and morphology of colonies, were isolated from V-Ti magnetite

mine tailings. Most of the strains were gram-positive, and their morphologies were predominantly rod-shaped (Yu et al., 2014). Among the 136 strains, only 18 strains exhibited the ability to dissolve the mycelia of *C. cassiicola* and form a boundary line on the PDA medium (Figure 1). Moreover, in the presence of these 18 strains, *C. cassiicola* colonies turned completely black, and the colonies were significantly smaller than those in the control (Figure 1). Thus, the 18 strains were considered antagonistic against *C. cassiicola*.

Effectiveness evaluation of antagonistic bacteria

To accurately determine the antagonistic effect, two kinds of antagonistic culture assay methods were used for the 18 strains antagonistic to *C. cassiicola* ACC10. The 18 bacteria strains exhibited varying degrees of antagonistic effects on *C. cassiicola* ACC10. The growth inhibitory rate (GIR) values of the 18 bacteria strains ranged from 14.71 to 51.43% (Table 1), with strain KT-58 exhibiting the greatest inhibitory effect. The antagonistic band (AB) of 18 bacteria strains against *C. cassiicola* ACC10 ranged from 1.0 to 3.2 cm in width (Table 1). Strain KT-10 showed the widest AB, while that of KT-52 was the narrowest. The bacteriostatic rate (RE) test revealed that the 18 strains of antagonistic bacteria displayed varying bacteriostatic rates against 20 *C. cassiicola* strains, with RE values ranging from 45 to 100% (Table 1). Strains KT-115 and KT-10 exhibited the maximum bacteriostatic rate of 100%, and the RE values of both KT-71 and KT-60 were 90%. The RE of each of the other eleven strains was lower than 80%, with KT-121 having the lowest RE. Based on the three parameters estimated, strain KT-10 demonstrated a high antagonistic effect against *C. cassiicola*.

Phylogeny of antagonistic bacteria in V-Ti magnetite mine tailings

For BOX-A1R clustering fingerprint analysis, the 18 antagonistic strains were classified into two groups, labeled I and II, which contained 13 and five strains, respectively, at a 74% similarity level (Figure 2), indicating a diverse population of antagonistic bacteria was present in the mine tailings. Group I was further divided into five subgroups, while Group II was divided into two subgroups. The similarity among KT-10, KT-97, and KT-99 on one branch was 100%, and that between KT-58 and KT-71, between KT-113 and KT-115, and between KT-60 and KT-65 on three different branches was also 100%, respectively.

Based on the BOX-A1R clustering tree, 13 representative antagonistic strains were selected at the 100% similarity level for 16S rRNA sequencing analysis. As BLASTn analysis of the GenBank database showed that the 16S rRNA sequences of the 13 strains were 99%−100% similar to the 16S rRNA sequences of *Bacillus*, the strains were preliminarily identified as *Bacillus* sp. The phylogenetic tree of the 16S rRNA sequences revealed that the 13 strains could be divided into three clades and thus belonged to different taxa (Figure 3). Among them, KT-53, KT-60, KT-103, KT-52, KT-71, KT-64, KT-83, KT-10, and KT-113 were located in the same clade as *Bacillus subtilis* and *Bacillus tequilensis*, indicating a high degree of homology and close genetic distance. Strains KT-70 and *Bacillus licheniformis* were in the same clade, and KT-121, KT-102, and KT-72 were in the same clade as *Bacillus pumilus*. However, it should be noted that using only 16S rRNA sequences may not enable the accurate identification of the species level for bacteria.

Production time of bacterial antagonistic toxin

The strains KT-10, KT-60, KT-71, KT-83, and KT-115 displayed strong antagonistic effects and were thus selected to analyze the time of antagonistic toxin production (Supplementary Table S2). Strains KT-10 and KT-115 began producing antagonistic toxins after 32 h of culture and continued to increase toxin production after 40 h (Figure 4A). Strains KT-60 and KT83 also started producing toxins after 32 h, but their toxin levels did not increase after 40 h, and the toxicity of KT-60 disappeared by 48 h. KT-71 began toxin production at 40 h, but there was no increase at 48 h. Thus, there was substantial diversity in the antagonistic toxin production time among the strains. KT-10 exhibited a strong inhibition effect on the spread of kiwifruit brown spots, effectively preventing and controlling the expansion of the kiwifruit brown leaf spot disease pathogen. The toxin secretion by KT-10 and its antifungal effect was enhanced with prolonged culture duration (Figure 4B).

Control effect of KT-10 on kiwifruit brown leaf spots in greenhouse conditions

Based on the assays of antagonistic effectiveness and antagonistic toxin production time, KT-10, the strain with the strongest antagonistic effect, was selected to characterize its control effect on the kiwifruit brown leaf spot disease caused by *C. cassiicola* ACC10. The brown spots on kiwifruit leaves began to expand 10 days after being sprayed with the strain KT-10, while in the control (CK) conditions without antagonistic bacteria, the spots began to expand just 5 days after spraying. The spread rate of brown spots in the KT-10 treatment was slow, with an average spot size of only 7.2 mm in diameter, which is 1.44 times that of the initial ACC10 mycelial plugs on day 30 (Figure 5B). In contrast, the brown spots in the CK treatment rapidly expanded to 15.3 mm on day 30, reaching a diameter more than three times the initial 5-mm diameter of the mycelial plugs of the ACC10 (Figure 5B). Thus, strain KT-10 had a substantial control effect on kiwifruit brown leaf spots (Figure 5A).

Control effect of KT-10 on kiwifruit brown leaf spots in field conditions

To further assess the control effect of *Bacillus* sp. KT-10 on kiwifruit brown leaf spots, the strain was applied to kiwifruit in field conditions. After 7 days of the first spraying, the disease index (DI)

10.3389/fmicb.2024.1280333

TABLE 1 Antagonistic effects of 18 tailings-isolated bacterial strains against *Corynespora cassiicola*.

Strain	GIR (%)	AB (cm)	RE (%)	Strain	GIR (%)	AB (cm)	RE (%)
KT-10	37.9 ± 1.5c	3.2 ± 0.4**a**	100 ± 0.0*a*	KT-60	26.3 ± 1.8ef	1.8 ± 0.1**cd**	90.1 ± 1.8*b*
KT-102	26.3 ± 1.2ef	1.8 ± 0.3**cd**	85.4 ± 1.4*c*	KT-64	26.8 ± 0.9e	1.8 ± 0.2**cd**	55.1 ± 1.9*i*
KT-103	25.0 ± 0.4ef	1.9 ± 0.4**bcd**	75.1 ± 2.9*e*	KT-65	23.8 ± 0.8fgh	1.9 ± 0.5**bcd**	59.9 ± 1.9*h*
KT-113	41.7 ± 1.1b	2.9 ± 0.3**a**	60.0 ± 3.4*h*	KT-70	16.0 ± 1.9j	1.9 ± 0.1**bcd**	69.7 ± 2.7*f*
KT-115	26.2 ± 2.2ef	2.3 ± 0.3**bc**	100 ± 0.0*a*	KT-71	20.5 ± 1.6i	2.0 ± 0.3**bcd**	90.3 ± 4.4*b*
KT-121	20.9 ± 2.1h	1.5 ± 0.2**de**	45.1 ± 1.7*k*	KT-72	21.4 ± 1.2gh	1.6 ± 0.2**d**	74.7 ± 1.8*e*
KT-52	25.0 ± 1.2ef	1.0 ± 0.2**e**	50.2 ± 2.0*j*	KT-83	18.2 ± 0.3i	2.4 ± 0.2**b**	85.2 ± 1.6*c*
KT-53	34.2 ± 1.4d	1.8 ± 0.2**cd**	50.2 ± 2.7*j*	KT-97	14.7 ± 0.6j	2.2 ± 0.3**bc**	80.2 ± 2.9*d*
KT-58	51.4 ± 3.4a	2.0 ± 0.2**bcd**	65.3 ± 2.8*g*	KT-99	25.0 ± 0.9ef	2.3 ± 0.4**bc**	69.8 ± 2.4*f*

GIR and AB were determined for *C. cassiicola* ACC10, and RE was tested using 20 pathogenic *C. cassiicola* strains.
GIR, growth inhibition rate; AB, antagonistic band; RE, bacteriostatic rate.
Values in the same column that are labeled with different letters were significantly different at $P < 0.05$.

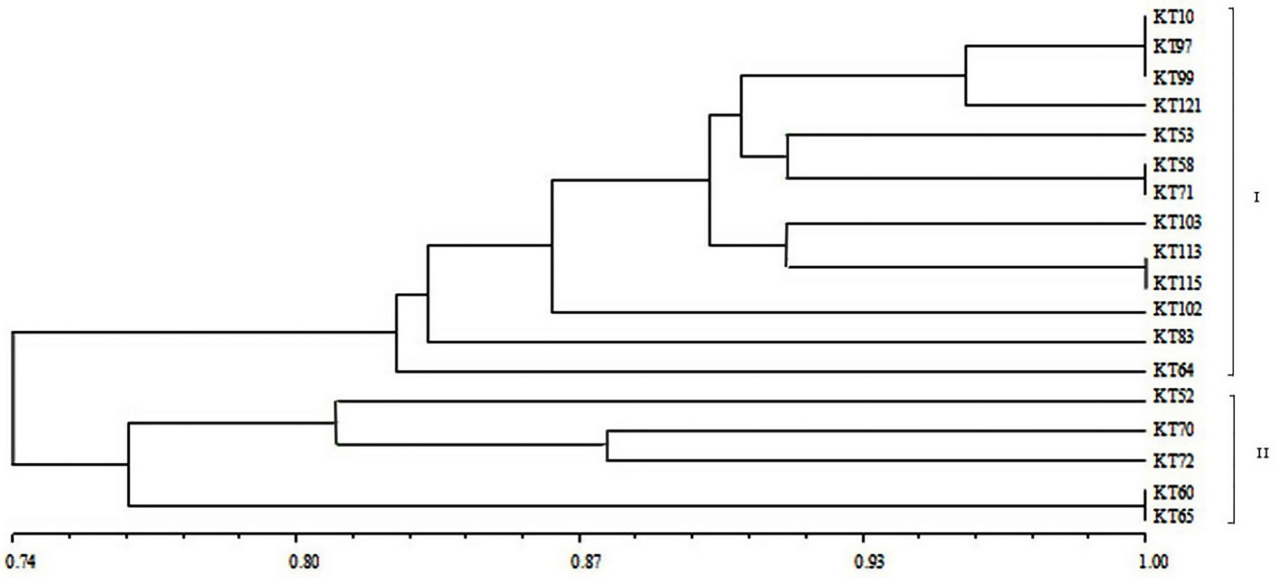

FIGURE 2
BOX-A1R cluster diagram of the antagonistic strains isolated from V-Ti magnetite mine tailings.

of kiwifruit brown leaf spots in the KT-10 treatment had increased from the initial value of 3.36–4.08; meanwhile, DI had increased from 2.82 to 15.91 in the CK treatment, and the relative control effect of KT-10 was 78.48% (Figure 6A). Seven days after the last spraying, DI was 8.36 in the KT-10 treatment and 43.54 in the CK treatment; therefore, the relative control effect of KT-10 was 83.89%. Thus, the kiwifruit brown leaf spot disease became more severe without any control measures. However, *Bacillus* sp. KT-10 effectively controlled the disease in the field (Figures 6B, C).

Discussion

Plant diseases pose a serious threat to agricultural production, and the primary approach to their prevention and control has traditionally been the application of chemical pesticides. However, the long-term and extensive use of chemical pesticides has led to issues such as pesticide residues, environmental pollution, human health consequences, and the disruption of ecological balance (Lata et al., 2021). Accordingly, biological control methods have gained widespread acceptance and application owing to their advantages, including highly reduced environmental pollution, safety, an absence of chemical product residues, high specificity to pathogens, avoidance of pesticide resistance, and high efficiency (Pérez-Sánchez et al., 2018). Beneficial microorganisms, such as *Bacillus*, *Pantoea*, *Streptomyces*, *Trichoderma*, *Clonostachys*, *Pseudomonas*, *Burkholderia*, certain yeasts, and their metabolites, are primarily employed in biological control agents (Lahlali et al., 2022).

Some beneficial bacteria with effects that include plant growth promotion, resistance enhancement, and bioremediation of heavy metals have previously been isolated from V-Ti magnetite mine tailings, which are characterized by their extreme conditions

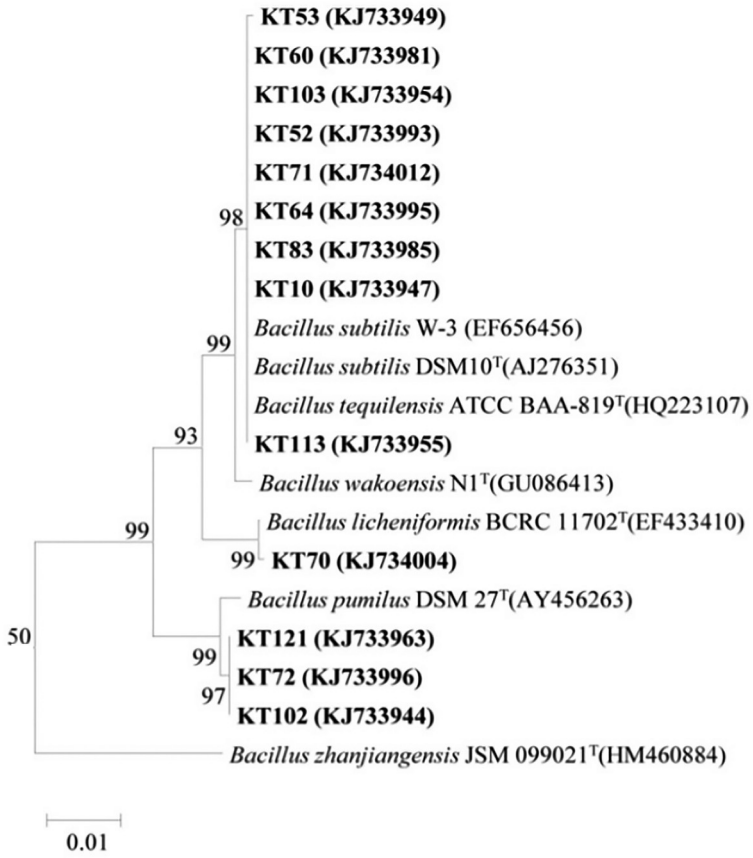

FIGURE 3
Phylogenetic tree generated from the 16S rRNA sequences of the representative antagonistic strains and reference strains by the neighbor-joining method.

of heavy metal contamination and nutrient scarcity (Yu et al., 2014, 2017). Extremophiles are relevant to a broad range of fields, spanning biotechnology, biodegradation, bioremediation, biorefining, and astrobiology, as well as various industries, such as agriculture and the production of pharmaceuticals, food, cosmetics, and textiles (Kochhar et al., 2022). V-Ti magnetite mine tailings can harbor an abundance of plant-growth-promoting microorganisms, including nitrogen-fixing rhizobia and indoleacetic acid-producing, siderophore-secreting, and heavy metal-tolerant microbes (Yu et al., 2014; Shen et al., 2023). In the present study, 18 bacterial strains isolated from the V-Ti magnetite mine tailings displayed various antagonistic effects on kiwifruit brown spot disease. This indicates that a diverse population of beneficial bacteria with antagonistic effects can thrive in extreme environments such as V-Ti magnetite mine tailings. Among these 18 antagonistic bacterial strains, KT-10 demonstrated substantial antagonistic and control effects and could potentially serve as a biocontrol agent for kiwifruit brown spot disease.

The kiwifruit leaf brown spot disease is a severe issue in both Sichuan Province and Guangxi Zhuang Autonomous Region, with *C. cassiicola* as the predominant pathogen (Yuan et al., 2014; Cui et al., 2015). *Corynespora cassiicola* infects a wide range of host species and has diverse transmission routes, making rapid and effective control measures essential for agricultural production (Shimomoto et al., 2011). In severe cases, *C. cassiicola* can infect the flowers, fruits, and stems (Qi et al., 2009). *Corynespora cassiicola* was even observed to infect soybeans [*Glycine max* (L.) Merr.], extracting nutrients from leaves, stems, pods, seeds, and roots or surviving in an endophytic relationship with soybeans (Edwards Molina et al., 2022).

Various naturally occurring microorganisms have been isolated that are capable of antagonizing or eradicating pathogenic microorganisms to achieve biological control of diseases. Biocontrol microorganisms work through mechanisms that include competition, antagonism, and the stimulation of plant defense mechanisms against pathogens, thereby inducing plant resistance mechanisms (Zehra et al., 2021). The most effective bioagents studied are those that employ multiple mechanisms, as seen in *Pseudomonas*, which utilizes both antibiosis and the induction of host resistance to suppress disease-causing microorganisms (Junaid et al., 2013). Genera such as *Bacillus* and *Pseudomonas* and their bioactive secondary metabolites have been considered beneficial bio-controllers of plant diseases through direct antibiosis, plant growth promotion, and the induction of systemic resistance in plant hosts (Dimkić et al., 2022). Bacteriophages, actinomycetes, and *Bacillus* spp. have shown biocontrol potential against *P. syringae*, the pathogen responsible for kiwifruit bacterial canker disease (Tu et al., 2011;

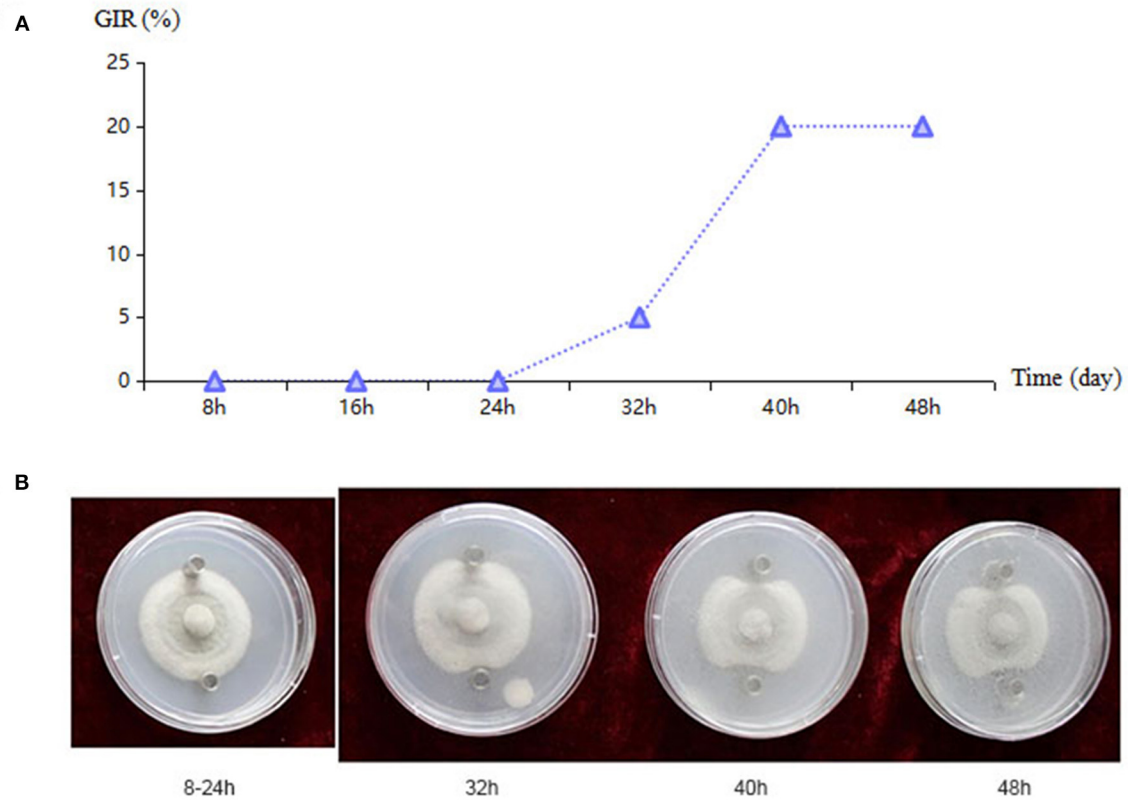

FIGURE 4
Bacillus sp. KT-10 antagonizing *Corynespora cassiicola* ACC10 in an Oxford cup experiment. **(A)** The growth inhibitory rate (GIR) for the antagonistic toxin of bacteria at different culture times. **(B)** Antagonistic effect of KT-10 toxin as observed in a time series of images of the Oxford cup experiment.

Biondi et al., 2012; Frampton et al., 2014). However, the resources for bio-control microorganisms against kiwifruit leaf spot remain limited. In the present study, 18 bacterial strains among the 136 strains isolated from V-Ti magnetite tailings were antagonistic to kiwifruit leaf brown spot disease. The rare antagonistic bacteria in the V-Ti magnetite mine tailings could be one of the reasons for the prolonged absence of plant growth in that area. However, differences in the antagonistic effects of the 18 bacteria strains were observed, despite the strains all belonging to the genus *Bacillus*.

The utilization of *Bacillus* for biological control of plant diseases has been an active research area (Comby et al., 2017). Among the extensively studied *Bacillus* species, *B. subtilis* is well documented for its roles as a growth promoter and antagonist of various pathogens. The disease suppression mechanisms employed by *B. subtilis* include plant growth promotion, antibiosis, competition for space and nutrients, lysis of pathogen hyphae, and the induction of systemic resistance (Wang X. Q. et al., 2018). For example, *B. subtilis* (at 10^8 CFU/ml) exhibited a remarkable 68.20% inhibition rate against spore germination of *Hemileia vastatrix*, the causative agent of coffee rust (Daivasikamani, 2009). *Bacillus* species have also been explored as a biological tool for enhancing crop performance across adverse environments through the induction of biomolecular changes (Radhakrishnan et al., 2017). In this study, 13 representative antagonistic bacterial strains from V-Ti magnetite mine tailings were identified as *B. licheniformis*, three strains as *B. pumilus*, and seven strains as *B. subtilis* or *B. tequilensis*. *Bacillus tequilensis* is closely related to *B. subtilis*, obstructing the positive identification of strains as belonging to one species or the other based on 16S rRNA sequence analysis alone (Gatson et al., 2006). Moreover, sequence similarity of at least 99% in 16S rRNA full-length sequences has been previously recommended as a genus-level threshold (Robert, 2018). Hence, all of the representative antagonistic strains were determined to belong to the genus *Bacillus*, which is characterized by its strong adaptability and resistance to heavy metals and barren environments (Yu et al., 2014).

Corynespora cassiicola, as a broad-spectrum pathogen, can cause spot disease in many host plant species. However, several microorganisms have been found to antagonize or control this pathogen. For example, a strain of *Meyerozyma caribbica* isolated from *C. cassiicola*-infected soybean plants inhibited *C. cassiicola* mycelial growth by producing antifungal phenethyl alcohol, suggesting a novel biocontrol method for managing target spot disease in soybean (Zhang et al., 2023). *Trichoderma spirale*, through producing antifungal alcohols and pyran compounds, displayed biocontrol activity against leaf spot disease caused by *C. cassiicola* in lettuce (*Lactuca sativa* L.) (Baiyee et al., 2019). In the present study, a toxin production test showed that the strain KT-10 produced toxin at 32 h, with toxin production gradually increasing at both 40 and 48 h. This suggests that KT-10 can produce toxins during its growth stages to inhibit the growth of *C. cassiicola*, which affects crops beyond kiwifruit. *Corynespora cassiicola* can cause target spot diseases in cotton (*Gossypium hirsutum* L.) and soybean, with isolates from a single location in Tennessee

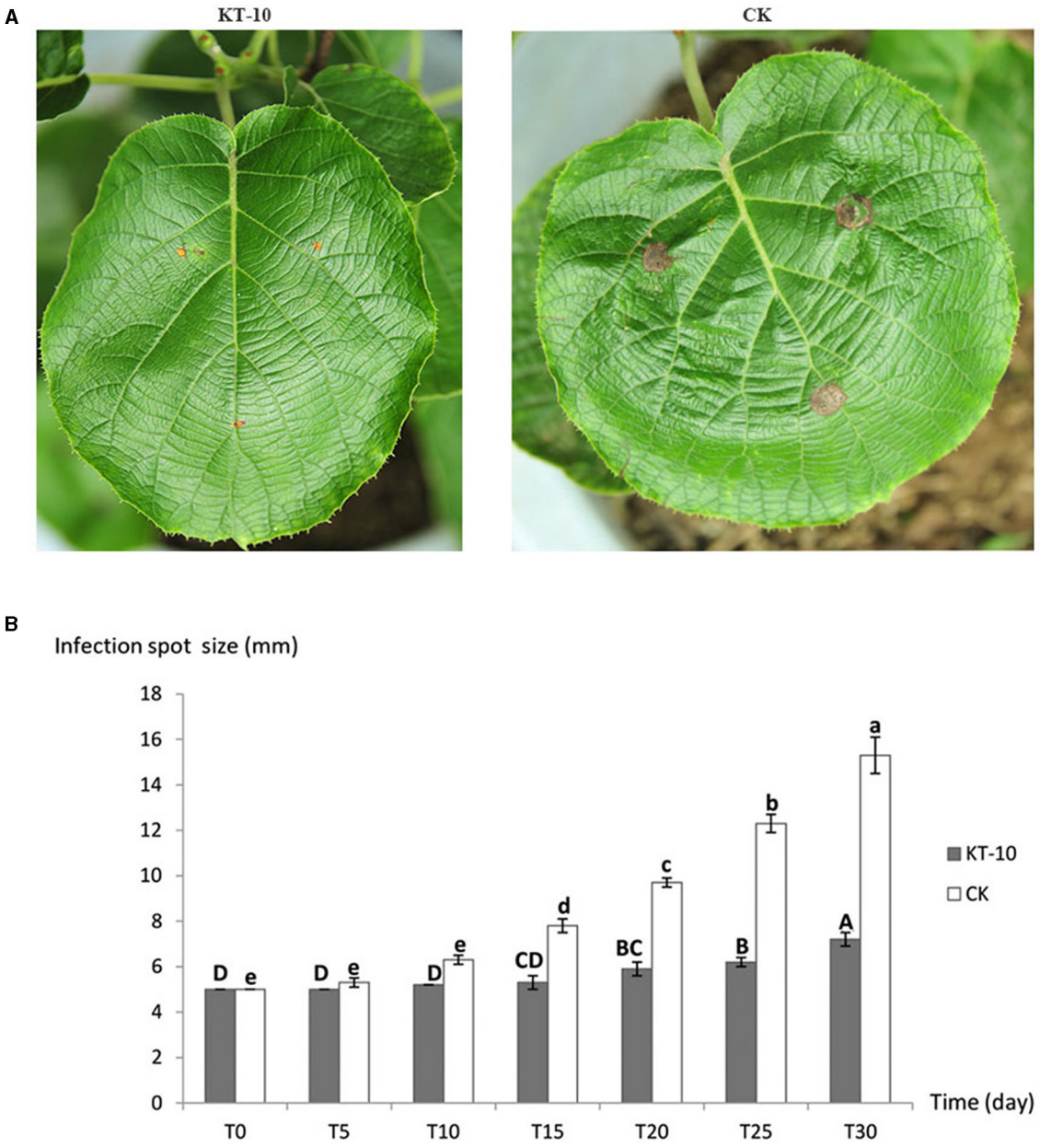

FIGURE 5
Control effect of *Bacillus* sp. KT-10 on the spread rate of *Corynespora cassiicola* ACC10 on kiwifruit leaves in the pot experiment. **(A)** Images showing the typical control effect for kiwifruit brown leaf spot on a plant grown in a pot. **(B)** Infection spot size at different times. Different letters indicate a significant difference ($p < 0.05$) among different infection time.

including eight unique multilocus genotypes, reflecting the genetic diversity of C. *cassiicola* isolates (Rondon and Lawrence, 2021). In this study, we used antagonistic bacteria against 20 strains of *C. cassiicola* randomly selected from 20 different disease outbreak sites throughout Sichuan to assess the antagonistic effect of KT-10 against different pathogen genotypes. The varying bacteriostatic rates also indicate that the 20 strains of *C. cassiicola* from different sites in Sichuan exhibit meaningful phenotypic diversity (Xu et al., 2023). The observed 100% bacteriostatic rate (RE) also showed that *Bacillus* sp. KT-10 had relatively broad control against *C. cassiicola*.

Despite the relatively common occurrence of kiwifruit leaf brown spots in Sichuan, effective prevention and control measures remain elusive. Recently, a maize biochar-zinc oxide (MB-ZnO) nanocomposite was considered an environmentally friendly method for managing kiwifruit leaf spot disease, achieving the highest growth inhibition (79%) at a 19 mg/ml nanoparticle dose (Kamal et al., 2023). Biological control, especially using antagonistic microorganisms, has become a widely adopted strategy in the control of plant diseases. Among the 18 antagonistic strains isolated from V-Ti magnetite mine tailings in the present study, KT-10 demonstrated the most pronounced growth inhibition against the

10.3389/fmicb.2024.1280333

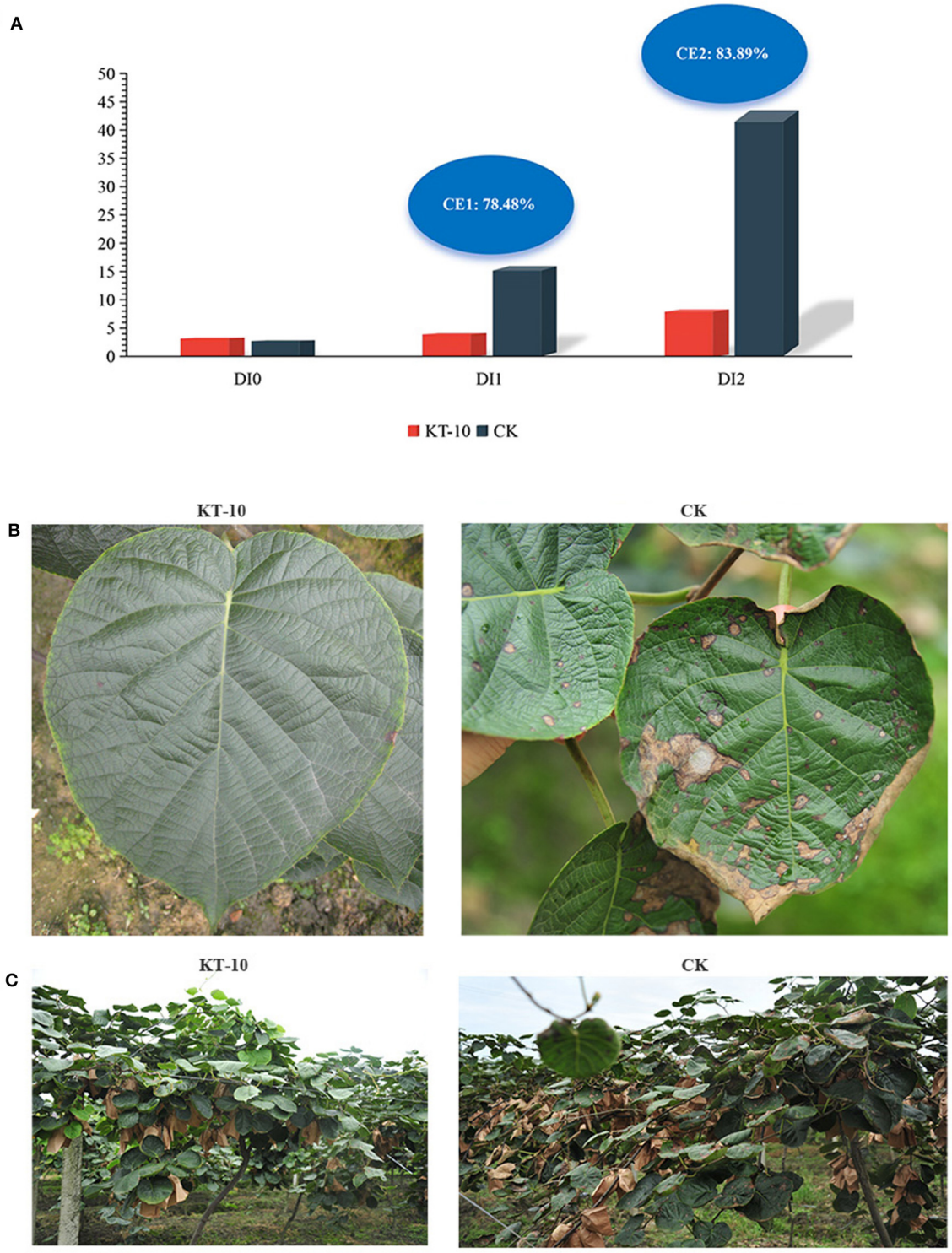

FIGURE 6
Control effect of *Bacillus* sp. KT-10 on the brown leaf spot of kiwifruit in the field. **(A)** Disease index (DI) and control effect (CE) of the kiwifruit brown spot disease. **(B)** Image showing the typical control effect of kiwifruit brown leaf spots in the field. **(C)** Field control effect of kiwifruit brown leaf spot. DI0, DI value before spraying KT-10; DI1, DI value at 7 days after first spraying KT-10; DI2, DI value at 7 days after last spraying KT-10; CE1, CE value at 7 days after first spraying KT-10; CE2, CE at 7 days after the last spraying of KT-10.

20 pathogenic *C. cassiicola* strains assayed, reaching a rate of 100% bacteriostatic rate (RE), with an antagonistic bandwidth of up to 3.2 cm and an inhibitory rate of up to 100%. Therefore, *Bacillus* sp. KT-10 can be considered an effective antagonistic microbe against *C. cassiicola*. Moreover, the inhibitory effects of strain KT-10 on kiwifruit brown spots were verified in both pot and field experiments. The strain KT-10 exhibited significant effects in the assessment of kiwifruit brown spot control in the pot

experiment, inhibiting and preventing the expansion of kiwifruit brown spot symptoms. Although the DI slightly increased after KT-10 application in the field experiment, the control effect reached 84% after the third application, far surpassing the control treatment in terms of reduced symptom onset at 30 days. This demonstrated that *B. subtilis* KT-10 can effectively control kiwifruit brown spots in the field, establishing its potential application in brown spot disease management.

Conclusion

We identified several bacterial strains, previously isolated from V-Ti magnetite mine tailings, which exhibited antagonistic effects against the pathogenic fungus *C. cassiicola*, the causal agent of kiwifruit brown leaf spot disease. All of these strains were identified as belonging to the *Bacillus* genus. However, these antagonistic bacteria showed varying control effects and toxin production times. Among them, strain KT-10 showed the most significant effect on kiwifruit brown leaf spot disease and therefore has the potential to be a biocontrol agent. Moreover, the present results indicate that biological control microorganisms can be found in extreme soil environments such as V-Ti magnetite mine tailings. The present results suggest the application of KT-10 in kiwifruit production could represent a breakthrough in brown spot disease control.

Data availability statement

The datasets presented in this study can be found in online repositories. The names of the repository/repositories and accession number(s) can be found at: https://www.ncbi.nlm.nih.gov/genbank/, KJ733949, KJ733981, KJ733954, KJ733993, KJ734012, KJ733995, KJ733985, KJ733947, KJ733955, KJ734004, KJ733963, KJ733996, KJ733944.

Author contributions

YC: Writing—review & editing, Writing—original draft, Data curation, Formal analysis, Investigation, Methodology, Visualization. YZ: Data curation, Formal analysis, Investigation, Methodology, Visualization, Writing—original draft. GD: Data curation, Formal analysis, Investigation, Methodology, Writing—review & editing. YL: Data curation, Formal analysis, Investigation, Methodology, Writing—review & editing. JX: Data curation, Formal analysis, Investigation, Methodology, Writing—review & editing. ZC: Investigation, Writing—review & editing. LL: Investigation, Writing—review & editing. GG: Writing—review & editing, Supervision. XY: Supervision, Writing—review & editing, Data curation, Formal analysis, Investigation, Project administration, Writing—original draft.

Funding

The author(s) declare financial support was received for the research, authorship, and/or publication of this article. This research was supported by the Demonstration Project of Transfer and Transformation of Scientific and Technological Achievements in Sichuan Province [2022ZHCG0030], the Basic Scientific Research Operating Expenses Project of Sichuan Province [2022JDKY0022], the Key Research Project of Deyang City [2022NZ015], Science and technology projects in Sichuan Province [2021YFN0035], Wild Plants Sharing and Service Platform of Sichuan Province, and Sichuan Province talent introduction and cultivation project.

Acknowledgments

The authors acknowledge Associate Professor Petri Penttinen of Sichuan Agricultural University for his help in revising the manuscript.

Conflict of interest

The authors declare that the research was conducted in the absence of any commercial or financial relationships that could be construed as a potential conflict of interest.

Publisher's note

Supplementary material

The Supplementary Material for this article can be found online at: https://www.frontiersin.org/articles/10.3389/fmicb.2024.1280333/full#supplementary-material

References

Baiyee, B., Pornsuriya, C., Ito, S. I., and Sunpapao, A. (2019). *Trichoderma spirale* T76-1 displays biocontrol activity against leaf spot on lettuce (*Lactuca sativa* L.) caused by *Corynespora cassiicola* or Curvularia aeria. *Biol. Control* 129, 195–200. doi: 10.1016/j.biocontrol.2018.10.018

Biondi, E., Kuzmanovic, N., Galeone, A., Ladurner, E., Benuzzi, M., Minardi, P., et al. (2012). Potential of *Bacillus amyloliquefaciens* strain d747 as control agent against *Pseudomonas syringae* pv. Actinidiae. *J. Plant Pathol.* 94:58.

Bu, S., Munir, S., He, P., Li, Y., Wu, Y., Li, X., et al. (2021). *Bacillus subtilis* L1-21 as a biocontrol agent for postharvest gray mold of tomato caused by *Botrytis cinerea*. *Biol. Control* 157:104568. doi: 10.1016/j.biocontrol.2021.104568

Comby, M., Gacoin, M., Robineau, M., Rabenoelina, F., Ptas, S., Dupont, J., et al. (2017). Screening of wheat endophytes as biological control agents against *Fusarium* head blight using two different *in vitro* tests. *Microbiol. Res.* 202, 11–20. doi: 10.1016/j.micres.2017.04.014

Cui, Y., Gong, G., Yu, X., Xu, J., Wen, X., Zhang, M., et al. (2015). First report of brown leaf spot on kiwifruit caused by *Corynespora cassiicola* in Sichuan, China. *Plant Dis.* 99, 725–725. doi: 10.1094/PDIS-08-14-0808-PDN

Daivasikamani, S. (2009). Biological control of coffee leaf rust pathogen, *Hemileia vastatrix* Berkeley and Broome using *Bacillus subtilis* and *Pseudomonas fluorescens*. *J. Biopestic.* 2, 94–98.

Dimkić, I., Janakiev, T., Petrović, M., Degrassi, G., and Fira, D. (2022). Plant-associated *Bacillus* and *Pseudomonas* antimicrobial activities in plant disease suppression via biological control mechanisms-a review. *Physiol. Mol. Plant Pathol.* 117:101754. doi: 10.1016/j.pmpp.2021.101754

Drummond, L. (2013). The composition and nutritional value of kiwifruit. *Adv. Food Nutr. Res.* 68, 33–57. doi: 10.1016/B978-0-12-394294-4.00003-1

Edwards Molina, J. P., Navarro, B. L., Allen, T. W., and Godoy, C. V. (2022). Soybean target spot caused by *Corynespora cassiicola*: a resurgent disease in the Americas. *Trop. Plant Pathol.* 47, 315–331. doi: 10.1007/s40858-022-00495-z

Frampton, R. A., Taylor, C., Holguín Moreno, A. V., Visnovsky, S. B., Petty, N. K., Pitman, A. R., et al. (2014). Identification of bacteriophages for biocontrol of the kiwifruit canker phytopathogen *Pseudomonas syringae* pv. actinidiae. *Appl. Environ. Microbiol.* 80, 2216–2228. doi: 10.1128/AEM.00062-14

Gatson, J. W., Benz, B. F., Chandrasekaran, C., Satomi, M., Venkateswaran, K., Hart, M. E., et al. (2006). *Bacillus tequilensis* sp. nov., isolated from a 2000-year-old Mexican shaft-tomb, is closely related to *Bacillus subtilis*. *Int. J. Syst. Evol. Microbiol.* 56, 1475–1484. doi: 10.1099/ijs.0.63946-0

Jeong, I. H., Lim, M. T., Kim, G. H., Han, T. W., Kim, H. C., Kim, M. J., et al. (2008). Incidences of leaf spots and blights on kiwifruit in Korea. *Plant Pathol. J.* 24, 125–130. doi: 10.5423/PPJ.2008.24.2.125

Junaid, J. M., Dar, N. A., Bhat, T. A., Bhat, A. H., and Bhat, M. A. (2013). Commercial biocontrol agents and their mechanism of action in the management of plant pathogens. *Int. J. Mod. Plant Anim. Sci.* 1, 39–57.

Kamal, A., Ali, M., Farraj, D. A. A., Al-Zaidi, E. M., Khizar, M., Aljaaidi, R. A., et al. (2023). Diagnosis and control of brown leaf spot of kiwi (*Actinidia deliciosa*) using biochar-zinc oxide nanocomposite (MB-ZnO) as a non-toxic bio-fungicides. *Crystals* 13:98. doi: 10.3390/cryst13010098

Kochhar, N., Shrivastava, S., Ghosh, A., Rawat, V. S., Sodhi, K. K., and Kumar, M. (2022). Perspectives on the microorganism of extreme environments and their applications. *Curr. Res. Microb. Sci.* 3:100134. doi: 10.1016/j.crmicr.2022.100134

Lahlali, R., Ezrari, S., Radouane, N., Kenfaoui, J., Esmaeel, Q., El Hamss, H., et al. (2022). Biological control of plant pathogens: a global perspective. *Microorganisms* 10:596. doi: 10.3390/microorganisms10030596

Lata, R., Komal, T., Neha, K., Neelam, S., Sukhbir, S., Ajmer, S. G., et al. (2021). An extensive review on the consequences of chemical pesticides on human health and environment. *J. Clean. Prod.* 283:124657. doi: 10.1016/j.jclepro.2020.124657

Li, X., Zeng, S., Liu, J., Wang, Y., and Sui, Y. (2022). Introduction and multiplex management strategies of postharvest fungal diseases of kiwifruit: a review. *Biol. Control* 176:105096. doi: 10.1016/j.biocontrol.2022.105096

Pérez-Sánchez, T., Mora-Sánchez, B., and Balcázar, J. L. (2018). Biological approaches for disease control in aquaculture: advantages, limitations and challenges. *Trends Microbiol.* 26, 896–903. doi: 10.1016/j.tim.2018.05.002

Qi, Y., Xie, Y., Zhang, X., Pu, J., Zhang, H., Huang, S., et al. (2009). Molecular and pathogenic variation identified among isolates of *Corynespora cassiicola*. *Mol. Biotechnol.* 41, 145–151. doi: 10.1007/s12033-008-9109-9

Qiu, J., Zhao, L., Jiang, S., Godana, E. A., Zhang, X., Zhang, H., et al. (2022).Efficacy of *Meyerozyma caribbica* in the biocontrol of blue mold in kiwifruit and mechanisms involved. *Biol. Control* 173:105000. doi: 10.1016/j.biocontrol.2022.105000

Radhakrishnan, R., Hashem, A., and Abd_Allah, E. F. (2017) *Bacillus*: a biological tool for crop improvement through bio-molecular changes in adverse environments. *Front. Physiol.* 8:667. doi: 10.3389/fphys.2017.00667

Ren, A. M., Zhang, L. K., and Memg, X. G. (2010). Research progress and existing problems of endophytic. *Guangdong Agricult. Sci.* 2, 103–106. doi: 10.3724/SP.J.1142.2010.40521

Richardson, D. P., Ansell, J., and Drummond, L. N. (2018). The nutritional and health attributes of kiwifruit: a review. *Eur. J. Nutr.* 57, 2659–2676. doi: 10.1007/s00394-018-1627-z

Robert, C. E. (2018). Updating the 97% identity threshold for 16S ribosomal RNA OTUs. *Bioinformatics* 34, 2371–2375. doi: 10.1093/bioinformatics/bty113

Rondon, N. M., and Lawrence, K. (2021). The fungal pathogen *Corynespora cassiicola*: a review and insights for target spot management on cotton and soyabean. *J. Phytopathol.* 169, 329–338. doi: 10.1111/jph.12992

Shen, T., Jin, R., Yan, J., Cheng, X., Zeng, L., Chen, Q., et al. (2023). Study on diversity, nitrogen-fixing capacity, and heavy metal tolerance of culturable *Pongamia pinnata* rhizobia in the vanadium-titanium magnetite tailings. *Front. Microbiol.* 14:1078333. doi: 10.3389/fmicb.2023.1078333

Shimomoto, Y., Sato, T., Hojo, H., Morita, Y., Takeuchi, S., Mizumoto, H., et al. (2011). Pathogenic and genetic variation among isolates of *Corynespora cassiicola* in Japan. *Plant Pathol.* 60:253–260. doi: 10.1111/j.1365-3059.2010.02374.x

Tamura, K., Peterson, D., Peterson, N., Stecher, G., Nei, M., Kumar, S., et al. (2011). MEGA5: molecular evolutionary genetics analysis using maximum likelihood, evolutionary distance, and maximum parsimony methods. *Mol. Biol. Evol.* 28, 2731–2739. doi: 10.1093/molbev/msr121

Tu, X., Shen, Z., Gao, Z., Kang, Z., and Huang, L. (2011). Investigation of kiwifruit bacterial canker disease (*Pseudomonas syringae* pv. Actinidiae Takikawa) in Guanzhong area of Shanxi Province and its biological control. *Plant Dis. Pests* 2, 17–20.

Wang, Q., Zhang, C., Long, Y., Wu, X., Su, Y., Lei, Y., et al. (2021). Bioactivity and control efficacy of the novel antibiotic tetramycin against various kiwifruit diseases. *Antibiotics* 10:289. doi: 10.3390/antibiotics10030289

Wang, X. Q., Zhao, D. L., Shen, L. L., Jing, C. L., and Zhang, C. S. (2018). Application and mechanisms of *Bacillus subtilis* in biological control of plant disease. *Role of Rhizospheric Microbes in Soil: Volume 1: Stress Management and Agricultural Sustainability*, ed V. Singh Meena (New York, NY: Springer), 225–250. doi: 10.1007/978-981-10-8402-7_9

Wang, Y., Luo, Y., Sui, Y., Xie, Z., Liu, Y., Jiang, M., et al. (2018). Exposure of *Candida oleophil*a to sublethal salt stress induces an antioxidant response and improves biocontrol efficacy. *Biol. Control* 127, 109–115. doi: 10.1016/j.biocontrol.2018.09.002

Wicaksono, W. A., Jones, E. E., Casonato, S., Monk, J., and Ridgway, J. H. (2018). Biological control of *Pseudomonas syringae* pv. *actinidiae* (Psa), the causal agent of bacterial canker of kiwifruit, using endophytic bacteria recovered from a medicinal plant. *Biol. Control* 116, 103–112. doi: 10.1016/j.biocontrol.2017.03.003

Xu, J., Gong, G. S., Cui, Y. L., Zhu, Y. H., Wang, J., Yao, K. K., et al. (2023). Comparison and correlation of *Corynespora cassiicola* populations from kiwifruit and other hosts based on morphology, phylogeny, and pathogenicity *Plant Dis.* 107, 1979–1992. doi: 10.1094/PDIS-04-22-0937-RE

Yu, X., Li, Y., Cui, Y., Liu, R., Li, Y., Chen, Q., et al. (2017). An indoleacetic acid-producing *Ochrobactrum* sp. MGJ11 counteracts cadmium effect on soybean by promoting plant growth. *J. Appl. Microbiol.* 122, 987–996. doi: 10.1111/jam.13379

Yu, X., Li, Y., Zhang, C., Liu, H., Liu, J., Zheng, W., et al. (2014). Culturable heavy metal-resistant and plant growth promoting bacteria in V-Ti magnetite mine tailing soil from Panzhihua, China. *PLoS ONE* 9:e106618. doi: 10.1371/journal.pone.0106618

Yuan, G. Q., Xie, Y. L., Tan, D. C., Li, Q. Q., and Lin, W. (2014). First report of leaf spot caused by *Corynespora cassiicola* on kiwifruit (*Actinidia chinensis*) in China. *Plant Dis.* 98, 1586–1586. doi: 10.1094/PDIS-06-14-0604-PDN

Zehra, A., Raytekar, N. A., Meena, M., and Swapnil, P. (2021). Efficiency of microbial bio-agents as elicitors in plant defense mechanism under biotic stress: a review. *Curr. Res. Microb. Sci.* 2:100054. doi: 10.1016/j.crmicr.2021.100054

Zhang, C., Cai, K., Li, M., Zheng, J., and Han, Y. (2022). Plant-growth-promoting potential of PGPE isolated from *Dactylis glomerata* L. *Microorganisms* 10:731. doi: 10.3390/microorganisms10040731

Zhang, C., Long, Y. H., Li, J. H., Li, M., Xing, D. K., An, H. M., et al. (2020). A Chitosan composite film sprayed before pathogen infection effectively controls postharvest soft rot in kiwifruit. *Agronomy* 10:265. doi: 10.3390/agronomy10020265

Zhang, G., Li, X., Gu, H., Zhang, W., Si, S., Li, R., et al. (2021). Pathogenic identification of leaf tip blight of red-fleshed kiwifruit in Qiandongnan prefecture. *Plant Dis. Pests* 12, 1–4. doi: 10.19579/j.cnki.plant-d.p.2021.02.001

Zhang, S. L., Sun, Q., Cao, Y., Ji, Y. P., Zhang, Y. J., Herrera-Balandrano, D. D., et al. (2023). Biocontrol of *Corynespora cassiicola* in soybean using a new phenethyl alcohol-producing *Meyerozyma caribbica* strain. *Biol. Control* 184:105287. doi: 10.1016/j.biocontrol.2023.105287

Zhou, J., Xie, Y., Liao, Y., Li, X., Li, Y., Li, S., et al. (2022). Characterization of a *Bacillus velezensis* strain isolated from *Bolbostemmatis rhizoma* displaying strong antagonistic activities against a variety of rice pathogens. *Front. Microbiol.* 13:983781. doi: 10.3389/fmicb.2022.983781

frontiers | Frontiers in Microbiology

TYPE Original Research
PUBLISHED 11 April 2024
DOI 10.3389/fmicb.2024.1307966

OPEN ACCESS

EDITED BY
Xiao Lin Wang,
Chinese Academy of Sciences (CAS), China

REVIEWED BY
An-Hui Ge,
Chinese Academy of Sciences (CAS), China
Jian-Wei Guo,
Kunming University, China

*CORRESPONDENCE
Yinquan Wang
✉ kjkfpp@163.com
Ling Jin
✉ yxyjl@163.com

RECEIVED 05 October 2023
ACCEPTED 25 March 2024
PUBLISHED 11 April 2024

CITATION
Liu C, Wang Y, Jin L, Wang Y and Liu D (2024) Morphological, molecular, and biological characterization of bulb rot pathogens in stored Lanzhou lily and the *in vitro* antifungal efficacy of three plant essential oils. *Front. Microbiol.* 15:1307966. doi: 10.3389/fmicb.2024.1307966

Morphological, molecular, and biological characterization of bulb rot pathogens in stored Lanzhou lily and the *in vitro* antifungal efficacy of three plant essential oils

Chaoqun Liu[1], Yinquan Wang[1,2]*, Ling Jin[1,2]*, Yan Wang[1] and Dongling Liu[1]

[1]College of Pharmacy, Gansu University of Chinese Medicine, Lanzhou, China, [2]Northwest Collaborative Innovation Center for Traditional Chinese Medicine Co-Constructed by Gansu Province and MOE of PRC, Lanzhou, China

Lanzhou lily (*Lilium davidii* var. *willmottiae*) is an exclusive sweet lily variety indigenous to China, which is susceptible to bulbous rot caused by fungal infection during storage. This experiment tests the pathogenicity of the pure culture isolated from the diseased tissue was confirmed in accordance with Koch's postulates, and the pathomycetes were identified based on their morphological and molecular characteristics. Furthermore, the biological characteristics of the pathogens were investigated, followed by an evaluation of the antifungal effects of three plant essential oils against them. The results showed that two strains of fungi were isolated from Lanzhou lily rot, which were identified as *Fusarium oxysporum* Schl. and *Aspergillus sydowii* (Bain. Et sart.). In addition, the pathogenicity of these two strains of fungi was demonstrated that only *F. oxysporum* induced rot with similar symptoms during the post-harvest storage period. The biological characteristics of *F. oxysporum* indicated the potato maltose agar and lily dextrose agar were identified as the most suitable media. Sucrose was determined to be the optimal carbon source, while ammonium nitrate was found to be the best nitrogen source for the growth of *F. oxysporum*. Mycelial growth and sporulation of *F. oxysporum* occurred at an optimum pH value of 6. Total darkness facilitated mycelial growth and conidial germination. The ideal temperature for growth was found to be 28°C, while relative humidity did not significantly impact mycelial growth; however, a relative humidity of 55% was most favorable for spore production. Among the three essential oils tested, cinnamon essential oil displayed superior antifungal efficacy against *F. oxysporum*, whereas angelica essential oil and tea tree essential oil also exhibited moderate inhibitory effects against this pathogen. This research provides valuable theoretical insights for disease control during the storage and transportation of Lanzhou lily.

KEYWORDS

Lilium davidii* var. *willmottiae **(E. H. Wilson) Raffill, bulb rot disease, *Fusarium oxysporum*, biological characteristics, anti-fungal effect, plant essential oils**

Introduction

Over 200 species belonging to the *Lilium L.* family can be found worldwide, and China serves as the primary geography for *Lilium* as 55 *Lilium* species are grown here (Kong et al., 2017). Lanzhou lily (*Lilium davidii* var. *willmottiae*) represents a variety of *L. davidii* within the *Liliaceae* family (Hu et al., 2020). It is just an exclusive sweet lily variety native to China characterized by its white color and sweet taste. Moreover, it contains significant amounts of natural phospholipids, alkaline elements, pectin, abundant cellulose, and plant protein. Lanzhou lily possesses various medicinal effects such as fortifying the spleen and nourishing the stomach while also acting as an anti-aging agent and offering protection against atherosclerosis. Additionally, it exhibits numerous bioactivities as an antioxidant and also bestows antitumor effects, glucose-lowering benefits, and immunomodulatory effects (Gao D. et al., 2022). Therefore, Lanzhou lily has been utilized for both medicinal and culinary purposes for more than 400 years in China. Lanzhou, situated in the northwestern region of the Chinese Loess Plateau in Gansu, boasts a dry climate and high altitude with significant temperature fluctuations between day and night. These conditions provide an ideal environment for the accumulation of nutritional and bioactive substances in plants, therefore conducive to the cultivation of high-value economic vegetables. As such, it has been recognized by the General Administration of Quality Supervision, Inspection, and Quarantine of the People's Republic of China as a geographical indication protected product (Li et al., 2020). The cultivation area of Lanzhou lily has currently expanded to 13,000 hectares, yielding approximately 80,000 tons. This industry serves as the cornerstone for farmers' prosperity in the primary production regions.

Lanzhou lily is vulnerable to mechanical damages during harvesting, storage, and transportation and pathogenic fungi infiltrate through wounds on its succulent roots or bulbs, resulting in bulb discoloration and decay (Janisiewicz and Conway, 2010). Statistical data indicates an estimated annual post-harvest loss of Lanzhou lily ranging from 20 to 25%. Fungal infection is the major factor contributing to changes in safety and sensory attributes, degradation of functional compounds, production of odors, and reduction in edible quality during the storage of Lanzhou lily (Sanches-Silva et al., 2014).

The occurrence of bulb rot disease (BRD) is commonly associated with bulb damage, a humid storage environment, and poor ventilation. Typically, it manifests as brown sunken spots on the outer bulb, with the central part of the spot exhibiting rotting, which spreads to the surrounding area. The affected tissue continues to decay until the entire bulb undergoes dry rotting (Bian, 2016; Jiao et al., 2021). BRD and wilt in the *Lilium* oriental hybrid cultivar "Sorbonne" are caused by *Fusarium tricinctum* (Corda) Sacc., *Fusarium oxysporum*, and *Fusarium solani* (Li et al., 2013; Cao et al., 2018). In addition, *F. tricinctum* and *Aspergillus flavus* not only cause wilt disease in Chinese ornamental lilies but also affect edible lilies in Lanzhou (Shang et al., 2014; Gong et al., 2015). In binucleate bulbs afflicted by BRD in Israel, fungal pathogens such as *Rhizoctonia solani* Kühn, *Pythium oligandrum* Drechsler, *Fusarium proliferatum*, and *F. oxysporum* have been identified. Among them, *R.* AG-A, *P. oligandrum*, and *F. proliferatum* can cause significant damage to bulbs (Sara et al., 2014; Xing et al., 2022). *F. oxysporum* f.sp. Lilii has been found responsible for medical lily bulb rot in Hunan, Jiangxi, Zhejiang, and Beijing in China. *F. solani* causes BRD in Zhejiang and Jiangxi, while *F. proliferatum* and *F. commune* are the agents causing this disease in Jiangxi. *Curvularia pseudobrachyspora* has been reported as a causal agent for *Lilium brownii* var. *viridulum* BRD in Jiangxi (Zeng et al., 2020; Jiao et al., 2021). Obviously, a majority of these pathogens were isolated from the decaying bulbs of ornamental lilies, with limited research being conducted on BRD in Lanzhou lily bulbs during storage.

The use of fungicides to prevent or treat plant phytopathogenic fungi has given rise to the development of resistant strains of fungal pathogens and has consequently engendered a plethora of health hazards, including an escalated risk of cancer and environmental contamination (Panjehkeh and Jahani Hossein-Abadi, 2011). With increasing focus on food safety, there is a growing demand for broad-spectrum, efficient, environmentally friendly, and safe food preservatives (Wei et al., 2018). Natural plant ingredients possessing antifungal properties are expected to serve as alternatives to chemical fungicides (Zhu et al., 2019). Plant essential oils represent a class of plant secondary metabolites that exhibit diverse biological activities and can be abundantly found in the roots, stems, leaves, flowers, and fruits of plants (Maffei, 2010). Approximately 60 plant families encompass species that produce essential oils. The Apiaceae, Asteraceae, Lamiaceae, Lauraceae, and Camelliaceae families are particularly significant due to their essential oils possessing anti-fungal and anti-bacterial effects and other properties (Vigan, 2010; Hammer and Carson, 2011). However, there is currently no available literature documenting the utilization of cinnamon essential oil, tea tree essential oil, and angelica essential oil for the prevention and control of storage diseases in Lanzhou lily bulbs.

The objective of this research was to isolate and identify the pathogen that causes BRD in Lanzhou lily and investigate its morphological, molecular, and biological characteristics. Additionally, we assessed the potential of antifungal plant essential oils against BRD *in vitro*. This research serves as a valuable theoretical reference for disease control during the storage and transportation of Lanzhou lily bulbs.

Materials and methods

Sample collection

Lanzhou lily bulb rot samples were collected from Yuanjiawan Village, Xiguoyuan, Qilihe District, Lanzhou, China (36.065915°N, 103.785866°E) in late October in 2022 and stored at −4°C in the bottom fresh-keeping refrigerator. The bulb rot collected had diseased plants with typical symptoms of BRD.

Isolation and purification of fungus

Approximately 50 rotten bulbs with typical BRD symptoms during storage were collected and pathogenic fungi were isolated by tissue separation. The bulb rot was washed with water, cut 4

× 4 mm in size at the place where diseased, and healthy tissues were placed in the ultraclean workbench. The surface of the diseased bulb was disinfected with 75% absolute alcohol for 30 s, washed three times with sterilized water, disinfected with 2% (v/v) sodium hypochlorite solution for 2.5 min, rinsed three times with sterile water, placed on potato dextrose agar (PDA) medium, and incubated at 28°C for 3–5 days. The edge of the colony with a hole punch was picked up and placed on the PDA medium for purification. After the mycelium grows out, the purified colony was then isolated and cultured for a single spore.

Pathogenicity test

To confirm the pathogenicity of pure culture isolated from the lily samples with BRD, Koch's postulates were performed (Gao D. et al., 2022; Gao Z. Y. et al., 2022). In this experiment, conidia obtained from the 1-week-old culture medium that carried with fungal isolate were used. First, the surface of 35 asymptomatic lily bulb samples was disinfected with 75% alcohol, washed with sterile distilled water, then disinfected by sodium hypochlorite solution (2%, v/v) for 2.5 min. Subsequently, sterile distilled water was used to rinse them to complete surface disinfection. The bulbs were air-dried for 10 min at room temperature (25 ± 2°C; De Oliveira et al., 2014). The sterilized inoculum was used to puncture the healthy bulb. The fungi cake with PDA culture medium were pasted on the hole as the injured inoculation, and the fungi cake with PDA culture medium were pasted on the bulb slice without puncture as the uninjured inoculation. The healthy bulb slice was treated as the control and five bulbs per group were placed. This process was repeated seven times. The bulbs were put into the culture dish for moisture culture. All bulbs were incubated at 28°C under light/dark for 12 h and 60–70% relative humidity after inoculation. After 15 days, the disease incidence was recorded to determine the pathogenicity of the pathogen to the bulbs. The aforementioned single-spore isolation and purification were used to re-isolate fungi from each group of lesions observed on the inoculated corms to prove Koch's hypothesis.

Pathogen identification

Morphological identification

The appearance of colonies and morphology of the fungal isolates were surveyed after placing them in a biochemical incubator at light/dark for 12 h at 28°C for a week. The representative isolate was used for microscopic observations. The morphological characteristics of the hyphae and spores of the pathogenic fungi were observed and photographed with a fluorescence microscope system (Leica DM4000B LED, Germany). The size and morphological information related to the characteristics of the strain (e.g., hypha, macroconidium, and microconidium) were measured with all 50–60 numbers of each structure.

Molecular identification

DNA extraction, amplification, and sequencing

The total genomic DNA of a 5-day-old fungal isolate cultivated on a PDA medium at 28°C was extracted using a fungal/bacterial DNA kit™ (Favorgen, Taiwan). Polymerase chain reaction (PCR) amplification of ITS, Tef-1, Cam, PRB1, PRB2, TUB2, BenA, Mcm7, and Tsr1 was performed using the primer pairs according to the methods described earlier (Bian et al., 2022; Sklenár et al., 2022; Nuangmek et al., 2023). The relevant gene sequences are listed in Table 1 (Wang et al., 2022). The amplification of nine genes was completed in an independent PCR reaction. The program employed for amplification is as follows: one initial step of 3 min at 95°C; the second step of 35 cycles for 30 s at 95°C, next, annealing step for 50 s at 60°C and 30 s at 59°C or 1 min at 52°C; finally, the extension step lasting 10 min at 72°C. The PCR products were directly sequenced followed by final purification. Sequencing reactions were carried out and the aforementioned PCR primers were employed in the ABI Prism 3130 genetic analyzer (Applied Biosystems) according to the manufacturer's instructions.

TABLE 1 Primers identified in the PCR amplification of the seven loci.

Locus	Primer	Sequence of primer (5′-3′)
ITS	ITS5	GGAAGTAAAAGTCGTAACAAGG
	ITS4	TCCTCCGCTTATTGATATGC
Tef1	EF1	ATGGGTAAGGARGACAAGAC
	EF2	GGARGTACCAGTSATCATG
Ccam	CL1	GARTWCAAGGAGGCCTTCTC
	CL2A	TTTTTGCATCATGAGTTGGAC
RPB1	RPB1-Fa	CAYAARGARTCYATGATGGGWC
	RPB1-G2R	GTCATYTGDGTDGCDGGYTCDCC
RPB2	RPB2-5f2	GGGGWGAYCAGAAGAAGGC
	RPB2-11ar	GCRTGGATCTTRTCRTCSACC
Tub2	T1	AACATGCGTGAGATTGTAAGT
	T2	TAGTGACCCTTGGCCCAGTTG

Phylogenetic analyses

The genes such as Cam, Tef-1, PRB1, PRB2, TUB2, BenA, Mcm7, and Tsr1 obtained from the sequences were compared with those from the NCBI for similarity analysis via http://blast.ncbi.nlm.nih.gov (accessed on January 13, 2024). Multiple proofreads were arranged by edgar (Nuangmek et al., 2023) and alignment was manually adjusted if necessary. The obtained data about Tef-1, Cam, PRB1, PRB2, TUB2, BenA, Mcm7, and Tsr1 was used for multi-gene phylogenetic analysis (Sklenár et al., 2022; Nuangmek et al., 2023). Phylogenetic analysis was performed using maximum likelihood (ML) and Bayesian inference (BI) methods. Nucleotide substituted Gtrcat model on RAxML-HPC2 version 8.2.12 (Nuangmek et al., 2023) on the Cipres internet portal (Miller et al., 2010) was employed. The best pattern for nucleotide substitution was derived using the J-Modeltest V.2.3 (Darriba et al., 2012) on the basis of the designated method (Ronquist et al., 2012). The BI analysis was conducted following the protocol of Wang et al. (2019). Using MrBayes V. 3.2.6 (Ronquist et al., 2012) in combinatorial analysis, each locus is optimized into a partition. All characters have equal weights, and blank spaces are considered missing data. The phylogenetic trees were visualized using FigTree v1.4.0 (Rambaut, 2019).

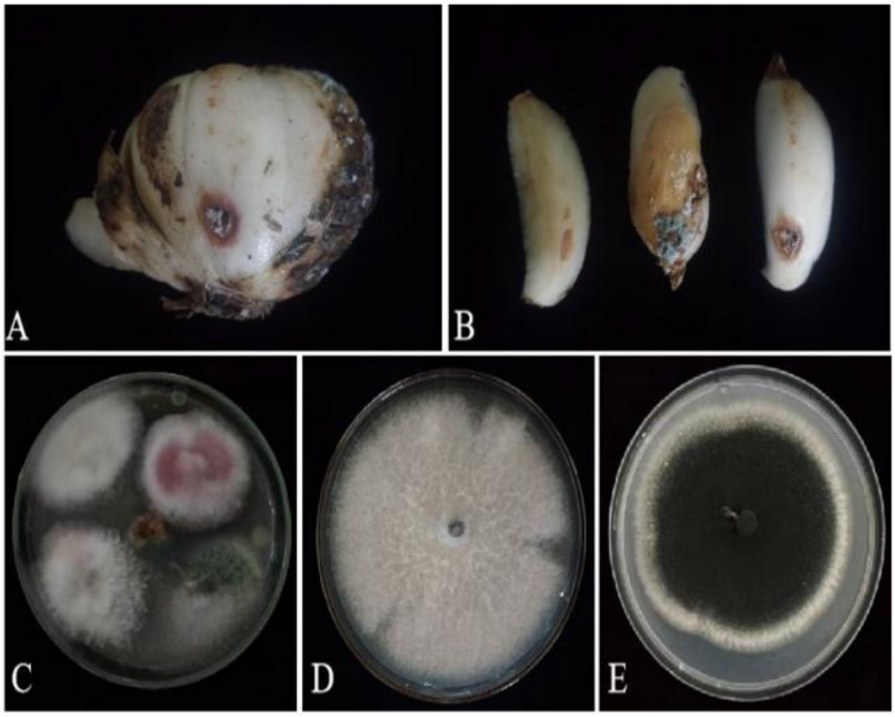

FIGURE 1
Lily samples with BRD **(A, B)**, separators of lily samples **(C)**, and pathogens of lily separators **(D, E)**.

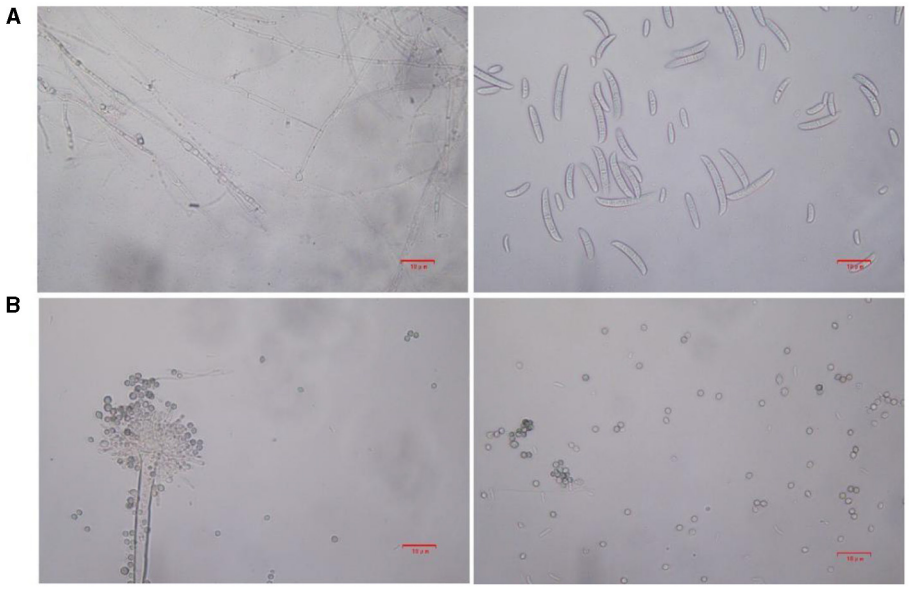

FIGURE 2
The microstructure of strains 201 and 202 in the logarithmic phase. **(A)** The effect of strain 201 on separating mycelium and spore under 400×, scale bars: D–G = 10 μm. **(B)** The effect of strain 202 on separating mycelium and spore under 400X, scale bars: D–G = 10 μm.

Influence of different culture media on mycelium growth and sporulation quantity

A 1-week-old fungi block with a diameter of ~6 mm was placed in the middle of different types of tested media, such as PDA medium, potato maltose agar (PMA) medium, lily agar (LA) medium and lily dextrose agar (LDA) medium. Then the culture was developed at 28°C for 3–5 days under light/dark for 12 h. The diameter of mycelium is usually measured using the cross-shaped method on the 3rd day. The blood cell counting plate method is used to measure the spore yield 5 days later.

TABLE 2 Details of the *Fusarium* species complex sequences used in the molecular phylogenetic analysis.

Fungal taxa	Strain/isolate	GenBank accession number		
		Tef-1	RPB1	RPB2
Fusarium	CBS 258.50	MH484964.1	MW928820.1	MH484873.1
Fusarium	CBS 193.65	MN170450.1	MW928800.1	MN170383.1
F. curvatum	CBS 238.94	MH484984.1	MW928804.1	MH484893.1
F. cugenangense	LC4496	MW594324	MW024599	MW474557
F. cugenangense	LC13736	MW594321	MW024596	MW474554
F. curvatum	LC13739	MW594325	MW024600	MW474558
F. duoseptatum	LC13740	MW594326	MW024601	MW474559
F. duoseptatum	LC13741	MW594327	MW024602	MW474560
F. fabacearum	LC13743	MW594329	MW024604	MW474562
F. nirenbergiae	LC13760	MW594346	MW024621	MW474579
F. odoratissimum	LC13761	MW594348	MW024623	MW474581
F. oxysporum	LC13766	MW594353	MW024628	MW474586
F. libertatis	LLC1736	OP487222.1	OP486375.1	OP486790.1
N. solani	LC13841	MW620188	MW024757	MW474713

TABLE 3 Details of the *Aspergillus* species complex sequences used in the molecular phylogenetic analysis.

Fungal taxa	Strain/isolate	GenBank accession number				
		BenA	CaM	RPB2	Mcm7	Tsr1
A. versicolor	NRRL 238	LC589363	EF652354	EF652178	JN854079	JN853911
A. versicolor	DTO 019-A2	ON807694	ON807829	ON808133	ON807971	ON808262
A. versicolor	NRRL 4838	EF652304	EF652392	EF652216	JN854074	JN853907
A. versicolor	EMSL 4779	ON807705	ON807840	ON808143	ON807985	ON808274
A. versicolor	NRRL 233	JN853963	JN854025	JN853814	JN854086	JN853916
A. versicolor	DTO 237-D1	ON807716	ON807852	ON808155	ON807998	OP688454
A. versicolor	NRRL 3505	EF652284	EF652372	EF652196	JN854088	LC004923
A. versicolor	DTO 337-C3	ON807682	ON807818	ON808122	ON807959	ON808251
A. versicolor	EMSL 4723	ON807683	ON807819	ON808123	ON807960	ON808252
A. versicolor	NRRL 4791	EF652302	EF652390	EF652214	JN854084	JN853922
A. versicolor	DTO 019-D2	ON807675	ON807811	ON808115	ON807951	ON808243
A. sydowii	CGMCC 3.06723	ON807742	ON807878	ON808178	ON808035	ON808308
A. sydowii	UTHSCSA 12-934	LN898879	LN898802	LN898956	ON808032	ON808305
A. subversicolor	NRRL 58999	JN853970	JN854010	JN853799	JN854069	JN853857
A. creber	EMSL 4759	ON807791	ON807928	ON808221	ON808090	ON808362
A. creber	NRRL 58592	JN853980	JN854043	JN853832	JQ301890	JN853887

Utilization of different carbon and nitrogen sources

As mycelium grows from carbon and nitrogen sources, 7-day-old colonies were placed in the pivot of the culture. The growth of mycelium and sporulation yield of the pathogen from various nitrogen sources and carbon sources were calculated by Cha's solid (PTT) medium (Li et al., 2021). To sum up, two different types of carbon sources were used, namely, sucrose (ZT) and fructose (GT). No carbon source was treated as the control (PTT) group. At the same time, the method for setting nitrogen source groups were the same as above using ammonium nitrate (XSA) and ammonium sulfate (LSA). No nitrogen source was treated as the control (PTT). The experiments were repeated three times for each group and then mycelial development was observed at 28°C for 3–5 days under light/dark for 12 h. Mycelial growth and spore production were measured on the basis of the above method.

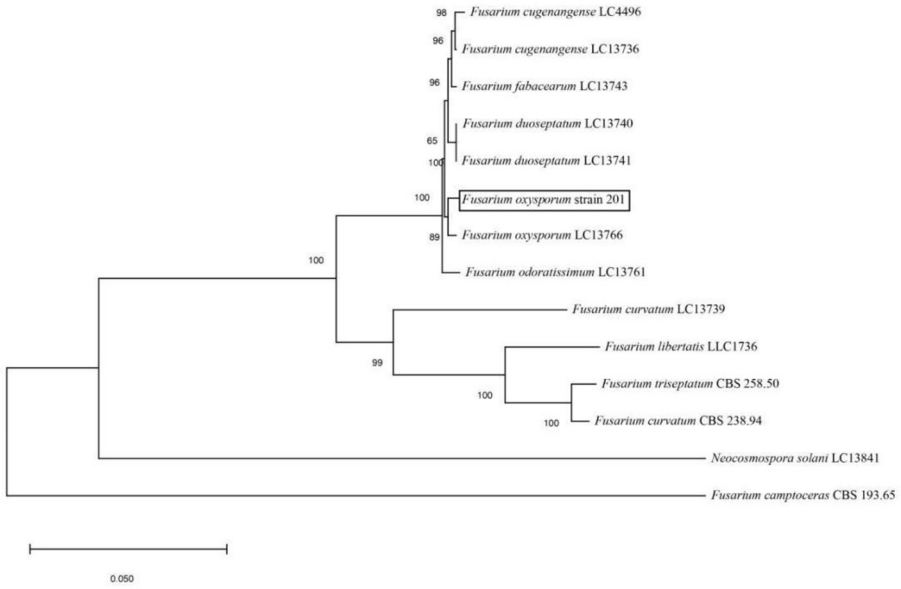

FIGURE 3
Phylogenetic analysis of concatenated sequences of Tef-1, RPB1, and RPB2 from this study and reference sequences of *Fusarium* spp. Specimens using the maximum likelihood method (1,000 bootstrap iterations).

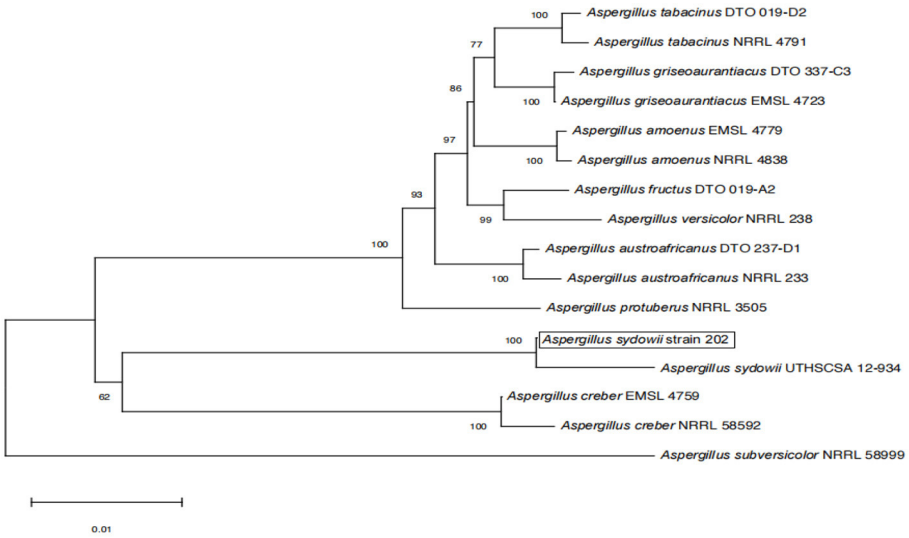

FIGURE 4
Phylogenetic analysis of concatenated sequences of BenA, Cam, RPB2, Mcm7, and Tsr1 from this study and references sequences of *Aspergillus* spp. Specimens using the maximum likelihood method (1,000 bootstrap iterations).

Effect of temperature and relative humidity (RH) on mycelium growth and sporulation quantity

The effect of temperature and RH on the growth of mycelium and sporulation quantity was tested on PDA medium, by incubating the culture at temperatures of 4, 15, 28, and 37°C and at relative humidity ranging from 55 to 85% at 15% intervals. A mature colony of 6 mm in diameter was placed at the center of the medium, which was then incubated at different temperatures and RH. The growth of mycelial was tested on the 3rd day. The sporulation quantity under different temperatures and relative humidity was determined.

Influence of pH on mycelium growth and sporulation quantity

To study the influence of pH on mycelium growth and sporulation quantity, the culture was incubated at pH ranging

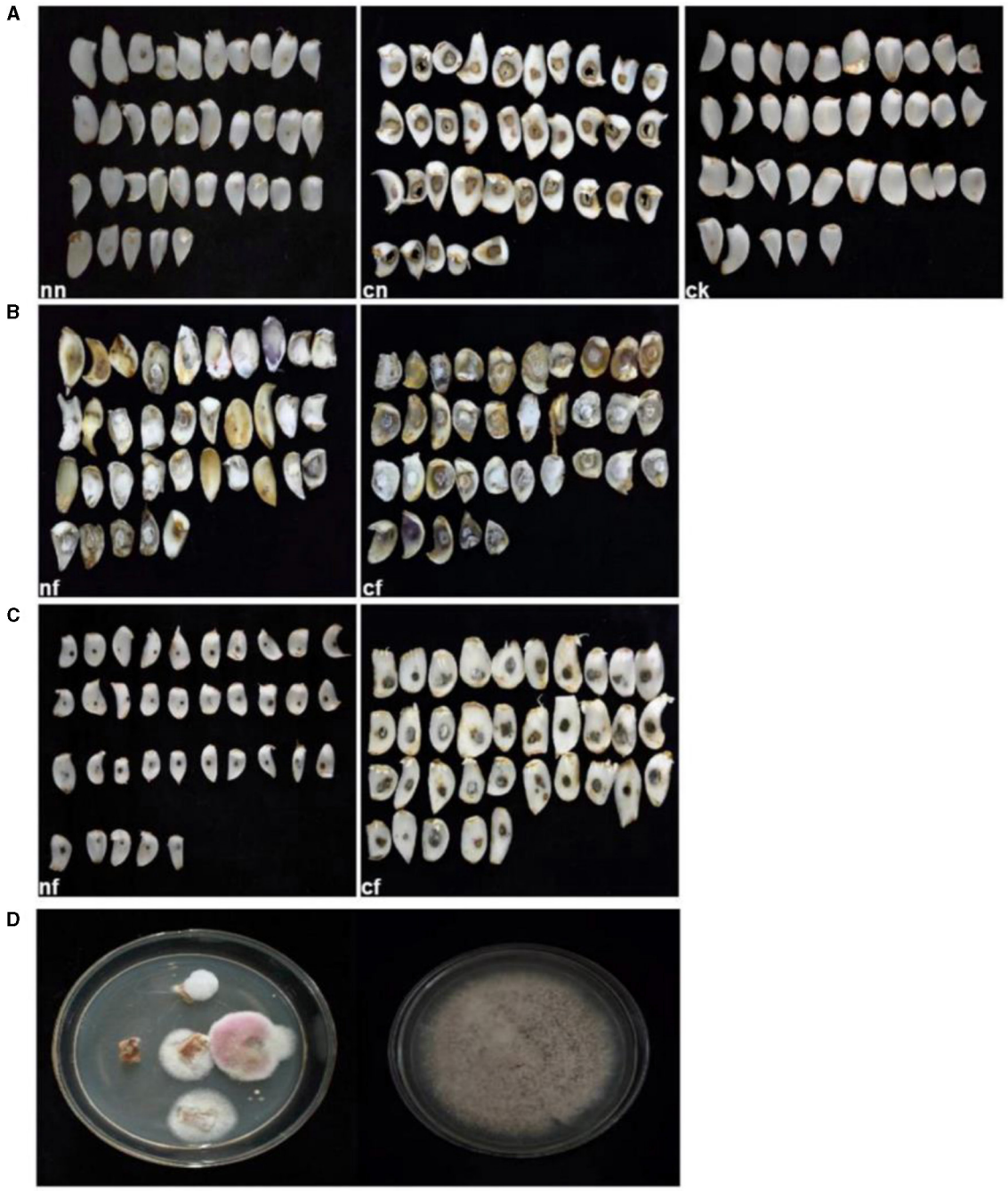

FIGURE 5
Pathogenicity test results of lily bulbs. **(A)** Represents the control group; **(B)** represents strain 201; **(C)** represents strain 202. **(D)** Pathogenicity test bulbs were reisolated and purified. **ck**, control group (fresh and undamaged bulb); **nn**, uninjured blank group (blank medium was placed in uninjured bulb slices); **cn**, stab blank group (blank medium was placed at the stab); **nf**, harmless fungus group (culture medium with the fungus was placed in the harmless bulb); **cf**, puncture fungus group (fungal culture medium placed at the puncture site).

from 5 to 9. A mature colony, which contained the isolated strains, was placed in PDA medium with a diameter about 6 mm and then incubated at 28°C. The spore yield was measured by blood cell counting plate at 7 days, and colony growth was measured by cross method as an indicator of mycelial growth.

Influence of photoperiod on mycelium growth and sporulation quantity

To understand the influence of illumination by light, the PDA medium was placed in incubators at 28°C under three light conditions of full light, full darkness, and light/dark for 12 h, respectively, which was then inoculated by pathogenic fungi blocks

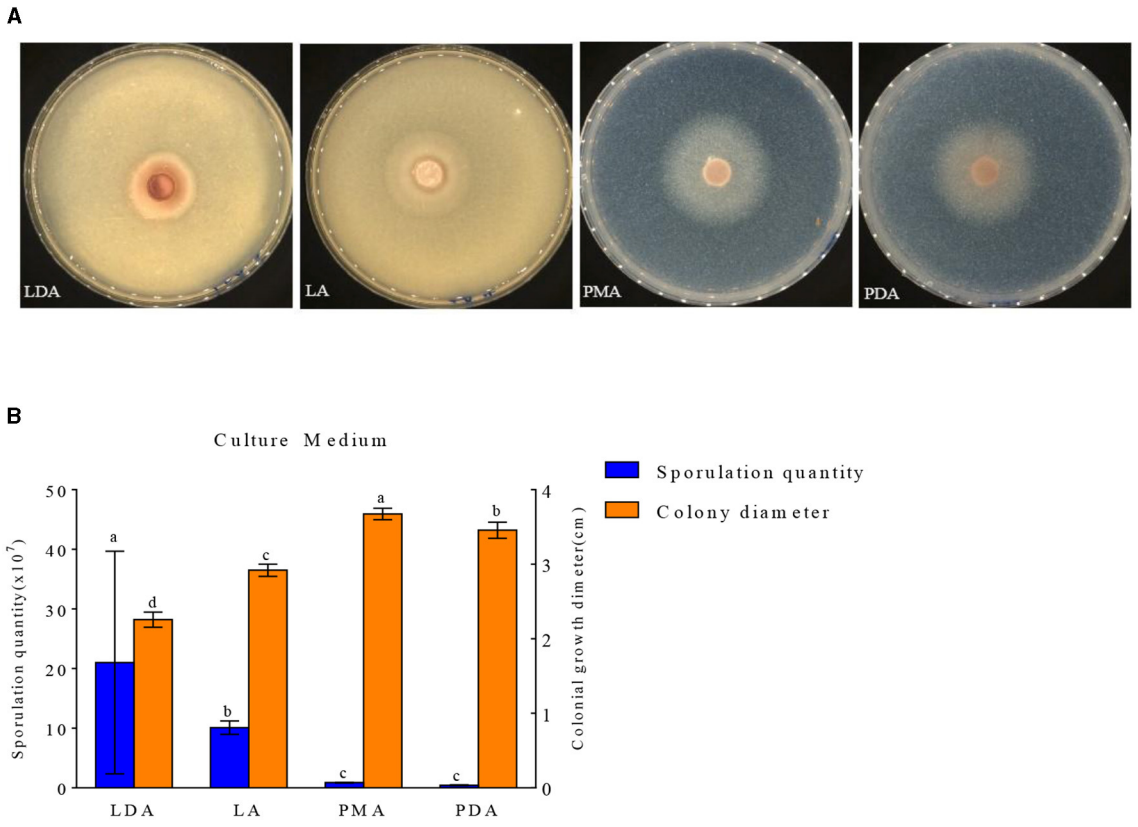

FIGURE 6
Effect of culture media on the mycelia growth and sporulation of strain 201. **(A)** The growth state of strain 201 on different media; **(B)** Histogram of the effect of different media on the mycelial growth and spore production of strain 201. Different letters indicate significant differences between groups.

TABLE 4 **Effect of culture media on the mycelia growth and sporulation of strain 201.**

Medium type	Spore yield ($\times 10^7$ cfu/mL)	Colony diameter (cm)
LDA	21.02 ± 17.61a	2.25 ± 0.08d
LA	10.09 ± 1.06b	2.92 ± 0.06c
PMA	0.88 ± 0.06c	3.67 ± 0.06a
PDA	0.46 ± 0.05c	3.45 ± 0.09b

Different letters indicate significant differences between groups ($P < 0.05$).

at 6 mm centrally. Each process was repeated three times. The mycelial growth and spore production were measured on the basis of the abovementioned method.

In vitro antifungal susceptibility of plant essential oils on mycelial growth

The growth of mycelium reflects the antifungal susceptibility of fungicides (Xin et al., 2020) to a certain degree. The various of anti-fungal agents were blended with the liquid culture of PDA medium at different concentrations in a moderate temperature. A comparable sterile water and carbendazim were added to the PDA medium, which served as the control group and positive control group, respectively. Meanwhile, PDA medium was taken as a blank control group. Afterward, a colony with fungi was placed in the blank control group, cultured at the conditions of 28°C and 55% RH for 7 days under light/dark for 12 h. Next the diameter of the mycelial growth (cm) was measured by a ruler. The employed essential oils were cinnamon essential oils (CEOs), tea tree essential oils (TEOs), and angelica essential oils (AEOs), which extracted from the stems and leaves of cinnamon, tea trees, and *Angelica sinensis* and carbendazim purchased from Sichuan Runer Technology Co., Ltd. (Pesticide registration number: PD85150-35).

Data analysis

SPSS 22.0 statistical software was utilized for one-way analysis of variance (ANOVA), Data analysis and plotting were performed using GraphPad Prism 8.0.2 and Duncan's new multiple range method was employed to test the significance of differences among treatments. The level of significance was set at $P = 0.05$.

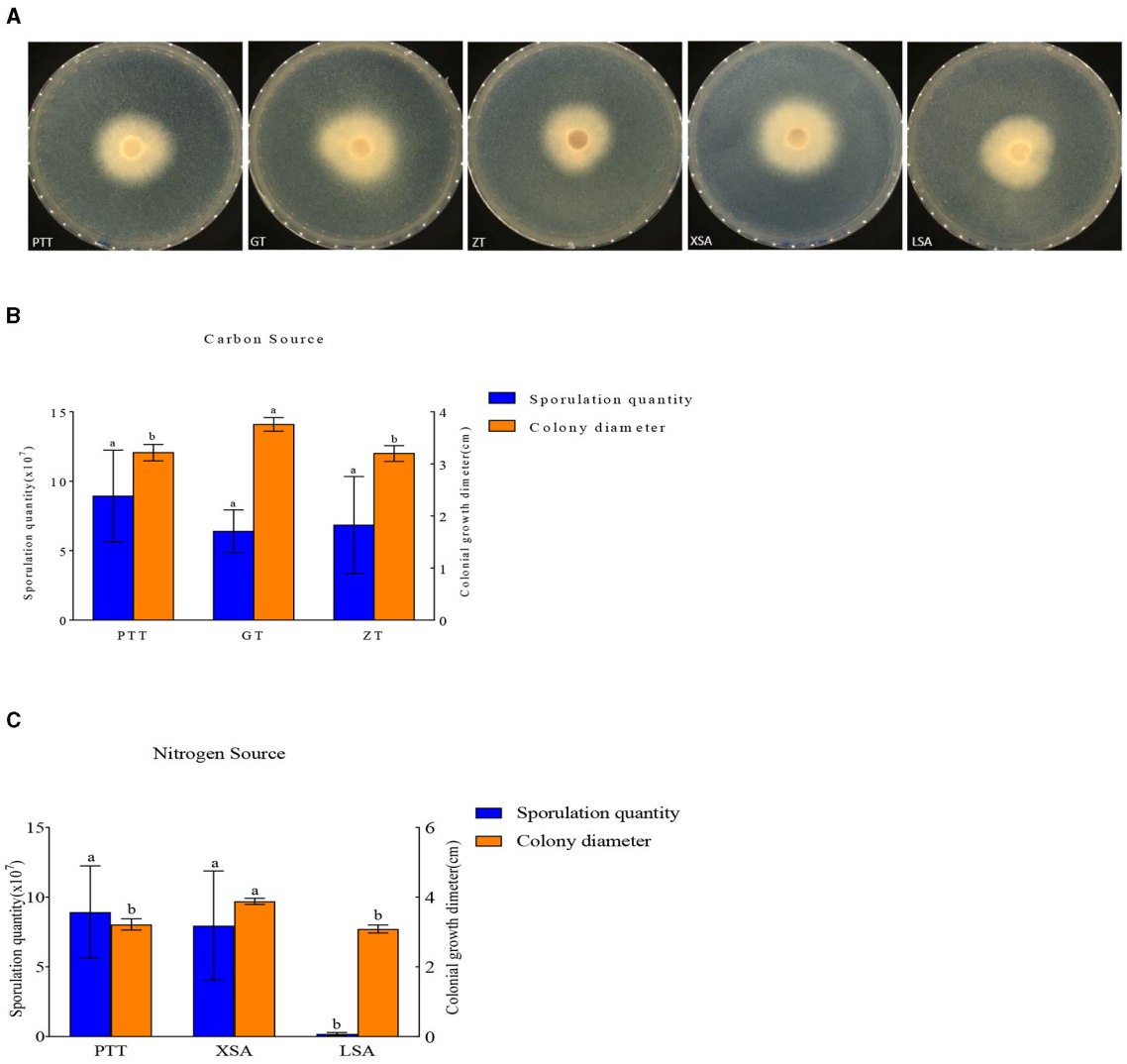

FIGURE 7
Effect of carbon and nitrogen source on the mycelia growth and sporulation of strain 201. **(A)** The growth status of strain 201 on different carbon and nitrogen sources; **(B, C)** Histogram of the effect of carbon and nitrogen sources on the mycelial growth and spore production of strain 201. Different letters indicate significant differences between groups.

Results

Pathogen identification

Morphological observations

Based on lily samples with BRD symptoms (Figures 1A, B), we used tissue separation method to obtain isolated strains (Figure 1C). The two strains (hereafter referred to as strains 201 and 202) were obtained through tissue isolation, and two colonies of each isolate were placed on PDA medium at a temperature of 28°C for 1 week. Strain 201 exhibited a white color with a regular circular shape, accompanied by the exudate in the early stage. The central part appeared flocculent, dense, and velvety, gradually transitioning from colorless to light yellow and becoming fluffy after 7 days. The phenomenon of light yellow pigmentation can be seen on the back surface of the PDA medium (Figure 1D). On the other hand, strain 202 displayed blue-green colonies that were dense and fluffy, with hyphae appearing white or grayish green (Figure 1E). In microscopic observations, strain 201 showed solitary characteristics: the hyphae have septa, the conidiophore are colorless, there are a few

TABLE 5 Effect of carbon and nitrogen sources on the mycelia growth and sporulation of strain 201.

Medium type		Spore yield ($\times 10^7$ cfu/mL)	Colony diameter (cm)
Control	PTT	8.90 ± 3.13a	3.21 ± 0.13b
	GT	6.40 ± 1.46a	3.76 ± 0.11a
Control source	ZT	0.68 ± 3.30a	3.20 ± 0.13b
	XSA	8.00 ± 3.70a	3.88 ± 0.07a
Nitrogen source	LSA	0.19 ± 0.10b	3.08 ± 0.10b

Different letters indicate significant differences between groups ($P < 0.05$).

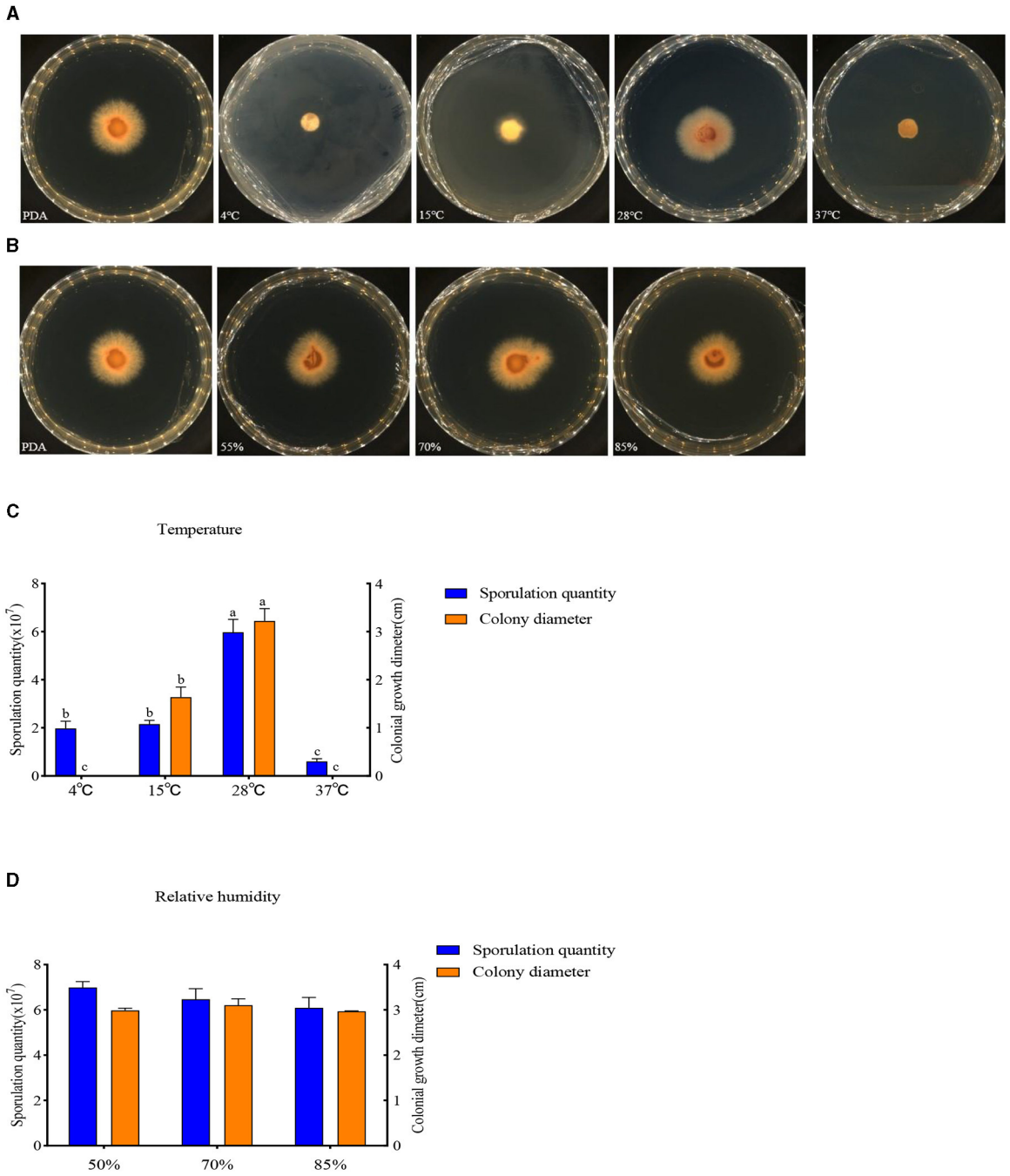

FIGURE 8
Effect of temperature and relative humidity on the mycelia growth and sporulation of strain 20. **(A, B)** The growth state of strain 201 under different temperatures and relative humidity values; **(C, D)** Histogram of the effect of temperature and relative humidity on the mycelial growth and spore production of strain 201. Different letters indicate significant differences between groups.

of branches that are sharp and angular, and many circular contents can be seen inside the hyphae. Microconidia are colorless, elliptical, ovoid, and columnar, with a wide center and gradually narrowing at both ends. Meanwhile, macroconidia are achromatic, sickle shaped, slender, with 0–5 septa and mostly 2–3 septa (Figure 2A). In contrast, strain 202 exhibited a complete spore-producing structure with a double layer. Sporangia resembled broom-like branching structures attached in chain-like formations. These sporangia appeared spherical or elliptical in shape and as short columns. Conidia are spherical or nearly spherical in shape, with rough walls and small spines (Figure 2B). Based on these morphological characteristics, it was initially determined that isolated strain 201 belonged to the genus *Fusarium* while strain 202 corresponded to *Aspergillus* species. Subsequently, phylogenetic analysis confirmed the identification of these fungi.

TABLE 6 Effect of temperature and relative humidity on the mycelia growth and sporulation of strain 201.

Type	Spore yield ($\times 10^7$ cfu/mL)		Colony diameter (cm)
Temperature	4°C	1.83 ± 0.49b	0.00c
	15°C	2.13 ± 0.35b	1.64 ± 0.21b
	28°C	6.24 ± 0.87a	3.22 ± 0.26a
	37°C	0.51 ± 0.18c	0.00c
Relative humidity	55%	6.78 ± 0.50	2.98 ± 0.05
	70%	6.16 ± 0.54	3.10 ± 0.14
	85%	6.10 ± 0.68	2.96 ± 0.01

Different letters indicate significant differences between groups ($P < 0.05$).

Phylogenetic analysis

The amplified sequences obtained from the two isolated fungal strains in our work were deposited into the GenBank (Tables 2, 3). The basic local alignment search tool (BLAST), were used to assign strains 201 and 202 to belong to the *Fusarium* species complex and *Aspergillus* species complex, respectively. Furthermore, fungal bioassay was performed through phylogenetic analysis. In our work, two phylogenetic trees were constructed for *Fusarium* and *Aspergillus* species complex. Consequently, the maximum likelihood (ML) analysis-generated phylogenetic trees are presented here. The phylogenetic tree successfully established monophyletic branches for the two fungal isolates (strains 201 and 202) evaluated in this study. Based on this tree, we can see that strain 201 and *F. oxysporum* as well as strain 202 and *A. sydowii* were on the same branches. Both have a high statistical support rate (100% BS; Figures 3, 4).

Pathogenicity test

After 15 days of inoculation, typical symptoms of BRD became visible on the bulbs. In contrast, the control group and strain 202 group remained asymptomatic (Figures 5A, C). Especially for the strain 202, there was a slight decay in the pricked area, where the fungal cake was placed in the cf group[1]. We speculated that this rot may be caused by prick injury rather than strain 202 (Figure 5C). The inoculated group pathogens of strain 201, whether injured or not, exhibited severe external damage characterized by the diseased spots of dark brown and brown lesions during infection. Surrounded by hyphae, these spots gradually expanded to form round or irregular shapes and eventually developed a rotten appearance with a visible layer of brown mold (Figure 5B). Thirty-five samples were used for the pathogenicity test, which is equivalent to 35 replicates and they consistently yielded similar results. To confirm the main pathogen, the cultures were isolated again from rot bulbs (Figure 5D) and identified to be *F. oxysporum* using the aforementioned morphological and molecular methods.

Based on the aforementioned findings, strain 201 is identified as *F. oxysporum*, while strain 202 is classified as *A. sydowii*. Because strain 201 can cause lily bulb rot and strain 202 cannot, simultaneously strain 201 can be obtained through re-isolation according to the pathogenicity test. Consequently, it can be inferred that *F. oxysporum* serves as the primary pathogenic fungi responsible for BRD in Lanzhou lily. Henceforth, the subsequent research was exclusively focused on *F. oxysporum*.

Influence of different culture media on mycelium growth and spore yield

The growth of mycelial growth and spore yield of *F. oxysporum* were significantly influenced by different media (Figures 6A, B). *F. oxysporum* can grow on all test media. The PMA medium and LDA medium are suitable culture media for *F. oxysporum*. It was observed that the colony diameter reached 3.68 cm after 3 days of cultivation on the PMA medium, and the spore yield was measured as 2.10×10^7 cfu/mL after a duration of 7 days on the LDA medium. Secondly, LA medium showed a significant decrease in mycelial growth and an increase in spore production compared to PDA medium, but both PMA and PDA media have a cholesterol-lowering effect on the spore yield of *F. oxysporum* (Table 4). In conclusion, both PMA and LDA media demonstrate suitability for cultivating pathogenic fungi.

Use of different carbon and nitrogen sources

The used carbon and nitrogen sources in all the experiments supported mycelium growth (Figure 7). Compared with the control medium (PTT), *F. oxysporum* exhibited the fastest mycelium growth and produced the highest spores on a culture medium with ammonium nitrate (XSA) as the nitrogen source, with a colony diameter of 3.88 cm after 3 days and the spore production of 8.00×10^7 cfu/mL after 7 days. On the other hand, the fastest growth and highest spore production of *F. oxysporum* were observed on the culture medium using fructose (GT) as the carbon source, in which the colony diameter was 3.76 cm after 3 days, and the spore production was 6.4×10^7 cfu/mL after 7 days, with statistically significant differences observed (Table 5). Overall, the conditions of XSA as the nitrogen source and GT as the carbon source are more favorable for the growth of *F. oxysporum*.

Effect of temperature and relative humidity

The buildup of *F. oxysporum* is significantly influenced by temperature especially (Figure 8). At temperatures of 4, 15, 28, and 37°C, mycelial growth and spore production were observed. At 4 and 37°C, the mycelium stops growing and the spore production decreases; the optimal temperature for the growth of *F. oxysporum* is 28°C, with the fastest mycelium growth and maximum spore production, followed by 15°C. *F. oxysporum* grows at intervals of 15% in the relative humidity range of 55–85%. Notably, RH did not have an obvious impact on the buildup of *F. oxysporum*. However, the spore production was most mutative when the relative humidity was 55% (Table 6). On the whole, the temperature of 28°C and relative humidity of 55% were the best conditions for the growth of mycelium and the spore production of *F. oxysporum*.

1 "cf" group refers to the fungi cake with PDA culture medium were pasted on the hole as the injured inoculation,means inoculate pathogenic fungi at the puncture site (here pathogenic fungi are strain 201 and strain 202).

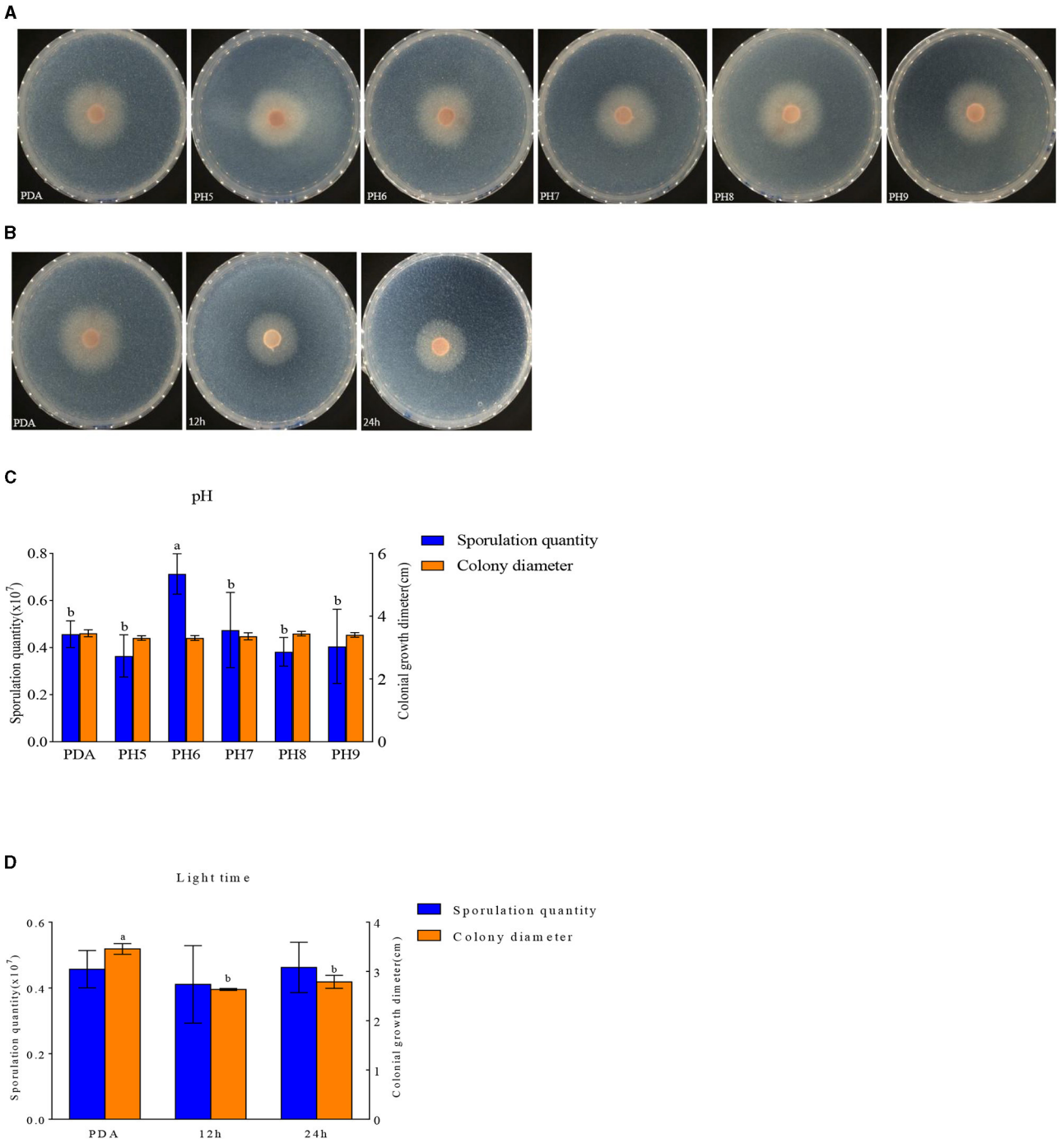

FIGURE 9
Effect of pH and light treatment on the mycelia growth and sporulation of strain 201. **(A, B)** Growth state of strain 201 under different pH and light; **(C, D)** Histogram of the effect of pH and light on the mycelial growth and spore production of strain 201. Different letters indicate significant differences between groups.

Influence of pH and photoperiod on mycelium growth and spore yield

F. oxysporum exhibits the ability to thrive in the pH range of 5–9 (Figures 9A, C). Other pH values have no effect on the growth of *F. oxysporum*, but the spore production of *F. oxysporum* is highest reaching 0.71 × 10^7 cfu/mL when pH is 6 (Table 7). Photoperiod also plays an important role on the growth of *F. oxysporum* (Figures 9B, D). It was observed that the light conditions favorable for *F. oxysporum* growth and spore yield of *F. oxysporum* are completely dark, followed by the conditions of complete light, and finally light/dark for 12 h. Based on the comprehensive analysis, the pH of 6 and

completely dark were the most suitable factors for the growth of *F. oxysporum*.

Fungicide assays

The representative isolate *F. oxysporum* exhibited varying sensitivities to the three plant essential oils (Figure 10). Among the tested essential oils, cinnamon essential oil demonstrated the highest inhibition rate, exhibiting a comparable antifungal effect to carbendazim within a specific range. Next was angelica essential oil, which also displayed suppressive effects against *F. oxysporum*. In contrast, when compared to cinnamon essential oil and *Angelica sinensis* essential oil, tea tree essential oil exhibits the weakest inhibitory effect on *F. oxysporum*. These findings indicate that *F. oxysporum* is most susceptible to cinnamon essential oil and least susceptible to tea tree essential oil (Table 8).

TABLE 7 Effect of pH and light treatment on the mycelia growth and sporulation of strain 201.

Type	Spore yield ($\times 10^7$ cfu/mL)		Colony diameter (cm)
pH	PDA	0.46 ± 0.05b	3.46 ± 0.09
	5	0.36 ± 0.08b	3.33 ± 0.02
	6	0.71 ± 0.08a	3.30 ± 0.06
	7	0.47 ± 0.15b	3.36 ± 0.09
	8	0.38 ± 0.06b	3.44 ± 0.06
	9	0.41 ± 0.11b	3.40 ± 0.06
Light time	PDA	0.46 ± 0.05	3.46 ± 0.09a
	12 h	0.41 ± 0.11	2.63 ± 0.02b
	24 h	0.46 ± 0.07	2.79 ± 0.12b

Different letters indicate significant differences between groups ($P < 0.05$).

Discussion

In this study, we isolated two strains of fungi from the rotten bulbs of Lanzhou lilies, namely, *F. oxysporum* and *A. sydowii*. *F. oxysporum* was identified as the main causative factor of BRD in Lanzhou lily based on comprehensive morphological and molecular characterization along with rigorous pathogenicity tests. Previous research (Bian et al., 2016) has reported the isolation of pathogenic fungi such as *F. oxysporum* from Lanzhou lily planted in Lintao County, Gansu Province. *F. oxysporum* could also cause scale rot of Lanzhou lily in the process of air culture, and the incidence rate was 95% (Hu et al., 2022), which is consistent with our findings regarding the isolation of pathogenic fungi.

A. sydowii, a species of *Aspergillus*, is widely distributed in nature due to its strong survival ability (Yu, 2015). Based on existing literature, research on *A. sydowii* has mostly focused on marine *A. sydowii* and tobacco products, as marine *A. sydowii* can produce various bioactive secondary metabolites (Sun, 2022). In addition, researchers have isolated *A. sydowii* in tobacco products (Huang et al., 2022; Zhu et al., 2023). For our study, *A. sydowii* was isolated for the first time. To our knowledge, this is one of the few reports on the isolation of *A. sydowii* from Lanzhou lily with BRD.

Furthermore, we characterized the influence of various carbon and nitrogen sources on the mycelium growth and spore production of *F. oxysporum*. Studies on biological characteristics have shown that the growth of *F. oxysporum* is the fastest on PMA medium, and the spore yield is the highest on the LDA medium. This indicates that the nutrition of maltose and lily bulbs themselves are beneficial for the reproduction of *F. oxysporum*,

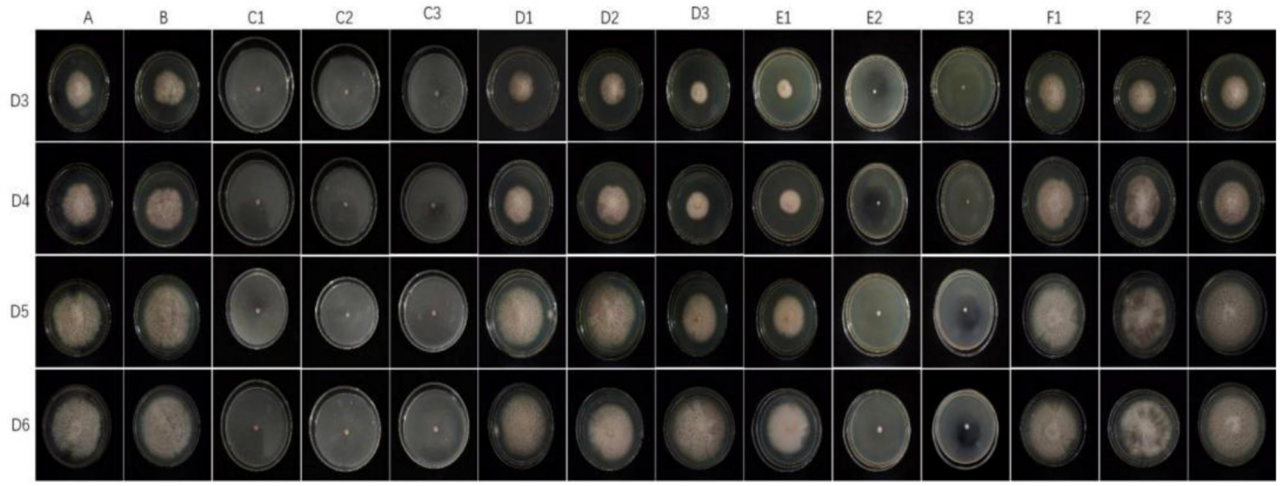

FIGURE 10
Effect of different antifungal agents on strain 201. Mycelial growth of strain 201 on PDA plates incubated for 3–6 days in the control group (A: blank medium, B: medium+water), positive control group (C: carbendazim, C1: 0.14 μL/mL, C2: 0.17 μL/mL, C3: 0.2 μL/mL), presence of different concentrations of angelica essential oil (D1: 0.14 μL/mL, D2: 0.17 μL/mL, D3: 0.2 μL/mL), cinnamon essential oil (E1: 0.14 μL/mL, E2: 0.17 μL/mL, E3: 0.2 μL/mL), and tea tree essential oil (F1: 0.14 μL/mL, F2: 0.17 μL/mL, F3: 0.2 μL/mL).

TABLE 8 Effect of the treatment with different plant essential oils on the mycelia growth of strain 201 (cm).

	D3	D4	D5	D6
A	4.67 ± 0.03	5.82 ± 0.06	7.52 ± 0.06	8.06 ± 0.05
B	5.18 ± 0.02[a]	5.85 ± 0.24	7.40 ± 0.08	8.28 ± 0.06
C1	0.60[ab]	0.60[ab]	0.60[ab]	0.60[ab]
C2	0.60[ab]	0.60[ab]	0.60[ab]	0.60[ab]
C3	0.60[ab]	0.60[ab]	0.60[ab]	0.60[ab]
D1	4.02 ± 0.06[a]	5.23 ± 0.22[a]	6.65 ± 0.08[a]	7.52 ± 0.05[a]
D2	3.02 ± 0.07[ac]	3.83 ± 0.10[ac]	5.30 ± 0.01[ac]	6.02 ± 0.05[ac]
D3	4.23 ± 0.02[ac]	5.38 ± 0.02[a]	6.90 ± 0.04[ac]	7.90 ± 0.04[c]
E1	2.60 ± 0.08[a]	3.50 ± 0.12[ac]	4.78 ± 0.18[a]	6.05 ± 0.16[a]
E2	0.60[ad]	0.60[ad]	0.60[ad]	0.61 ± 0.11[ad]
E3	0.60[ad]	0.60[ad]	0.60[ad]	0.60[ad]
F1	5.13 ± 0.14[a]	6.40 ± 0.08[a]	7.93 ± 0.14[a]	8.32 ± 0.07
F2	4.89 ± 0.06[a]	6.19 ± 0.05[ae]	6.85 ± 0.04[ae]	8.05 ± 0.16
F3	4.60 ± 0.05[d]	5.89 ± 0.04[d]	7.62 ± 0.06[d]	8.39 ± 0.05[ae]

[a]Represents the comparison between each group and Group A.
[b]Represents the comparison between C1, C2, and C3.
[c]Represents the comparison between D1, D2, and D3.
[d]Represents the comparison between E1, E2, and E3.
[e]Represents the comparison between F1, F2, and F3, $P < 0.05$.

which can infect lily bulbs and cause rot disease. In our study, ammonium nitrate as the nitrogen resource can promote mycelium growth and spore production of *F. oxysporum*. For this reason, we recommend that careful consideration should be given to the application of ammonium nitrate as a fertilizer in the fields of Lanzhou lily affected by *F. oxysporum* in China. In addition, we found that the tested carbon sources supported mycelium growth and spore production. Yet, compared to other carbon resources, the pathogen exhibits higher speed of growth and spore production on fructose. Other reports have shown that sucrose is one of the best carbon sources for producing enrofloxacin in *F. oxysporum* isolates (Cao et al., 2018; Ya et al., 2018), but both fructose and sucrose can alter the biosynthesis of fungal toxins and affect the quality of lilies. In the future research, it will be vital to study how carbon and nitrogen resources other than NH_4NO_3 and fructose affect lily BRD and explore how these resources can be considered and utilized in lily cultivation and storage. At the same time, carbon and nitrogen resources supporting BRD development and fungal toxin production should be reduced, which can provide new solutions for sustainable management of lily bulb diseases and storage.

The mycelial growth of *F. oxysporum* was influenced heavily by temperature. The mycelium stops growing and the spore production decreases at 4 and 37°C. *F. oxysporum* can produce spores when the temperature is between 4 and 37°C. The optimal growth temperature range for mycelium growth is 15–28°C, but 28°C is the appropriate temperature for mycelial growth as well as spore production. This finding agrees with Bian et al.'s (2016) and Cao et al. (2018) research on the biological characteristics of *F. oxysporum*, which revealed that the optimal temperature for mycelial growth and spore production was 25°C. In addition, humidity is an important environmental factor having a certain impact on the occurrence of BRD in Lanzhou lily. In this study, a relative humidity of 55% was found to be optimal for mycelial growth and spore production of *F. oxysporum*. Therefore, we should fully consider the prevention of BRD in Lanzhou lily by varying the temperature and relative humidity during its storage.

According to reports, photoperiod as a key external environmental variable may affect the plant pathogens and their biological characteristics (Costa et al., 2021; Macioszek et al., 2021). In our present work, full darkness (no illumination) was conducive to the buildup of *F. oxysporum*. For some isolates of *F. oxysporum*, total darkness was also clearly causing hyphal growth and/or spore yield (Pan et al., 2011; Jin et al., 2019). This is different from the observation of Cao Xing, who have indicated that the light and dark environment affects its mycelial growth and conidia germination (Cao et al., 2018). Accordingly, within *Fusarium* sp., strain specificity reactions to photoperiod may extensively exist. When the pH increases between pH 5 and 9, there is no significant change in the size of the colony diameter and spore production of *F. oxysporum*. But the spore production reaches its maximum value at pH 6. Moreover, pH 6–7 is conducive to mycelial growth and spore production, with pH 6 being the optimal value. These findings agree with Zhao (2012), who found the optimal pH of 6 for the mycelial growth of *F. oxysporum*, a pathogen of green hybrid bamboo wilt disease, and also consistent with Feng's (2014) description of the optimal pH 6 for *F. oxysporum*, a pathogen of Acacia wilt disease. Consequently, it is necessary to explore the effects of ultraviolet radiation and soil pH on bulb diseases of Lanzhou lily during storage.

The utilization of natural plant ingredients with antifungal properties as potential alternatives to chemical fungicides is preferred. Consequently, we conducted an investigation on the antifungal efficacy of three plant essential oils against *F. oxysporum*. Among the three tested essential oils, cinnamon essential oil showed the best inhibition rates. The results were consistent with the research findings that cinnamon essential oil was good for inhibiting the growth of bacteria and fungi (Mao, 2018; He, 2019; Yang et al., 2021; Zhao et al., 2023). Some researchers have proven that angelica essential oil has an inhibitory effect on pathogenic bacteria (Prakash et al., 2015; Qiao et al., 2022). Our results indicated that angelica essential oil s also showed an inhibition ability against *F. oxysporum*. Similar to our research findings, several biological fungicides and their mixtures were shown to inhibit the growth of *F. oxysporum* isolates (Jiang et al., 2021). Therefore, it is necessary to conduct in-depth and systematic research in the future to determine whether a mixture of various plant essential oils can more effectively inhibit the fungal diseases of Lanzhou lily during storage.

Data availability statement

The original contributions presented in the study are included in the article/supplementary material, further inquiries can be directed to the corresponding author.

Author contributions

CL: Writing—original draft, Writing—review & editing. YiW: Writing—review & editing, Project administration, Supervision. LJ: Project administration, Writing—review & editing. YaW: Writing—review & editing. DL: Writing—review & editing.

Funding

The author(s) declare that financial support was received for the research, authorship, and/or publication of this article. This work was supported by the earmarked fund for National Modern Agricultural Industry Technology System Grant (CARS-21) of the Ministry of Finance and the Ministry of Agriculture and Rural Affairs of the People's Republic of China, the Strategic Research and Consulting Project of the Chinese Academy of Engineering (GS2021ZDA06), Double First-Class Major Scientific Research Project of the Gansu Provincial Department of Education (GSSYLXM-05), Evaluation of the Toxicity of Rotten Lilies Based on the Elegant *Caenorhabditis elegans* (2022CX12), and Gansu Province Science and Technology Major Special Project (23ZDFA013-1).

Acknowledgments

The authors acknowledge Xiaodan Zhang (Wuhan Luming Biology Co., Ltd.) for his assistance in the identification of pathogenic fungi.

Conflict of interest

The authors declare that the research was conducted in the absence of any commercial or financial relationships that could be construed as a potential conflict of interest.

Publisher's note

All claims expressed in this article are solely those of the authors and do not necessarily represent those of their affiliated organizations, or those of the publisher, the editors and the reviewers. Any product that may be evaluated in this article, or claim that may be made by its manufacturer, is not guaranteed or endorsed by the publisher.

References

Bian, C., Kusuya, Y., Sklenár, F., D'hooge, E., Yaguchi, T., Ban, S., et al. (2022). Reducing the number of accepted species in *Aspergillus series* Nigri. *Stud. Mycol.* 102, 95–132. doi: 10.3114/sim.2022.102.03

Bian, X. R. (2016). *Identification of the Pathogen of Lily Fusarium wilt in Lanzhou and Study on the Biological Characteristics of the Pathogen* (Master's thesis), Gansu Agricultural University. Available online at: https://kns.cnki.net/KCMS/detail/detail.aspx?dbname=CMFD201602&filename=1016902580.nh

Bian, X. R., Shi, G. Y., Liang, Q. L., Sun, H. Q., Fan,. S. F., and Chen, J. L. (2016). Isolation, identification and pathogenicity determination of lily fusarium wilt pathogen in Lanzhou. *J. Gansu Agri. Univ.* 4, 58–64. doi: 10.3969/j.issn.1003-4315.2016.04.010

Cao, X., Liu, N. N., Hu, Y. N., Yi, M. F., and Wang, G. Q. (2018). Identification and biological characteristics of the pathogen of lily bulb rot disease. *Henan Agri. Sci.* 12, 96–101. doi: 10.15933/j.cnki.1004-3268.2018.12.015

Costa, T. P., Rodrigues, E. M., Dias, L. P., Pupin, B., Ferreira, P. C., and Rangel, D. E. (2021). Different wavelengths of visible light influence the conidia production and tolerance to ultra-violet radiation of the plant pathogens *Colletotrichum acutatum* and *Fusarium fujikuroi*. *Eur. J. Plant Pathol.* 159, 105–115. doi: 10.1007/s10658-020-02146-y

Darriba, D., Taboada, G. L., Doallo, R., and Posada, D. (2012). jModelTest 2: more models, new heuristics and parallel computing. *Nat. Methods* 9:772. doi: 10.1038/nmeth.2109

De Oliveira, M. J., Laranjeira, D., Câmara, M. P. S., Laranjeira, F. F., Armengol, J., and Michereff, S. J. (2014). Effects of wounding, humidity, temperature, and inoculum concentrations on the severity of corky dry rot caused by *Fusarium semitectum* in melon fruits. *ActaSci. Agron.* 36, 281–289 doi: 10.4025/actasciagron.v36i3.17656

Feng, X. (2014). *Master's Thesis on the Biological Characteristics and Screening of Control Agents of Fusarium oxysporum wilt Disease in* Acacia. Wuhan: Huazhong Agricultural University.

Gao, D., Chen, H., Liu, H., Yang, X., Guo, P., Cao, X., et al. (2022). Structure characterization and antioxidant activity analysis of polysaccharides from Lanzhou Lily. *Front. Nutr.* 9:976607. doi: 10.3389/fnut.2022.976607

Gao, Z. Y., Xue, J., Yang, F. P., Zhang, M. F., Zhang, X. H., and Dong, R. (2022). Isolation, identification of pathogens of Lanzhou lily and the pathogenicity determination of scales. *Mol. Plant Breed.* 1–9. Available online at: https://kns.cnki.net/kcms/detail/46.1068.S.20220729.1728.027.html

Gong, H. L., Sun, A. J., Li, Q., Tang, G. G., Yuan, H. J., Feng, Z. P., et al. (2015). Identification of the pathogen from stored Lanzhou lily bulb rot disease and biological characteristics. *Sci. Technol. Food Indus.* 20, 97–106. doi: 10.13386/j.issn.1002-0306.2015.20.011

Hammer, K. A., and Carson, C. F. (2011). "Antibacterial and antifungal activities of essential oils," in *Lipids and Essential Oils as Antimicrobial Agents*, ed T. Halldor (Hoboken, NJ: Wiley).

He, J. L. (2019). *Research on the Inhibition Mechanism and Application of Cinnamon Essential Oil on Two Postharvest Pathogens of Red Yang Kiwifruit*. (Doctoral Dissertation), Sichuan Agricultural Science. Available online at: https://kns.cnki.net/KCMS/detail/detail.aspx?dbname=CDFDLAST2021&~filename$=$1019676742.nh

Hu, Y., Cao, C., Lv, L. Z., and Ju, X. T. (2022). Isolation and identification of pathogenic bacteria of lily scale rot disease in Lanzhou. *Hubei Agric. Sci.* 18, 84–87. doi: 10.14088/j.cnki.issn0439-8114.2022.18.013

Hu, Y., Ren, J., Liu, Y., Zhang, M., and Zhang, X. (2020). Evaluating the genetic relationship of lilium species/cultivars based on target region amplification polymorphism (trap). *Genet. Resour. Crop Evol.* 67, 503–513. doi: 10.1007/s10722-019-00880-9

Huang, M. M., Chen, M. Z., Chen, J., and Zheng, W. W. (2022). Isolation, identification and conidial development of an endophytic fungus from Man Jianghong. *Subtrop. Plant Sci.* 1, 26–33. doi: 10.3969/j.issn.1009-7791.2022.01.004

Janisiewicz, W. J., and Conway, W. S. (2010). Combining biological control with physical and chemical treatments to control fruit decay after harvest. *Stewart Postharv. Rev.* 6, 1–16. doi: 10.2212/spr.2010.1.3

Jiang, Y. L., Liang, Q. L., Wei, L. X., Meng, X. P., Lin, K., and Yue, Y. (2021). Prevention and control effects of several biopesticides and their mixtures on bulb rot disease of Lanzhou lilies during storage. *Chin. J. Biol. Contr.* 5, 1041–1049. doi: 10.16409/j.cnki.2095-039x.2021.06.002

Jiao, X. L., Zhang, X. M., and Zhou, Y. H. (2021). Research progress on bulb diseases of medicinal lily. *China Plant Protect. Guide* 41, 30–37. doi: 10.3969/j.issn.1672-6820.2021.10.005

Jin, X. M., Luo, Y. H., Qin, Z. C., Li, X. Y., Yan, H. X., and Liu, X. P. (2019). Biological characteristics and virulence of *Fusarium oxysporum*. *Chin. J. Grassl.* 41, 144–151.

Kong, Y., Bai, J., Lang, L., Bao, F., Dou, X., and Wang, H. (2017). Floral scents produced by lilium and cardiocrinum species native to china. *Biochem. Systemat. Ecol.* 70, 222–229. doi: 10.1016/j.bse.2016.11.001

Li, F., Matloob, M., Nzabanita, C., and Li, Y. (2021). Growth, sporulation and germination of *Verticillium alfalfae* on media. *Eur. Plant Pathol.* 161, 383–395. doi: 10.1007/s10658-021-02330-8

Li, Y., Wang, H., Zhang, W., Wu, H., and Wang, Z. (2020). Evaluation of nutrition components in Lanzhou lily bulb by confocal Raman microscopy. *Spectrochim. Acta A Mol. Biomol. Spectrosc.* 244:118837. doi: 10.1016/j.saa.2020.118837

Li, Y. Y., Wang, Y. J., Xie, Z. K., Wang, R. Y., Qiu, Y., Pan, H. Q., et al. (2013). First report of lily blight and wilt caused by *Fusarium tricinctum* in China. *Plant Dis.* 97:993. doi: 10.1094/PDIS-11-12-1010-PDN

Macioszek, V. K., Sobczak, M., Skoczowski, A., Oliwa, J., Michlewska, S., and Gapi'nska, M. A. (2021). The effect of photoperiod on necrosis development, photosynthetic efficiency and 'Green Islands' formation in *Brassica juncea* infectedwith *Alternaria brassicicola*. *Int. J. Mol. Sci.* 22:8435. doi: 10.3390/ijms22168435

Maffei, M. E. (2010). Sites of synthesis, biochemistry and functional role of plant volatiles. *South Afri. J. Bot*. 76, 612–631. doi: 10.1016/j.sajb.2010.03.003

Mao, X. L. (2018). *Study on the Inhibition and Preservation Effect of Cinnamon Essential Oil on Some Postharvest Pathogens of Jufeng Grape*. (Master's Thesis), Central South University of Forestry and Technology. Available online at: https://kns.cnki.net/KCMS/detail.aspxdbname=CMFD201802&filename=1018112669.nh (accessed February 25, 2024).

Miller, M. A., Pfeiffer, W., and Schwartz, T. (2010). Creating the CIPRES Science Gateway for inference of large phylogenetic trees. *Grid Comput. Environ.* 2010:5676129. doi: 10.1109/GCE.2010.5676129

Nuangmek, W., Kumla, J., Khuna, S., Lumyong, S., and Suwannarach, N. (2023). Identification and characterization of fusarium species causing watermelon fruit rot in Northern Thailand. *Plants* 12:956. doi: 10.3390/plants12040956

Pan, H., Guan, F. Z., Wu, G. W., Song, X. X., Jiang, W. D., and Wang, L. Q. (2011). *Fusarium oxysporum* type flax specialization biological characteristics research. *J. Northeast Agric. Univer*. 42, 50–56. doi: 10.3969/j.issn.1005-9369.2011.07.009

Panjehkeh, N., and Jahani Hossein-Abadi, Z. (2011). Inhibitory effects of essential oils of medicinal plants from growth of plant pathogenic fungi. *Commun. Agri. Appl. Biol. Sci.* 76, 705–714. doi: 10.21608/jpd.2014.42648

Prakash, B., Kenla, A., and Mishra, P. K. (2015). Plant essential oils as food preservatives to control moulds, mycotoxin contamination and oxidative deterioration of agri-food commoditiese: potentials and challenges. *Food Control* 47, 381–391 doi: 10.1016/j.foodcont.2014.07.023

Qiao, C. H., Li, B. S., Zhang, Z., Bi, Y., Li, Z. H., Zhu, Y. T., et al. (2022). The inhibitory activity of *Angelica sinensis* stem and leaf essential oil on four types of post harvest spoilage fungi in fruits and vegetables. *Food Ferment. Indus.* 11, 206–212. doi: 10.13995/j.cnki.11-1802/ts.029680

Rambaut, A. (2019). *FigTree Tree Figure Drawing Tool Version 13*. Edinburgh: Institute of Evolutionary 623 Biology, University of Edinburgh. Available online at: http://treebioedacuk/software/figtree (accessed February 25, 2024).

Ronquist, F., Teslenko, M., Van der Mark, P., Ayres, D. L., Darling, A., Höhna, S., et al. (2012). MrBayes 3.2: efficient Bayesian phylogenetic inference and model choice across a large model space. *Systemat. Biol.* 61, 539–542. doi: 10.1093/sysbio/sys029

Sanches-Silva, A., Costa, D., Albuquerque, T. G., Buonocore, G. G., Ramos, F., Castilho, M. C., et al. (2014). Trends in the use of natural antioxidants in active food packaging: a review. *Food Additiv. Contaminant. A Chem. Anal. Contr. Exposure Risk Assess.* 31, 374–395. doi: 10.1080/19440049.2013.879215

Sara, L. M., Orly, E., and Marcel, M. (2014). Bulb and root rot in lily (*Lilium longiflorum*) and onion (*Allium cepa*) in Israel. *J. Phytopathol.* 162, 466–471. doi: 10.1111/jph.12214

Shang, Q. H., Zhao, X., and Li, Y. Y. (2014). First report of *Fusarium tricinctum* causing stem and root rot on Lanzhou lily (*Lilium davidii* var. unicolor) in China. *Plant Dis.* 98, 999. doi: 10.1094/PDIS-11-13-1146-PDN

Sklenár, F., Glässnerová, K., Jurjević, Ž., Houbraken, J., Samson, R. A., Visagie, C. M., et al. (2022). Taxonomy of *Aspergillus series* Versicolores: species reduction and lessons learned about intraspecific variability. *Stud. Mycol.* 102, 53–93. doi: 10.3114/sim.2022.102.02

Sun, Y. (2022). *Study on Co culture Inducing Secondary Metabolite Production and Its Mechanism in Aspergillus polymorphus*. Dalian: Dalian University of Technology.

Vigan, M. (2010). Essential oils: renewal of interest and toxicity. *Eur. J. Dermatol.* 20, 685–692. doi: 10.1684/ejd.2010.1066

Wang, M. M., Chen, Q., Diao, Y. Z., Duan, W. J., and Cai, L. (2019). *Fusarium incarnatum*-equiseti complex from China. *Persoonia* 43, 70–89. doi: 10.3767/persoonia.2019.43.03

Wang, M. M., Crous, P. W., and Sandoval-Denis, M. (2022). Fusarium and allied genera from China: species diversity and distribution. *Persoonia* 48, 1–53. doi: 10.3767/persoonia.2022.48.01

Wei, Y. Z., Wei, Y. Y., and Xu, F. (2018). The combined effects of tea tree oil and hot air treatment on the quality and sensory characteristics and decay of strawberry. *Postharv. Biol. Technol.* 136, 139–144. doi: 10.1016/j.postharvbio.2017.11.008

Xin, W., Mao, Y., Lu, F., Li, T., Wang, J., and Duan, Y. (2020). *In vitro* fungicidal activity and in planta control efficacy of coumoxystrobin against *Magnaporthe oryzae*. *Pestic. Biochem. Physiol*. 162, 78–85. doi: 10.1016/j.pestbp.2019.09.004

Xing, L., Chen, X. X., Zhou, Y. H., Li, Y., Guo, J., Huang, Y. W., et al. (2022). Pathogenic identification of medicinal lily bulb rot disease in Beijing. *Chin. Medicinal Mater.* 9, 2060–2065. doi: 10.13863/j.issn1001-4454.2022.09.005

Ya, X. Z., Chen, Y. Y., Li, F. X., Cao, H., Xin, F. L., Du, F., et al. (2018). Identification and biological characteristics of a lily fusarium wilt pathogen. *J. Shanxi Agri. Univ.* 5, 1–6. doi: 10.13842/j.cnki.issn1671-8151.201712009

Yang, R. P., Miao, J. Y., and Shen, Y. T. (2021). Antifungal effect of cinnamaldehyde, eugenol and carvacrol nanoemulsion against *Penicillium digitatum* and application in postharvest preservation of Citrusfruit. *LWT* 141:110924. doi: 10.1016/j.lwt.2021.110924

Yu, H. (2015). *Study on the Chemical Constituents of Trichoderma and Aspergillus Polysaccharide*. Baoding: Hebei University.

Zeng, H., Li, R., Lu, Q., and Yan, D. (2020). First report of bulb rot on lily caused by Curvularia pseudobrachyspora in China. *Plant Dis.* 104:291. doi: 10.1094/PDIS-05-19-0943-PDN

Zhao, D. B., Wang, S. D., and Wang, W. W. (2023). Preparation and antibacterial activity study of cinnamon essential oil nanoemulsion Chinese. *Seasonings* 4, 194–199. doi: 10.3969/j.issn.1000-9973.2023.04.034

Zhao, J. Y. (2012). *Support × Master's Thesis on the Identification and Biological Characteristics of the Pathogen of Green Hybrid Bamboo Wilt Disease*. Sichuan Agricultural University. Available online at: https://kns.cnki.net/kcms2/article/abstract?v=mRajgomPiinxx_xGdmaWU9MQbkLaE-Muzc7fxKFrnBIuZttkcksOkT9I7UZdaFfQqZpYgSMXhB5n_G-crNnh-d5A0fJwrACucgbOHwt6ml~RsgKjS8fB5SHRyVWY545qPFje0M6LhfpA6hv21INyQ==uniplatform=NZKPTlanguage=CHS (accessed February 25, 2024).

Zhu, B. B., Huang, K., Xue, F., An, H. Q., Ye, C. W., Li, D., et al. (2023). Isolation, identification and biological characteristics of main fungi in handmade cigars. *Chin. J. Tobacco* 6, 93–101. doi: 10.16472/j.chinatobacco.2022.208

Zhu, C. Y., Lei, M. Y., and Mebeaselassie, A. (2019). Antifungal activity and mechanism of action of tannic acid against *Penicillium digitatum*. *Physiol. Mol. Plant Pathol*. 107, 46–50. doi: 10.1016/j.pmpp.2019.04.009

Frontiers in Microbiology

Explores the habitable world and the potential of microbial life

The largest and most cited microbiology journal which advances our understanding of the role microbes play in addressing global challenges such as healthcare, food security, and climate change.

Discover the latest Research Topics

See more →

Frontiers

Avenue du Tribunal-Fédéral 34
1005 Lausanne, Switzerland
frontiersin.org

Contact us

+41 (0)21 510 17 00
frontiersin.org/about/contact